2016

Effects Of Process Variants On Metallurgical And Mechanical Properties In Friction Stir Welding Of Aluminum Alloys

Xiaomin Huang
University of South Carolina

EFFECTS OF PROCESS VARIANTS ON METALLURGICAL AND MECHANICAL PROPERTIES IN FRICTION STIR WELDING OF ALUMINUM ALLOYS

by

Xiaomin Huang

Bachelor of Science
Wuhan University of Technology, 2008

Master of Science
Wuhan University of Technology, 2011

Submitted in Partial Fulfillment of the Requirements

For the Degree of Doctor of Philosophy in

Mechanical Engineering

College of Engineering and Computing

University of South Carolina

2016

Accepted by:

Anthony P. Reynolds, Major Professor

Jamil A. Khan, Committee Member

Chen Li, Committee Member

Xiao-Dong Zhou, Committee Member

Cheryl L. Addy, Vice Provost and Dean of the Graduate School

DEDICATION

To my father Guoyou and mother Jinzhen, for giving me life

To my sister Min and brother Rui, for growing together

To my husband Peng, for listening, accompanying and loving

To my son Austin, for giving me hope and power

ACKNOWLEDGMENTS

It has been five and a half years since I arrived at USC and began my Ph.D. study in USC. Deep in my heart, this is the most special journey and experience in my life so far, which has a particular meaning for myself, my professional career and the personal growth in the future. I grow from an outsider of friction stir welding to a professional researcher, and I'm so proud to become a professional FSWer. I survived from extreme sorrow in losing loved ones, and enjoy the great joy and happiness of a new born life. I learn how to insist especially during hard times and will conquer every challenge in future. I'm lucky and glad to meet another ME and am learning to be a better myself. Love in advancing side, life in retreating side. Looking back on the past and right into the future, I am deeply grateful. I would like to specially appreciate those persons and organizations who shape the person that I am today during my research and life.

I would like to gratefully and sincerely appreciate my advisor, Professor Anthony P. Reynolds, for your continuous guidance, support, understanding, patience and invaluable advices during my graduate study at University of South Carolina. I've learned a lot from you, your erudite knowledge, critical thinking, dedication to work, and optimistic attitude to life. Your mentorship was paramount in shaping my dissertation and understanding of science research especially in friction stir welding, fostering my professional development, and providing a well-rounded experience consistent with my career goals in long term. I also gratefully acknowledge the financial support from the

Center for Friction Stir Processing (CFSP) which is a National Science Foundation-Industry/University Cooperative Research Centers (NSF-I/UCRC) supported by Grant No. EEC-0437341.

I would like to thank Dr. Wei Tang and Associate Lab Engineer Daniel Wilhelm. Dr. Tang, thank you for your assistance in training me to be an FSWer, planning and executing experiments, laboratory testing and also your help for getting me along with the study and living in Columbia. I still miss the enjoyable holiday parties and delicious food shared with your family. Dan, you are such a nice, professional and great engineer and machinist. I've always been surprised by and grateful for your generous selfless help in my research. Thank you for making my welds and experiments possible, and giving me the chance to watch the flight show of those cool and amazing model planes you made. I will never forget the beautiful scene: the airplane soaring and diving in the blue summer sky, Lake Murray shining brightly in the sunshine, and people talking, laughing and sharing.

I also appreciate my committee members, Professor Jamil Khan, Professor Chen Li and Professor Xiao-Dong Zhou, for their comments, suggestions, time and effort while going through the research proposal and dissertation.

I would like to specially acknowledge administrative personnel of the Department of Mechanical Engineering at USC: Professor Jamil A. Khan (Chair), Mr. Glenn Severt (IT Manager), Ms. Renee Jenkins (Admin. Assist.), Ms. Misty O'Donnell (Admin. Assist.), Ms. Lalitha Ravi (Admin. Assist.) for their help in many academic affairs.

Special thanks to my group members, also my comrades and partners in FSW lab at USC: Piyush, Reza, Clinton, Joel, Hussein, Xiao, Hejun, Dawei, Ryan, Marie, Mathieu,

Corbin, Ilana, Jeffery, Matthew for their help, suggestions and contributions in academic area and daily life. I also thank all my friends who make my life in USC enjoyable and colorful.

I reserve my thanks for my parents and family members for accompany, support, encouragement, patience and unconditional love during my study and life. My dear parents, you are the enlightenment to me. Dad, I would be no one without your encouragement. I will always remember what you told me: delve into your interested research and enjoy it. I MISS YOU SO MUCH. Mom, thank you for your moral support and love, and I am happy that I could make you and dad proud. My mother in law, thank you so much for your caring and help, otherwise I couldn't have much time working on my research. My dear son Austin, thank you for staying with me, growing healthy and bringing me endless happiness, hope and power all the time especially when I was busied with my research. Finally I appreciate my husband Peng for his accompany, support and love. Without you, I couldn't go through those extremely bad times in my life, not to mention continuing my Ph.D. study and graduating successfully.

ABSTRACT

Conventional shoulder friction stir welding (CSFSW) produces uneven heat input through welded material thickness: higher close to the top and lower close to the bottom. When CSFSW is applied on certain aluminum alloys, such as 7xxx and 2xxx series high strength aluminum alloys which contain low melting point intermetallic, overheating and local melting may happen close to weld crown. Stationary shoulder friction stir welding (SSFSW) may generate much more uniform heat input through plate thickness than CSFSW due to the non-rotating shoulder and rotating pin. Therefore, overheating and local melting are expected to be avoided in SSFSW. Furthermore, local properties of joint made by SSFSW should be more uniform through its thickness than those of joint made by CSFSW.

In this study, thermal management was mainly approached by applying a rotating shoulder tool (CSFSW) and a stationary shoulder tool (SSFSW) in FSW. Beside the thermal management implemented by the shoulder, single pass (SP) FSW, dual-pass (DP) FSW, various pin features such as flats and flutes, have also been introduced in this investigation to achieve different thermal distribution.

A series of 24.9 mm and 25.4 mm thick AA7099-T7651, 32 mm thick AA7050-T7451 and 25.4 mm thick AA6061-T651 aluminum alloy plates have been friction stir welded using four different process variants. The process variants used are: stationary shoulder single pass (SSSP), conventional shoulder single pass (CSSP),

stationary shoulder dual pass (SSDP), and conventional shoulder dual pass (CSDP). FSW parameters, such as speeds, forces, temperatures, torques, powers and grain size, have been recorded, calculated and analyzed. Welding quality, material flow and deformation, as well as microstructure have been examined by various metallographic means. Mechanical examinations have been adopted to test mechanical properties of joints made with CSFSW and SSFSW. The TPM model implemented in COMSOL MULTIPHYSICS 4.0/4.4 has also been adopted in this research to simulate thermal distributions in FSW process when different process variants are applied.

Goals of this study include further understanding CSFSW and SSFSW mechanical, thermal and metallurgical processes, producing high quality thick plate SSFSW joint on 7xxx aluminum alloys, as well as investigating the influences of thermal management, pin features, process control parameters and different process variants in process response parameters, achievable welding speeds, thermal distribution and history in welded joint metallurgical and mechanical properties.

TABLE OF CONTENTS

Dedication iii

Acknowledgments iv

Abstract vii

List of Tables xi

List of Figures xii

Chapter 1 Introduction and background 1

1.1 Introduction 1

1.2 Motivation, Objective and Methodology 3

1.3 Dissertation Layout 7

Chapter 2 Literature review 9

2.1 Friction Stir Welding 9

2.2 Weld microstructure 12

2.3 Effects of control parameter & thermal managements on response parameters, microstructure and properties 13

2.4 State of the Art in FSW Process Modeling 41

Chapter 3 Materials and experimental Procedures 48

3.1 Experimental Materials 48

3.2 Experimental Facilities 52

3.3 Details of Weld Run 54
Chapter 4 Results and discussions 68
4.1 Single Pass Half Penetration FSW in AA7099 68
4.2 Single Pass Full Penetration FSW in AA7099 87
4.3 Dual Pass Full Penetration FSW 163
4.4 Stationary Shoulder Single Pass FSW in different alloys 243
4.5 Simulation Work 259
Chapter 5 Summary, Conclusions and future work 309
5.1 Summary 309
5.2 Conclusions 311
5.3 Recommendations for future Work 315
BIBLIOGRAPHY 316
Appendix A - Summary of FSW Tool Parameters 326
Appendix B - Summary of TBCs and FSW Control Parameters 327
Appendix C - Summary of Defect Examination Results 330

LIST OF TABLES

Table 3.1 Nominal Chemical Composition (WT%) of Considered Al Alloys 48

Table 3.2 Relevant Properties of Considered Aluminum Alloys 48

Table 3.3 Dimension Chart 65

Table 4.1 Summary of Experimental Control and Response Parameters 261

Table 4.2 Summary of Tool Parameters 262

Table 4.3 Thermal conductivity, heat capacity and density of materials adopted 264

Table 4.4 Temperature dependent flow stress of workpiece adopted in Simulation 265

Table 4.5 Boundary convection coefficients of interfaces adopted in Simulation. 265

LIST OF FIGURES

Figure 2.1 A Schematic diagram of typical FSW process 10

Figure 2.2 Typical transverse cross section of metallographic FSW sample. 12

Figure 2.3 Torque and power as functions of weld pitch in dissimilar welds 15

Figure 2.4 Process parameters and grain size as functions of rotation rate 16

Figure 2.5 X force and spindle torque as functions of weld position 16

Figure 2.6 Peak T distribution adjacent to a FSW of AA7075 20

Figure 2.7 Thermocouple embedded in weld path of FSW in AA6063 22

Figure 2.8 Temperature in FSW joints of AA6063 22

Figure 2.9 Thermocouple placed at various locations inside tool 24

Figure 2.10 Typical hardness profiles on traverse cross section. 26

Figure 2.11 Mechanical properties as functions of peak T for simulated HAZ 27

Figure 2.12 a) Average nugget hardness and b) Volume fraction of coarse second phase precipitate as a function of rotation rate measured at various depths from AA7010 weld crown produced with different welding speeds 28

Figure 2.13 Average nugget hardness and HAZ minimum hardness as function of welding speed in AA7050 welds 29

Figure 2.14 Joint hardness as a function of peak T from input torque FEM model 30

Figure 2.15 SAXS maps of volume fraction and precipitate size in FSW of AA7449 31

Figure 2.16 Typical thermal management methods applied in FSW..... 33

Figure 2.17 Joint efficiency and elongation as function of upset pressure for in air and underwater friction welded AA6061 35

Figure 3.1 Water spray in the wake of the FSW tool..... 55

Figure 3.2 Composite Backing Plate 55

Figure 3.3 Schematic Fixture for Semi-Guided-Bend Test Arrangement-One End Held-Force Applied Near Mandrel 60

Figure 3.4 Face bending samples: before testing 61

Figure 3.5 Crown bending samples: before testing 62

Figure 3.6 Normal scale transversal tensile test before testing 63

Figure 3.7 Normal scale transversal tensile test: DIC sprayed speckle pattern 64

Figure 3.8 Normal scale longitudinal tensile testing: after test 64

Figure 3.9 Longitudinal tensile testing: schematic diagram of dimensions 65

Figure 3.10 Subscale longitudinal tensile testing: DIC sprayed speckle pattern 65

Figure 3.11 Subscale longitudinal tensile testing device 66

Figure 3.12 Schematic Diagram of Residual Stress Test 67

Figure 4.1 Joint surfaces of SPH in AA7099 70

Figure 4.2 Macro Transverse Cross Sections of SPH in AA7099 72

Figure 4.3 Weld Crowns with bad surface defects of SSSPH 73

Figure 4.4 Response parameters and GS at center NG for SPH 76

Figure 4.5 Response parameters as functions of the rotating speed in CSSPH with T+3F pins with two different flat depths: 1.35mm and 2.7mm 78

Figure 4.6 Through thickness grain size on the weld centerline in SPH 80

Figure 4.7 Through thickness hardness on the weld centerline in SPH 81

Figure 4.8 Transverse hardness profiles of SPH 85

Figure 4.9 HAZ min hardness, Nugget average hardness, and HAZ width of SPH 85

Figure 4.10 Joint surfaces of CSSP: T+3F pin 89

Figure 4.11 Joint surfaces of SSSP: T+3F pin 90

Figure 4.12 Joint surfaces of SSSP: T+3CT pin 90

Figure 4.13 Macro Transverse Cross Sections of CSSP: different speeds 95

Figure 4.14 Macro Transverse Cross Sections of CSSP: different TBCs..... 96

Figure 4.15 Macro Transverse Cross Sections of SSSP: different speeds and tools..... 97

Figure 4.16 Macro Transverse Cross Sections of SSSP: different forge forces..... 99

Figure 4.17 Macro Transverse Cross Sections of SP..... 99

Figure 4.18 Response parameters and GS as functions of tool rotation rate for CSSP .. 101

Figure 4.19 Temperature as functions of power input for CSSP..... 103

Figure 4.20 Response parameters as functions of tool rotation rate for SSSP 105

Figure 4.21 Response parameters for SSSP: T+3CT pin..... 107

Figure 4.22 Temperature and grain size at center for SSSP: 51 mm/min, 69 KN..... 108

Figure 4.23 Temperature and grain size at center for SSSP: 160 rpm, 51 mm/min..... 109

Figure 4.24 Response parameters and GS at center nugget for SP: a welding speed of 51 mm/min, a flat/flute depth of 0.9 mm..... 111

Figure 4.25 Temperature at pin center and GS at center nugget for SP 112

Figure 4.26 Grain size at center nugget for SP 113

Figure 4.27 Through thickness hardness in CSSP: different welding speeds..... 114

Figure 4.28 Through thickness hardness in CSSP: different conditions 115

Figure 4.29 Through thickness hardness in CSSP: different TBCs..... 117

Figure 4.30 Through thickness hardness of SP..... 118

Figure 4.31 Transverse hardness profiles of CSSP..... 122

Figure 4.32 Transverse hardness profiles of SSSP..... 123

Figure 4.33 (a) HAZ min hardness at AS and RS, (b) HAZ min hardness, (c) HAZ width, and (d) Nugget average hardness at mid-plane of CSSP..... 123

Figure 4.34 (a) HAZ min hardness at AS and RS, (b) HAZ min hardness, (c) HAZ width, and (d) Nugget average hardness of CSSP..... 125

Figure 4.35 (a) HAZ min hardness at AS and RS, (b) HAZ min hardness, (c) HAZ width, and (d) Nugget average hardness of SSSP: different rotation rates..... 129

Figure 4.36 (a) HAZ min hardness at AS and RS, (b) HAZ min hardness, (c) HAZ width, and (d) Nugget average hardness of SP 133

Figure 4.37 Engineering stress and strain curves of transverse tensile testing in CSSP 138

Figure 4.38 (a) Ultimate tensile strength, (b) yield strength and (c) elongation of transverse tensile testing performed in CSSP: different TBCs 139

Figure 4.39 (a) Ultimate tensile strength, (b) yield strength and (c) elongation of transverse tensile testing performed in CSSP: different speeds..... 140

Figure 4.40 Engineering stress and strain curves of transverse tensile testing in SSSP: different forge forces..... 142

Figure 4.41 (a) UTS, (b) YS and (c) EL of transverse tensile testing performed on SSSP joints: same speeds, different forge forces..... 143

Figure 4.42 (a) UTS, (b) YS and (c) EL of transverse tensile testing in comparable SP 144

Figure 4.43 Engineering stress and strain curves of longitudinal tensile testing in CSSP: PWHT 146

Figure 4.44 (a) UTS, (b) YS and (c) EL of longitudinal tensile testing in CSSP as functions of forge forces: different TBCs and welding speeds, a setup of 1 °, a T+3F pin with a flat depth of 0.9 mm, a rotation rate of 160 RPM, PWHT 147

Figure 4.45 Engineering stress and strain curves of longitudinal testing in SSSP as functions of rotation rates: different rotation rates and pins, a welding speed of 51 mm/min, PWHT (#4306) 148

Figure 4.46 Ultimate tensile strength of longitudinal testing in SSSP as functions of rotation rates: different rotation rates and pins, a welding speed of 51 mm/min, PWHT 148

Figure 4.47 (a) Ultimate tensile strength, (b) yield strength and (c) elongation of longditudinal tensile testing in comparable CSSP (#4299) and SSSP (#4306) joints: different tool shoulder and pin features, PWHT, a setup of 1 °, a pin flat/flute depth of 0.9 mm, a rotation rate of 160 rpm, a welding speed of 51 mm/min 150

Figure 4.48 Through thickness average, longitudinal, residual stress profiles in SP: different tool shoulders and pin features, AW and PWHT, 1 °setup, rotation rate 160 rpm 152

Figure 4.49 (a) Peak residual stress, (b) FWHM, (c) tension area of through thickness average, longitudinal, residual stress profiles in both AW and PWHT conditions, and (d) unit weld energy of CSSP and SSSP joints as a function of welding speeds: 1 ° setup, a rotation rate of 160 rpm, different pin features, 0.9 mm flat/flute depth... 153

Figure 4.50 (a) Peak residual stress, (b) FWHM, (c) tension area of through thickness average, longitudinal, residual stress profiles in AW and PWHT conditions, and (d) unit weld energy of SP joints as a function of power: 160 rpm, different pin features 154

Figure 4.51 (a) Peak residual stress, (b) FWHM, and (c) tension area of through thickness average, longitudinal, residual stress profiles in both AW and PWHT conditions of CSSP and SSSP joints as a function of the unit weld energy: 160 rpm, different pin features 155

Figure 4.52 Specimens of SP joints after the face bending testing: AW and PWHT..... 158

Figure 4.53 Schematic diagram of defect free area in SSSP: different tools and control parameters, PWHT, the same welding speed of 51 mm/min..... 161

Figure 4.54 Specimens of defect free parts of SSSP after face bending testing: PWHT 162

Figure 4.55 Macro defects in specimen #3975B-2 failed in the face bending testing.... 163

Figure 4.56 Joint surfaces of DP: T+3F pin for CSDP, T+3CT for SSDP, 1 °tilt..... 167

Figure 4.57 Macro Transverse Cross Sections of CSDP: different speeds, T+3CT pin, 1.3 mm flute depth, 1^0 tilt 170

Figure 4.58 Macro Transverse Cross Sections of CSDP: different TBCs and tool shoulders, 1^0 tilt, T+3F pin, 1.3 mm flat depth, 160 rpm, 102 mm/min..... 170

Figure 4.59 Macro Transverse Cross Sections of CSDP: different tool pins and layouts, 1^0 tilt, T+3F pin, 1.3 mm flat depth, 200 rpm, 203 mm/min 171

Figure 4.60 Macro Transverse Cross Sections of DP: 1.3 mm flat depth, 1^0 tilt 172

Figure 4.61 Reaction forces, torque, power, peak temperatures at pin center as functions of tool rotation rate in the 1^{st} pass of CSDP (CSDP-1): a setup of 1 °, a flat/flute depth of 1.35 mm 174

Figure 4.62 T at center pin as a function of power input in the 1^{st} pass of CSDP (CSDP-1): a setup of 1 °, a flat/flute depth of 1.35 mm 176

Figure 4.63 Reaction forces, torque, power, peak T and GS at pin center as functions of tool rotation rate in the 1^{st} pass of DP (DP-1) and the 2^{nd} pass of DP (DP-2): a setup of 1 °, a flat/flute depth of 1.35 mm..... 178

Figure 4.64 (a) Temperature at center pin and (b) GS at center nugget as functions of power input in the 1^{st} pass of DP (DP-1) and the 2^{nd} pass of DP (DP-2): a setup of 1 °, a flat/flute depth of 1.35 mm..... 181

Figure 4.65 GS at center nugget as a function of Temperature at center pin in the 1st pass of DP (DP-1) and the 2nd pass of DP (DP-2): a setup of 1 °, a flat/flute depth of 1.35 mm 182

Figure 4.66 Hardness as a function of distance from crown of each pass on the weld centerline in CSDP: different TBCs, PWHT, same T+3F pin, 200 RPM, 203 mm/min 183

Figure 4.67 Hardness as a function of distance from crown of each pass on the weld centerline of CSDP: different speeds, AW and PWHT, T+3F pin, 1.3 mm flat depth 185

Figure 4.68 Hardness as a function of distance from crown of each pass on the weld centerline of SSDP: different speeds, AW and PWHT, T+3CT pin, 1.3 mm flat depth..... 188

Figure 4.69 Through thickness hardness on the weld centerline of DP: different pin features and speeds, AW and PWHT, 1.3 mm flat/flute depth..... 191

Figure 4.70 Transverse hardness profiles of each pass at various depths at mid-plane (6mm below crown), and at root (12mm below crown) in PWHT condition of CSDP with different TBCs: T+3F pin, 1.3 mm flat depth, 200 RPM, 203 mm/min..... 194

Figure 4.71 Hardness profiles of each pass transverse to weld at various depths near crown (3mm below crown), at mid-plane (6mm below crown), near root (9mm below crown) and at root (12mm below crown) in AW and PWHT conditions of CSDP with different speeds: T+3F pin, 1.3 mm flat depth 195

Figure 4.72 Hardness profiles of each pass transverse to weld at various depths near crown (3mm below crown), at mid-plane (6mm below crown), near root (9mm below crown) and at root (12mm below crown) in AW and PWHT conditions of SSDP with different speeds: T+3F pin, 1.3 mm flat depth..... 196

Figure 4.73 (a) HAZ min hardness at AS and RS, (b) HAZ min hardness, (c) HAZ width, and (d) Nugget average hardness as functions of distance from crown of the pass of transverse CSDP joints in PWHT condition with different thermal boundary conditions: T+3F pin, 1.3 mm flat depth, 200 RPM, 203 mm/min 197

Figure 4.74 (a) HAZ min hardness, (b) HAZ width and (c) Nugget average hardness as functions of distance from crown of the pass of transverse CSDP joints in AW and PWHT conditions with different speeds: T+3F pin, 1.3 mm flat depth 200

Figure 4.75 Effect of speeds on (a) HAZ min hardness, (b) Nugget average hardness and (c) HAZ width as functions ofdistance from crown of the pass of transverse CSDP joints in AW and PWHT conditions with different speeds: T+3F pin, 1.3 mm flat depth..... 201

Figure 4.76 Effect of the 2nd pass on (a) HAZ min hardness, (b) Nugget average hardness and (c) HAZ width as functions ofdistance from crown of the pass of transverse CSDP joints in AW and PWHT conditions with different speeds: T+3F pin, 1.3 mm flat depth 202

Figure 4.77 Effect of PWHT on (a) HAZ min hardness, (b) Nugget average hardness and (c) HAZ width as functions of distance from crown of the pass of transverse CSDP joints in AW and PWHT conditions with different speeds: T+3F pin, 1.3 mm flat depth..... 205

Figure 4.78 (a) HAZ min hardness, (b) HAZ width and (c) Nugget average hardness as functions of distance from crown of the pass of transverse SSDP joints in AW and PWHT conditions with different speeds: T+3CT pin, 1.3 mm flat depth 208

Figure 4.79 Effect of speeds on (a) HAZ min hardness, (b) Nugget average hardness and (c) HAZ width as functions ofdistance from crown of the pass of transverse SSDP joints in AW and PWHT conditions with different speeds: T+3F pin, 1.3 mm flat depth..... 209

Figure 4.80 Effect of the 2nd pass on (a) HAZ min hardness, (b) Nugget average hardness and (c) HAZ width as functions ofdistance from crown of the pass of transverse SSDP joints in AW and PWHT conditions with different speeds: T+3F pin, 1.3 mm flat depth 211

Figure 4.81 Effect of PWHT on (a) HAZ min hardness, (b) Nugget average hardness and (c) HAZ width as functions ofdistance from crown of the pass of transverse SSDP joints in AW and PWHT conditions with different speeds: T+3F pin, 1.3 mm flat depth..... 214

Figure 4.82 (a) HAZ min hardness, (b) HAZ width and (c) Nugget average hardness as functions ofdistance from crown of the pass of transverse CSDP and SSDP joints in AW conditions with different pin features and speeds: 1.3 mm flat/flute depth 216

Figure 4.83 (a) HAZ min hardness, (b) HAZ width and (c) Nugget average hardness as functions ofdistance from crown of the pass of transverse CSDP and SSDP joints in PWHT conditions with different pin features and speeds: 1.3 mm flat/flute depth 217

Figure 4.84 Effect of speeds on (a) HAZ min hardness, (b) Nugget average hardness and (c) HAZ width as functions ofdistance from crown of the pass of transverse DP joints in AW and PWHT conditions with different speeds: T+3F pin, 1.3 mm flat depth..... 218

Figure 4.85 Effect of the 2nd pass on (a) HAZ min hardness, (b) Nugget average hardness and (c) HAZ width as functions ofdistance from crown of the pass of transverse DP joints in AW and PWHT conditions with different speeds: T+3F pin, 1.3 mm flat depth..... 221

Figure 4.86 Effect of PWHT on (a) HAZ min hardness, (b) Nugget average hardness and (c) HAZ width as functions ofdistance from crown of the pass of transverse DP joints in AW and PWHT conditions with different speeds: T+3F pin, 1.3 mm flat depth..... 224

Figure 4.87 Engineering stress and strain curves of transverse tensile testing on CSDP joints in AW and PWHT conditions 227

Figure 4.88 Engineering stress and strain curves of transverse tensile testing on SSDP joints in AW and PWHT conditions 228

Figure 4.89 Ultimate tensile strength of transverse tensile testing as a function of welding speed of CSDP joints in PWHT condition: IA 228

Figure 4.90 Ultimate tensile strength of transverse tensile testing as a function of shoulder diameter of CSDP joints in PWHT condition: T+3F, 200 RPM, 203 mm/min..... 229

Figure 4.91 (a) Ultimate Tensile Strength, (b) Yield Strength and (c) Elongation of transverse tensile testing as a function of welding speed of CSDP and SSDP joints in AW and PWHT conditions: IA..... 230

Figure 4.92 Engineering stress and strain curves of longitudinal tensile testing on CSDP joints in PWHT condition 232

Figure 4.93 Engineering stress and strain curves of longitudinal tensile testing on SSDP joints in PWHT condition: T+3CT tool..... 233

Figure 4.94 (a) Ultimate Tensile Strength, (b) Yield Strength and (c) Elongation of subscale longitudinal tensile testing as a function of welding speed of CSDP and SSDP joints in PWHT condition: IA 233

Figure 4.95 Through thickness average, longitudinal, residual stress profiles in both AW and PWHT conditions of CSDP and SSDP joints produced with different speeds, shoulders and pin features: 1 °setup, 0.9 mm flat/flute depth..... 236

Figure 4.96 (a) Peak residual stress, (b) FWHM, (c) tension area of through thickness average, longitudinal, residual stress profiles in both AW and PWHT conditions, and (d) unit weld energy of DP as a function of welding speeds: 1 °setup, 0.9 mm flat/flute depth..... 237

Figure 4.97 (a) Peak residual stress, (b) FWHM, (c) tension area of through thickness average, longitudinal, residual stress profiles in both AW and PWHT conditions, and (d) unit weld energy of DP joints as a function of power: 1 °setup, 0.9 mm flat/flute depth..... 238

Figure 4.98 (a) Peak residual stress, (b) FWHM, (c) tension area of through thickness average, longitudinal, residual stress profiles in both AW and PWHT conditions, and

(d) unit weld energy of DP joints as a function of unit weld energy: 1 °setup, 0.9mm depth..... 238

Figure 4.99 Specimens of DP joints in AW and PWHT conditions after the face bending testing. From left to right in (a): #4229&#4230, #4229&#4231, #4232A&#4233A,#4232B&#4233B: PWHT..... 241

Figure 4.100 Joint surfaces of SSSP in AA7099: 0 °tilt, T+3F pin, 1.7 mm flat depth, 51 mm/min, Fz 71.2 KN: (a) 200 RPM and (b) 160 RPM 244

Figure 4.101 Joint surfaces of SSSP in AA7099: 1 °tilt, T+3CT pin, 1.7 mm flat depth, 51 mm/min, Fz 69 KN: (a) 200 RPM and (b) 160 RPM 244

Figure 4.102 Joint surfaces of SSSP in AA7099: 1 °tilt, T+3CT pin, 0.9 mm flat depth, 51 mm/min, Fz 69 KN: (a) 200 RPM and (b) 160 RPM 245

Figure 4.103 Joint surfaces of SSSP in AA7050: 0 °tilt, T+3F pin, 1.7 mm flat depth, 51 mm/min, Fz 66.7 KN: (a) 200 RPM and (b) 160 RPM 245

Figure 4.104 Joint surfaces of SSSP in AA6061: 1 °tilt, T+3CT pin, 0.9 mm flute depth, 203 mm/min, Fz 66.7 KN: (a) 480 RPM and (b) 400 RPM 246

Figure 4.105 Macro Transverse Cross Sections of SSSP in AA7099: 1 °tilt, T+3CT, 0.9 mm deep flutes, 51 mm/min, 69 KN, different rotation rates..... 250

Figure 4.106 Macro Transverse Cross Sections of SSSP in AA6061: 1 °tilt, T+3CT, 0.9 mm deep flats, 203 mm/min, 66.7 KN, different rotation rates..... 251

Figure 4.107 Macro Transverse Cross Sections of SSSP in AA6061: 1 °tilt, T+3CT, 0.9 mm deep flats, 320 RPM, 203 mm/min, different forge forces..... 252

Figure 4.108 Macro Transverse Cross Sections of SSSP in different alloys..... 252

Figure 4.109 Reaction forces, torque, power and GS as functions of tool rotation rate for comparable SSSP joints in AA7099 and AA7050: the same welding speed of 51 mm/min..... 254

Figure 4.110 Reaction forces, torque, power, peak T and GS as functions of tool rotation rate for comparable SSSP joints in AA7099 and AA6061: 1 °tilt, T+3CT, 0.9 mm deep flute, the welding speed of 51 mm/min for AA7099 and 203 mm/min for AA6061..... 257

Figure 4.111 T at center pin as a function of power input for comparable SSSP joints in AA7099 and AA6061: 1 °tilt, T+3CT, 0.9 mm deep flute, the welding speed of 51 mm/min for AA7099 and 203 mm/min for AA6061..... 257

Figure 4.112 A snapshot of COMSOL Graphical User Interface..... 267

Figure 4.113 Typical TPM model for SPFSW 268

Figure 4.114 Typical Cross Sections in y-z plane of TPM model..... 269

Figure 4.115 Snapshot of meshed geometry inside COMSOL..... 270

Figure 4.116 Thermal field of the TPM model obtained through simulation..... 271

Figure 4.117 Simulated and measured T and power as a function of alpha on pin in SSSP: alpha on shoulder is 0 272

Figure 4.118 (a) Simulated and measured T and power as a function of alpha on shoulder, and (b) simulated power generated by pin, shoulder, and total power in CSSP: alpha on pin is 0.4..... 273

Figure 4.119 Simulated and measured T and power as a function of alpha on pin in SSDP-1: alpha on shoulder is 0 274

Figure 4.120 (a) Simulated and measured T and power as a function of alpha on shoulder, and (b) simulated power generated by pin, shoulder, and total power in CSDP-1: alpha on pin is 0.5 275

Figure 4.121 Simulated T at pin center and power in SP 277

Figure 4.122 Simulated T at pin center and power in DP-1 281

Figure 4.123 Determination of HAZ width and time of T staying among 200~350℃ .. 284

Figure 4.124 Typical 3D view of T field obtained from TPM model of SP joints..... 285

Figure 4.125 Typical contour plots of temperature at transverse cross-section of SP.... 286

Figure 4.126 Typical 3D view of T field obtained from TPM model of DP-1 joints..... 286

Figure 4.127 Typical contour plots of temperature at transverse cross-section of DP-1 287

Figure 4.128 Simulated (a) T at pin center and (b) power as a function of welding speed with different h of SP joints..... 288

Figure 4.129 Simulated (a) T at pin center and (b) power as a function of welding speed with different h of DP-1 joints..... 288

Figure 4.130 HAZ width as a function of welding speed with different h of SP joints: (a) at crown, (b) at mid-plane and (c) at root..... 290

Figure 4.131 HAZ width as a function of welding speed with different h of DP-1 joints: (a) at crown, (b) at mid-plane and (c) at root 290

Figure 4.132 Simulated T at pin center as a function of distance to weld center with different welding speeds and h of SP 292

Figure 4.133 Simulated T at pin center as a function of distance to weld center with different welding speeds and h of DP-1 294

Figure 4.134 HAZ T history as a function of process time at various depths with different h applied at WP surface of SP: 0.85 mm/s..... 295

Figure 4.135 HAZ T history as a function of process time at various depths with different h applied at WP surface of SP: 1.275 mm/s..... 296

Figure 4.136 HAZ T history as a function of process time at various depths with different h applied at WP surface obtained from TPM model of SP: 1.7 mm/s..... 297

Figure 4.137 HAZ T history as a function of process time at various depths with different h applied at WP surface of SP: a welding speed of 2.125 mm/s..... 298

Figure 4.138 HAZ T history as a function of process time at various depths with different h applied at WP surface of DP-1: a welding speed of 1.7 mm/s..... 298

Figure 4.139 HAZ T history as a function of process time at various depths with different h applied at WP surface of DP-1: welding speed 2.125 mm/s..... 299

Figure 4.140 HAZ T history as a function of process time at various depths with different h applied at WP surface of DP-1: welding speed of 2.55 mm/s 300

Figure 4.141 HAZ T history as a function of process time at various depths with different h applied at WP surface of DP-1: welding speed 2.975 mm/s..... 301

Figure 4.142 HAZ T history as a function of process time at various depths with different h applied at WP surface of DP-1: a welding speed of 3.4 mm/s..... 301

Figure 4.143 HAZ T history as a function of process time at various depths with different h applied at WP surface of DP-1: welding speed 3.825 mm/s..... 302

Figure 4.144 HAZ T history as a function of process time at various depths with different h applied at WP surface of DP-1: welding speed 4.25 mm/s..... 303

Figure 4.145 Time of T staying among 200~350℃ with different h: SP..... 304

Figure 4.146 Time of T staying among 200~350℃ at various depths: SP..... 304

Figure 4.147 Time of T staying among 200~350℃ with different h: DP-1..... 305

Figure 4.148 Time of T staying among 200~350℃ at various depths: DP-1..... 306

Figure 4.149 Simulated T at pin center and power of DP joints as a function of ΔK..... 308

CHAPTER 1

INTRODUCTION AND BACKGROUND

1.1 Introduction

Joining of two components plays a significant role and has been widely applied in structural manufacturing. Development of joining mainly aims at improving joint performance and reducing cost. There are several possible ways to meet those requirements, such as selection and development of advancing methods, technology, material, and so on.

Various joining methods have been developed and applied in manufacturing process in air, under water, and even in outer space. During the last decades, most joining of two components have been performed by adhesive bonding, mechanical joining (SV gasket joining, brazing, corrugated stainless steel tube fittings, flanged, grooved, hubless coupling, press joining) and welding. Welding joins materials like metals and thermoplastics by causing coalescence. Compared with adhesive bonding and mechanical joining, welding produces a stronger joint with less weight. Common welding methods include solvent weld, heat fusion weld, shielded metal arc welding, gas tungsten arc welding, flux-cored arc welding, gas metal arc welding, submerged arc welding, electroslag welding, etc. Various energy sources have been applied in welding, such as an electric arc, a gas flame, an electron beam, a laser, friction and ultrasound. Forge welding

was invented until the end of the 19th century, then followed arc welding, oxyfuel welding, and electric resistance welding. In late 20th century, electron beam welding, laser beam welding, magnetic pulse welding, and friction stir welding have been invented, which boosted the joining in manufacturing [1]. Friction Stir Welding (FSW), invented by The Welding Institute (TWI) UK in December 1991, has been considered as the innovative breakthrough of the state-of-the-art manufacturing process for joining aluminum, magnesium, steel, copper, nickel and titanium alloys.

Friction stir welding (FSW) is a solid state thermo-mechanical welding process without melting. In FSW process, a non-consumable rotating tool plunges into a pre-drilled hole of the two abutting workpieces, and then travels along the seam line. Friction between tool and workpieces generates frictional heat, which softens material nearby the FSW tool to enable tool travelling, heats material in two work pieces around it to a sufficient temperature, plasticizes, moves and mixes it through relative motions between the rotating-translating tool and work pieces to form a joint. FSW has distinct advantages relative to conventional welding methods. FSW is energy conservation and consumption reduction, and more environment-friendly. FSW can reduce the component weight since mechanical fastenings like riveted or bolted joints are no longer necessary [2], [3]. Since there is no melting involved in FSW, relative to fusion processes, FSW can be applied in all the aluminum alloys without hot cracking, element loss, porosity and so on. Also, damage to the base metal is minimized in FSW compared with other welding methods. Filling material is unnecessary which can reduce weight and cost. More importantly, friction stir welding (FSW) has enabled the joining of high strength aerospace aluminum alloys like 7XXX aluminum alloys which were formerly considered

unweldable by most fusion welding techniques. Generally speaking, relative to other conventional welding methods, FSW can produce highly repeatable joints with higher strengths, less consumption, lower weight, and lower cost.

FSW materials with good properties (especially high specific strengths) and light weight, like aluminum, magnesium, and titanium alloys have been studied to improve joint performance, reduce cost and bloom manufacturing industries like aerospace, automotive, ship building, railways, robotics, personal computers, etc. [4], [5].

1.2 Motivation, Objective and Methodology

1.2.1 Motivation

Friction stir welding (FSW) has enabled the joining of high strength aerospace aluminum alloys which were formerly considered unweldable by most fusion welding techniques. However, in order to reap the benefits of these high strength alloys in welded structure, it is important to produce welds which do not excessively degrade the strength. Thermal history and welding speed are crucial to the joint's strength, stated as following.

1.2.1.1 Temperature

When a conventional FSW tool is applied, friction heat is generated by friction between the rotating shoulder and work-piece surface, and friction between the rotating pin and weld material. The rotating shoulder prevents expulsion of material and produces friction heat, therefore near crown materials receive a lot of power input. It's obvious that conventional shoulder friction stir welding (CSFSW) produces uneven heat input through welded material thickness due to the rotating shoulder and pin: higher close to the top and lower close to the bottom. When CSFSW is applied on certain aluminum alloys, such as 7xxx and 2xxx series high strength aluminum alloys which contain low melting point

intermetallic, overheating and local melting may happen close near weld crown while underheating may occur near weld root, which as well as defects reduce joint properties significantly.

To avoid overheating in FSW, stationary shoulder FSW (SSFSW) will be adopted and studied in this research. Stationary shoulder (SS) is expected to avoid overheating especially near crown and achieve homogeneities in thermal distribution and microstructure through thickness. Stationary shoulder friction stir welding (SSFSW) generates much more uniform heat input through plate thickness than CSFSW due to the non-rotating shoulder and rotating pin. Therefore, overheating and local melting are easy to avoid in SSFSW. Furthermore, local properties of joint made by SSFSW should be more uniform through its thickness than those of joint made by CSFSW.

To avoid overheating in FSW, thermal managements like water-spray at work-piece surface and backing plates with different thermal conductivities have also been adopted to enhance heat dissipation during FSW process.

1.2.1.2 Welding Speed

Copious previous work has demonstrated the importance of welding speed in determining attainable strength. A typical measure of weld strength is the transverse tensile test. Joint strength of 7XXX alloy welds in transverse tension is strongly correlated with heat affected zone (HAZ) minimum hardness [6]. Minimum hardness has been shown to be increased by welding at high speeds and may also be affected by application of various thermal boundary conditions designed to increase quench rates in the HAZ [6],[7],[8],[9],[10],[11]. Welding speed is limited in practice primarily by two factors: (1) in-plane force on the weld tool increases with increasing welding speed and

ultimately at sufficient speed the tool will fail and (2) increasing welding speed normally requires increased weld power, weld power is closely correlated with peak weld temperature, and peak weld temperature must be maintained below the incipient melting point of the alloy being welded or else the weld nugget ductility and strength will be compromised.

So, there is a tension between welding at the highest possible speed to minimize HAZ overaging and maintaining weld peak T below the incipient melting temperature. Process modifications which would enable welding at reasonably high speeds without exceeding incipient melting temperatures are desirable.

When single pass (SP) full penetration FSW is applied in 25.4 mm thick high strength 7XXX aluminum alloys plate, welding speed is limited and it's likely to overheat near crown and also may result defective joints, which reduce joint strength. On the other hand, single pass half penetration (SPH) FSW is more easily to produce defect free joints, allows much higher speeds, improves weldability and maintains nugget temperature below the incipient melting temperature, which together increase the joint's strengths, especially the UTS. Therefore, dual pass (DP) FSW has been considered and adopted in this research. In the DP processes, welds are made from both sides of the plate one by one by a 12.7 mm long pin with each pass having a weld penetration of slightly greater than half of the plate thickness (24.9 mm).

1.2.2 Objectives

Objectives of this research are to: (a) improve weldability of FSW in 7XXX aluminum alloys and produce high quality FSW joint in 25.4 mm thick AA7xxx plate, (b) further understand mechanical and metallurgical processes using different shoulders (CS

and SS) and different process variants (SPH, SP and DP), (c) investigate effect of control parameters and thermal managements on response parameters and properties, (d) investigate the influence of thermal distribution and history in welded joint's metallurgical and mechanical properties, and (e) study SSSP in different aluminum alloys.

1.2.3 Methodology

Based on previous discussion, stationary shoulder (SS) welding might alleviate overheating problems, and double pass (DP) welding might enable faster welding.

In this research, as for full penetrated FSW, we explore four process variants in the welding of a 25.4 mm (for SP) or 24.9 mm (for DP) thick high strength aerospace aluminum alloy with the goal of maximizing transverse properties while preventing overheating. The process variants used include CSSP, SSSP, CSDP and SSDP. Single pass welds will be performed on 25.4 mm thick AA7099-T7651 plates. Dual pass welds will be made on 24.9 mm thick plates machined from the 25.4 mm thick AA7099-T7651 plates. In both of the dual pass processes, welds are made from both sides of the plate one by one with each pass having a weld penetration of slightly greater than half of the plate thickness. Water spray and different backing plates will also be applied for comparison study. SSSP will also be performed on 32 mm thick AA7050-T7451 plates and 25.4 mm thick AA6061-T651 plates.

FSW control and response parameters, such as speeds, forces, temperatures, torques, and powers, will be recorded and analyzed. Welding quality, material flow and deformation, as well as microstructure will be examined by various metallographic means.

Mechanical examinations and analysis will be adopted to test global and local properties of joints made in this research.

1.3 Dissertation Layout

This dissertation is divided into five chapters:

(1) **Chapter 1** presents a general background of joining processes in manufacturing, briefly introduces friction stir welding including advantages relative to traditional joining technologies, current and potential applications, and elucidates the motivation, objectives and methodology of this dissertation.

(2) Literature review has been presented in **Chapter 2** for depicting a thorough background and reviewing relevant studies in several aspects. First, basic background of FSW like history of invention and developments, process advantages and disadvantages relative to other joining technologies, process parameters, and weld microstructure are reviewed to provide this research work a general background. Then to offer a general idea about the crucial mechanism in FSW and how to tailor the process variables to obtain sound and defect-free weld joints depend on specific applications, effects of primary control parameters (like tool rotation rate, travelling speed, and forge force) on response parameters (torque, temperature), thermal history and properties, effects of temperature and its transients on weld properties, as well as temperature measuring methods are reviewed. Thermal managements in FSW especially the modification of thermal boundary conditions are also reviewed to better understand the thermal managements applied in this research. Finally, state of the art of FSW modeling is reviewed to widen and deepen understanding of simulation about FSW process.

(3) **Chapter 3** consists of materials, experimental and testing procedures adopted in this dissertation. Metallurgy of experimental materials including AA7099-T7651, AA7050-T7451 and AA6061 are reviewed and studied. Experimental facilities like FSW and data acquisition are further introduced. Details of weld run are explained and listed including thermal managements, FSW preparation, PWHT, metallographic sample preparation, and relevant mechanical testing procedures.

(4) **Chapter 4** states and discusses obtained research results in experimental and simulated results. According to different process variants and weld materials applied, FSW experiments can be divided into the following four categories: a) single pass half penetration FSW in AA7099, b) single pass full penetration FSW in AA7099, c) dual pass full penetration FSW in AA7099, and d) stationary shoulder single pass full penetration FSW in different alloys. In each category, macro and microstructure, process responses, mechanical properties like hardness, tensile testing and bending properties, residual stress are studied and discussed. Comparison study is performed to further understand FSW mechanism in aluminum alloys. Simulation work is also performed on selected comparable joints to study thermal distributions in FSW. This part explains the adopted TPM model, states motivation and goals, illustrates material properties selection, simulation procedures and discusses the simulation results.

(5) **Chapter 5** presents summary and conclusions of this research, and proposes future works for further research directions.

CHAPTER 2

LITERATURE REVIEW

2.1 Friction Stir Welding

Friction stir welding (FSW) is a solid-state thermo-mechanical welding process without melting. In a typical FSW process performed in Aluminum alloys, a non-consumable tool consisting of a rotating or non-rotating shoulder and a rotating probe heats material in the two work-pieces around the tool up to a sufficient temperature (below the melting temperature of the base metal), plasticize, move and mix it through relative motions between the rotating-translating tool and the still work-pieces. Figure 2.1 illuminates the typical friction stir welding process and corresponding terminologies. Readers are referred to a recent paper written by Threadgill [12] which clearly illustrates general terminologies adopted in FSW.

Atomic-level analysis of bond formation in FSW has been studied by Oosterkamp [13], Tylecote [14], Lawrence H. Van Vlack [15] and Li [16]. Take Aluminum alloys plates for example. Before the FSW process, strong metallic bonds generated by interatomic attractive forces held atoms inside two work-pieces together. During the FSW process, larger heat input generates huge energy, which is absorbed by atoms near the work-piece interface. Those atoms then have larger mean spacing, become more active and are ready for moving with the rotating-translating pin from one work-piece to another.

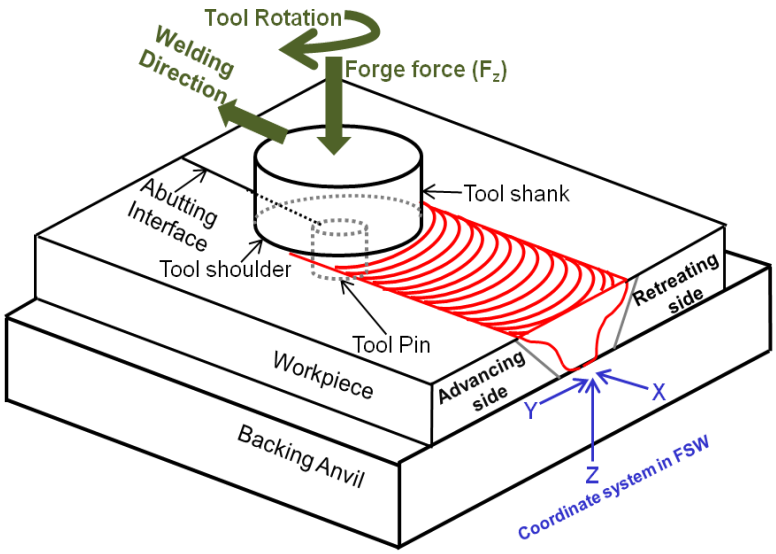

Figure 2.1 A Schematic diagram of typical FSW process with corresponding terminologies [12]

Then intense atom diffusion and mixing at the atomic level or plastic deformation in the macroscopic scale occur. The atom diffusion will be further enhanced by elevated temperature and intense plastic deformation, allowing new strong metallurgical bonds between diffused atoms with adjacent atoms under high hydrostatic pressure formed by the shoulder and applied large forge force. Material in front of the pin will suffer from intense plastic deformation and gradually deposit behind the pin with the pin rotating and travelling along the joint line. Then a FSW joint forms [13],[14],[15],[16]. The shoulder will also restrain plasticized material inside the weld to prevent the plasticized material from being oxidized, and reduce flash and possibility of forming volumetric defects.

FSW enables the joining of high strength aluminum alloys therefore has been widely applied in aerospace and automotive industries. The process of FSW performed on aluminum alloys causes a recrystallized nugget zone and a heat affected zone (HAZ), which experience different thermal history then exhibit different microstructures and properties relative to the base metal. However, relative to other joining techniques for

aluminum alloys, FSW has still been considered as superior because of its intrinsic advantages, like resistance to hot cracking, preservation of base material properties, better dimensional stability, etc. [17], [18], [19].

Primary process control parameters, like tool rotation rate, welding speed, forge force, tool geometry, can be tailored to obtain sound and defect-free weld joints depend on specific applications. Other control parameters includes tool tilt angle and tool features. Thermal managements include welding environment, backing plates and welding methods (partial or full penetration, single or dual pass, conventional or stationary shoulder). In-plane forces and torque experienced by the tool, power input and joint temperature constitute process response variables. Weldability, macro and micro structure, thermal distribution, transverse and through thickness hardness distributions and other mechanical properties of joints are of primary interest.

In this research, to increase joint's strength, most efforts are made to apply higher welding speed, get a sound defect free joint, and keep peak joint temperature below the alloy's incipient melting temperature which might reduce typical undesirable effects of FSW processes. In conventional shoulder FSW, the tool is of a two piece design with a rotating shoulder and a rotating pin during FSW process. It will generate much heat near weld crown due to the rotating shoulder, which indicates overheating near crown often occurs. To avoid this, stationary shoulder FSW during which process the shoulder keeps stationary is introduced in this research. Also, to allow higher welding speeds, dual pass (DP) FSW is introduced. In the DP processes, welds are made from both sides of the plate one by one by a pin with each pass having a weld penetration of slightly greater than half of the plate thickness.

Control parameters together with thermal managements have significant influence in FSW joint's material flow, microstructural and thermal distribution, which determine joint's quality and properties. In this research, all parameters are considered to produce sound defect free joints. Control parameters like tilt angle and pin features are not the primary study interest. Primary control parameters and thermal managements are the focal points of this research. All the welds are made with similar and comparable tool geometries and features as detailed in section 3.3 and Appendix.

2.2 Weld microstructure

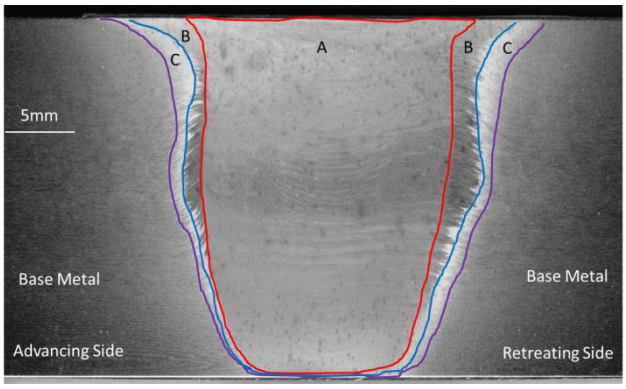

Figure 2.2 Typical transverse cross section of metallographic sample friction stir welded on 25.4 mm thick AA7099 plates after polishing and etching. Regions indicated by lines with different colors are: A) nugget, B) TMAZ, and C) HAZ.

As shown in Figure 2.2, the typical macrostructure of a FSW joint transverse cross section after polishing and etching consists of three distinct local regions: the nugget, TMAZ (Thermal Mechanically Affected Zone) and HAZ (Heat Affected Zone). During the FSW process, the central region underneath the weld seam experiences intense plastic deformation and temperature there increases quite close to but generally below the incipient melting temperature of base metal, resulting in a fine grained recrystallized area referred to as nugget, dynamically recrystallized zone or

stir/deformation zone. The shape and size of the applied tool probe which stirs the joint during FSW process significantly determines the shape and size of the nugget. A typical nugget of FSW joint in aluminum alloy is featured with equiaxed grains of few (2-10) microns with high angle grain boundaries and low dislocation density [9], [20]. Next to the nugget zone on either size is the TMAZ, which experiences some plastic deformation and significant thermal cycle. Usually the grain structure in TMAZ consists of considerably deformed parent grain structure with distinct subgrains visible without any recrystallization. At the advancing side, there is always a distinct boundary between nugget and TMAZ; however, at the retreating side the microstructure transitions gradually. Next to the TMAZ is the HAZ, which experiences significant thermal cycle without plastic deformation due to its distance from the weld zone. In HAZ there is no apparent change in the grain structure, and it is normally characterized by the changes in hardness response. HAZ is the weakest area of the joint due to overaging in a typical precipitation hardening aluminum alloy (for instance AA7099) welds.

2.3 Effects of control parameter & thermal managements on response parameters, microstructure and properties

Primary process control parameters in FSW include tool rotation rate, tool travelling speed, forge force and tool geometry. Other secondary control parameters include tool tilt angle and tool features. Thermal managements includes thermal boundary conditions (BCs) (welding environment and backing plates), and welding process variants (partial or full penetration, single or dual pass, conventional or stationary shoulder). In-plane forces and torque experienced by the tool, power input and joint temperature constitute process response variables. Weldability, macro and micro

structure, temperature distribution, transverse and through thickness hardness distributions and other mechanical properties like yield strength, tensile strength and residual stress of joints are of primary interest.

Process control parameters as well as thermal managements will affect thermal history during FSW process, which will affect heating, cooling, history and sequence of precipitation and dissolution, which will finally determine local and global microstructure and properties. In other words, better understanding of effects of control parameters and thermal managements on process response variables and joint properties will help us to tailor control parameters and thermal managements to obtain sound, defect-free weld joints with optimized properties depending on specific applications.

2.3.1 Effects of Primary control parameters on response parameters and properties

2.3.1.1 Torque & forces

In FSW, the rate of heat generation 'Q' is equal to the mechanical power associated with the tool, which is equal to the torque times the angular velocity of tool. Specific energy (energy per unit length) can be calculated by dividing the power by the welding speed. Both specific energy and power can be related to the total heat input and hence the thermal distribution, therefore they are significant parameters for analytical and computational modeling. Power and torque cannot be directly controlled, and torque depends on control parameters like rotation rate, welding speed, forge force, etc. Torque and forces will also affect the tool longevity and will be considered during FSW parameter choosing. Power and torque significantly affect deformation zone temperature, and it's vital in FSW study to understand interrelationships among torque, power, temperature, control and response parameters [21].

Another significant response parameter during FSW comes to forces experienced by the tool especially in the pin. Exploring effects of control parameters and other welding conditions on tool forces can help better understanding of the material flow and consolidation in FSW. Quantification of tool forces is also vital for tool and machine design to avoid failure of tool or machine during FSW. The tool shoulder and pin geometries, pin features, control parameters and BCs which can minimize the tool forces while maintaining superior mechanical properties are desirable [22].

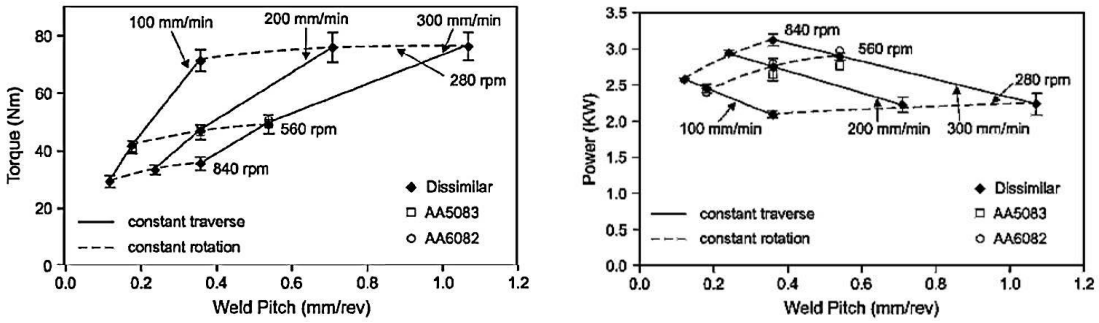

(a) Steady state torque (b) Steady state power

Figure 2.3 Torque and power as functions of weld pitch in dissimilar welds. Adapted from Peel et al. [23]

Peel et al. [23] performed dissimilar FSW in 3 mm thick AA5083 and AA6082 sheets with a series of systematically varied speeds to study several process response parameters. Figure 2.3 shows the torque and power trends in steady state with weld pitch increasing. It's shown that torque is more sensitive to the rotation rate than to the welding speed, and larger rotation rate results in larger power input. It also shows that the effect of rotation rate on torque is higher at low rotation rate regime than at high rotation rate regime, which trend is similar to temperature in deformed zone discussed previously. Long et al. [8] studied response parameters like torque and forces of several welds made with rotation rates ranging from 100 rpm to 800 rpm and a constant welding speed of

1.27 mm/s in three different plates: 9.5 mm thick AA5083, 8.3 mm thick AA2219 and 9.5 mm thick AA7050. Average forces in X axis and torque are plotted against the rotation rate, as shown in Figure 2.4. With the increasing of rotation rate, torque decreased sharply at low rotation rate regime and then decreased more and more slowly with the further increase in rotation rate. When rotation rate increased, X force also decreased sharply at the low rotation rate regime, then it began to increase slowly after it reached a minimum value at an intermediate rotation rate level.

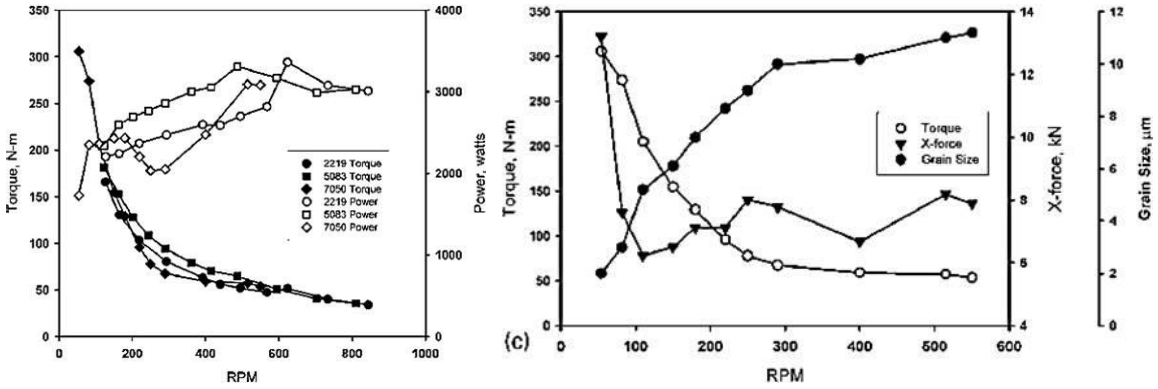

Figure 2.4 Left: Torque and power as functions of rotation rate for different alloys. Right: Torque, X force and grain size as functions of rotation rate in AA7050 welds. Adapted from Longy et al. [8]

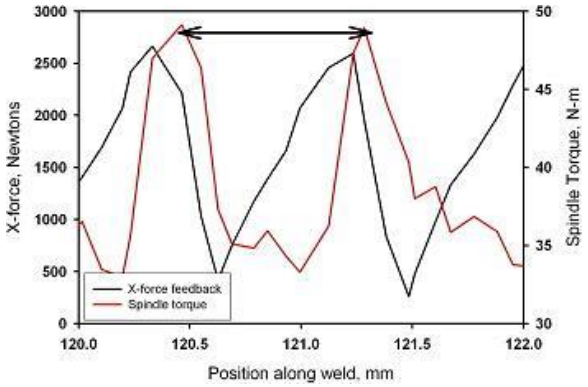

Figure 2.5 X force and spindle torque as functions of weld position. Adapted from Reynolds [24]

It's worthy to note that the discontinuous material flow in FSW results in discontinuous torque and tool forces, which are not monotonic response parameters and

roughly follow the sinusoidal pattern, as shown in Figure 2.5. The amplitude of the signal depends on several control parameters. However, the wavelength has been reported to be equal to the advance per revolution [24], [25]. It has also been reported that the banded microstructure spacing in FSW of AA2524 and AA2024 correlated well with oscillating frequency of the forces [25]. Recently there have been increased studies of periodicity of the tool forces. Blignault et al. [26] reported a work of measuring process force footprint with the use of multi-axial force transducer. Subsequently Hattingh et al. [27] from the same research group examined the effects of tool geometry and process parameters in FSW by analyzing the polar plots of process forces. Boldsaikhan et al. [28] performed phase space analysis of time series force data to develop algorithms using computational methods to detect wormhole defects. However, study of exploring relationships between process forces and welding parameters is still in the early stage. Theories and assumptions to describe the material flow in the joint should be capable to relate the dynamic changes in the tool forces since the material flow is examined through tool forces.

2.3.1.2 Effects of Temperature on response parameters & properties

During FSW, the weld joint material undergoes intense thermo-mechanical deformation and temperature cycle. In precipitation hardened aluminum alloys, thermal history in the joint cross section significantly affects the microstructural distribution, which affects the relevant joint properties. Therefore, experimentally measured temperature history especially at weld nugget and heat affected zone, which is determined by primary control parameters like weld speeds and forge force, are of utmost significance in study of FSW joint properties. Understanding and finally establishing the

relationship between control parameters and temperature history probably realize the tailoring of desired specific properties in FSW joints.

Unfortunately, temperature measurement of locations inside the FSW process zone is highly problematic. During FSW process, the tool rotates and travels along the joint seam line, resulting materials around the probe moving under the severe thermomechanical influence, which leads to limited locations for temperature measuring, steep temperature gradients, etc. Therefore, it is hardly possible to measure actual transient temperatures in the deformation zone.

Several methods for temperature measurements are not applicable in measuring temperature history inside the joint. Surface radiation technologies of physical contact and non-contact with the measured objects, like laser-ultrasonic technique and infrared temperature sensors, are complicated by variations in local emissivity. They are applied to measure surface temperature instead of temperature inside the joint [29],[30],[31],[32]. Kosugi et al. [33] developed a new noncontact method, the laser-ultrasonic technique, to monitor temperature distribution of a heated rotating cylindrical object. Measured surface temperature of the cylindrical object and heat conduction analyses were combined together to quantitatively evaluate temperature distribution of the cylindrical object in the radial direction. However, this rotating object was not like the FSW tool which is inside the joint, so this method is not applicable in measuring temperature inside FSW joints. Recently, Woo et al. [34] exploited the deep penetration capacity of neutrons into most metallic materials, and applied the *in-situ* neutron diffraction method to reveal thermal stresses and the real time temperature in the stir zone of AA6061-T6 during FSW process. However, this method requires high cost, significant efforts and instrumentation,

which makes it not cost-effective to be applied on a regular basis of temperature measurement.

From above review, it has been illustrated that directly measuring real time temperature inside the joint is extremely challenging, since many measurement techniques are inapplicable due to the intense thermomechanical deformation associated with the FSW process. Currently, thermocouples (TCs) have become the most practicable means to obtain real time temperature inside the joint. TCs can be either placed directly in the weld path or embedded inside the FSW tool. Few studies have reported tool temperature measurements since it is difficult and complicate to accurately measure the real time temperature of a rotating and travelling body surrounded by deformed metal materials. The method measuring temperature by embedding TCs in the weld path has been employed mostly by researchers to measure experimental temperature. Typical applications of experimental temperature measurement results include analyzing the thermal distribution during FSW process based on heat transfer theories, correlating them with specific welding parameters for effect study, validating and evaluating numerical and analytical simulation models. However, embedding TCs in the weld path to measure temperature still has intrinsic disadvantages. When TCs are embedded in the weld path, during the FSW process the deformed metal material and/or moving probe will undoubtedly affect TCs locations by displacing or even destroying them, which raises several problems, like uncertainty of TCs actual location where temperature data is from, and uncertainty of actual value of temperature recorded. Therefore, when TCs are right in the path of the FSW tool in which case TCs will be destroyed, care must be taken to analysis and conclusions based on those temperature measurement results. When TCs are

not in the deformation zone, for instance TCs are embedded in the HAZ, there will be much less uncertainty of TCs locations. However, due to the specific thermal distribution, a larger temperature gradient existing in and around the deformation zone results a large error in the temperature measurement where there is even a small uncertainty of TC location.

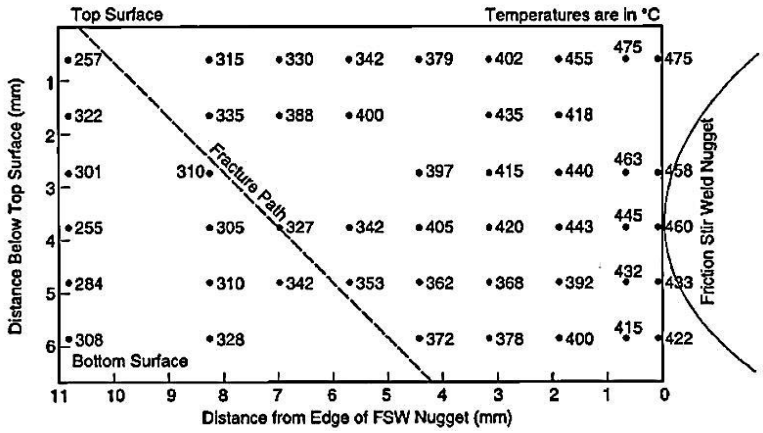

Figure 2.6 Peak T distribution adjacent to a FSW of AA7075-T651. Adapted from Mahoney et al. [35]

One of the earliest works that expounded thermal distribution in FSW by measuring temperature using TCs was performed by Mahoney et al [35]. In his study, full penetration FSW butt weld was performed in 6.35 mm thick AA7075-T651 sheet with a welding speed of 2.12 mm/s. Temperatures were measured as function of both the distance from weld nugget and through the thickness of the sheet by embedding TCs proximate to the weld nugget. Peak temperature was measured at different locations adjacent to the weld nugget, as shown in Figure 2.6. Peak temperatures outside the weld nugget varied from 422 ℃ to 475 ℃ at the edge of the nugget to 257 ℃ to 308 ℃ at a distance of ~11 mm from the nugget. Maximum peak temperature was observed at the edge of the stir zone near weld crown. A decreasing trend of peak temperatures was found when distance from weld crown increased due to heat generated by tool shoulder,

and/or when distance from nugget edge increased due to heat extraction by the backing plate. The fracture path in the tensile samples followed the isothermal contour in the cross section of the joint, which contour angled from the weld crown toward the nugget as it approached the weld root. Since then, similar experiments with embedded TCs placed at various locations at the far field, in and around the deformation zone, have been conducted by several researchers such as Tang et al.[36], Frigaard et al. [37], Kwon et al. [38], Sato et al. [39], Fonda and Lambrakos [40], Chao et al. [41], Chen and Kovacevic [42], Hassan et al. [43] and Simar et al. [44]. Tang et al. [36] performed FSW in 6.4 mm thick AA6061-T6 plates with a constant welding speed of 2 mm/s and a rotation rate ranging from 300 rpm to 1200 rpm to investigate heat input and temperature distribution during FSW process. Temperatures at various positions through thickness and along transverse direction were measured by imbedded TCs in a series of small holes with different depths at different distances from the weld seamline drilled to the workpiece bottom. It was found that the maximum peak temperature which occurred at the weld center was about 80% of the base metal melting temperature. When a constant welding speed was applied, higher forge force and larger rotation rate resulted in higher peak temperature. At higher rotation rate, the incremental effect of rotation rate on peak temperature decreased since increased temperature reduced the metal flow stress and the torque which limited any power generation increase. Sato et al. [39] applied FSW in 4 mm thick AA6063-T5 and AA6063-T4 sheets with various rotation rates (800~3600 rpm) and a constant welding speed of 6 mm/s to examine thermal history and distributions of micro-structure and hardness. During welding process, thermal cycles were measured in the stir zone using a K-type TC placed at the bottom of the butt line (see Figure 2.7).

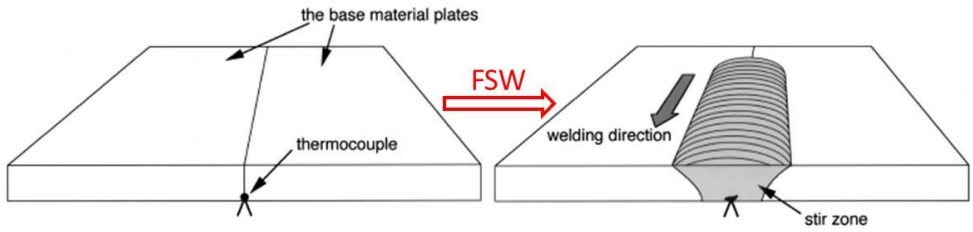

(a) Schematic graphs of thermocouple located at weld plate bottom

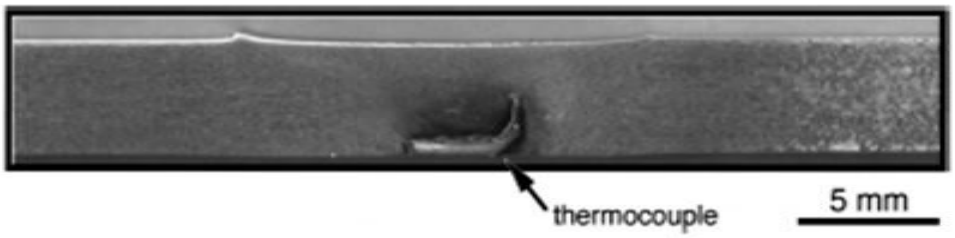

(b) Transverse cross section with the stirred thermocouple after FSW

Figure 2.7 Thermocouple embedded in weld path of FSW in AA6063. Adapted from Sato et al. [39]

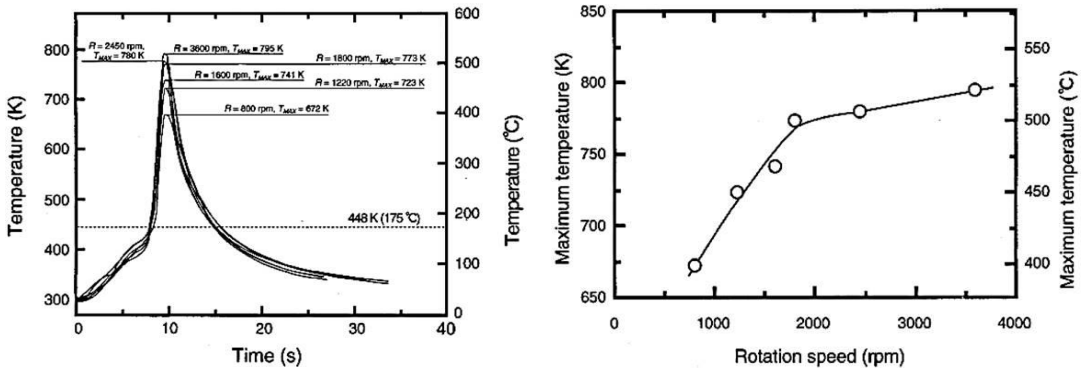

(a) (b)

Figure 2.8 a) Temperature as a function of time, and b) peak temperature as functions of rotation rate for FSW joints of 4 mm thick AA6063. Adapted from Sato et al. [39]

Temperature results as plotted in Figure 2.8 showed that, the maximum temperature rose sharply with increasing rotation speed up to 2000 rpm, beyond which it gradually rose, which trend is similar to results stated by Tang et al [36]. However, in this research possible effects of forge force on thermal, microstructure and hardness distributions were not considered, since there might have been adjustments in forge force due to variations in rotation rates. It has been believed and proved by many researchers like Thomas et al.

[45], Fonda et al. [40], Colligan et al. [46] and Rajakumar et al. [47] that forge force plays a significant role in FSW. It also stated that constant welding speed resulted in the same temperature transient, which presents the time at a given elevated temperature. Simar et al. [48] performed FSW in 6 mm thick 6005A with a welding speed ranging from 200 mm/s to 1000 mm/s and a constant rotation rate. It's found that when welding speed increased, the measured peak temperature drops gradually, which is consistent with both experimental results [47] and simulation results [7], [49].

All the above works discussed assess temperature history and distribution in the stir zone by embedding TCs either directly in the weld path or very close to the stir zone. On the other hand, as mentioned earlier, measuring temperature of the joint by placing TCs inside or at the tool probe has been employed in only few researches. Simar et al. [44] placed two TCs at different locations (3 mm and 13 mm) from the interface of shoulder and workpiece to measure peak temperatures during FSW. Leinert et al. [50] reported results of FSW in 6.3 mm thick hot-rolled AISI 1018 mild steel at a welding speed of 0.42 mm/s by employing similar temperature measuring method. Temperature cycles were measured on the workpiece and tool during welding using thermocouples and an infrared camera system. Some TCs were located at ~3.2 mm from the edge of the stir zone on the top surface of the workpiece, other TCs were also attached to the outer circumference of the tool at various distances (6.35 mm and 9.65 mm) above the shoulder. Covington [51] measured temperature during welding process by placing TCs at different positions like the probe core and locations away from the shoulder interface. The measured temperature results were used to validate a thermal model by using a parametric study. With the aim of applying closed loop control of deformation zone

temperature in FSW of copper canisters, Cederqvist [52] used similar arrangement of thermocouples at the shoulder and probe as seen in Figure 2.9.

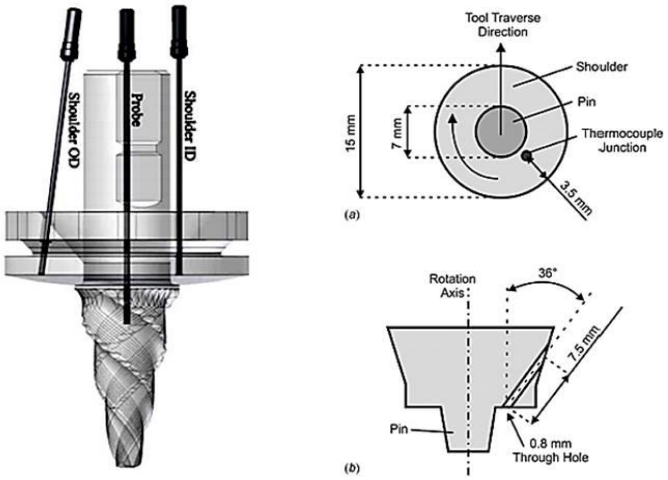

Figure 2.9 Thermocouple placed at various locations inside tool. Adapted from Fehrenbacher et al. [53] and Cederqvist [52]

In the above studies temperature was measured by imbedding TCs inside the tool, which has also been employed at the USC FSW lab for thermal history study [54], [6]. However, it could be argued that when tool is embedded inside the tool, the thermal conditions of tool may affect the temperature measurement. Gerlich et al. [21] measured temperature in friction stir spot welding from TC tip which directly contacted with deformed material. TCs were fed into two through holes: one flush with shoulder interface, and another outside the probe. Relative to TCs embedding inside the tool, TCs in direct contact with deformed material is probably more reflective of the deformed zone temperature since it might avoid the effect of thermal condition on the tool compared to the TC situated at the tool interior [21]. Similar method has been employed by Fehrenbacher et al. [31] recently to measure temperature at the shoulder interface. The above stated studies employed TCs to measure temperature in welding. TCs placed in the plate measure temperature at a given point, while TCs inside tool can measure

temperature history of deformation zone along seamline during the entire welding process. TCs embedded inside the tool can guarantee the repeatability of temperature measurement due to no displacement in TCs. However, thermal condition around the TC in the tool will somehow affect the temperature measurement, which value can only be considered as some measure of average temperature of the material around the tool. Also, the measured temperature by tool TC is probably a little lower than the actual deformed zone temperature at steady state.

In a summary, above literature about temperature in FSW indicates that, keeping other parameters constant, when the weld is performed in air without extra thermal managements, the tool rotation rate proportionally affects the peak temperature in the joint, while the tool welding speed affects the heating and cooling rate and hence length of time of staying above a certain temperature. Reynolds et al. [7] reported the effect of welding speed on the transient length of thermal history by simulating thermal distribution in FSW. Thermal managements have also been introduced in FSW to enhance the heat extraction and modify thermal conditions, which help tailor FSW parameters to obtain desired joint properties. Nelson et al. [55] demonstrated that employing rapid cooling techniques like welding under cold fluids can enhance the heat extraction rate. Upadhyay et al. [56] pointed out that increased convection from the top surface reduced nugget temperature, increased torque, and increased cooling rate in the HAZ, which resulted in higher HAZ minimum hardness and higher tensile strength of tested transverse weld cross-sections. Also, thermal BCs at the workpiece bottom can be varied by employing backing plates with different thermal conductivities. Upadhyay et al. [56] also stated that a high-thermal diffusivity BP can enhance cooling rates in the HAZ,

resulting in improved HAZ minimum hardness. Thermal managements will be discussed later in section 2.3.2.

2.3.1.3 Effect of Temperature and its Transients on Weld Properties

Microstructure of the joint is highly affected by the thermal cycle experienced by the material during the welding process. This cycle will cause decrease in strength and other desired properties by dissolving precipitates, diffusing solute, forming non-strengthening phases and coarsening or dissolving strengthening precipitates to some degree. Most researches in FSW tried to minimize this negative effect and produce joints with desired properties at an acceptable production rate. To achieve this goal micro hardness test on the joint cross section has been examined since it is a window to material behavior during FSW.

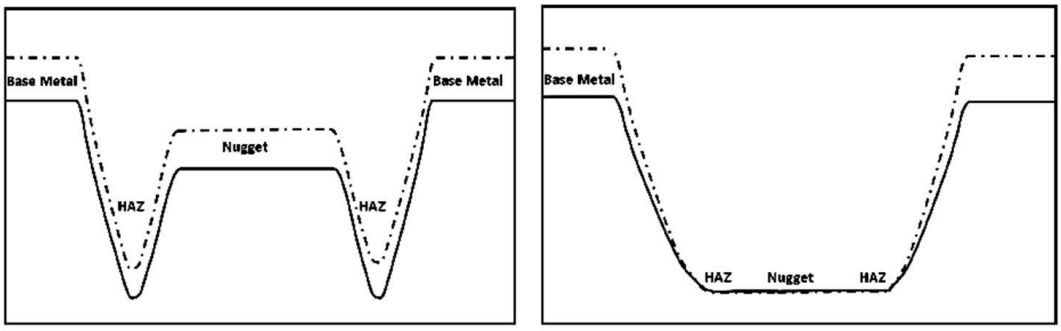

(a) (b)

Figure 2.10 Typical hardness profiles on traverse cross section for a) joints with peak T sufficiently high close to solution treatment T, and b) joints with peak T around 350 ℃ in as welded condition (solid lines) and naturally or artificially aged condition (dashed and dotted lines). [6],[7],[38],[57],[58].

In precipitation hardening alloy, nugget temperature that is close to SHT will result in a typical "W" shape hardness profile in the transverse cross section of the joint, as shown in Figure 2.10(a). With such peak temperature, the nugget would be in a condition quite similar to the nugget after solution heat treatment and aging, therefore, strengthening phases may re-precipitate during post weld cooling and subsequent natural

or artificial aging processes. Several works reported the trend of hardness recovery, which is the greatest at nugget and less at HAZ [7],[38]. For a typical "W" shape hardness profile, hardness drops rapidly on either side of the nugget, continuously decreases across the TMAZ and then reaches the global minima at HAZ [43],[59],[60]. If a low welding power is applied in FSW to keep nugget temperature at around 350 ℃, the typical hardness profile will be characterized with a flat U shaped profile as shown in Figure 2.10(b) instead of the W shaped profile, due to similar hardness values at HAZ and the nugget with a weld peak temperature around 350 ℃. It has been reported that, in precipitation hardening alloys, peak temperature of ~350 ℃ is the most damaging to strength. Mahoney et al. [35] performed tensile testing on FSW joints of AA7010 and reported that during the testing failure occurred along HAZ where the measured peak T ranged from 300℃ to 350℃ (as shown in Figure 2.6). Subsequent TEM analysis of the fracture surface indicated the presence of coarsened strengthening precipitates. Both

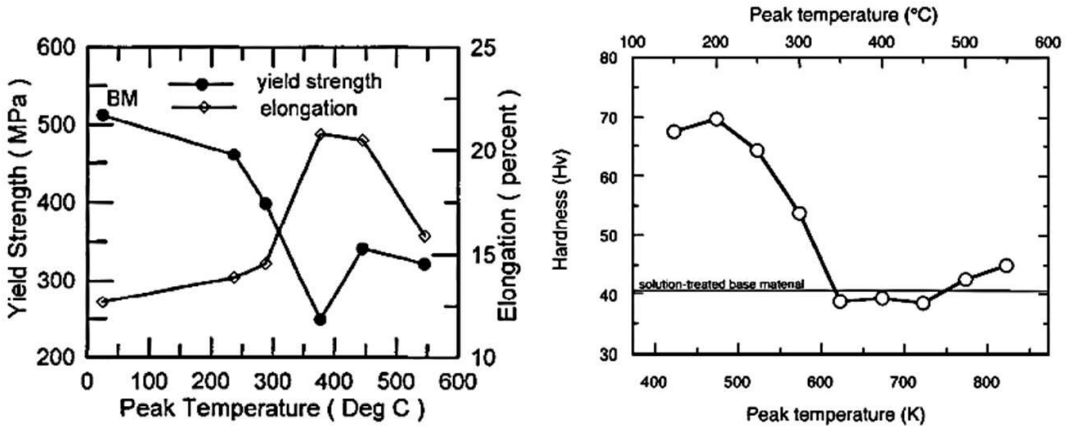

(a) (b)

Figure 2.11 Mechanical properties as functions of peak T for simulated HAZ. Adapted from a) Hwang and Chou [61], and b) Sato et al. [60]

Hwang and Chou [61] and Sato [60] simulated the thermal cycles at HAZ under different peal temperature in joints of AA7075 and AA6063 and reported mechanical properties as

shown in Figure 2.11. Hwang and Chou reported that the minimum strength occurred with a peak T of about 377 ℃, as shown in Figure 2.11(a), and Sato et al. reported that a temperature ranging from 350 ℃ to 450 ℃ (test was done without subsequent aging) was shown to be most damaging to the properties, which both corroborate Mahoney's [35] observation that the temperature of ~350 ℃ is responsible for the biggest decrease in strength. When the peak temperature is significantly larger than 350℃, the hardness at joint nugget will increase with the temperature increasing. Hassan et al. [43] reported

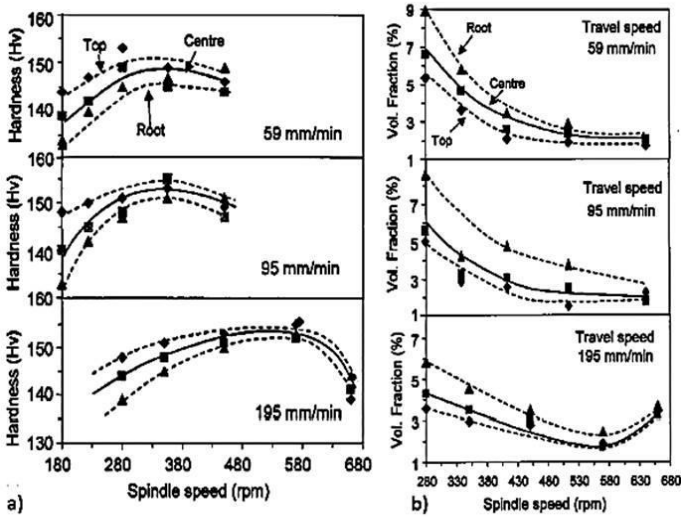

Figure 2.12 a) Average nugget hardness and b) Volume fraction of coarse 2nd phase precipitate as a function of rotation rate measured at various depths from AA7010 weld crown produced with different welding speeds. Adapted from Hassan et al. [43]

that, when speeds increase, nugget hardness generally increases until reaching a plateau, as shown in Figure 2.12. It shows an excellent reciprocal correlation between the volume fraction of coarse 2nd phase precipitates and the nugget hardness values. It indicates that fewer coarse precipitates result in larger solute availability for strengthening phase precipitation in nugget, which leads to larger hardness in the nugget. Reynolds et al. [7] systematically studied effects of weld parameters on joint properties and reported similar results with FSW of AA7050 as shown in Figure 2.13: when speeds increased the

average nugget hardness increased until reaching a plateau. It also reported that higher welding speed resulted in larger HAZ minimum hardness, which effect was less relative to the effect of welding speed on average nugget hardness.

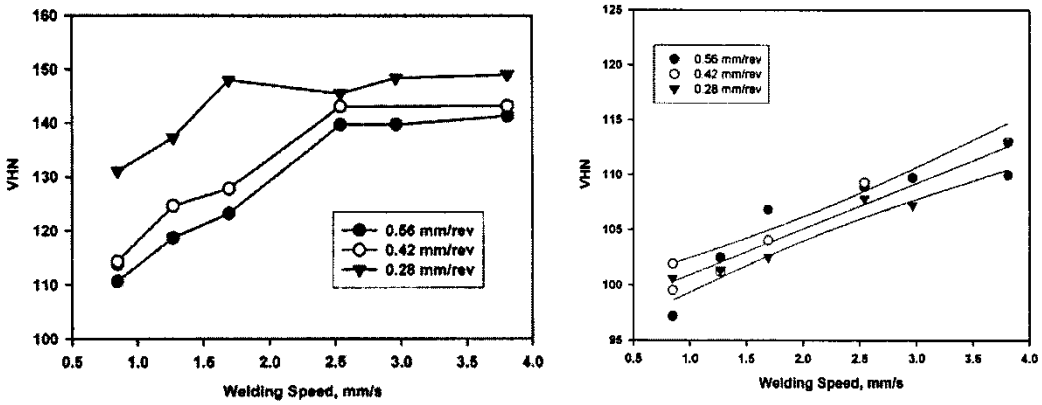

(a) Average nugget hardness: as welded (b) HAZ minimum hardness: PWHT

Figure 2.13 Average nugget hardness and HAZ minimum hardness as function of welding speed in AA7050 welds. Adapted from Reynolds et al. [7]

Thermal history a joint goes through is the most effective key to understand effects of weld parameters on joint properties, which has been considered and studied in only few researches. Reynolds et al. [7] extracted peak temperatures (as shown in Figure 2.14) from input torque model and reported a linear correlation between the peak temperature and the nugget hardness. When the peak temperature is around 350℃, the strengthening precipitations are coarsened which leads to a weak nugget (data points inside the circle) and complicates this linear correlation. It also reported a general increase in hardness when peak temperature increased, indicating a positive response of the average nugget hardness to the post weld heat treatment (PWHT). Nelson et al. [55] and Fuller et al. [57] also reported a similar positive response of nugget hardness to natural aging. Relative to nugget average hardness, the HAZ minimum hardness has a

negative response to PWHT due to precipitate coarsening and disappearance of strengthening precipitates.

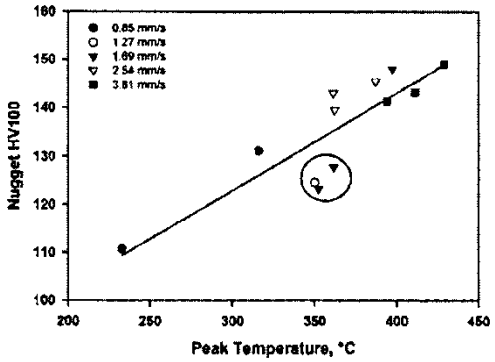

(a) PWHT average nugget hardness vs peak T. Circled data are supposed to be in overaged condition.

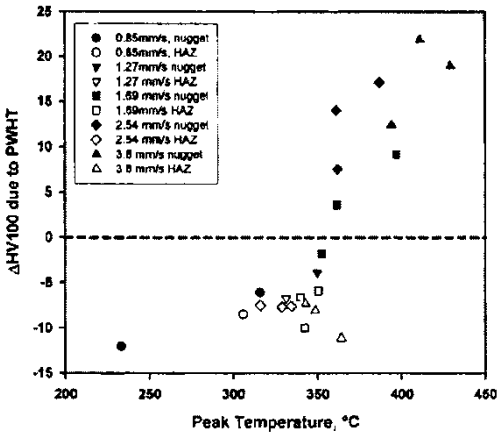

(b) Change in average nugget hardness (closed symbols) and HAZ hardness (open symbols) due to PWHT vs peak T. Symbol shapes indicates various welding speeds.

Figure 2.14 Joint hardness as a function of peak T extracted from input torque FEM model. Adapted from Reynolds et al. [7]

Recently new technologies like transmission electron microscopy (TEM), selected area (electron) diffraction (SAD) and small-angle X-ray scattering (SAXS) have significantly enhanced investigations of precipitation and dissolution behaviors and then strength variations at the NG, TMAZ and HAZ [59],[60],[61],[62],[63],[64],[65]. Jata et al. [59] investigated the joint of AA7050 by TEM both in AW and PWHT (T6, 120 ℃) conditions. In the AW joint, very little precipitates were observed in the nugget; while in

the HAZ fine strengthening precipitate and precipitate free zone (PFZ) were coarsened by a factor of five relative to the base metal. In the PWHT joint, fine strengthening precipitates similar to the one shown in base metal were observed in the nugget, while PWHT had little influence in HAZ, which still consisted of non-strengthening coarsened precipitates and large PFZ. Together with very similar observation from Su et al. [66], those studies corroborate that natural or artificial aging has little influence in HAZ minimum hardness while a significant improvement in the average nugget hardness. Dumont et al. [67] reported quantitative data of volume fraction and precipitate size in different zones of the joint as shown in Figure 2.15 based on SAXS. Compared to

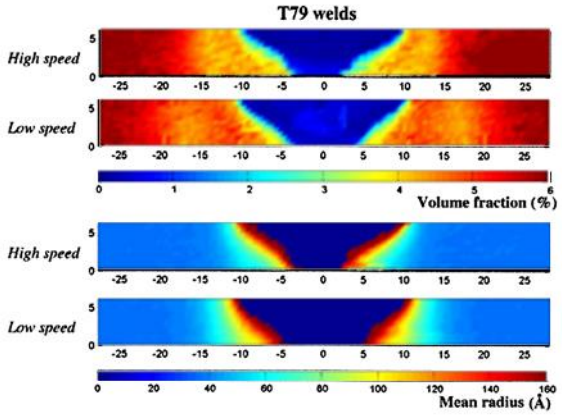

Figure 2.15 SAXS maps of precipitate size and volume fraction in FSW of AA7449-T79 at high and low welding speeds. [67]

precipitates with mean radius of 40~60 Å in base metal, precipitates in HAZ have coarsened to 120-160Å. In the nugget the volume fraction of precipitates is close to zero, which validates the assertion that almost all the precipitates will be dissolved when the weld is made at the peak temperature around the solutionizing temperature. Svensson and Karlson [65] studied the precipitation and dissolution behavior in different zones of joint in AA6082 in which alloy β ''(Mg_5Si_6) fine precipitate is the primary hardening precipitate. Similar to observations in 7XXX series aluminum alloys, in the AW

condition, in HAZ the hardening precipitates were not observed while β'($Mg_{1.7}Si$) were observed to form on dispersoids. In the nugget, β' were not observed since all the precipitates were dissolved into matrix due to high peak temperature.

In a sum, 6XXX and 7XXX series aluminum alloys share a common sequence of precipitation and dissolution. The kinetics of precipitate coarsening, which is the rate of non-strengthening phase (η phase in 7XXX series and β'phase in 6XXX series) formation, is maximized when peak temperature is around 350 ℃. During the formation of non-strengthening phases, those non-strengthening phase (β'/η) particles decrease the strength by taking away from the matrix a lot of solute which otherwise would have been available for the re-precipitation of strengthening phase (β''/η') during the post weld aging. At regions with peak T around 350 ℃, like the nuggets with relatively low weld power and most HAZ areas, material there remains in the formation of non-strengthening phases (β'/η), which causes strength loss. Lower welding speed will remain the material in the above regions for a relatively longer time, aggravate this situation and cause more strength loss. At regions with peak T much higher than 350 ℃, when the peak T increases to the solutionizing T, more precipitates dissolve into matrix, which avoids precipitate coarsening, and increases the nugget zone strength due to the formation of fine strengthening precipitates during the subsequent heat treatment process.

2.3.2 THERMAL MANAGEMENTS IN FSW

2.3.2.1 Modification of Thermal Boundary Conditions

Figure 2.16 shows typical heat transfer in FSW/P and systematic thermal management techniques which can be applied to modify thermal conditions at tool,

workpiece and backing plate boundaries, etc. In this section, the thermal management here means modification of thermal BCs. The thermal management is another aspect that has a significant influence on joint properties in FSW [67], [69]. Keeping everything else constant, the applied thermal management technique can either enhance or reduce the heat transfer rate, indicating by the "+" and "-"signs, relatively. Primary heat transfer methods considered in FSW/P are conduction (solid arrows) and convention (dotted arrows). Modifying the welding process by implementing thermal management techniques to improve joint properties and ease the process has been studied over decades. To improve the properties of AISI 304 stainless steel joints applied in gas storage tanks and rocket combustion chamber, the use of acetone/dry ice mixture and liquid nitrogen was discussed in a patent [70] in 1966. In this section the background and history of thermal managements will be comprehensively reviewed and discussed.

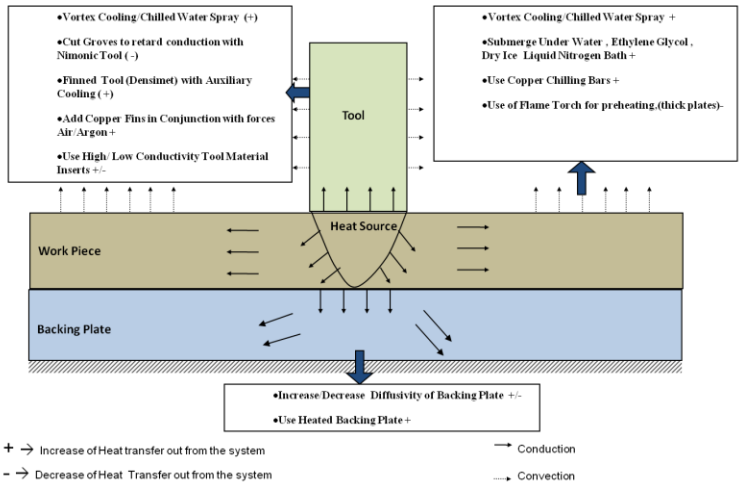

Figure 2.16 Typical thermal management methods applied in FSW [68]

Modification of thermal BCs in most literature is aimed at improving desired joint property like increasing mechanical properties, decreasing residual stress or corrosion susceptibility, etc. Rapid quenching has also been employed by some researchers to examine fundamental mechanism of fine grain evolution. Benavides et al. [71], [72]

welded AA2024 plates submerging in liquid nitrogen to investigate the viability of FSW at very low temperature. Temperature measuring results at far field indicated that the submerged cold joints were up to 81 ℃ colder than the room temperature. Reasonably the joint was defective, characterized with a large worm-hole defect, since the material flow was limited due to too low temperature. However, the average grain size at stir zone was significantly decreased to 0.8μm relative to regular size of ~10μm.

Rapid heat extraction has been applied in several works on the joint immediately after welding to reduce residual stresses and then better fracture and fatigue properties. Van der Aa et al. [73] and Richards et al. [74] employed coolants like liquid CO_2 for local cooling to obtain dynamically controlled low stress no-distortion (DCLSND) in fusion welding. Staron et al. [75] applied CO_2 to cool material near the weld seam in FSW. It's reported that tensile residual stress in the center of 6.35 mm thick AA2024 plate was significantly reduced. In 2007, DCLSND technology was also applied in FSW (water jet device applied in the wake of weld) was reported to decrease residual tensile stress by 60% at joint center [76]. It seems feasible to reduce residual stress by employing higher heat extraction rate in the welding process. Recently Richards et al. [74] investigated the effect of active cooling methods on the welding stresses during FSW by finite element modelling. Various active cooling methods using liquid CO_2 cooling systems as the cooling sink in practically feasible locations during FSW have been examined. The simulation work indicated that, for a given flow rate of cooling source, to optimize the cooling effect, there is an optimum operating window depending on the size, power and positioning of the cooling sinks. Besides reducing residual stress, rapid cooling of workpiece has also been employed for other goals in following researches.

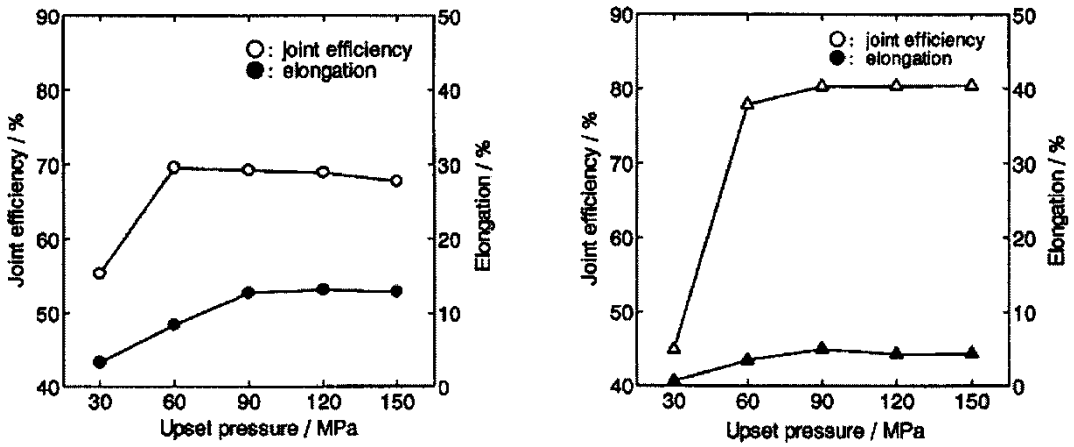

(a) atmospheric joint (b) underwater joint

Figure 2.17 Joint efficiency and elongation as function of upset pressure for in air and underwater friction welded AA6061. [68]

Sakurada et al. [77] welded cylindrical AA6061 plates under water using inertia friction welding. As shown in Figure 2.17, relative to the weld made in air, in this under water joint, joint efficiency was increased by 14% and the width of HAZ was reduced. Nelson et al. [55] performed FSW by externally heating and cooling the parent plate and anvil to examine the effect of quench rate on AA7075 and AA2195. Cold water and mist were applied behind the tool to chill welding plates. After the welding process, AA7075 joints were natural aged for 1000 hours for following tensile testing. Tensile strength was increased up to 10% compared to conventional FSW of AA7075. Su et al. [78] used a mixture of water, dry ice and methanol behind the tool to quench the AA7075 sheet and reported production of nano and ultra fine grains. Hoffman et al. [79] reported similar results of AA6061 welded under water. Fratini et al. [80] performed welds using three sets of welding parameters on 3 mm thick AA7075 sheets at three FSW environments: normal, forced air and water submerged. It's visually observed that in submerged joints, the size of the soft zone was slightly decreased, which possibly resulted in the slightly increased strength. Hossein and Manesh [81] welded accumulative roll bonded aluminum

alloy under water, and reported narrower HAZ region, lower grain size at nugget, and slight increase in tensile and yield strengths. Bloodworth et al. [82] performed welds with three sets of welding parameters both in air and under water. It's reported that welding under water required larger torque (20% increase) and then more power input, and increased the tensile strength slightly. Temperature at deformed zones has also been controlled by cooling methods using forced air or cooling liquids. Those methods have also been claimed to enhance the window of welding speeds and decrease the surface irregularity [83], detailed observations and results of which claim however haven't been found in open literature.

Preheating the workpiece, as another type of thermal management, enjoys several advantages like easing the machining, allowing higher speeds, decreasing process forces the tool experiences and thus improving tool life, etc. [84],[85],[86]. Preheating is typically helpful for high temperature alloys, while not applicable in precipitation hardening aluminum alloys which are sensitive to thermal history. Therefore preheating will not be discussed at length.

Modification of thermal BCs at the bottom of workpiece during FSW affects thermal history in the joint, which will definitely influence the joint microstructure and properties. Rosales et al. [87] performed FSW on AA2024 and AA6013 plates with a constant forge force and three sets of rotating and welding speeds. Three backing plates coated with steel, copper and ceramic were applied to study the effect of thermal BCs of backing plate. When different backing plates were employed, the measured results of far field in-plate temperature changed significantly due to the effect of different thermal conductivities of backing plate. Nelson et al. [55] employed a heated backing plate in the

welding of AA7075 and reported a higher peak temperature, lower cooling rate and therefore inferior mechanical properties. Su et al. [88] employed both conventional steel and mica clamp and backing plate in friction stir spot welding (FSSW) of 1.3 mm thick AA6111. Relative to the conventional steel clamp and backing plate, when the mica clamp and backing plate (with smaller thermal conductivity and greater insulation) were employed in the welding, a larger fraction ranging from 12.5% to 50% of heat generated by tool was transferred into the joint as heat energy due to less the heat dissipating into the backing plate. Bakavos et al. [89] performed a similar study in FSW of 0.9 mm thick AA6111, and reported 45 ℃ increase of peak temperature while 15% reduction in lap shear strength when a ceramic backing plate was employed relative to conventional steel backing plate. Upadhyay [56] applied different backing plates with different thermal diffusivities in FSW of 25.4 mm thick AA6061 and 4.2 mm thick AA6056 to investigate effects of process control parameters and TBCs on response parameters and joint properties. Thermal diffusivity of backing plate material significantly affected peak temperature of the joint and the cooling rate in the HAZ which resulted in a significant variation in weld properties, and other process variables. The use of low thermal conductivity backing plate enhanced the through thickness homogeneity of micro-hardness and grain size in up to 25.4 mm thick joints. Relative to conventional monolithic steel backing plate, the use of composite backing plate which consisted of steel strip with low thermal diffusivity at center and aluminum bars with high thermal diffusivity at side increased cooling rates in the HAZ, resulting in increased HAZ minimum hardness and therefore superior joint property.

Thermal management in FSW has been proved as helpful and necessary in tailoring the welding process to obtain desired specific properties of joints. It's important to put more efforts to further understand the correlations among thermal BCs and process variables like process forces, torque, temperature, grain size, hardness, strength and so on, to provide comprehensive information of effectively and accurately tailor the joint properties through thermal managements.

2.3.2.2 Process Variants in FSW

Process variants can change the thermal history during FSW and are another type of thermal management. Process variants employed in this research include half (partial) and full penetration FSW, single pass and dual pass FSW, conventional and stationary shoulder FSW. Relative to full penetration FSW, partial penetration FSW enjoys several advantages, like improving the weldability, being more likely to produce defect free joint, allowing higher FSW speeds, causing smaller process forces and requiring less torque. Partial penetration FSW is more beneficial than full penetration especially in high strength alloys like 7XXX series aluminum alloys. Therefore, to reap the benefits of partial penetration while completely joining the workpieces, dual pass (DP) FSW with half penetration welds sequentially made on both of the workpiece is proposed to perform the FSW joining process, and is expected to have more advantages than single pass (SP) full penetration FSW. However, DP also brings complications into understanding of mechanism especially the thermal history in the joint since thermal BCs for the 2^{nd} pass has changed to be inhomogeneous compared to the 1^{st} pass and also the 2^{nd} pass will heat treat the 1^{st} pass. Unfortunately, there is few systematic investigation in comparing DP with SP FSW, and this dissertation is a first step to the goal.

In conventional shoulder (CS) FSW, both the tool shoulder and pin rotate to generate heat, soften material and allow the tool to translate along the seam line. It has been argued that, heat generated by the rotating shoulder dominates during FSW process. Wu et al.[90] reported that, in CSFSW with a constant rotation rate, the power generated by shoulder is typically 3~5 times of that of the tool pin. Schmidt et al. [91] simulated the heat generation in a FSW joint of AA2024-T3 using an analytical model. The simulation result showed that, shoulder contribution to heat generation is larger than 85% of total depending on tool geometry. Chao et al. [92] reported that for constant shoulder diameter and two pin lengths, shoulder heat inputs is 56.5% of total (long pin) and 86% of total (short pin). Again, tool geometry is the only thing considered. Shercliff and Colegrove in chapter 10 of Friction Stir Welding and Processing [93] stated that heat generated by pin is negligible in thin sheet and may be more than 10% of total heat generation in thick plate. However, thickness of thick plate and thin sheet was not defined. Khandkar et al. [94] proposed a novel input torque based model to study thermal distribution during FSW. Through power equations developed in this study, it can be calculated that, for a shoulder with a diameter of 23 mm, and a 6.4 mm long pin with a diameter of 11 mm, the ratio of shoulder power to pin power is 1.8; for a shoulder with a diameter of 35 mm, and a 32 mm long pin with a diameter of 19 mm, the ratio of shoulder power to pin power is 0.5. Therefore, in general, the conventional wisdom is that shoulder heating dominates based mainly on tool geometry. More sophisticated approaches are possible but contact conditions between tool and workpiece remain difficult to define.

It has also been argued that the rotating shoulder may generate too much heat in the joint near the crown, which will cause less homogeneity in thermal / microstructure /

hardness distributions through thickness [95], [96]. According to the literature view by Neto et al. [97], in CSFSW the tool shoulder generated about 60%~80% of the heat and the probe accounted for the rest. This high contribution of the shoulder to the total process power resulted in a wide HAZ at the weld crown, and a significant temperature gradient between the joint crown and root, thus less homogeneity in joint's thermal history, microstructure and properties distribution through thickness.

The new process variant stationary shoulder (SS) FSW with a stationary shoulder and a rotating probe has been developed with the goal of enhancing through-thickness thermal homogeneity and therefore minimizing microstructure and strength heterogeneities through thickness. SSFSW was first proposed by Russell et al. [98] to reduce the significant thermal gradient through joint thickness in the FSW of titanium alloys which have very low thermal conductivities. As a relatively new concept, SSFSW in Aluminum alloys is also expected to be advantageous in following aspects compared to CSFSW: (a) enabling the production of welds with smaller total heat input than in otherwise similar conventional shoulder welds, (b) improving surface finish [99], (c) producing narrower joint nugget and HAZ, (d) producing a narrower more parallel through-thickness thermal field, which should lead to more homogeneous through thickness microstructure and properties, and (e) minimizing distortion of welded parts, since the shoulder does not generate heat during welding [98],[90]. Wu et al. [100] performed butt FSW in 6.3 mm thick AA7050-T7651 plates by CS and SS welding tools that had near-identical geometries for a systematical comparison study. It reported that under optimum process conditions, relative to CS, SS reduced the process heat input by about 30%, and produced joints with a far superior surface finish, a narrower, more

parallel, HAZ and larger homogeneity in thermal, microstructure and property distributions through thickness, and better properties like transverse tensile strengths. DIC analysis of the strain distribution demonstrated that a narrower HAZ helped prevent premature failure by imposing greater constraint on the localization of plastic strain during deformation. Thermal simulation and hardness modelling confirmed that a more uniform heat source in SS FSW was attributed to the above benefits. In the dissertation Md. Reza-E-Rabby [101] investigated and compared the weld quality and process response variables of FSW with an identical pin (a coarse threaded conical pin with three shallow flats) and different tool shoulders(CS and SS). It's reported that: (a) With the same pin, SS produced defect free welds with smooth surface finish, while CS produced defect free welds with rough surface due to the shoulder mark leaving by the rotating shoulder in CSFSW. (b) Relative to CSFSW, in SSFSW, the required forge force and the X-axis force were higher and X-force was primarily governed by the applied forge force. (c) However, CS and SS caused little difference in torque, weld power and temperature. This conclusion challenges the popular proclamation that "shoulder predominantly generates frictional heat", which is not applicable to all cases. This phenomenon mostly depends on the applied forge force and present experience and technologies of producing sound welds with good quality and properties by FSW.

2.4 State of the Art in FSW Process Modeling

2.4.1 Global Introduction

During FSW, the weld joint material undergoes intense thermo-mechanical deformation and temperature cycle. In precipitation hardened aluminum alloys, thermal history in the joint cross section significantly affects the microstructural distribution,

which affects the relevant joint properties. Thermal history a joint goes through is the most effective key to understand effects of weld parameters on joint properties. Therefore, temperature history especially at weld nugget and heat affected zone, which is determined by primary control parameters like weld speeds and forge force, are of utmost significance in study of FSW joint properties. Understanding and finally establishing the relationship between control parameters and temperature history probably realize the tailoring of desired specific properties in FSW joints. Better understanding of FSW process, response parameters and resulting joint properties requires more systematic experimental and/or simulation data. Temperature history can be experimentally measured by imbedding TCs inside the tool and/or theoretically simulated by software. Unfortunately, it is hardly possible to measure actual transient temperatures in the deformation zone. Relative to experimental data, the reliable simulation research can help reduce time, energy, efficiency and cost, etc. Therefore thermal history of FSW with different process variants will be theoretically simulated based on reliable simulation model to investigate the effect of process variants, material properties such as flow stress, thermal conductivity, and heat capacity, thermal boundary conditions, variations in control parameters like rotation rate and welding speed on thermal distribution and power generation.

2.4.2 FSW Process Modeling

Since FSW was invented by Wayne Thomas in TWI in 1991 [102], a lot of research has been conducted to simulate the FSW process [68], [101], [103], [104], [105], [106],[107],[108],[109],[92],[110],[111],[112]. Those models ranging from simple heat

flow models to fully coupled thermo-mechanical models have their own advantages and disadvantages.

Accuracy in analytical and numerical modeling is hard to obtain. Friction stir processing is a highly coupled solid thermo-mechanical process, which causes significant material deformations and steep temperature gradients shortly. Process control and response parameters interact with each other complicatedly, resulting difficulties in accurate analytical and numerical modeling.

Relatively simple thermal models rely much less heavily on experimental data like heat input or temperature measurement to calibrate the models. Temperature field is the mostly expected outcome. Those models can simulate the far field thermal distribution accurately. However, in the near field, the heat source geometry affects the simulation accuracy of thermal distribution sensitively. Also, predictive capability of those models is limited due to limited outputs. Fully coupled thermo-mechanical models should perform the best in predictive capability, at the price of consuming plenty of computational power and time. Meanwhile, generality of those models is unfortunately decreased by heavily relying on experimental data.

A general thermal-mechanical model should include thermo-visco-elasto-plasticity relationships, which inevitably causes computational complexity and rigor. An essential problem of general thermal-mechanical models is how to properly describe heat generation in FSW process.

Conceptualizing the heat generation as a function of several principle process control parameters is an easy way to describe the heat source. Arbegast [113] assumed that, keeping other control parameters the same, heat generation during FSW is in

proportion to the square of angular velocity and is inversely proportional to the travelling speed. A pseudo heat index $w = \omega^2/v$ was introduced to describe the heat input. Here ω is the angular velocity, and v is the travelling speed of tool. Roy et al. [114], Balasubramanium et al. [115] and Kalya et al. [116] also proposed similar heat indices to describe heat generation during FSW process. However, those empirical heat indices are unrepresentative. The contact condition at the interface of the tool and workpiece was adopted by Schmidt [91] to describe the heat generation. The contact condition (either sticking or sliding) was determined by the contact shear stress which was estimated by Classical Coulombs law of friction.

A new model termed as Thermal Pseudo-Mechanical (TPM) model was proposed by Schmidt et al. [103],[91] to predict the thermal field. The TPM model is a combination of simple thermal model and fully coupled thermos-mechanical model: material flow is excluded in modelling while heat source is included in solution outcome. In the TPM model, all input parameters (including some thermal and mechanical properties of materials) are adopted to simulate the FSW process, yielding results of the joint's thermal field, not mechanical properties. The TPM model implemented in COMSOL MULTIPHYSICS 4.0/4.4 has been adopted in this dissertation to simulate thermal distributions in FSW process when different process variants are applied, therefore thermal modeling based on TPM model will be discussed in details in the following.

2.4.3 TPM Model: Introduction, advantages and disadvantages

Strength of local heat source in an infinitesimal element is stated in equation 2.1 [104]:

$$q = \omega r \tau_{contact} = \omega r\left(\delta \tau_{yield} + (1-\delta)\tau_{friction}\right) = \omega r\left(\delta \tau_{yield} + (1-\delta)\mu P\right) \quad \text{Eq (2.1)}$$

Here, q is the local strength of heat source generated on the tool surface. ω is the tool rotating speed in radians per second. r is the radial distance from the simulated location to tool rotation axis. τ_{contact} includes two components due to yield and/or friction depending on actual contact condition according to conceptualization proposed by Schmidt et al. [91]. τ_{yield} is the temperature dependent shear flow stress of the workpiece material. δ is a dimensionless slip rate ranging from 0 to 1, and is expressed as $\delta = V_{matrix}/V_{tool}$. Here V_{tool} is the tool surface velocity, and V_{matrix} is the matrix material (or deforming material) velocity at the interface of workpiece/tool. $\tau_{friction}$ is the shear stress component caused by friction, and is expressed as $\tau_{friction} = \mu P$. Here μ is the coulomb friction coefficient, and P is the contact pressure at the shoulder. The global heat generation is the integration of equation 2.1 over the tool (both shoulder and probe) surface contacting with matrix material. The global torque is given by the integration $\iint r\tau_{contact}$ over the tool (both shoulder and probe) surface contacting with matrix material.

The advantage of the TPM model is that the local heat generation rate is solved for iteratively by making the strength of the heat source dependent on the temperature (which the heat source is generating). Therefore, the heat source, as in real FSW, is self-limiting and is not prescribed a priori. Here, slip rate (contact condition) is an adjustable parameter that can be varied spatially (for example different values on shoulder and pin), and is used to achieve reasonable matching between experimentally observed weld power and probe T.

In equation 2.1, if sticking condition is dominant, then $V_{matrix} = V_{tool}$ and $\delta = 1$, which means that the local, temperature dependent yield stress of matrix material equals to the uniform shoulder pressure. Thus equation 2.1 can be expressed as following:

$$q = \omega r \tau(T) \qquad \text{Eq (2.2)}$$

Here $\tau(T)$ is the temperature dependent flow stress of the involved workpiece material. The details of the temperature dependence of the flow stress may also be used as an adjustable parameter. Equation 2.2 shows that, when sticking condition is dominant, heat generation during FSW process only depends on the temperature dependent flow stress of matrix material, while is independent of shoulder pressure, slip rate and coulomb friction coefficient. Since the temperature dependent flow stress is the only input required by this expression of heat source, the TPM model appears significantly convenient relative to other models stated above. However, in this case, the contact condition is assumed as fully sticking, which is not always the actual situation, thus effects of shoulder pressure which depends on forge force couldn't be considered. Reynolds et al. [117] have considered the effect of forge force in their research by introducing the δ as a ratio of shoulder contact pressure to the local temperature dependent yield stress.

Accurate description of thermal boundary conditions is also significantly crucial for reliable FSW simulation. More accurate description of heat transfer coefficient or thermal contact conductance at different interfaces, especially between the work piece and backing plate. [118],[119],[120] can help build more reliable model of FSW process simulation.

It's needed to determine the contact conductance at the interface of backing plate and workpiece (h_{bp}) when backing plate is modeled. h_{bp} has been assigned by different

researchers with different values ranging from 0.2 to 10^5 W/(m^2 K) [94],[118], [121],[109],[92]. For instance, Colegrove reported a good consistency with experimental measurements [109] when a h_{bp} of 25×10^3 W/(m^2 K) was used on the workpiece/backing plate interface under the tool and a h_{bp} of 10^3 W/(m^2 K) was applied everywhere else on the interface. Some researchers [119] adopted temperature dependent heat transfer coefficient in the simulation. Some other researchers tried to use several variables like local temperature, contact pressure and shoulder roughness, etc to determine heat transfer coefficient in the simulation [122].

CHAPTER 3

MATERIALS AND EXPERIMENTAL PROCEDURES

3.1 Experimental Materials

In this research, FSW in AA7099-T7651, AA7050-T7451 and AA6061-T651 have been produced and studied. Table 3.1 and

Table 3.2 list the nominal compositions and relevant properties of the alloys considered in this research.

Table 3.1 Nominal Chemical Composition (WT%) of Considered Al Alloys [123],[124],[125]

Alloy	Zn	Mg	Cu	Mn	Cr	Fe	Zr	Si	Ti
AA7099 -T7651	7.4~ 8.4	1.6~ 2.3	1.4~ 2.1	≤ 0.04	≤ 0.04	≤ 0.15	0.05~ 0.15	≤ 0.12	≤ 0.06
AA7050 -T7451	5.7~ 6.7	1.9~ 2.6	2.0~ 2.6	≤ 0.1	≤ 0.04	≤ 0.15	0.08~ 0.15	≤ 0.12	≤ 0.06
AA6061 -T651	≤0.25	0.8~ 1.2	0.15~ 0.4	≤ 0.15	0.04~ 0.35	≤ 0.7	-	0.4~ 0.8	≤ 0.15

Table 3.2 Relevant Properties of Considered Aluminum Alloys [123],[124],[125]

Alloy	Incipient Melting T (℃)	SHT (℃)	Strength			
			UTS (MPa)	Yield (MPa)	Elongation (%)	Hardness (Vickers)
AA7099-T7651	480	474	572	545	11	192
AA7050-T7451	488	477	524	469	11	162
AA6061-T651	582	529	310	276	12~17	107

The above alloys can be strengthened through precipitations of several metastable phases, therefore it's critical to understand and then control precipitation during artificial aging to achieve optimal properties.

3.1.1 Metallurgy of AA7099 and AA7050

The following information of 7xxx series alloys is from TOTAL MATERIAL [126]: *As typical Al-Zn-Mg-Cu alloy system alloys with Zn and Mg as primary alloying element, 7xxx family of aluminum alloy have the highest strength and have greater response to heat treatment relative to other alloys. In Al-Zn-Mg 7xxx family alloys, Mg substantially enhances the strength. Cu decreases the quench sensitivity thus increases strength, and possibly increases the resistance to stress corrosion, while decrease the resistance to general corrosion. Increasing amount of Si and Fe may reduce the fracture toughness. Maximized content of Cr and Mn increases the quench sensitivity and decreases the overall strength in the 7xxx family alloy.*

AA7050-T7451 has high strength, good fracture toughness and fatigue resistance, good stress corrosion cracking (SCC) resistance and exfoliation corrosion resistance [127]. AA7050-T7451 has been extensively applied in aerospace applications including fuselage skin, circumferential frames, bulkheads, stringers, wing components such as wing skin, spars and ribs [68].

The following information of AA7099-T7651 is from Kaiser Al [123]: *AA7099-T7651 is recently developed by Kaiser Aluminum to achieve an optimum combination of high strength, good fracture toughness, and good SCC resistance. Compared with most other aerospace alloys, it's a less quench sensitive Al-Mg-Zn-Cu-Zr alloy. AA7099-T7651 has up to 15% higher ultimate strength and up to 20% higher yield*

strength relative to AA7050-T7451, and has superior flatness, lot to lot consistency, and low, repeatable, reduced distortion during and after machining. Those advantages facilitate the machining process, reduce part repositioning, increase metal removal rates, while maintaining dimensional tolerances of the final machined part. Through a two stage aging treatment, the over-aged T7651 temper is achieved to obtain high strength and corrosion performance through thickness. AA7099-T7651 is especially suited for applications in aerospace engineering like lightweight airframe, fuselage applications such as frames and floor beams, wing structures such as ribs, spars and skins, etc.

The precipitation sequence of 7xxx series aluminum alloy are as follows:

$$SSS \rightarrow GP\ zones \rightarrow \eta' \rightarrow \eta\ (MgZn_2)$$

In AA7050-T7 stable η phase ($MgZn_2$) and/or $Mg_3Zn_3Al_2$ and metastable strengthening phase η' Mg (Zn_2; Al; Cu) are the major precipitate phases. η' precipitates as well as some GP zones are responsible for strengthening, while formation of non-strengthening η phase and coarsened η' deplete solute from the matrix and cause overaging as well as strength decrease [68].

Due to various temperature ranges in the thermal cycles introduced by FSW, there possibly exist the other phases in 7xxx series alloys [128]: (1) T phase (Al_6CuMg_4 & Al_2Mg_3Zn) existing in all systems including ternary and quaternary, (2) M phase ($MgZn_2$ & AlCuMg) existing in quaternary system, (3) Z phase ($A_{l5}Cu_6Mg_2$ & Mg_2Zn_{11}), (4) S phase (Al_2CuMg) with 46% Cu and 17% Mg, and (5) Θ phase (Al_2Cu).

It's worthy to note that, the solubility of Zn and Mg decreases when temperature drops which considerably affects precipitation hardening due to meta-stable modification

of the phase Al_2Mg_3Zn (T′) and η', thus solidification in 7xxx series alloys occurs with the formation of non-equilibrium eutectic at temperature 465℃-469℃ [129].

3.1.2 Metallurgy of AA6061

As a medium strength aluminum alloy, AA6061 is one of the most common alloys of aluminum widely applied in aerospace, automotive and general engineering fields due to its excellent formability, machinability, weldability and corrosion resistance compared to other alloys. A ternary alloy system (Al-Mg-Si), the general precipitation sequence of 6XXX series alloys, has been roughly reported as follows [130],[131]:

$$\alpha(SSS) \rightarrow \text{GP zones} \rightarrow \beta''(\text{Needle Shaped}) \rightarrow \beta'(\text{Rod Shaped}) \rightarrow \beta(Mg_2Si)$$

Here α(SSS) is the supersaturated solid solution; GP zones (or clusters) are the spherical precipitate with uncertain structure; β" are the fine needle-shaped precipitates along $<100>_{Al}$ with a monoclinic structure [132],[133]; β' are the rod-shaped precipitates along $<100>_{Al}$ with circular cross sections and a hexagonal crystal structure (a=0.705 nm and c=0.405 nm) [134],[135]; β(Mg_2Si) is usually formed as platelets on {100} of Al with the CaF_2 structure (a=0.639 nm) [135].

Thanks to advent and application of advanced techniques (TEM, SAD, DSC, SAXS, etc.), recently AA6061 has been considered as quaternary system due to presence of Cu which may affect the precipitation sequence in the Al alloy system [136],[137],[138],[139]. It has been reported the precipitation hardening kinetics can be increased by the addition of Cu [140],[141],[142],[143],[144],[145], which has been attributed to the refined microstructure [140],[141],[142] in some investigations while influence of Cu on the precipitation sequence in other studies [143],[144],[145]. 6XXX series alloys have distinctive properties partly due to a phase designated as Q, which is

stable only as a quaternary compound [136]. As an important precursor of the Q phase, the lath-shaped Q' phase, originally observed in AA6061 by Dumult et al. [145],[146], was reported to occur in increasing amount when Cu content increased [147]. The metastable phase Q' has similar composition and the same crystal system as Q. In Al-Mg-Si-Cu quaternary alloys, the lath shaped, hexagonal precursor phase to Q' as well as the β'' phase may be significantly responsible for strengthening [136]. In a typical 6022 alloy, different precipitation sequences caused by different Cu contents have been reported as following [148]:

$$\alpha(SSS) \rightarrow GP\ zones \rightarrow \beta''(Needle\ Shaped) \rightarrow \beta'(Rod\ Shaped) + Q'\ (Lath\ Shaped) \rightarrow \beta(Mg_2Si) + Si \quad (Cu\ content: 0.07\ wt\ pct)$$

$$\alpha(SSS) \rightarrow GP\ zones \rightarrow \beta''(Needle\ Shaped) \rightarrow Q'\ (Lath\ Shaped) \rightarrow Q + Si\ (Cu\ content: 0.91\ wt\ pct)$$

Therefore more complex precipitation sequence as follows in AA6061 has also been proposed:

$$\alpha(SSS) \rightarrow GP\ zones \rightarrow \beta''(Needle\ Shaped) \rightarrow \beta'(Rod\ Shaped) + Q' \rightarrow \beta(Mg_2Si) + Q$$

3.2 Experimental Facilities

3.2.1 Friction Stir Welding

All welds were produced by a hydraulically powered MTS FSW Process Development System (PDS). The PDS can be operated semi-automatically using customizable scripts, in which all the process control parameters like welding and rotational speeds, forge force, and tool displacement can be preprogrammed. Other control parameters like tilt angle and gear box ratio can be adjusted manually. The PDS is theoretically capable of applying a maximum vertical force of 135 kN, a maximum

traverse force in the X-axis direction of 66 kN, a maximum torque of 475 N m, a maximum rotational speed of 3000 rpm and a maximum traverse speed of 38 mm/sec. The PDS is capable of producing welds in both force control and displacement control modes. In force controlled mode, the vertical forge force of the tool can be controlled and adjusted during the process, while in position controlled mode, the vertical position of tool can be kept constant during the process. In this research, z-axis force control mode was preferred and adopted. The welding direction was parallel to plate rolling direction. Tool tilt was varied between 0 ° and 1 °.

3.2.2 Data acquisition of Process Response Variables

During welding process, the PDS recorded relevant process data as a function of time with an adjustable data collecting frequency up to 1000 Hz. The recorded process data includes both control and response parameters of tool, including position, traverse speed, rotational speed, forge force (in Z-axis, both command and feedback values), transverse force (in X-axis) and longitudinal force (in Y-axis). X axis forces were recorded from the signal produced from the piston pressure transducer on the X-axis hydraulic actuator. Y axis forces were obtained from the load cell in the spindle carriage. Resultant in-plane forces were calculated from average values of the X axis force and Y axis force. Real time torque was measured by a torque transducer attached to the spindle, and the FSW torque was calculated by substracting real time torque from free running torque of the tool under the same rotational speed. FSW power was calculated by FSW torque and rotational speed as shown in equation 3.1. Here P is the power in units of Watts (W), R is the rotation rate in units of rotations per minute (RPM), and T is the measured torque in units of Newton meters (N m). Probe temperature during FSW was

monitored and recorded by a k-type thermocouple connected to a HOBO data logger. The thermocouple was spot welded into the probe at the probe mid-plane and/or near root height on the rotation axis. It's expected that the tool temperature measured in this location is an accurate relative measure of the process zone temperature.

$$P = 2 \cdot \pi \cdot R \cdot T/60 \qquad \text{Eq (3.1)}$$

3.3 Details of Weld Run

3.3.1 Variations in Thermal Managements

3.3.1.1 FSW Tool

The tools used for performing all conventional shoulder welds were of a two piece design with a rotating shoulder and a rotating pin. The tools used for performing all stationary shoulder welds were of a two piece design with a stationary shoulder and a rotating pin.

The tool shoulder was fabricated out of H13 tool steel and then oil quenched or precipitation hardened. Tool shoulder for performing CSFSW was single scrolled and tool shoulder for performing SSFSW was smooth.

The 8 ºor 9 ºtapered tool pin in the shape of a truncated cone was fabricated out of H13 tool steel or MP-159. Tool pins with three different features were used: a pin with threads and 3 flats (T+3F), a pin with threads and 3 co-flow flutes (T+3C), and a pin with threads and 3 counter-flow flutes (T+3CT). With the chosen tool rotation direction, threads push material down, co-flow flutes push material down while counter-flow flutes pull material up. Flats are expected to be essentially neutral with regard to vertical flow.

3.3.1.2 Thermal Boundary Conditions

Welds were made either in lab air (IA) with an approximate ambient temperature of 23℃, or with a water spray (WS) in the wake of tool with a flow rate of 19 ml/s (0.3 gal/min), as shown in Figure 3.1. A 914mm x 152mm x 8mm backing plate (steel BP)

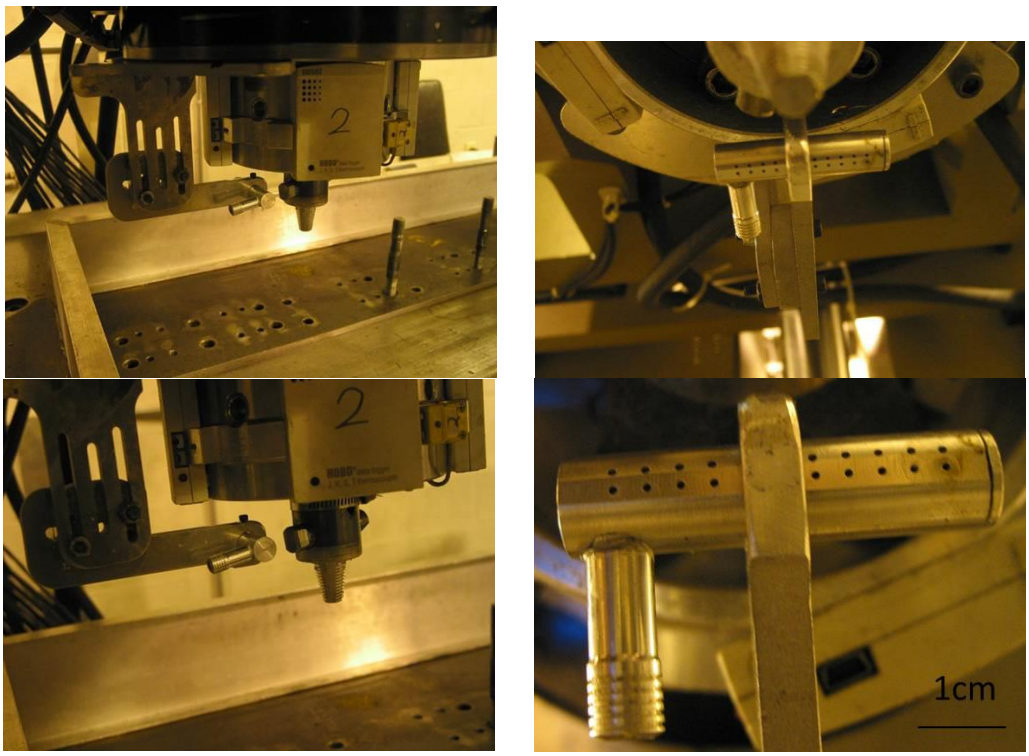

Figure 3.1 Water spray in the wake of the FSW tool

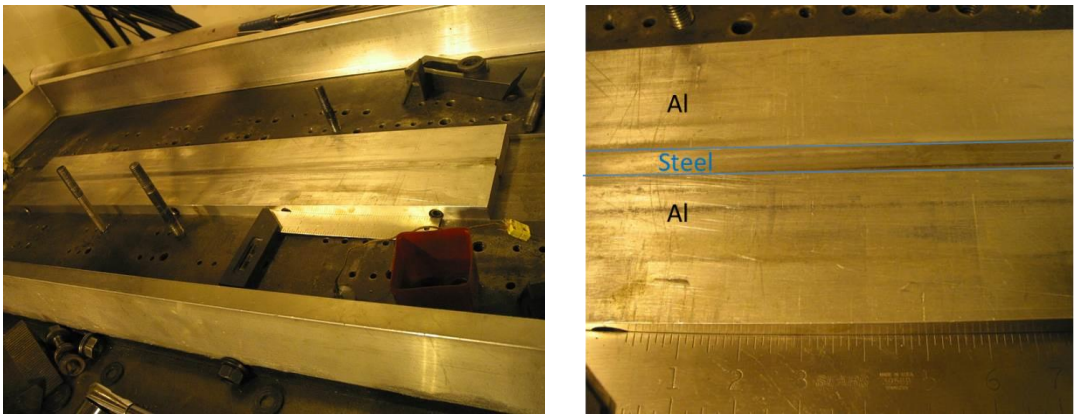

Figure 3.2 Composite Backing Plate

made of O1 tool steel was used in most cases to make welds in the air, while a 914mm x 152mm x 25mm composite backing plate (composite BP, as shown in Figure 3.2) (70mm wide AA6061 plate+12.7mm wide centered O1 tool steel plate+70mm wide AA6061 plate) was applied in some cases. Relative to steel BP, this composite BP consists of Al and steel, and has a higher general thermal conductivity. Narrow steel plate instead of Al is put right under the weld to avoid sticking between work-piece and BP when high temperature is generated during FSW.

3.3.1.3 Single Pass and Dual Pass FSW

Single pass welds were performed on 25.4 mm thick AA7099-T7651 plates, 32 mm thick AA7050-T7451 plates, and 25.4 mm thick AA6061-T651 plates. Dual pass welds were made on 24.9 mm thick plates machined from the 25.4 mm thick AA7099-T7651 plates. The thinner plates for dual pass welding were utilized to facilitate the use of a tool originally designed for welding 12.5 mm thick plate while producing some overlap between the first and second pass weld regions. In the dual pass processes, both passes were performed in the same direction with the same settings, producing joints in which the advancing side of the first pass was on the same side of the joint as the retreating side of the second pass. After the 1st pass being welded, the clamped plate was released and totally cooled to the ambient temperature, and then was turned over to perform the 2nd pass on it. Generally, different types of FSW process with different combinations of each thermal management were applied as follows:

(1) Conventional/Stationary shoulder single pass half penetration: CSSPH/SSSPH

(2) Conventional/Stationary shoulder single pass full penetration: CSSP/SSSP

(3) Conventional/Stationary shoulder dual pass full penetration: CSDP/SSDP

Summary of FSW tool parameters and control parameters are tabulated in Appendix A and B. DP-1 and DP-2 mean the 1_{st} and 2_{nd} pass of the dual pass weld.

3.3.2 FSW Preparation

Bead on plate friction stir welding were performed on AA7099-T7651, AA 7050-T7451 and AA6061-T651 plates with desired thickness using different sets of thermal managements and control parameters. The effects of welding directions of two passes (same or different, symmetric or asymmetric) in the dual pass FSW were also considered. For some weld parameter sets, forge force (Z axis force) was adjusted to make a good contact between shoulder and work piece surface to avoid obvious flashes which lead to volumetric defects inside welds.

All the work pieces were cut by radial saw. Oxidations on the top surface of those plates were removed by a hand grinder with a nylon bristle disk. Those plates were then machined to desired size and placed in butt joint arrangements. To ease plunging stage during FSW, pre-drilled holes were made at the beginning of the weld in following steps: (a) for half penetration: 7 ° tapered endmill with 9.5mm tip plunged 12.2mm deep, then over-drilled with 12.7mm cylindrical drill bit plunged 11.4mm deep; (b) for full penetration: 7 ° tapered endmill with 9.5mm tip plunged 24.9mm deep. Plates were aligned and clamped by finger and side clamps on different backing plates. All the welds were performed at 0 ° or 1 ° spindle tilt angle.

3.3.3 Post Weld Heat Treatment (PWHT)

All metallographic examination and mechanical tests were performed in as-welded (AW) and/or artificial post weld heat treatment (PWHT) conditions. PWHT was employed to examine effects of the artificial aging heat treatment on material's

properties. AA7099-T7651 welded samples were artificially heat treated after welding in oil bath at 121℃ for 4 hours, per instructions from Kaiser Aluminium. AA7050-T7451 welded samples were artificially heat treated after welding in Blue M Electric Oven at 121℃ for 24 hours. AA6061-T651 welded samples were artificially heat treated after welding in oil bath at 160℃ for 18 hours.

3.3.4 Metallographic Sample Preparations and Examinations

3.3.4.1 Sample Preparations

Metallographic samples were prepared according to standard techniques to satisfy requirements of optical characterization, taking macro and microstructural pictures and performing hardness testing. Under each set of process control parameters, metallographic specimens were cut with abrasive water jet inside corresponding area under steady state which is characterized with steady temperature measured by TCs. Testing cross sections were further machined by milling. Then specimens were automatically and/or manually ground with 240, 400, 600, 800, 1200 grit abrasive silicon carbide paper and polished using Aluminum oxide powder of 5 μm and 3μm, finishing with colloidal silica (< 0.05 μm). Macro and micro structural observation was performed on specimens chemically etched by the Keller's reagent (95% balance distilled water, 2.5% HNO_3, 1.5% HCl, and 1% HF). Different alloys intrinsically react diversely during friction stir welding, therefore etching time was adjusted depending on microstructural evaluation: relatively short time for AA7050 and AA7099 (10-20 sec) and long time for AA 6061(90-120 sec).

3.3.4.2 Grain Size

Macro and microstructures of the weld nuggets were evaluated. Transverse macrostructures were obtained by scanning cross-sections of the testing samples. Micrographs were obtained by a LECO Olympus PME3 inverted Metallurgical Microscope and/or Keyence Digital Microscope VHX-5000. Mean linear intercept (MLI) method [149] and/or the measuring function of Keyence Digital Microscope VHX-5000 were employed to measure grain sizes mostly at the nugget center and additionally at locations near the weld crown and root in some cases. By MLI method, these measurements were performed with 4~5 micrographs from the same vicinity using five lines randomly placed on each micrograph.

3.3.5 Mechanical Testing

3.3.5.1 Micro Hardness

Metallographic samples were later used for Vickers hardness testing performed on transverse cross-sections at different thicknesses (primarily in the midplane) to examine variations in mechanical properties of the joint in AW and/or PWHT conditions. An indent interval of 0.64 mm, a load of 200gf and a loading time of 10 seconds were employed in the hardness testing conducted by a "Buehler Micromet 1" hardness testing machine with a diamond shaped indenter. The Vickers hardness was calculated using the equation: $HV = 1854*P/(d^2)$ [150]. Here 'P' is the applied load in units of gf, and 'd' is the size of the indent in units of μm, which is the average value of the measured distances between two opposite vertices of the diamond-shaped indent.

It's worthy to note that, a minimum indent interval (2.5 times the indent size) is suggested by the ASTM standard to avoid residual stress field due to existing indents,

and this minimum indent interval intrinsically determines that this hardness measurement is discontinuous/discreet [150]. Larger applied load leads to larger indent size and then greater precision of measurement. On the other hand, larger indent size also means a larger minimum indent interval and more scattered hardness data. Therefore the applied load should be chosen based on overall consideration of spatial resolution and scatter in hardness data: in the region where there is a large gradient in the hardness like the HAZ, the spatial resolution becomes more significant so a relatively small load is recommended; while in the region where hardness is not expected to vary significantly, a relatively large load is suggested since the spatial resolution becomes less important.

3.3.5.2 Bending testing

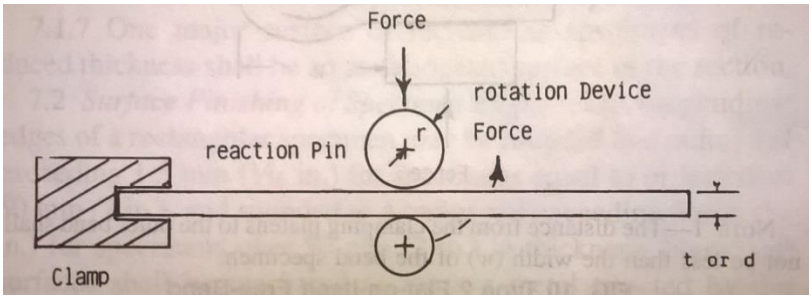

Figure 3.3 Schematic Fixture for Semi-Guided-Bend Test Arrangement-One End Held-Force Applied Near Mandrel [151]

In this research, bending tests were performed using 5T Mandrel bending test (bending radius r = 5* Thickness), as shown in Figure 3.3. Bending tests for ductility here include face and crown bending tests. Specimens for testing were cut and machined in following steps:

(1) Three 127mm x 12.7mm x 25.4 mm (length x width x thickness) samples were cut by abrasive water-jet;

(2) The 127mm x 12.7mm x 25.4 mm samples were machined into 127mm x 6.4mm x 25.4mm (or 4.6 mm, 7.6 mm) for face bending test. Figure 3.4 shows face bending samples before and after testing.

(3) The 127mm x 12.7mm x 25.4 mm samples were machined into 127mm x 12.7mm x 6.4mm for crown bending test. Extra material was machined off from the bottom to reduce the thickness. Figure 3.5 shows crown bending samples before and after testing.

Before testing, one end of the specimen was securely clamped. Then a stationary mandrel in contact with the outer surface of the bend was employed. The mandrel was rotated under force in an arc to bend the specimen. The bending was continued until the specimen successfully reached the specified angle or until failure in the bend occurs. This method may exert a small tension force in the bend.

Figure 3.4 Face bending samples: before testing

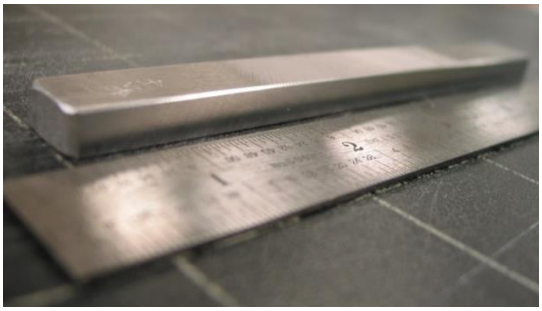

Figure 3.5 Crown bending samples: before testing

3.3.5.3 Tensile Testing

In this research, normal scale transverse and longitudinal tensile testing, and subscale longitudinal tensile testing were performed in selected conditions. Three samples under each condition were cut by abrasive water-jet and then further machined by milling to the desired dimensions. Dimensions of samples before testing were measured and recorded as initial area data.

Extensometer was used to record the strain during the normal scale tensile testing. As a more precise technology to examine strain distribution, Digital Image Correlation (DIC) technology was also applied in normal scale and subscale tensile testing. It's expedient here to refer readers to the book written by Sutton [152] which provides theories, methods, techniques and procedures of DIC testing and post analysis. Then properties like the ultimate tensile strength, yield strength and elongation were calculated based on engineering stress and engineering strain.

3.3.5.4 Normal scale Transverse Tensile Testing (TTT)

There are some difficulties of interpretation at the outset of transverse tensile testing. Due to the non-homogeneity of the weld zone, mechanical properties like ultimate tensile strength (UTS), yield strength (YS) and elongation (EL) undoubtedly vary significantly among different local regions of the weld. Therefore generally two

tensile testing methods can be adopted: a) local tensile tests consisting of miniature sample from different locations of the weld, and b) transverse tensile test where all the regions of the weld are stressed at the same time. Method (b) was applied in this research to conduct the tensile testing.

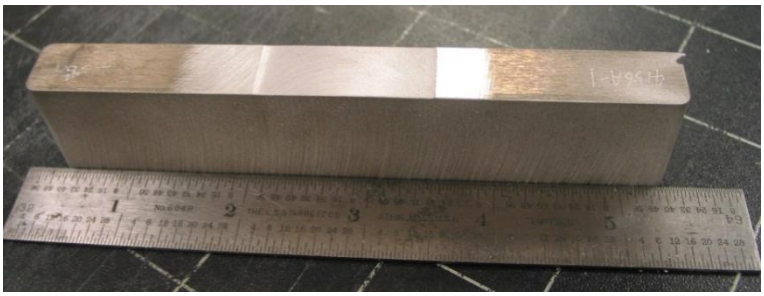

Figure 3.6 Normal scale transversal tensile test before testing

Rectangular samples for normal scale transverse tensile testing has a gauge length of 203mm, a width of 12.5mm and a thickness of 25.4mm, as shown in 错误!未找到引用源。. Specimens for normal scale transverse tensile testing with the desired dimensions then were prepared in the hood for DIC in the following procedures: Clean the testing surface using methanol or acetone. Shake the black and white Rust-Oleum spray paints until thoroughly mixed. Spray the white paint to the testing surface to form a thin and continuous layer and wait until the surface becomes dry. Then spray the black paint to the testing surface to form a randomly scattered speckle pattern as shown Figure 3.7 and wait until the surface becomes dry. It's necessary to keep the environment clean to avoid the sprayed surface being contaminated by particles, pollens, chips, etc.

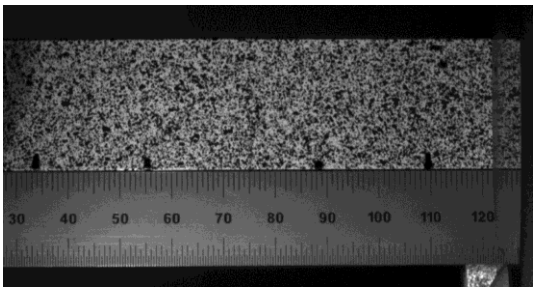

Figure 3.7 Normal scale transversal tensile test: DIC sprayed speckle pattern before test

Normal scale transverse tensile tests were performed using an initial load rate of 0.025 mm/sec on the MTS TESTSTAR machine with a maximum load of 222.4 KN. History of load was recorded both by the TESTSTAR system and the DIC system. Images of the testing surface with sprayed particles were captured using the Dolphin Digital interface camera produced by the Allied Vision Technologies, with a 28mm Nikon lens and a aperture number ranging from 11~16. Data of strain was analyzed and calculated by DIC software Vic-2D 2009 according to the captured digital images. It's expedient here to refer readers to the Vic-2D Reference Manual [153] provided by CorrelatedSolutions, Inc. for post analysis of DIC testing.

3.3.5.5 Longitudinal Tensile Testing (LTT)

Dimensions of dog-bone shaped specimens for normal scale and subscale longitudinal tensile testing were as shown in Figure 3.8, Figure 3.9 and Table 3.3.

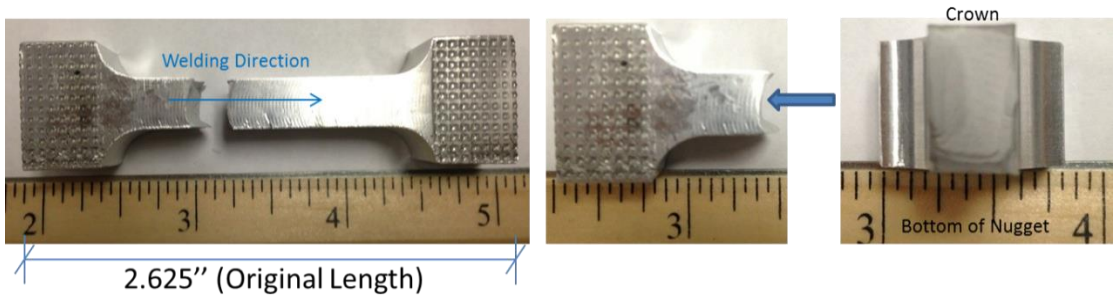

Figure 3.8 Normal scale longitudinal tensile testing: after test

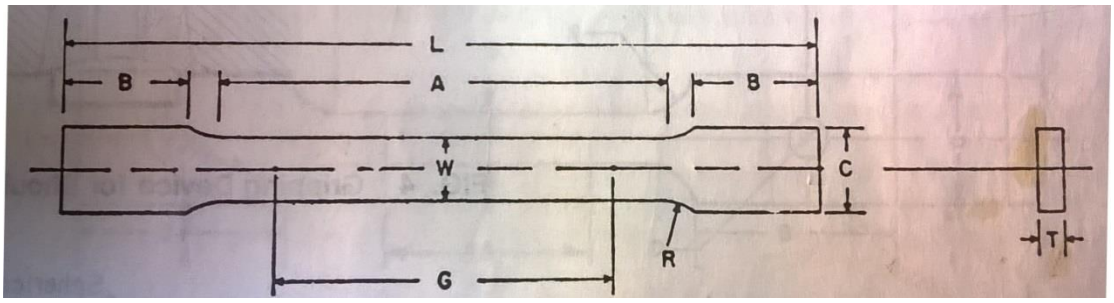

Figure 3.9 Longitudinal tensile testing: schematic diagram of dimensions [154]

Table 3.3 Dimension Chart [154]

ASTM Standard E 8M-04 (mm)	Standard Specimen	Subsize Specimen
G-Gage length	50.8	12 ±0.05
W-Width	12.7	3.0 ±0.05
T-Thickness	25.4	0.75 ±0.05
R-Radius of fillet	25.4	-
L-Overall length	203	24
A-Length of reduced section	83.8	16
B-Length of grip section	50.8	8
C-Width of grip section	19.1	4-6

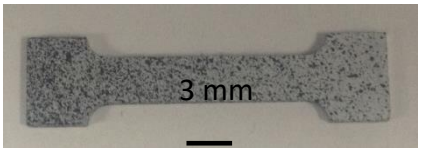

Figure 3.10 Subscale longitudinal tensile testing: DIC sprayed speckle pattern before test

Specimens for normal scale LTT with the desired dimensions were prepared in the hood for DIC and then tested in the same ways as the normal scale TTT. Specimens for subscale LTT were cut at the TC height (almost the mid-plate height) in the longitudinal direction, and then were manually ground using 320 and 400 grit abrasive silicon carbide paper with the desired dimensions. Those ground specimens were prepared in the hood for DIC in the same ways as the normal scale TTT, and the DIC sprayed speckle pattern was shown in Figure 3.10.

Subscale LTT were conducted by a subscale tensile test frame which gives 0.1~0.2 mm/min displacement control. The testing device was shown in Figure 3.11. The

load frame was controlled by a Labview program. Forces were measured and recorded by a load cell which had been calibrated before the test. Images of the testing surface with sprayed particles were captured using the Point grey Gras-50s5m-c camera with a 55mm Nikon lens and an aperture number of 16. Data of strain was also analyzed and calculated by DIC software Vic-2D 2009 according to the captured digital images.

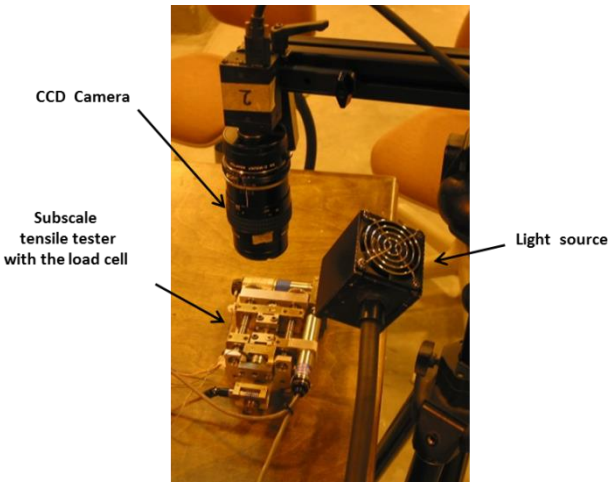

Figure 3.11 Subscale longitudinal tensile testing device

3.3.5.6 Residual Stress Testing

Through thickness average, longitudinal, residual stress was measured in both AW and PWHT conditions for selected weld conditions. The stress was measured using the cut-compliance method developed by Cheng [155], Schindler [156] and Prime [157] as described in Canaday et al. [95] following procedures and details of the residual stress testing performed in this dissertation also referred to Prime [157], Schindler [158] and standard testing methods provided in ASTM E647-91 [159]. Sample geometry and strain gage placements are shown in Figure 3.12. The strain gage was mounted using Micro-Measurements M-Bond 200 and the appropriate surface preparation products in the center of the back face of the specimen to measure strain opposite the notch of length on the rear face of the tested specimen [160]. In this experiment, a Vishay

Micro-Measurements gage model CEA-06-250UN-120 with a nominal resistance of 120 ohms and a gage factor of 2.085 was employed. Notch pre-cracking with an initial slot length of 40mm and the following cutting with an interval advancing distance of 0.76mm were performed by a 2.38mm diameter miniature end-mill chucked in milling machine on the fixed sample. The weld centerline was located in the transverse mid-plane and the slot was advanced from the retreating to advancing side. Wire leads were employed to connect the strain gage to an appropriately calibrated strain indicator, data shown on which device during the testing was recorded for residual stress calculating by MathCAD. Calculating method refers to the background part in the paper of Canaday et al. [95].

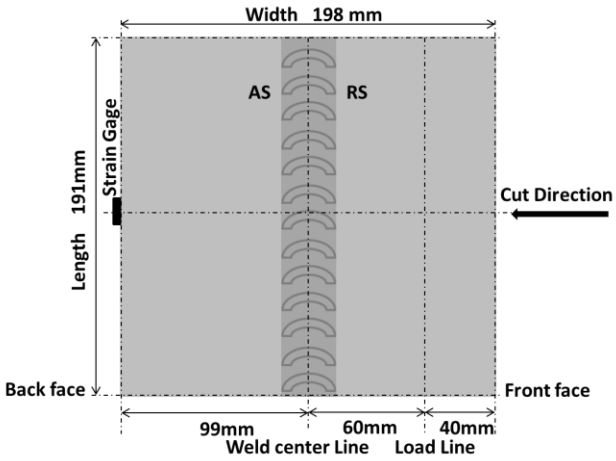

Figure 3.12 Schematic Diagram of Residual Stress Test

CHAPTER 4

RESULTS AND DISCUSSIONS

4.1 Single Pass Half Penetration FSW in AA7099

In this section, conventional shoulder single pass half penetration (CSSPH) FSW and stationary shoulder single pass half penetration (SSSPH) FSW have been studied in following aspects: macrostructure including investigation of surface finish, defect and nugget shape, microstructure, effect of control parameters on response parameters, grain size and hardness distribution, etc. The first passes of dual pass (DP) FSW in some cases were considered as single pass half penetration (SPH) and therefore were also included in this section. It should be noted that, for those first passes of DP (DP-1), the response parameters obtained during the welding like forces, torque and temperature can be comparable with those parameters of the single pass half penetration (SPH) welds. However, some properties of DP-1 welds like microstructure, hardness and strength which might have been affected by the second passes are not comparable to the SPH. Joints #4094A~C and #4098A~C were produced and provided by Md. Reza-E-Rabby for relative study in this section.

4.1.1 Macrostructure

In this section, effects of control parameters in FSW and the inserted pin features like right handed threads, flats, co-flow flutes and counter-flow flutes, on material flow

which will produce joints with different macrostructures should be considered. When the pin rotates counter clockwise (CCW) (as viewed from above), the right handed threads on the pin will push material downward toward the weld root and therefore can eliminate near root wormhole defects [101]. The inserted co-flow flutes are expect to move material downward to the weld root while the counter-flow flutes are expect to move material upward to the weld crown. Moderate downward thrust can help eliminating wormhole defects near the weld root, while too much downward thrust may cause surface defects [101]. Moderate upward thrust can help eliminating surface defects, while too much upward thrust may cause volumetric defects inside the nugget. Higher rotating speed will enhance those trends of material movements. When forge force is not enough, material will escape as flash therefore defects inside the nugget and surface defects will form.

4.1.1.1 Surface finish

In 2013, Liu et al. [99] reported that a stationary shoulder employed in FSW can produce a superior surface finish, relative to some flash and regular semi-circular marks on the joint surface caused by the rotating shoulder of CSFSW [9]. In this section similar results were found in SPH FSW, as shown in Figure 4.1. Figure 4.1 (a) and (b) show joint surfaces of CSSPH, produced by the same T+3F pin with the same setup of 0° tilt angle, the same welding speed of 102 mm/min, and rotating speeds of 200 RPM and 160 RPM, respectively. The obvious semi-circular marks can be seen on the joint surfaces. Figure 4.1 (c) and (d) show joint surfaces of SSSPH, produced by the same T+3F pin with the same setup of 0° tilt angle, the same welding speed of 102 mm/min, and rotating speeds of 200 RPM and 160 RPM, respectively. Relative to the CSSPH joint surfaces, these

SSSPH joint surfaces were smoother, and the semi-circular marks on the surfaces were less clear and complete. It indicates that relative to CSSPH, SSSPH can produce joints with better surface finish due to the absence of shoulder rotation during SSFSW process.

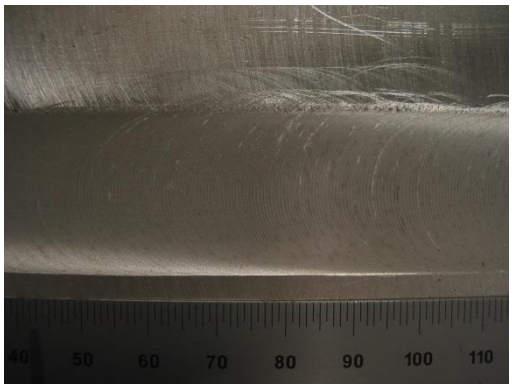

(a) CSSPH, T+3F, 200 rpm, 102mm/min

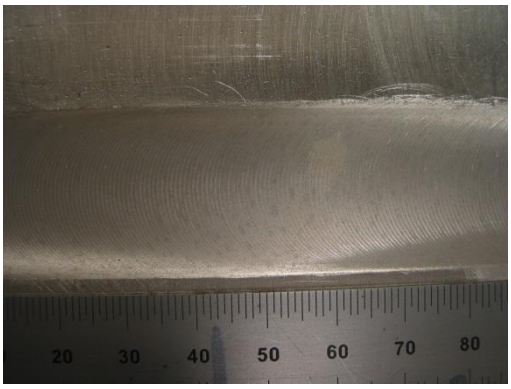

(b) CSSPH, T+3F, 160 rpm, 102mm/min

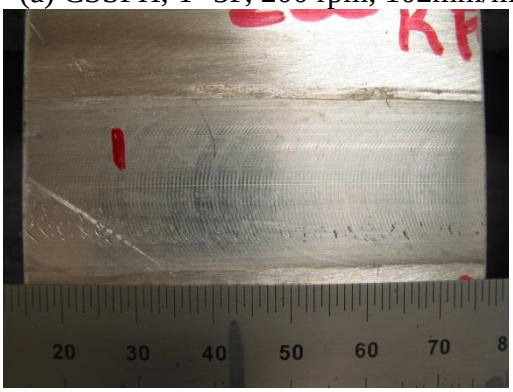

(c) SSSPH, T+3F, 200 rpm, 102mm/min

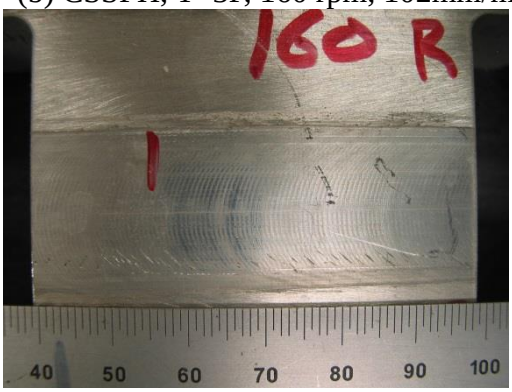

(d) SSSPH, T+3F, 160 rpm, 102mm/min

Figure 4.1 Joint surfaces of (a~b) CSSPH and (c~d) SSSPH in AA7099

4.1.1.2 Defect investigation

Material flow is affected by various factors, like FSW setup, FSW tool, control parameters, thermal boundary conditions and so on. Not sound material flow during the welding process results in defective joints. Not good surface finish may also result in defects if too much material escapes as flash.

The result of defect examination of SPH welds is listed in Appendix C. Here “SD” means “surface defect”. It shows that it’s highly possible to produce sound joints in both

CSSPH and SSSPH with similar FSW envelope which might because the half penetration FSW in high strength alloy AA7099 is highly feasible.

Defect examination results show that, in CSSPH, T+3F pin produced joints with good surface finishing and defect free nuggets, while T+3CT pin produced some defective joints with surface defects and/or defective nuggets possibly due to not sound material flow caused by right hand threads, inserted counter-flow flutes rotating CCW with too high speeds and/or not enough forge force. When T+3CT pin was applied, 160 rpm&102mm/min produced defect free welds; 200rpm&102mm/min caused small holes at mid-plane AS, which might due to not enough forge force; 240rpm&203mm/min and 320rpm&203mm/min caused surface defects and volumetric defects like holes between mid-plane and bottom (not sound vertical material movement) possibly due to too high speeds. Under too high rotating speed, right handed threads moved too much material to the weld root while the counter-flow flutes moved too much material to the weld crown, which were likely to cause defects inside the nugget. Material escaped as flash during welding due to upward movement and not enough forge force, which might be accounted for the formation of surface defects. It indicates that, to get better surface finish in CSSPH, high tool rotating speed and tools with T+3CT pin are not recommended. With lower tool rotating speeds (200 & 160 rpm, 102mm/min), pins featured with both T+3F and T+3CT can produce defect free welds, while pins featured with T+3F allow higher welding speeds.

In SSSPH, high tool rotating speed (400, 500 rpm) caused bad surface defects. When T+3F pin was applied, 160 rpm & 102 mm/min and 200 rpm & 102 mm/min produced defect free welds; when higher rotating speed or lower forge force was applied,

surface defects appeared. When T+3CT pin was applied, 160 rpm & 102 mm/min, 200 rpm & 102 mm/min and 300 rpm & 102 mm/min produced defect free welds, which indicates that the balance between upward material movement caused by counter-flow flutes and downward material movement caused by right-hand thread when the pin rotates CCW was achieved by FSW speeds, pin feature and forge forces in the above conditions. When T+3C pin was applied, 160 rpm & 102 mm/min, 200 rpm & 102 mm/min and 300 rpm & 102 mm/min produced welds with surface defects and defect free nuggets, which might because the right handed threads and co-flow flutes caused too much material moving downward. It indicates that, to get better surface finish in SSSPH, high tool rotating speed and tools with T+3C pin are not recommended.

4.1.1.3 Nugget

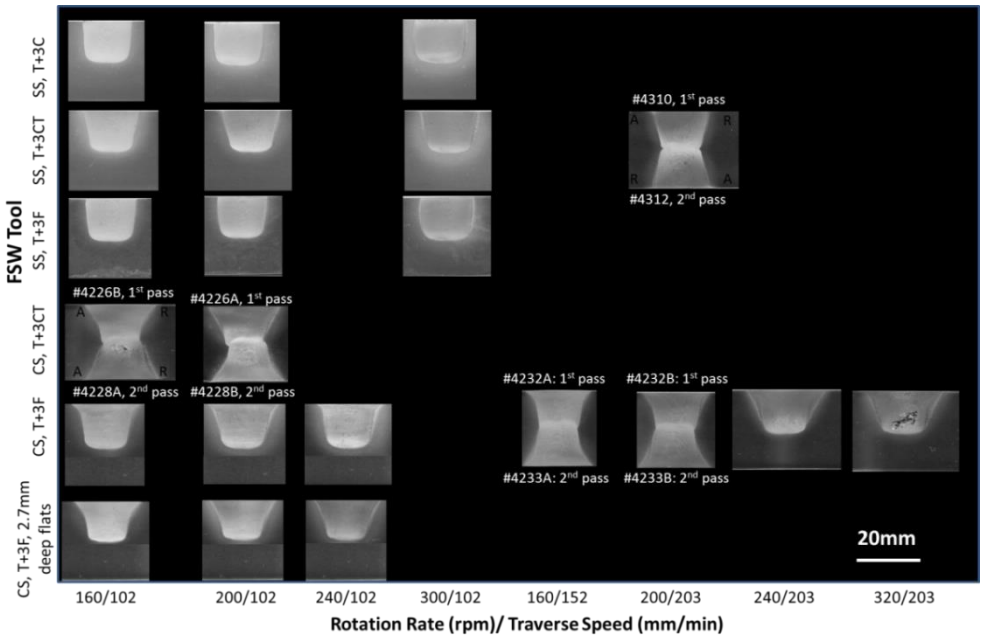

Figure 4.2 Macro Transverse Cross Sections of CSSPH and SSSPH in AA7099

Nugget shape on the transverse cross section of the joint will also be affected by material flow. Figure 4.2 shows the macro images of transverse cross sections of both

CSSPH and SSSPH welds in thick AA7099-T7651 plates (25.4 mm for SPH and 24.1 mm for DP). In SPH and the 1st pass of the DP (DP-1), the advancing sides (AS) are on the left in each image of the cross section. Images of transverse cross sections in each column are with a particular combination of rotation rate (rpm) and welding speed (mm/min), while images in each row are with a particular combination of FSW shoulder and pin features employed. The three joints located at the bottom of Figure 4.2 were produced by the T+3F pin with a flat depth of 2.7 mm, while other joints were produced by pins with a flat or flute depth of 1.35 mm. In SSSPH, when the T+3F pin was employed, high rotation rates (400 rpm and 500 rpm) caused very bad surface defects as shown in Figure 4.3 (a~b), therefore transverse cross sections of these two conditions were not studied.

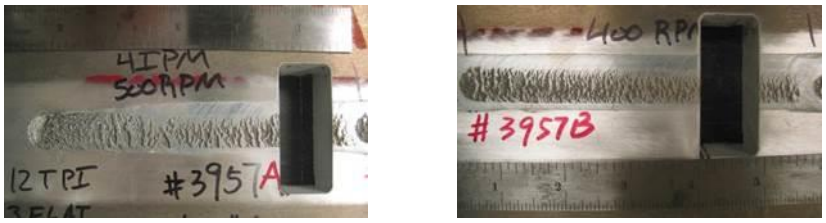

Figure 4.3 Weld Crowns with bad surface defects of SSSPH under (a) 400 rpm & 102 mm/min and (b) 500 rpm & 102 mm/min

The macrographs in Figure 4.2 indicate that relative to CSSPH, SSSPH results a nugget shape more consistent to the pin shape and leads to narrower HAZ near crown which may because the absence of shoulder rotation results in different heat source distributions especially near crown in SSSPH.

In CSSPH, under the same rotating speed, nuggets made by T+3CT pins were more tapered than nuggets made by T+3F pins due to less material moved downward by T+3CT pin. In nuggets made by T+3F pins, under the same welding speed, at lower rotation rates (160 rpm, 200 rpm), width of the nugget near crown was larger than that at

the mid-plane; while at higher rotation rate (240 rpm), width of the nugget near crown was just a little larger than that at the mid-plane. It might because right hand threads on the pin moved more material downward under larger rotating speed. At high rotation rate (240 rpm), when T+3F pin was employed, larger welding speed produced more tapered nuggets due to larger thermal gradients. Under the same FSW speeds, T+3F pin with 2.7mm deep flats produced nuggets more taper than those welded by T+3F pin with 1.35mm deep flats, which might because deeper flats resulted in less right hand threads contacting with material, therefore less material moved downward.

In SSSPH, under the same forge force, with the increasing rotating speed, nugget boundaries became more blurry, which might because that material surrounding the pin surface was moved farther under a larger angular velocity, resulting in wider TMAZ areas; under the same forge force and rotating speed, nuggets made by T+3CT pins were more tapered than nuggets made by T+3F and T+3C pins due to less material moved downward by T+3CT pin. In nuggets made by T+3F and T+3C pins, under the same welding speed, at lower rotation rates (160 rpm, 200 rpm), width of the nugget near crown was a little larger than or even similar to that at the mid-plane; while at higher rotation rate (300 rpm), width of the nugget near crown was a little smaller than that at the mid-plane. It's because T+3F and T+3C pins moved more material downward to the weld root under a larger rotating speed. Welding speed had little effect on nugget shape.

4.1.2 Process Responses

Process response parameters include in plane reaction forces (F_x, F_y and the resultant force F_{xy}), torque, power, peak temperature measured at pin center (which was also considered as the peak T measured at center NG due to pretty close position) and

grain size (GS) measured at center NG. Process response parameters were collected and calculated. Process response parameters as a function of tool rotation rate are shown in Figure 4.4 (a~g) for SPH welds. Various symbols represent for different FSW variables including rotating/stationary shoulder, pin types, tilt angle, and welding speeds.

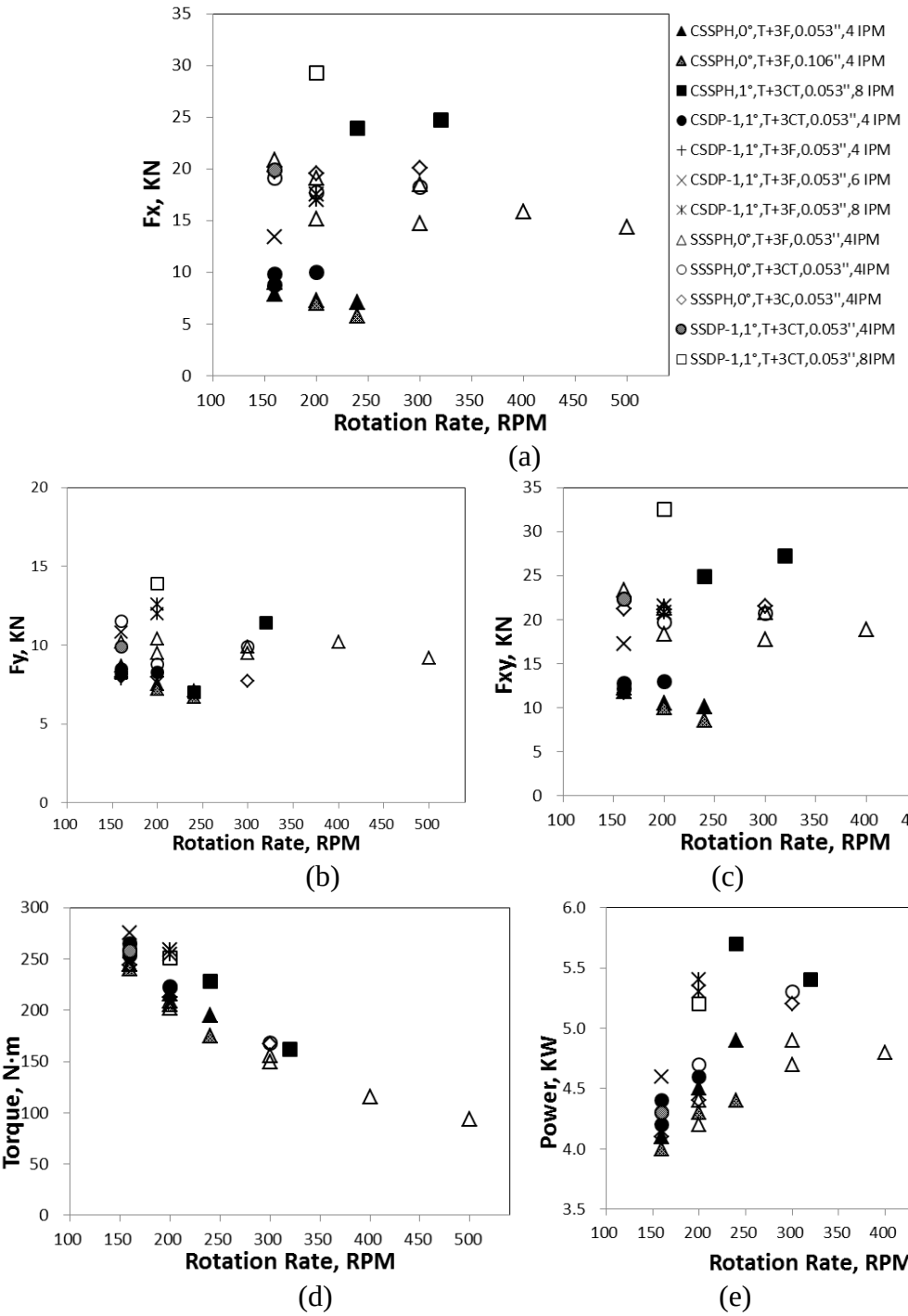

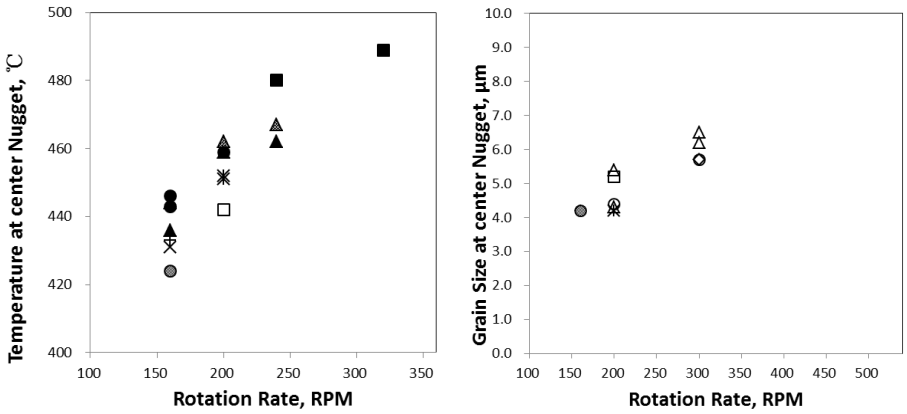

(f) (g)

Figure 4.4 Reaction forces, torque, power, peak T and GS at center NG as functions of tool rotation rate for CSSPH and SSSPH bead on plate welds on AA7099

4.1.2.1 CSSPH: Process Responses

Figure 4.4 a~g show the effects of control parameters on response parameters in CSSPH and SSSPH. It shows some trends in CSSPH:

When the T+3F pin was employed, with the same welding speed, when rotating speed increased, in-plane forces and torque decreased due to smaller required forge force and more softened material, power and then temperature increased because of larger rotation rate.

With the same rotation rate, when the welding speed increased, higher forge force was required to generate more frictional heat to ease the faster welding, then in plane forces increased, torque increased, power increased a little and pin temperature at center were similar.

When both the rotating speed and welding speed increased, the required forge force and in plane forces increased, torque were similar, power increased, then pin temperature at center increased, while GS at center NG were similar.

Relative to the flat depth of 1.35 mm employed in most cases, a larger flat depth of 2.7mm was also applied in some cases to investigate the influence of flat depth in FSW process response parameters as shown in 错误!未找到引用源。 a~g. Results show that deeper flat depth reduced the required forge force a little, while had little influence in other response parameters like in-plane forces, torque, power and temperature at pin center. When the T+3CT pin was employed, with the same forge force and welding speed (102 mm/min), when rotating speed increased, in-plane forces were similar, torque decreased due to more soften material then smaller flow stress between the material and tool, power and then temperature at center increased due to the increase of rotation rate.

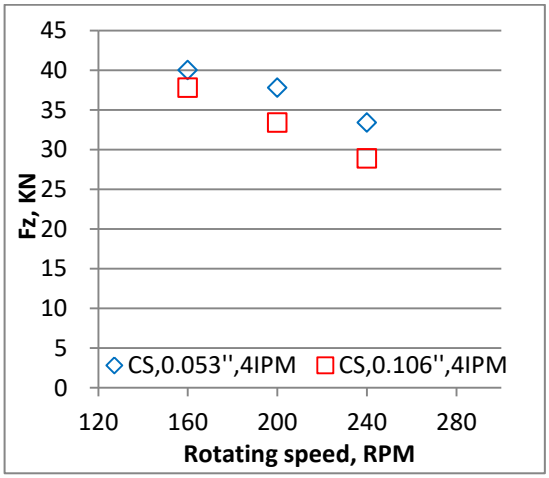

(a)

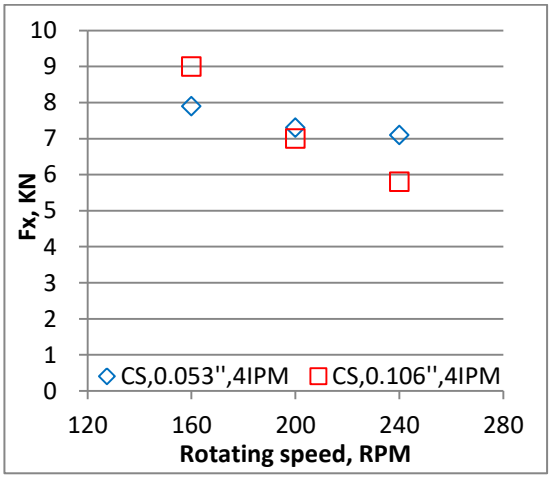

(b)

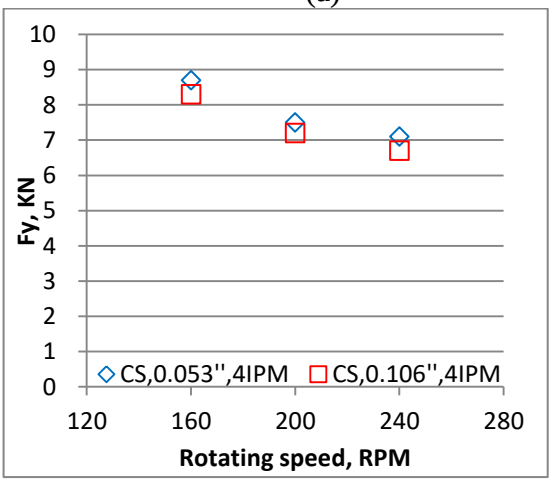

(c)

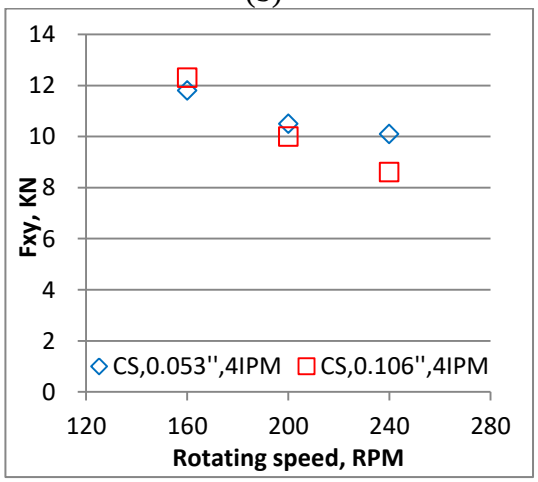

(d)

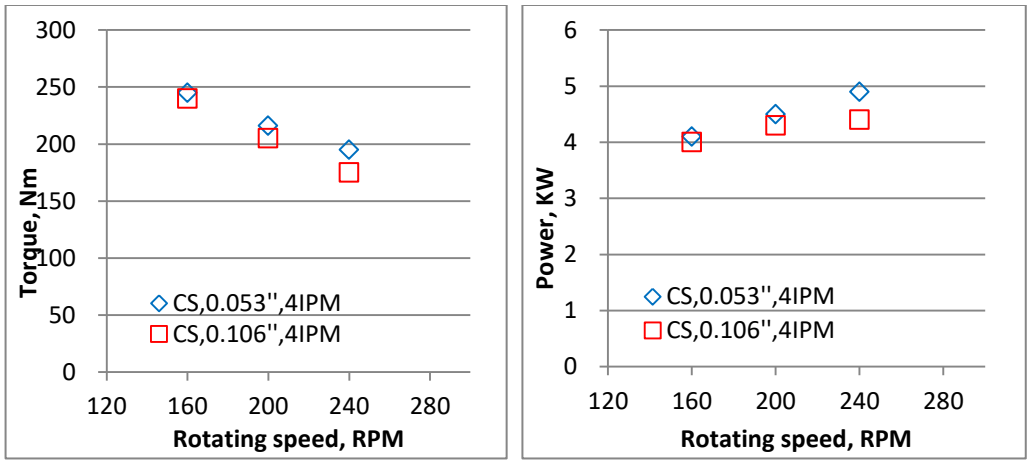

(e)

(f)

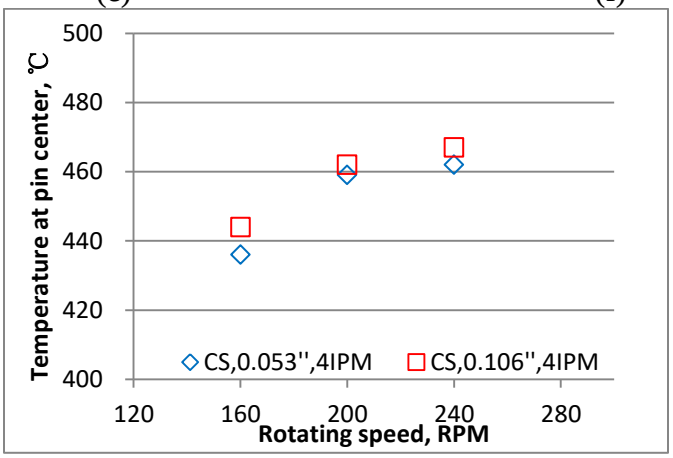

(g)

Figure 4.5 Response parameters as functions of rotating speed in CSSPH of AA7099 with T+3F pins with two different flat depths: 1.35mm and 2.7mm

4.1.2.2 SSSPH: Process Responses

In SSSPH, all the featured pins shared the same flat or flute depth of 1.35mm. When T+3F pin was employed, with an increasing of rotation rate, in-plane force decreased with a decreasing rate, torque decreased due to more softened material, and power increased due to increased rotation rate; with an increasing of forge force, F_x increased, F_y decreased a little, F_{xy} increased, torque and then power increased a little, while GS at center NG decreased a little. When T+3CT pin was employed, with an increasing of rotation rate, in-plane force decreased first, then increased after they arrived

a minimum, torque decrease due to more softened material, power increased due to increased rotation rate, and GS at center NG increased possibly due to larger power input and then higher temperature; When T+3C pin was employed, with the increasing of rotation rate, F_x increased a little, F_y and F_{xy} decreased a little, torque decreased due to more softened material, and power increased due to increased rotation rate. It indicates that different pin features caused different trends of in-plane forces which might due to effects of different pin features on material movements, and similar trends of torque and power when rotation rate increased. Under the same medium rotation rate (200 RPM), torque caused by T+3CT tool was a little larger than that of T+3C tool, which was a little larger than T+3F tool. When rotation rate was lower (160 RPM), difference in torque caused by T+3C tool and T+3F tool decreased; when rotation rate was higher (300 RPM), difference in torque caused by T+3C tool and T+3CT tool decreased. Under the same rotation rate (160&200 RPM), power caused by T+3CT tool was a little larger than that of T+3C tool, which was similar with T+3F tool. When rotation rate was higher (300 RPM), power caused by T+3CT tool was similar with that of T+3C tool, which was a little larger than that of T+3F tool. It indicates that under the same forge force and rotating speed, pin feature had little influence in torque and power.

4.1.2.3 CSSPH&SSSPH: Process Responses

Figure 4.4 a~g also show some similarities and differences in CSSPH and SSSPH. When T+3F pin were employed, under the same FSW speeds, compared to CSSPH with a setup of 0° or 1° tilt, SSSPH with a setup of 0° tilt required larger forge force to generate more frictional heat and ease the SSSPH FSW process, then lead to larger in-plane forces, while similar torque and power due to similar rotation rate. It indicates

that different setups of 0 °tilt or 1 °tilt had little effect on process parameters like required forge force, in-plane forces, torque, and power. When T+3CT pin was employed, in both CSSPH and SSSPH, with the increasing of rotating rate, torque decreased due to more softened material, power increased due to larger rotating speed, then temperature at pin center and GS at center NG increased due to more power input.

4.1.3 CSSPH&SSSPH: grain size and hardness distribution through thickness

Rotating and stationary shoulders result in different heat sources in FSW, affecting thermal distribution, microstructure and properties through thickness of joints. In this section, grain size and hardness variations on the weld centerline through thickness in CSSPH and SSSPH have been studied to investigate effects of CSSPH and SSSPH on variations of microstructure and property through thickness.

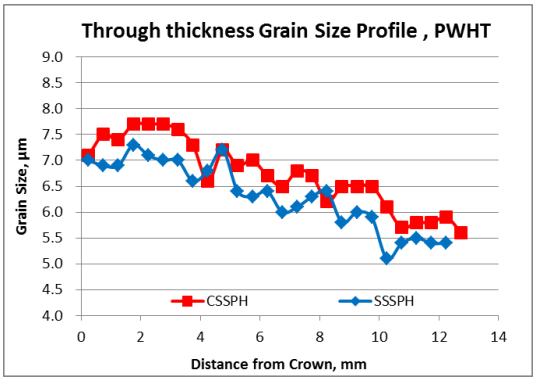

Figure 4.6 Through thickness grain size profiles on the weld centerline in SPH: PWHT

Figure 4.6 shows the grain size as a function of distance from the weld crown on the weld centerline in PWHT condition of CSSPH (#4094C) and SSSPH (#3960C). It indicates that, in both CSSPH and SSSPH, max grain size appeared near the weld crown, at z=0.07 T_n. Here z is the distance from the weld crown in units of mm, while T_n is the plate thickness in units of mm. Min grain sizes of CSSPH and SSSPH appeared near the weld root at z=0.42 T_n and z=0.4 T_n, respectively. Generally, with the increase of distance

from the weld crown, grain size increased a little and then decreased. Relative to CSSPH, SSSPH reduced grain size a little.

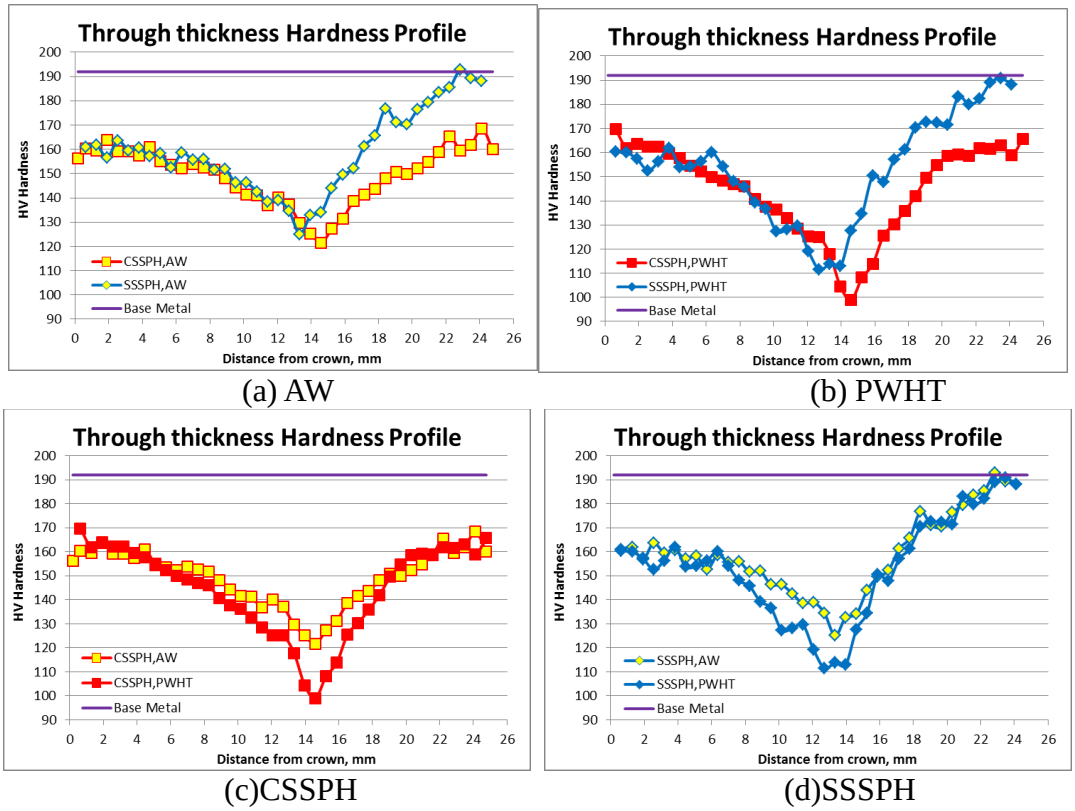

Figure 4.7 Through thickness hardness profiles on the weld centerline in SPH: (a) AW, (b) PWHT, (c) CSSPH and (d) SSSPH: rotation rate 160 rpm, welding speed of 102 mm/min.

Hardness test was also performed on the above joints (#4094C and #3960C) on the weld centerline through thickness (as shown in Figure 4.7) and transverse to weld at various depths through thickness (as shown in Figure 4.8, which will be discussed later). Figure 4.7 show the hardness as a function of distance from the weld crown on the weld centerline in AW and PWHT conditions of CSSPH and SSSPH.

Figure 4.7 (a) shows the hardness profiles through thickness in AW condition of CSSPH and SSSPH. With the increase of distance from the weld crown, inside the nuggets, hardness of CSSPH and SSSPH increased a little and then decreased. Max hardness of CSSPH and SSSPH appeared near the weld crown at z=0.07 T_n and z=0.1 T_n,

respectively. Min hardness of CSSPH and SSSPH appeared near the weld root at z=0.57 T_n and z=0.53 T_n, respectively. Relative to CSSPH, SSSPH had similar hardness, similar max hardness, a little larger min hardness, a little smaller hardness variation range, and a little less penetration. Beyond the nuggets, hardness began to increase in the area of base metal affected by the SPH process. Relative to CSSPH, hardness in SSSPH increased faster from a larger min hardness to a larger max hardness.

Figure 4.7 (b) shows the hardness profiles through thickness in PWHT condition of CSSPH and SSSPH. With the increase of distance from the weld crown, inside the nuggets, hardness of CSSPH and SSSPH generally decreased. Max hardness of CSSPH and SSSPH appeared near the weld crown at z=0.025 T_n and z=0.15 T_n, respectively. Min hardness of CSSPH and SSSPH appeared near the weld root at z=0.57 T_n and z=0.5 T_n, respectively. Relative to CSSPH, SSSPH had similar hardness, smaller max hardness, larger min hardness, smaller hardness variation range, and less penetration. Beyond the nuggets, hardness began to increase. Relative to CSSPH, hardness in SSSPH increased faster from a larger min hardness to a larger max hardness.

Hardness distributions were quite similar with grain size distribution inside the CSSPH and SSSPH nuggets through thickness, which were affected by temperature distribution inside the nugget through thickness. In FSW, heat generated will be generated inside the work pieces. Heat dissipates through convection from surfaces of the work pieces to the ambient, and conduction from bottom of the work pieces to the backing plate. Therefore with the distance from the weld crown increasing, nugget temperature at centerline increases first, reaching the maximum value slightly beneath the weld crown, and then decreases, arriving at the minimum value at the weld root.

Figure 4.7 (c) shows the hardness profiles through thickness in AW and PWHT conditions of CSSPH. It indicates that in CSSPH, relative to AW, PWHT increased the hardness near weld crown when $z \leqslant 0.05\ T_n$ and decreased the hardness for else when $z > 0.05\ T_n$, especially when $0.22\ T_n \leqslant z \leqslant 0.76\ T_n$., Inside the nugget, relative to AW, PWHT slightly increased the max hardness, decreased the min hardness by 18.2%, and increased the hardness variation range by 66%.

Figure 4.7 (d) shows the hardness profiles through thickness in AW and PWHT conditions of SSSPH. It indicates that in SSSPH, relative to AW, PWHT decreased hardness when $0.25\ T_n \leqslant z \leqslant 0.63\ T_n$., Inside nugget, relative to AW, PWHT affected the max hardness little, decreased the min hardness by 10.7%, and increased hardness variation range by 31%. It indicates that, relative to CS, SS was affected less by PWHT.

4.1.4 CSSPH&SSSPH: Transverse hardness distribution

Hardness tests were performed transverse to weld at depths of 3.2 mm (near crown), 6.4 mm (at mid-plane), 9.5 mm (near root) and 12.7 mm (at root) below the weld crown in both AW and PWHT conditions of CSSPH (#4094C) and SSSPH (#3960C). The power input of #4094C is 4.1 KW, resulting in a peak temperature measured at pin center of 436℃. The power input of #3960C is 4.3 KW. Figure 4.8 a~b show the hardness profiles transverse to weld at various depths through thickness of CSSPH in AW and PWHT conditions respectively. Figure 4.8 c~d show the hardness profiles transverse to weld at various depths through thickness of SSSPH in AW and PWHT conditions respectively. Those transverse hardness profiles all have characteristic “W” shape, which is typical hardness distribution of FSW in precipitation hardening aluminum alloys when the peak weld temperature is near or at the solution heat treat temperature

(474℃ for AA7099-T7651). Data including HAZ min hardness at AS and RS, nugget average hardness and HAZ width of CSSPH and SSSPH in AW and PWHT conditions were extracted from Figure 4.8 and was shown in Figure 4.9 (a~d).

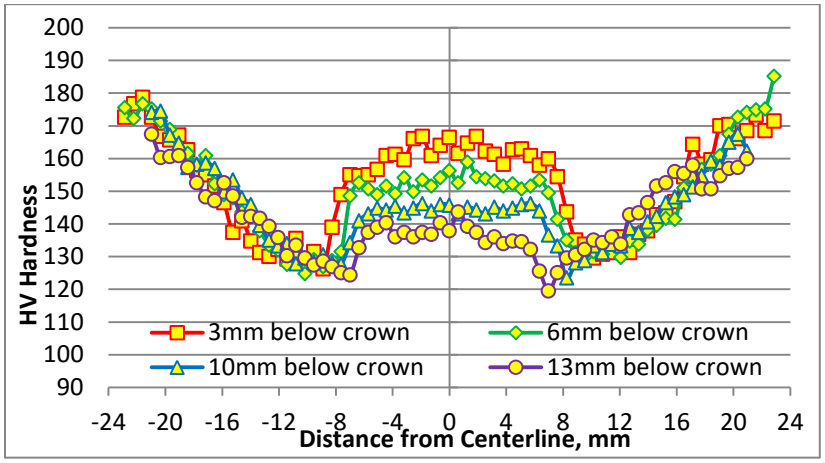

(a) CSSPH in AW condition

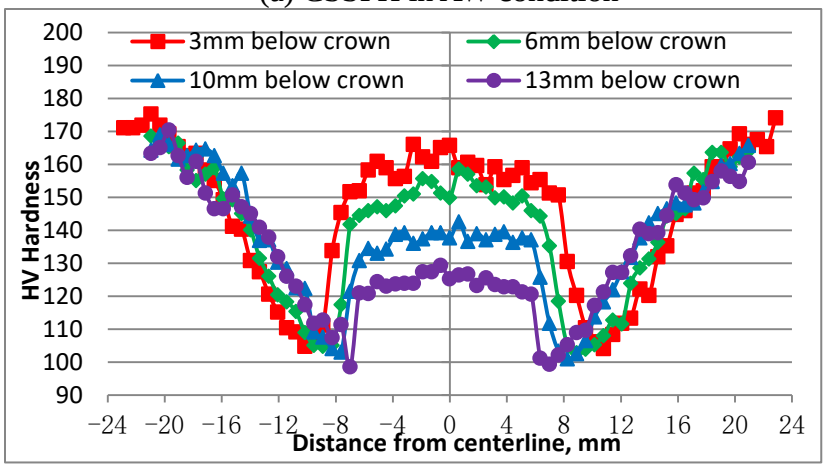

(b) CSSPH in PWHT condition

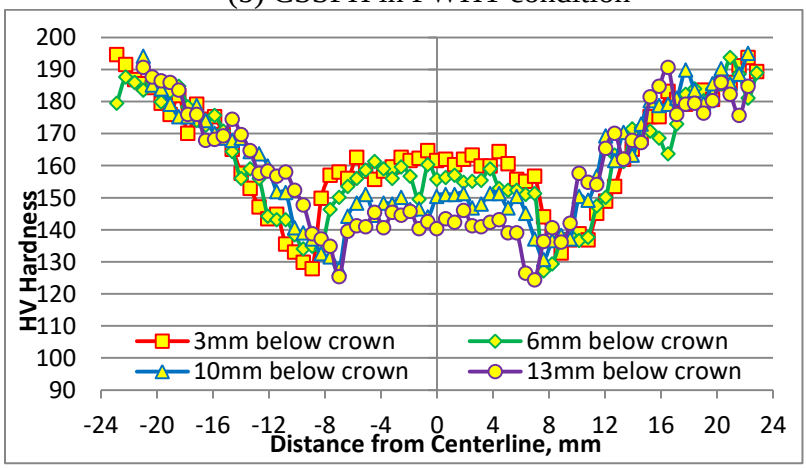

(c) SSSPH in AW condition

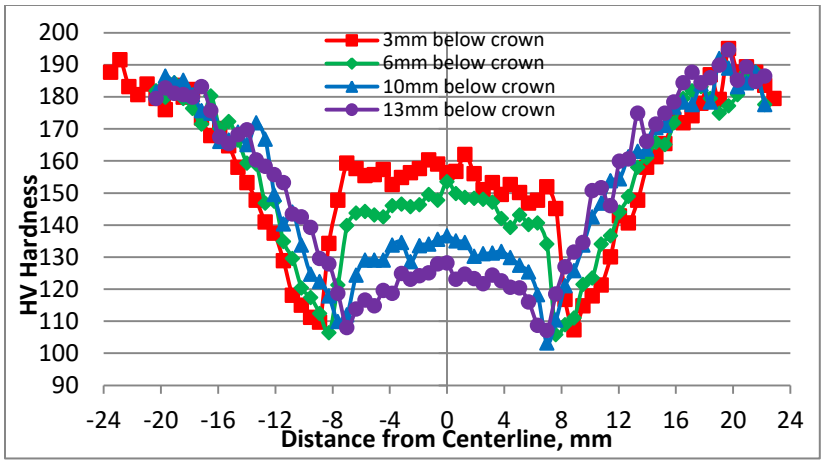

(d) SSSPH in PWHT condition

Figure 4.8 Transverse hardness profiles of SPH at various depths: AW and PWHT

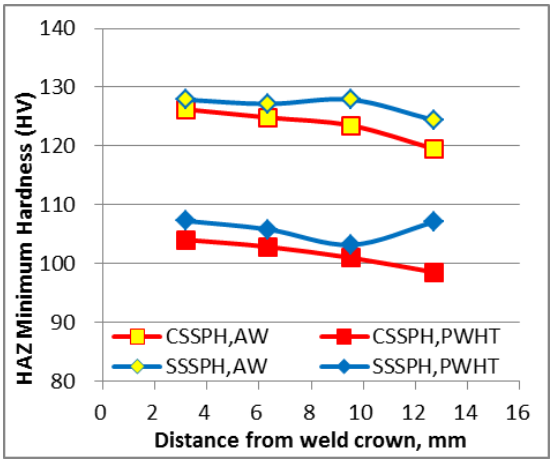

(a) HAZ min hardness

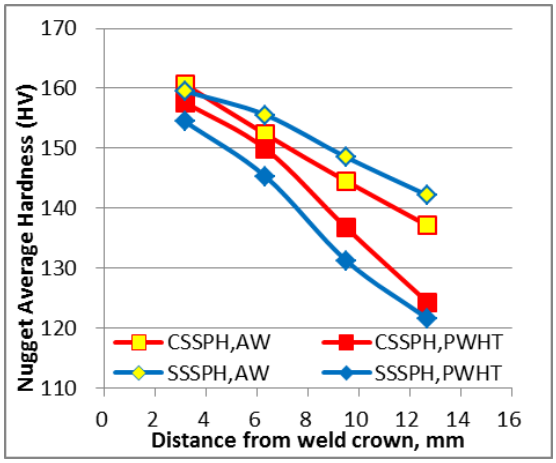

(b) Nugget average hardness

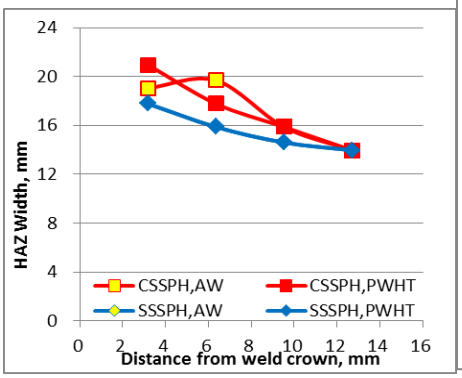

(c) HAZ width

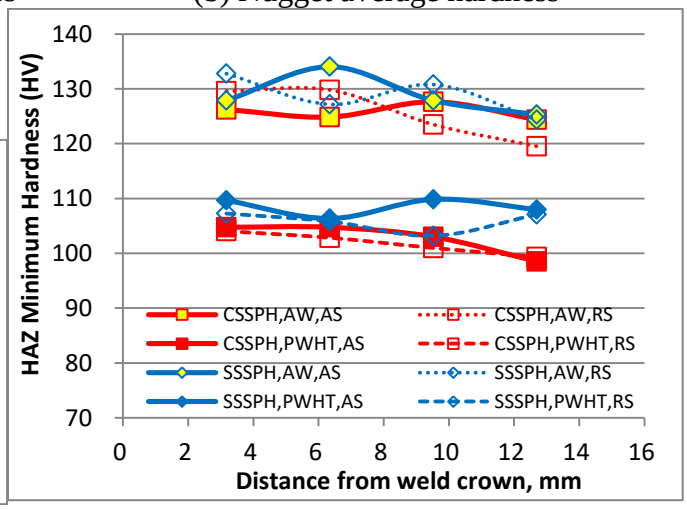

(d) HAZ min hardness at AS and RS

Figure 4.9 HAZ min hardness, Nugget average hardness, and HAZ width of SPH as a function of distance from weld crown: AW and PWHT conditions

Figure 4.9 (a~c) show that: In CSSPH, when the distance from weld crown increased, HAZ min hardnesses in both AW and PWHT conditions decreased slightly; nugget average hardnesses decreased while hardness in PWHT condition were smaller and decreased faster than those in AW conditon; HAZ widths in AW condition increased a little and then decreased, while HAZ width in PWHT decreased. In SSSPH, when the distance from weld crown increased, HAZ min hardnesses were similar in AW condition, while decreased slightly and then increased slightly in PWHT condition; nugget average hardnesses decreased while hardnesses in PWHT condition were smaller and decreased faster than those in AW conditon; HAZ widths in both AW and PWHT conditions decreased, and PWHT had little influence in HAZ width. Figure 4.9 (a~c) also show that: at the same distance from weld crown, relative to CSSPH, in SSSPH, HAZ min hardnesses in both AW and PWHT conditions were slightly larger, while the difference increased slightly when the distance from weld crown increased; nugget average hardnesses in AW condition were a little larger while in PWHT condition were a little smaller, while the difference increased when the distance from weld crown increased; HAZ widths in both AW and PWHT conditions were smaller, while the difference decreased when the distance from weld crown increased. Figure 4.9 (d) shows that in AW condition of CSSPH, relative to AS, at RS, HAZ min hardnessesses were larger near crown and at mid-plane while smaller near root and at root. In AW condition of SSSPH, relative to AS, at RS, HAZ min hardnessesses were larger near crown and near root, while smaller at mid-plane and similar at root. In PWHT condition, HAZ min hardnesses at AS were a little larger than those at RS.

4.2 Single Pass Full Penetration FSW in AA7099

Studies of SPH in chapter 4.1 indicate that, to get better surface finish in CSSPH, high tool rotating speed and tools with T+3CT pin are not recommended, while to get better surface finish in SSSPH, high tool rotating speed and tools with T+3C pin are not recommended. Here in CSSP, only T+3F tool pin with 0.9 mm deep flats was applied to investigate appropriate FSW control parameter windows. In SSSP, T+3F and T+3CT tool pins with various flute depths were applied to produce desired FSW joints.

Relative to SPH, in SP FSW, tool pin featured with right hand threads and inserted flats/flutes is longer and has a larger total surface interacting with material during FSW process. Therefore, under the same rotating speed, pin features affect material flow more significantly in SP than in SPH. Also, relative to SPH, full penetration SP means more material to be softened to enable the welding, thus more power input is required. Rotating speed should not be too high to avoid overheating inside the nugget, while welding speed will also be limited to avoid too large in-plane forces generated. Higher rotating speed leads to higher temperature and can lessen volumetric defects to some extent. However, it can result in overheating, especially near crown in CSSP, which will increase the brittleness and reduce mechanical strengths. Higher welding speed can help decrease temperature, increase strength, while it may cause volumetric defects due to not sufficiently plasticized material. Hence, in the following CSSP FSW, welding speed and rotating speed were adjusted (increased) to develop weld joints with better weld quality, or even defect free joints. Rotating speed was considered to be increased to increase the weld temperature, while welding speed to be increased to avoid overheating. Reducing temperature is significant to avoid

overheating inside joints. Therefore thermal boundary conditions varied by different welding environments of work piece surface (in air or cooled by water spray) and different backing plates with different thermal conductivities underneath the work piece bottom were applied in CSSP to examine effects of thermal managements on joint microstructure and properties. Water spray (WS) during FSW can enhances cooling of the plate, especially on the surface, which may also attributes to the increase in local HAZ minimum strength and UTS. WS may affect pin temperature near crown to some extent. Composite back plate (CBP) has a higher thermal conductivity K than steel back plate, which enhances heat conduction from Al plate bottom.

When composite BP, WS and 100rpm&102mm/min were applied in weld #4163, the required torque exceeded the FSW machine's limitation (600 N·m). This weld was aborted with a short weld length about 35.6 mm. For the consequent CSSP FSW, 160 RPM and 102 mm/min were adopted. Then CBP&WS were applied on 160 rpm&102mm/min weld (#4164), and it's found that, compared with welds with steel BP and 160 rpm&102mm/min, the torque increased from 383N*m to 541N*m, power increased from 6.4KW to 9.1KW, and at-center temperature decreased from 493℃ to 481 ℃. It indicates that, if a rotation rate higher than 160rpm is applied, at-center pin temperature will increase and possibly causes over-heating; if a rotation rate between 100rpm and 160 rpm is applied, the torque will exceed the machine limitation and the weld will be aborted. Thus CBP and/or WS were only applied on 160 rpm&102mm/min welds to evaluate influences of thermal managements on the surface and at the bottom of the work-piece in the welds macro and micro structures.

In this section, conventional shoulder single pass full penetration (CSSP) FSW and stationary shoulder single pass full penetration (SSSP) FSW have been studied in following aspects: macrostructure including investigation of surface finish, defect and nugget shape, microstructure, effect of control parameters on response parameters, grain size and hardness distribution, mechanical properties, etc.

4.2.1 Macrostructure

4.2.1.1 Surface finish

In this section surface finish in SP was examined. Figure 4.10 (a), (b) and (c) show joint surfaces of CSSP, produced by the same T+3F pin with the same flat depth of 0.9 mm, the same setup of 1 °tilt angle, the same forge force of 48.9 KN, the same welding speed of 51 mm/min, and rotating speeds of 200 RPM, 160 RPM and 120 RPM, respectively. The obvious semi-circular marks and flash can be seen on the joint surfaces.

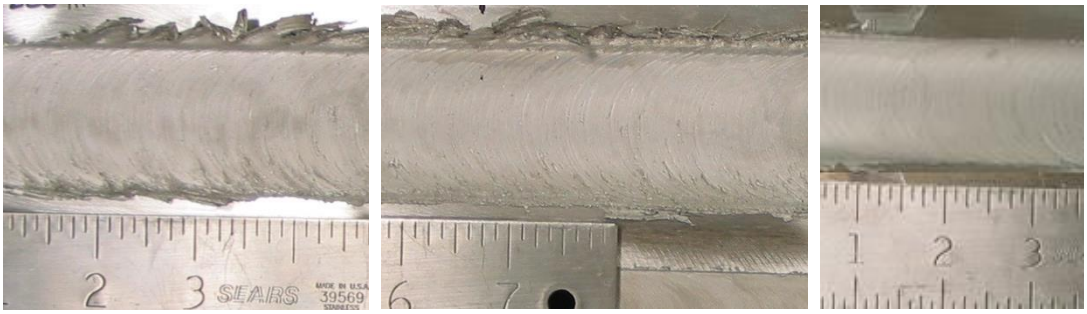

(a) #4153A, 200 rpm (b) #4153B, 160 rpm (c) #4153C, 120 rpm

Figure 4.10 Joint surfaces of CSSP: T+3F pin, 51 mm/min, Fz 48.9 KN, 1 °tilt

Figure 4.11 (a) and (b) show joint surfaces of SSSP, produced by the same T+3F pin with the same flat depth of 0.9 mm, the same setup of 0 °tilt angle, the same forge force of 73.4 KN, the same welding speed of 51 mm/min, and rotating speeds of 200 RPM and 160 RPM, respectively. In each condition, the surface is partially smooth and partially defective. In the smooth area, the semi-circular marks are less clear and

complete relative to those in CSSP as shown in Figure 4.10. Figure 4.12 (a), (b) and (c) show joint surfaces of SSSP, produced by the same T+3CT pin with the same flute depth of 0.9 mm, the same setup of 1 °tilt angle, the same forge force of 69 KN, the same welding speed of 51 mm/min, and rotating speeds of 200 RPM, 160 RPM and 120 RPM, respectively.

(a) #3963A, 200 rpm

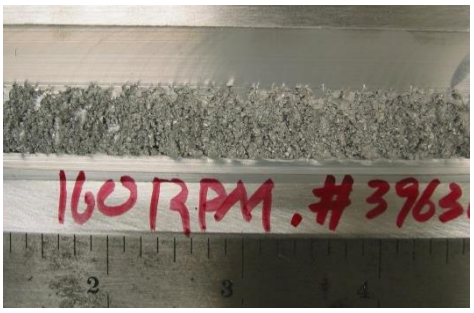

(b) #3963B, 160 rpm

Figure 4.11 Joint surfaces of SSSP: T+3F pin, 51 mm/min, Fz 73.4 KN, 0 °tilt

(a) #4167A, 200 rpm

(b) #4167B, 160 rpm

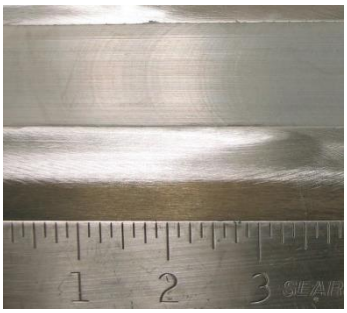

(c) #4167C, 120 rpm

Figure 4.12 Joint surfaces of SSSP: T+3CT pin, 51 mm/min, Fz 69 KN, 1 °tilt

Keeping other parameters the same, relative to surfaces of CSSP produced with T+3F tool, surfaces of SSSP produced with T+3CT tool are much smooth, and semi-circular marks on the surfaces are less clear and complete. Keeping other parameters the same, relative to surfaces of SSSP produced with T+3F tool and a setup of 0 ° tilt angle, surfaces of SSSP produced with T+3CT tool and a setup of 1 °tilt angle are defect free. It indicates that T+3F pin is suggested to be applied in CSSP while T+3CT

pin is suggested to be applied in SSSP. Relative to CSSP, SSSP can produce joints with better surface finish due to the absence of shoulder rotation during SSFSW process. Relative to setup of 0 °tilt angle, the setup of 1 °tilt angle can help produce defect free surface, especially in SSSP.

4.2.1.2 Defect investigation

The defect examination result of SP joints is listed in Appendix C. It shows that relative to SSSP, CSSP allows higher speeds and is more vulnerable to been overheated due to the rotating shoulder which will generate extra heat input during FSW.

In CSSP, only one type of tool was adopted: T+3F pin with a length of 25 mm and a flat depth of 0.9 mm. All joints were performed with the setup of 1 ° tilt. Defect examination results show that, in CSSP, when a lower welding speed (51 mm/min) was applied, only 100 rpm & 53.4 KN forge force produced welds with the lightest defects. Larger or smaller rotation rate and/or forge force caused surface defects and volumetric defects. Most of those welds had similar surface defects; some had similar wormhole defects at different location due to different rotation rate. Under similar forge forces, higher rotating speed leads to worse surface defects. When a higher welding speed (102 mm/min) was applied, there were no surface defects in most welds, which indicate that higher welding speed helps eliminate surface defects. Too low rotating speed (100 RPM, 120 RPM) causes wormhole defects inside the nugget at AS. Appropriate rotation rates (140 rpm, 160 rpm and 180 rpm) produced defect free nuggets with pin temperature higher than the incipient melting temperature (about 480℃). Some welds did not have volumetric defects, however, according to measured pin temperatures at center and near root (higher than the incipient melting temperature about 480℃), they were overheated

since the near crown part has higher temperature than at-center part when there was no water spray applied. In CSSP, among those welds produced with different thermal boundary conditions, it shows that any combination of different thermal boundary conditions produced joints without volumetric defects, while possibly been over heated according to the temperature measured at pin center. Details of thermal distribution in the whole transverse cross sections, which can be realized through thermal simulation, are needed to determine whether those joints have been over heated.

In SSSP, when a setup of 0 ° tilt, a T+3F pin and a welding speed of 51 mm/min were applied, under the same forge force (73.4 KN, #3963A & #3963B; #3964A & #3964B & #3964C), similar surface defects appeared at similar locations; higher rotating speed caused worse surface defects; lower rotating speed and/or deeper flat lead to less surface defects. When the pin rotates CCT, right-handed thread moves material downward, flat pin feature will interrupt this trend, co-flow flute will also move material downward, while counter-flow flute will move material upward. Deeper flat means more interruption of moving material downward, then less material moved downward from the crown, therefore less surface defect.

In SSSP, when a setup of 0 ° tilt, a T+3CT pin with a flute depth of 1.3 mm and a welding speed of 51 mm/min were applied, under the same forge force (69 KN, #3974A & #3974B & #3973A & #3973B), it shows that too high rotating speed leads to surface defects; lower rotating speed reduced/eliminated surface and reduced inside nugget defects, while there were still some wormhole defects near the weld root. Therefore, when a setup of 0 ° tilt was applied, changing the pin feature from flats to counter-flow flutes could help reduce/eliminate surface defect, while wouldn't eliminate worm hole

defects. When a setup of 0 °tilt, a T+3CT pin with a larger flute depth of 2.03 mm and a welding speed of 51 mm/min were applied, under the same forge force (69 KN, #3975A & #3975B), it shows that higher rotating speed (240 rpm) was more likely to cause surface defect; hole defects inside the nugget moved upward/from RS to AS when rotating speed increased. Keep other parameters the same, it's found that deeper flutes lead to less surface defects but worse worm hole defects inside the nugget, due to too much material moved upward by deeper counter-flow flutes when the pin rotates CCT.

In SSSP, when a setup of 1 °tilt, a T+3CT pin with a flute depth of 0.9 mm and a welding speed of 51 mm/min were applied, under the same forge force (69 KN, #4167ABC), too low rotating speed was not recommend since it caused wormhole defects which might due to not enough vertical material movement. It indicates that compared with 0 °tilt, 1 °tilt can significantly eliminate defects on surface and inside the nugget, produce defect free welds by providing more consolidation/forge at back of the shoulder. When a setup of 1 °tilt, a T+3CT pin with a flute depth of 0.9 mm and a welding speed of 51 mm/min were applied, under the same rotation rate (160 rpm, #4171B & 4171C & #4171D), too small forge force (35.6 KN) causes bad surface defects (large area), not full penetration and raises the crown. Among those applied forge forces, 53.4 KN is the minimum forge force that can produce defect free welds. Forge force larger than 53.4 KN also lead to defect free welds. Further tests are needed to verify whether forge force affects the defect free joint qualities (#4171AB, #4167B). When a setup of 1 °tilt, a T+3CT pin with a flute depth of 1.65 mm and a welding speed of 51 mm/min were applied, under the same forge force (69 KN, #4114 & #4116), 160 rpm caused wormhole defects at AS near root, while 200 RPM caused wormhole defects at AS near

mid-plane. The formation of wormhole defects inside the nugget might due to more material moved upward by a T+3CT pin with a flute depth of 1.65 mm, which is larger than the appropriate flute depth for sound material flow. It indicates that when rotating speed increased, wormhole defects moved upward, which might because when rotating speed increased, the velocity at upper part of the pin increased more than at lower part of the pin (due to different pin diameters), which increased the possibility of worm holes forming there (-need more similar cases). When a setup of 1 °tilt, a T+3CT pin, a rotation rate of 160 rpm and a welding speed of 51 mm/min were applied, under the same forge force (69 KN, #4116 & #4167B), 0.9 mm deep counter-flow flute produced defect free joint, while 1.65 mm deep counter-flow flute still caused wormhole defects inside the nugget. It indicates that, 1.65 mm counter-flow flute was too deep to produce a defect free weld. Based on current results, T+3CT with a flute depth of 0.9 mm (0.035'') is the best pin design for SSSP FSW.

In SSSP, when a setup of 0 ° tilt and a welding speed of 51 mm/min are applied, tools with T+3F pin are more easily to cause surface defects, while tools with T+3CT pin are more likely to cause defects in the nugget, especially at AS near root. When a setup of 0 ° tilt, a welding speed of 51 mm/min, and a T+3F pin are applied, it should be focused on how to eliminate surface defects. When a setup of 0 ° tilt, a welding speed of 51 mm/min, and a T+3CT pin are applied, it should focus on how to eliminate defects inside nuggets. Larger rotating speed leads to worse surface defects; counter-flow flutes with appropriate depth (0.9 mm) can reduce/eliminate surface defects and produce defect free joints. It indicates that, to get FSW welds with good welding quality, low tool rotation rate, T+3CT pin with a flute depth of 0.9 mm are recommended.

Defect investigation results also show that, pin features and shoulders have different effects on material flow in CSSP and SSSP. When a setup of 1 ℃tilt, a flat/flute depth of 0.9 mm, a rotating rate of 160 rpm and a welding speed of 51 mm/min were applied, T+3F pin is recommended for CSSP, while T+3CT is recommended for SSSP to enhance material vertical movements, improve weldability and produce defect free joints. When a setup of 1 ℃tilt, a flat/flute depth of 0.9 mm and a welding speed of 51 mm/min were applied, relative to CSSP, SSSP caused less surface defect.

4.2.1.3 Nugget

Figure 4.13~Figure 4.17 show the macro images of transverse cross sections of both CSSP and SSSP welds in 25.4 mm thick AA7099-T7651 plates. In CSSP and SSSP, the advancing sides (AS) are on the left in each image of the cross section.

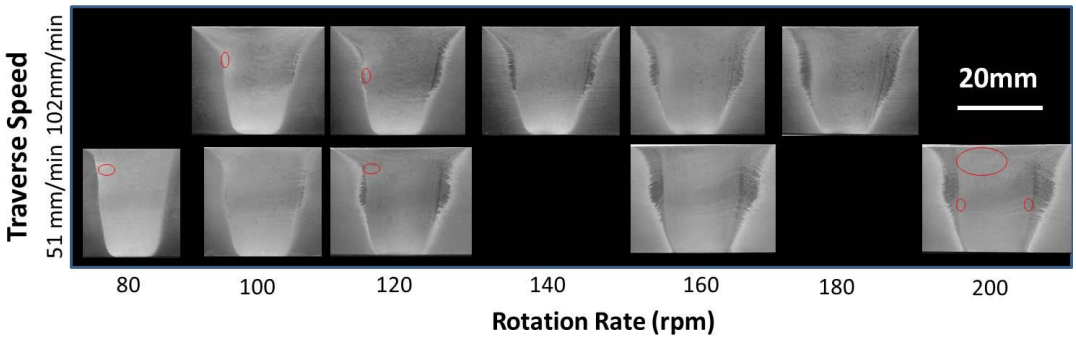

Figure 4.13 Macro Transverse Cross Sections of CSSP: Different speeds, T+3F pin, 0.9 mm deep flats

Figure 4.13 shows macro transverse cross sections of CSSP in AA7099, which were produced by a T+3F pin with a flat depth of 0.9 mm. Images of transverse cross sections in each column are with rotation rates (rpm), while images in each row are with welding speeds (mm/min). Those macro images show that, under the same rotating speed, relative to the lower welding speed (51 mm/min), the higher welding speed (102 mm/min) produced nuggets with smaller TMAZ area, and more clear HAZ boundary. When either

a lower welding speed (51 mm/min) or a higher welding speed (102 mm/min) was applied, under similar forge forces, higher rotating speed leads to larger TMAZ area, more blurry HAZ boundary, and a joint shape less similar to the pin.

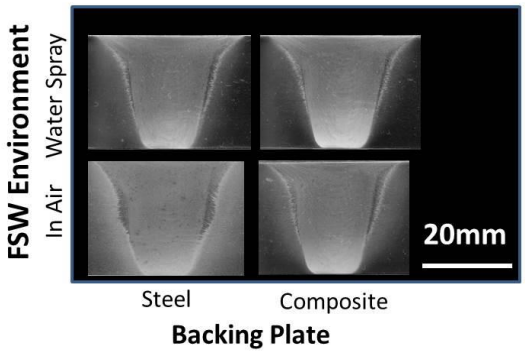

Figure 4.14 Macro Transverse Cross Sections of CSSP: different thermal boundary conditions, T+3F pin, 0.9 mm deep flats, 160 rpm, 102 mm/min

Figure 4.14 shows macro transverse cross sections of CSSP in AA7099, which were produced by a T+3F pin with a flat depth of 0.9 mm, a rotation rate of 160 rpm, and a welding speed of 102 mm/min under different thermal boundary conditions. Among those welds produced with different thermal boundary conditions, as shown in Figure 4.14, it shows that relative to the weld performed in air, the weld performed with WS has a smaller TMAZ area, clearer HAZ boundary especially near crown, and a joint shape more similar to the pin. Relative to the weld using steel backing plate, the weld performed with composite backing plate has a smaller TMAZ area, clearer HAZ boundary especially near root, and a joint shape more similar to the pin. Relative to the joint performed in air using steel backing plate, when both water spray and composite backing plate (as described in chapter 3 and shown in Figure 3.1 and Figure 3.2) were applied, the joint has a smaller TMAZ area, more clear HAZ boundary, and a joint shape more similar to the pin. Relative to composite backing plate, water spray produced a joint

with a little smaller TMAZ area, clearer HAZ boundary near crown, less clear HAZ boundary near root.

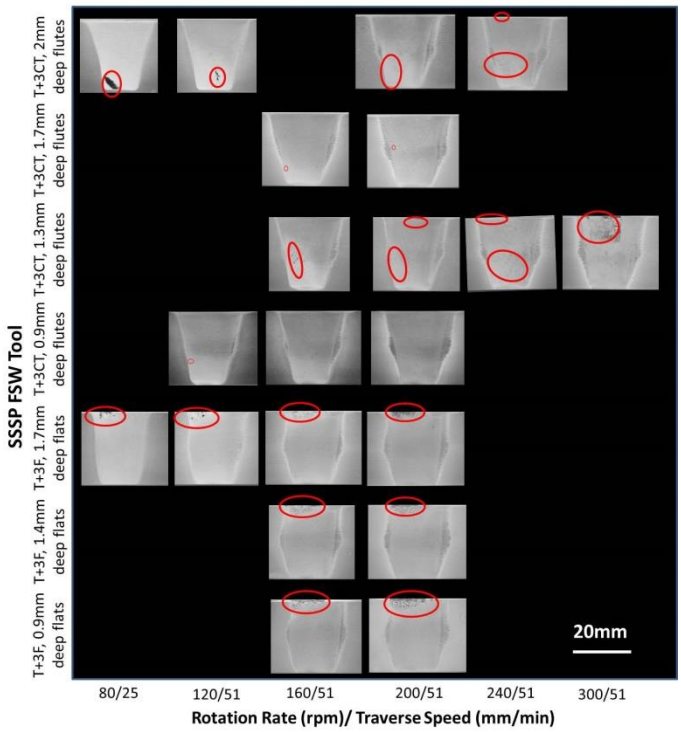

Figure 4.15 Macro Transverse Cross Sections of SSSP: different speeds and tools

Figure 4.15 shows macro transverse cross sections of SSSP in AA7099. Images of transverse cross sections in each column are with a particular combination of rotation rate (rpm) and welding speed (mm/min), while images in each row are with various FSW tools employed with various pin features and flat/flute depths. Figure 4.15 show that:

(1) When a setup of 0 °tilt, a T+3F pin and a welding speed of 51 mm/min were applied, under the same forge force (73.4 KN, #3963A & #3963B; #3964A & #3964B & #3964C), higher rotating speed caused larger TMAZ area; lower rotating speed and/or deeper flat lead to less TMAZ area.

(2) When a setup of 0 °tilt, a T+3CT pin with a flute depth of 1.3 mm and a welding speed of 51 mm/min were applied, under the same forge force (69 KN, #3974A

& #3974B & #3973A & #3973B), it shows that lower rotating speed leads to less TMAZ area. When a setup of 0 °tilt, a T+3CT pin with a larger flute depth of 2.03 mm and a welding speed of 51 mm/min were applied, under the same forge force (69 KN, #3975A & #3975B), it shows that higher rotating speed (240 rpm) was more likely to cause larger TMAZ area and more blurry boundaries; lower welding speed (25 mm/min) leads to a joint shape which was more similar with the pin.

(3) When a setup of 1 °tilt, a T+3CT pin with a flute depth of 0.9 mm and a welding speed of 51 mm/min were applied, under the same forge force (69 KN, #4167ABC), higher rotating speed caused larger TMAZ area. When a setup of 1 °tilt, a T+3CT pin with a flute depth of 1.65 mm and a welding speed of 51 mm/min were applied, under the same forge force (69 KN, #4114 & #4116), when rotating speed increased, TMAZ area increased, and nugget boundaries became more blurry.

(4) When a setup of 0 °tilt and a welding speed of 51 mm/min are applied, larger rotating speed leads to a larger TMAZ area.

Figure 4.16 shows macro transverse cross sections of SSSP in AA7099, which were produced by a T+3CT pin with a flat depth of 0.9 mm, a setup of 1 °tilt, a rotation rate of 160 rpm, and a welding speed of 51 mm/min under different forge forces. Higher forge force caused a little larger TMAZ area, especially at mid-plane RS.

Figure 4.17 shows macro transverse cross sections of CSSP and SSSP in AA7099, which were produced by pins with the same flat/flute depth of 0.9 mm, and the same welding speed of 51 mm/min. Figure 4.17 shows that, shoulders have different effects on material flow in CSSP and SSSP. When a setup of 1 °tilt, a flat/flute depth of 0.9 mm and a welding speed of 51 mm/min were applied, relative to CSSP, SSSP resulted in a nugget

shape more consistent to the pin shape and lead to narrower metallurgical zone and TMAZ zone especially near crown due to the shoulder effect. Different metallurgical geometries and shapes in CSSP and SSSP joints indicate different material flow, thermal temperature and strength distribution in joints.

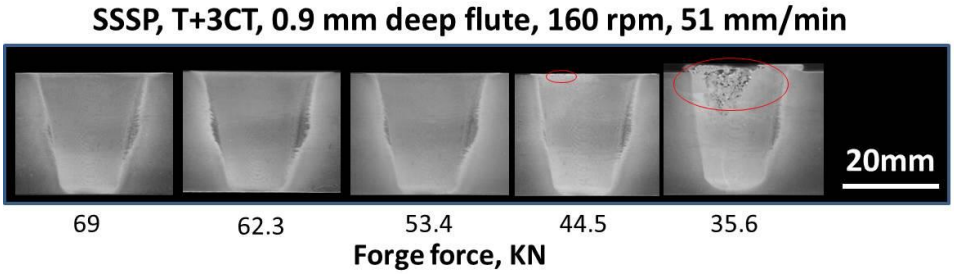

Figure 4.16 Macro Transverse Cross Sections of SSSP: different forge forces, T+3CT pin, 0.9 mm deep flutes, 160 rpm, 51 mm/min

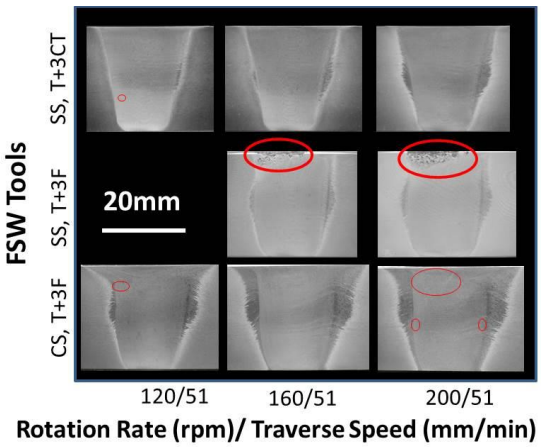

Figure 4.17 Macro Transverse Cross Sections of SP: 0.9 mm deep flats/flutes, 51 mm/min

4.2.2 Process Responses

Process response parameters include in plane reaction forces (F_x, F_y and the resultant force F_{xy}), torque, power, peak temperature measured at pin center (which was also considered as the peak temperature measured at center NG due to the pretty close positions) and grain size (GS) measured at center NG. Process response parameters were collected and calculated. Process response parameters as a function of tool rotation rate

are summarized and shown in Figure 4.18 for CSSP and Figure 4.20 for SSSP welds of AA7099. Figure 4.19 a~b show temperatures (a) at center pin and (b) near root as functions of power input for CSSP bead on plate welds on AA7099. Various symbols represent for different FSW conditions including rotating or stationary shoulder, pin types, tilt angle, welding speeds, and thermal boundary conditions. Here most welds were produced with normal thermal boundary conditions, which are in air environment nearby the work piece surface and the steel backing plate applying underneath the work piece bottom. "WS" and "CBP" were used to indicate welds made by different thermal boundary conditions. "WS" means welds were produced with water spray applying at work piece surface, "CBP" means welds were produced with composite backing plate applying underneath work piece bottom.

4.2.2.1 Process Responses of CSSP

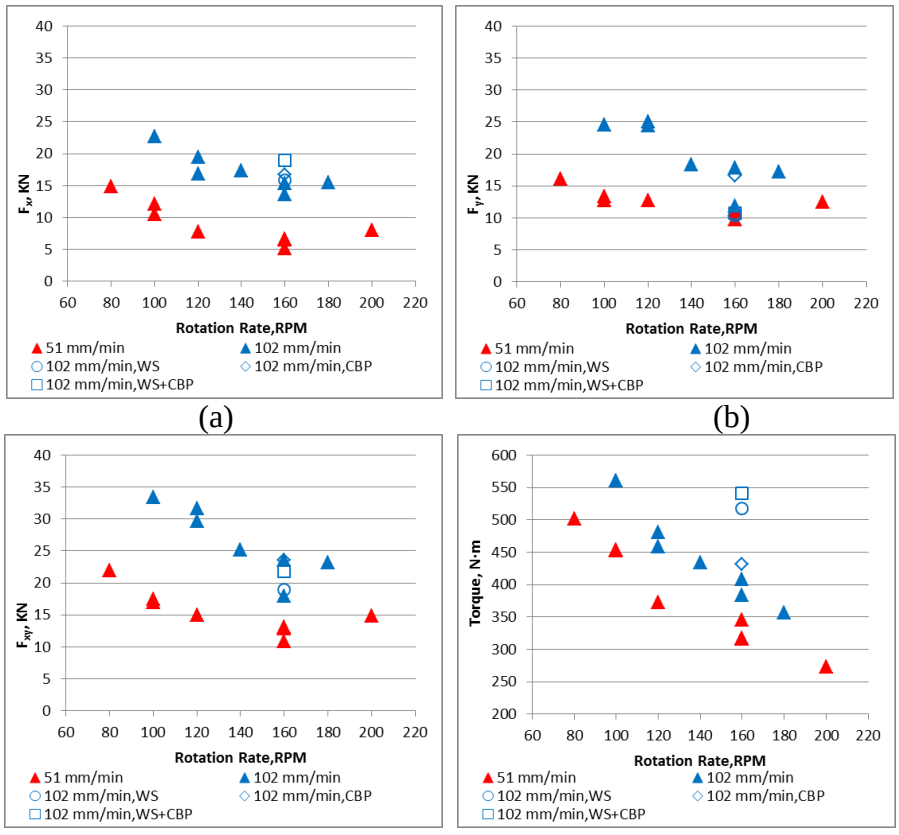

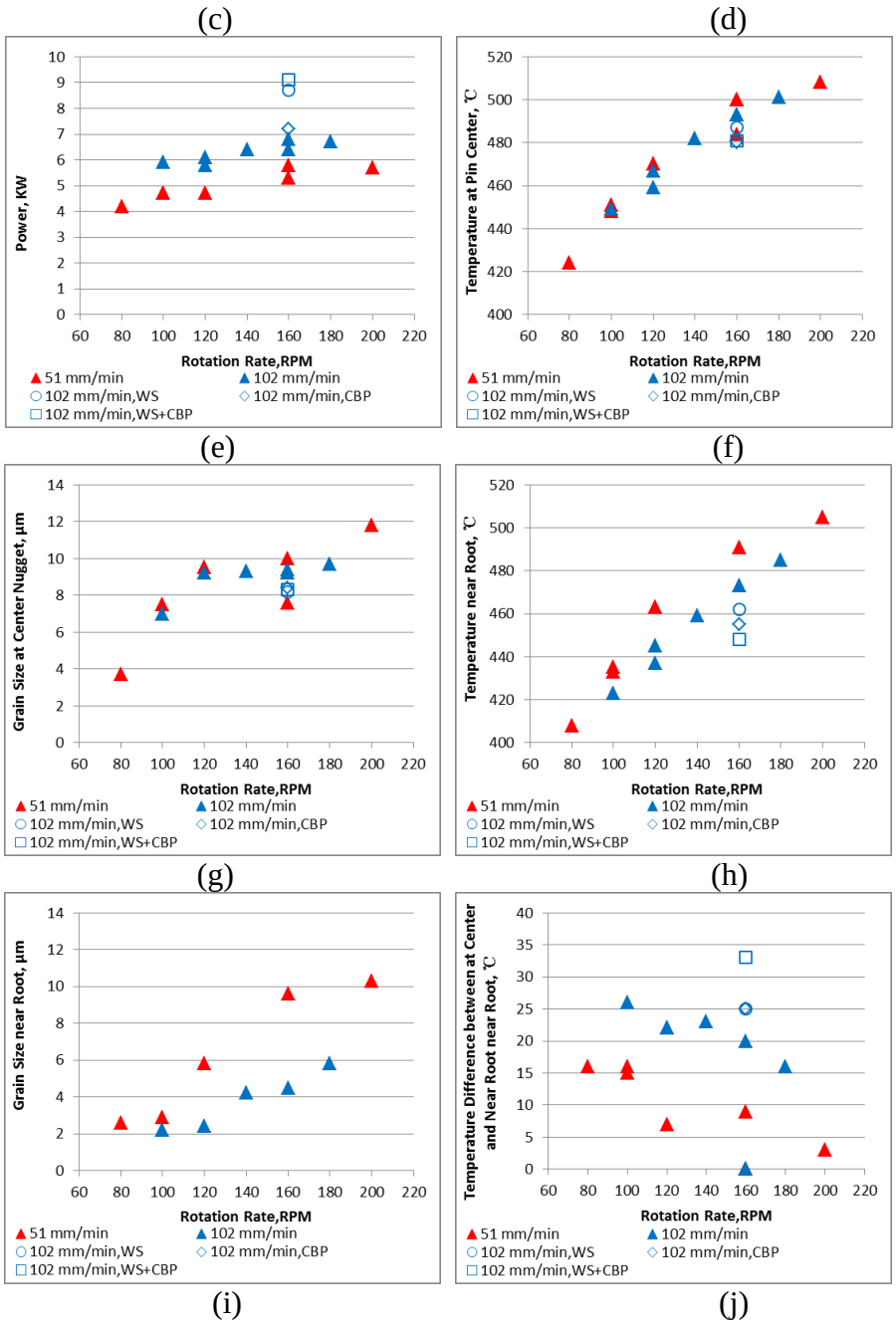

Figure 4.18 Reaction forces, torque, power, peak T and GS vs. tool rotation rate in CSSP

Figure 4.18 a~j show the response parameters as functions of tool rotation rate for CSSP bead on plate welds on AA7099. Solid symbols represent joints produced in air with steel backing plate underneath the work piece bottom. Open symbols represent joints produced with water spray applying on the work piece surface and/or with

composite backing plate underneath the work piece bottom. Figure 4.19 a~b show T (a) at center pin and (b) near root as functions of power input for CSSP bead on plate welds.

4.2.2.1.1 CSSP with the same Thermal Boundary Condition

Figure 4.18 a~j indicates that, in CSSP joints produced with the same thermal boundary conditions (in air, with steel backing plate underneath the work piece bottom):

(1) When the lower welding speed (51 mm/min) was applied, under the similar forge forces, when rotating speed increased, in-plane forces decreased first and then increased, and minima in-plane forces were obtained at the intermediate rotating speed (160 rpm). Torque decreased, power increased, then at-center and near-root pin temperatures and GS increased.

(2) When the higher welding speed (102 mm/min) was applied, under the similar forge forces, when rotating speed increased, required forge force decreased, then in-plane forces decreased. Torque decreased, power increased, then at-center and near-root pin temperatures increased. At-center GS was similar, while near-root GS increased.

(3) When rotating speed was large enough, T and GS gradually arrived a plateau.

(4) Higher welding speed required larger forge force, then caused larger in-plane forces, lead to higher torque, higher power, a little smaller at-center pin temperature and GS, and smaller near-root pin temperature and GS.

(5) In a joint, at-center pin temperature was larger than near-root pin temperature, and temperature difference at different locations was increased by higher welding speed and/or lower rotating speed.

Figure 4.19 a~b show that, in CSSP joints produced with the same thermal boundary conditions (in air, with steel backing plate underneath the work piece bottom),

under the similar forge forces, when power input increased, at-center and near-root pin temperatures increased at the same rate (steel BP, no WS) in CSSP joints produced with welding speed of either 51 mm/min and or 104 mm/min.

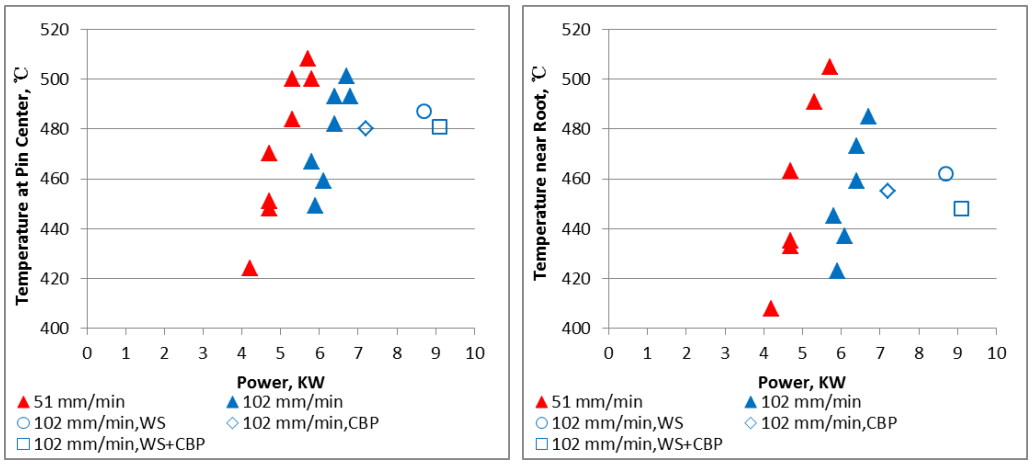

(a) (b)

Figure 4.19 Temperature (a) at center pin and (b) near root as functions of power: CSSP

4.2.2.1.2 CSSP with different Thermal Boundary Conditions

Figure 4.18 a~j indicates that, in CSSP joints produced with the same speeds and different thermal boundary conditions (with water spray (WS) applying on the work piece surface, and/or with composite backing plate (CBP) underneath the work piece bottom):

(1) When WS was applied, required forge force increased, F_x was similar, F_y and F_{xy} decreased, torque and power increased, at-center and near-root pin temperatures decreased a little, and at-center grain size decrease a little. When CBP was applied, required forge force and in-plane forces were similar, torque and power increased a little, center and near-root pin T and center grain size decrease.

(2) When both WS and CBP were applied, required forge force increased, F_x increased, F_y decreased and F_{xy} were similar, torque and power increased, at-center and near-root pin temperatures and at-center grain size decreased.

(3) CBP, WS, and CBP&WS have similar influence in at-center pin temperature and at-center GS.

(4) Application of either WS or CBP increased the required power input. CBP&WS required a higher power input than WS, which was larger than CBP.

(5) Relative to CBP, WS has a larger influence in increasing F_z, decreasing F_y and F_{xy}, and increasing torque, power. When temperature inside the joint is decreased, FSW torque will increase. It showed that water spray device has a more significant effect in reducing temperature near crown than composite BP. Relative to WS, CBP has a larger influence in decreasing at-center and near-root pin temperatures.

4.2.2.2 Process Responses of SSSP

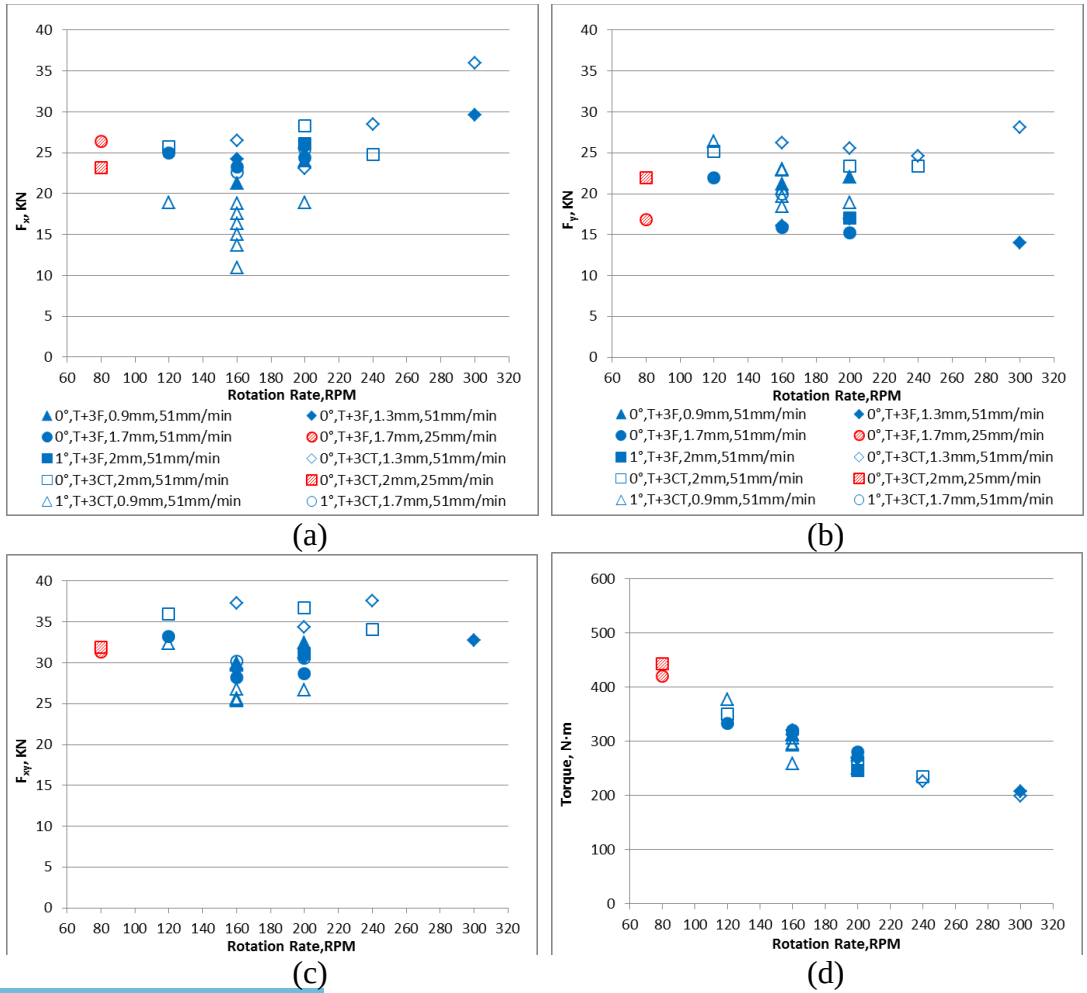

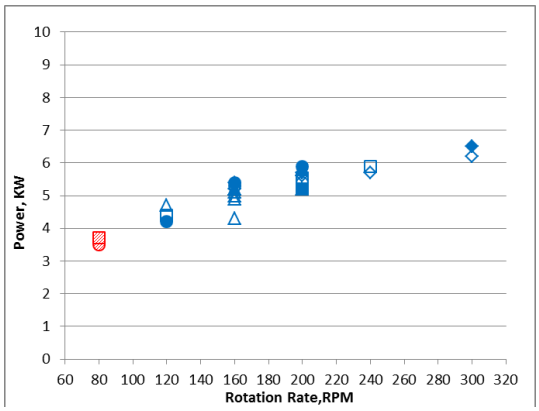

(e)

Figure 4.20 Reaction forces, torque and power as functions of tool rotation rate in SSSP

Figure 4.20 a~e show the response parameters as functions of tool rotation rate for SSSP bead on plate welds on AA7099. Generally, when rotating speed increased, torque decreased, and power increased.

When the T+3F pin was applied, almost all joints were defective. Surface defect was dominant, which might due to the pin feature which moved too much material downward to the weld root. When a T+3F pin with a flat depth of 0.9 mm, a setup of 0 ° tilt, and a welding speed of 51 mm/min were applied, under the same forge force (#3963A & #3963B), larger rotating speed lead to larger F_x (13%), similar F_y (4%), larger F_{xy} (8%), smaller torque (-12%), larger power (12%) and at-center GS (26%). When a T+3F pin with a flat depth of 1.3 mm, a setup of 0 ° tilt, and a welding speed of 51 mm/min were applied, under the same forge force (#3964B & #3964C), larger rotating speed lead to similar in-plane forces (5%), smaller torque (-16%), larger power (6%) and at-center GS (22%). When a T+3F pin with a flat depth of 1.7 mm, a setup of 0 ° tilt, and a welding speed of 51 mm/min were applied, under the same forge force (#3965A & #3965B), larger rotating speed lead to similar in-plane forces (F_x, 5%; F_y, -4%; F_{xy}, 2%), smaller torque (-12%), larger power (9%) and at-center GS (52%). It indicates that

different flat depths affect the influence of rotation rate increase in response parameters. When rotation rate increased, the flat depth of 0.9 mm caused larger in-plane forces, while the flat depths of 1.3 mm and 1.7 mm affected in-plane forces little. When rotation rate increased, the flat depths of 0.9 mm and 1.3 mm increased the grain size at center nugget by similar extents, while flat depth of 1.7 mm increased the grain size at center nugget by much larger extent.

When the T+3CT pin was applied, only the combination of 1 ° tilt, a T+3CT pin with a flute depth of 0.9 mm, a rotation rate of 160 rpm, a welding speed of 51 mm/min and a series of appropriate forge forces produced joints without volumetric defects.

When the T+3CT pin was applied, with the same welding speed of 51 mm/min, keep other control parameters the same, larger rotating speed lead to smaller torque, while larger power input, at-center pin T and GS. With a 0 ℃tilt setup, and the same forge force, the T+3CT pin with deeper flutes lead to larger F_x, a little smaller F_y, and then a little larger F_{xy}, similar torque, power and at-center GS; higher rotating speed lead to smaller F_x, similar F_y, smaller F_{xy}, smaller torque, higher power, and similar at-center GS.

As shown in Figure 4.21 a~e, with a setup of 1 ℃tilt, the same welding speed of 51 mm/min, and the same forge force, when the T+3CT pin with a flute depth of 0.9 mm was applied, higher rotating speed lead to similar F_x, smaller F_y, and smaller F_{xy}, smaller torque, larger power input and then higher at-center pin temperature and GS; when the T+3CT pin with a flute depth of 1.7 mm was applied, higher rotating speed lead to larger F_x, smaller F_y, and similar F_{xy}, smaller torque while larger power input. It indicates that, when rotating speed increased, the T+3CT pin with deeper flutes lead to larger F_x, a little smaller F_y and then a little larger F_{xy}, a little larger torque and power, and the differences

of torque decreased. It indicates that, different head angle setups caused different changes in F_x with rotating speed increasing due to different contact conditions between shoulder and plate surface.

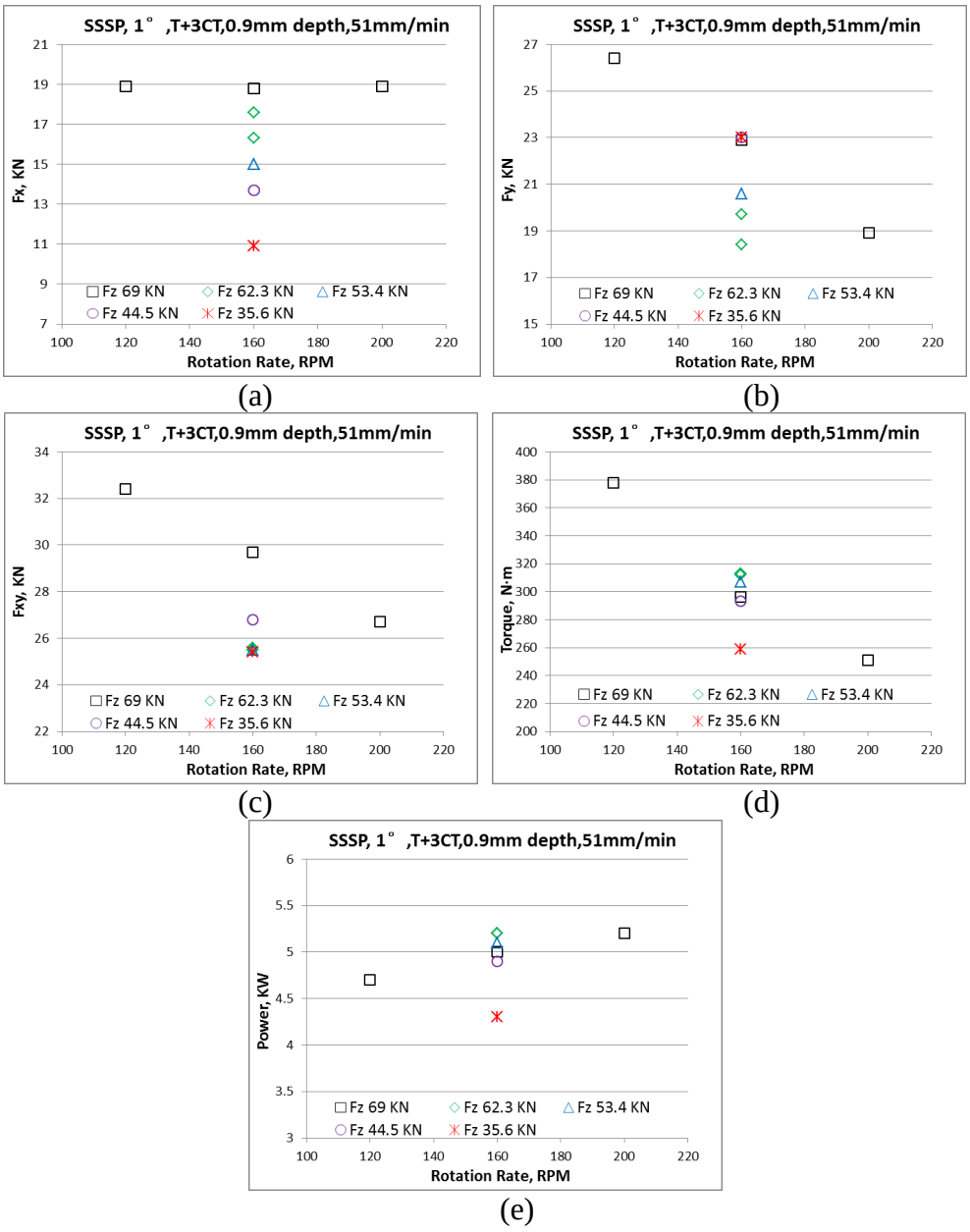

Figure 4.21 Reaction forces, torque and power as functions of tool rotation rate in SSSP: 1° tilt, T+3CT pin with a flute depth of 0.9 mm, a welding speed of 51 mm/min

As shown in Figure 4.21 a~e, with a setup of 1 °tilt, under the same rotating speed of 160 rpm, the same welding speed of 51 mm/min, and the same T+3CT pin with a flute

depth of 0.9 mm, when forge force increased, F_x increased a little, F_y decreased first then increased after F_z was larger than 62.3KN, F_{xy} was similar at first then increased after F_z was larger than 62.3KN. Torque, power and then at-center pin temperature and GS increased first then decreased after F_z was larger than 62.3KN. Minimum in-plane forces, maximum torque, power, at-center pin temperature and at-center GS were obtained under an intermediate forge force (62.3KN).

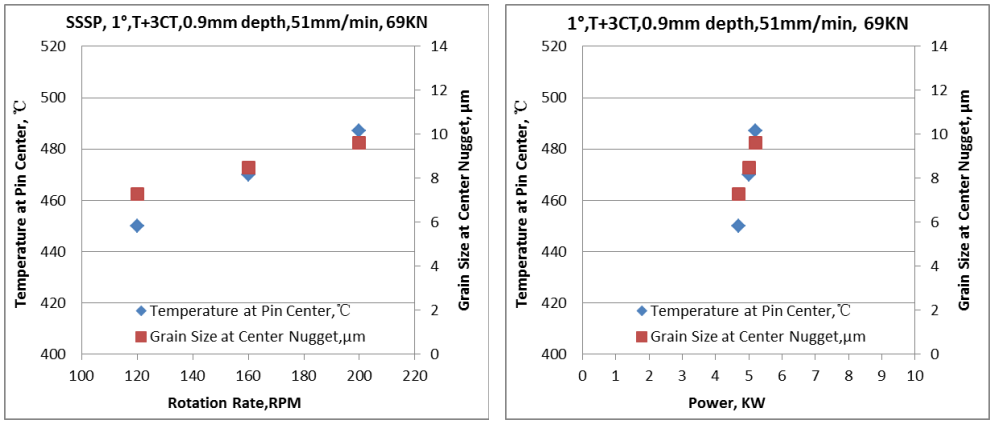

(a) (b)

Figure 4.22 Temperature and grain size at center as functions of (a) rotation rate and (b) power input in SSSP: 1° tilt, T+3CT pin with a flute depth of 0.9 mm, a welding speed of 51 mm/min, forge force 69 KN

Figure 4.22 a~b show temperature and grain size at center as functions of (a) rotation rate and (b) power input for SSSP bead on plate welds on AA7099 produced with the same welding speed of 51 mm/min and the same forge force of 69 KN. Figure 4.22 (a) shows that, under the same forge force, when rotating speed increased, temperature at pin center and grain size at center nugget increased due to decreased power and temperature at pin center. Figure 4.22 (b) shows that, under the same forge force, when power input increased, temperature at pin center and grain size at center nugget increased.

Figure 4.23 a~b show temperature and grain size at center as functions of (a) forge force and (b) power input for SSSP bead on plate welds on AA7099 produced with the same rotating speed of 160 rpm and the same welding speed of 51 mm/min. Figure 4.23 (a) shows that, under the same speeds, when forge force increased, temperature at pin center and grain size at center nugget increased first then decreased after F_z was larger than 62.3KN. Minimum at-center pin temperature and at-center GS were obtained under an intermediate forge force (62.3KN). Figure 4.23 (b) shows that, under the same speeds, when power input increased, temperature at pin center and grain size at center nugget increased.

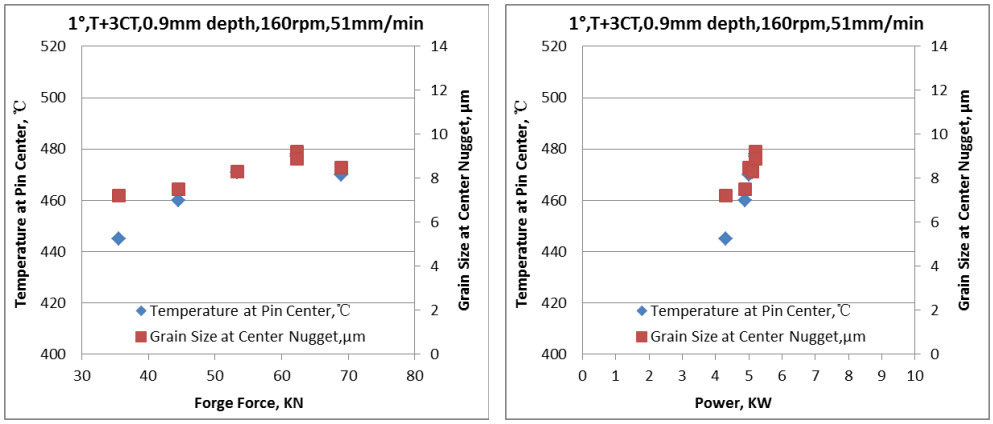

(a) (b)

Figure 4.23 Temperature and grain size at center as functions of (a) forge force and (b) power input in SSSP: 1° tilt, T+3CT pin with a flute depth of 0.9 mm, a rotation rate 160 rpm, a welding speed of 51 mm/min

4.2.2.3 Process Responses of CSSP and SSSP

The applicable speeds of CSSP and SSSP listed in Appendix B show that, relative to SSSP, CSSP allows higher welding speed which significantly increases PWHT UTS.

Figure 4.24 and Figure 4.25 also show similarities and differences in CSSP and SSSP.Figure 4.24 a~g show response parameters like reaction forces, torque, power, temperature at pin center and GS at center nugget as functions of tool rotation rate for

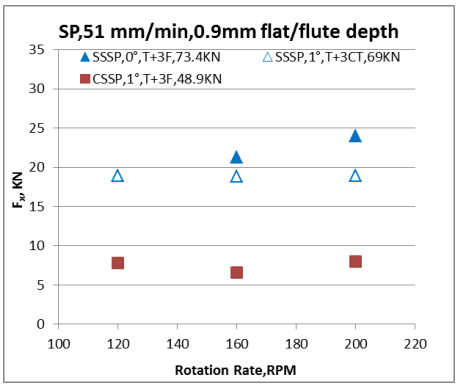

(a)

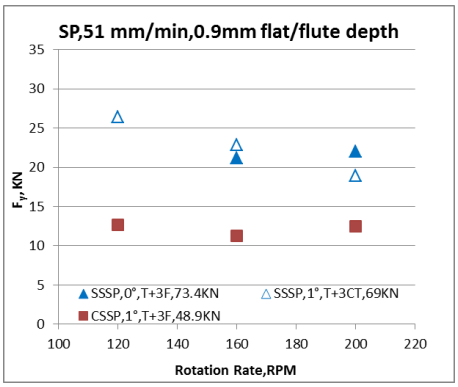

(b)

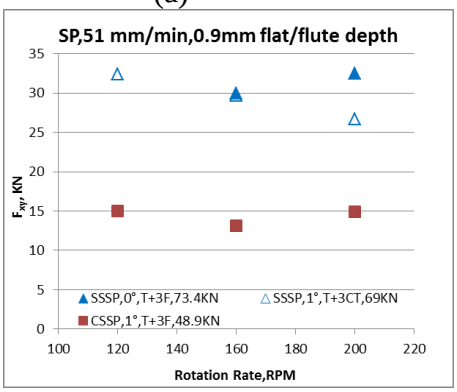

(c)

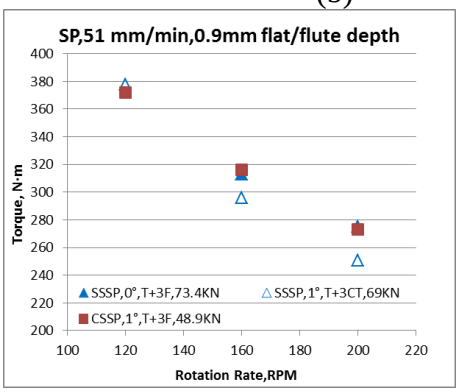

(d)

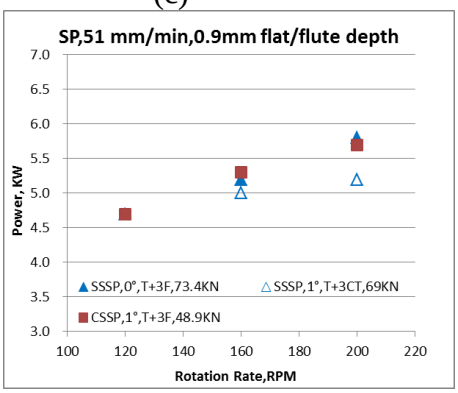

(e)

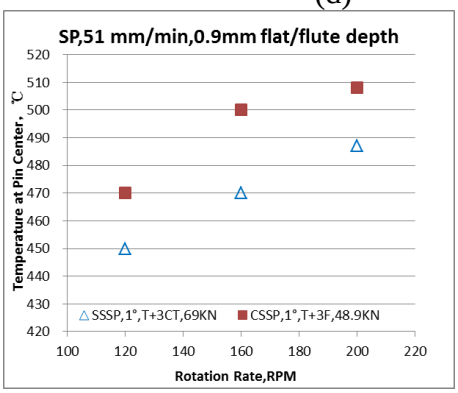

(f)

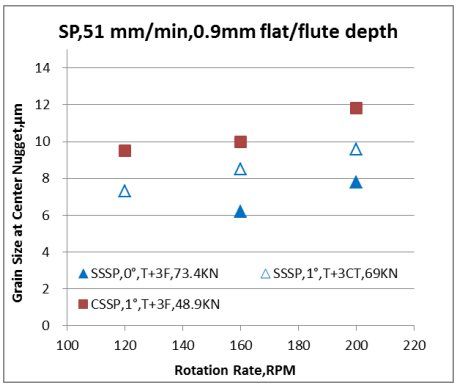

(g)

Figure 4.24 Reaction forces, torque, power, temperature at pin center and GS at center nugget as functions of tool rotation rate in SP: a welding speed of 51 mm/min, a flat/flute depth of 0.9 mm

CSSP and SSSP bead on plate welds on AA7099 which were produced by pins with the same flat/flute depth of 0.9 mm, and the same welding speed of 51 mm/min.

Figure 4.24 shows that, shoulders have different effects on response parameters in CSSP and SSSP. Generally, both in CSSP and SSSP, when rotating speed increased, torque decreased, power increased, T at pin center and GS at center nugget increased.

When the T+3F pin was applied, relative to CSSP joints produced with the setup of 1°, in SSSP joints produced with the setup of 0°, under the same rotation rate, SSSP required larger forge force, lead to larger in-plane forces, similar torque and power, and much smaller grain size at center nugget. When rotation rate increased, in CSSP, under the same forge force, in-plane forces were similar; while in SSSP, under the same forge force, F_x increased a little, F_y was similar, and then F_{xy} increased a little. When rotation rate increased, relative to CSSP, in SSSP, torque decreased at the similar slope, while power and grain size at center nugget increased at the similar slopes. Those similar trends in torque and power might due to the same pin feature (T+3F) adopted in those joints.

When the same setup of 1 ?ilt was applied, relative to CSSP joints produced with the T+3F pin, in SSSP joints produced with the T+3CT pin, under the same rotation rate, SSSP required larger forge force, lead to larger in-plane forces, a little smaller torque, smaller power, smaller temperature at pin center and grain size at center nugget. When rotation rate increased, in CSSP, under the same forge force, in-plane forces were similar; while in SSSP, under the same forge force, F_x was similar, F_y decreased, then F_{xy} decreased. When rotation rate increased, relative to CSSP, in SSSP, torque decreased

faster, power increased slower, temperature at pin center and grain size at center nugget increased at the similar slopes.

Figure 4.25 a~b show response parameters like temperature at pin center and grain size at center nugget as functions of power input for CSSP and SSSP bead on plate welds on AA7099 which were produced by pins with the same flat/flute depth of 0.9 mm, and the same welding speed of 51 mm/min. When power input increased, temperature at pin center and grain size at center nugget increased, and the increasing slope of SSSP was larger than that of CSSP. With similar power input, SSSP had a lower temperature at pin center than CSSP. To achieve the same T at pin center, SSSP requires more power input.

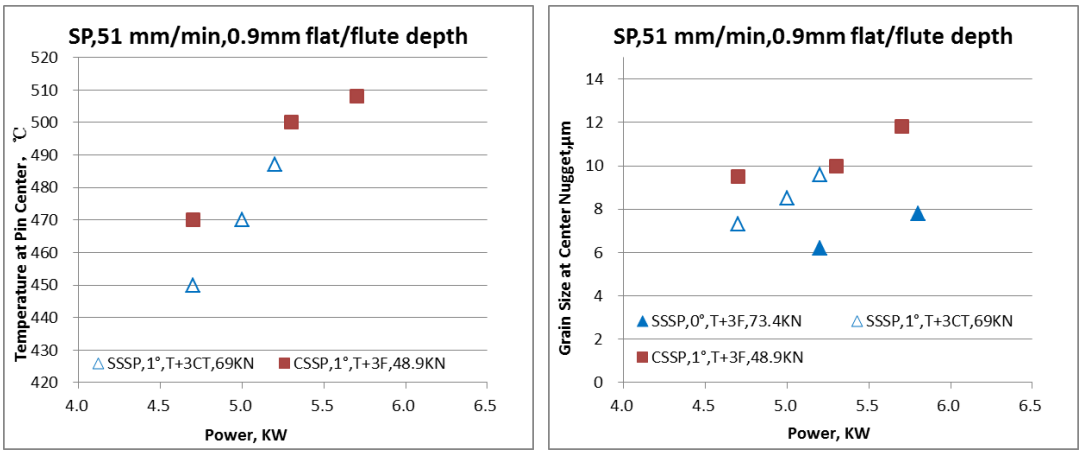

(a) (b)

Figure 4.25 Temperature at pin center and GS at center nugget as functions of power input in SP: a setup of 1° , a welding speed of 51 mm/min, a flat/flute depth of 0.9 mm

Figure 4.26 shows grain size at center nugget as function of temperature at pin center for CSSP and SSSP bead on plate welds on AA7099, which were produced with a setup of 1° , a welding speed of 51mm/min, a flat/flute depth of 0.9mm. When temperature at pin center increased, grain size at center nugget increased, and the increasing slope of SSSP was at first larger then smaller than that of CSSP. At the similar

temperature at pin center, SSSP had a smaller grain size at center nugget than CSSP. To achieve the same grain size at center nugget, SSSP requires more power input.

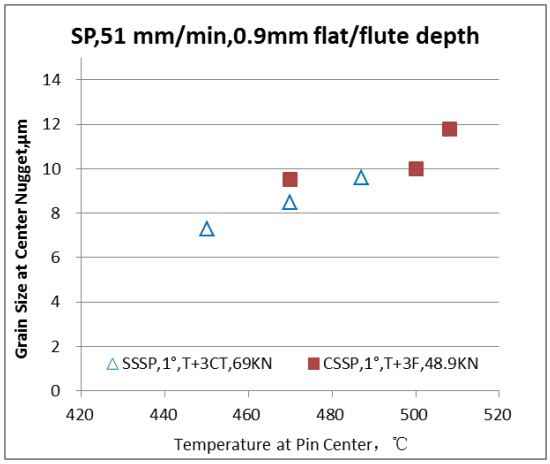

Figure 4.26 Grain size at center nugget as function of temperature at pin center in SP: a setup of 1°, a welding speed of 51 mm/min, a flat/flute depth of 0.9 mm

4.2.3 Hardness distribution through thickness

Rotating and stationary shoulders result in different heat sources in FSW, affecting thermal distribution, microstructure and properties through thickness of joints. In this section, hardness variations on the weld centerline through thickness in CSSP and SSSP have been studied to investigate effects of CSSP and SSSP on variations of property through thickness.

4.2.3.1 Hardness distribution through thickness of CSSP

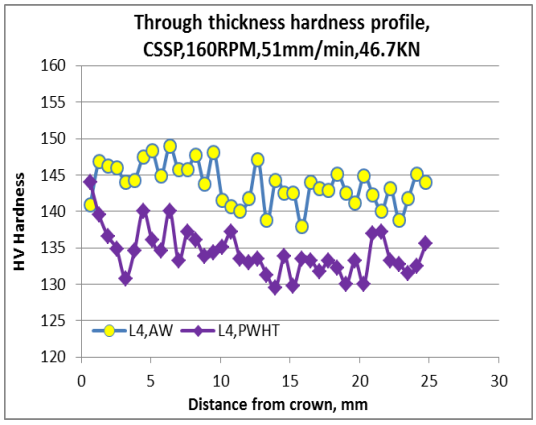

(a) CSSP: Fz 46.7 KN (#4299)

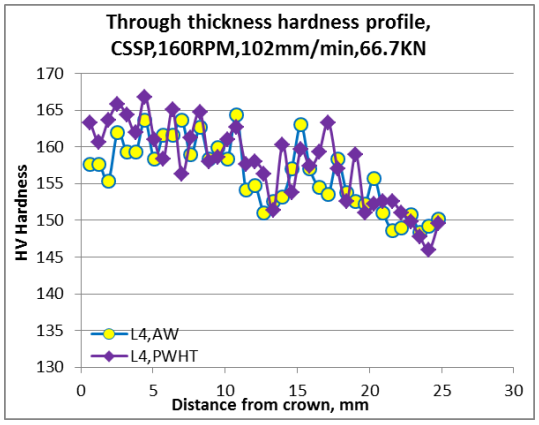

(b) CSSP: Fz 66.7 KN (#4300)

Figure 4.27 Through thickness hardness profiles on the weld centerline in CSSP with a welding speed of (a) 51 mm/min and (b) 102 mm/min: AW and PWHT, 160 RPM, T+3F pin, 0.9 mm flat depth

Figure 4.27 and Figure 4.28 show the hardness as a function of distance from the weld crown on the weld centerline in AW and PWHT conditions of CSSP joints.

Figure 4.27 (a) shows that, in the AW condition, the minimum hardness with a value of 138 appeared at a distance of 15.9mm from the weld crown, while the maximum hardness with a value of 149 appeared at a distance of 6.4 mm from the weld crown. In the PWHT condition, the minimum hardness with a value of 130 appeared at a distance of 15.2 mm from the weld crown, while the maximum hardness with a value of 144 appeared at a distance of 0.64 mm from the weld crown. It shows that, in both AW and PWHT conditions, minimum hardness appeared nearby the mid-plane of the joint in both AW and PWHT conditions, while maximum hardness in PWHT condition appeared at the location closer to the weld crown than that in AW condition. It shows that hardness varied with the similar range in AW and PWHT conditions. It also indicates that relative to AW condition, PWHT reduced hardness through thickness except the hardness measured 0.64 mm away from the weld crown.

Figure 4.27 (b) shows that, in the AW condition, the minimum hardness with a value of 148 appeared at a distance of 23.5 mm from the weld crown, while the maximum hardness with a value of 164 appeared at a distance of 10.8 mm from the weld crown. In the PWHT condition, the minimum hardness with a value of 146 appeared at a distance of 24.1 mm from the weld crown, while the maximum hardness with a value of 168 appeared at a distance of 4.4 mm from the weld crown. It shows that, in both AW and PWHT conditions, minimum hardness appeared near root in both AW and PWHT conditions, while maximum hardness in PWHT condition appeared at the location closer

to the weld crown than that in AW condition. It shows that relative to hardness in AW condition, hardness in PWHT conditions varied with a little larger/similar range. It also shows that hardness profiles through thickness were similar in AW and PWHT condition, which indicates that in joints produced by a larger welding speed (102 mm/min), PWHT had little effect on hardness profiles through thickness.

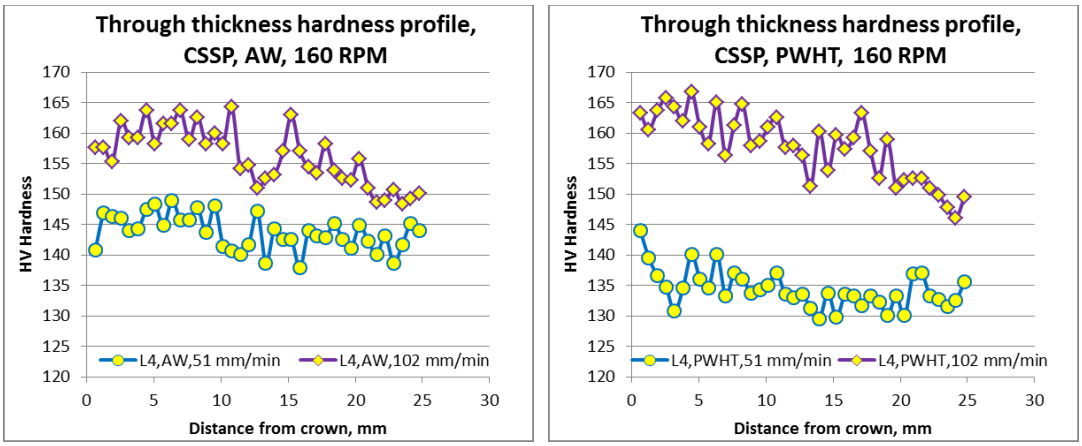

(a) CSSP: AW (#4299 & #4300) (b) CSSP: PWHT (#4299 & #4300)

Figure 4.28 Through thickness hardness profiles on the weld centerline in (a) AW and (b) PWHT conditions of CSSP with different welding speed: 160 RPM, T+3F pin

Figure 4.28 (#4299 & #4300) shows hardness profiles as a function of distance from the weld crown on the weld centerline in (a) AW and (b) PWHT conditions of CSSP with a welding speed of 51 mm/min and 102 mm/min: 160 RPM, T+3F pin, 0.9 mm flat depth. Both joints were produced with a setup of 1°, a rotation rate of 160 rpm, by a T+3F tool with a flat/flute depth of 0.9 mm. Figure 4.28 (a) and (b) show the differences in hardness profiles through thickness in AW and PWHT conditions of joints produced by different welding speeds.

Figure 4.28 (a) shows that, in AW conditions, relative to the joint produced by the lower welding speed (51 mm/min), in the joint produced by the higher welding speed (102 mm/min), hardness through thickness was at a little larger level and varied with a

little larger range. Generally, difference in hardness was similar from crown to the mid-plane, while decreased from mid-plane to the root. Hardness in two joints was quite similar at the mid-plane and near root. In the joint produced by the lower welding speed (51 mm/min), minimum hardness appeared nearby the mid-plane while max hardness appeared near the weld crown. In the joint produced by the higher welding speed (102 mm/min), minimum hardness appeared near the weld root, while max hardness appeared nearby the mid-plane.

Figure 4.28 (b) shows that, in PWHT conditions, relative to the joint produced by the lower welding speed (51 mm/min), in the joint produced by the higher welding speed (102 mm/min), hardness through thickness was at a larger level and varied with a larger range. Generally, difference in hardness gradually decreased from crown to the root. In the joint produced by the lower welding speed (51 mm/min), minimum hardness appeared nearby the mid-plane while max hardness appeared quite close to the weld crown. In the joint produced by the higher welding speed (102 mm/min), minimum hardness appeared near the weld root, while max hardness appeared near the crown.

Different thermal boundary conditions (TBCs) are described as following: “Original” TBC means steel backing plate was applied underneath the work-piece, and no water spray were applied on the work-piece surface; “CBP” TBC means the composite backing plate was applied underneath the work-piece, and no water spray were applied on the work-piece surface; “WS” TBC means the steel backing plate was applied underneath the work-piece, and water spray were applied on the work-piece surface; “WS+CBP” TBC means the composite backing plate was applied underneath the work-piece, and water spray were applied on the work-piece surface.

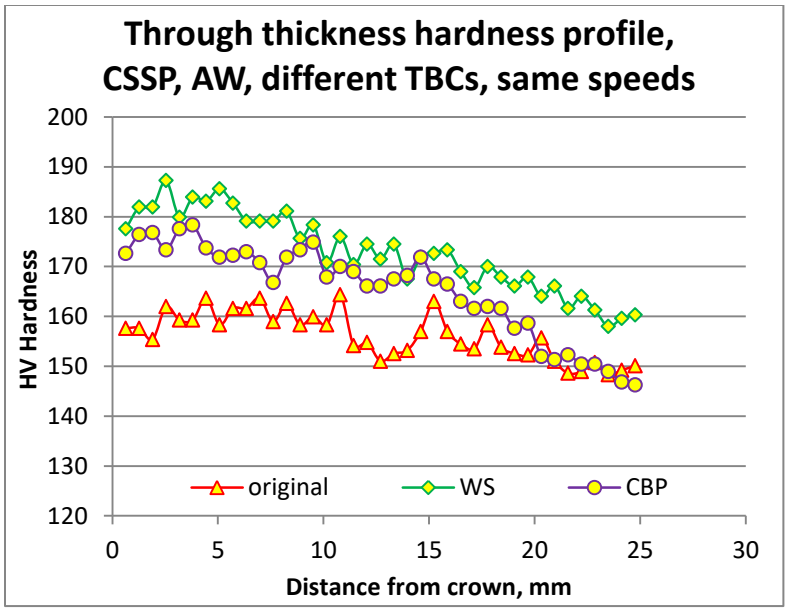

Figure 4.29 Through thickness hardness profiles on the weld centerline in CSSP: different thermal boundary conditions, AW, a rotation rate of 160 RPM, a welding speed of 102 mm/min, AW

Figure 4.29 (#4300, #4165 & #4166) shows through thickness hardness profiles as a function of distance from the weld crown on the weld centerline in AW condition of CSSP joints produced with different TBCs (original, WS, and CBP) and same speeds. All joints were produced with a setup of 1° , a rotation rate of 160 rpm, a welding speed of 102 mm/min, by a T+3F tool with a flat depth of 0.9 mm.

Figure 4.29 shows that, in AW conditions, under the same speeds, relative to the joint produced with the "original" TBCs, in the joint produced with "WS" TBCs, hardness through thickness was at larger level and varied with a larger range; relative to the joint produced with the "original" TBCs, in the joint produced with "CBP" TBCs, hardness through thickness was similar near root and at a little larger level at other heights, and varied with a larger range; relative to the joint produced with the "CBP" TBCs, in the joint produced with "WS" TBCs, hardness through thickness was a little larger near root and slightly larger at other heights, and varied with a slightly larger range.

It indicates that, relative to the "original" TBCs, both the "WS" TBCs and "CBP" TBCs increased the through thickness hardness and its variation range, except that the "CBP" TBCs had little effect on hardness near root.

4.2.3.2 Hardness distribution through thickness of CSSP and SSSP

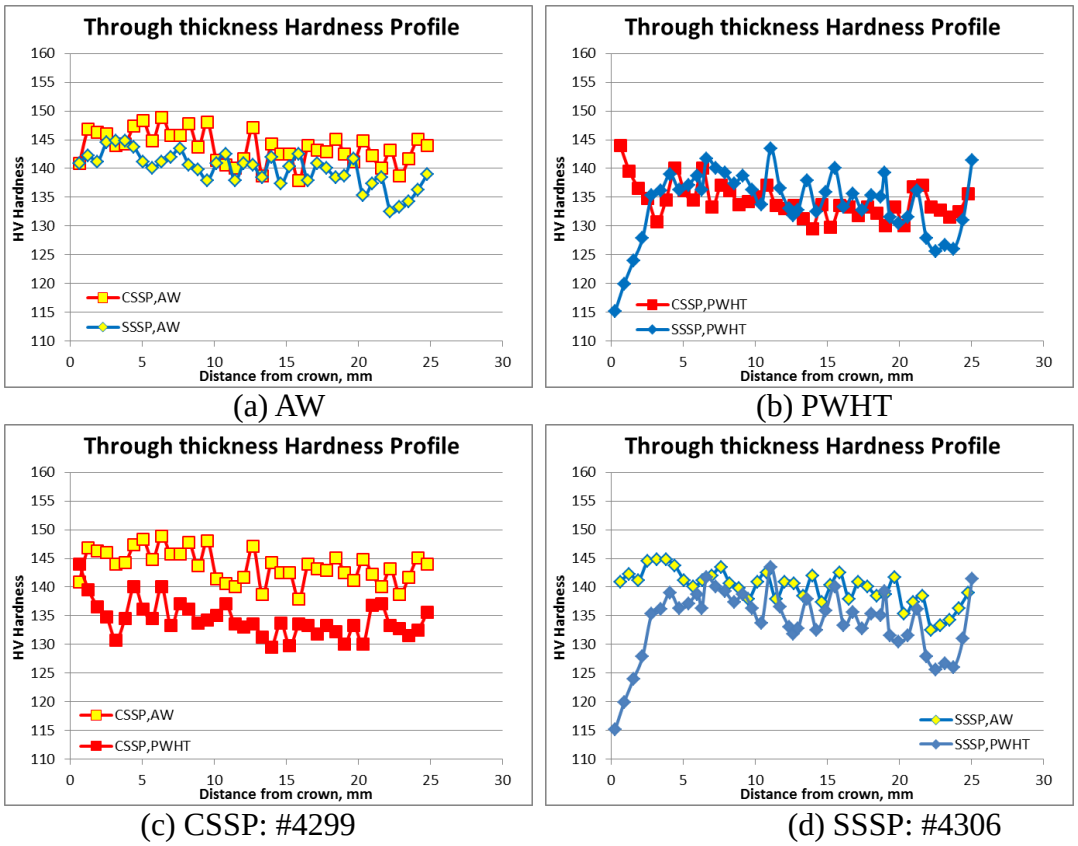

Figure 4.30 Through thickness hardness profiles on the weld centerline in conditions of CSSP (T+3F pin, #4299) and SSSP (T+3CT pin, #4306): (a) AW, (b) PWHT, (c) CSSP and (d) SSSP

Figure 4.30 shows hardness as a function of distance from weld crown on the weld centerline in AW and PWHT conditions of CSSP (#4299) and SSSP (#4306).

Figure 4.30 (a) shows the hardness profiles through thickness in AW condition of CSSP and SSSP. In the AW condition, relative to CSSP, hardness through thickness in SSSP was slightly smaller, and varied with a similar range. In both CSSP and SSSP, hardness increased slightly within a small distance from the weld crown. As for the CSSP

joint, the minimum hardness with a value of 138 appeared at a distance of 15.9 mm from the weld crown, while the maximum hardness with a value of 149 appeared at a distance of 6.4 mm from the weld crown. As for the SSSP joint, the minimum hardness with a value of 133 appeared near the root, at a distance of 22.2 mm from the weld crown, while the maximum hardness with a value of 145 appeared near crown, at a distance of 3.2 mm from the weld crown.

Figure 4.30 (b) shows the hardness profiles through thickness in PWHT condition of CSSP and SSSP. In the PWHT condition, relative to CSSP, hardness through thickness in SSSP was much smaller near crown, then be similar in the rest area, and varied with a much larger range. In CSSP, hardness decreased within a small distance from the weld crown. In SSSP, hardness increased within a small distance from the weld crown. As for the CSSP joint, the minimum hardness with a value of 130 appeared at a distance of 15.2 mm from the weld crown, while the maximum hardness with a value of 144 appeared at a distance of 0.64 mm from the weld crown. As for the SSSP joint, the minimum hardness with a value of 115 appeared quite near the root, at a distance of 0.3 mm from the weld crown, while the maximum hardness with a value of 141 appeared quite near the root, at a distance of 25 mm from the weld crown.

Figure 4.30 (c) shows the hardness profiles through thickness in AW and PWHT conditions of CSSP. It shows that, in the AW condition, the minimum hardness with a value of 138 appeared at a distance of 15.9 mm from the weld crown, while the maximum hardness with a value of 149 appeared at a distance of 6.4 mm from the weld crown. In the PWHT condition, the minimum hardness with a value of 130 appeared at a distance of 15.2 mm from the weld crown, while the maximum hardness with a value of

144 appeared at a distance of 0.64 mm from the weld crown. It shows that, in both AW and PWHT conditions, minimum hardness appeared nearby the mid-plane of the joint in both AW and PWHT conditions, while maximum hardness in PWHT condition appeared at the location closer to the weld crown than that in AW condition. It shows that hardness varied with the similar range in AW and PWHT conditions. It also indicates that relative to AW condition, PWHT reduced hardness through thickness except the hardness measured 0.64 mm away from the weld crown.

Figure 4.30 (d) shows the hardness profiles through thickness in AW and PWHT conditions of SSSP. It shows that, in the AW condition, the minimum hardness with a value of 133 appeared near the root, at a distance of 22.2 mm from the weld crown, while the maximum hardness with a value of 145 appeared near crown, at a distance of 3.2 mm from the weld crown. In the PWHT condition, the minimum hardness with a value of 115 appeared quite near the root, at a distance of 0.3 mm from the weld crown, while the maximum hardness with a value of 141 appeared quite near the root, at a distance of 25 mm from the weld crown. It indicates that, relative to AW, PWHT increased the hardness variation range, reduced the hardness through thickness in SSSP, especially near crown.

Figure 4.30 (c) and (d) indicate that, relative to AW, in CSSP, PWHT affected hardness variation range little, and reduced hardness through thickness except the hardness measured 0.64 mm away from weld crown. However, in SSSP, PWHT reduced hardness through thickness except hardness measured 0.64 mm away from weld crown.

4.2.4 Transverse hardness distribution

Hardness tests were performed transverse to weld at various depths near crown, at mid-plane, and near root in both AW and PWHT conditions of the CSSP and SSSP joints.

Transverse hardness profiles were shown in Figure 4.31 a~h for CSSP joints and Figure 4.32 a~e for SSSP joints. HAZ minimum hardness at AS and RS, HAZ width, nugget average hardness were extracted from those transverse hardness profiles and plotted in Figure 4.33~ Figure 4.36.

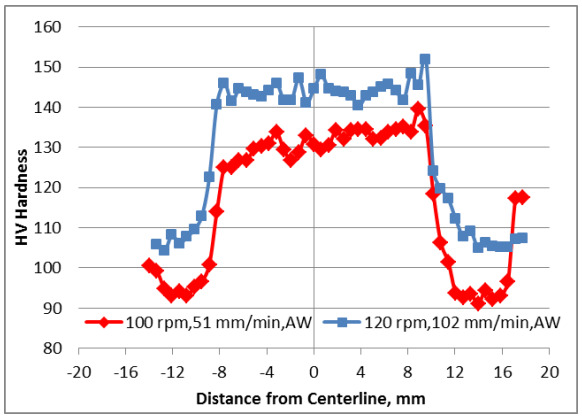

(a) #4154A: 51 mm/min; #4154C: 102 mm/min

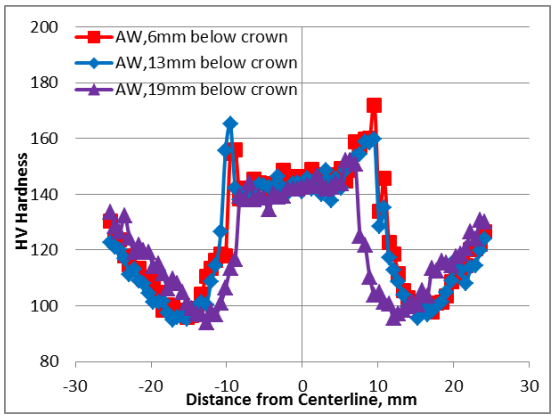

(b) #4299, AW

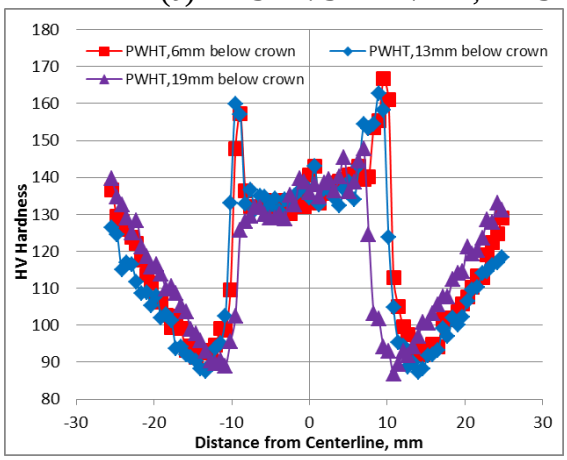

(c) #4299, PWHT

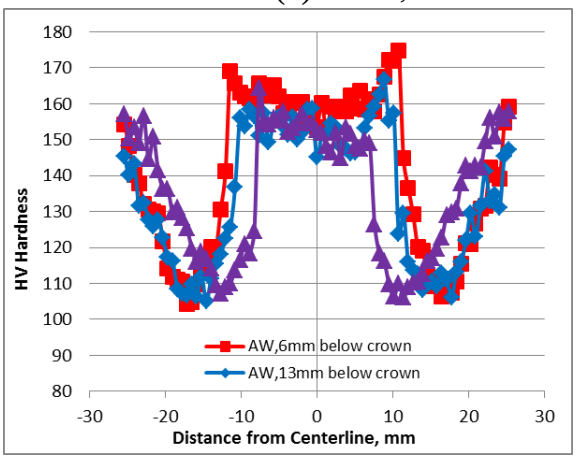

(d) #4300, AW

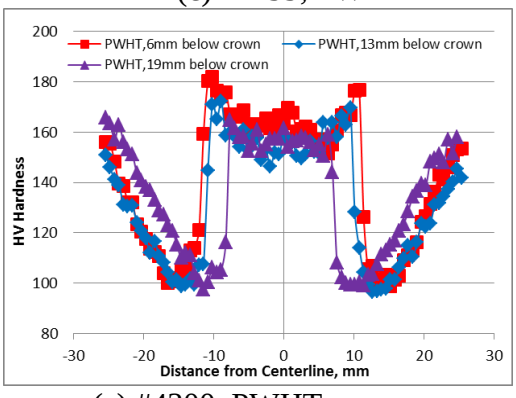

(e) #4300, PWHT

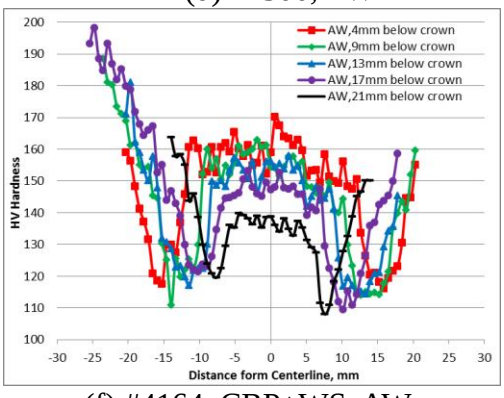

(f) #4164, CBP+WS, AW

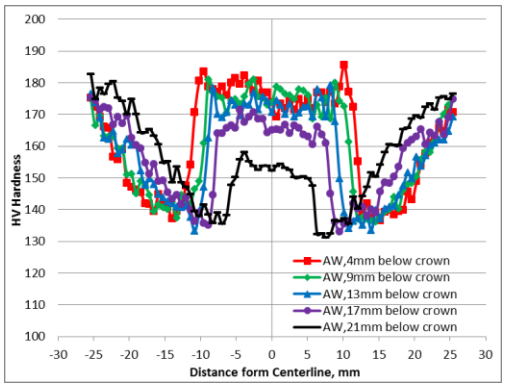

(g) #4165, CBP, AW

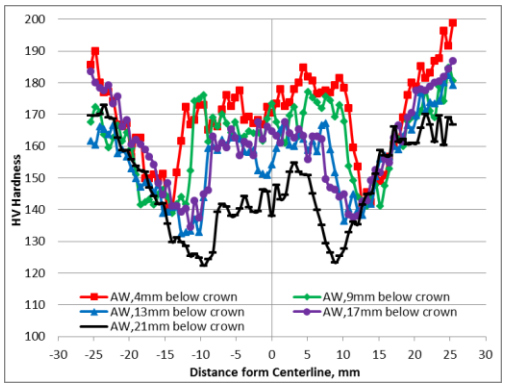

(h) #4166, WS, AW

Figure 4.31 Transverse hardness profiles of CSSP at various depths: near crown, at mid-plane, and near root in both AW and PWHT conditions

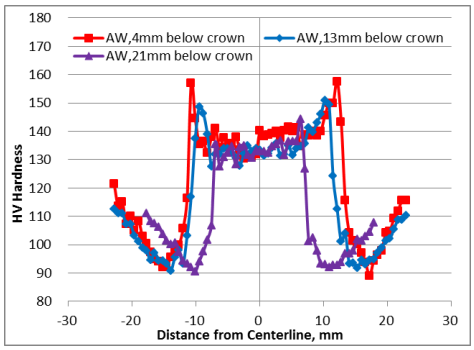

(a) #4167A, AW

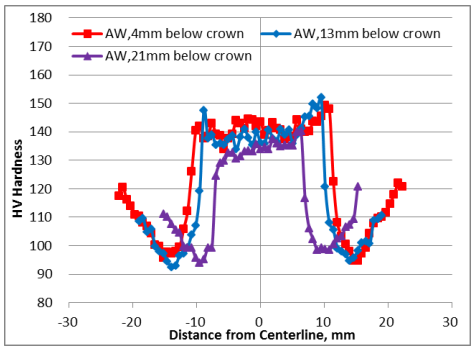

(b) #4167B, AW

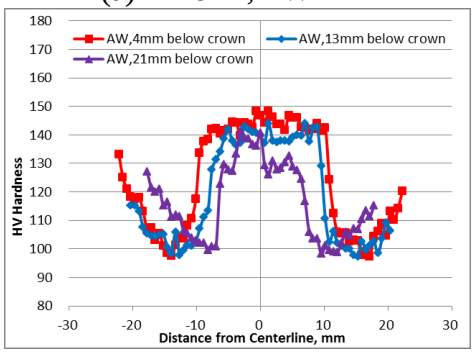

(c) #4167C, AW

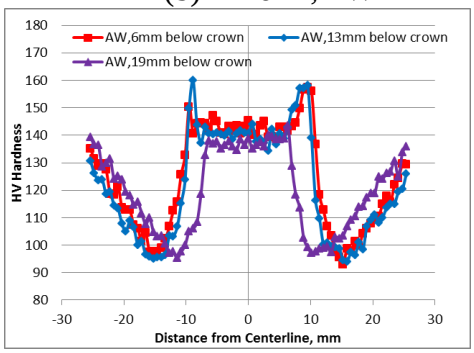

(d) #4306, AW

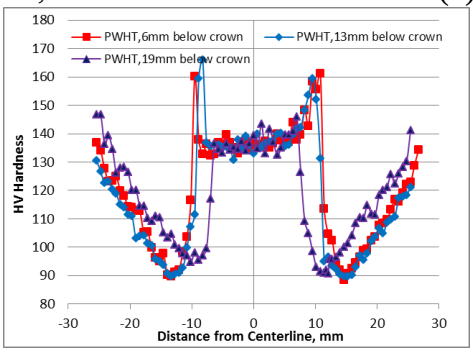

(e) #4306, PWHT

Figure 4.32 Transverse hardness profiles of SSSP at various depths near crown, at mid-plane, and near root in both AW and PWHT conditions

4.2.4.1 Transverse hardness distribution of CSSP

HAZ minimum hardness at AS and RS, HAZ width, nugget average hardness were extracted from transverse hardness profiles of CSSP joints and plotted in Figure 4.33 and Figure 4.34.

4.2.4.1.1 Effects of rotation rate and welding speed on transverse hardness in CSSP

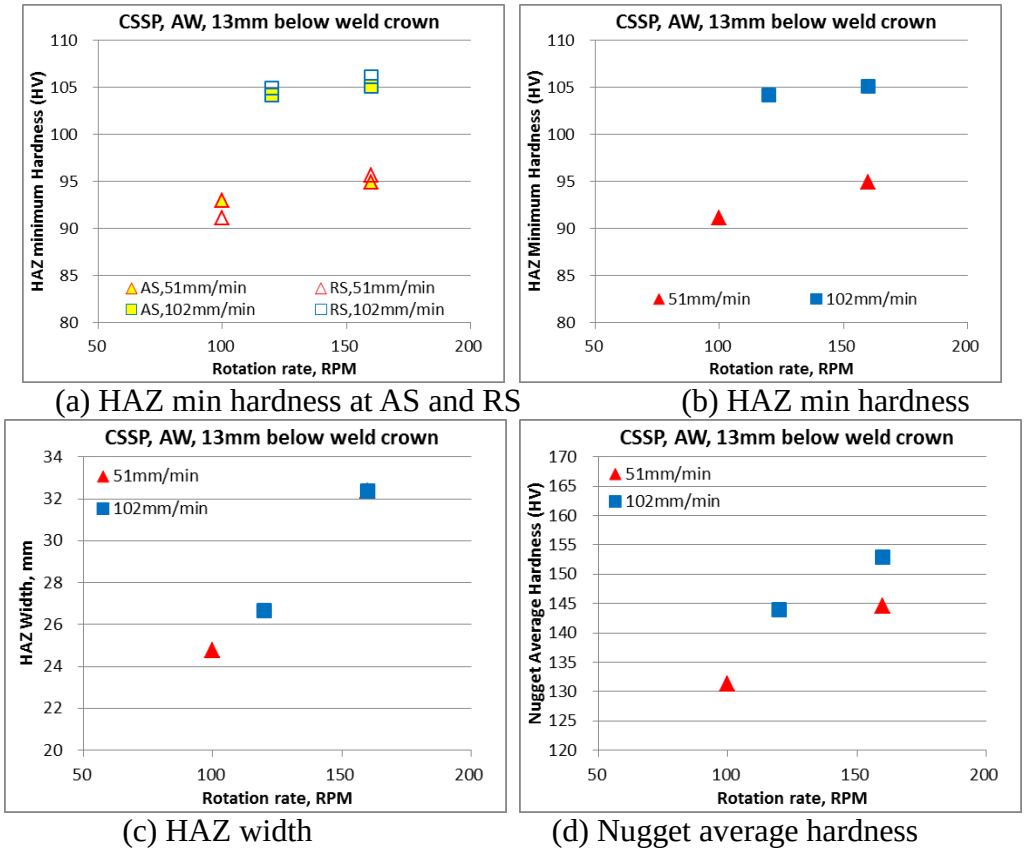

(a) HAZ min hardness at AS and RS (b) HAZ min hardness

(c) HAZ width (d) Nugget average hardness

Figure 4.33 (a) HAZ min hardness at AS and RS, (b) HAZ min hardness, (c) HAZ width, and (d) Nugget average hardness at mid-plane as functions of rotation rate of transverse CSSP: AW

Figure 4.33 shows effects of rotation rate and welding speed on transverse hardness in CSSP. Hardness tests were performed transverse to weld at depths of 13 mm

(at mid-plane) below the weld crown in AW condition of four CSSP joints: #4154A, #4299, #4154C and #4300.

Figure 4.33 (a) shows the HAZ min hardness at AS and RS at mid-plane (13 mm below the weld crown) of transverse CSSP joints in AW condition as functions of rotation rate. It shows that, under the same rotation rate, higher welding speed resulted in larger HAZ min hardness at either AS or RS. Under the same rotation rate, HAZ min hardness at AS and RS were similar in joints produced with different welding speed. When rotation rate increased, in the joints produced by the lower welding speed (51 mm/min), HAZ min hardness at AS and RS slightly increased ,while in the joints produced by the higher welding speed (102 mm/min), HAZ min hardness at AS and RS were similar.

Figure 4.33 (b) shows the HAZ min hardness at mid-plane (13 mm below the weld crown) of transverse CSSP joints in AW condition as functions of rotation rate. It shows that, under the same rotation rate, higher welding speed resulted in larger HAZ min hardness. When rotation rate increased, in the joints produced by the lower welding speed (51 mm/min), HAZ min hardness slightly increased ,while in the joints produced by higher welding speed (102 mm/min), HAZ min hardness at AS and RS were similar. It indicates that when lower welding speed (51 mm/min) was applied, HAZ min hardness was more sensitive to rotation rate, and increased faster with rotation rate increasing.

Figure 4.33 (c) shows the HAZ width at mid-plane (13 mm below the weld crown) of transverse CSSP joints in AW condition as functions of rotation rate. It shows that, under the same rotation rate, higher welding speed resulted in similar HAZ width. When rotation rate increased, HAZ width increased with the same slope in joints produced by

lower (51 mm/min) and higher welding speed (102 mm/min). It indicates that HAZ min hardness was more sensitive to rotation rate, while affected little by welding speed.

Figure 4.33 (d) shows the nugget average hardness at mid-plane (13 mm below the weld crown) of transverse CSSP joints in AW condition as functions of rotation rate. It shows that, under the same rotation rate, higher welding speed resulted in larger nugget average hardness. When rotation rate increased, nugget average hardness increased with the same slope in the joints produced by the lower welding speed (51 mm/min) and the higher welding speed (102 mm/min).

4.2.4.1.2 Effects of thermal boundary conditions on transverse hardness in CSSP

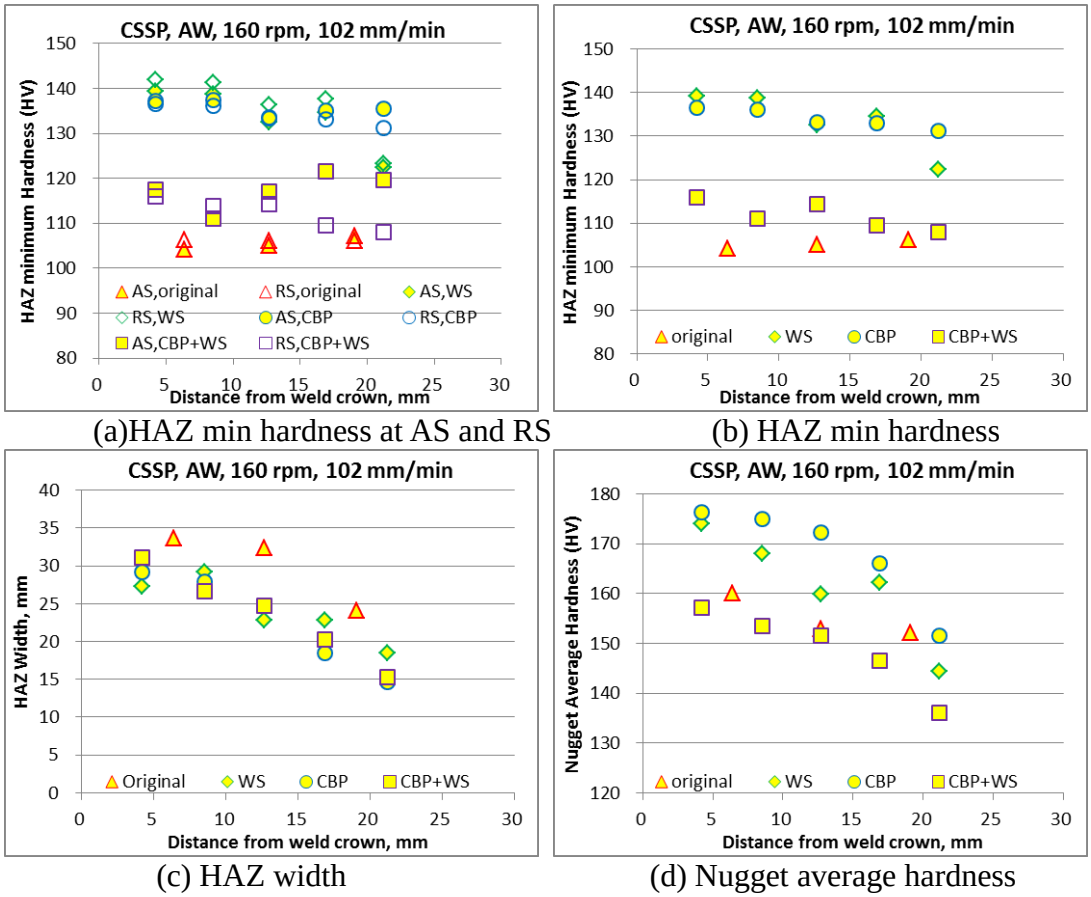

(a)HAZ min hardness at AS and RS (b) HAZ min hardness

(c) HAZ width (d) Nugget average hardness

Figure 4.34 (a) HAZ min hardness at AS and RS, (b) HAZ min hardness, (c) HAZ width, and (d) Nugget average hardness as functions of distance from weld crown of transverse CSSP: different TBCs, a rotation rate of 160 RPM, a welding speed of 102 mm/min, AW

Figure 4.34 shows effects of thermal boundary conditions on transverse hardness in CSSP. Hardness tests were performed transverse to weld from crown to root, at depths ranging from 4 mm to 21 mm below the weld crown in AW condition of four CSSP joints: #4164, #4165, #4166 and #4300.

Figure 4.34 (a) shows the HAZ min hardness at AS and RS at various depths of transverse CSSP joints produced with different thermal boundary conditions and same speeds as functions of distance from weld crown. It shows that:

When original TBCs (steel backing plate underneath the work-piece, and no water spray on the work-piece surface) were applied, at the same depth from crown, HAZ min hardness at AS and RS were similar; HAZ min hardness was affected little by the increase of the distance from weld crown. When WS TBCs (steel backing plate underneath the work-piece, and water spray on the work-piece surface) were applied, at the same depth from crown, HAZ min hardness at AS and RS were similar; With the increase of the distance from weld crown, HAZ min hardness was much smaller at root, while were similar at other depths. When CBP TBCs (composite backing plate underneath the work-piece, and no water spray on the WP surface) were applied, in the upper half transverse joint (within 12.7 mm below the crown), at the same depth from crown, HAZ min hardness at AS and RS were similar; in the lower half transverse joint (12.7~25.4 mm below the crown), at the same depth from crown, HAZ min hardness at AS was slightly larger than that at RS, which might due to the effect of CBP. When the distance from weld crown increased, HAZ min hardness at AS were similar, and HAZ min hardness at RS decreased slightly. When both WS and CBP were applied, in the upper half transverse joint (within 12.7 mm below the crown), at the same depth from

crown, HAZ min hardness at AS and RS were similar; in the lower half transverse joint (12.7~25.4 mm below the crown), at the same depth from crown, HAZ min hardness at AS was larger than that at RS, which might due to the effect of CBP. When the distance from weld crown increased, HAZ min hardness at AS decreased first then increased slightly, and HAZ min hardness at RS decreased slightly.

Figure 4.34 (b) shows the HAZ min hardness at various depths of transverse CSSP joints produced with different thermal boundary conditions and same speeds as functions of distance from weld crown. It shows that:

When original thermal boundary conditions (steel backing plate underneath the work-piece, and no water spray on the work-piece surface) were applied, HAZ min hardness was affected little by the increase of the distance from weld crown.

When WS thermal boundary conditions (steel backing plate underneath the work-piece, and water spray on the work-piece surface) were applied, with the increase of the distance from weld crown, HAZ min hardness was much smaller at root, while were similar at other depths.

When CBP thermal boundary conditions (composite backing plate underneath the work-piece, and no water spray on the work-piece surface) were applied, when the distance from weld crown increased, HAZ min hardness was similar.

When both WS and CBP were applied, with the distance from weld crown increasing, HAZ min hardness slightly decreased.

Figure 4.34 (c) shows the HAZ width at various depths of transverse CSSP joints produced with different thermal boundary conditions and same speeds as functions of the distance from weld crown. It shows that:

When original thermal boundary conditions (steel backing plate underneath the work-piece, and no water spray on the work-piece surface) were applied, with the distance from weld crown increasing, HAZ width decreased.

When WS thermal boundary conditions (steel backing plate underneath the work-piece, and water spray on the work-piece surface) were applied, with the increase of the distance from weld crown, HAZ width first increased slightly, then decreased.

When CBP thermal boundary conditions (composite backing plate underneath the work-piece, and no water spray on the work-piece surface) were applied, when the distance from weld crown increased, HAZ width decreased.

When both WS and CBP were applied, with the distance from weld crown increasing, HAZ width decreased.

Figure 4.34 (d) shows the nugget average hardness at various depths of transverse CSSP joints produced with different thermal boundary conditions and same speeds as functions of distance from weld crown. It shows that:

When original thermal boundary conditions (steel backing plate underneath the work-piece, and no water spray on the work-piece surface) were applied, with the distance from weld crown increasing, nugget average hardness decreased with a decreasing slope.

When WS thermal boundary conditions (steel backing plate underneath the work-piece, and water spray on the work-piece surface) were applied, with the increase of the distance from weld crown, nugget average hardness decreased.

When CBP thermal boundary conditions (composite backing plate underneath the work-piece, and no water spray on the work-piece surface) were applied, when the

distance from weld crown increased, nugget average hardness decreased with an increasing slope. When both WS and CBP were applied, with the distance from weld crown increasing, nugget average hardness decreased with an increasing slope.

4.2.4.2 Transverse hardness distribution of SSSP

HAZ minimum hardness, HAZ width, nugget average hardness were extracted from transverse hardness profiles of SSSP and plotted in Figure 4.35 and Figure 4.36.

4.2.4.2.1 Effects of rotation rate on transverse hardness in SSSP

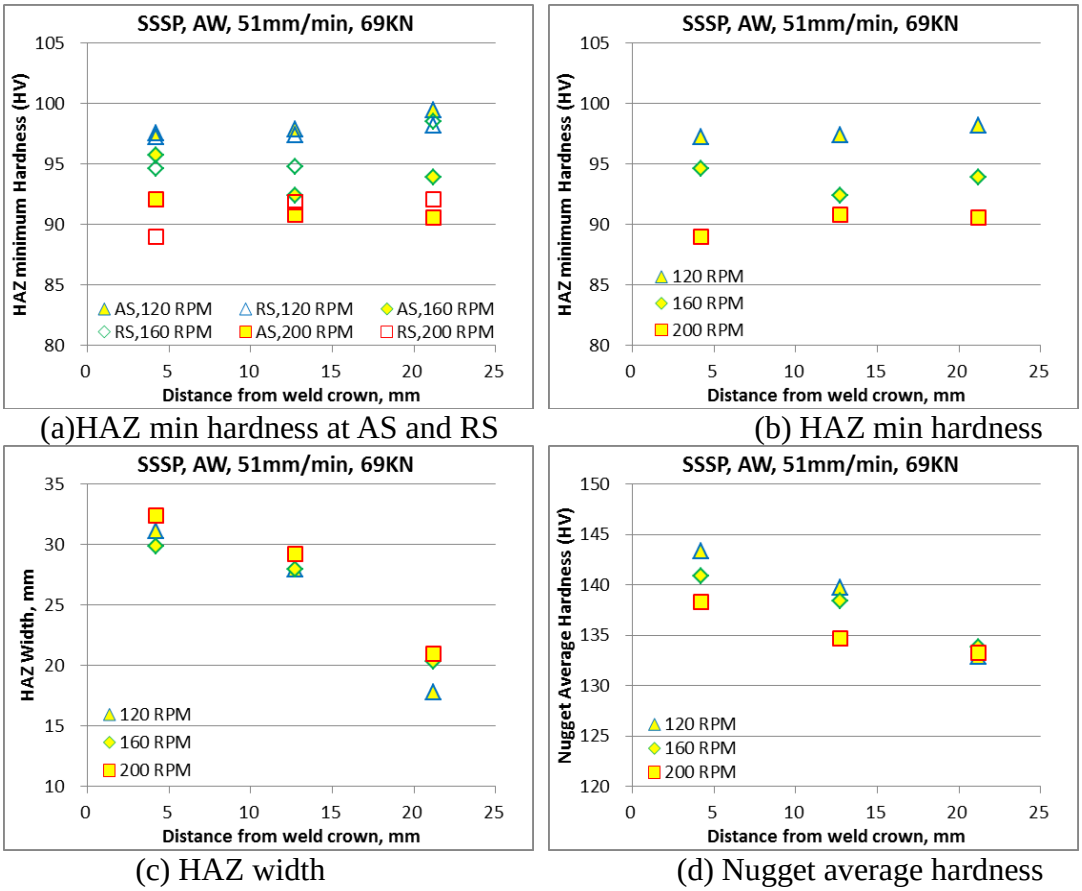

(a)HAZ min hardness at AS and RS (b) HAZ min hardness

(c) HAZ width (d) Nugget average hardness

Figure 4.35 (a) HAZ min hardness at AS and RS, (b) HAZ min hardness, (c) HAZ width, and (d) Nugget average hardness as functions of distance from weld crown of transverse SSSP: different rotation rates, the same welding speed of 102 mm/min, the same forge force of 69 KN, AW

Figure 4.35 shows effects of rotation rate on transverse hardness in SSSP. Hardness tests were performed transverse to weld at depths of 4 mm (near crown), 13

mm (at mid-plane) and 21 mm (near root) below the weld crown in AW condition of three SSSP joints: #4167A, #4167B, and #4167C.

Figure 4.35 (a) shows the HAZ min hardness at AS and RS at various depths of transverse SSSP joints produced with different rotation rates and same welding speed as functions of distance from weld crown. It shows that:

At the same depth below the weld crown, under the same rotation rate, HAZ min hardness at AS and RS were similar in the same joint;

At the same depth below the weld crown, when rotation rate increased, HAZ min hardness at AS and RS decreased.

Under the same rotation rate, when the distance from weld crown increased, in the joints produced with a rotation rate of 120 RPM, HAZ min hardness at AS and RS slightly increased; in the joints produced with a rotation rate of 160 RPM, HAZ min hardness at AS decreased first then increased, while HAZ min hardness at RS slightly increased; in the joints produced with a rotation rate of 200 RPM, HAZ min hardness at AS slightly decreased, while HAZ min hardness at RS slightly increased at a decreasing slope.

Figure 4.35 (b) shows the HAZ min hardness at various depths of transverse SSSP joints produced with different rotation rates and same welding speed as functions of distance from weld crown. It shows that: At the same depth below the weld crown, when rotation rate increased, HAZ min hardness decreased. Under the same rotation rate, when the distance from weld crown increased, in the joints produced with a rotation rate of 120 RPM, HAZ min hardness slightly increased; in the joints produced with a rotation rate of

160 RPM, HAZ min hardness decreased first then increased; in the joints produced with a rotation rate of 200 RPM, HAZ min hardness slightly increased at a decreasing slope.

Figure 4.35 (c) shows the HAZ width at various depths of transverse SSSP joints produced with different rotation rates and same welding speed as functions of distance from weld crown. It shows that: At the same depths below the weld crown, HAZ widths produced by different rotation rates were similar near crown (4 mm below the crown) and at mid-plane (13 mm below the crown); while near root (21 mm below crown), HAZ widths produced by 160 RPM and 200 RPM were similar and were a little larger than that produced by 120 RPM. When distance from weld crown increased, HAZ widths decreased with the similar slopes in joints produced by different rotation rates. It indicates that HAZ width was affected little by rotation rate.

Figure 4.35 (d) shows the nugget average hardness at various depths of transverse SSSP joints produced with different rotation rates and same welding speed as functions of distance from weld crown. It shows that: Nugget average hardness near crown (4 mm below the crown) decreased slightly with rotation rate increasing. At mid-plane (13 mm below the crown), nugget average hardness of joints produced by 120 RPM and 160 RPM were similar and a little larger than that produced by 200 RPM. Nugget average hardnesses near root (21 mm below the crown) were similar with rotation rate increasing. When distance from weld crown increased, nugget average hardness decreased at slopes which decreased when rotation rate increased. The nugget average hardness near root was smaller than at mid-plane or near crown, indicating that the peak temperature near root was likely lower than that at mid-plane and near crown. Results of GS at those different

locations are needed. It also indicates that the increase of distance from weld crown decreased the already slight effect of rotation rate on nugget average hardness.

4.2.4.3 Transverse hardness distribution of CSSP and SSSP

Hardness tests were performed transverse to weld at depths of 6.4 mm (near crown), 12.7 mm (at mid-plane), and 19.1 mm (near root) below the weld crown in both AW and PWHT conditions of CSSP (#4299) and SSSP (#4306). The power input of #4299 is 5.3 KW, resulting in a peak temperature measured at pin center of 484℃.Transverse hardness profiles at various depths of below the weld crown in both AW and PWHT conditions of this CSSP joint were shown in Figure 4.31(b) and Figure 4.31(c), respectively. The power input of #4306 is 5.2 KW, resulting in a peak temperature measured at pin center of 477℃. Transverse hardness profiles at various depths of below the weld crown in both AW and PWHT conditions of this SSSP joint were shown in Figure 4.32 (h) and Figure 4.32 (i), respectively. Those transverse hardness profiles all have characteristic "W" shape, which is typical hardness distribution of FSW in precipitation hardening aluminum alloys when the peak weld temperature is near or at the solution heat treat temperature (474℃ for AA7099-T7651). HAZ minimum hardness at AS and RS, HAZ width, nugget average hardness of the above comparable CSSP (#4299) and SSSP (#4306) joints were extracted from transverse hardness profiles and plotted in Figure 4.36, which shows effects of different FSW shoulders on transverse hardness in SP.

Figure 4.36(a) shows the HAZ min hardness at AS and RS at various depths of transverse SP joints produced with the same speeds as functions of distance from weld crown. It shows that:

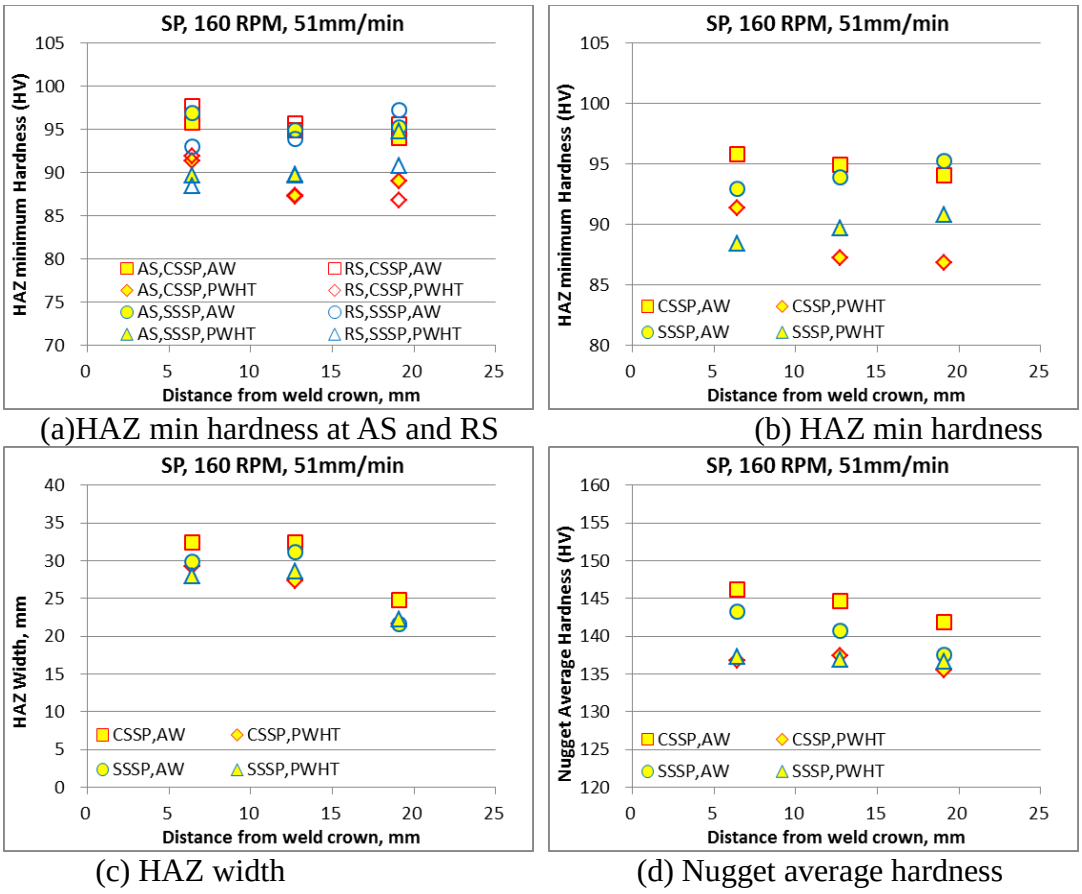

(a)HAZ min hardness at AS and RS (b) HAZ min hardness

(c) HAZ width (d) Nugget average hardness

Figure 4.36 (a) HAZ min hardness at AS and RS, (b) HAZ min hardness, (c) HAZ width, and (d) Nugget average hardness as functions of distance from weld crown of transverse SP: rotation rate 160 RPM, welding speed 51 mm/min, AW and PWHT

(1) In AW condition of CSSP, at different depths below the weld crown, HAZ min hardness at RS was a little larger than/similar with that at AS. When the distance from weld crown increased, HAZ min hardness at AS and RS decreased slightly.

(2) In AW condition of SSSP, relative to HAZ min hardness at RS, HAZ min hardness at AS was larger near crown, a little larger/similar at mid-plane, and a little smaller/similar near root. When distance from weld crown increased, HAZ min hardness slightly decreased with a decreasing slope at AS, increased slightly at RS.

(3) In PWHT condition of CSSP, relative to HAZ min hardness at RS, HAZ min hardness at AS was similar near crown and at mid-plane, and a little larger/similar near

root. When the distance from weld crown increased, HAZ min hardness at AS and RS slightly decreased with a decreasing slope.

(4) In PWHT condition of SSSP, relative to HAZ min hardness at RS, HAZ min hardness at AS was a little larger /similar near crown, similar at mid-plane, and larger near root. When the distance from weld crown increased, HAZ min hardness at AS and RS slightly decreased with a decreasing slope.

(5) In AW condition of SP, at AS, HAZ min hardness in SS were similar with that in CS at various depths below weld crown. When the distance from weld crown increased, HAZ min hardness at AS and RS slightly decreased.

(6) In PWHT condition of SP, at AS, relative to HAZ min hardness in CS, HAZ min hardness in SS was a little smaller /similar near crown, a little larger/similar at mid-plane, and larger near root. When the distance from weld crown increased, HAZ min hardness slightly decreased then increased slightly in CS, while slightly increased in SS.

(7) In AW condition of SP, at RS, relative to HAZ min hardness in CS, HAZ min hardness in SS was smaller near crown, a little smaller/similar at mid-plane, and a little larger/similar near root. When distance from weld crown increased, HAZ min hardness slightly decreased with a decreasing slope in CS, while slightly increased in SS.

(8) In PWHT condition of SP, at RS, relative to HAZ min hardness in CS, HAZ min hardness in SS was smaller near crown, a little larger/similar at mid-plane, and larger near root. When distance from weld crown increased, HAZ min hardness in CS slightly decreased with a decreasing slope, while HAZ min hardness in SS slightly increased.

Figure 4.36(b) shows HAZ min hardness at various depths of transverse SP joints produced with the same speeds as functions of distance from weld crown. It shows that:

(1) In AW condition, relative to HAZ min hardness of CSSP, HAZ min hardness of SSSP was smaller near crown, a little smaller/similar at mid-plane, and a little larger/similar near root. When distance from weld crown increased, HAZ min hardness of CSSP decreased slightly, while HAZ min hardness of SSSP increased slightly.

(2) In PWHT condition, relative to HAZ min hardness of CSSP, HAZ min hardness of SSSP was smaller near crown, a little larger/similar at mid-plane, and larger near root. When the distance from weld crown increased, HAZ min hardness of CSSP decreased with a decreasing slope, while HAZ min hardness of SSSP increased slightly.

(3) In CSSP, relative to AW, PWHT reduced HAZ minimum hardness, and the difference increased with the increase of distance from weld crown. In SSSP, relative to AW, PWHT reduced HAZ minimum hardness, and the difference was constant with the increase of distance from weld crown. Relative to CSSP, PWHT reduced the HAZ minimum hardness in SSSP by a less extent.

Figure 4.36(c) shows the HAZ width at various depths of transverse SP joints produced with the same speeds as functions of distance from weld crown. It shows that:

(1) In AW condition, relative to HAZ width of CSSP, HAZ width of SSSP was a little smaller /similar near crown, similar at mid-plane, and a little smaller/similar near root. When the distance from weld crown increased, HAZ width of CSSP kept constant then began to decrease, while HAZ width of SSSP increased slightly then decreased.

(2) In PWHT condition, relative to HAZ width of CSSP, HAZ width of SSSP was similar at various depths below the weld crown. When the distance from weld crown increased, HAZ width of CSSP and SSSP kept constant then began to decrease.

(3) In CSSP, relative to AW, PWHT reduced HAZ width, and the differences were near crown and root, which were a little smaller than the difference at mid-plane. In SSSP, relative to AW, PWHT reduced HAZ width a little near crown and at mid-plane, while PWHT affect HAZ width little near root. Relative to CSSP, PWHT reduced the HAZ width in SSSP by a less extent.

Figure 4.36(d) shows nugget average hardness at AS and RS at various depths of transverse single pass (SP) full penetrated joints produced with the same speeds as functions of distance from weld crown. It shows that:

(1) In AW condition, at various depths below the weld crown, nugget average hardness of SSSP was little smaller than that of CSSP. When the distance from weld crown increased, nugget average hardness of SP decreased, while nugget average hardness of SSSP decreased a little faster than that of CSSP.

(2) In PWHT condition, at various depths below the weld crown, nugget average hardness of SSSP was similar with that of CSSP. When the distance from weld crown increased, HAZ width of CSSP and SSSP kept constant.

(3) In CSSP, relative to AW, PWHT reduced nugget average hardness, and the differences decreased from weld crow to root. In SSSP, relative to AW, PWHT reduced nugget average hardness a little, and the differences decreased from weld crow to root. Relative to CSSP, PWHT reduced HAZ width in SSSP by a less extent.

4.2.5 Tensile Testing Properties

Rotating and stationary shoulders result in different heat sources in FSW, affecting thermal distribution, microstructure and properties through thickness of joints.

In this section, transverse and longitudinal tensile testing in SP have been performed to investigate effects of CS and SS on joint's tensile properties like UTS, YS and EL.

4.2.5.1 Transverse Tensile Testing (AW&PWHT)

4.2.5.1.1 CSSP: Transverse Tensile Testing

Figure 4.37 a~j show the engineering stress as a function of engineering strain of transverse tensile testing on CSSP joints in AW and PWHT conditions. In each condition, there were 1~3 samples from the same joint tested. In this section, transverse tensile

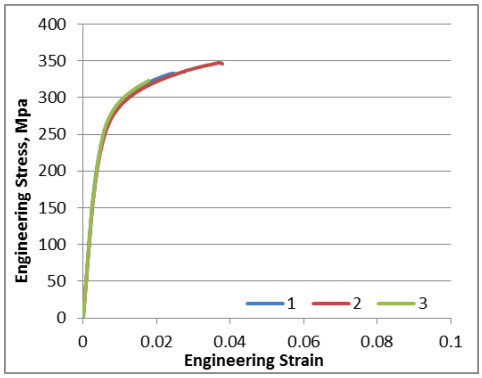

(a)#4156A, PWHT

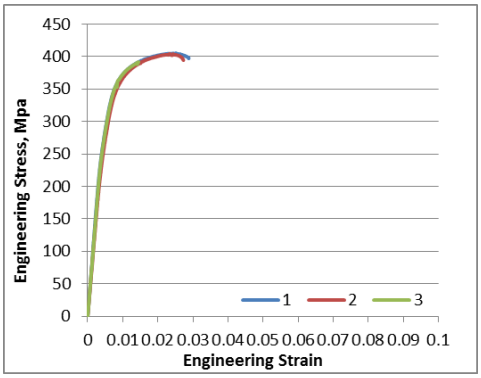

(b) #4156B, PWHT

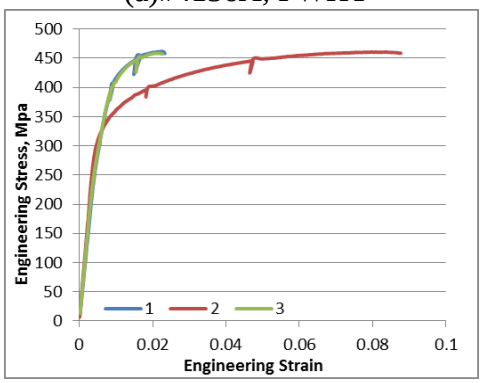

(c) #4164, PWHT

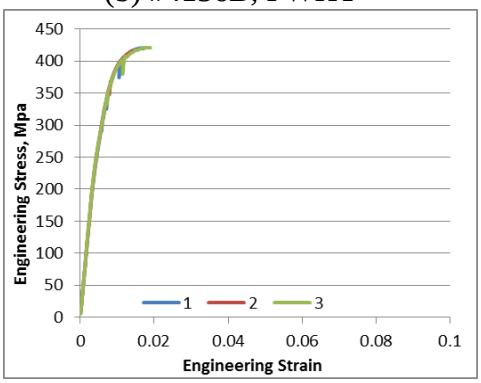

(d) #4165, PWHT

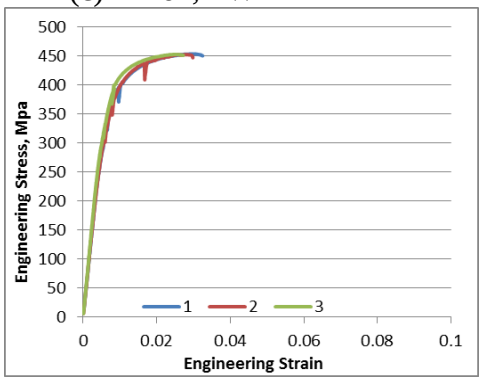

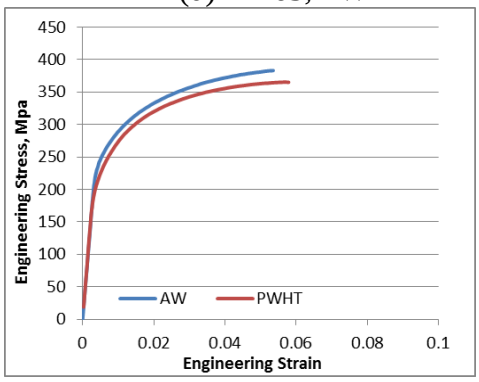

(e) #4166, PWHT (f) #4299

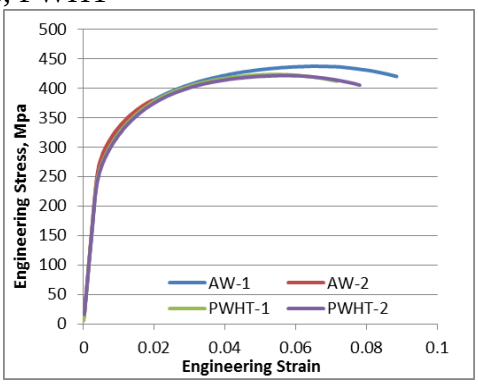

(g) #4300

Figure 4.37 Engineering stress and strain curves of transverse tensile testing in CSSP

testing was performed on some CSSP joints as following: #4156A (100 rpm, 51 mm/min, Original), #4156B (120 rpm, 102 mm/min, Original), #4164 (160 rpm, 102 mm/min, WS+CBP), #4165 (160 rpm, 102 mm/min, CBP), #4166 (160 rpm, 102 mm/min, WS), #4299 (160 rpm, 51 mm/min, Original), and #4300 (160 rpm, 102 mm/min, Original). Different thermal boundary conditions are described as following: “Original” thermal boundary condition means steel backing plate was applied underneath the work-piece, and no water spray were applied on the work-piece surface; “CBP” thermal boundary condition means the composite backing plate was applied underneath the work-piece, and no water spray were applied on the work-piece surface; “WS” thermal boundary condition means the steel backing plate was applied underneath the work-piece, and water spray were applied on the work-piece surface; “WS+CBP” thermal boundary condition means the composite backing plate was applied underneath the work-piece, and water spray were applied on the work-piece surface. Through those engineering stress and strain curves shown in Figure 4.37, characteristic values like ultimate tensile strength (UTS), yield strength (YS) and elongation (EL) were calculated and average values were shown in Figure 4.38~Figure 4.39.

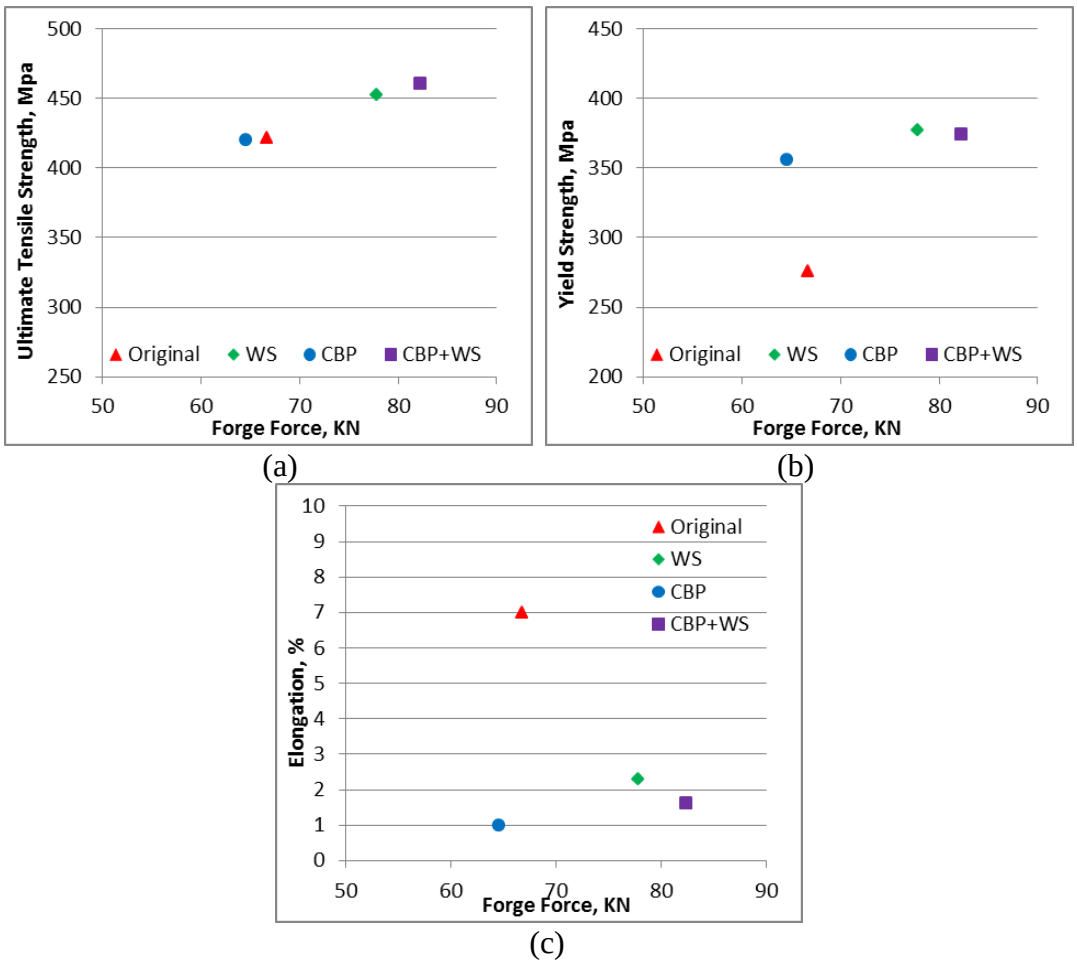

Figure 4.38 (a) Ultimate tensile strength, (b) yield strength and (c) elongation of transverse tensile testing in CSSP: different TBCs, a rotation rate of 160 RPM, a welding speed of 102 mm/min, PWHT

Figure 4.38 shows (a) ultimate tensile strength, (b) yield strength and (c) elongation of transverse tensile testing performed on CSSP joints in PWHT condition produced the same rotation rate of 160 RPM, the same welding speed of 102 mm/min, with different thermal boundary conditions as functions of applied forge forces. Figure 4.38 (a)~(c) show that, under the same speeds, relative to "original" TBCs, "WS" TBCs increased the UTS (7%), increased the YS (37%), and decreased the EL (-67%); "CBP" TBCs affected the UTS little, increased the YS (29%), and decreased the EL (-86%); "WS+CBP" TBCs increased the UTS (9%), increased the YS (36%), and decreased the

EL (-77%). It indicates that, both WS and CBP increased YS and decreased EL, and WS increased UTS to some extent while CBP affect the UTS little.

Figure 4.39 shows (a) ultimate tensile strength, (b) yield strength and (c) elongation of transverse tensile testing performed on CSSP joints in PWHT condition produced with different speeds with the same thermal boundary conditions (steel backing plate applied underneath the work-piece, and no water spray applied on the work-piece surface) in AW and PWHT conditions as functions of rotation rate.

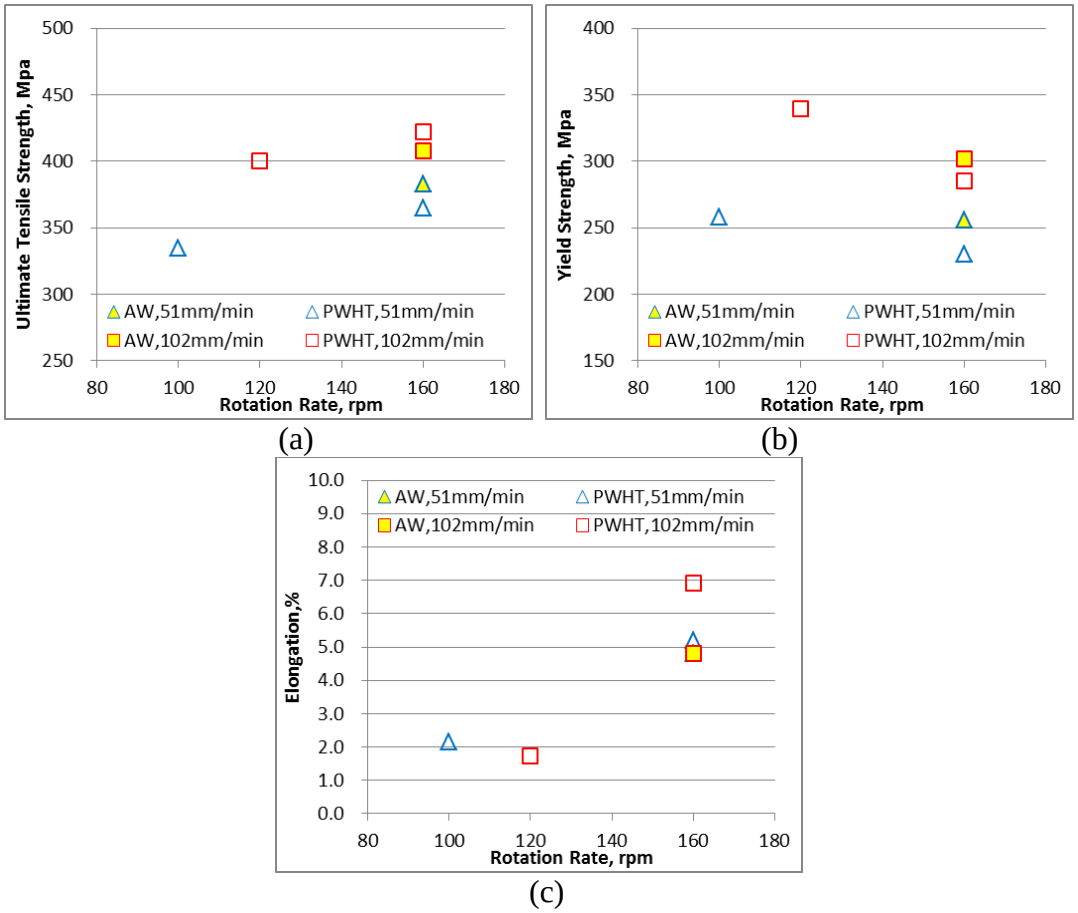

Figure 4.39 (a) UTS, (b) yield strength and (c) elongation of transverse tensile testing in CSSP as functions of rotation rate: different speeds, AW and PWHT, steel backing plate applied underneath the work-piece, and no water spray applied on the work-piece surface

Figure 4.39 (a)~(c) show that, when the welding speed of 51 mm/min was applied, relative to the rotation rate of 100 rpm, the rotation rate of 160 rpm increased UTS (9%),

decreased YS (-11%), and increased the EL (140%). When the welding speed of 102 mm/min was applied, relative to the rotation rate of 120 rpm, the rotation rate of 160 rpm increased UTS (5%), decreased YS (-16%), and increased the EL (298%). When the rotation rate of 160 rpm was applied, relative to the welding speed of 51 mm/min, the welding speed of 102 mm/min increased UTS (7%), increased YS (18%), and affected EL little in AW condition, while increased UTS (16%), increased YS (24%), and increased the EL (33%) in PWHT condition. When the rotation rate of 160 rpm and the welding speed of 51 mm/min were applied, relative to AW condition, PWHT condition decreased UTS (-5%), decreased YS (-10%), and increased EL (8%). When the rotation rate of 160 rpm and the welding speed of 102 mm/min were applied, relative to AW condition, PWHT condition increased UTS (3%), decreased YS (-5%), and increased EL (44%). It indicates that:

(1) In PWHT conditions, when rotation rate increased, under the same welding speed, UTS increased a little, YS decreased a little, and EL increased significantly; when rotation rate increased, relative to joints produced by the lower welding speed (51 mm/min), in joints produced by the higher welding speed (102 mm/min), UTS increased slower, YS decreased faster and EL increased faster.

(2) Under the same rotation rate, relative to lower welding speed (51 mm/min), higher welding speed (102 mm/min) increased UTS a little, increased YS and affected EL little in AW conditions, while increased UTS, YS and EL in PWHT conditions (by larger extents relative to AW conditions).

(3) Under the same rotation rate (160 rpm), relative to AW conditions, in joints produced by lower welding speed (51 mm/min), PWHT decreased UTS and YS a little,

and increased EL a little; in the joints produced by the higher welding speed (102 mm/min), PWHT increased UTS a little, decreased YS a little while increased EL significantly. When higher welding speed was applied, PWHT had a little larger effect on increasing UTS and EL, while had similar effect on decreasing YS.

4.2.5.1.2 SSSP: Transverse Tensile Testing

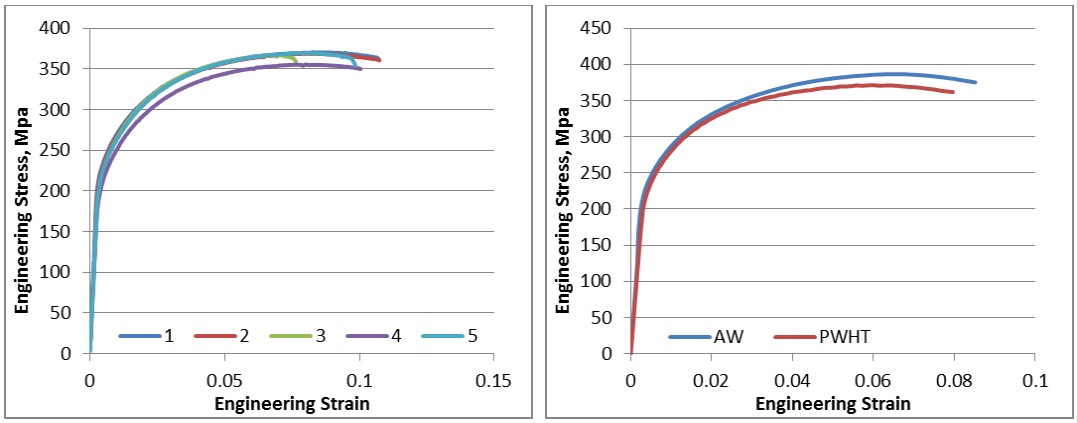

(a) #4171B, PWHT (b) #4306

Figure 4.40 Engineering stress and strain curves of transverse tensile testing in SSSP as functions of applied forge force: different forge forces, AW and PWHT, 1 setup, by a T+3CT pin with a flute depth of 0.9 mm, rotation rate 160 rpm,welding speed 51 mm/min

Figure 4.40 a~b show the engineering stress as a function of engineering strain of transverse tensile testing on SSSP joints produced with the same speeds and different forge forces in AW and PWHT conditions. In each conditions, there were 1~5 samples from the same joint tested. In this section, transverse tensile testing was performed on some SSSP joints as following: #4171B (160 rpm, 51 mm/min, F_z 53.4 KN), and #4306 (160 rpm, 51 mm/min, F_z 62.3 KN).

Through those engineering stress and strain curves shown in Figure 4.40, characteristic values like ultimate tensile strength (UTS), yield strength (YS) and elongation (EL) were calculated and average values were shown in Figure 4.41. Figure 4.41 shows (a) ultimate tensile strength, (b) yield strength and (c) elongation of

transverse tensile testing performed on SSSP joints produced with the same speeds and different forge forces in AW and PWHT conditions as functions of applied forge force.

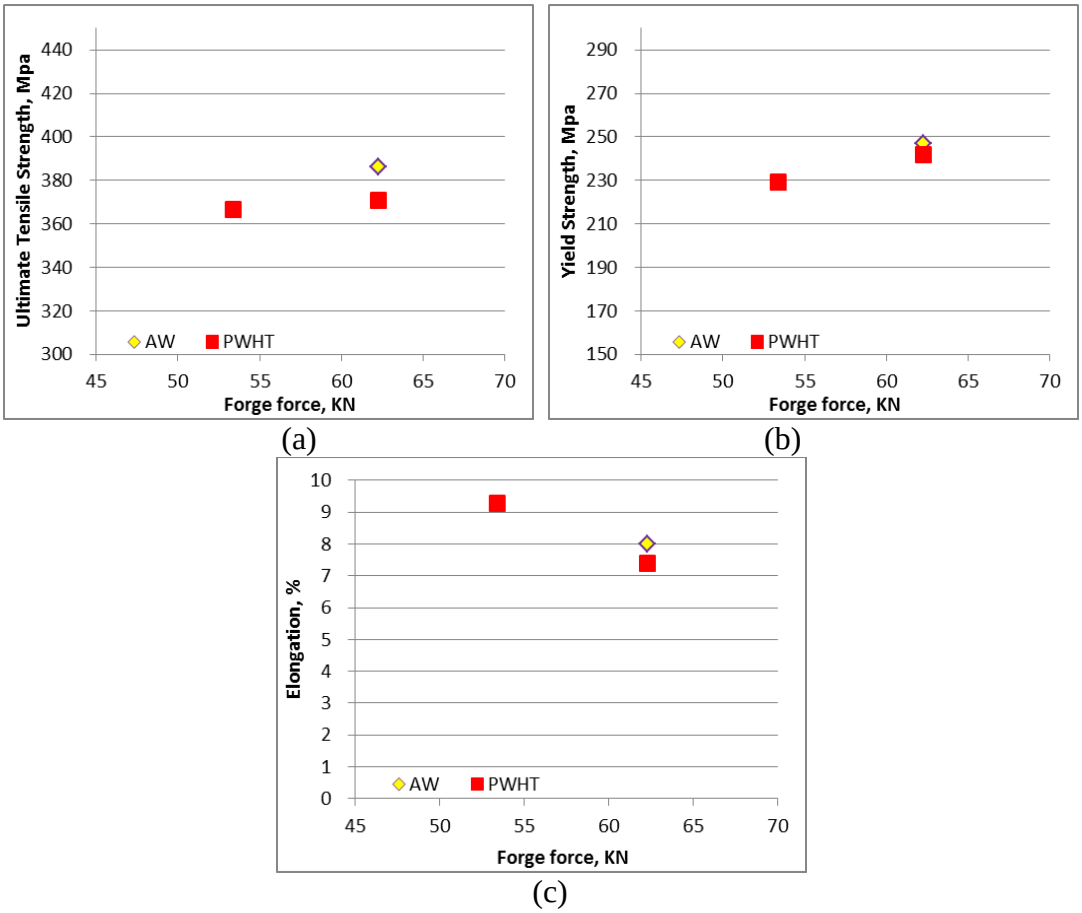

Figure 4.41 (a) Ultimate tensile strength, (b) yield strength and (c) elongation of transverse tensile testing in SSSP as functions of applied forge force: different forge forces, AW and PWHT, a setup of 1 °, by a T+3CT pin with a flute depth of 0.9 mm, a rotation rate of 160 rpm, a welding speed of 51 mm/min

Figure 4.41 (a)~(c) show that, in PWHT condition, relative to the lower forge force (53.4 KN), the a little higher (62.3 KN) affected UTS little (1%), increased YS (5%), and decreased EL (-20%). When the higher forge force (62.3 KN) was applied, relative to AW condition, the PWHT condition reduced UTS (-4%), affected YS little (-2%), and reduced EL (-8%). It indicates that, a little larger forge forces affect UTS and YS little, while decreasing EL by some extent; PWHT affects UTS, YS and EL little.

4.2.5.1.3 CSSP and SSSP: Transverse Tensile Testing

Engineering stress as a function of engineering strain of transverse tensile testing on comparable CSSP (#4299) and SSSP (#4306) joints produced with the same speeds and tools with different shoulder and pin features in AW and PWHT conditions were shown in Figure 4.37 (f) and Figure 4.40 (b), respectively. In each condition, there was one sample tested. In this section, transverse tensile testing was performed on comparable CSSP (#4299) and SSSP (#4306) joints.

Through those engineering stress and strain curves shown in Figure 4.37 (f) and Figure 4.40 (b), characteristic values like ultimate tensile strength (UTS), yield strength (YS) and elongation (EL) were calculated and average values were shown in Figure 4.42.

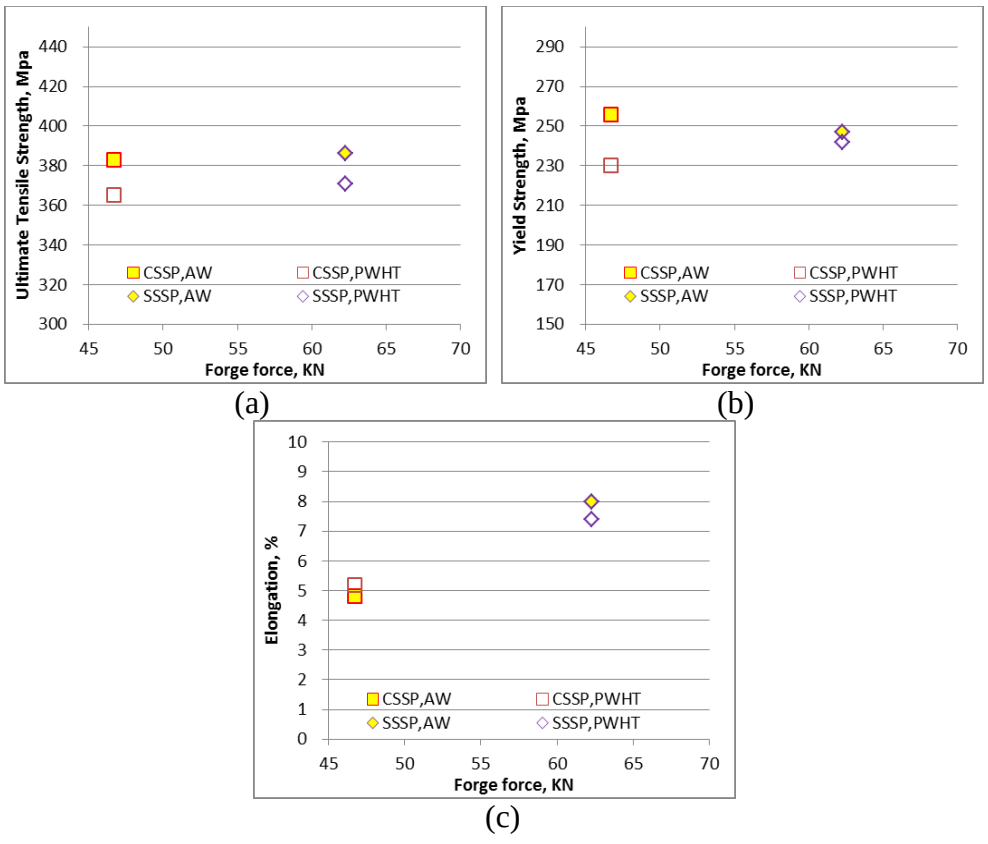

Figure 4.42 (a) UTS, (b) YS and (c) EL of transverse tensile testing in comparable CSSP (#4299) and SSSP (#4306): different tool shoulder and pin features, AW and PWHT, a setup of 1 °, a flat/flute depth of 0.9 mm, rotation rate 160 rpm, welding speed 51 mm/min

Figure 4.42 shows (a) ultimate tensile strength, (b) yield strength and (c) elongation of transverse tensile testing performed on comparable CSSP (#4299) and SSSP (#4306) joints produced with the same speeds and tools with different shoulder and pin features in AW and PWHT conditions. Figure 4.42(a)~(c) show that, in both AW and PWHT conditions, relative to CSSP, SSSP produced joints with the similar UTS and YS, while the larger EL, and EL increased more in AW (67%) than in PWHT (42%) condition. In both CSSP and SSSP, relative to AW condition, PWHT had little effect on UTS and YS; PWTH increased EL significantly (44%) in CSSP, while affected EL in SSSP slightly (8%).

4.2.5.2 Longitudinal Tensile Testing (AW&PWHT)

4.2.5.2.1 CSSP: Longitudinal Tensile Testing

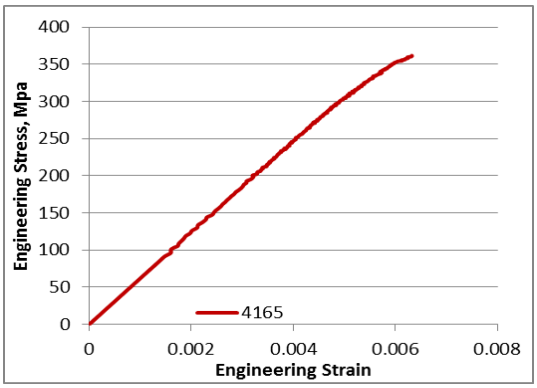

(a) #4165, normal scale LTT

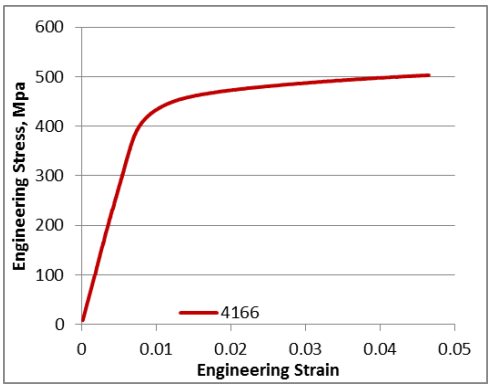

(b) #4166, normal scale LTT

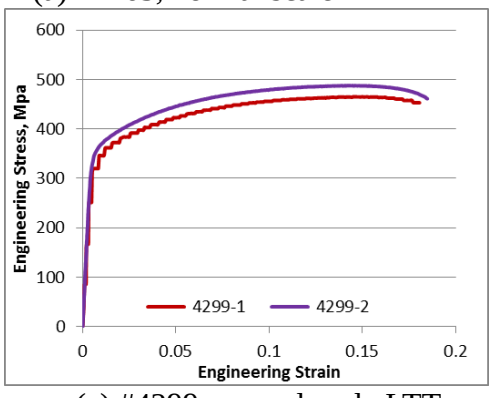

(c) #4299, normal scale LTT

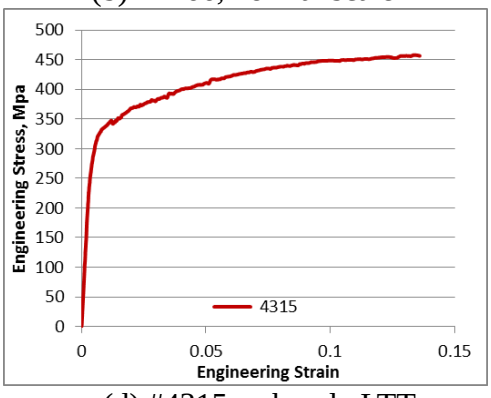

(d) #4315, subscale LTT

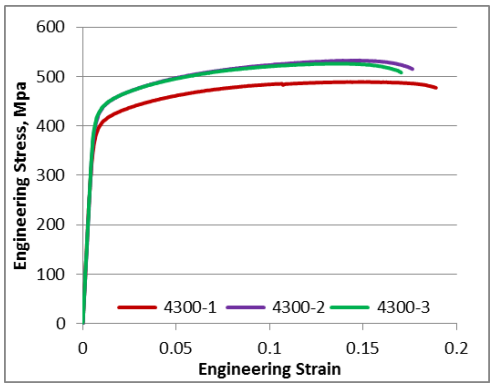

(e) #4300, subscale LTT

Figure 4.43 Engineering stress and strain curves of longitudinal tensile testing in CSSP: PWHT

Figure 4.43 a~e show the engineering stress as a function of engineering strain of longitudinal tensile testing on CSSP joints in PWHT condition. In each conditions, there were 1~3 samples from the same joint tested. In this section, longitudinal tensile testing was performed on some CSSP joints as following: #4165 (160 rpm, 102 mm/min, CBP), #4166 (160 rpm, 102 mm/min, WS), #4299 (160 rpm, 51 mm/min, F_z 46.7 KN, Original), #4315 (160 rpm, 51 mm/min, F_z 55.6 KN, Original), and #4300 (160 rpm, 102 mm/min, Original). Through those engineering stress and strain curves shown in Figure 4.43, characteristic values like ultimate tensile strength (UTS), yield strength (YS) and elongation (EL) were calculated and average values were shown in Figure 4.44. Figure 4.44 shows (a) Ultimate tensile strength, (b) yield strength and (c) elongation of longitudinal tensile testing performed on CSSP joints in PWHT condition produced with different thermal boundary conditions (original, WS, and CBP) and welding speeds (51 mm/min, and 102 mm/min) as functions of forge forces. Figure 4.44 (a)~(c) show that, under the same speeds, relative to original TBCs, WS decreased UTS little (-2%), increased YS little (4%), while decreased EL significantly (-77%); CBP decreased UTS (-30%), and decreased EL significantly (-99%). With the same rotation rates and TBCs,

higher welding speed (102 mm/min) increased UTS a little (8~13%), increased YS (22~31%), while decreased EL (-6~31%). With the same speeds and TBCs, a little higher forge force (55.6 KN) decreased UTS slightly (-4%), decreased YS slightly (-7%), and decreased EL a little (-28%).

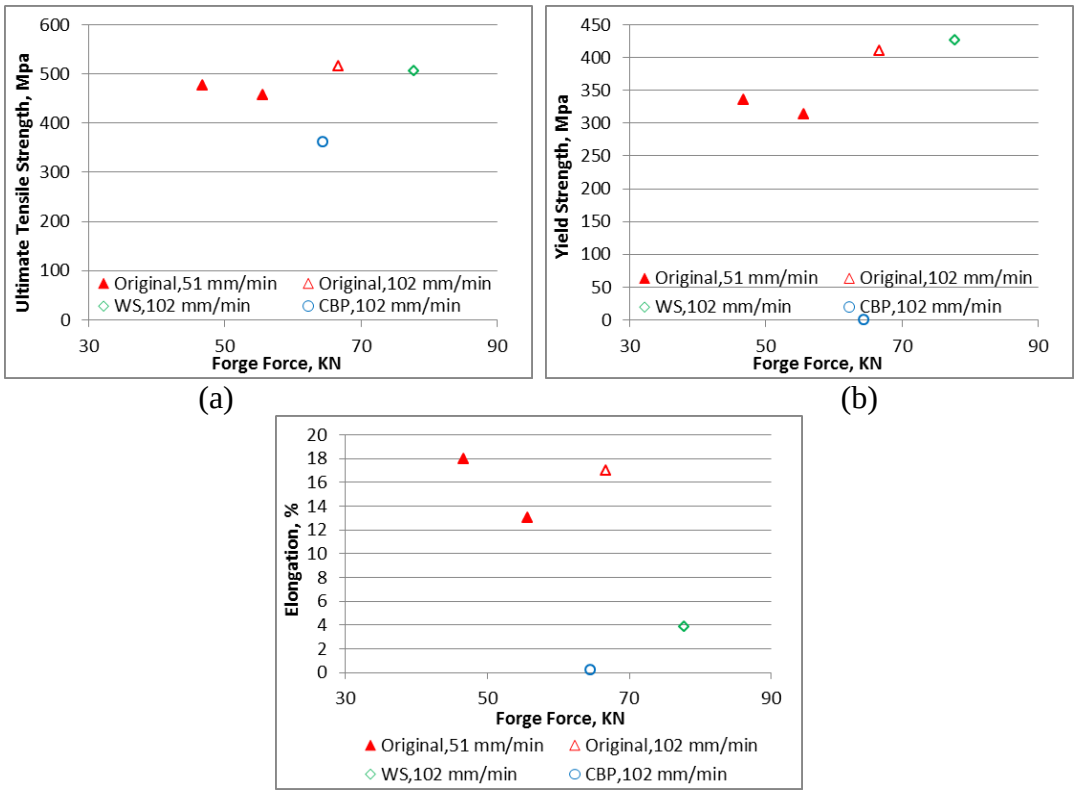

Figure 4.44 (a) UTS, (b) YS and (c) EL of longitudinal tensile testing in CSSP as functions of forge forces: different TBCs and welding speeds, a setup of 1° , a T+3F pin with a flat depth of 0.9 mm, a rotation rate of 160 RPM, PWHT

4.2.5.2.2 SSSP: Longitudinal Tensile Testing

In this section, longitudinal tensile testing was performed on some SSSP joints as following: #3965A, #3965B, #3973A, #3975A, #3975B, and #4306. In each conditions, there were 1~3 samples from the same joint tested. Engineering strain data of #3965A, #3965B, #3973A, #3975A and #3975B (normal scale LTT) was not reliable, while the engineering stress data was reliable, so only the engineering stress as a function of

engineering strain of longitudinal tensile testing on #4306 joint (subscale LTT) in PWHT conditions was shown in Figure 4.45. Through those engineering stress data, and the engineering stress-strain curves shown in Figure 4.45, characteristic values like ultimate tensile strength (UTS), yield strength (YS) and elongation (EL) were calculated and average values were shown in Figure 4.46.

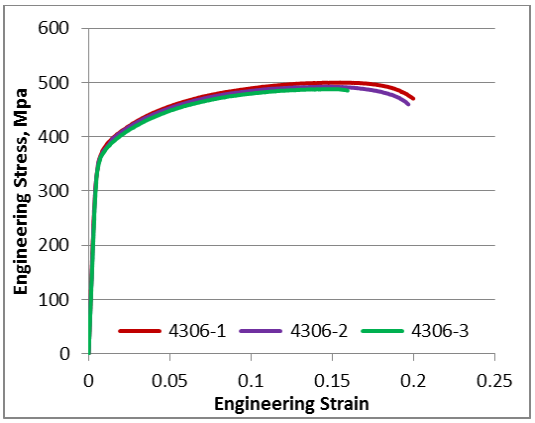

Figure 4.45 Engineering stress and strain curves of longitudinal testing in SSSP as functions of rotation rates: different rotation rates and pins, a welding speed of 51 mm/min, PWHT (#4306)

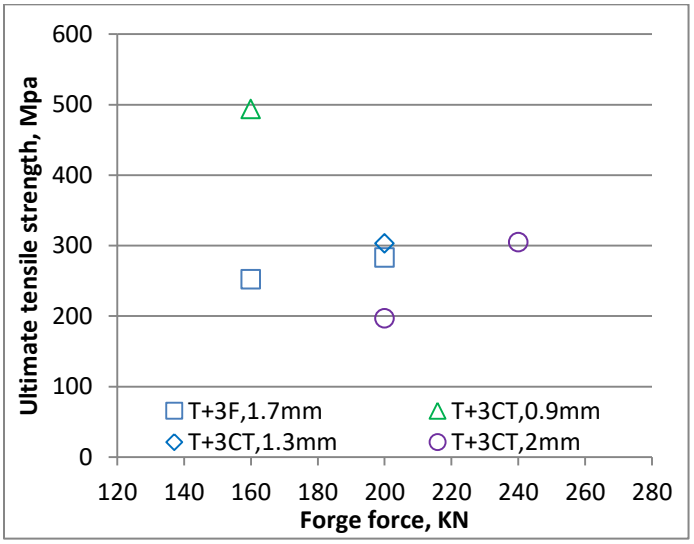

Figure 4.46 Ultimate tensile strength of longitudinal testing in SSSP as functions of rotation rates: different rotation rates and pins, a welding speed of 51 mm/min, PWHT

Figure 4.46 shows (a) ultimate tensile strength, (b) yield strength and (c) elongation of longitudinal testing performed on SSSP joints in PWHT condition produced with the same welding speeds (51 mm/min), different rotation rates and pins as functions of rotation rates. Figure 4.46(a)~(c) show that, in PWHT condition, when the same tool (T+3F pin with a flat depth of 1.7 mm) was adopted, 25% larger rotation rate increased UTS by 12%. When the same tool (T+3CT pin with a flute depth of 2 mm) was adopted, 20% larger rotation rate increased UTS by 55%. Under the same speeds, relative to the joint produced by the T+3CT pin with a flute depth of 2 mm (#3975B), the joint produced by the T+3CT pin with a flute depth of 1.3 mm (#3973A) had a 54% larger UTS, while the joint produced by the T+3F pin with a flute depth of 1.7 mm (#3965A) had a 44% larger UTS. The joint produced by a T+3CT pin with a flute depth of 0.9 mm and a rotation rate of 160 rpm (#4306) had a much larger UTS, which might due to the appropriate pin feature with the appropriate flute depth, or may because that the longitudinal tensile testing was performed by a subscale tensile tester on subscale tensile samples, while other joints were tested by a normal tensile tester on normal scale tensile samples. It indicates that, higher rotation rate increased the UTS; appropriate flat/flute depths resulted in good UTS, while too deeper flat/flute decreased the UTS: the deeper, the larger.

4.2.5.2.3 CSSP and SSSP: Longitudinal Tensile Testing

Engineering stress as a function of engineering strain of longitudinal tensile testing on comparable CSSP (#4299) and SSSP (#4306) joints produced with the same speeds and tools with different shoulder and pin features in PWHT condition were shown in Figure 4.43 (c) and Figure 4.45, respectively. In each condition, there was one sample

tested. In this section, longitudinal tensile testing was performed by a subscale tensile tester on comparable CSSP (#4299) and SSSP (#4306) joints.

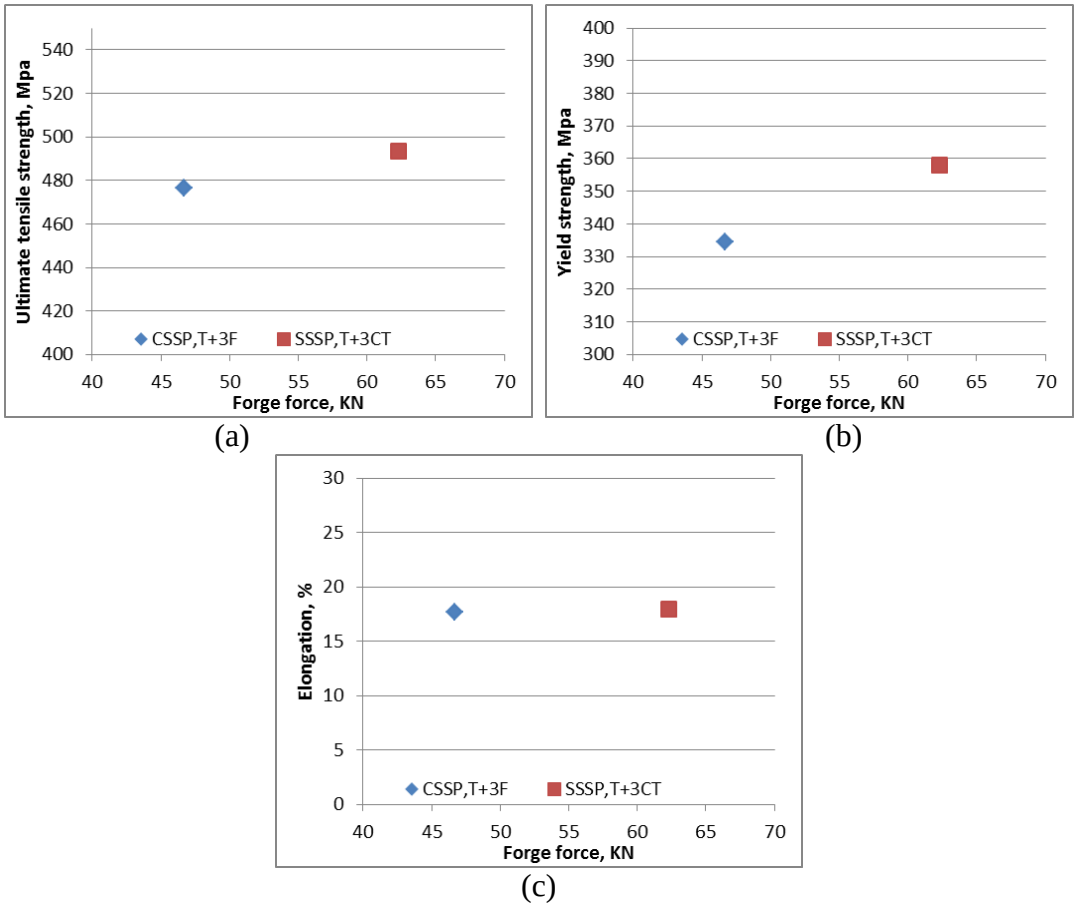

Figure 4.47 (a) Ultimate tensile strength, (b) yield strength and (c) elongation of longditudinal tensile testing in comparable CSSP (#4299) and SSSP (#4306) joints: different tool shoulder and pin features, PWHT, a setup of 1 °, a pin flat/flute depth of 0.9 mm, a rotation rate of 160 rpm, a welding speed of 51 mm/min

Through those engineering stress and strain curves shown in Figure 4.43 (c) and Figure 4.45, characteristic values like ultimate tensile strength (UTS), yield strength (YS) and elongation (EL) were calculated and average values were shown in Figure 4.47. Figure 4.47 shows (a) ultimate tensile strength, (b) yield strength and (c) elongation of longitudinal tensile testing performed on comparable CSSP (#4299) and SSSP (#4306) joints produced with the same speeds and tools with different shoulder and pin features in

PWHT conditions. Figure 4.47(a)~(c) show that, relative to CSSP, SSSP increased UTS by 4%, increased YS by 7% and increased EL by 2% in PWHT condition. It indicates that, in PWHT conditions, relative to CS, SS affected UTS, YS and EL little.

Subscale longitudinal tensile testing was performed on both #4306 and #4300 in the PWHT condition by the same subscale tensile tester. Both joints were defect free. Testing results show that, #4306 had a UTS of 494 MPa, a YS of 358 MPa, and an EL of 18%, while #4300 had a UTS of 516 MPa, a YS of 407 MPa, and an EL of 17%. It shows that, relative to SSSP, CSSP allows higher welding speeds, which increased the UTS (5%), increased the YS (14%), and decreased EL (-4%). It indicates that, in subscale longitudinal tensile testing of SP joints in PWHT condition, under the same rotation rate, higher welding speed increased UTS slightly, increased YS, and decreased EL slightly.

4.2.6 Residual Stress (AW&PWHT)

In this section, residual stress distribution in the CSSP and SSSP joints will be studied to investigate effects of CSSP and SSSP, different control parameters and PWHT on residual stress profiles in joints. Through thickness average, longitudinal, residual stress was measured in both AW and PWHT conditions for selected CSSP and SSSP joints as following: #4299, #4315, #4300 and #4306. Through those residual stress profiles of above tested CSSP and SSSP joints in both AW and PWHT conditions shown in Figure 4.48, characteristic values like the peak residual stress (PRS), full width at half maximum (FWHM) and tension area (TA) were calculated and shown in Figure 4.49~Figure 4.51, which also include Unit weld energy (UWE). PRS is in units of MPa, FWHM is in units of mm, TA is in units of KJ/m^2, while UWE is in units of KW/(m/s). UWE equals to power in units of W be divided by welding speed in units of mm/s.

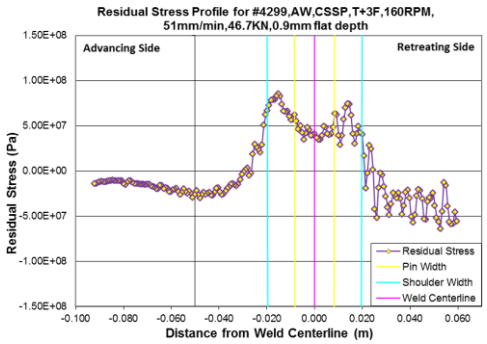

(a) #4299, AW

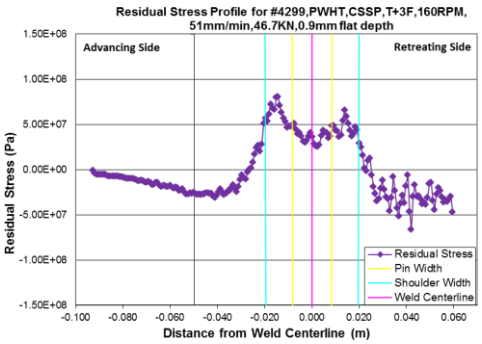

(b) #4299, PWHT

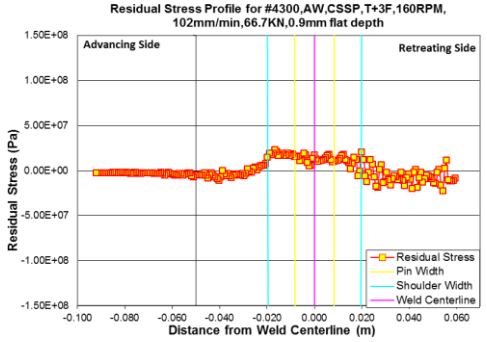

(c) #4300, AW

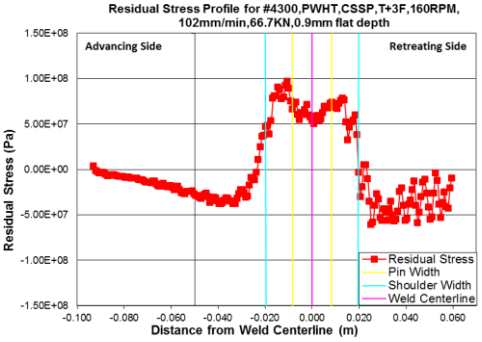

(d) #4300, PWHT

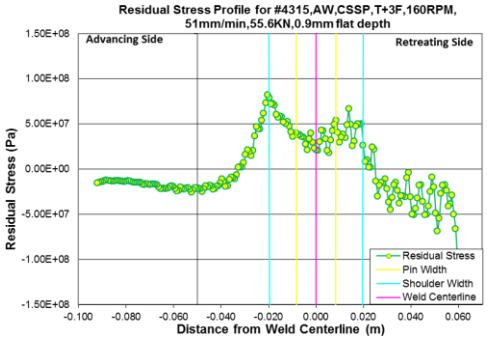

(e) #4315, AW

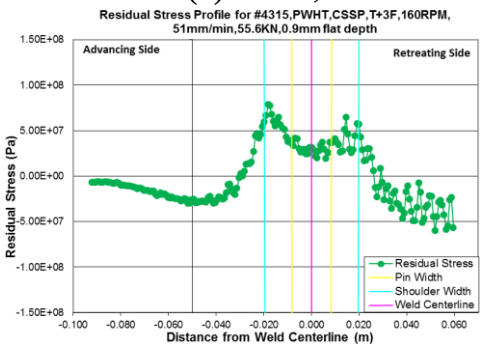

(f) #4315, PWHT

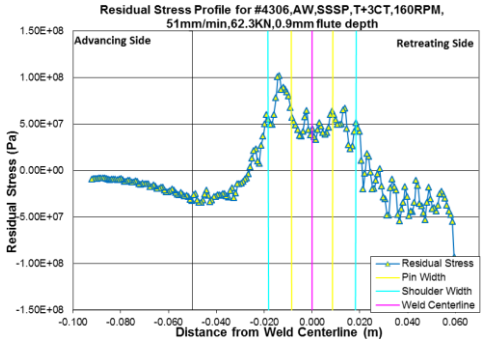

(g) #4306, AW

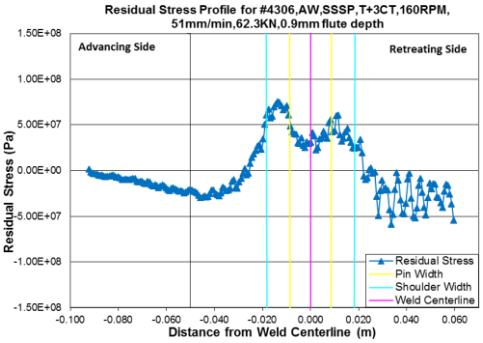

(h) #4306, PWHT

Figure 4.48 Through thickness average, longitudinal, residual stress profiles in SP: different tool shoulders and pin features, AW and PWHT, 1 °setup, rotation rate 160 rpm

Figure 4.48 (except (c)) shows that, relative to AW condition, PWHT affects the residual stress profiles little. Residual stress profile of the #4300 joint in AW condition shown in Figure 4.48(c) is not reliable. However, it's assumed to be similar with the #4300 joint in PWHT condition, according to results of all other tested samples. PRS, FWHM and TA of #4300 joint in AW condition will not be discussed in this section.

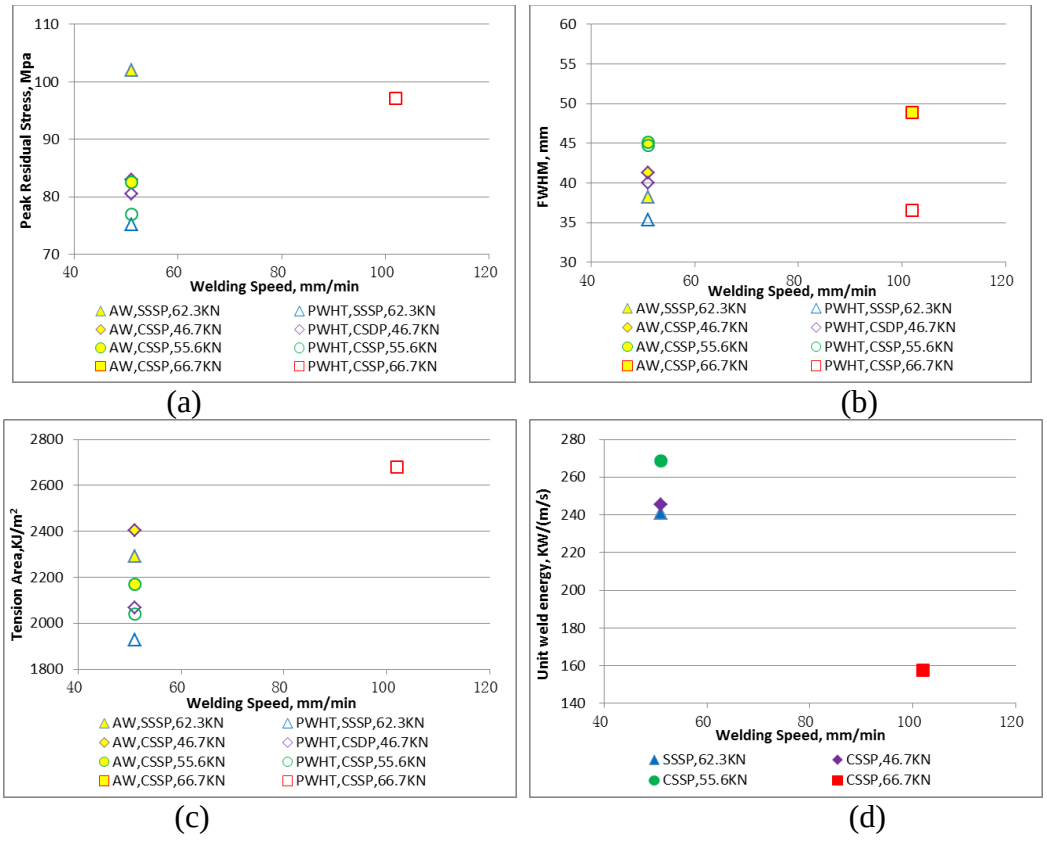

Figure 4.49 (a) Peak residual stress, (b) FWHM, (c) tension area of through thickness average, longitudinal, residual stress profiles in both AW and PWHT conditions, and (d) unit weld energy of CSSP and SSSP joints as a function of welding speeds: 1 ° setup, a rotation rate of 160 rpm, different pin features, 0.9 mm flat/flute depth

Figure 4.49 shows (a) Peak residual stress, (b) FWHM, (c) tension area of through thickness average, longitudinal, residual stress profiles in both AW and PWHT conditions, and (d) unit weld energy of CSSP and SSSP joints as a function of welding speeds. Figure 4.50 shows (a) Peak residual stress, (b) FWHM, (c) tension area of

through thickness average, longitudinal, residual stress profiles in both AW and PWHT conditions, and (d) unit weld energy of CSSP and SSSP joints as a function of power. Figure 4.51 shows (a) Peak residual stress, (b) FWHM, and (c) tension area of through thickness average, longitudinal, residual stress profiles in both AW and PWHT conditions of CSSP and SSSP joints as a function of the unit weld energy.

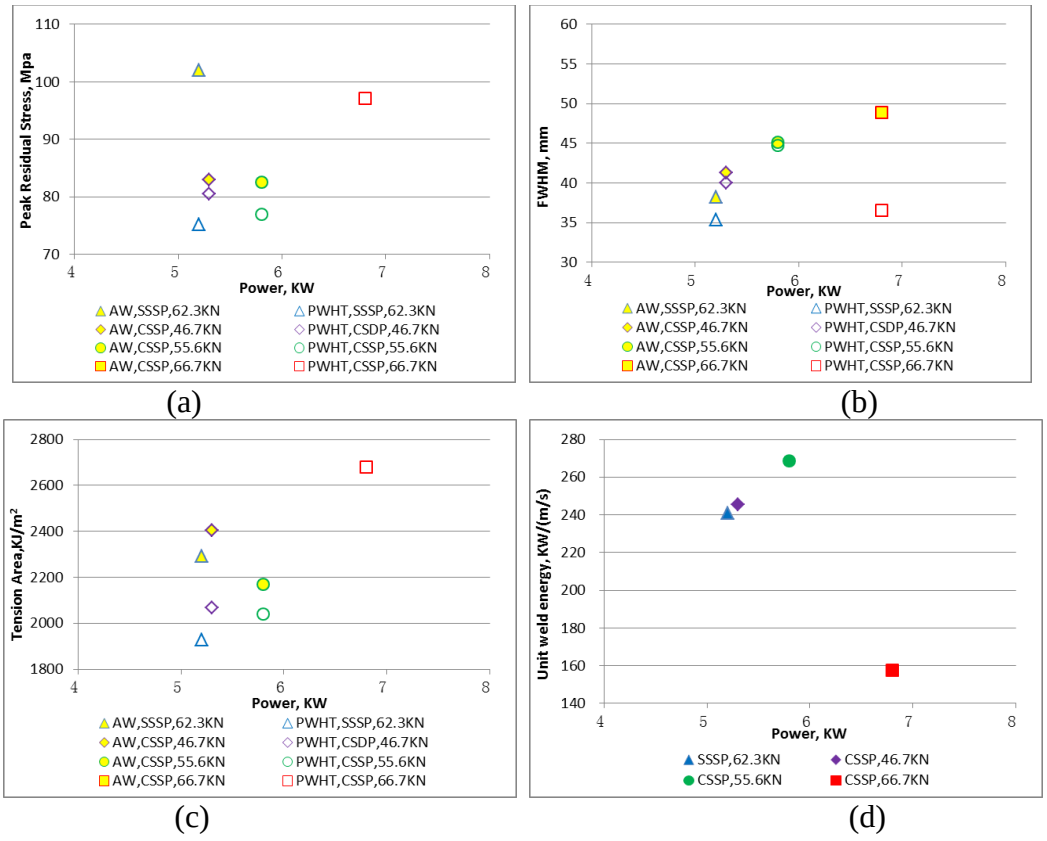

Figure 4.50 (a) Peak residual stress, (b) FWHM, (c) tension area of through thickness average, longitudinal, residual stress profiles in AW and PWHT conditions, and (d) unit weld energy of SP joints as a function of power: 160 rpm, different pin features

Figure 4.49~Figure 4.51 show that:

(1) Under the same speeds, in AW conditions, a little higher forge force increased FWHM a little (9%), decreased TA a little (-10%), while had little effect on PRS; in PWHT conditions, a little higher forge force decreased PRS slightly (-4%), increased

FWHM a little (12%), while had little effect on TA. A little higher forge force also increased the UWE a little (9%) due to a little larger power input. (#4299, #4315)

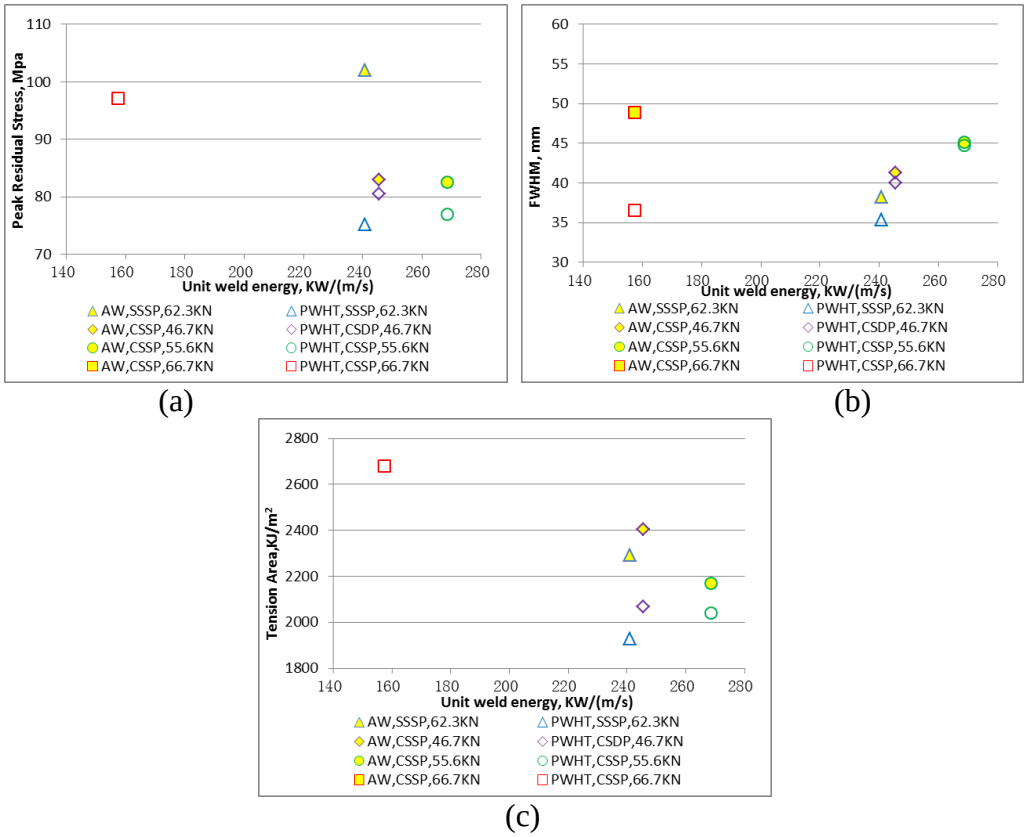

Figure 4.51 (a) Peak residual stress, (b) FWHM, and (c) tension area of through thickness average, longitudinal, residual stress profiles in both AW and PWHT conditions of CSSP and SSSP joints as a function of the unit weld energy: 160 rpm, different pin features

(2) Under the same rotation rates, higher welding speed increased PRS (21%), decreased FWHM a little (-9%), and increased TA (30%) in PWHT conditions. Higher welding speed also decreased the UWE (-36%) due to a little larger power input and much larger welding speed. (#4299, #4300)

(3) Under the same speeds, relative to CSSP, SSSP increased PRS (23%), decreased FWHM (-8%) and TA (-5%) slightly in AW conditions, while decreased PRS (-7%) and TA (-7%) slightly, and decreased FWHM a little (-12%) in PWHT conditions.

SSSP affected UWE little due to the similar power input and the same welding speed. (#4299, #4306)

(4) Under the same rotation rates, relative to SSSP, CSSP with higher welding speed increased PRS (29%) and TA (39%), while affected FWHM little in PWHT conditions. CSSP with higher welding speed also decreased the UWE (-35%) due to larger power input and much larger welding speed. (#4306, #4300)

(5) When the welding speed of 51 mm/min was applied, relative to AW, in SSSP, PWHT decreased PRS (-26%) and TA (-16%), and decreased FWHM a little (-7%); in CSSP, PWHT decreased TA (-6~14%) a little while affected PRS and FWHM little.

(6) When UWE increased, PRS decreased, and FWHM increased a little. When power increased, PRS increased, UWE decreased due to larger welding speed.

4.2.7 Face Bending Testing Properties

In this section, face bending tests were performed on CSSP and SSSP entire joints as following in AW and PWHT conditions produced by different control parameters and TBCs to investigate effects of different shoulders, tools, control parameters and TBCs on joint's face bending properties: #4156A (CSSP, 100 rpm, 51 mm/min, Original), #4156B (CSSP, 120 rpm, 102 mm/min, Original), #4164 (CSSP, 160 rpm, 102 mm/min, CBP+WS), #4165 (CSSP, 160 rpm, 102 mm/min, CBP), #4166 (CSSP, 160 rpm, 102 mm/min, WS), #4299 (CSSP, 160 rpm, 51 mm/min, F_z 46.7 KN, Original), #4315 (CSSP, 160 rpm, 51 mm/min, F_z 55.6 KN, Original), #4300 (CSSP, 160 rpm, 102 mm/min, Original), and #4306 (SSSP, 160 rpm, 51 mm/min, Original). Results of face bending tests of the above joints (127mm x 6.4mm x 25.4mm) for face bending test in AW and PWHT conditions, as shown in Figure 4.52, were summarized as following:

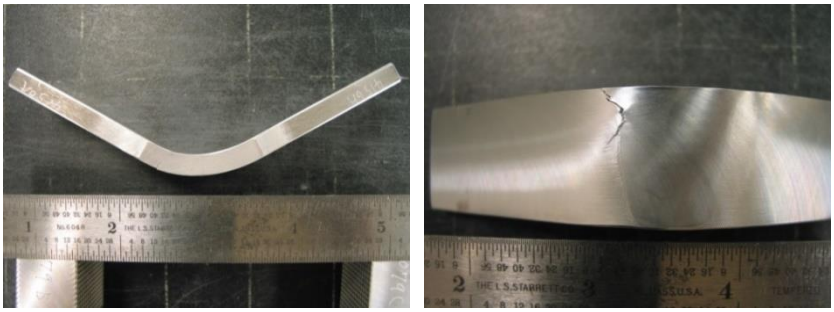

(a) #4156A, PWHT

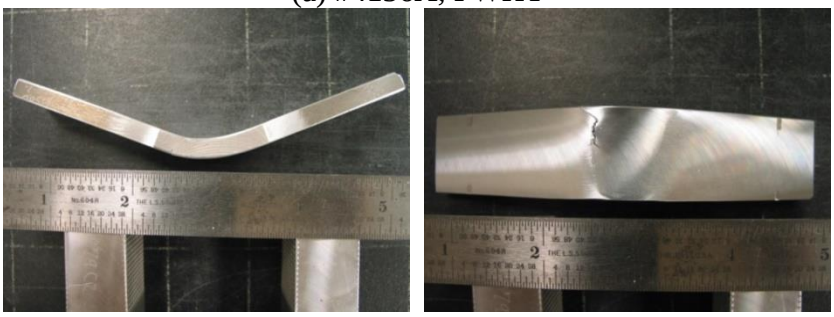

(b) #4156B, PWHT

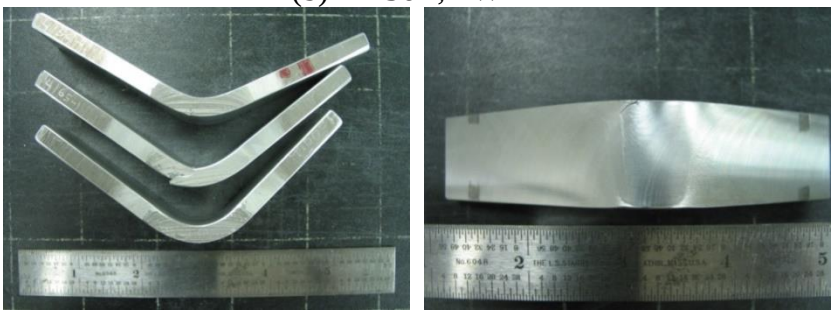

(c) #4164 (the top one in the left picture), PWHT

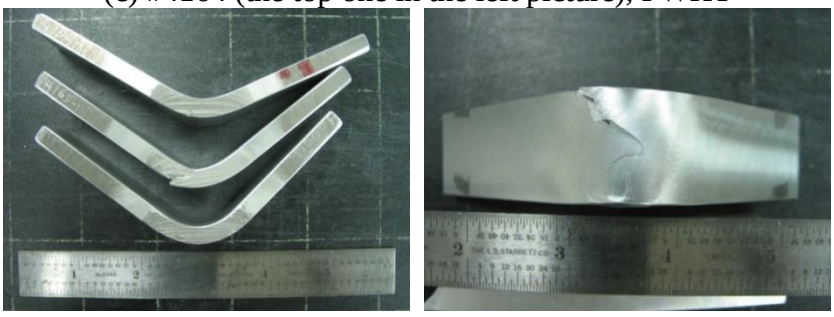

(d) #4165 (the middle one in the left picture), PWHT

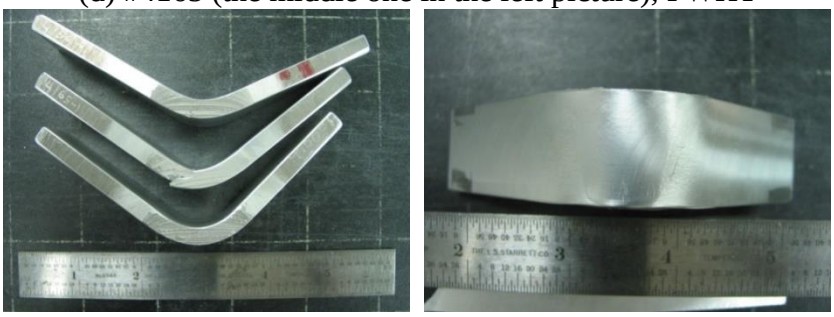

(e) #4166 (the bottom one in the left picture), PWHT

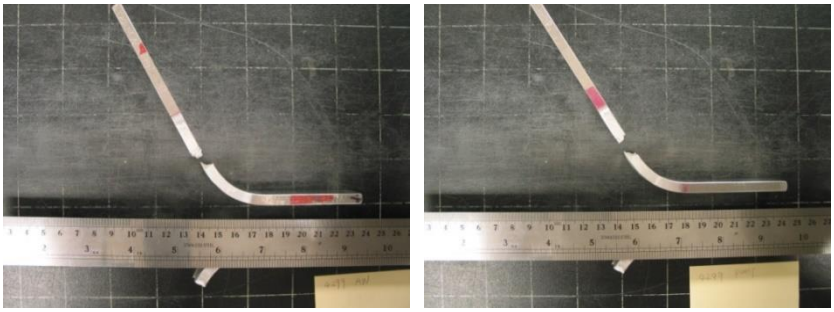

(f) #4299, AW (left) and PWHT (right)

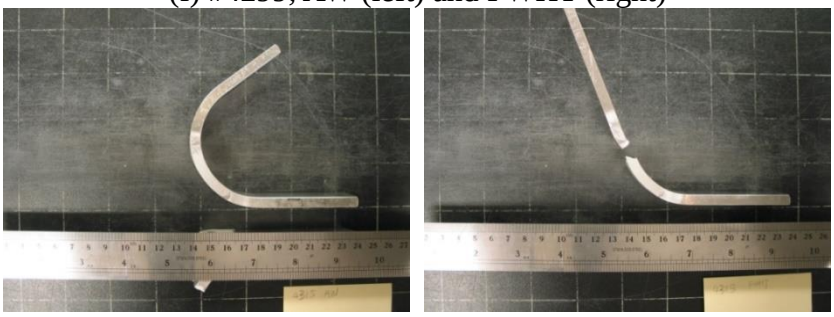

(g) #4315, AW (left) and PWHT (right)

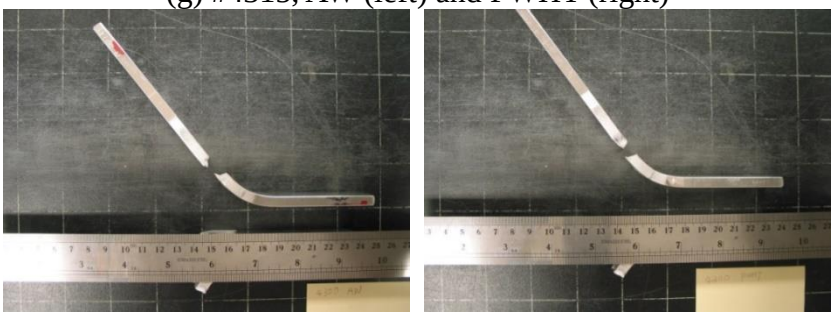

(h) #4300, AW (left) and PWHT (right)

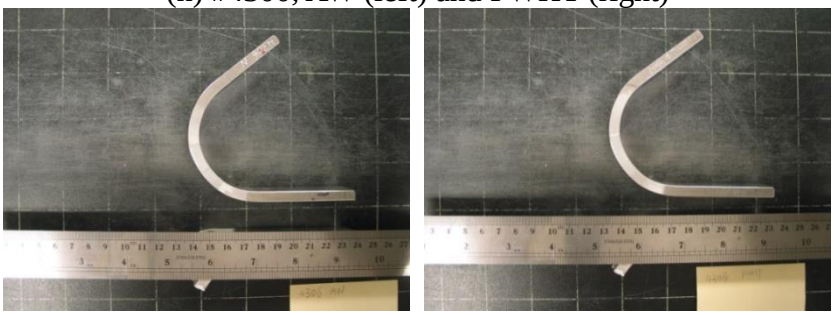

(i) #4306, AW (left) and PWHT (right)

Figure 4.52 Specimens of SP joints after the face bending testing: AW and PWHT

Passed: #4156A in PWHT (cracks at AS from crown to mid-plane), #4156B in PWHT (cracks at AS from crown to mid-plane), #4164 in PWHT (cracks at AS near crown), #4166 in PWHT, #4315 in AW, and #4306 in AW and PWHT.

Failed: #4165 in PWHT (almost broke, with large cracks at AS near crown), #4299 in AW and PWHT, #4315 in PWHT, and #4300 in AW and PWHT.

Results of CSSP joints (#4156A, #4156B, #4299, #4315 and #4300) produced with different speeds and the same TBCs in PWHT condition show that, the rotation rate of 160 rpm produced joints (#4299, #4315 and #4300) failing in the face bending test, when the welding speed of either 51 mm/min or 102 mm/min was applied. #4300 joint had no volumetric defects. Measured temperatures at center pin of #4299, #4315 and #4300 are 484℃, 500℃ and 493℃, respectively. Those temperatures are higher than the incipient melting temperature of AA7099-T7651, which is 480℃. It indicates that the rotation rate of 160 rpm is high for CSSP and caused overheating inside the CSSP joints, where fractography study is needed for further conclusion. Both 100 rpm & 51 mm/min (#4156A) and 120 rpm & 102 mm/min (#4156B) produced joints passing the face bending testing, though cracks appeared at locations of volumetric defects in each joint. Measured temperatures at center pin of #4156A and #4156B are 451℃ and 459℃, respectively. Measured temperatures near pin root of #4156A and #4156B are 435℃ and 437℃, respectively. It indicates that, lower rotation rate (100 rpm or 120 rpm) produced CSSP joints which might have not been overheated, where fractography study is needed for further conclusion.

Results of CSSP joints (#4164, #4165, #4166 and #4300) produced with the same speeds and different TBCs in PWHT condition show that, in those four joints without volumetric defects, only when WS was applied on the work-piece surface, the produced joints passed the face bending testing. TBCs of #4164, #4165, #4166 and #4300 are "CBP+WS", "CBP", "WS" and "original", respectively. Measured temperatures at center

pin of #4164, #4165, #4166 and #4300 are 481℃, 480℃, 487℃ and 493℃, respectively. Measured temperatures near pin root of #4164, #4165 and #4166 are 448℃, 455℃ and 462℃, respectively. Data of temperature at pin center indicates that all those four joints have been possibly overheated, while only joints produced with WS applied on the work-piece surface passed the face bending testing. It indicates that, the application of WS on work-piece surface can improve the performance of CSSP joints in face bending testing, even when overheating occurs.

Results of CSSP and SSSP joints (#4299, #4315 and #4306) produced with the same speeds and different tools with the same flat/flute depth in AW and PWHT condition show that, only the SSSP joint (#4306) in both AW and PWHT conditions, and the CSSP joint (#4315) in AW condition passed the face bending testing. Measured temperatures at center pin of #4299, #4315 and #4306 are 484℃, 500℃ and 477℃, respectively. The CSSP joints have been overheated, while the SSSP might also have been overheated. It indicates that, relative to CS, the process variant of SS improves the performance of SP joints in face bending testing. It also indicates that relative to AW, PWHT worsens the performance of SP, especially in CSSP joints in face bending testing.

The above results also show that locations of cracks during testing correlate to volumetric defects in each joint.

Face bending tests were also performed on defect free parts (without volumetric defects) of some SSSP joints as following in PWHT conditions produced by the same welding speed of 51 mm/min, different tools and control parameters a to investigate effects of different tools, control parameters and TBCs on SSSP joint's face bending properties: #3965A (200 rpm, 51 mm/min, 71.2 KN), #3965B (160 rpm, 51 mm/min,

71.2 KN), #3973A (200 rpm, 51 mm/min, 69 KN), #3975A (240 rpm, 51 mm/min, 69 KN), #3975B (200 rpm, 51 mm/min, 69 KN), and #4114 (200 rpm, 51 mm/min, 69 KN). All the above listed SSSP joints are defective. Macro and micro defects of those joints have been studied to find the area without volumetric defects as shown in Figure 4.53, which shows that there are two parts in those joints are defect free: (1) near crown part, 3.8 mm~11.4 mm away from the weld crown, as indicated as "-1", and (2) near root part, 4.6 mm~7.6 mm away from the weld root, as indicated as "-2". All the tested samples have a length of 127mm, a width of 6.4mm, and a height of 4.6 mm or 7.6 mm for face bending test.

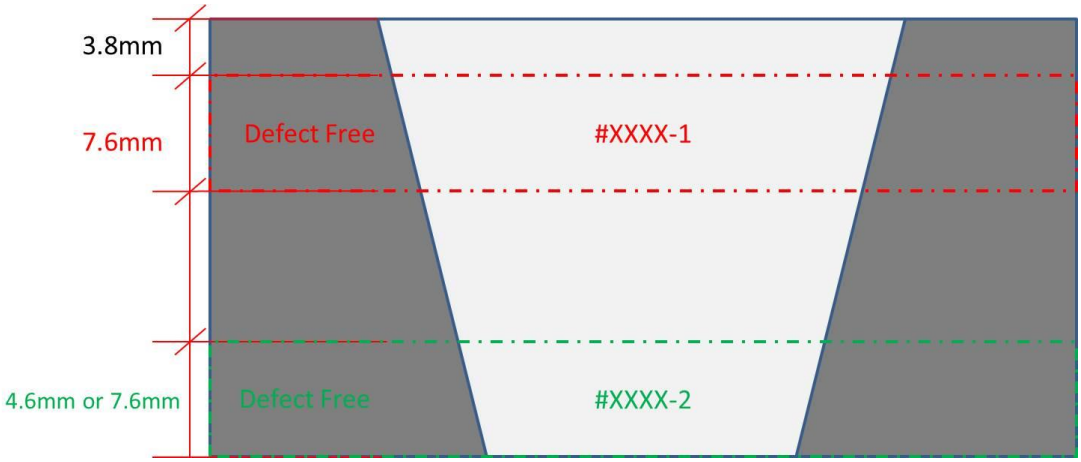

Figure 4.53 Schematic diagram of defect free area in SSSP: different tools and control parameters, PWHT, the same welding speed of 51 mm/min

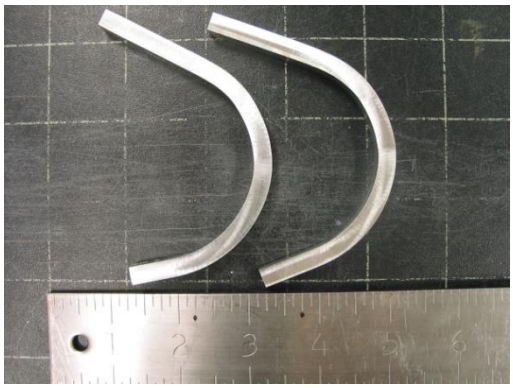

(a) #3965A-1 (left) and #3965A-2 (right)

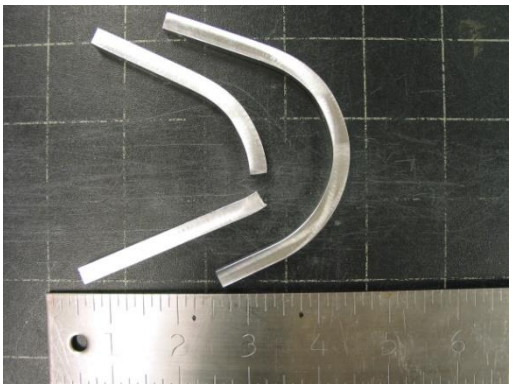

(b) #3965B-1 (left) and #3965B-2 (right)

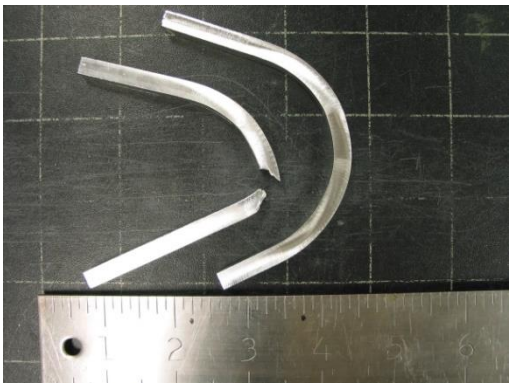

(c) #3973A-1 (left) and #3973A-2 (right)

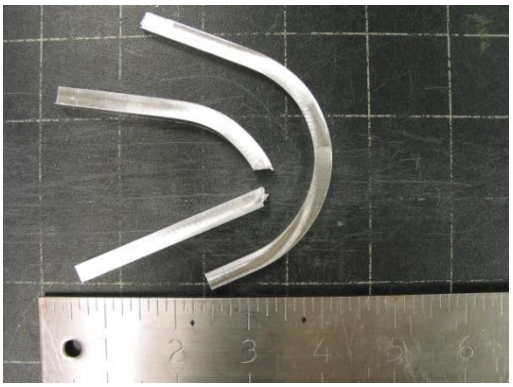

(d) #3975A-1 (left) and #3975A-2 (right)

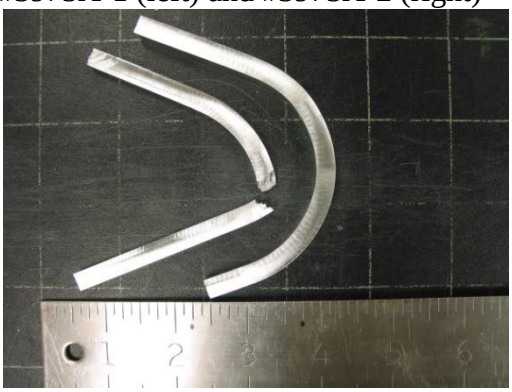

(e) #3975B-1 (right) and #3975B-2 (left)

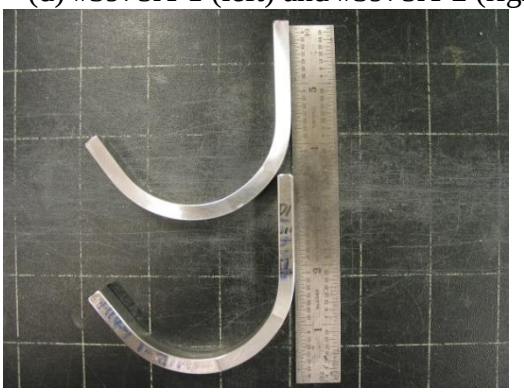

(g) #4114-1 (bottom) and #4114-2 (top)

Figure 4.54 Specimens of defect free parts of SSSP after face bending testing: PWHT

Heights and results of face bending tests of partial defect free parts of above joints in PWHT condition, as shown in Figure 4.54, were summarized as following:

(a) #3965A-1: 7.6 mm high; passed; #3965A-2: 7.6 mm high; passed;

(b) #3965B-1: 7.6 mm high; failed; #3965B-2: 7.6 mm high; passed;

(c) #3973A-1: 7.6 mm high; failed; #3973A-2: 7.6 mm high; passed;

(d) #3975A-1: 7.6 mm high; failed; #3975A-2: 4.6 mm high; passed;

(e) #3975B-1: 7.6 mm high; passed, with small crack at AS from mid-plane to root; #3975B-2: 4.6 mm high; failed;

(g) #4114-1: 7.6 mm high; passed; #4114-2: 7.6 mm high; passed;

Results of DF parts of SSSP joints (#3965A, #3965B, #3973A, #3975A, #3975B and #4114) produced with the same welding speed of 51 mm/min, the same TBCs and

different tools and rotation rates in PWHT condition show that, in one case of the near crown specimens, no failure was observed (3965A-1); in one case of the near root specimens, failure was observed (3975B-2). Fractography is needed to ascertain the reason(s) for failure in broken specimens. Overheating (microstructural features) may be the culprit in some cases of the near crown specimens. Weld defects present in #3975B-2 (as shown in Figure 4.55), which might be caused by too deep flutes of the T+3CT pin tool, may have led to failure in the face bending testing.

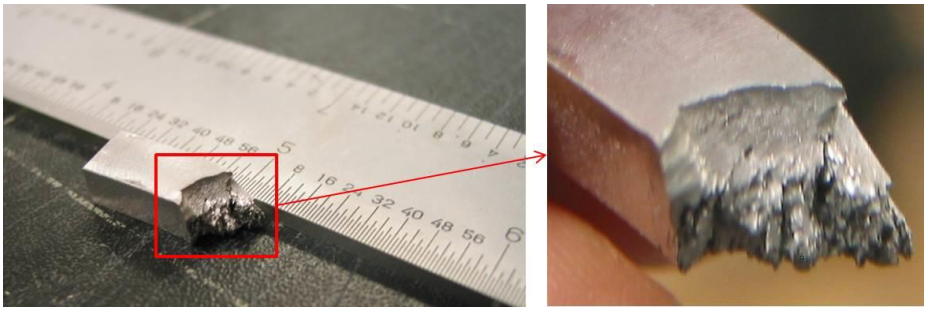

Figure 4.55 Macro defects in specimen #3975B-2 failed in the face bending testing

4.3 Dual Pass Full Penetration FSW

Single pass half penetration (SPH) FSW allows high speeds with the joint partially penetrated. Relative to SPH, single pass full penetration (SP) FSW fully penetrates the joint, while limits speeds which are much smaller. It's known that higher welding speed produces stronger joints. To produce fully penetrated joints welded by higher speeds, another process variant, dual pass full penetration (DP) FSW, has been proposed. In DP, the same welding direction of the 1st and the 2nd passed results in asymmetric nuggets with AS/RS at the opposite sides, as shown in Figure 4.59 (#4229&#4230), while different welding directions of the 1st and the 2nd passed result in symmetric nuggets with AS/RS at the same side, as shown in Figure 4.59 (#4229&#4231). In DP, most joints were produced with a shoulder diameter of 25.4 mm,

the asymmetric layout of two passes, and without WS applied on the work-piece surface. Two passes in the joints #4226A&#4228B, #4226B&#4228A, and #4229&#4231 were symmetric. #4237&#4238 and #4243&#4244 were produced with WS. #4241&#4242 and #4243&#4244 were produced with a shoulder diameter of 30.5 mm.

Through previous study on SPH and SP, 1° setup, 12.7 mm long FSW tools with 1.3 mm flat/flute depth were applied in DP. In CSDP, different pin features (T+3CT and T+3F), FSW speeds, thermal boundary conditions (with/without water spray on the work-piece surface), welding directions of two passes (same or different), shoulder diameter were applied to investigate the appropriate FSW control parameter window and obtain desired CSDP joints. In SSDP, T+3F tool and different speeds were applied, to make desired SSDP joints which are also comparable to the sound CSDP joints.

Firstly, some trial welds as following were made to obtain appropriate speeds for CSDP: #4226A (200 rpm, 102 mm/min), #4226B (160 rpm, 102 mm/min), #4227A (320 rpm, 203 mm/min), #4227B (240 rpm, 203 mm/min), #4228A (240 rpm, 152 mm/min, symmetric), and #4228B (160 rpm, 152 mm/min, symmetric). Among the above joints, only when a rotation rate of 160 rpm and a welding speed of 102 mm/min produced defect free welds (as shown in Appendix C).

Then this set of speeds was applied in the following welds to determine which layout of passes and which pin feature are better for CSDP: #4229&#4230 (160 rpm, 102 mm/min), #4229&#4231 (symmetric, 160 rpm, 102 mm/min), #4232A&#4233A (asymmetric, 160 rpm, 152 mm/min), and #4232B&#4233B (asymmetric, 200 rpm, 203 mm/min). The above four CSDP joints were all defect free, and #4229&#4230 and #4229&#4231 have the PWHT UTS of 412 MPa and 406 MPa, respectively. It indicates

that, under the same speeds with the same tool, relative to a symmetric layout of passes, the asymmetric layout of CSDP passes increased the PWHT UTS a little. Relative to the T+3CT pin, with the same speeds and the same layout of passes (asymmetric), the T+3F allows much larger speeds, producing DF joints which are stronger. Therefore, the asymmetric layout and the T+3F pin were adopted for the following CSDP welds with the same speeds (200 rpm, 203 mm/min) while different TBCs and shoulder diameters: #4237&#4238 (WS, shoulder diameter 25.4 mm), #4241&#4242 (IA, shoulder diameter 30.5 mm), and #4243&#4244 (WS, shoulder diameter 30.5 mm).

Among the above joints, #4237, #4243 and #4244 were defective, as shown in Appendix C. #4232B&#4233B, #4237&#4238 and #4241&#4242 have PWHT UTS of 480 MPa, 470 MPa, and 433 MPa, respectively. It indicates that, with the same shoulder diameter, relative to the joint without WS, when WS was applied on the work-piece surface, it's difficult to produce defect free joints, and the PWHT UTS was reduced by 2%. What's more, relative to SP, in DP, temperature and power in each pass will be reduced by half penetration which involves much less material, hence overheating is much less likely to occur in DP. It also indicates that, without WS applied, relative to the shoulder diameter of 25.4 mm, the large shoulder diameter (30.5 mm) also produced DF joints, while reduced the PWHT UTS (-10%). Therefore WS will not be considered, and the shoulder diameter of 25.4 mm will be adopted in following CSDP joints: #4302&#4304 (160 rpm, 102 mm/min), and #4301&#4303 (200 rpm, 203 mm/min). In SSDP, the T+3F tool and different speeds were applied, to make the following desired SSDP joints which are also comparable to the sound CSDP joints: #4309&#4311 (160 rpm, 102 mm/min), and #4310&#4312 (200 rpm, 203 mm/min).

The 1st pass of DP (DP-1) before the welding of the 2nd pass (DP-2) on the same plate is the same with the SPH. They share the same effects of pin features, control parameters and thermal boundary conditions on material flow, thermal distribution, microstructure and properties. When the 1st pass is ready for welding, the plate is in the T7 condition, as same as the parent plate. When the 2nd pass is ready for welding, the plate has been affected the 1st pass. Especially, material inside the nugget of the 1st pass has been solution heat treated and therefore has changed from the T7 condition to the W condition, which will cause differences in physical, thermal and mechanical properties.

In this section, effects of shoulder types (CS and SS), pin features (T+3CT and T+3F), shoulder diameters (25.4 mm and 30.5 mm), FSW speeds, thermal boundary conditions (IA and WS), layouts of two passes and effect of the 2nd pass on DP joints have been studied in following aspects: macrostructure including investigation of surface finish, defect and nugget shape, microstructure, effect of control parameters on response parameters, grain size and hardness distribution, mechanical properties, etc.

4.3.1 Macrostructure

4.3.1.1 Surface finish

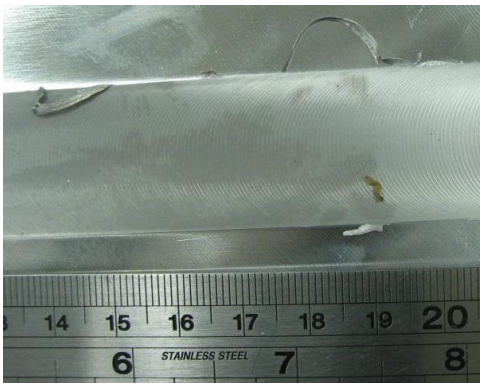

(a) #4302, 160 rpm, 102 mm/min, CSDP-1

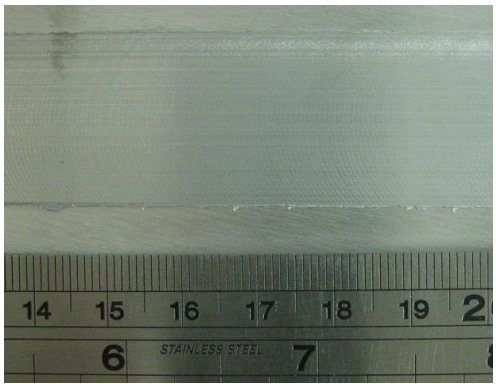

(b) #4309, 160 rpm, 102 mm/min, SSDP-1

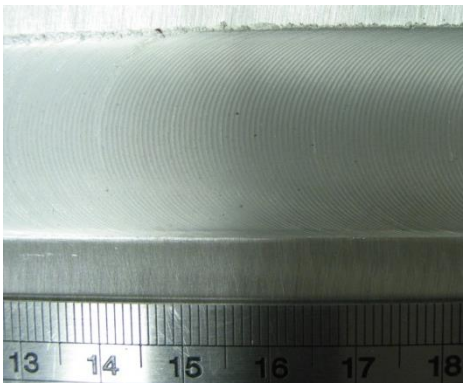

(c) #4304, 160 rpm, 102 mm/min, CSDP-2

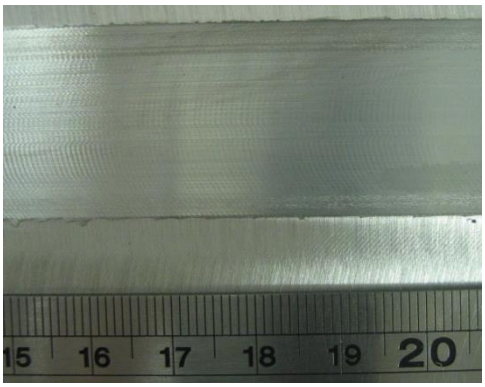

(d) #4311, 160 rpm, 102 mm/min, SSDP-2

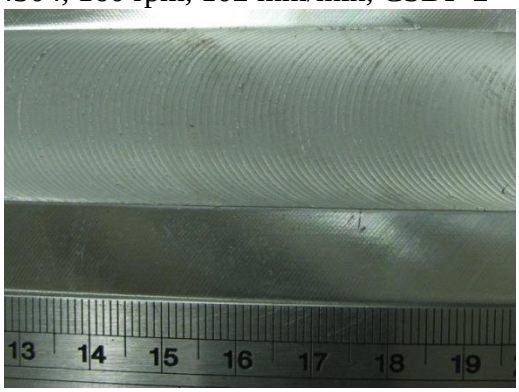

(e) #4301, 200 rpm, 203 mm/min, CSDP-1

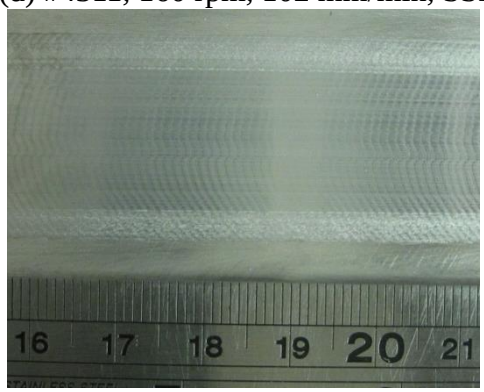

(f) #4310, 200 rpm, 203 mm/min, SSDP-1

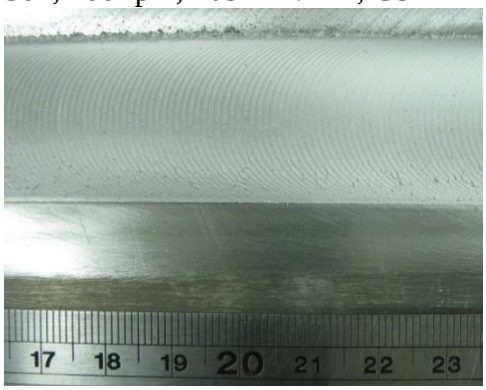

(g) #4303, 200 rpm, 203 mm/min, CSDP-2

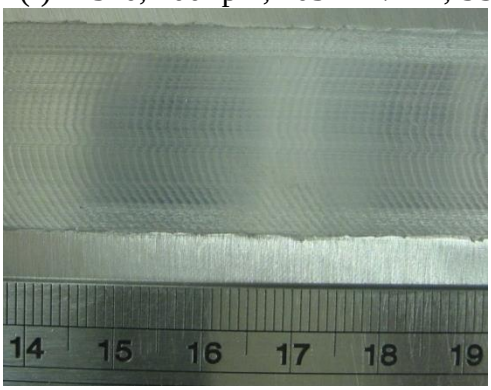

(h) #4312, 200 rpm, 203 mm/min, SSDP-2

Figure 4.56 Joint surfaces of DP: T+3F pin for CSDP, T+3CT for SSDP, 1 ℃ilt

In this section surface finish in DP was examined. Figure 4.56 shows joint surfaces of the 1st and 2nd passes in CSDP and SSDP, produced by the T+3F or T+3CT pins, with the same setup of 1° , with the same flat/flute depth of 1.3 mm and different speeds. All surfaces are smooth. The obvious semi-circular marks and flash (mostly at RS) can be seen on the CSDP joint surfaces. Keeping other parameters the same, relative to

CSDP produced with T+3F tool, in SSDP produced with T+3CT tool, the semi-circular marks on the surfaces are less clear and complete. Relative to CSDP, SSDP can produce joints with better surface finish due to the absence of shoulder rotation during SSFSW process. However, the difference SS caused in DP is much less than in SP due to the different amount of material involved in the welding process.

4.3.1.2 Defect investigation

The result of defect examination of DP joints is listed in Appendix C. It shows that, both CSDP and SSDP produced DF joints with the same speeds: (a) 160 rpm and 102 mm/min, and (b) 200 rpm and 203 mm/min.

In CSDP, when the T+3CT pin was applied, only the set of 160 rpm and 102 mm/min produced DF joints, which might due to the effect of pin features on material flow: when the FSW speed is too large, too much material will be moved downward to the weld root by the right-handed threads and upward to the weld crown by the counter-flow flutes, resulting surface defects and volumetric defects inside the nuggets, especially near the mid-plane. When the same T+3F tool, the same speeds (200 rpm, 203 mm/min) and the shoulder diameter of 25.4 mm were applied, WS applied on the work-piece surface caused the 1st pass defective (#4237, small holes at AS near crown and mid-plane) and the 2nd pass DF. When the same T+3F tool, the same speeds (200 rpm, 203 mm/min) and the shoulder diameter of 30.5 mm were applied, WS applied on the work-piece surface caused both the 1st pass (#4243, holes near mid-plane AS) and the 2nd pass (#4244, surface defect at AS) defective. It indicates that, WS applied at work-piece surface was difficult to produce DF joints. When the same T+3F tool, the same speeds (200 rpm, 203 mm/min) were applied, both the shoulder diameters of 25.4

mm and 30.5 mm produced DF joints. When the same T+3F tool, the same speeds (200 rpm, 203 mm/min) and the WS were applied, both the shoulder diameters of 25.4 mm and 30.5 mm produced defective joints, while the larger shoulder worsened the defects. Therefore WS will not be considered, and the shoulder diameter of 25.4 mm will be adopted in CSDP joints. When the T+3F pin was applied, both sets of speeds produced DF joints: (a) 160 rpm and 102 mm/min, and (b) 200 rpm and 203 mm/min.

In SSDP, when T+3CT pin was applied, the set of 160 rpm and 102 mm/min produced DF joints, while the set of 200 rpm and 203 mm/min produced the joint of which the 1st pass DF and the 2nd pass defective (#4312, worm holes at mid AS near crown). It indicates that in SSDP, higher speeds were more likely to cause defects near crown, especially in the 2nd pass.

4.3.1.3 Nugget

Figure 4.57~Figure 4.60 show the macro images of transverse cross sections of both CSDP and SSDP welds in 24.9 mm and 25.4 mm thick AA7099-T7651 plates. As for the asymmetric DP (in most cases), the AS of the 1st pass is on the left while the AS of the 2nd pass is on the right in each image of the cross section ,as shown in Figure 4.60. As for the symmetric DP (in one case: #4229&#4231), the AS of both the 1st pass and the 2nd pass are on the left in each image of the cross section, as shown in Figure 4.60.

Figure 4.57 shows macro transverse cross sections of CSDP in AA7099, which were produced with a setup of 1° tilt, by a T+3CT pin with a flute depth of 1.3 mm. Images of transverse cross sections in each column are with rotation rates (rpm), while images in each row are with welding speeds (mm/min). It shows that, under the same welding speed, higher rotation rate produced less tapered nuggets with similar HAZ

width near crown, more blurry NG boundary and larger TMAZ area. Under the same rotation rate (240 rpm), lower and higher welding speeds produced similar nuggets.

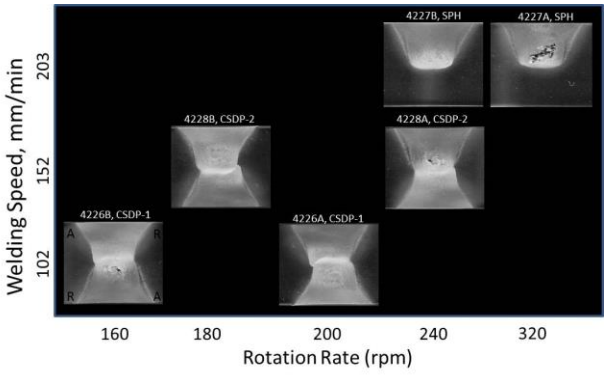

Figure 4.57 Macro Transverse Cross Sections of CSDP: different speeds, T+3CT pin, 1.3 mm flute depth, 1^0 tilt

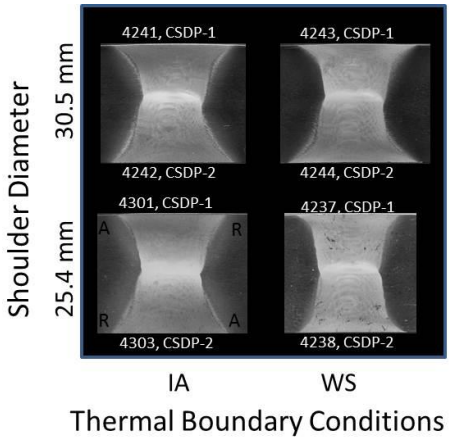

Figure 4.58 Macro Transverse Cross Sections of CSDP: different TBCs and tool shoulders, 1^0 tilt, T+3F pin, 1.3 mm flat depth, 160 rpm, 102 mm/min

Figure 4.58 shows macro transverse cross sections of CSDP in AA7099, which were produced with a setup of 1° tilt, by a T+3F pin with a flat depth of 1.3 mm, a rotation rate of 160 rpm, and a welding speed of 102 mm/min. Those macro images show that, relative to the weld made in air (IA), the weld produced with WS had a nugget with a little narrower HAZ near crown, more clear NG boundary and less TMAZ area. Relative to the shoulder diameter of 25.4 mm, larger shoulder diameter (30.5 mm)

produced joints with more tapered nugget, larger HAZ near crown, less clear NG boundary and a little larger TMAZ area.

Figure 4.59 shows macro transverse cross sections of CSDP in AA7099, which were produced with a setup of 1° tilt, by a T+3F pin with a flat depth of 1.3 mm, a rotation rate of 200 rpm, and a welding speed of 203 mm/min. Those macro images show that, when the T+3CT pin was applied, relative to symmetric CSDP, asymmetric CSDP produced the similar nugget, with a less offset between the 1st pass and the 2nd pass. When the asymmetric layout of passes was adopted, relative to the T+3CT pin, the T+3F pin produced the joint with a less tapered nugget, a little narrower HAZ at crown, and more clear NG boundary. That might because relative to the T+3CT pin, the T+3F pin moved less material upward.

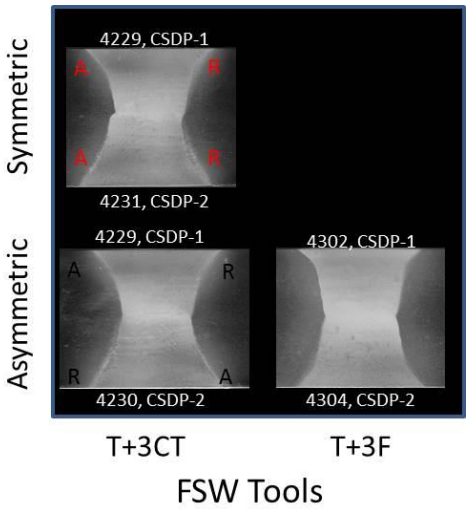

Figure 4.59 Macro Transverse Cross Sections of CSDP: different tool pins and layouts, 1^0 tilt, T+3F pin, 1.3 mm flat depth, 200 rpm, 203 mm/min

Figure 4.60 shows macro transverse cross sections of CSDP and SSDP in AA7099, which were produced with a setup of 1° tilt, by a T+3F pin or T+3CT pin with a flat depth of 1.3 mm. Those macro images show that, under the same speeds, relative to

CSDP, SSDP produced joints with a nugget shape more consistent to the pin shape, a narrower HAZ at crown, and a little less TMAZ area. All those differences may due to the absence of shoulder rotation results in different heat source distribution especially near crown in SSDP.

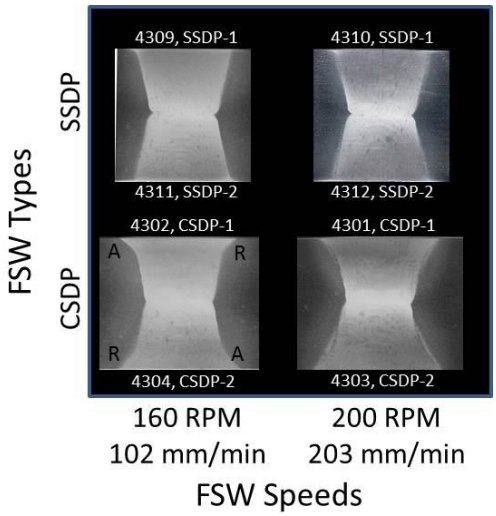

Figure 4.60 Macro Transverse Cross Sections of DP: 1.3 mm flat depth, 1^0 tilt

Figure 4.58~Figure 4.60 also show that relative to the 1st pass, the 2nd pass had a nugget with a little larger HAZ near crown, less clear NG boundary and a little larger TMAZ area.

4.3.2 Process Responses

Process response parameters include in plane reaction forces (F_x, F_y and the resultant force F_{xy}), torque, power, peak temperature measured at pin center (which was also considered as the peak temperature measured at center NG due to the pretty close positions) and grain size (GS) measured at center NG. Process response parameters were collected and calculated. Process response parameters as a function of tool rotation rate are summarized and shown in Figure 4.61 for CSDP-1 and Figure 4.63 for comparable DP welds of AA7099. Relationships among power input, temperature at pin center, and

GS at center nugget are summarized and shown in Figure 4.62 for CSDP-1, Figure 4.64 and Figure 4.65 for CSDP and SSDP.

In Figure 4.61~Figure 4.62, various symbols represent for different tools, welding speeds, TBCs, and shoulder diameters. Here most welds were produced with a normal shoulder diameter of 25.4 mm, and with normal thermal boundary conditions, which are in air environment nearby the work piece surface and the steel backing plate applying underneath the work piece bottom. “SD 30.5mm” was used to indicate welds were produced by a shoulder with a shoulder diameter of 30.5 mm. “WS” was used to indicate welds were produced with water spray applying at work piece surface.

In Figure 4.63~Figure 4.65, various symbols represent for different shoulder types (CS or SS), welding speeds, and the 1st or the 2nd pass. Here “DP-1” indicates the weld is the 1st pass of the DP, and “DP-2” indicates the weld is the 2nd pass of the DP.

4.3.2.1 Process Responses of CSDP

Figure 4.61 a~f show the response parameters as functions of tool rotation rate for the 1st pass of CSDP (CSDP-1) bead on plate welds on AA7099, produced with a setup of 1° , by a T+3CT or T+3F tool with a flat/flute depth of 1.35 mm. It shows that:

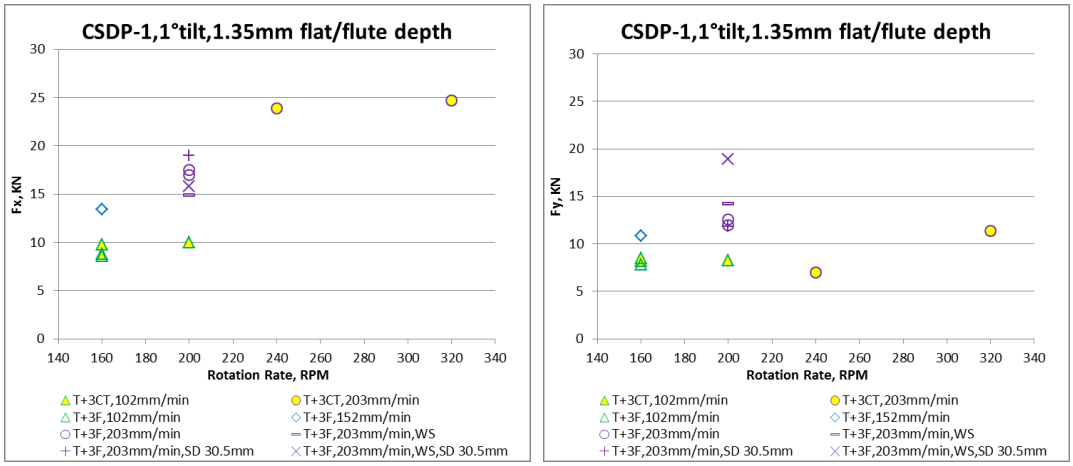

(a) (b)

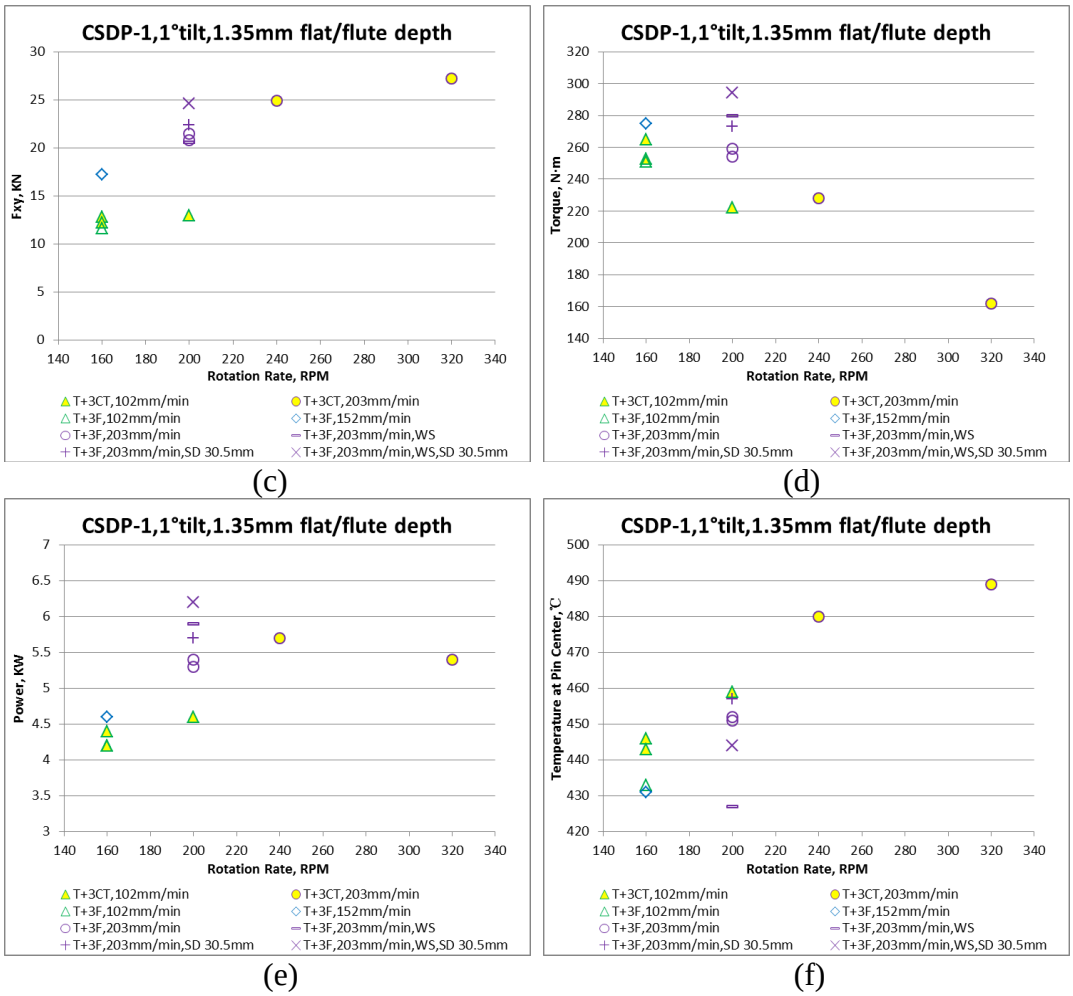

Figure 4.61 Reaction forces, torque, power, peak temperatures at pin center as functions of tool rotation rate in the 1st pass of CSDP (CSDP-1): a setup of 1° , a flat/flute depth of 1.35 mm

(1) When the T+3CT pin was applied, under the same welding speed (102 mm/min) and the same forge force (40 KN), higher rotation rate (200 rpm) affected F_y little, increased F_x (14%) and then F_{xy} a little (7%), decreased torque a little (-12%), increased power a little (10%) and then increased T at pin center slightly (4%).

(2) When the T+3CT pin was applied, under the same welding speed (203 mm/min), higher rotation rate (320 rpm) required a smaller F_z (-19%), then affected F_x little, increased F_y (63%), and increased F_{xy} a little (9%); decreased torque (-29%), and then decreased power (-5%) and temperature at pin center (-2%) slightly.

(3) When the T+3CT pin was applied, with the increasing of rotation rate, in the lower welding speed (102 mm/min), reaction forces were similar, torque decreased a little, power increased a little, and temperature at pin center increased a little. In the higher welding speed (203 mm/min), F_x and F_{xy} were similar, while F_y increased faster than that in the lower welding speed; torque increased at the similar slope with that in the lower welding speed joint; power decreased slightly, while temperature increased slower than that in the lower welding speed joint. When the power input increased, in the lower welding speed (102 mm/min), temperature at pin center increased a little; in the higher welding speed (203 mm/min), temperature at pin center decreased a little.

(4) With the same speeds (160 rpm, 102 mm/min) applied, relative to the T+3CT tool (#4229), the T+3F tool (#4302) required a little higher forge force (6%), decreased reaction forces a little (F_x: -2%; F_y: -8%; F_{xy}: -5%), affected torque and power little, and decreased the temperature at pin center slightly (-2%).

(5) When the same tool of T+3F and the same rotation rate (160 rpm) were applied, the higher welding speed (152 mm/min) required higher F_z (16%), then increased reaction forces (F_x: 56%; F_y: 39%; F_{xy}: 48%), increased torque (10%) and power (10%) a little, while affected temperature at pin center little.

(6) When the same tool of T+3F and the same speeds (200 rpm, 203 mm/min) were applied, relative to the CSDP-1 produced in air (IA) with a shoulder diameter of 25.4 mm, WS increased F_y (13%) a little while decreased F_z (-4%) and other reaction forces (F_x: -15%; F_{xy}: -4%), increased torque (8%) and power (9%) a little, while decreased the temperature at pin center a little (-5%); the shoulder with a diameter of 30.5 mm decreased F_y (-6%), while increased F_z (4%) and other reaction forces (F_x: 9%; F_{xy}:

4%), increased torque (5%) and power (7%) a little, while affected the temperature at pin center slightly (1%); when both WS and the larger shoulder (30.5 mm) were applied, F_x decreased (-10%), F_y (50%) and F_{xy} (14%) increased, torque (14%) and power (15%) increased, and temperature at pin center was affected slightly (-2%). When WS was applied, T at pin center was decreased to some extent, which also caused volumetric defects inside the joints, according to the defect investigation results in section 4.3.1.2.

Figure 4.62 shows temperature at center pin as a function of power input for the 1st pass of CSDP (CSDP-1) bead on plate welds on AA7099, produced with a setup of 1°, by a T+3CT or T+3F tool with a flat/flute depth of 1.35 mm. It indicates that power affected temperature at pin center little.

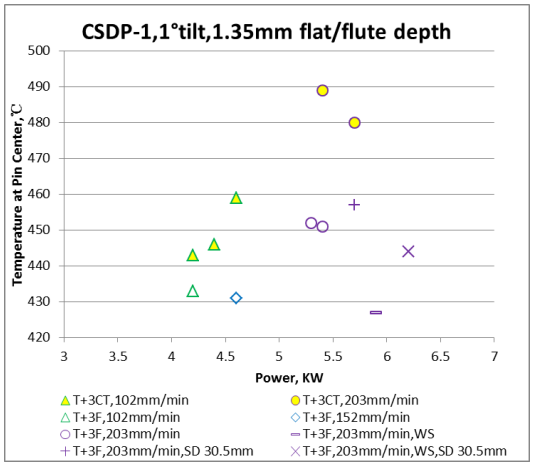

Figure 4.62 T at center pin as a function of power input in the 1st pass of CSDP (CSDP-1): a setup of 1°, a flat/flute depth of 1.35 mm

4.3.2.2 Process Responses of CSDP and SSDP

The applicable speeds of CSDP and SSDP listed in Appendix B show that, the T+3F tool is better for CSDP and the T+3CT tool is better for SSDP to allow similar welding parameter windows and produce desired joints. Figure 4.63 and Figure 4.64

show some the response parameters of the 1st passes and the 2nd passed of comparable CSDP and SSDP joints.

Figure 4.63 a~g show the response parameters as functions of tool rotation rate for the 1st pass of DP (DP-1) and the 2nd pass of DP (DP-2) bead on plate welds on AA7099, produced with a setup of 1° , by a T+3CT or T+3F tool with a flat/flute depth of 1.35 mm. It indicates that:

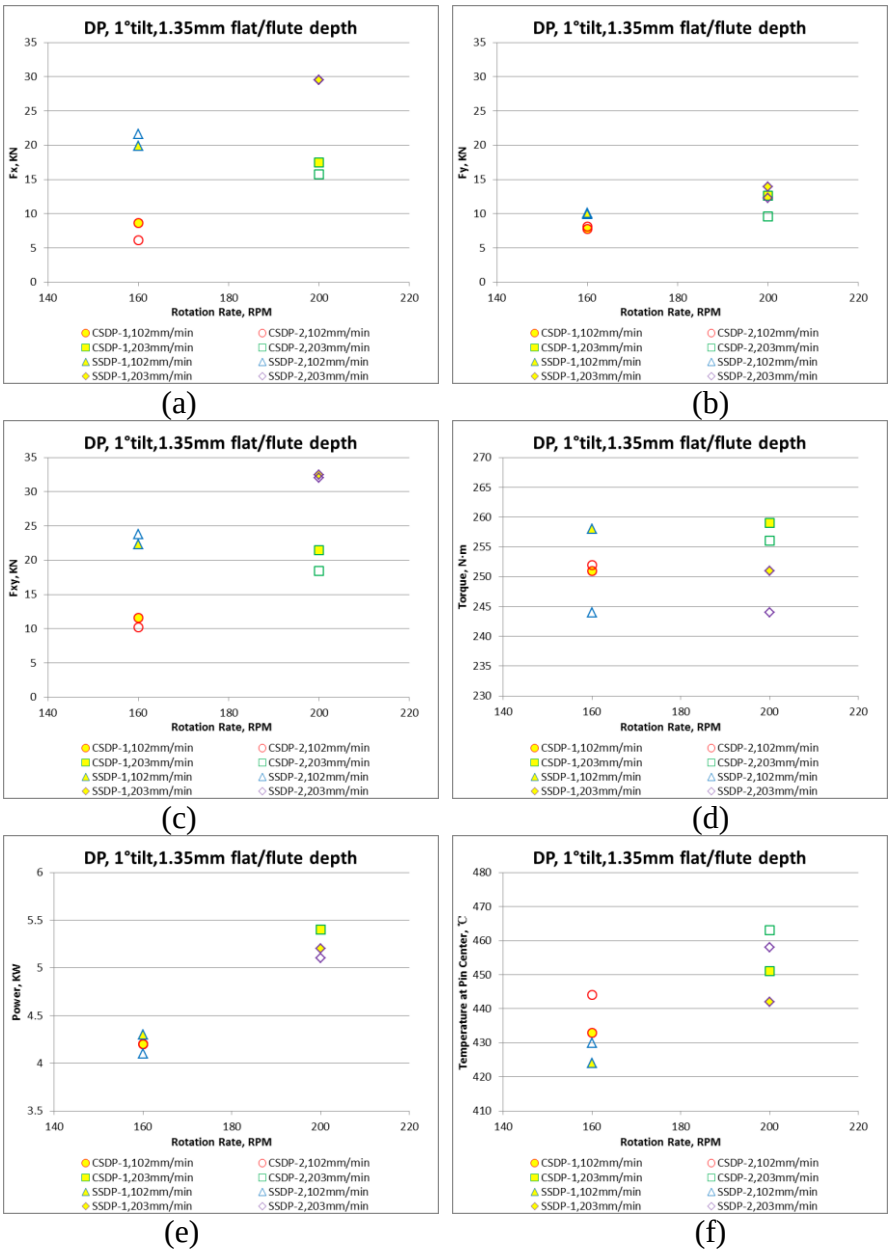

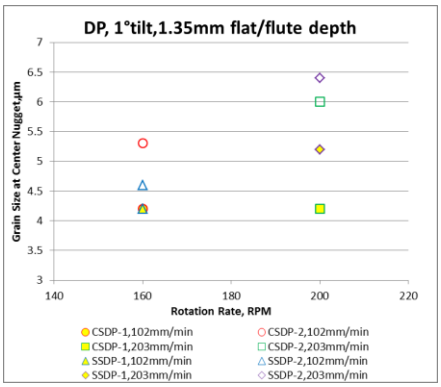

(g)

Figure 4.63 Reaction forces, torque, power, peak T and GS at pin center as functions of tool rotation rate in the 1st pass of DP (DP-1) and the 2nd pass of DP (DP-2): a setup of 1° , a flat/flute depth of 1.35 mm

(1) In CSDP-1, higher speeds required 31% higher F_z, increased F_x by 104%, increased F_y by 62%, increased F_{xy} by 85%, increased torque by 3%, increased power by 29%, increased temperature at pin center by 4%, and affected GS at center NG little. In CSDP-2, higher speeds required 34% higher F_z, increased F_x by 157%, increased F_y by 19%, increased F_{xy} by 80%, increased torque by 2%, increased power by 29%, increased temperature at pin center by 4%, and increased GS at center NG by 13%.

(2) In SSDP-1, higher speeds required 22% higher F_z, increased F_x by 48%, increased F_y by 40%, increased F_{xy} by 46%, decreased torque by 3%, increased power by 21%, increased temperature at pin center by 4%, and increased GS at center NG by 24%. In SSDP-2, higher speeds required 22% higher F_z, increased F_x by 37%, increased F_y by 22%, increased F_{xy} by 35%, affected torque little, increased power by 24%, increased temperature at pin center by 7%, and increased GS at center NG by 39%.

(3) In CSDP, when the lower speeds were applied, relative to the 1st pass, the 2nd pass required 5% lower F_z, decreased F_x by 29%, increased F_y by 4%, decreased F_{xy} by 12%, affected torque and power little, increased temperature at pin center by 3%, and

increased GS at center NG by 26%. In CSDP, when the higher speeds were applied, relative to the 1st pass, the 2nd pass required 4% lower F_z, decreased F_x by 10%, decreased F_y by 24%, decreased F_{xy} by 14%, decreased torque by 1%, affected power little, increased temperature at pin center by 3%, and increased GS at center NG by 43%.

(4) In SSDP, when the lower speeds were applied, relative to the 1st pass, the 2nd pass required the same F_z, increased F_x by 9%, increased F_y by 2%, increased F_{xy} by 7%, decreased torque by 5%, decreased power by 5%, increased temperature at pin center by 1%, and increased GS at center NG by 10%. In SSDP, when the higher speeds were applied, relative to the 1st pass, the 2nd pass required the same F_z, affected F_x little, decreased F_y by 12%, decreased F_{xy} by 2%, decreased torque by 3%, decreased power by 2%, increased temperature at pin center by 4%, and increased GS at center NG by 23%.

(5) In DP-1, when the lower speeds were applied, relative to CS, SS decreased the required F_z by 15%, increased F_x by 131%, increased F_y by 27%, increased F_{xy} by 92%, increased torque by 3%, increased power by 2%, decreased temperature at pin center by 2%, and affected GS at center NG little; In DP-1, when the higher speeds were applied, relative to CS, SS decreased the required F_z by 22%, increased F_x by 69%, increased F_y by 10%, increased F_{xy} by 51%, decreased torque by 3%, decreased power by 4%, decreased temperature at pin center by 2%, and increased GS at center NG by 24%.

(6) In DP-2, when the lower speeds were applied, relative to CS, SS decreased the required F_z by 11%, increased F_x by 254%, increased F_y by 25%, increased F_{xy} by 133%, decreased torque by 3%, decreased power by 2%, decreased temperature at pin center by 3%, and decreased GS at center NG by 13%; In DP-2, when the higher speeds were applied, relative to CS, SS decreased the required F_z by 19%, increased F_x by 88%,

increased F_y by 28%, increased F_{xy} by 74%, decreased torque by 5%, decreased power by 6%, decreased temperature at pin center by 1%, and increased GS at center NG by 7%.

The above observations indicate that,

(1) In CSDP, higher speeds required higher F_z, increased reaction forces a lot, increased torque a little, increased power, and increased temperature at pin center. When speeds increased, relative to CSDP-1, in CSDP-2, F_x increased more, F_y increased much less; GS at center NG of CSDP-1 kept the same while that of CSDP-2 increased. In CSDP, relative to CSDP-1, in CSDP-2, required F_z decreased a little, F_x decreased, F_{xy} decreased, torque and power were similar, temperature at pin center increased slightly, and GS at center NG increased. When the lower speeds were applied, F_x decreased more, F_y increased slightly, and GS at center NG increased less. When the higher speeds were applied, F_y decreased.

(2) In SSDP, higher speeds required the same F_z, increased reaction forces, affected torque little, increased power, increased temperature at pin center a little, and increased GS at center NG. When speeds increased, relative to SSDP-1, in SSDP-2, reaction forces increased less, power, temperature at pin center and GS at center NG increased a little more. In SSDP, relative to SSDP-1, in SSDP-2, required F_z was the same, reaction forces increased a little when the lower speeds were applied, while F_x and F_{xy} were similar, F_y decreased when the higher speeds were applied; torque and power decreased a little, while temperature at pin center and GS at center NG increased a little. When the lower speeds were applied, torque and power decreased more, while temperature and GS increased less.

(3) In DP, relative to CS, SS decreased the required F_z, increased reaction forces (the difference was larger when the lower speeds were applied, and/or in the 2nd pass), affected torque, power and temperature little, affected GS little in DP-1 with lower speeds, increased GS in DP-1 with higher speeds, decreased GS in DP-2 with lower speeds, and increased GS a little in DP-2 with higher speeds.

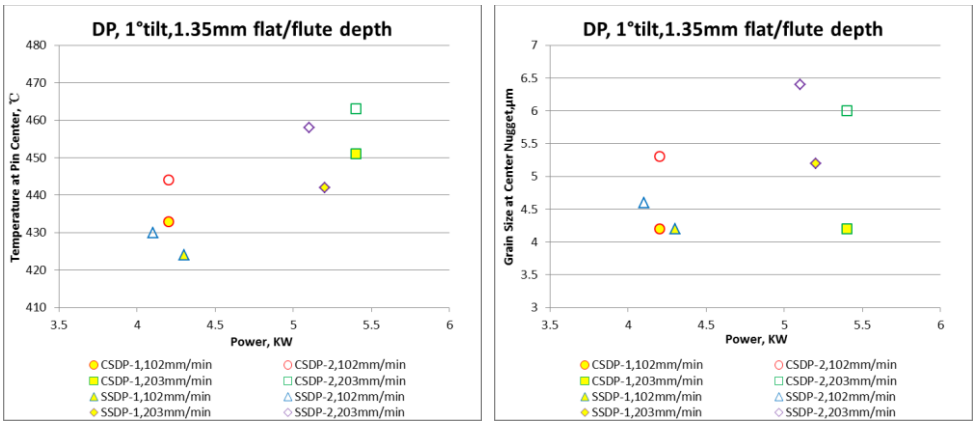

(a) (b)

Figure 4.64 (a) Temperature at center pin and (b) GS at center nugget as functions of power input in the 1st pass of DP (DP-1) and the 2nd pass of DP (DP-2): a setup of 1° , a flat/flute depth of 1.35 mm

Figure 4.64 shows (a) temperature at center pin and (b) GS at center nugget as functions of power input for the 1st pass of DP (DP-1) and the 2nd pass of DP (DP-2) bead on plate welds on AA7099, produced with a setup of 1° , by a T+3CT or T+3F tool with a flat/flute depth of 1.35 mm. It shows that:

(1) Relative to CSDP-1, in CSDP-2, power was similar, temperature at pin center was a little higher, and GS at center NG was larger. When speeds increased, temperature difference kept the same, while GS difference increased. Relative to SSDP-1, in SSDP-2, power and T at pin center were a little higher, and GS at center NG was larger. When speeds increased, power difference decreased, T difference and GS difference increased.

(2) When speeds increased, power increased, temperature at pin center increased, GS at center NG increased (except in the CSDP-1 which kept the similar).

(3) Relative to CSDP, in SSDP, when the lower speeds were applied, power was a little larger, temperature was a little lower, GS in the 1st pass was similar, while GS in the 2nd pass was smaller; when the higher speeds were applied, power was a little smaller, and temperature was a little lower, GS was larger and the GS difference was smaller in the 2nd pass relative to the 1st pass.

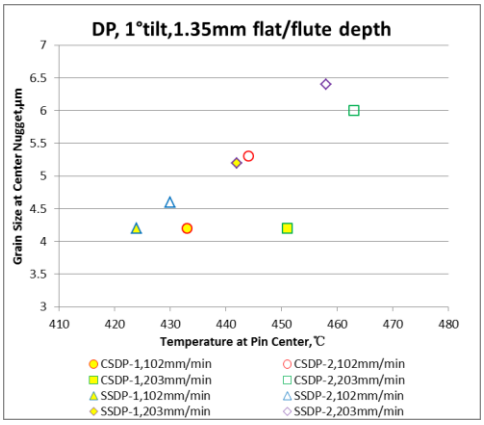

Figure 4.65 GS at center nugget as a function of Temperature at center pin in the 1st pass of DP (DP-1) and the 2nd pass of DP (DP-2): a setup of 1° , a flat/flute depth of 1.35 mm

Figure 4.65 shows GS at center nugget as a function of T at center pin for the 1st pass of DP (DP-1) and the 2nd pass of DP (DP-2) bead on plate welds on AA7099, produced with a setup of 1° , by a T+3CT or T+3F tool with a flat/flute depth of 1.35 mm. It shows that, when temperature at pin center increased, GS at center NG increased.

4.3.3 Hardness distribution through thickness

In this section, hardness on weld centerline through thickness in DP have been studied to investigate effects of shoulders on property variations through thickness.

4.3.3.1 Hardness distribution through thickness of CSDP

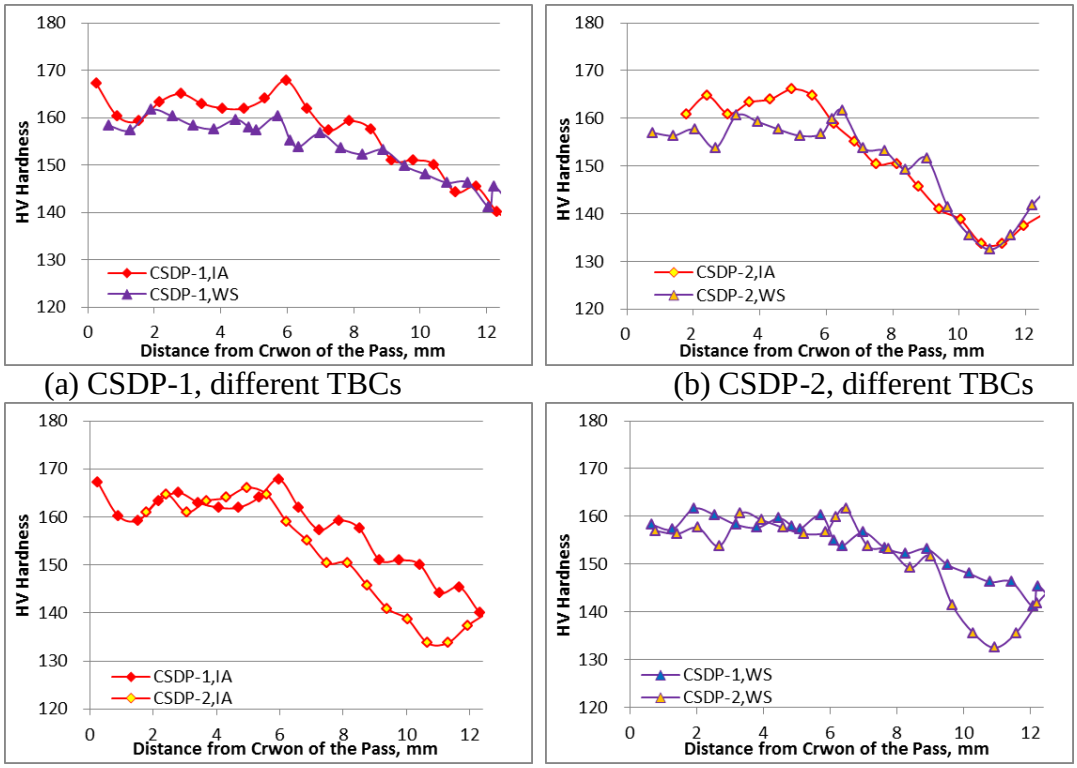

(a) CSDP-1, different TBCs (b) CSDP-2, different TBCs

(c) CSDP, IA: #4232B&#4233B (d) CSDP, WS: #4237&#4238

Figure 4.66 Hardness as a function of distance from crown of each pass on the weld centerline in CSDP: different TBCs, PWHT, same T+3F pin, 200 RPM, 203 mm/min

Figure 4.66 shows the hardness as a function of distance from crown of each pass on the weld centerline in PWHT condition of CSDP joints produced with the same T+3F tool, the same rotation rate of 200 rpm, the same welding speed of 203 mm/min, and different thermal boundary conditions indicated as “IA” and “WS”. “IA” and “WS” were used to indicate welds were produced without and with water spray applying at work piece surface, respectively. Those joints were produced with the same tool (T+3F), same speeds (200 rpm, 203 mm/min) and different TBCs as following: #4232B&#4233B (IA), and #4237&#4238 (WS). Figure 4.66 indicates that:

(1) Effects of different TBCs:

Relative to joints produced without water spray (IA), in CSDP-1, water spray (WS) affected the minimum hardness values little, which was a little closer (-7%) to the weld crown of the 1st pass; WS affected the maximum hardness values little, which was much closer (-68%) to the weld crown of the 1st pass; WS also significantly decreased range of hardness variation through thickness (-33%). In CSDP-2, WS affected the minimum hardness values little, which was a little closer (-3%) to the weld crown of the 2nd pass; WS affected the maximum hardness values little, which was further (30%) from the weld crown of the 2nd pass; WS also decreased range of hardness variation through thickness a little (-10%). WS decreased the distance of maximum hardness location to the weld crown of pass in CSDP-1, while increased the distance of maximum hardness location to the weld crown of pass in CSDP-2. WS had a larger effect on the 1st pass, especially on decreasing the hardness variation range.

(2) Effect of the 2nd pass

When joints were produced without water spray (IA), relative to the CSDP-1, the CSDP-2 affected the minimum hardness values little, which was closer (-13%) to the weld crown of the passes; the CSDP-2 affected the maximum hardness values little, which was closer (-16%) to the weld crown of the passes; the CSDP-2 slightly increased the range of hardness variation through thickness (6%). When joints were produced with water spray (WS), relative to the CSDP-1, the CSDP-2 decreased the minimum hardness values a little (-6%), which was closer (-10%) to the weld crown of the passes; the CSDP-2 affected the maximum hardness values little, which was much further (240%) from the weld crown of the passes; the CSDP-2 significantly increased the range of hardness variation through thickness (43%).

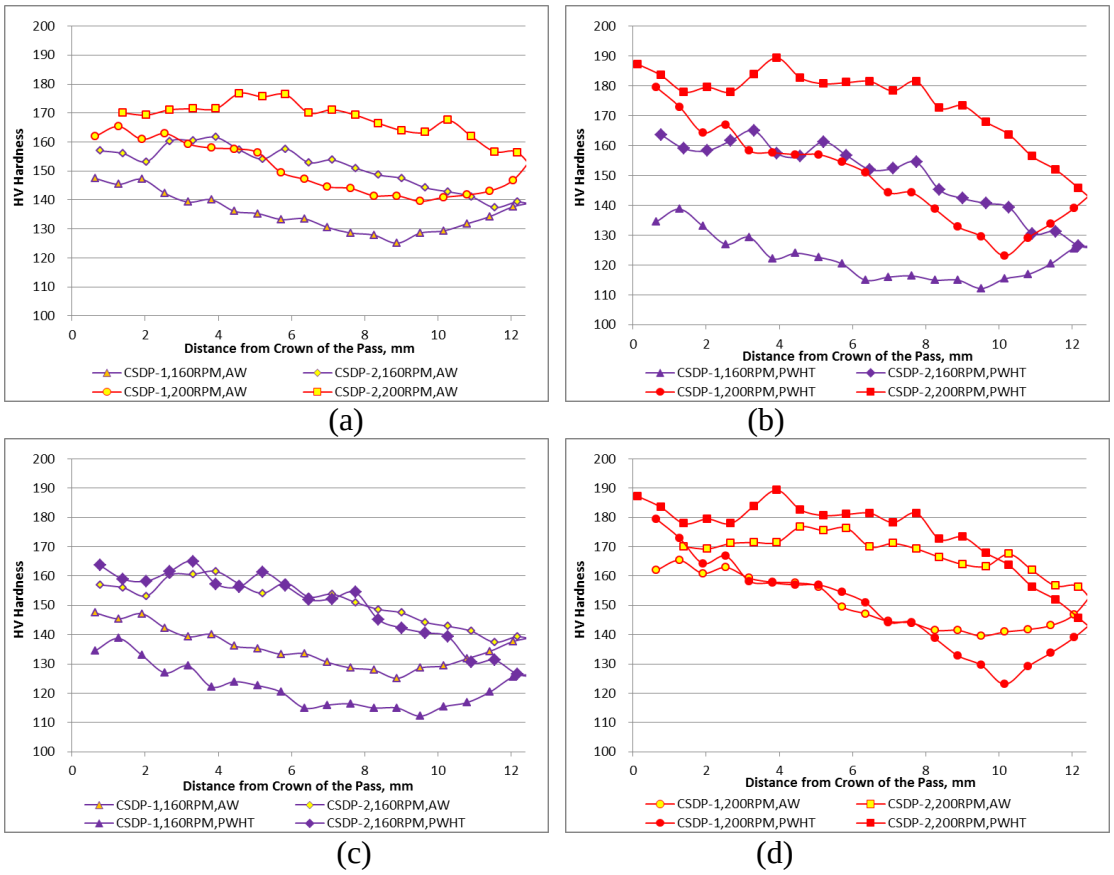

Figure 4.67 Hardness as a function of distance from crown of each pass on the weld centerline of CSDP: different speeds, AW and PWHT, T+3F pin, 1.3 mm flat depth

Figure 4.67 shows the hardness as a function of distance from crown of each pass on the weld centerline in AW and PWHT conditions of CSDP produced with the same T+3F tool and different speeds as following: #4302&#4304 (160 rpm, 102 mm/min), and #4301&#4303 (200 rpm, 203 mm/min). Figure 4.67 indicates that:

(1) Effects of different speeds

When joints were produced by higher speeds, in AW CSDP-1, higher speeds increased the minimum hardness a little (12%), which was a little further (7%) from the weld crown of the 1st pass; higher speeds increased the maximum hardness a little (12%), which was much further (100%) from the weld crown of the 1st pass; higher speeds also increased the range of hardness variation (16%). In PWHT CSDP-1, higher speeds

increased the minimum hardness a little (10%), which was a little further (7%) from the weld crown of the 1st pass; higher speeds increased the maximum hardness (29%), which was much closer (-50%) to the weld crown of the 1st pass; higher speeds also significantly increased the range of hardness variation (113%). In AW CSDP-2, higher speeds increased the minimum hardness a little (14%), which was slightly further (5%) from the weld crown of the 2nd pass; higher speeds increased the maximum hardness a little (9%), which was further (18%) from the weld crown of the 2nd pass; higher speeds also decreased the range of hardness variation a little (-15%). In PWHT CSDP-2, higher speeds increased the minimum hardness a little (15%), with the same distance from the weld crown of the 2nd pass; higher speeds increased the maximum hardness a little (15%), which was further (18%) from the weld crown of the 2nd pass; higher speeds also increased the range of hardness variation a little (14%).

(2) Effect of the 2nd pass

Relative to CSDP-1, when AW joints were produced by lower speeds, CSDP-2 increased the minimum hardness a little (10%), which was further (31%) from weld crown of the passes; CSDP-2 increased the maximum hardness a little (10%), which was significantly further (514%) from weld crown of the passes; CSDP-2 also increased the range of hardness variation a little (9%). When PWHT joints were produced by lower speeds, CSDP-2 increased the minimum hardness a little (13%), which was further (28%) from weld crown of the passes; CSDP-2 increased the maximum hardness (19%), which was significantly further (160%) from weld crown of the passes; CSDP-2 also significantly increased the range of hardness variation (45%). When AW joints were produced by higher speeds, CSDP-2 increased the minimum hardness a little (12%),

which was further (28%) from weld crown of the passes; CSDP-2 increased the maximum hardness slightly (7%), which was significantly further (262%) from weld crown of the passes; CSDP-2 also decreased the range of hardness variation (-21%). When PWHT joints were produced by higher speeds, CSDP-2 increased the minimum hardness (19%), which was further (20%) from weld crown of the passes; CSDP-2 increased the maximum hardness slightly (6%), which was significantly further (514%) from weld crown of passes; CSDP-2 also decreased range of hardness variation (-23%).

(3) Effect of PWHT

Relative to AW condition, when CSDP-1 joints were produced by lower speeds, PWHT decreased the minimum hardness a little (10%), which was a little further (7%) from the weld crown of the 1st pass; PWHT decreased the maximum hardness slightly (-6%), which was much further (100%) from the weld crown of the 1st pass; PWHT also increased the range of hardness variation (19%). When CSDP-1 joints were produced by higher speeds, PWHT decreased the minimum hardness a little (-12%), which was slightly further (7%) from the weld crown of the 1st pass; PWHT increased the maximum hardness slightly (9%), which was much closer (-50%) to the weld crown of the 1st pass; PWHT also significantly increased the range of hardness variation (118%). When CSDP-2 joints were produced by lower speeds, PWHT decreased the minimum hardness slightly (-8%), which was slightly further (5%) from the weld crown of the 2nd pass; PWHT affected the maximum hardness little, which was a little closer (-15%) to the weld crown of the 2nd pass; PWHT also significantly increased the range of hardness variation (59%). When CSDP-2 joints were produced by higher speeds, PWHT decreased the minimum hardness slightly (-7%), with the same distance from the weld crown of the 2nd

pass; PWHT increased the maximum hardness slightly (7%), which was a little closer (-15%) to the weld crown of the 2nd pass; PWHT also significantly increased the range of hardness variation (113%).

4.3.3.2 Hardness distribution through thickness of SSDP

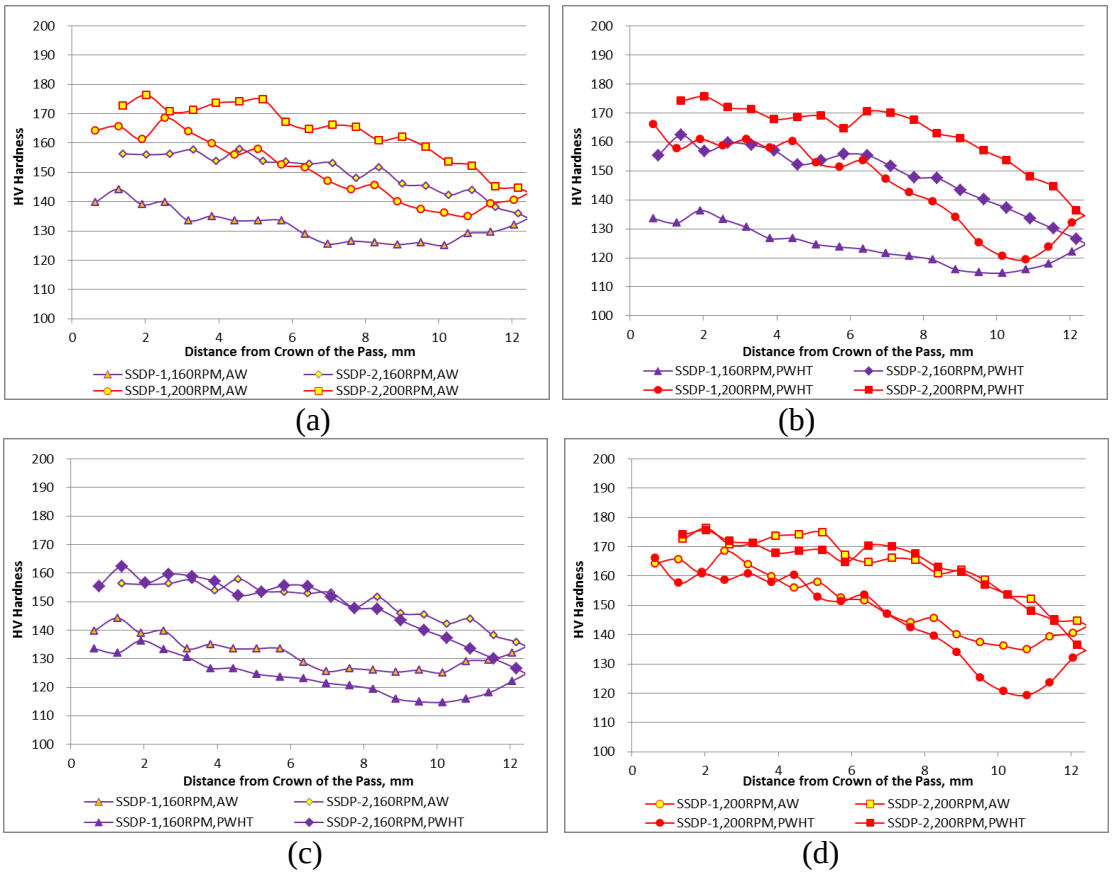

Figure 4.68 Hardness as a function of distance from crown of each pass on the weld centerline of SSDP: different speeds, AW and PWHT, T+3CT pin, 1.3 mm flat depth

Figure 4.68 shows the hardness as a function of distance from crown of each pass on the weld centerline in AW and PWHT conditions of SSDP produced with the same T+3CT tool and different speeds as following: #4309&#4311 (160 rpm, 102 mm/min), and #4310&#4312 (200 rpm, 203 mm/min). Figure 4.68 indicates that:

(1) Effects of different speeds

When joints were produced by higher speeds, in AW SSDP-1, higher speeds increased the minimum hardness increased slightly (8%), which was slightly further (6%) from the weld crown of the 1st pass; higher speeds increased the maximum hardness a little (17%), which was much further (100%) from the weld crown of the 1st pass; higher speeds also significantly increased the range of hardness variation (75%). In PWHT SSDP-1, higher speeds increased the minimum hardness slightly (4%), which was slightly further (6%) from the weld crown of the 1st pass; higher speeds increased the maximum hardness (22%), which was significantly closer (-67%) to the weld crown of the 1st pass; higher speeds also significantly increased the range of hardness variation (117%). In AW SSDP-2, higher speeds increased the minimum hardness slightly (6%), with the same distance from the weld crown of the 2nd pass; higher speeds increased the maximum hardness a little (12%), which was significantly closer (-57%) to the weld crown of the 2nd pass; higher speeds also significantly increased the range of hardness variation (44%). In PWHT SSDP-2, higher speeds increased the minimum hardness slightly (8%), with the same distance from the weld crown of the 2nd pass; higher speeds increased the maximum hardness slightly (8%), which was significantly further (43%) from the weld crown of the 2nd pass; higher speeds also increased the range of hardness variation slightly (10%).

(2) Effect of the 2nd pass

Relative to SSDP-1, when AW joints were produced by lower speeds, SSDP-2 increased the minimum hardness slightly (9%), which was further (20%) from weld crown of the passes; SSDP-2 increased the maximum hardness slightly (10%), which was significantly further (262%) from weld crown of the passes; SSDP-2 also increased the

range of hardness variation a little (16%). When PWHT joints were produced by lower speeds, SSDP-2 increased the minimum hardness a little (10%), which was further (20%) from weld crown of the passes; SSDP-2 increased the maximum hardness (19%), which was closer (-27%) to weld crown of the passes; SSDP-2 also significantly increased the range of hardness variation (66%). When AW joints were produced by higher speeds, SSDP-2 increased the minimum hardness slightly (7%), which was a little further (13%) from weld crown of the passes; SSDP-2 increased the maximum hardness slightly (5%), which was closer (-21%) to weld crown of the passes; SSDP-2 also decreased the range of hardness variation slightly (-5%). When PWHT joints were produced by higher speeds, SSDP-2 increased the minimum hardness a little (14%), which was a little further (13%) from weld crown of the passes; SSDP-2 increased the maximum hardness slightly (6%), which was significantly further (215%) from weld crown of the passes; SSDP-2 also decreased the range of hardness variation a little (-16%).

(3) Effect of PWHT

Relative to AW condition, when SSDP-1 joints were produced by lower speeds, PWHT decreased the minimum hardness slightly (-8%), with the same distance from the weld crown of the 1st pass; PWHT decreased the maximum hardness slightly (-6%), which was much further (50%) from the weld crown of the 1st pass; PWHT also increased the range of hardness variation a little (13%). When SSDP-1 joints were produced by higher speeds, PWHT decreased the minimum hardness a little (-12%), with the same distance from the weld crown of the 1st pass; PWHT affected the maximum hardness little, which was much closer (-75%) to the weld crown of the 1st pass; PWHT also significantly increased the range of hardness variation (39%). When SSDP-2 joints

were produced by lower speeds, PWHT decreased the minimum hardness slightly (-7%), with the same distance from the weld crown of the 2nd pass; PWHT affected the maximum hardness little, which was much closer (-70%) to the weld crown of the 2nd pass; PWHT also significantly increased the range of hardness variation (61%). When SSDP-2 joints were produced by higher speeds, PWHT decreased the minimum hardness slightly (-6%), with the same distance from the weld crown of the 2nd pass; PWHT affected the maximum hardness little, with the same distance from the weld crown of the 2nd pass; PWHT also increased the range of hardness variation 23(%).

4.3.3.3 Hardness distribution through thickness of CSDP and SSDP

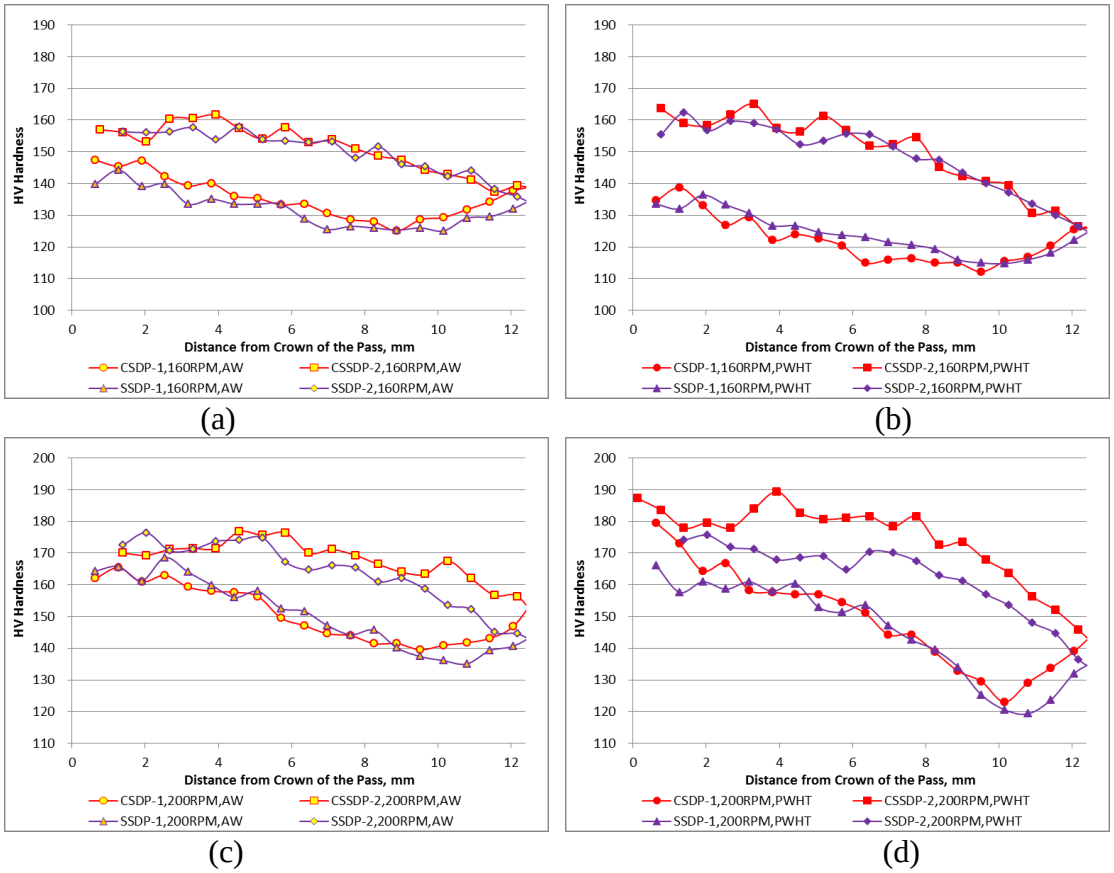

Figure 4.69 Through thickness hardness on the weld centerline of DP: different pin features and speeds, AW and PWHT, 1.3 mm flat/flute depth

Figure 4.69 shows the hardness as a function of distance from crown of each pass on the weld centerline in AW and PWHT conditions of CSDP and SSDP produced with different speeds and pin features with the same flat/flute depth of 1.3mm. Weld information of those joints, #4302&#4304, #4301&#4303, #4309&#4311 and #4310&#4312, has been listed in section 4.3.3.1 and section 4.3.3.2.

Figure 4.69 show that: Relative to CS, when AW DP-1 joints were produced by lower speeds, SS affected the minimum hardness little, which was a little further (14%) from the weld crown of the 1st pass; SS affected the maximum hardness little, which was significantly further (100%) from the weld crown of the 1st pass; SS also decreased the range of hardness variation a little (-14%). When PWHT DP-1 joints were produced by lower speeds, SS affected the minimum hardness little, which a slightly further (7%) from the weld crown of the 1st pass; SS affected the maximum hardness little, which was significantly further (50%) from the weld crown of the 1st pass; SS also decreased the range of hardness variation (-19%). When AW DP-1 joints were produced by higher speeds, SS affected the minimum hardness little which was slightly further (5%) from the weld crown of the 1st pass; SS affected the maximum hardness little, which was further (18%) from the weld crown of the 1st pass; SS also decreased the range of hardness variation slightly (-8%). When PWHT DP-1 joints were produced by higher speeds, affected the minimum hardness little, with the same distance from the weld crown of the 1st pass; SS affected the maximum hardness little, which was significantly closer (-58%) to the weld crown of the 1st pass; SS also decreased the range of hardness variation slightly (-7%). When AW DP-2 joints were produced by lower speeds, SS affected the minimum hardness little, which was a little further (13%) from the weld crown of the 2nd

pass; SS affected the maximum hardness little, which was significantly further (100%) from the weld crown of the 2nd pass; SS also increased the range of hardness variation (30%). When PWHT DP-2 joints were produced by lower speeds, SS affected the minimum hardness little, which was slightly further (6%) from the weld crown of the 2nd pass; SS decreased the maximum hardness slightly (-8%), with the same distance from the weld crown of the 2nd pass; SS also decreased the range of hardness variation (-17%). When AW DP-2 joints were produced by higher speeds, SS slightly decreased the minimum hardness (-8%), with the same distance from the weld crown of the 2nd pass; SS affected the maximum hardness little, which was significantly closer (-57%) to the weld crown of the 2nd pass; SS also significantly increased the range of hardness variation (56%). When PWHT DP-2 joints were produced by higher speeds, SS slightly decreased the minimum hardness (-7%), with the same distance from the weld crown of the 2nd pass; SS slightly decreased the maximum hardness (-7%), which was significantly closer (-49%) to the weld crown of the 2nd pass; SS also slightly decreased the range of hardness variation (-10%).

4.3.4 Transverse hardness distribution

Hardness tests were performed transverse to weld at various depths near crown, at mid-plane, near root and at root in both AW and PWHT conditions of the 1st and 2nd passed of CSDP and SSDP joints. Transverse hardness profiles were shown in **错误!未找到引用源。** a~d and Figure 4.71 a~h for CSDP joints and Figure 4.72 a~h for SSDP joints. HAZ minimum hardness at AS and RS, HAZ width, nugget average hardness were extracted from those transverse hardness profiles and plotted in Figure 4.73, Figure 4.74, Figure 4.78, Figure 4.82and Figure 4.83. Effects of speeds, the 2nd pass, and PWHT on

HAZ minimum hardness, nugget average hardness and HAZ width at various depths of DP joints were plotted in Figure 4.75~Figure 4.77, Figure 4.79~Figure 4.81, and Figure 4.84~Figure 4.86, where positive values indicate the effect of increasing and negative values indicate the effect of decreasing.

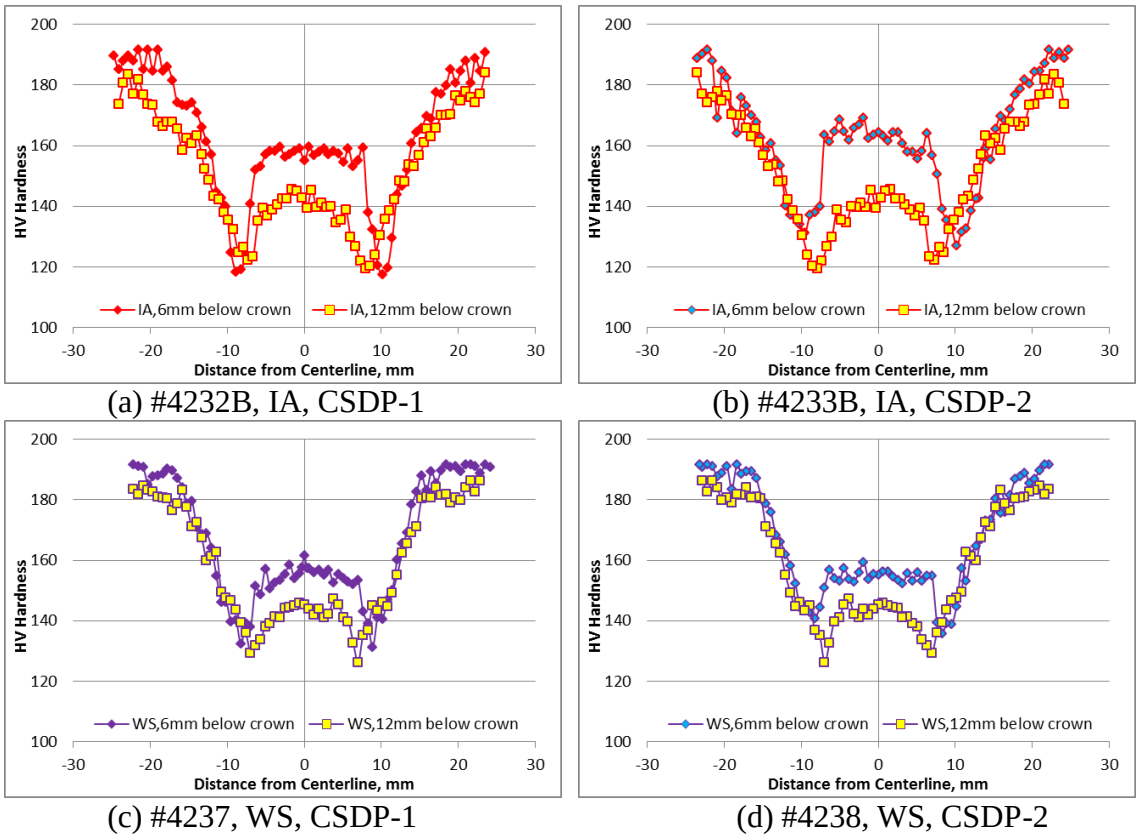

(a) #4232B, IA, CSDP-1 (b) #4233B, IA, CSDP-2

(c) #4237, WS, CSDP-1 (d) #4238, WS, CSDP-2

Figure 4.70 Transverse hardness profiles of each pass at various depths at mid-plane (6mm below crown), and at root (12mm below crown) in PWHT condition of CSDP with different TBCs: T+3F pin, 1.3 mm flat depth, 200 RPM, 203 mm/min

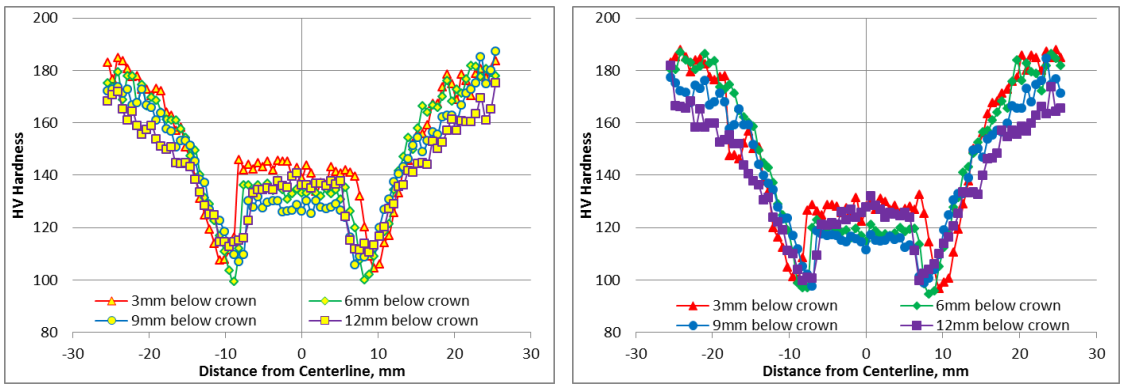

(a) #4302, CSDP-1, 160 RPM, AW (b) #4302, CSDP-1, 160 RPM, PWHT

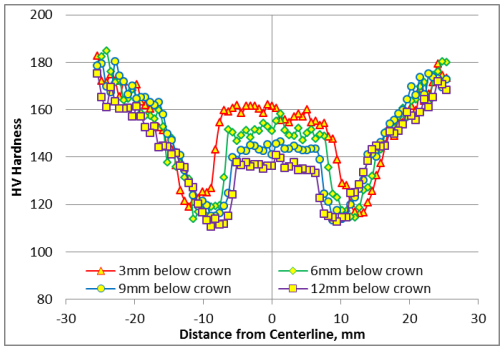

(c) #4304, CSDP-2, 160 RPM, AW

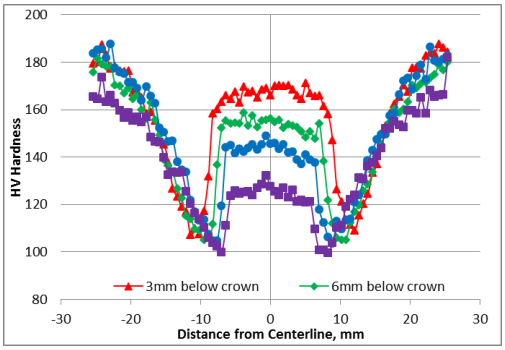

(d) #4304, CSDP-2, 160 RPM, PWHT

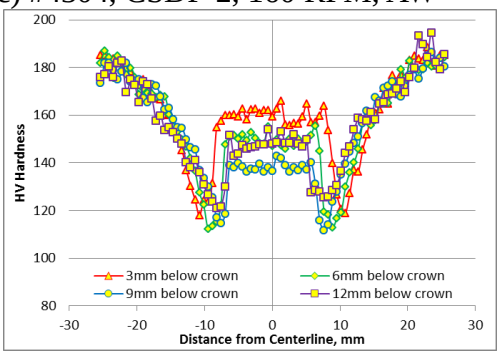

(e) #4301, CSDP-1, 200 RPM, AW

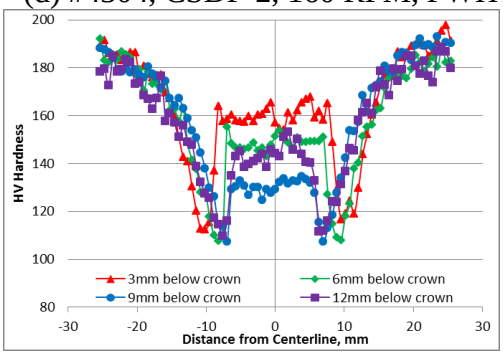

(f) #4301, CSDP-1, 200 RPM, PWHT

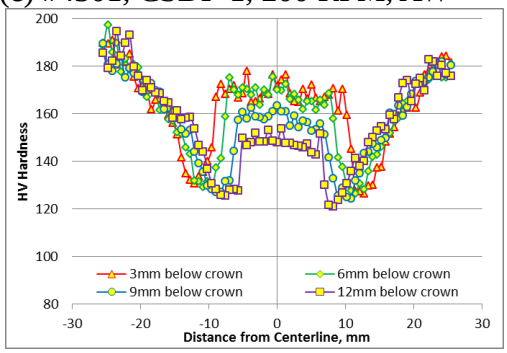

(g) #4303, CSDP-2, 200 RPM, AW

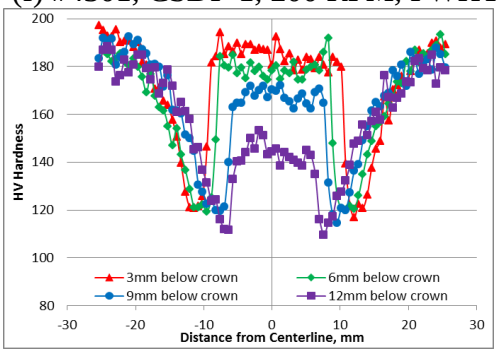

(h) #4303, CSDP-2, 200 RPM, PWHT

Figure 4.71 Hardness profiles of each pass transverse to weld at various depths near crown (3mm below crown), at mid-plane (6mm below crown), near root (9mm below crown) and at root (12mm below crown) in AW and PWHT conditions of CSDP with different speeds: T+3F pin, 1.3 mm flat depth

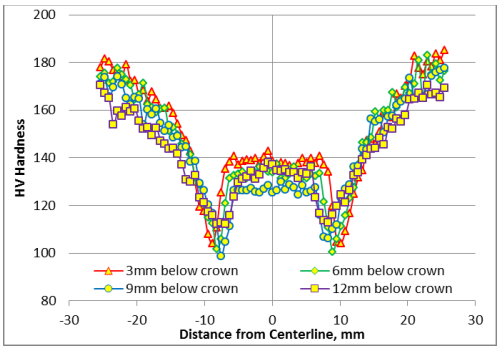

(a) #4309, SSDP-1, 160 RPM, AW

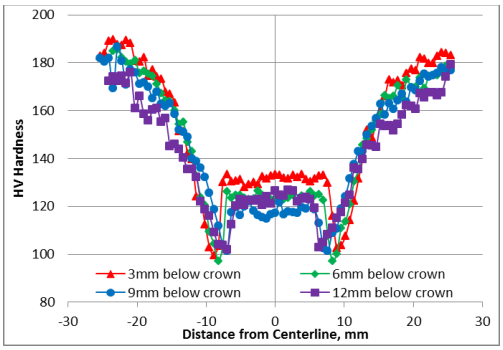

(b) #4309, SSDP-1, 160 RPM, PWHT

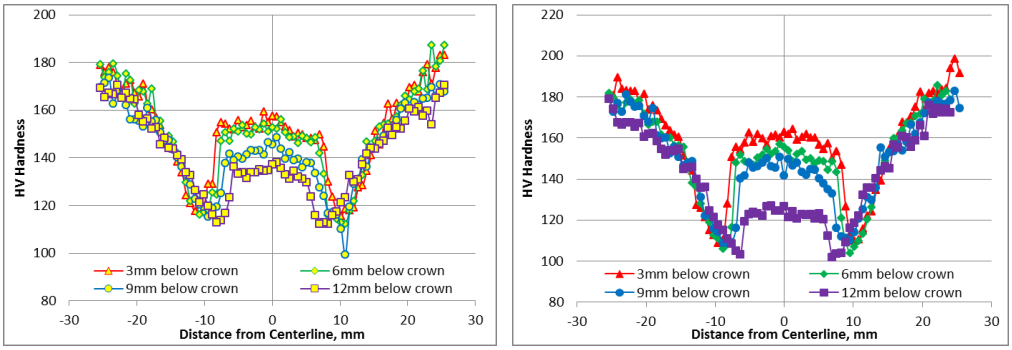

(c) #4311, SSDP-2, 160 RPM, AW (d) #4311, SSDP-2, 160 RPM, PWHT

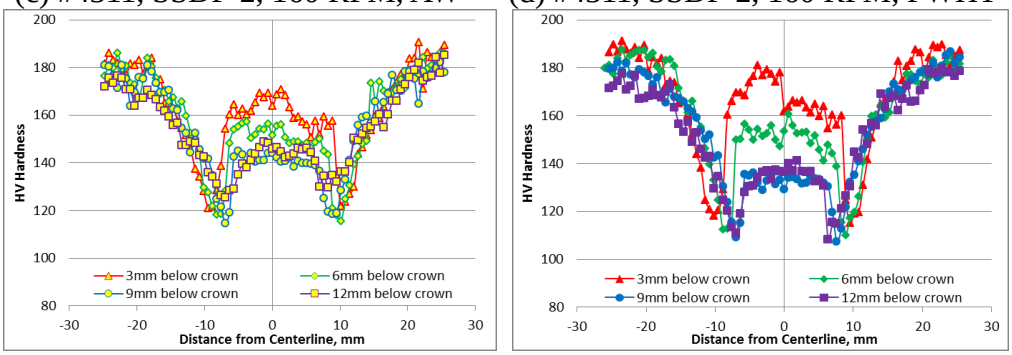

(e) #4310, SSDP-1, 200 RPM, AW (f) #4310, SSDP-1, 200 RPM, PWHT

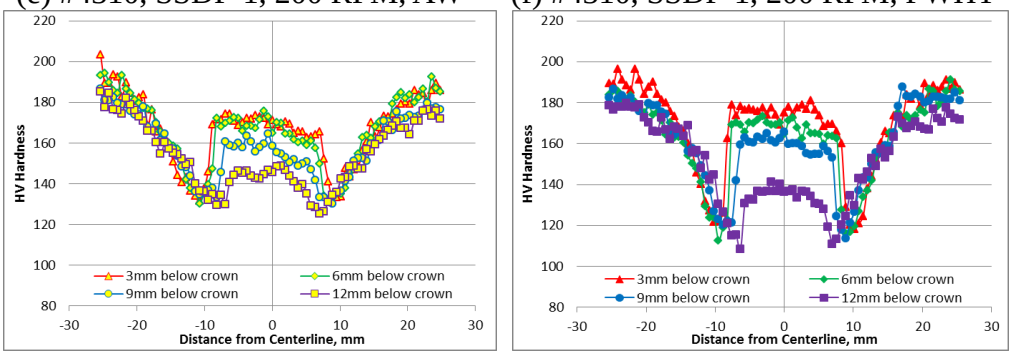

(g) #4312, SSDP-2, 200 RPM, AW (h) #4312, SSDP-2, 200 RPM, PWHT

Figure 4.72 Hardness profiles of each pass transverse to weld at various depths near crown (3mm below crown), at mid-plane (6mm below crown), near root (9mm below crown) and at root (12mm below crown) in AW and PWHT conditions of SSDP with different speeds: T+3F pin, 1.3 mm flat depth

4.3.4.1 Transverse hardness distribution of CSDP

HAZ minimum hardness at AS and RS, HAZ width, nugget average hardness were extracted from transverse hardness profiles of CSDP joints and plotted in Figure 4.73 and Figure 4.74.

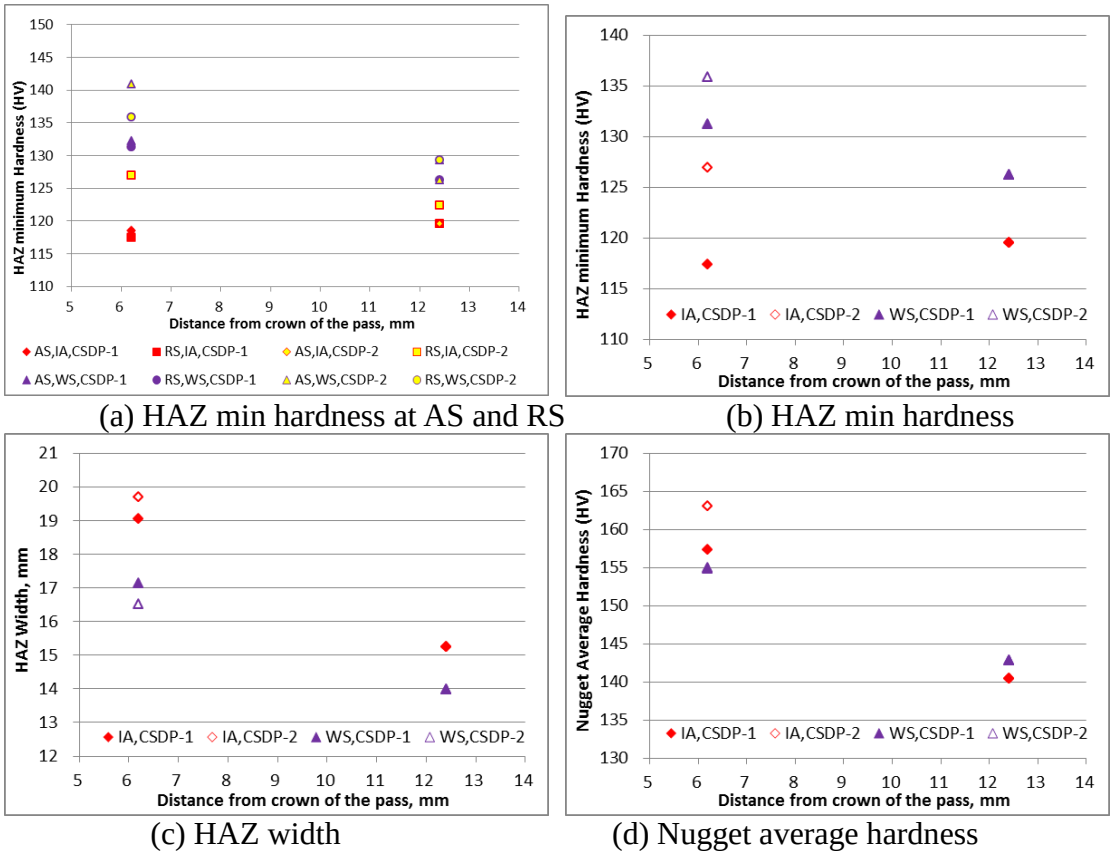

(a) HAZ min hardness at AS and RS (b) HAZ min hardness

(c) HAZ width (d) Nugget average hardness

Figure 4.73 (a) HAZ min hardness at AS and RS, (b) HAZ min hardness, (c) HAZ width, and (d) Nugget average hardness as functions of distance from crown of the pass of transverse CSDP joints in PWHT condition with different thermal boundary conditions: T+3F pin, 1.3 mm flat depth, 200 RPM, 203 mm/min

Figure 4.73 shows (a) HAZ min hardness at AS and RS, (b) HAZ min hardness, (c) HAZ width and (d) Nugget average hardness at mid-plane (6mm below crown), and at root (12mm below crown) as functions of distance from crown of the pass of transverse CSDP joints in PWHT condition produced with the same T+3F tool, the same rotation rate of 200 rpm, the same welding speed of 203 mm/min, and different thermal boundary conditions indicated as “IA” and “WS”. “IA” and “WS” were used to indicate welds were produced without and with water spray applying at work piece surface, respectively. Those joints were produced with the same tool, same speeds (200 rpm, 203 mm/min) and different TBCs as following: #4232B&#4233B (IA), and #4237&#4238 (WS).

4.3.4.1.1 Effect of different locations

Figure 4.73 shows that, in the same joints, relative to the root of the weld, at mid-plane, in IA CSDP-1, HAZ minimum hardness was affected little, nugget average hardness increased a little (12%), and HAZ width increased (25%); in IA CSDP-2, HAZ minimum hardness increased slightly (6%), nugget average hardness increased as little (16%), and HAZ width increased (29%); in WS CSDP-1, HAZ minimum hardness was affected little, nugget average hardness increased slightly (8%), and HAZ width increased (23%); in WS CSDP-2, HAZ minimum hardness increased slightly (8%), nugget average hardness increased slightly (8%), and HAZ width increased a little (18%). It indicates that, in the same joints, relative to the root of the weld, at mid-plane, HAZ minimum hardness was about the similar, nugget average hardness increased a little, and HAZ width increased.

4.3.4.1.2 Effect of the 2nd pass

Figure 4.73 shows that, relative to IA CSDP-1, in IA CSDP-2, at the mid-plane, HAZ minimum hardness increased by 8%, nugget average hardness increased by 4%, and HAZ width increased by 3%; at the root, HAZ minimum hardness, nugget average hardness and HAZ width were the same; Relative to WS CSDP-1, in WS CSDP-2, at the mid-plane, HAZ minimum hardness increased by 4%, nugget average hardness was the same, and HAZ width decreased by 4%; at the root, HAZ minimum hardness, nugget average hardness and HAZ width were the same. It shows that, relative to CSDP-1, in CSDP-2, either when WS was applied or not, either at the mid-plane or at root of the weld, HAZ minimum hardness increased slightly, nugget average hardness and HAZ width were affected little.

4.3.4.1.3 Effects of different TBCs

Figure 4.73 shows that, relative to IA CSDP-1, in WS CSDP-1, at the mid-plane, HAZ minimum hardness increased a little (12%), nugget average hardness was affected little, and HAZ width decreased a little (-10%); at the root, HAZ minimum hardness increased slightly (6%), nugget average hardness was affected little, and HAZ width decreased slightly (-8%). Relative to IA CSDP-2, in WS CSDP-2, at the mid-plane, HAZ minimum hardness increased slightly (7%), nugget average hardness decreased slightly (-5%), and HAZ width decreased a little (-16%); at the root, HAZ minimum hardness increased slightly (6%), nugget average hardness was affected little, and HAZ width decreased slightly (-8%). Figure 4.73(a) also shows that, in the same joints, HAZ minimum hardness at AS and RS are quite similar.

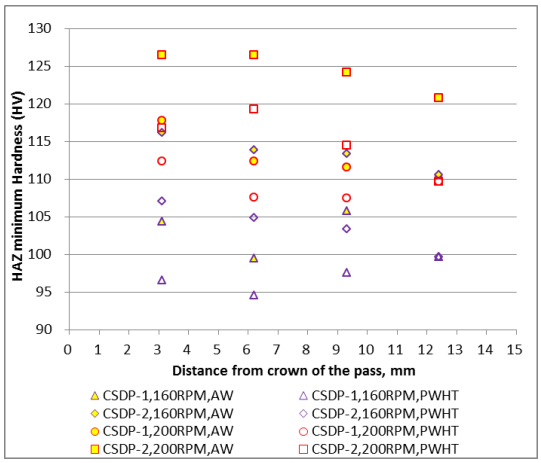

(a) HAZ min hardness

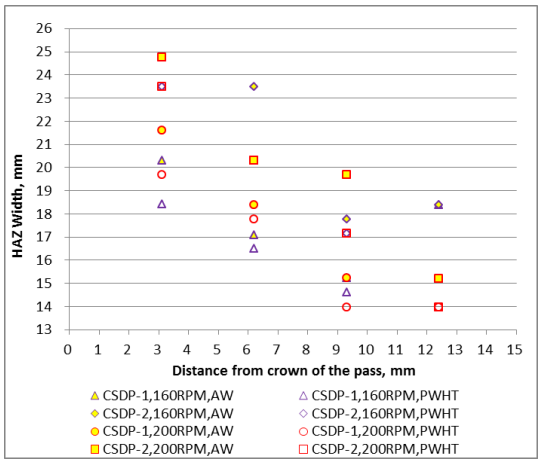

(b) HAZ width

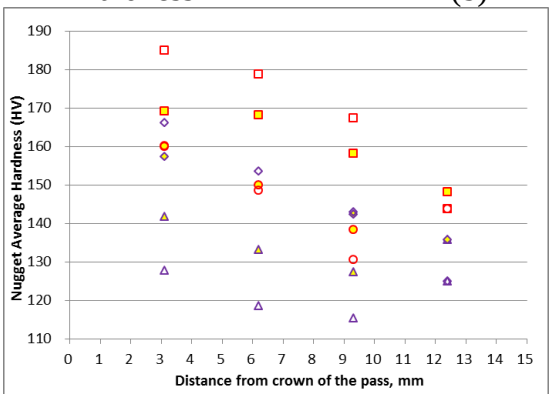

(c) Nugget average hardness

Figure 4.74 (a) HAZ min hardness, (b) HAZ width and (c) Nugget average hardness as functions of distance from crown of the pass of transverse CSDP joints in AW and PWHT conditions with different speeds: T+3F pin, 1.3 mm flat depth

Figure 4.74 shows (a) HAZ min hardness, (b) HAZ width, and (c) Nugget average hardness near crown (3mm below crown), at mid-plane (6mm below crown), near root (9mm below crown) and at root (12mm below crown) as functions of distance from crown of the pass of transverse CSDP joints in AW and PWHT conditions produced with the same T+3F tool, the same TBCs (IA) and different speeds. Effects of speeds, the 2nd pass, and PWHT on (a) HAZ minimum hardness, (b) nugget average hardness and (c) HAZ width were plotted in Figure 4.75, Figure 4.76 and Figure 4.77, respectively. Those joints were produced with the same tool and different speeds as following: #4302&#4304 (160rpm, 102mm/min), and #4301&#4303 (200rpm, 203mm/min).

4.3.4.1.4 Effects of different speeds

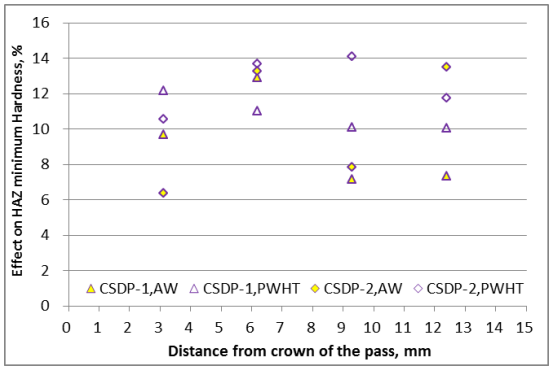

(a) HAZ minimum hardness

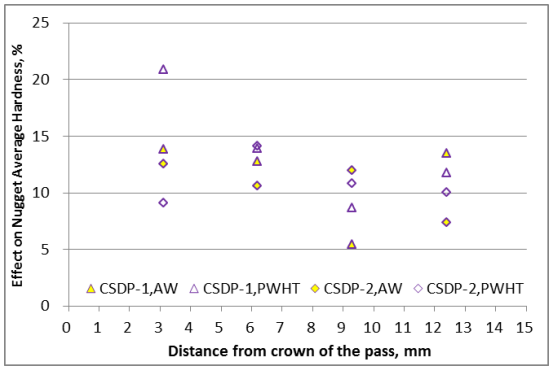

(b) Nugget average hardness

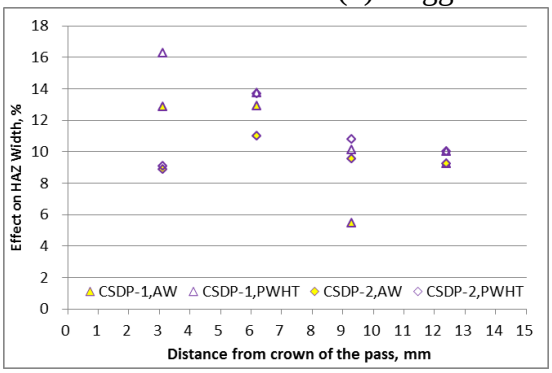

(c) HAZ width

Figure 4.75 Effect of speeds on (a) HAZ min hardness, (b) Nugget average hardness and (c) HAZ width as functions ofdistance from crown of the pass of transverse CSDP joints in AW and PWHT conditions with different speeds: T+3F pin, 1.3 mm flat depth

Figure 4.75 shows the effect of speeds on (a) HAZ minimum hardness, (b) nugget average hardness and (c) HAZ width as functions of distance from crown of the pass of transverse CSDP joints in AW and PWHT conditions produced with the same tool while different speeds. Figure 4.75 shows that:

In DP, higher FSW speeds increased HZA minimum hardness, nugget average hardness and HAZ width a little.

In AW CSDP-1, the increasing effect of higher speeds on HAZ minimum hardness slightly increased from near crown to the mid-plane, then slightly decreased to a constant value near root and at root; the increasing effects of higher speeds on nugget average hardness near crown, at mid-plane and at root were similar, which were a little larger than that near root; the increasing effects of higher speeds on HAZ width were similar near crown and at mid-plane, decreased near root and slightly increased at root.

In PWHT CSDP-1, the increasing effect of higher speeds on HAZ minimum hardness slightly and gradually decreased from near crown location to root; the increasing effects of higher speeds on nugget average hardness decreased a little from near crown location to the near root location, then slightly decreased to the root; the increasing effects of higher speeds on HAZ width slightly decreased from near crown location to near root location, then kept similar at root.

In AW CSDP-2, the increasing effect of higher speeds on HAZ minimum hardness near crown and near root were similar, which were slightly smaller than the similar increasing effects at mid-plane and at root; the increasing effects of higher speeds on nugget average hardness near crown, at mid-plane and near root were similar, which

were slightly larger than that at root; the increasing effects of higher speeds on HAZ width near crown, near root and at root were similar, which were slightly smaller than that at mid-plane.

In PWHT CSDP-2, the increasing effect of higher speeds on HAZ minimum hardness slightly and gradually increased from near crown to mid-plane, then decreased slightly at root; the increasing effects of higher speeds on nugget average hardness slightly increased from near crown location to the mid-plane, then slightly and gradually decreased to the root; the increasing effects of higher speeds on HAZ width near crown, near root and at root were similar, which were a little smaller than that at mid-plane.

4.3.4.1.5 Effect of the 2nd pass

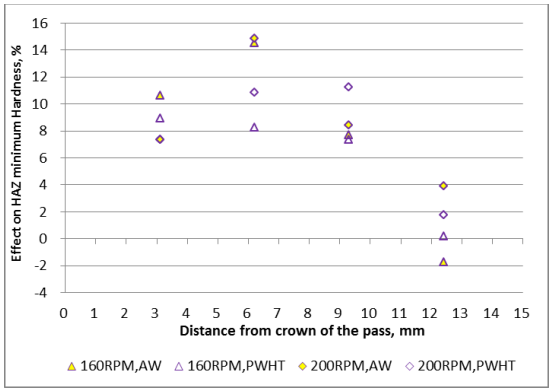

(a) HAZ minimum hardness

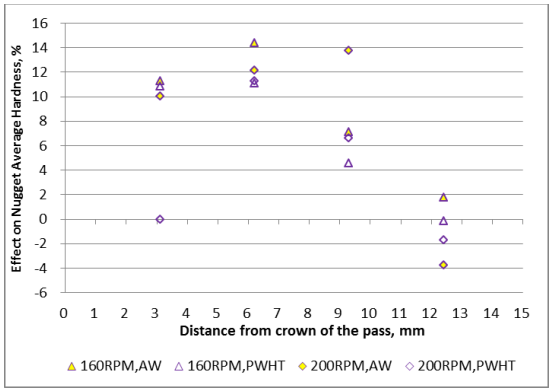

(b) Nugget average hardness

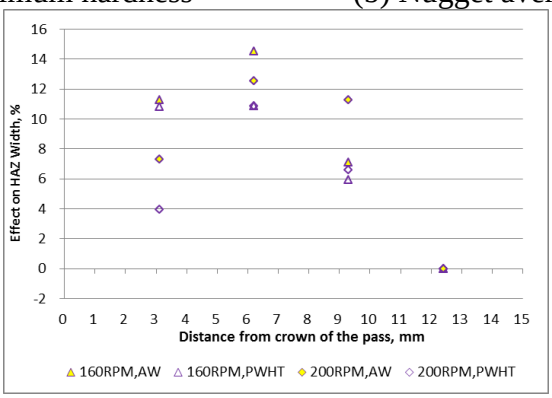

(c) HAZ width

Figure 4.76 Effect of the 2nd pass on (a) HAZ min hardness, (b) Nugget average hardness and (c) HAZ width as functions ofdistance from crown of the pass of transverse CSDP joints in AW and PWHT conditions with different speeds: T+3F pin, 1.3 mm flat depth

Figure 4.76 shows the effect of the 2nd pass on (a) HAZ minimum hardness, (b) nugget average hardness and (c) HAZ width as functions of distance from crown of the pass of transverse CSDP joints in AW and PWHT conditions produced with the same tool while different speeds. Figure 4.76 shows that:

(1) In AW CSDP produced with the lower FSW speeds, the 2nd pass increased HZA minimum hardness near crown, at mid-plane and near root a little, while decreased HAZ minimum hardness at root slightly. The increasing effect slightly increased from near crown location to the mid-plane, then slightly decreased near root. In AW CSDP produced with the lower FSW speeds, the 2nd pass increased nugget average hardness near crown, at mid-plane, and near root a little, while affected nugget average hardness at root little. The increasing effects increased a little from near crown location to the mid-plane, then decreased to the root. In AW CSDP produced with the lower FSW speeds, the 2nd pass increased HAZ width near crown and at mid-plane a little, increased HAZ width near root slightly, and affected HAZ width little at root. The increasing effects increased a little from near crown to the mid-plane, then decreased to the root.

(2) In PWHT CSDP produced with the lower FSW speeds, the 2nd pass increased HZA minimum hardness slightly near crown, at mid-plane, and near root, while affected HZA minimum hardness little at root. The increasing effect slightly and gradually decreased from near crown location to near root location. In PWHT CSDP produced with the lower FSW speeds, the 2nd pass increased nugget average hardness near crown, at mid-plane and near root a little, while affected nugget average hardness at root little. The increasing effects slightly increased from near crown location to the mid-plane, then decreased to the root. In PWHT CSDP produced with the lower FSW speeds, the 2nd pass

increased HAZ width near crown and at mid-plane a little, increased HAZ width near root slightly, and affected HAZ width little at root. The increasing effects were similar near crown and at the mid-plane, then decreased to the root.

(3) In AW CSDP produced with the higher FSW speeds, the 2nd pass increased HZA minimum hardness at mid-plane a little, while increased HAZ minimum hardness near crown, near root and at root slightly. The increasing effects increased from near crown location to the mid-plane, then decreased to the root. In AW CSDP produced with the higher FSW speeds, the 2nd pass increased nugget average hardness near crown, at mid-plane and near root a little, while decreased nugget average hardness at root slightly. The increasing effects increased a little from near crown location to near root location, then decreased at the root. In AW CSDP produced with the higher FSW speeds, the 2nd pass increased HAZ width near crown slightly, increased HAZ width at mid-plane and near root a little, and affected HAZ width at root little. The increasing effects increased a little from near crown location to the mid-plane, then decreased with an increasing slope to the root.

(4) In PWHT CSDP produced with the higher FSW speeds, the 2nd pass increased HZA minimum hardness a little near crown, at mid-plane, and near root, while increased HZA minimum hardness at root slightly. The increasing effects slightly and gradually increased from near crown location to near root location, then decreased at root. In PWHT CSDP produced with the higher FSW speeds, the 2nd pass affected nugget average hardness near crown and at root little, increased nugget average hardness at mid-plane a little, and increased nugget average hardness near root slightly. In PWHT CSDP produced with the higher FSW speeds, the 2nd pass increased HAZ width at mid-plane a

little, increased HAZ width slightly near crown and near root, while affected HAZ width little at root. The increasing effects increased a little from near crown location to the mid-plane, then decreased to the root.

4.3.4.1.6 Effect of PWHT

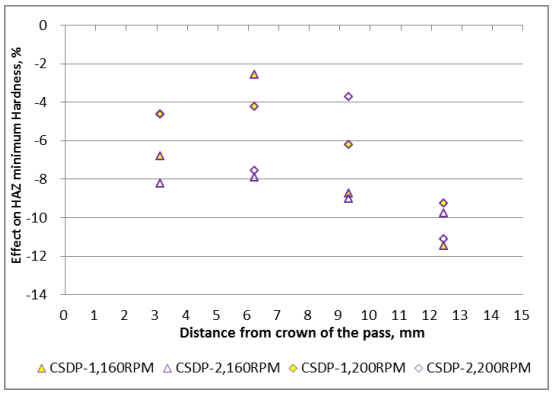

(a) HAZ minimum hardness

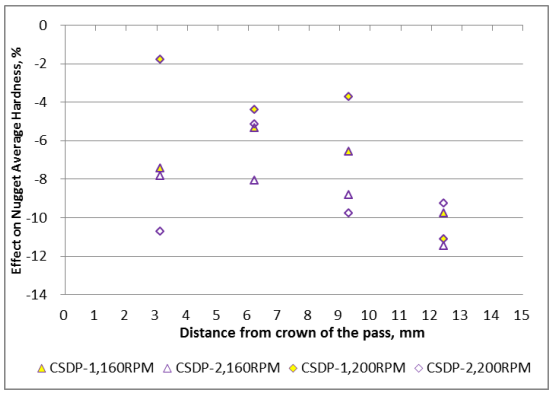

(b) Nugget average hardness

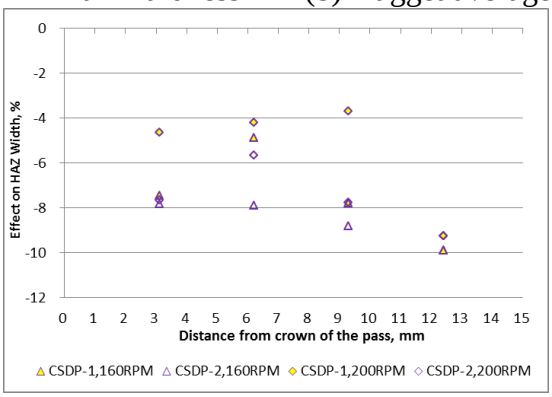

(c) HAZ width

Figure 4.77 Effect of PWHT on (a) HAZ min hardness, (b) Nugget average hardness and (c) HAZ width as functions of distance from crown of the pass of transverse CSDP joints in AW and PWHT conditions with different speeds: T+3F pin, 1.3 mm flat depth

Figure 4.77 shows the effect of PWHT on (a) HAZ minimum hardness, (b) nugget average hardness and (c) HAZ width as functions of distance from crown of the pass of transverse CSDP joints in AW and PWHT conditions produced with the same tool while different speeds. Figure 4.77 shows that:

(1) In CSDP-1 produced with the lower FSW speeds, PWHT decreased HZA minimum hardness slightly near crown and near root, affected HZA minimum hardness

little at mid-plane, and decreased HZA minimum hardness a little at root. The decreasing effect decreased from near crown location to the mid-plane, then increased to the root.

In CSDP-1 produced with the lower FSW speeds, PWHT decreased nugget average hardness slightly. The decreasing effect decreased a little from near crown location to the mid-plane, then increased to the root. In CSDP-1 produced with the lower FSW speeds, PWHT decreased HAZ width slightly. The decreasing effects decreased a little from near crown location to the mid-plane, then increased to the root.

(2) In CSDP-2 produced with the lower FSW speeds, PWHT decreased HZA minimum hardness slightly. The decreasing effects were similar near crown, at mid-plane, near root and at root. In CSDP-2 produced with the lower FSW speeds, PWHT decreased nugget average hardness near crown, at mid-plane and near root slightly, while decreased nugget average hardness a little at root. The decreasing effects gradually increased from near crown location to the root. In CSDP-2 produced with the lower FSW speeds, PWHT decreased HAZ width slightly. The decreasing effects were similar near crown, at the mid-plane, near root and at root.

(3) In CSDP-1 produced with the higher FSW speeds, PWHT decreased HZA minimum hardness slightly. The decreasing effects decreased slightly from near crown location to the mid-plane, then increased to the root. In CSDP-1 produced with the higher FSW speeds, PWHT affected nugget average hardness near crown, at mid-plane and near root little, while decreased nugget average hardness at root a little. The decreasing effects near crown, at mid-plane and near root were similar, which were smaller than that at root.

In CSDP-1 produced with the higher FSW speeds, PWHT affected HAZ width little near crown, at mid-plane and near root, and decreased HAZ width at root slightly.

The decreasing effects were similar near crown, at mid-plane and near root, which were smaller than that at root.

(4) In CSDP-2 produced with the higher FSW speeds, PWHT decreased HZA minimum hardness slightly near crown and at mid-plane, affected HZA minimum hardness little near root, and decreased HZA minimum hardness a little at root. The decreasing effects near crown and near root were similar, and were smaller than that at mid-plane, which was smaller than that at root. In CSDP-2 produced with the higher FSW speeds, PWHT decreased nugget average hardness slightly. The decreasing effects near crown, near root and at root were similar, which were larger than that at mid-plane.

In CSDP-2 produced with the higher FSW speeds, PWHT decreased HAZ width slightly. The decreasing effects decreased a little from near crown location to the mid-plane, then increased to the root.

4.3.4.2 Transverse hardness distribution of SSDP

HAZ minimum hardness at AS and RS, HAZ width, nugget average hardness were extracted from transverse hardness profiles of SSDP joints and plotted in Figure 4.78.

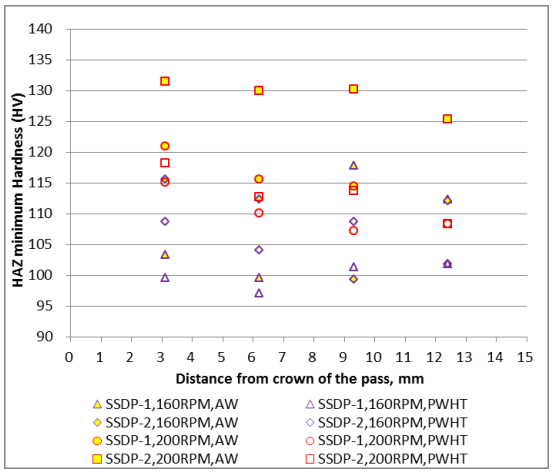

(a) HAZ min hardness

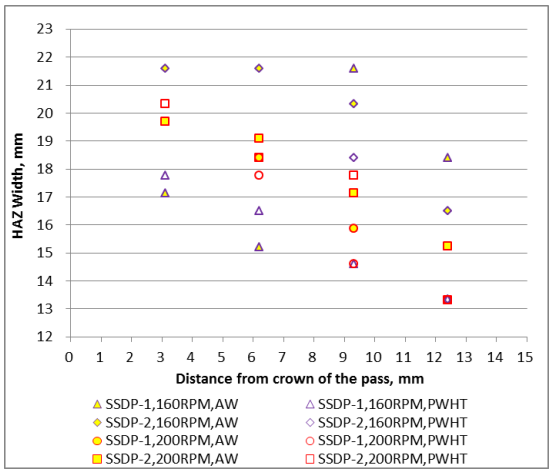

(b) HAZ width

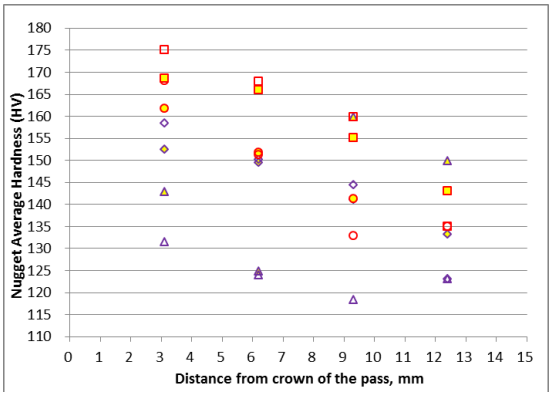

(c) Nugget average hardness

Figure 4.78 (a) HAZ min hardness, (b) HAZ width and (c) Nugget average hardness as functions of distance from crown of the pass of transverse SSDP joints in AW and PWHT conditions with different speeds: T+3CT pin, 1.3 mm flat depth

Figure 4.78 shows (a) HAZ min hardness, (b) HAZ width, and (c) Nugget average hardness near crown (3mm below crown), at mid-plane (6mm below crown), near root (9mm below crown) and at root (12mm below crown) as functions of distance from crown of the pass of transverse SSDP joints in AW and PWHT conditions produced with the same T+3CT tool, the same TBCs (IA) and different speeds. Effects of speeds, the 2nd pass, and PWHT on (a) HAZ minimum hardness, (b) nugget average hardness and (c) HAZ width were plotted in Figure 4.79, Figure 4.80 and Figure 4.81, respectively. Those joints were produced with the same tool and different speeds as following: #4309&#4311 (160 rpm, 102 mm/min), and #4310&#4312 (200 rpm, 203 mm/min).

4.3.4.2.1 Effects of different speeds

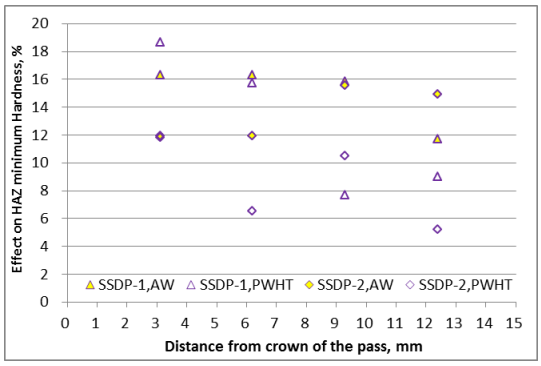

(a) HAZ minimum hardness

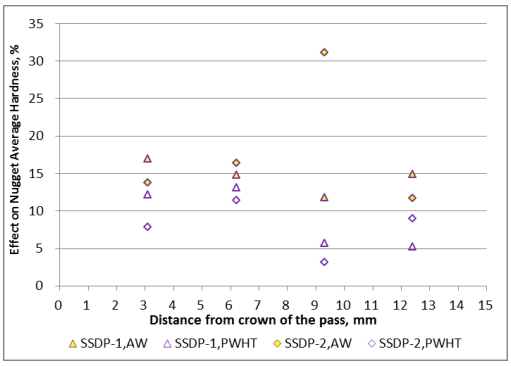

(b) Nugget average hardness

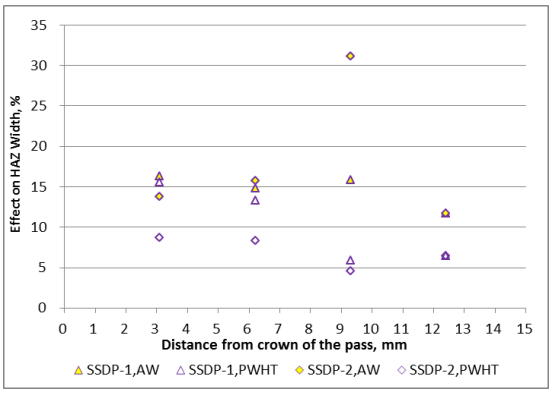

(c) HAZ width

Figure 4.79 Effect of speeds on (a) HAZ min hardness, (b) Nugget average hardness and (c) HAZ width as functions ofdistance from crown of the pass of transverse SSDP joints in AW and PWHT conditions with different speeds: T+3F pin, 1.3 mm flat depth

Figure 4.79 shows the effect of speeds on (a) HAZ minimum hardness, (b) nugget average hardness and (c) HAZ width as functions of distance from crown of the pass of transverse SSDP joints in AW and PWHT conditions produced with the same tool while different speeds. Figure 4.79 shows that:

(1) In AW SSDP-1, higher FSW speeds increased HZA minimum hardness a little. The increasing effects were similar near crown, at mid-plane and near root, which were larger than that at root. In AW SSDP-1, higher FSW speeds increased nugget average hardness a little. The increasing effects slightly decreased from near crown location to near root location, then slightly increased to the root. In AW SSDP-1, higher FSW speeds increased HAZ width a little. The increasing effects were similar near crown, at mid-plane and near root, which were a little larger than that at root.

(2) In PWHT SSDP-1, higher FSW speeds increased HZA minimum hardness a little near crown and at mid-plane, and increased HZA minimum hardness slightly near root and at root. The increasing effect decreased from near crown location to near root location, then slightly increased to the root. In PWHT SSDP-1, higher FSW speeds

increased nugget average hardness a little near crown and at mid-plane, and increased nugget average hardness slightly near root and at root. The increasing effects near crown and at mid-plane were similar, which were larger than the similar increasing effects near root and at root. In PWHT SSDP-1, higher FSW speeds increased HAZ width a little near crown and at mid-plane, and increased HAZ width slightly near root and at root. The increasing effects decreased from near crown location to near root location, then kept similar at root.

(3) In AW SSDP-2, higher FSW speeds increased HZA minimum hardness a little. The increasing effects near crown and at mid-plane were similar, which were a little smaller than the similar increasing effects near root and at root. In AW SSDP-2, higher FSW speeds increased nugget average hardness. The increasing effects increased with an increasing slope from near crown location to near root location, then decreased at root. In AW SSDP-2, higher FSW speeds increased HAZ width. The increasing effects increased with an increasing slope from near crown to near root location, then decreased to the root.

(4) In PWHT SSDP-2, higher FSW speeds increased HZA minimum hardness a little near crown and near root, and increased HZA minimum hardness slightly at mid-plane and at root. The increasing effects near crown and near root were similar, which were larger than the similar increasing effects at mid-plane and at root. In PWHT SSDP-2, higher FSW speeds increased nugget average hardness a little at mid-plane, increased nugget average hardness slightly near crown and at root, and affected nugget average hardness little near root. In PWHT SSDP-2, higher FSW speeds increased HAZ width slightly. The increasing effects slightly decreased with an increasing slope from near crown location to near root location, then slightly increased at root.

4.3.4.2.2 Effect of the 2nd pass

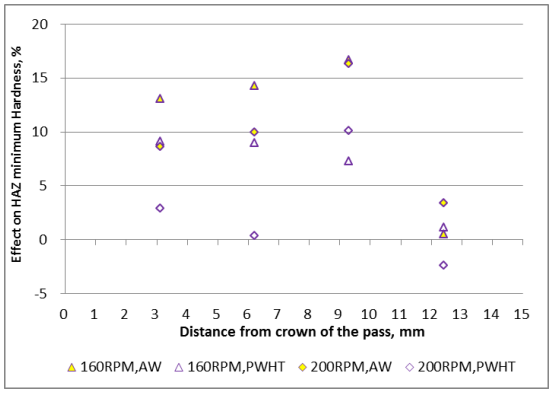

(a) HAZ minimum hardness

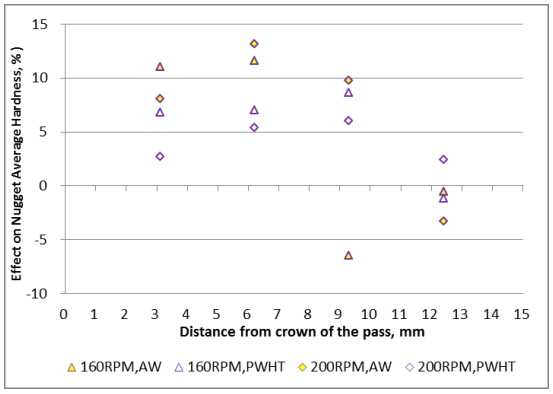

(b) Nugget average hardness

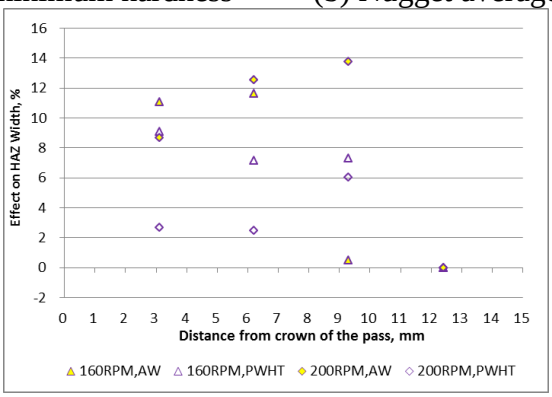

(c) HAZ width

Figure 4.80 Effect of the 2nd pass on (a) HAZ min hardness, (b) Nugget average hardness and (c) HAZ width as functions ofdistance from crown of the pass of transverse SSDP joints in AW and PWHT conditions with different speeds: T+3F pin, 1.3 mm flat depth

Figure 4.80 shows the effect of the 2nd pass on (a) HAZ minimum hardness, (b) nugget average hardness and (c) HAZ width as functions of distance from crown of the pass of transverse SSDP joints in AW and PWHT conditions produced with the same tool while different speeds. Figure 4.80 shows that:

(1) In AW SSDP produced with the lower FSW speeds, the 2nd pass increased HZA minimum hardness near crown, at mid-plane and near root a little, while affected HAZ minimum hardness at root little. The increasing effect increased a little with an increasing slope from near crown location to near root location, then decreased to almost zero at root. In AW SSDP produced with the lower FSW speeds, the 2nd pass increased

nugget average hardness a little near crown and at mid-plane, decreased nugget average hardness slightly near root, while affected nugget average hardness at root little. The increasing effects near crown and at mid-plane were similar. In AW SSDP produced with the lower FSW speeds, the 2nd pass increased HAZ width near crown and at mid-plane a little, and affected HAZ width little near root and at root. The increasing effects near crown and at mid-plane were similar.

(2) In PWHT SSDP produced with the lower FSW speeds, the 2nd pass increased HZA minimum hardness slightly near crown, at mid-plane, and near root, while affected HZA minimum hardness little at root. The increasing effect gradually decreased from near crown location to the root. In PWHT SSDP produced with the lower FSW speeds, the 2nd pass increased nugget average hardness near crown, at mid-plane and near root slightly, while affected nugget average hardness at root little. The increasing effect near crown was a little larger than the similar increasing effects at mid-plane and near root. In PWHT SSDP produced with the lower FSW speeds, the 2nd pass increased HAZ width near crown, at mid-plane and near root slightly, and affected HAZ width little at root. The increasing effects were similar near crown and at the mid-plane, which were a little smaller than that near root.

(3) In AW SSDP produced with the higher FSW speeds, the 2nd pass increased HZA minimum hardness near crown and at mid-plane slightly, increased HAZ minimum hardness a little near root, while affected HAZ minimum hardness little at root. The increasing effects increased with an increasing slope from near crown location to near root location, then decreased at the root. In AW SSDP produced with the higher FSW speeds, the 2nd pass increased nugget average hardness near crown slightly, increased

nugget average hardness at mid-plane and near root a little, while affected nugget average hardness at root little. The increasing effects increased a little from near crown location to the mid-plane, then decreased to the root. In AW SSDP produced with the higher FSW speeds, the 2nd pass increased HAZ width near crown slightly, increased HAZ width at mid-plane and near root a little, and affected HAZ width at root little. The increasing effects increased with an decreasing slope from near crown location to near root location, then decreased to almost zero at the root.

(4) In PWHT SSDP produced with the higher FSW speeds, the 2nd pass increased HZA minimum hardness a little near root, while affected HZA minimum hardness little near crown, at mid-plane and at root. In PWHT SSDP produced with the higher FSW speeds, the 2nd pass affected nugget average hardness near crown and at root little, while increased nugget average hardness at mid-plane and near root slightly. The increasing effects increased slightly from near crown location to near root location, then slightly decreased at root. In PWHT SSDP produced with the higher FSW speeds, the 2nd pass increased HAZ width near root slightly, while affected HAZ width little near crown, at mid-plane and at root.

4.3.4.2.3 Effect of PWHT

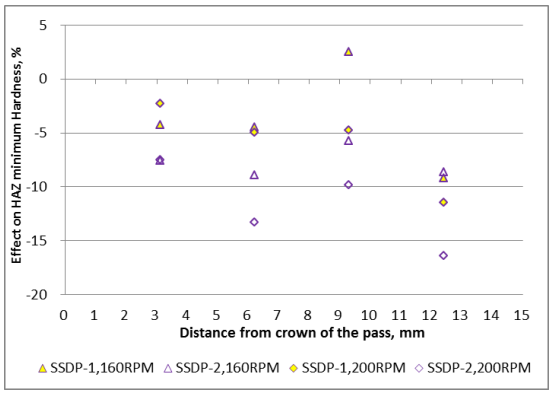

(a) HAZ minimum hardness

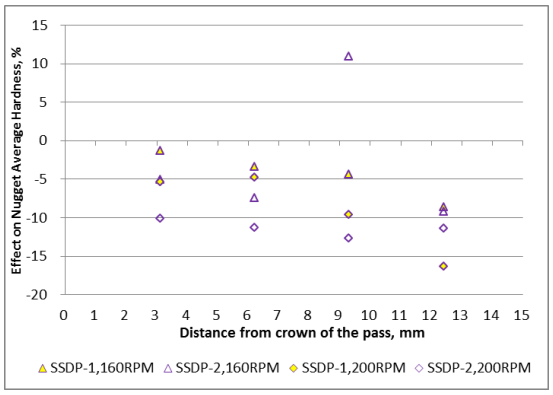

(b) Nugget average hardness

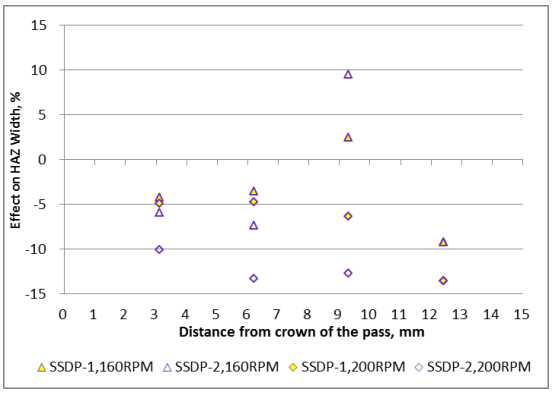

(c) HAZ width

Figure 4.81 Effect of PWHT on (a) HAZ min hardness, (b) Nugget average hardness and (c) HAZ width as functions ofdistance from crown of the pass of transverse SSDP joints in AW and PWHT conditions with different speeds: T+3F pin, 1.3 mm flat depth

Figure 4.81 shows the effect of PWHT on (a) HAZ minimum hardness, (b) nugget average hardness and (c) HAZ width as functions of distance from crown of the pass of transverse SSDP joints in AW and PWHT conditions produced with the same tool while different speeds. Figure 4.81 shows that:

(1) In SSDP-1 produced with the lower FSW speeds, PWHT decreased HZA minimum hardness slightly near crown, at mid-plane and at root, while affected HZA minimum hardness little near root. The decreasing effects near crown and at mid-plane were similar, which were smaller than that at root. In SSDP-1 produced with the lower FSW speeds, PWHT affected nugget average hardness little near crown and at mid-plane, while decreased nugget average hardness slightly near root and at root. The decreasing effect slightly increased from near crown location to the root. In SSDP-1 produced with the lower FSW speeds, PWHT decreased HAZ width slightly near crown, affected HAZ width little at mid-plane and near root, while decreased HAZ width a little at root.

(2) In SSDP-2 produced with the lower FSW speeds, PWHT decreased HZA minimum hardness slightly. The decreasing effects were similar near crown, at mid-plane

and at root, which were a little larger than that near root. In SSDP-2 produced with the lower FSW speeds, PWHT decreased nugget average hardness near crown, at mid-plane and at root slightly, while increased nugget average hardness a little near root. In SSDP-2 produced with the lower FSW speeds, PWHT decreased HAZ width slightly near crown, at mid-plane and at root, while increased HAZ width slightly near root.

(3) In SSDP-1 produced with the higher FSW speeds, PWHT affected HZA minimum hardness little near crown, decreased HZA minimum hardness slightly at mid-plane and near root, and decreased HZA minimum hardness a little at root. The decreasing effects at mid-plane and near root were similar, which were smaller than that at root. In SSDP-1 produced with the higher FSW speeds, PWHT decreased nugget average hardness slightly near crown and at mid-plane, while decreased nugget average hardness near root and at root a little. The decreasing effects near crown and at mid-plane were similar, which began to increase from the mid-plane to the root. In SSDP-1 produced with higher FSW speeds, PWHT decreased HAZ width slightly near crown, at mid-plane and near root, and decreased HAZ width at root a little. The decreasing effects were similar near crown, at mid-plane and near root, which were smaller than that at root.

(4) In SSDP-2 produced with the higher FSW speeds, PWHT decreased HZA minimum hardness slightly near crown, and decreased HZA minimum hardness a little at mid-plane, near root and at root. The decreasing effects had the following descending order: at root, at mid-plane, near root, then near crown. In SSDP-2 produced with the higher FSW speeds, PWHT decreased nugget average hardness a little. The decreasing effect slightly and gradually increased from near crown location to near root location, then decreased slightly at root. In SSDP-2 produced with the higher FSW speeds, PWHT

decreased HAZ width a little. The decreasing effects were similar at mid-plane, near root and at root, which were a little larger than that near crown.

4.3.4.3 Transverse hardness distribution of CSDP and SSDP

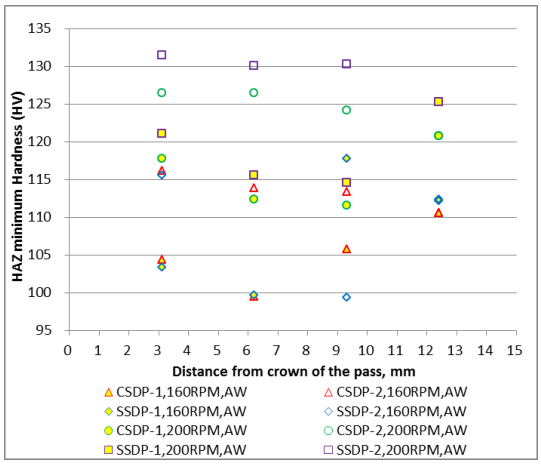

(a) HAZ min hardness

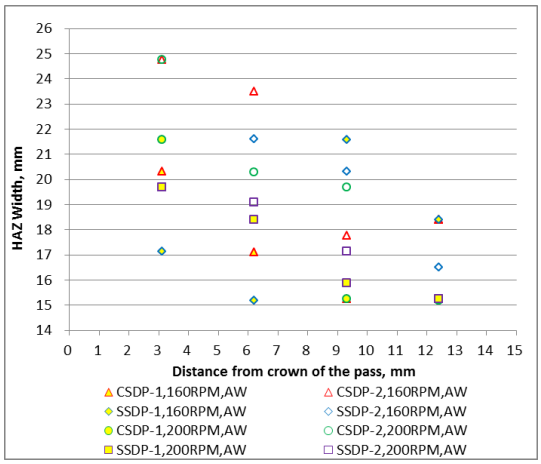

(b) HAZ width

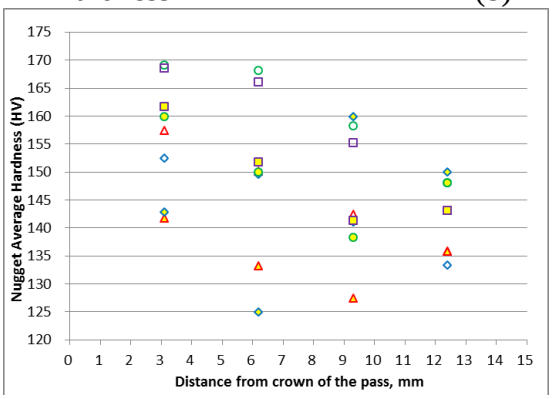

(c) Nugget average hardness

Figure 4.82 (a) HAZ min hardness, (b) HAZ width and (c) Nugget average hardness as functions ofdistance from crown of the pass of transverse CSDP and SSDP joints in AW conditions with different pin features and speeds: 1.3 mm flat/flute depth

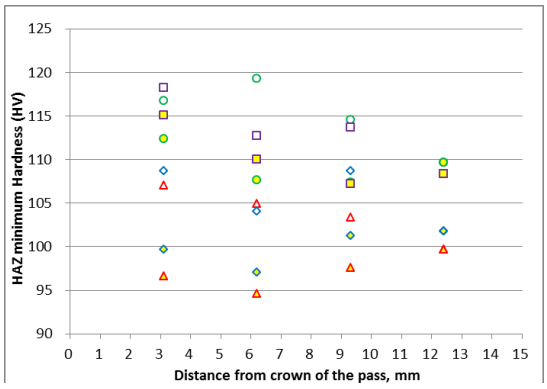

(a) HAZ min hardness

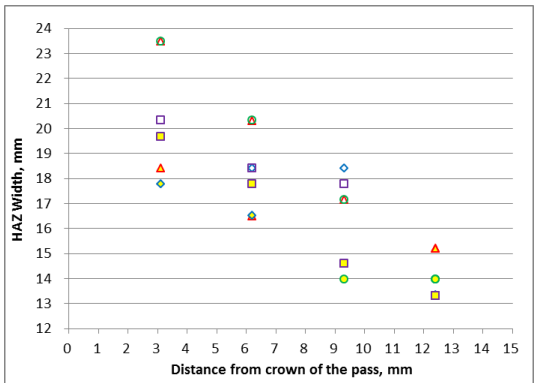

(b) HAZ width

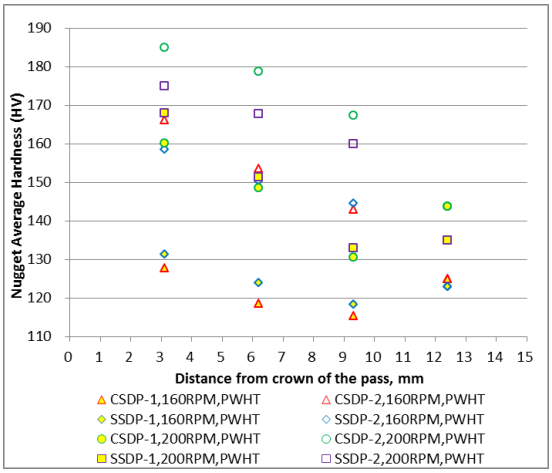

(c) Nugget average hardness

Figure 4.83 (a) HAZ min hardness, (b) HAZ width and (c) Nugget average hardness as functions ofdistance from crown of the pass of transverse CSDP and SSDP joints in PWHT conditions with different pin features and speeds: 1.3 mm flat/flute depth

HAZ minimum hardness, HAZ width, and nugget average hardness were extracted from transverse hardness profiles of comparable DP joints and plotted in Figure 4.82 and Figure 4.83. Figure 4.82 shows (a) HAZ min hardness, (b) HAZ width and (c) Nugget average hardness near crown (3mm below crown), at mid-plane (6mm below crown), near root (9mm below crown) and at root (12mm below crown) as functions of distance from crown of the pass of transverse CSDP and SSDP joints in AW conditions produced with different pin features and speeds. Figure 4.83 shows (a) HAZ min hardness, (b) HAZ width and (c) nugget average hardness near crown (3mm below crown), at mid-plane (6mm below crown), near root (9mm below crown) and at root (12mm below crown) as functions of distance from crown of the pass of transverse CSDP and SSDP joints in PWHT conditions produced with different pin features and speeds. Those CSDP joints were #4302&#4304 and #4301&#4303. Those SSDP joints were #4309&#4311 and #4310&#4312. Details of weld information of the above comparable CSDP and SSDP joints have been listed in section 4.3.4.1 and 4.3.4.2. Effects of speeds,

the 2nd pass, and PWHT on (a) HAZ minimum hardness, (b) nugget average hardness and (c) HAZ width were plotted in Figure 4.84, Figure 4.85 and Figure 4.86, respectively.

4.3.4.2.4 Effect of speeds

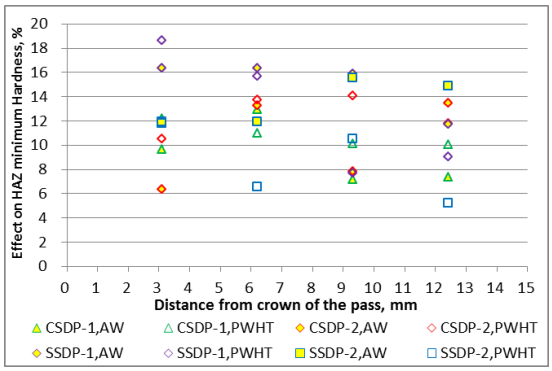

(a) HAZ minimum hardness

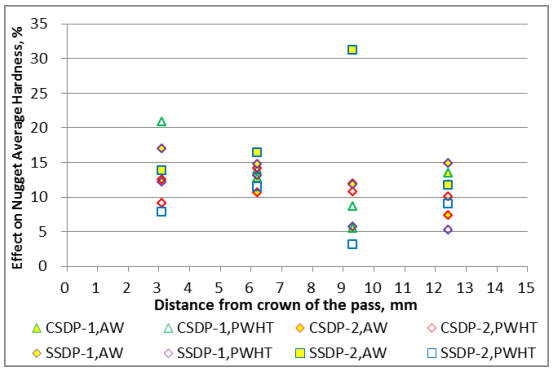

(b) Nugget average hardness

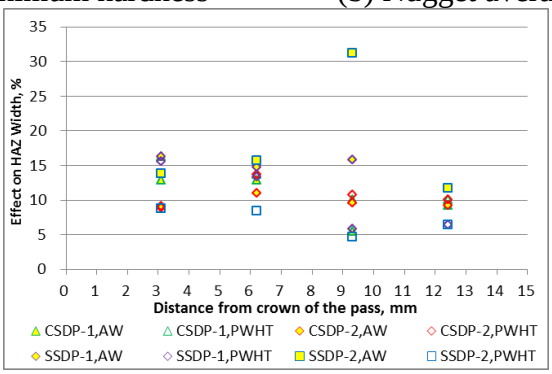

(c) HAZ width

Figure 4.84 Effect of speeds on (a) HAZ min hardness, (b) Nugget average hardness and (c) HAZ width as functions ofdistance from crown of the pass of transverse DP joints in AW and PWHT conditions with different speeds: T+3F pin, 1.3 mm flat depth

Figure 4.84 shows the effect of speeds on (a) HAZ minimum hardness, (b) nugget average hardness and (c) HAZ width as functions of distance from crown of the pass of transverse DP joints in AW and PWHT conditions produced with different tools and speeds. Figure 4.84 shows that:

(1) In both AW CSDP-1 and AW SSDP-1, higher FSW speeds increased HZA minimum hardness a little. Relative to AW CSDP-1, in AW SSDP-1, the increasing effects were larger near crown and near root, and the increasing effects were a little larger

at mid-plane and at root. In both AW CSDP-1 and AW SSDP-1, higher FSW speeds increased nugget average hardness a little, and the minimum of increasing effect appeared near root. Relative to AW CSDP-1, in AW SSDP-1, the increasing effects were a little larger near crown, at mid-plane and at root, while the increasing effect was larger near root. In AW DP-1, higher FSW speeds increased HAZ width a little. Relative to AW CSDP-1, in AW SSDP-1, the increasing effects were a little larger near crown, at mid-plane and at root, while the increasing effect was much larger near root.

(2) In both PWHT CSDP-1 and PWHT SSDP-1, higher FSW speeds increased HZA minimum hardness a little. Relative to PWHT CSDP-1, in PWHT SSDP-1, the increasing effects were larger near crown and at mid-plane, a little smaller near root, and similar at root. In both PWHT CSDP-1 and PWHT SSDP-1, higher FSW speeds increased nugget average hardness a little. Relative to PWHT CSDP-1, in PWHT SSDP-1, the increasing effects were smaller near crown and at root, a little smaller near root, and similar at mid-plane. In PWHT DP-1, higher FSW speeds increased HAZ width a little. Relative to PWHT CSDP-1, in PWHT SSDP-1, the increasing effects were similar near crown and at mid-plane, while smaller near root and at root.

(3) In both AW CSDP-2 and AW SSDP-2, higher FSW speeds increased HZA minimum hardness a little. Relative to AW CSDP-2, in AW SSDP-2, the increasing effects were larger near crown and near root, while similar at mid-plane and at root. In both AW CSDP-2 and AW SSDP-2, higher FSW speeds increased nugget average hardness a little. Relative to AW CSDP-2, in AW SSDP-2, the increasing effect was similar near crown, a little larger at mid-plane and at root, and much larger near root. In both AW CSDP-2 and AW SSDP-2, higher FSW speeds increased HAZ width a little.

Relative to AW CSDP-2, in AW SSDP-2, the increasing effects were a little larger near crown and at mid-plane, much larger near root, while similar at root.

(4) In both PWHT CSDP-2 and PWHT SSDP-2, higher FSW speeds increased HZA width a little. Relative to PWHT CSDP-2, in PWHT SSDP-2, the increasing effects were smaller at mid-plane and at root, a little smaller near root, and similar near crown. In both PWHT CSDP-2 and PWHT SSDP-2, higher FSW speeds increased nugget average hardness a little. Relative to PWHT CSDP-2, in PWHT SSDP-2, the increasing effects were similar near crown and at root, a little smaller at mid-plane, and much smaller near root. In PWHT DP-2, higher FSW speeds increased HAZ width a little. Relative to PWHT CSDP-2, in PWHT SSDP-2, the increasing effects were smaller near crown and at mid-plane, and similar near root and at root.

4.3.4.2.5 Effect of 2nd pass

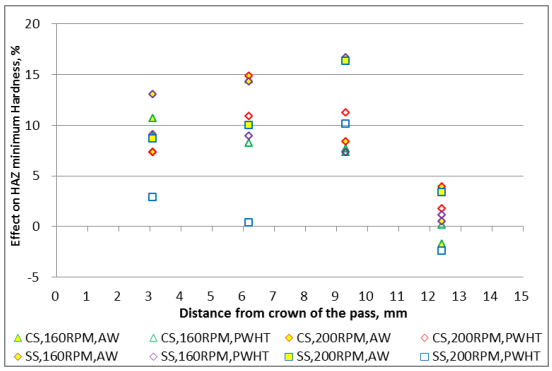

(a) HAZ minimum hardness

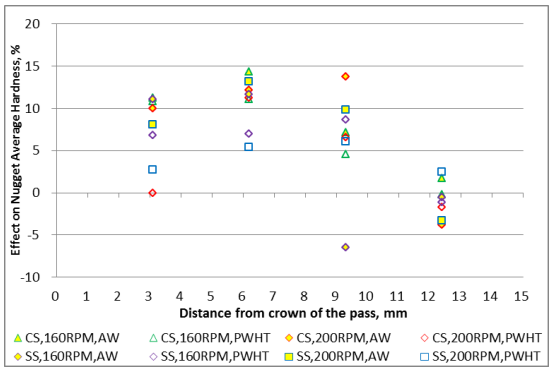

(b) Nugget average hardness

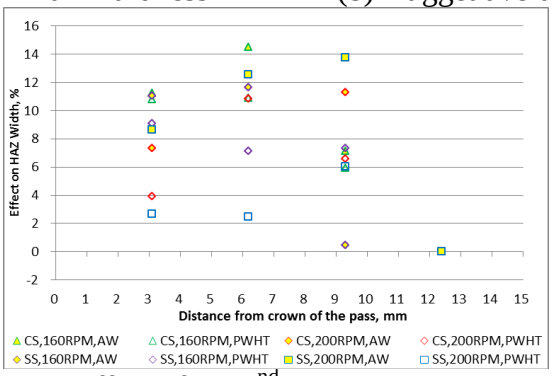

(c) Effect of the 2nd pass on HAZ width

Figure 4.85 Effect of the 2nd pass on (a) HAZ min hardness, (b) Nugget average hardness and (c) HAZ width as functions ofdistance from crown of the pass of transverse DP joints in AW and PWHT conditions with different speeds: T+3F pin, 1.3 mm flat depth

Figure 4.85 shows the effect of the 2nd pass on (a) HAZ minimum hardness, (b) nugget average hardness and (c) HAZ width as functions of distance from crown of the pass of transverse DP joints in AW and PWHT conditions produced with different tools and speeds. Figure 4.85 shows that:

(1) In both AW CSDP and AW SSDP produced with the lower FSW speeds, the 2nd pass increased HZA minimum hardness near crown, at mid-plane and near root a little, while affected HAZ minimum hardness at root little. Relative to AW CSDP produced with the lower FSW speeds, in AW SSDP produced with the lower FSW speeds, the increasing effect was a little larger near crown, similar at mid-plane, and much larger near root. Relative to AW CSDP produced with the lower FSW speeds, in AW SSDP produced with the lower FSW speeds, the increasing effects were similar near crown, at mid-plane and at root. Near root, in AW CSDP produced with the lower FSW speeds, the 2nd pass increased nugget average hardness slightly, while in AW SSDP produced with the lower FSW speeds, the 2nd pass decreased nugget average hardness slightly. In both AW CSDP and AW SSDP produced with the lower FSW speeds, the 2nd pass increased HZA width a little near crown and at mid-plane, and affected HZA width little at root. Near root, in AW CSDP produced with the lower FSW speeds, the 2nd pass increased HZA width slightly, while in AW SSDP produced with the lower FSW speeds, the 2nd pass affected HZA width little.

(2) In both PWHT CSDP and PWHT SSDP produced with the lower FSW speeds, the 2nd pass increased HZA minimum hardness near crown, at mid-plane and near root slightly, while affected HAZ minimum hardness at root little. Relative to PWHT CSDP

produced with the lower FSW speeds, in PWHT SSDP produced with the lower FSW speeds, the increasing effects were similar. In both PWHT CSDP and PWHT SSDP produced with the lower FSW speeds, the 2nd pass increased nugget average hardness near crown, at mid-plane and near root slightly, while affected nugget average hardness at root little. Relative to PWHT CSDP produced with the lower FSW speeds, in PWHT SSDP produced with the lower FSW speeds, the increasing effects were smaller near crown and at mid-plane, larger near root, while similar at root. In both PWHT CSDP and PWHT SSDP produced with the lower FSW speeds, the 2nd pass increased HAZ width slightly near crown, at mid-plane and near root, while affected HAZ width at root little. Relative to PWHT CSDP produced with the lower FSW speeds, in PWHT SSDP produced with the lower FSW speeds, the increasing effects were similar near crown and near root, while a little smaller at mid-plane.

(3) In both AW CSDP and AW SSDP produced with the higher FSW speeds, the 2nd pass increased HZA minimum hardness near crown, at mid-plane and near root slightly, while affected HAZ minimum hardness at root little. Relative to AW CSDP produced with the higher FSW speeds, in AW SSDP produced with the higher FSW speeds, the increasing effects were similar near crown and at root, smaller at mid-plane, and larger near root. In both AW CSDP and AW SSDP produced with the higher FSW speeds, the 2nd pass increased nugget average hardness near crown, at mid-plane and near root a little, while affected nugget average hardness at root little. Relative to AW CSDP produced with the higher FSW speeds, in AW SSDP produced with the higher FSW speeds, the increasing effects were similar near crown and at mid-plane, while a little smaller near root. In both AW CSDP and AW SSDP produced with the higher FSW

speeds, the 2nd pass increased HAZ width near crown, at mid-plane and near root a little, while affected HAZ width at root little. Relative to AW CSDP produced with the higher FSW speeds, in AW SSDP produced with the higher FSW speeds, the increasing effects were similar near crown and at mid-plane, while a little larger near root.

(4) Relative to PWHT CSDP produced with the higher FSW speeds, in PWHT SSDP produced with the higher FSW speeds, the increasing effects were smaller near crown, at mid-plane and at root, while similar near root. In both PWHT CSDP and PWHT SSDP produced with the higher FSW speeds, the 2nd pass affected nugget average hardness little near crown and at root, and increased nugget average hardness a little at mid-plane and near root. Relative to PWHT CSDP produced with the higher FSW speeds, in PWHT SSDP produced with the higher FSW speeds, the increasing effects were smaller at mid-plane and similar near root. PWHT DP produced with the higher FSW speeds, the 2nd pass affected HAZ width little near crown and at root, and increased HAZ width slightly near root. At the mid-plane, in PWHT CSDP produced with the higher FSW speeds, the 2nd pass increased HAZ width a little, while in PWHT SSDP produced with the higher FSW speeds, the 2nd pass affected HAZ width little.

4.3.4.2.6 Effect of PWHT

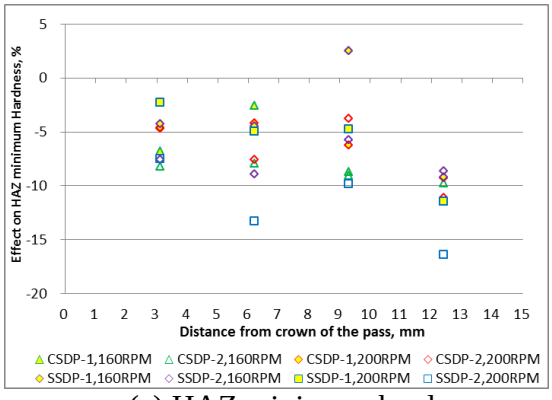

(a) HAZ minimum hardness

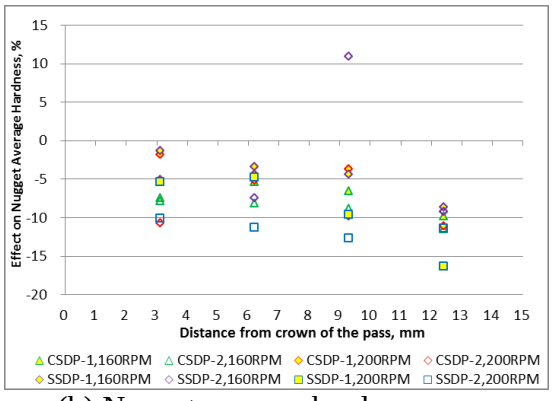

(b) Nugget average hardness

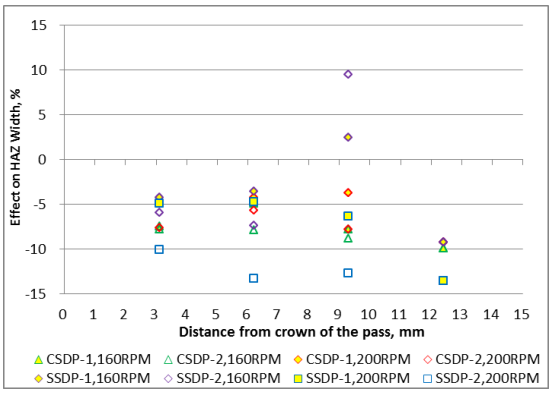

(c) HAZ width

Figure 4.86 Effect of PWHT on (a) HAZ min hardness, (b) Nugget average hardness and (c) HAZ width as functions ofdistance from crown of the pass of transverse DP joints in AW and PWHT conditions with different speeds: T+3F pin, 1.3 mm flat depth

Figure 4.86 shows the effect of PWHT on (a) HAZ minimum hardness, (b) nugget average hardness and (c) HAZ width as functions of distance from crown of the pass of transverse DP joints in AW and PWHT conditions produced with different tools and speeds. Figure 4.86 shows that:

(1) In both CSDP-1 and SSDP-1 produced with the lower FSW speeds, PWHT decreased HZA minimum hardness slightly near crown, affected HZA minimum hardness little at mid-plane, and decreased HZA minimum hardness a little at root. Near root, in CSDP-1 produced with the lower FSW speeds, PWHT decreased HZA minimum hardness slightly, while in SSDP-1 produced with the lower FSW speeds, PWHT affected HZA minimum hardness little. In both CSDP-1 and SSDP-1 produced with the lower FSW speeds, PWHT decreased nugget average hardness slightly. Relative to CSDP-1 produced with the lower FSW speeds, in SSDP-1 produced with the lower FSW speeds, the decreasing effects were smaller near crown, a little smaller at mid-plane and near root, while similar at root. In both CSDP-1 and SSDP-1 produced with the lower FSW speeds, PWHT decreased HAZ width slightly near crown, at mid-plane and at root. Relative to

CSDP-1 produced with the lower FSW speeds, in SSDP-1 produced with the lower FSW speeds, the decreasing effect was a little smaller near crown, and similar at mid-plane and at root. Near root, in joints produced with the lower FSW speeds, PWHT affected HAZ width little in CSDP-1, while decreased HAZ width slightly in SSDP-1.

(2) In both CSDP-2 and SSDP-2 produced with the lower FSW speeds, PWHT decreased HZA minimum hardness slightly. Relative to CSDP-2 produced with the lower FSW speeds, in SSDP-2 produced with the lower FSW speeds, the decreasing effects were similar near crown, at mid-plane and at root, while a little smaller near root. In both CSDP-2 and SSDP-2 produced with the lower FSW speeds, PWHT decreased nugget average hardness slightly near crown, at mid-plane and at root. Relative to CSDP-2 produced with the lower FSW speeds, in SSDP-2 produced with the lower FSW speeds, the decreasing effects were similar near crown, at mid-plane and at root. Near root, in CSDP-2 produced with the lower FSW speeds, PWHT decreased nugget average hardness slightly, while in SSDP-2 produced with the lower FSW speeds, PWHT increased nugget average hardness a little. In both CSDP-2 and SSDP-2 produced with the lower FSW speeds, PWHT decreased HAZ width slightly near crown, at mid-plane and at root. Relative to CSDP-2 produced with lower FSW speeds, in SSDP-2 produced with the lower FSW speeds, the decreasing effects were similar near crown, at mid-plane and at root. Near root, in joints produced with the lower FSW speeds, PWHT increased HAZ width slightly in CSDP-2, while decreased HAZ width slightly in SSDP-2.

(3) In both CSDP-1 and SSDP-1 produced with the higher FSW speeds, PWHT affected HZA minimum hardness little near crown and at mid-plane, decreased HZA minimum hardness slightly near root, and decreased HZA minimum hardness a little at

root. Relative to CSDP-1 produced with the higher FSW speeds, in SSDP-1 produced with the higher FSW speeds, the decreasing effect was a little smaller near crown, similar at mid-plane and near root, while a little larger at root. In both CSDP-1 and SSDP-1 produced with the higher FSW speeds, PWHT decreased nugget average hardness slightly at mid-plane and decreased nugget average hardness a little at root. Relative to CSDP-1 produced with the higher FSW speeds, in SSDP-1 produced with the higher FSW speeds, the decreasing effect was similar at mid-plane while larger at root. Near crown and near root, in CSDP-1 produced with the higher FSW speeds, PWHT affected nugget average hardness little, while in SSDP-1 produced with the higher FSW speeds, PWHT decreased nugget average hardness slightly. In both CSDP-1 and SSDP-1 produced with the higher FSW speeds, PWHT decreased HAZ width slightly. In joints produced with the higher FSW speeds, relative to CSDP-1, in SSDP-1, the decreasing effects were similar near crown and at md-plane, while a little larger near root and at root.

(4) In both CSDP-2 and SSDP-2 produced with the higher FSW speeds, PWHT decreased HZA minimum hardness slightly. Relative to CSDP-2 produced with the higher FSW speeds, in SSDP-2 produced with the higher FSW speeds, the decreasing effects was a little larger near crown and were larger at mid-plane, near root and at root. Relative to CSDP-2 produced with the higher FSW speeds, in SSDP-2 produced with the higher FSW speeds, the decreasing effects was similar near crown, larger at md-plane, while a little larger near root and at root. Relative to CSDP-2 produced with the higher FSW speeds, in SSDP-2 produced with the higher FSW speeds, the decreasing effects were a little larger near crown, and larger at mid-plane, near root and at root.

4.3.5 Tensile Testing Properties

Rotating and stationary shoulders result in different heat sources in FSW, affecting thermal distribution, microstructure and properties through thickness of joints. In this section, transverse and longitudinal tensile testing results in CSDP and SSDP have been studied to investigate effects of CSDP and SSDP on joint's tensile properties like ultimate tensile strength, yield strength and elongation.

4.3.5.1 Transverse Tensile Testing (AW&PWHT)

Transverse tensile tests have been performed on some CSDP joints in PWHT condition. Unfortunately during those tests the strain data was not obtained successfully, leaving only the stress data through which the UTS was calculated. Transverse tensile tests have also been performed on some CSDP and SSDP joints in AW and PWHT conditions. Engineering stress as a function of engineering strain of transverse tensile testing on CSDP and SSDP joints in AW and PWHT conditions were shown in Figure 4.87 and Figure 4.88. Results of transverse tensile testing on CSDP and SSDP joints in AW and/or PWHT conditions were plotted in Figure 4.89~Figure 4.91.

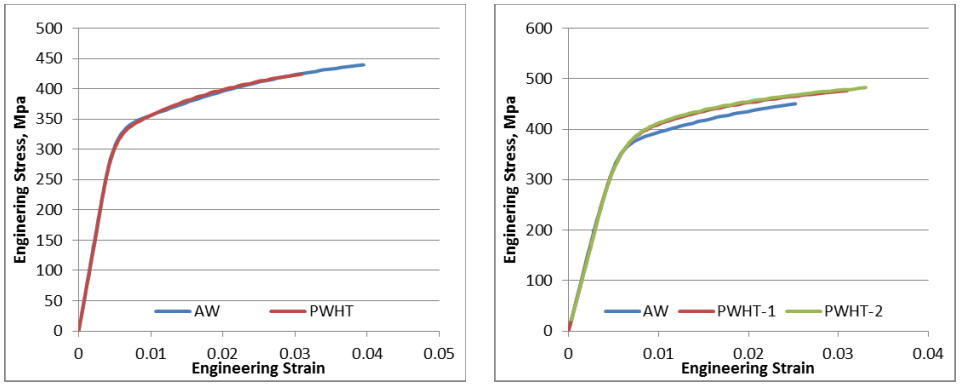

(a) #4302&#4304, 160 RPM, 102 mm/min (b) #4301&#4303, 200 RPM, 203 mm/min

Figure 4.87 Engineering stress and strain curves of transverse tensile testing on CSDP joints in AW and PWHT conditions

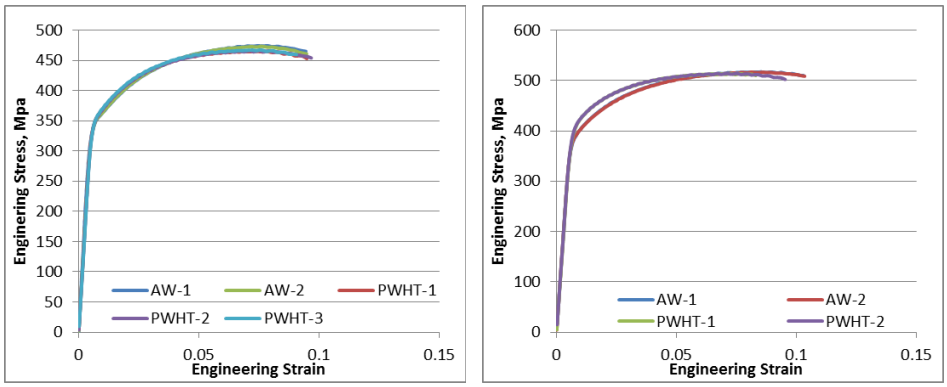

(a) #4309&#4311, 160 RPM, 102 mm/min (b) #4310&#4312, 200 RPM, 203 mm/min

Figure 4.88 Engineering stress and strain curves of transverse tensile testing on SSDP joints in AW and PWHT conditions

4.3.5.1.1 CSDP: Transverse Tensile Testing

Compared with the CSDP #4229&#4231 (symmetric layout), in the CSDP #4229&#4230 (asymmetric layout), the PWHT UTS increased by 1.5%. It indicates that, under the same speeds, in CSDP, relative to symmetric layout, the asymmetric layout increased PWHT UTS slightly.

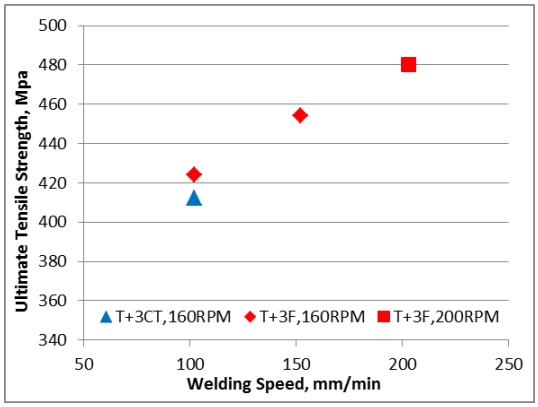

Figure 4.89 Ultimate tensile strength of transverse tensile testing as a function of welding speed of CSDP joints in PWHT condition: IA

Figure 4.89 shows the ultimate tensile strength of transverse tensile testing as a function of welding speed of CSDP joints in PWHT condition. Figure 4.89 shows that, under the same speeds (160 rpm, 102 mm/min), relative to the T+3CT tool, T+3F tool increased the PWHT UTS slightly (3%). When the same T+3F tool was applied, under

the same rotation rate, higher welding speed increased the PWHT UTS a little (7%). When the same T+3F tool was applied, higher FSW speeds increased the PWHT UTS a little (6%), and the increasing effect of welding speed on PWHT UTS was larger than that of RPM. Figure 4.89 also shows that, relative to the T+3CT tool, T+3F tool allows higher FSW speeds which increased the PWHT UTS a little.

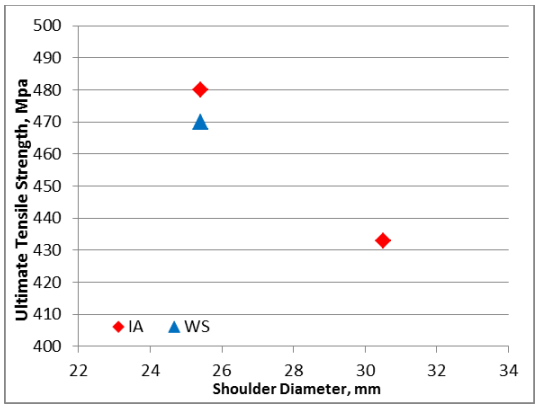

Figure 4.90 Ultimate tensile strength of transverse tensile testing as a function of shoulder diameter of CSDP joints in PWHT condition: T+3F, 200 RPM, 203 mm/min

Figure 4.90 shows the ultimate tensile strength of transverse tensile testing as a function of shoulder diameter of CSDP joints in PWHT condition produced by the same T+3F tool, with the same rotation rate of 200 rpm, and the same welding speed of 203 mm/min. Figure 4.90 shows that, with the same shoulder diameter, relative to IA, WS decreased the PWHT UTS slightly (-2%), which might due to the volumetric defects in the 1st pass caused by WS (#4237, small holes at AS near crown and mid-plane). When WS was not applied, relative to the shoulder diameter of 25.4 mm, the larger shoulder diameter (30.5 mm) decreased the PWHT UTS a little (-10%) even when the joints were defect free.

Figure 4.91 shows (a) Ultimate Tensile Strength, (b) Yield Strength and (c) Elongation of transverse tensile testing as a function of welding speed of CSDP and

SSDP joints in AW and PWHT conditions. Figure 4.91 shows that: In AW CSDP, higher FSW speeds increased UTS slightly (2%), increased YS a little 11(%), and decreased EL significantly (-42%). In PWHT CSDP, higher FSW speeds increased UTS (13%) and YS (15%) a little, and increased EL slightly (4%). When the lower FSW speeds (160 rpm, 102 mm/min) were applied, relative to AW, PWHT decreased UTS slightly (-4%), affected YS little, and decreased EL (-24%). When the higher FSW speeds (200 rpm, 203 mm/min) were applied, relative to AW, PWHT increased UTS (7%) and YS (4%) slightly, and increased EL (37%).

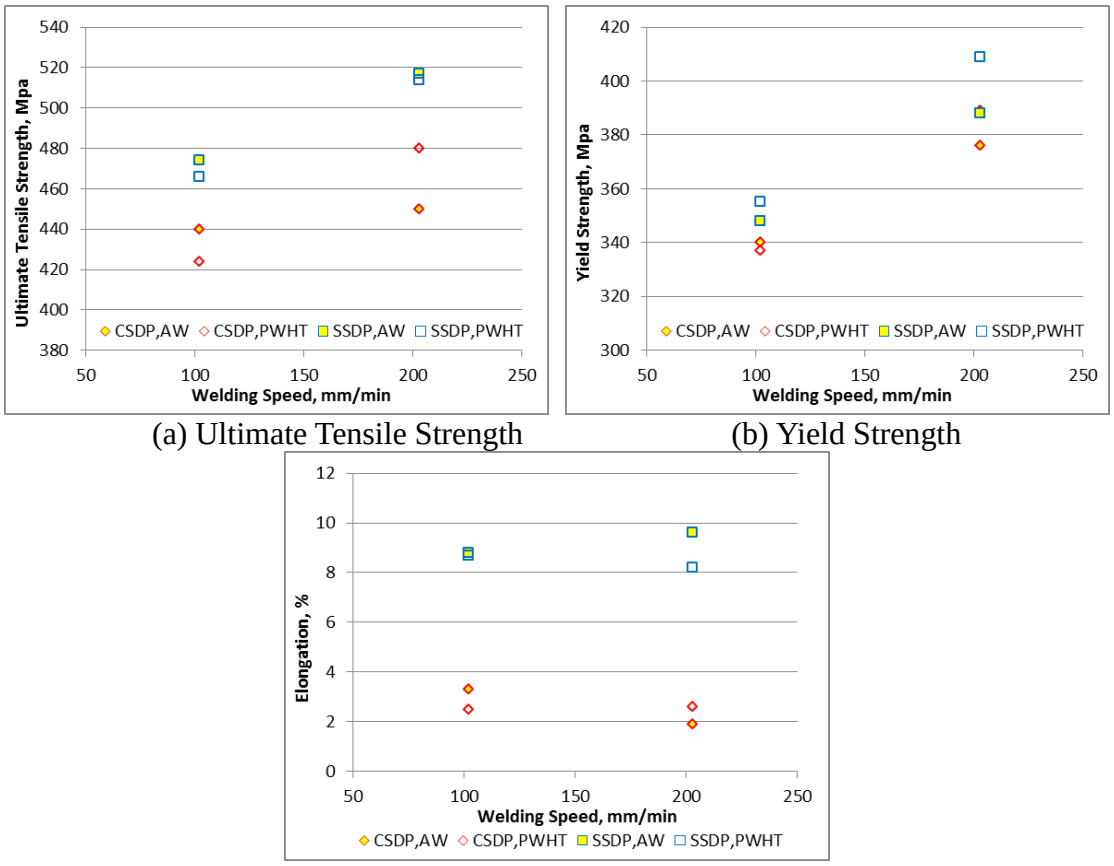

(a) Ultimate Tensile Strength (b) Yield Strength

(c) Elongation

Figure 4.91 (a) Ultimate Tensile Strength, (b) Yield Strength and (c) Elongation of transverse tensile testing as a function of welding speed of CSDP and SSDP joints in AW and PWHT conditions: IA

4.3.5.1.2 SSDP: Transverse Tensile Testing

Figure 4.91 shows (a) Ultimate Tensile Strength, (b) Yield Strength and (c) Elongation of transverse tensile testing as a function of welding speed of CSDP and SSDP joints in AW and PWHT conditions. Figure 4.91 shows that: In AW SSDP, higher FSW speeds increased UTS (9%), YS (12%) and EL (9%) a little. In PWHT SSDP, higher FSW speeds increased UTS (10%) and YS (15%) a little, while decreased EL slightly (-6%). When the lower FSW speeds (160 rpm, 102 mm/min) were applied, relative to AW, PWHT affected UTS, YS and EL little. When the higher FSW speeds (200 rpm, 203 mm/min) were applied, relative to AW, PWHT affected UTS little, increased YS slightly (5%), and decreased EL a little (-15%).

4.3.5.1.3 CSDP and SSDP: Transverse Tensile Testing

Figure 4.91 shows (a) Ultimate Tensile Strength, (b) Yield Strength and (c) Elongation of transverse tensile testing as a function of welding speed of CSDP and SSDP joints in AW and PWHT conditions. Figure 4.91 shows that, when the lower FSW speeds (160 rpm, 102 mm/min) were applied, in AW, relative to CSDP, SSDP increased UTS slightly (8%), affected YS little, and increased EL significantly (167%); in PWHT, relative to CSDP, SSDP increased UTS a little (10%), increased YS slightly (5%), and increased EL significantly (248%). When the higher FSW speeds (200 rpm, 203 mm/min) were applied, in AW, relative to CSDP, SSDP increased UTS a little (15%), affected YS little, and increased EL significantly (405%); in PWHT, relative to CSDP, SSDP increased UTS (7%) and YS (5%) slightly, and increased EL significantly (215%).

4.3.5.2 Longitudinal Tensile Testing (PWHT)

Subscale longitudinal tensile tests have been performed on the 1st passes and the 2nd passes of some CSDP and SSDP joints in PWHT condition. Engineering stress as a function of engineering strain of longitudinal tensile testing on CSDP and SSDP joints in PWHT condition were shown in Figure 4.92 and Figure 4.93. Results of longitudinal tensile testing on CSDP and SSDP joints in PWHT condition were plotted in Figure 4.94.

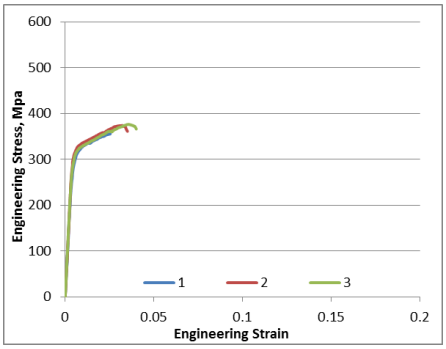

(a) #4302, CSDP-1, 160 RPM, 102 mm/min

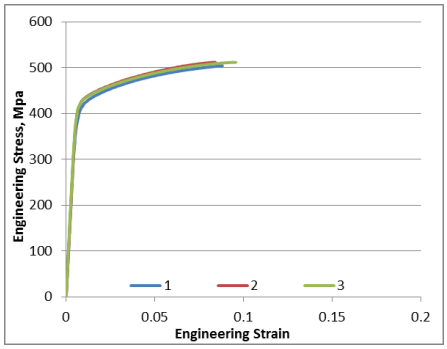

(b) #4304, CSDP-2, 160 RPM, 102 mm/min

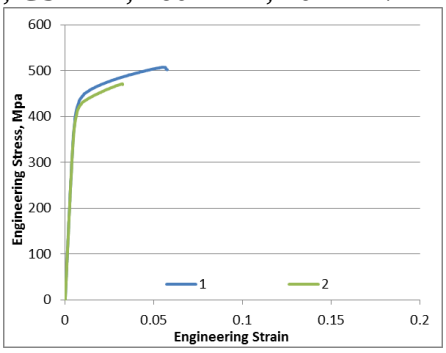

(c) #4301, CSDP-1, 200 RPM, 203mm/min

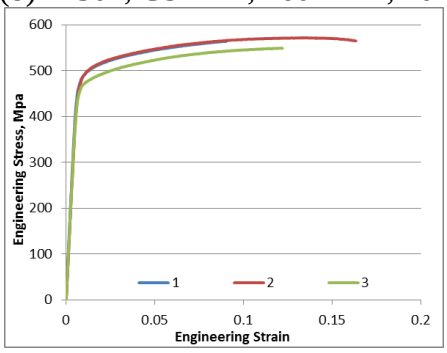

(d) #4303, CSDP-2, 200 RPM, 203 mm/min

Figure 4.92 Engineering stress and strain curves of longitudinal tensile testing on CSDP joints in PWHT condition

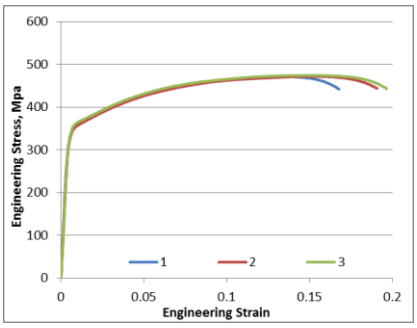

(a) #4309, SSDP-1, 160 RPM, 102mm/min

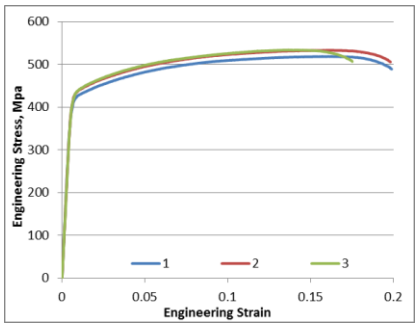

(b) #4311, SSDP-2, 160 RPM, 102 mm/min

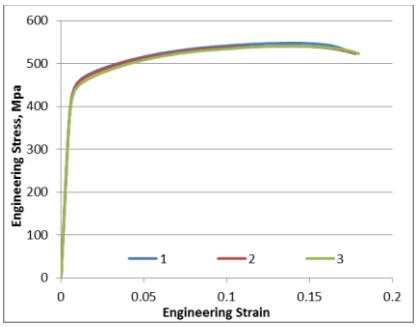

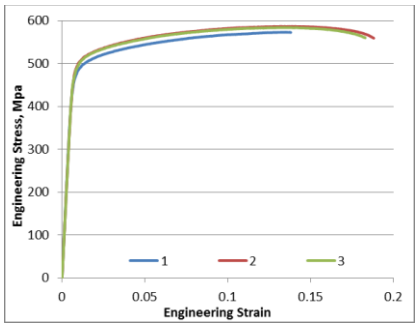

(c) #4310, SSDP-1, 200 RPM, 203mm/min (d) #4312, SSDP-2, 200 RPM, 203 mm/min

Figure 4.93 Engineering stress and strain curves of longitudinal tensile testing on SSDP joints in PWHT condition: T+3CT tool

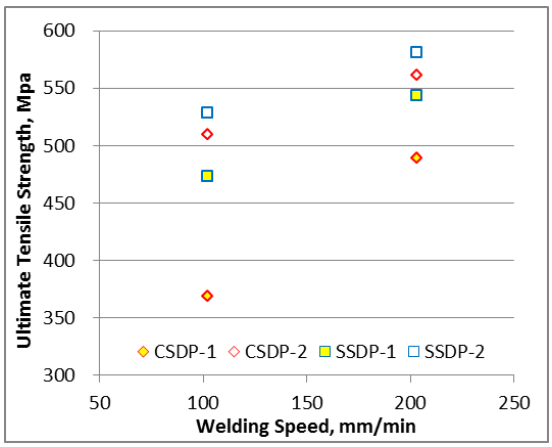

(a) Ultimate Tensile Strength

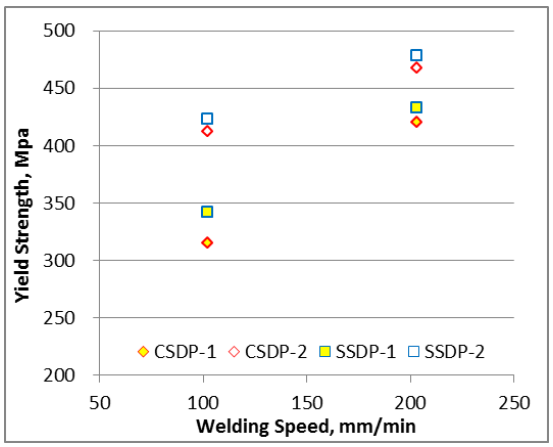

(b) Yield Strength

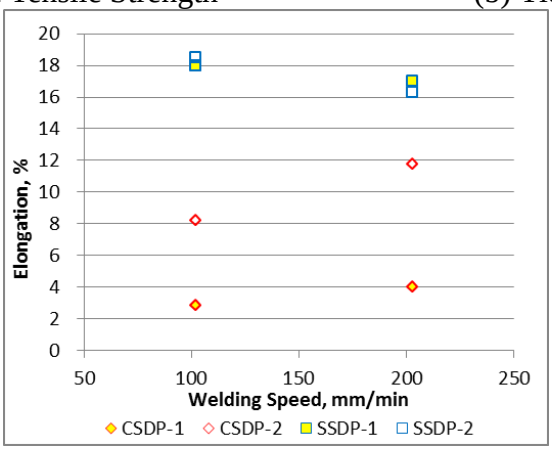

(c) Elongation

Figure 4.94 (a) Ultimate Tensile Strength, (b) Yield Strength and (c) Elongation of subscale longitudinal tensile testing as a function of welding speed of CSDP and SSDP joints in PWHT condition: IA

Figure 4.94 shows (a) Ultimate Tensile Strength, (b) Yield Strength and (c) Elongation of subscale longitudinal tensile testing as a function of welding speed of

CSDP and SSDP joints in PWHT condition. Figure 4.94 shows the following results of PWHT CSDP and SSDP:

In CSDP-1, higher FSW speeds increased UTS (33%), YS (33%) and EL (40%). In CSDP-2, higher FSW speeds increased UTS (10%) and YS (13%) a little, and increased EL (43%). When the lower FSW (160 rpm, 102 mm/min) speeds were applied, relative to the 1st pass, the 2nd pass increased UTS (38%) and YS (31%), and increased EL significantly (187%). When the higher FSW speeds (200 rpm, 203 mm/min) were applied, relative to the 1st pass, the 2nd pass increased UTS (15%) and YS (11%) a little, and increased EL significantly (195%).

In SSDP-1, higher FSW speeds increased UTS a little (15%), increased YS (27%), and decreased EL slightly (-5%). In SSDP-2, higher FSW speeds increased UTS (10%) and YS (13%) a little, while decreased EL a little (-12%). When the lower FSW speeds (160 rpm, 102 mm/min) were applied, relative to the 1st pass, the 2nd pass increased UTS a little (12%), increased YS (24%), and affected EL little. When the higher FSW speeds (200 rpm, 203 mm/min) were applied, relative to the 1st pass, the 2nd pass increased UTS slightly (7%), increased YS a little (11%), and affected EL little (-4%).

When the lower FSW speeds (160 rpm, 102 mm/min) were applied, in DP-1, relative to CS, SS increased UTS (28%), increased YS slightly (9%), and increased EL significantly (527%); in DP-2, relative to CS, SS affected UTS and YS little, and increased EL significantly (124%). When the higher FSW speeds (200 rpm, 203 mm/min) were applied, in DP-1, relative to CS, SS increased UTS a little (11%), affected YS little, and increased EL significantly (325%); in DP-2, relative to CS, SS affected UTS and YS little, and increased EL (38%).

4.3.6 Residual Stress (AW&PWHT)

In this section, residual stress distribution in the CSDP and SSDP joints will be studied to investigate effects of CSDP and SSDP, different control parameters and PWHT on residual stress profiles in joints. Through thickness average, longitudinal, residual stress was measured in both AW and PWHT conditions for selected CSDP and SSDP joints as following: #4302&#4304, #4301&#4303, #4309&#4311 and #4310&#4312. Through those residual stress profiles of above tested CSDP and SSDP joints in both AW and PWHT conditions shown in Figure 4.95, characteristic values like the peak residual stress (PRS), full width at half maximum (FWHM) and tension area (TA) were calculated and shown in Figure 4.96~Figure 4.98. Unit weld energy (UWE) was also calculated and shown in Figure 4.96~Figure 4.98. PRS is in units of MPa, FWHM is in units of mm, TA is in units of KJ/m^2, while UWE is in units of KW/(m/s). UWE equals to power in units of W be divided by the welding speed in units of mm/s.

Figure 4.95 shows through thickness average, longitudinal, residual stress profiles in both AW and PWHT conditions of CSDP and SSDP joints produced with different speeds, shoulders and pin features. Figure 4.95 shows that, relative to AW condition, PWHT affects the residual stress profiles little.

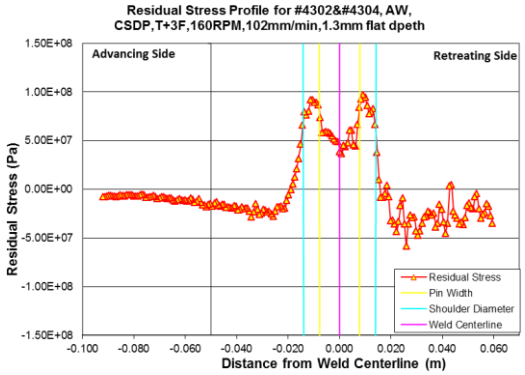

(a) #4302&#4304, AW

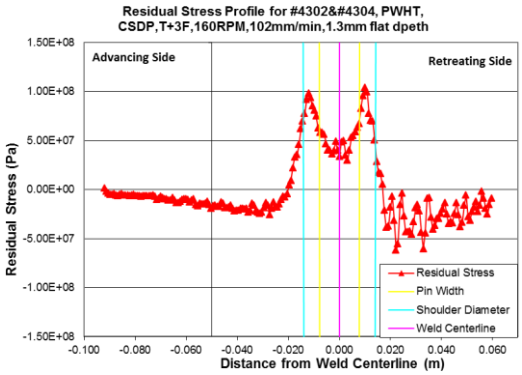

(b) #4302&#4304, PWHT

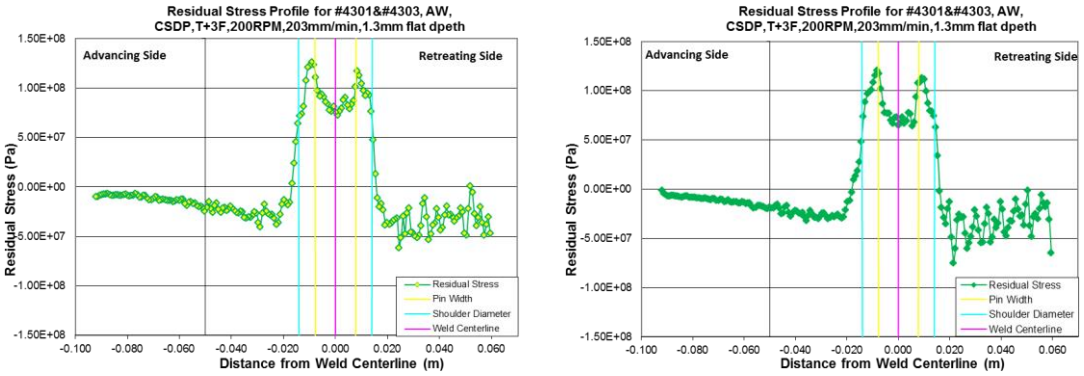

(c) #4301&#4303, AW

(d) #4301&#4303, PWHT

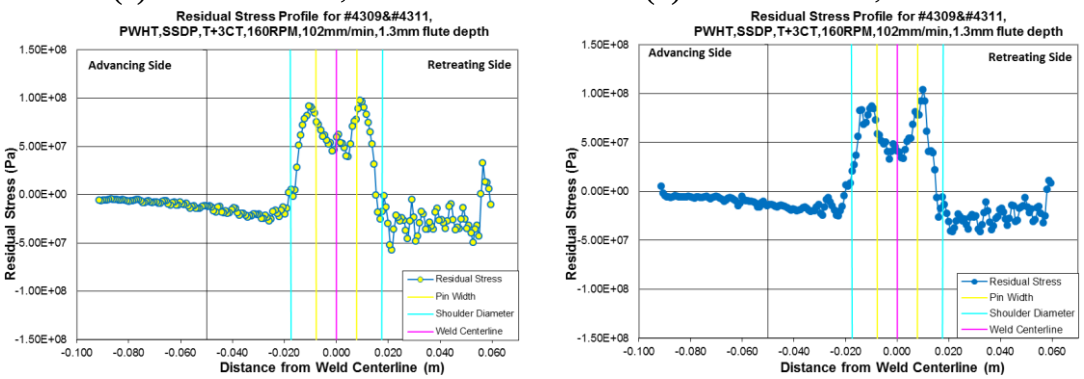

(e) #4309&#4311, AW

(f) #4309&#4311, PWHT

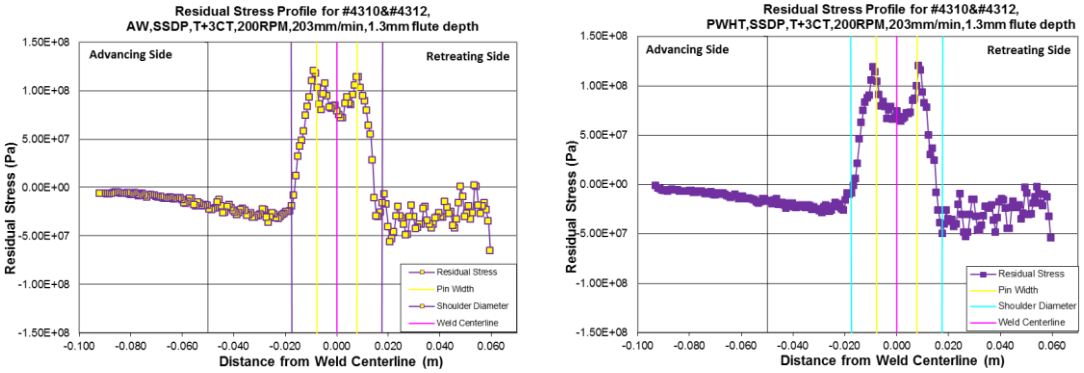

(g) #4310&#4312, AW

(h) #4310&#4312, PWHT

Figure 4.95 Through thickness average, longitudinal, residual stress profiles in both AW and PWHT conditions of CSDP and SSDP joints produced with different speeds, shoulders and pin features: 1 °setup, 0.9 mm flat/flute depth

Figure 4.96 shows (a) Peak residual stress, (b) FWHM, (c) tension area of through thickness average, longitudinal, residual stress profiles in both AW and PWHT conditions, and (d) unit weld energy of CSDP and SSDP joints as a function of welding speeds.

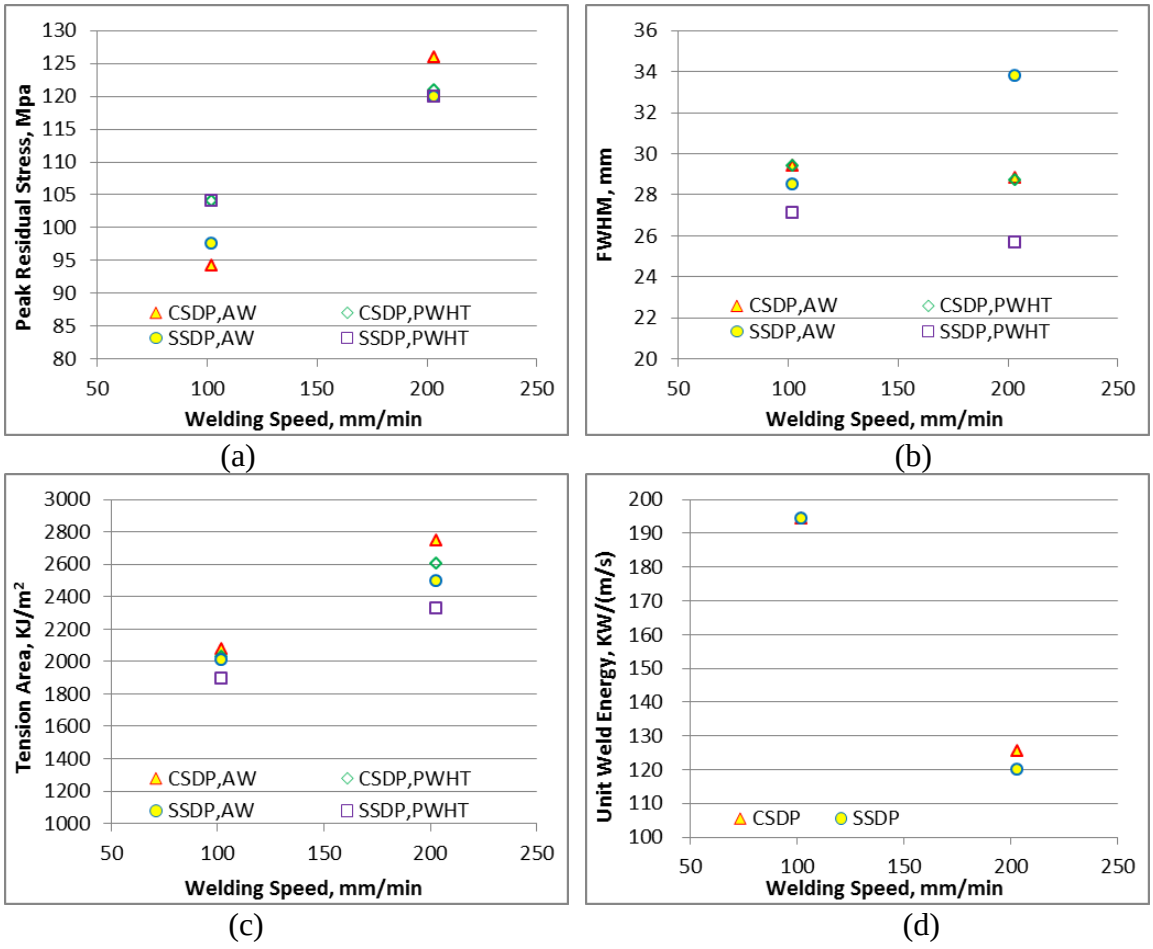

Figure 4.96 (a) Peak residual stress, (b) FWHM, (c) tension area of through thickness average, longitudinal, residual stress profiles in both AW and PWHT conditions, and (d) unit weld energy of DP as a function of welding speeds: 1 °setup, 0.9 mm flat/flute depth

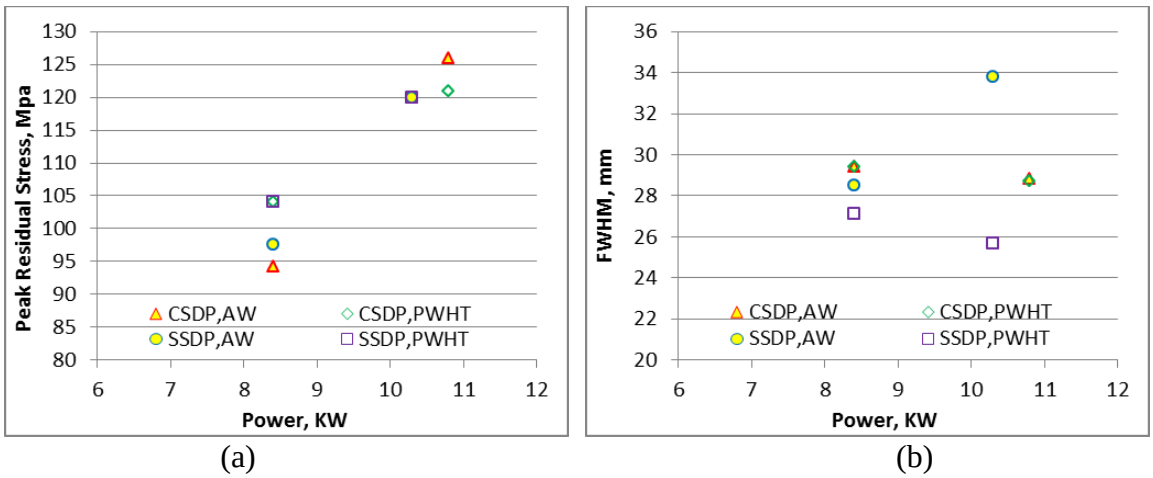

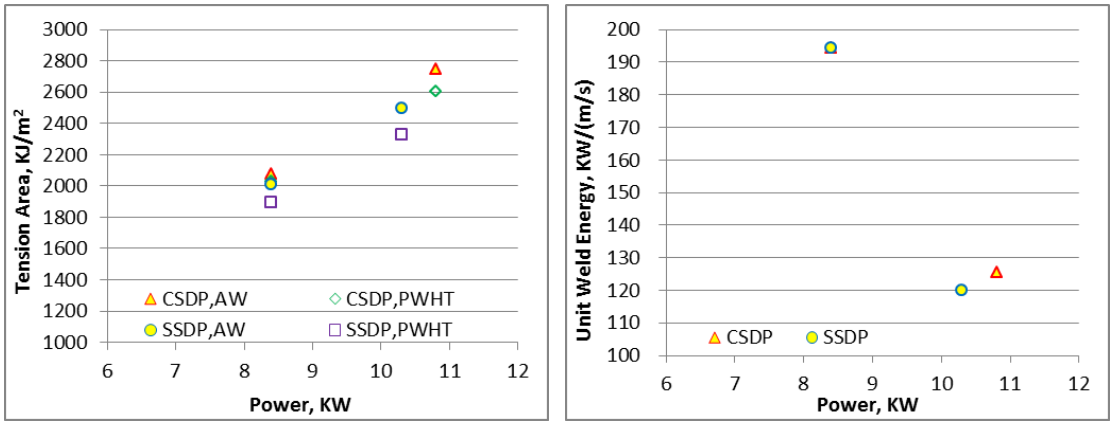

(c) (d)

Figure 4.97 (a) Peak residual stress, (b) FWHM, (c) tension area of through thickness average, longitudinal, residual stress profiles in both AW and PWHT conditions, and (d) unit weld energy of DP joints as a function of power: 1 °setup, 0.9 mm flat/flute depth

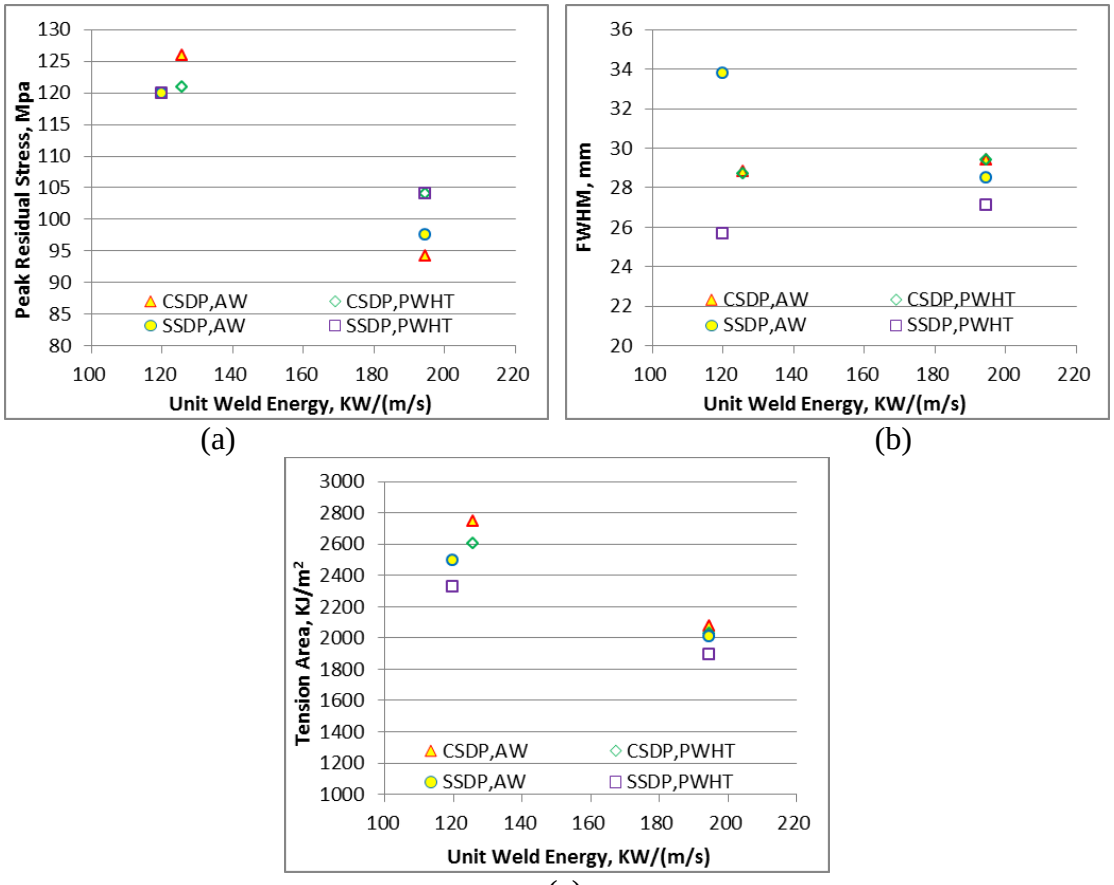

(a) (b)

(c)

Figure 4.98 (a) Peak residual stress, (b) FWHM, (c) tension area of through thickness average, longitudinal, residual stress profiles in both AW and PWHT conditions, and (d) unit weld energy of DP joints as a function of unit weld energy: 1 °setup, 0.9mm depth

Figure 4.97 shows (a) Peak residual stress, (b) FWHM, (c) tension area of through thickness average, longitudinal, residual stress profiles in both AW and PWHT conditions, and (d) unit weld energy of CSDP and SSDP joints as a function of power. Figure 4.98shows (a) Peak residual stress, (b) FWHM, and (c) tension area of through thickness average, longitudinal, residual stress profiles in both AW and PWHT conditions of CSDP and SSDP joints as a function of the unit weld energy.

Figure 4.96~Figure 4.98 show that:

(1) In AW CSDP, higher FSW speeds increased PRS (34%) and TA (32%), while affected FWHM little; In PWHT CSDP, higher FSW speeds increased PRS a little (16%), affected FWHM little, and increased TA (28%). In CSDP, higher FSW speeds decreased UWE (-35%). When the lower FSW speeds (160 RPM, 102 mm/min) were applied, relative to AW, PWHT increased PRS a little (10%), affected FWHM and TA little. When the higher FSW speeds (200 RPM, 203 mm/min) were applied, relative to AW, PWHT affected PRS and FWHM little, and decreased TA slightly (-5%).

(2) In AW SSDP, higher FSW speeds increased PRS (23%), FWHM (19%) and TA (24%); In PWHT SSDP, higher FSW speeds increased PRS a little (15%), decreased FWHM slightly (-5%), and increased TA (23%). In SSDP, higher FSW speeds decreased UWE (-38%). When lower FSW speeds (160 RPM, 102 mm/min) were applied, relative to AW, PWHT increased PRS slightly (7%), while decreased FWHM (-7%) and TA (-6%) slightly. When higher FSW speeds (200RPM, 203mm/min) were applied, relative to AW, PWHT affected PRS little, decreased FWHM (-24%), and decreased TA slightly (-7%).

(3) When the lower FSW speeds (160 RPM, 102 mm/min) were applied, in AW DP, relative to CS, SS affected PRS, FWHM and TA little; in PWHT DP, relative to CS,

SS affected PRS little, while decreased FWHM (-8%) and TA (-7%) slightly; in DP, relative to CS, SS affected UWE little. When the higher FSW speeds (200 RPM, 203 mm/min) were applied, in AW DP, relative to CS, SS decreased PRS (-5%) and TA (-5%) slightly, while increased FWHM a little (17%); in PWHT DP, relative to CS, SS affected PRS little, decreased FWHM (-10%) and TA (-11%) a little; in DP, relative to CS, SS decreased UWE slightly (-5%).

4.3.7 Face Bending Testing Properties

In this section, face bending tests were performed on CSDP and SSDP entire joints as following in AW and PWHT conditions produced by different control parameters and TBCs to investigate effects of different shoulders, tools, layouts, control parameters and TBCs on joint's face bending properties: #4229&#4230 (PWHT), #4229&#4231(PWHT), #4232A&#4233A (PWHT), #4232B&#4233B (PWHT), #4237&#4238 (PWHT), #4302&#4304 (AW&PWHT), #4301&#4303 (AW&PWHT), #4309&#4311 (AW&PWHT), and #4310&#4312 (AW&PWHT). Details of weld information of the above joints have been listed in section 4.3.5.1.

Results of face bending tests of the above joints (127mm x 6.4mm x 24.9mm) for face bending test in AW and PWHT conditions, as shown in Figure 4.99, were summarized as following:

Passed: #4229&#4230 (PWHT), #4229&#4231(PWHT), #4232A&#4233A (PWHT), #4232B&#4233B (PWHT), #4309&#4311 (AW&PWHT), and #4310&#4312 (AW)

Failed: #4237&#4238 (PWHT), #4302&#4304 (AW&PWHT), #4301&#4303 (AW&PWHT), #4310&#4312 (PWHT)

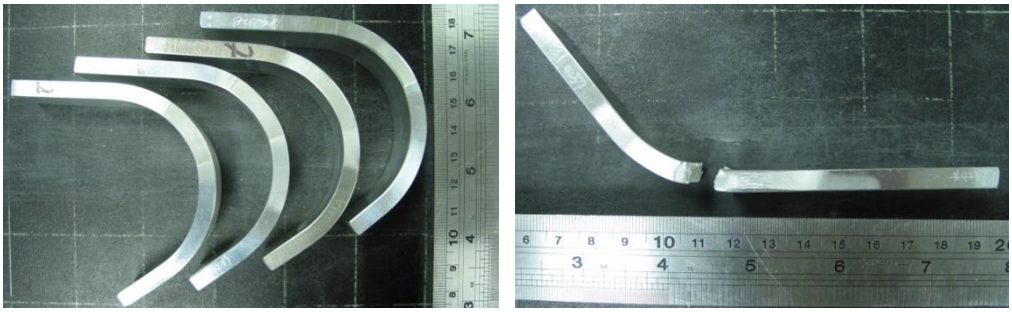

(a) (b) #4237&#4238, PWHT

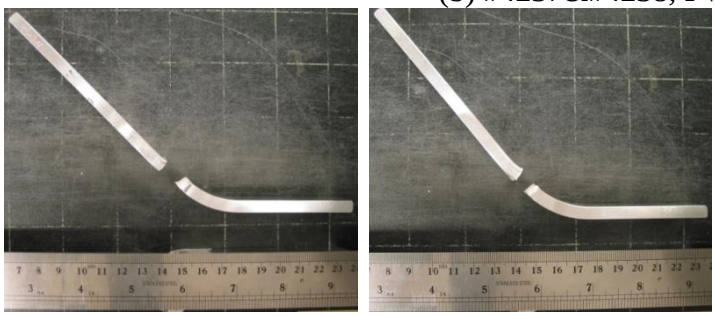

(c) #4302&#4304, AW (d) #4302&#4304, PWHT

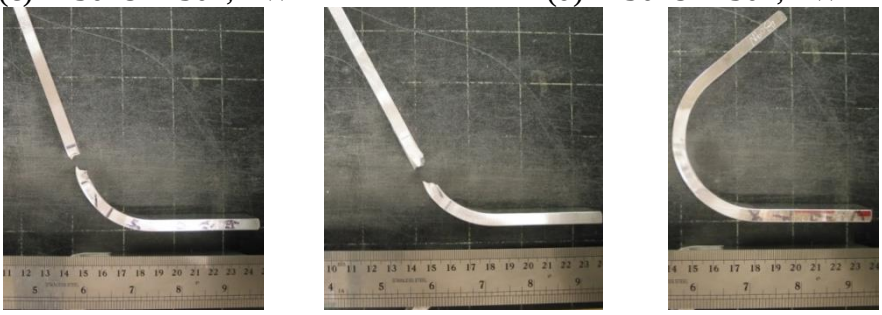

(e) #4301&#4303, AW (f) #4301&#4303, PWHT (g) #4309&#4311, AW

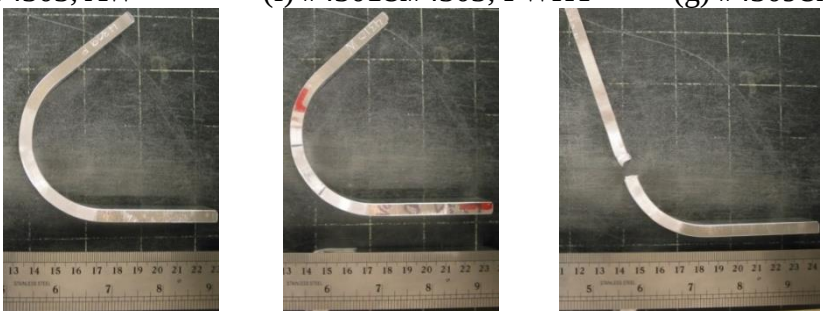

(h) #4309&#4311, PWHT (i) #4310&#4312, AW (j) #4310&#4312, PWHT

Figure 4.99 Specimens of DP joints in AW and PWHT conditions after the face bending testing. From left to right in (a): #4229&#4230, #4229&#4231, #4232A&#4233A,#4232B&#4233B: PWHT

In the above joints, all are defect free except #4237 (small holes at AS near crown and mid-plane) and #4312 (wormholes at mid AS near crown). The above results of face bending testing show that:

(1) In PWHT CSDP, when joints were produced by the same T+3CT tool with a rotation rate of 160 rpm and a welding speed of 102 mm/min, the CSDP joints with both symmetric and asymmetric layouts passed the face bending testing;

(2) In PWHT CSDP, when joints were produced by the same T+3F tool with a rotation rate of 200 rpm and a welding speed of 203 mm/min, the IA CSDP joint passed the face bending testing, while the WS CSDP joint failed the face bending testing, which possibly due to the defect in the 1st pass of WS CSDP.

(3) In PWHT CSDP, the joint produced by the T+3CT tool with a rotation rate of 160 rpm and a welding speed of 102 mm/min passed the face bending testing; the joint produced by the T+3F tool with a rotation rate of 160 rpm and a welding speed of 152 mm/min passed the face bending testing; the joint produced by the T+3F tool with a rotation rate of 160 rpm and a welding speed of 102 mm/min failed the face bending testing. It indicates that, in PWHT CSDP, with a rotation rate of 160 rpm and a welding speed of 152 mm/min, the T+3CT produced defect free joints which passed the face bending testing, while the T+3F tools produced defect free joints which failed the face bending testing, which might because that relative to the T+3CT tool, the T+3F tool produced a 14% higher power in total though similar temperatures at pin center; however, relative to the T+3CT tool, the T+3F tool allows higher speeds to produce defect free joints which passed the face bending testing.

(4) In PWHT CSDP, when the joints were produced by the T+3F tool with a rotation rate of 200 rpm and a welding speed of 203 mm/min, one passed the face bending testing and another failed.

(5) In comparable CSDP and SSDP joints, all the CSDP joints produced with the same T+3F tool and different speeds in AW and PWHT conditions failed the face bending testing. All the SSDP joints produced with the same T+3CT tool and different speeds in AW and PWHT conditions failed the face bending testing, except one case: the SSDP joint produced with a rotation rate of 200 rpm and a welding speed of 203 mm/min in PWHT condition, which might due to the defective 2nd pass of this SSDP. It indicates that, under the same speeds and the same TBCs, relative to CSDP, SSDP improved the joint's performance in the face bending testing. It also indicates that the performance during face bending testing was also affected by volumetric defects and PWHT. When the joint is defective, PWHT will worsen the performance.

4.4 Stationary Shoulder Single Pass FSW in different alloys

In section 4.2, SSSP in AA7099 has been investigated. SSSP has also been performed in other alloys to investigate the effect of different base metals on properties of SSSP joints. Control parameters and tool information have been tabulated in Appendix B in the Appendix. In this section, SSSP FSW in different alloys has been studied in following aspects: macrostructure including investigation of surface finish, defect and nugget shape, microstructure, effect of control parameters on response parameters, and grain size, etc.

4.4.1 Macrostructure

4.4.1.1 Surface finish

In this section surface finish of SSSP in different alloys was examined. Figure 4.100 (a) and (b) show joint surfaces of SSSP in AA7099-T7651, produced by the same

T+3F pin with the same flat depth of 1.7 mm, the same setup of 0 ° tilt angle, the same forge force of 71.2 KN, the same welding speed of 51 mm/min, and rotating speeds of 200 RPM and 160 RPM, respectively. In each condition, the surface is partially smooth and partially defective. In the smooth area, the semi-circular marks are smooth, not obvious and not complete. Figure 4.101 (a) and (b) show joint surfaces of SSSP in AA7099-T7651, produced by the same T+3CT pin with the same flat depth of 1.7 mm, the same setup of 1 ° tilt angle, the same forge force of 69 KN, the same welding speed of 51 mm/min, and rotating speeds of 200 RPM and 160 RPM, respectively. In each condition, surface is smooth and semi-circular marks are not obvious and not complete.

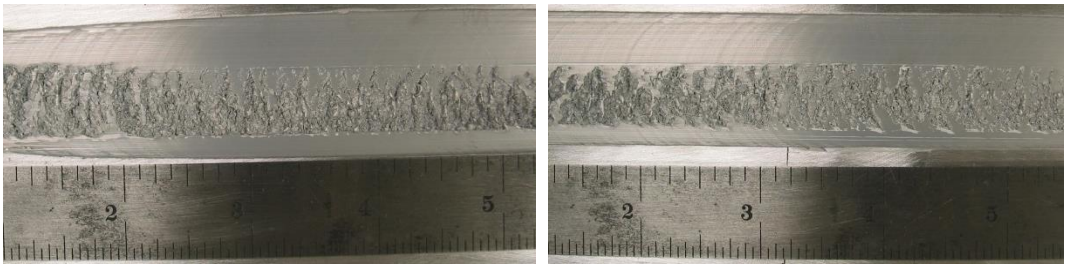

(a) #3965A (b) #3965B

Figure 4.100 Joint surfaces of SSSP in AA7099: 0 ° tilt, T+3F pin, 1.7 mm flat depth, 51 mm/min, Fz 71.2 KN: (a) 200 RPM and (b) 160 RPM

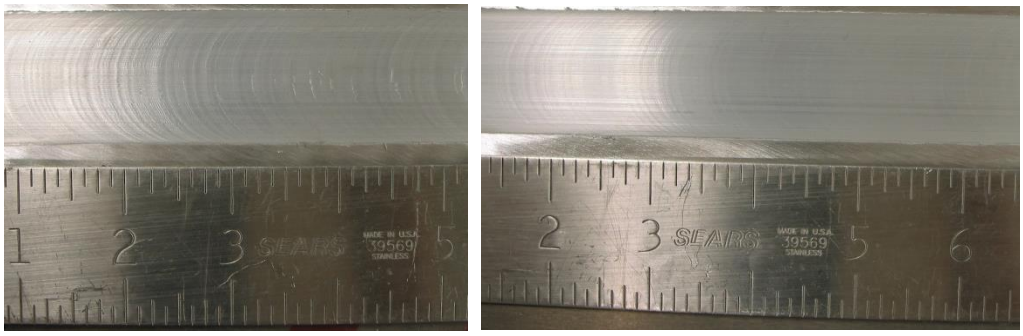

(a) #4114 (b) #4116

Figure 4.101 Joint surfaces of SSSP in AA7099: 1 ° tilt, T+3CT pin, 1.7 mm flat depth, 51 mm/min, Fz 69 KN: (a) 200 RPM and (b) 160 RPM

Figure 4.102 (a) and (b) show joint surfaces of SSSP in AA7099-T7651, produced by the same T+3CT pin with the same flat depth of 0.9 mm, the same setup of 1 ° tilt angle,

the same forge force of 69 KN, the same welding speed of 51 mm/min, and rotating speeds of 200 RPM and 160 RPM, respectively. In each condition, the surface is smooth and the semi-circular marks are not obvious and not complete.

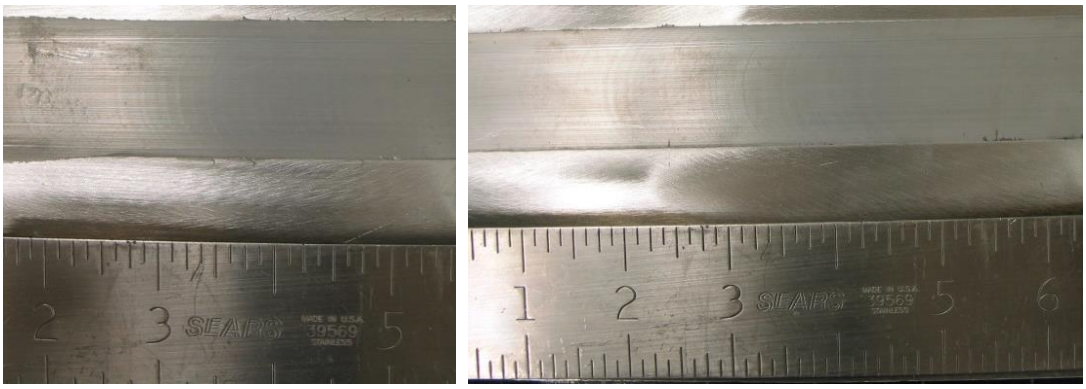

(a) #4167A (b) #4167B

Figure 4.102 Joint surfaces of SSSP in AA7099: 1 °tilt, T+3CT pin, 0.9 mm flat depth, 51 mm/min, Fz 69 KN: (a) 200 RPM and (b) 160 RPM

It indicates that, in SSSP in AA7099-T7651, relative to the T+3F tool with a setup of 0° and a flat depth of 1.3 mm, the T+3CT tool with a setup of 1° and a flat depth of 1.3 mm can significantly improve the surface finish, and decrease the surface defect significantly, though there were some small holes or cracks inside the nugget; relative to the T+3CT tool with a setup of 1° and a flat depth of 1.3 mm, the T+3CT tool with a setup of 1° and a flat depth of 0.9 mm eliminate the volumetric defects inside the nugget, while keep the good and smooth surface finish.

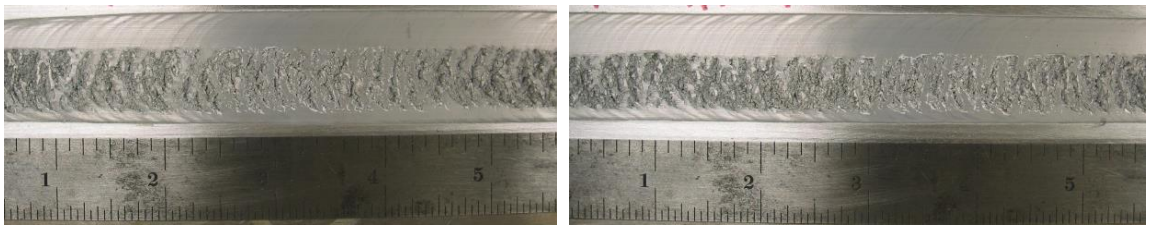

(a) #3966A (b) #3966B

Figure 4.103 Joint surfaces of SSSP in AA7050: 0 °tilt, T+3F pin, 1.7 mm flat depth, 51 mm/min, Fz 66.7 KN: (a) 200 RPM and (b) 160 RPM

Figure 4.103 (a) and (b) show joint surfaces of SSSP in AA7050-T7451, produced by the same T+3F pin (flat depth 1.7 mm), the same 0 °tilt setup, the same forge force of 66.7 KN, welding speed of 51 mm/min, and rotating speeds of 200 RPM and 160 RPM, respectively. In each condition, surface is partially smooth and partially defective. In the smooth area, semi-circular marks are smooth, not obvious and not complete.

Figure 4.104 (a) and (b) show joint surfaces of SSSP in AA6061-T651, produced by the same T+3CT pin with the same flute depth of 0.9 mm, the same setup of 1 °tilt angle, the same forge force of 66.7 KN, the same welding speed of 203 mm/min, and rotating speeds of 480 RPM and 400 RPM, respectively. In each condition, the surface is smooth and the semi-circular marks are not obvious and not complete.

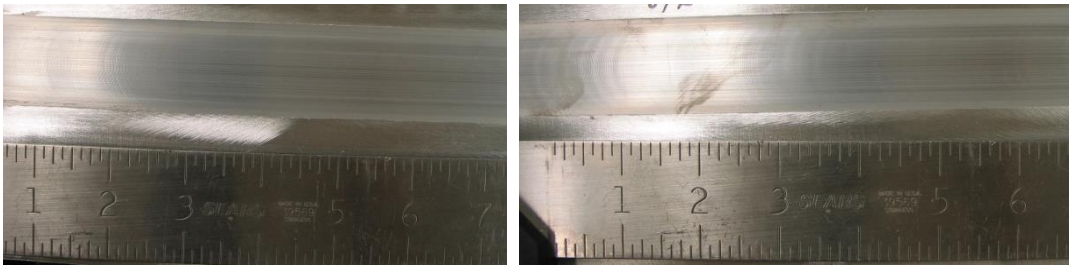

(a) #4168A (b) #4168B

Figure 4.104 Joint surfaces of SSSP in AA6061: 1 °tilt, T+3CT pin, 0.9 mm flute depth, 203 mm/min, Fz 66.7 KN: (a) 480 RPM and (b) 400 RPM

It indicates that, in the above cases, SSSP in AA7099 and AA7050 allows similar FSW welding speed windows, resulting similar surface finish, which is half smooth while half smooth when the T+3F tool with a setup of 0° was applied. T+3CT tool with a setup of 1° and a flute depth of 0.9 mm produced defect free SSSP joints in AA7099, which might also possibly produced defect free SSSP joints in AA7050. However, relative to SSSP in AA7099 and AA7050, SSSP in AA6061 allows much higher FSW speeds, resulting smooth and perfect surface finish. Different surface finishes might due

to the setup of 1° in SSSP of AA6061 which helps eliminate the surface defect, as well as the reason that AA6061 is much softer relative to the other two 7XXX alloys.

4.4.1.2 Defect investigation

The result of defect examination of SSSP joints in different alloys is listed in Appendix C. It shows that:

In SSSP of AA7099, when a setup of 0 °tilt, a T+3F pin and a welding speed of 51 mm/min were applied, under the same forge force (73.4 KN), similar surface defects appeared at similar locations; higher rotating speed caused worse surface defects; lower rotating speed and/or deeper flat lead to less surface defects. When the pin rotates CCT, right-handed thread moves material downward, flat pin feature will interrupt this trend, co-flow flute will also move material downward, while counter-flow flute will move material upward. Deeper flat means more interruption of moving material downward, then less material moved downward from the crown, therefore less surface defect.

In SSSP of AA7099, when a setup of 0 °tilt, a T+3CT pin with a flute depth of 1.3 mm and a welding speed of 51 mm/min were applied, under the same forge force (69 KN), it shows that too high rotating speed leads to surface defects; lower rotating speed reduced/eliminated surface and reduced inside nugget defects, while there were still some wormhole defects near the weld root. Therefore, when a setup of 0 °tilt was applied, changing the pin feature from flats to counter-flow flutes could help reduce/eliminate surface defect, while wouldn't eliminate worm hole defects. When a setup of 0 °tilt, a T+3CT pin with a larger flute depth of 2.03 mm and a welding speed of 51 mm/min were applied, under the same forge force (69 KN), it shows that higher rotating speed (240 rpm) was more likely to cause surface defect; hole defects inside the nugget moved

upward/from RS to AS when rotating speed increased. Keep other parameters the same, it's found that deeper flutes lead to less surface defects but worse worm hole defects inside the nugget, due to too much material moved upward by deeper counter-flow flutes when the pin rotates CCT.

In SSSP of AA7099, when a setup of 1 ℃tilt, a T+3CT pin with a flute depth of 0.9 mm and a welding speed of 51 mm/min were applied, under the same forge force (69 KN), too low rotating speed was not recommend since it caused wormhole defects which might due to not enough vertical material movement. It indicates that compared with 0 ℃tilt, 1 ℃tilt can significantly eliminate defects on surface and inside the nugget, produce defect free welds by providing more consolidation/forge at back of the shoulder. When a setup of 1 ℃tilt, a T+3CT pin with a flute depth of 0.9 mm and a welding speed of 51 mm/min were applied, under the same rotation rate (160 rpm), too small forge force (35.6KN) causes bad surface defects (large area), not full penetration and raises the crown. Among those applied forge forces, 53.4 KN is the minimum forge force that can produce defect free welds. Forge force larger than 53.4 KN also lead to defect free welds. Further tests are needed to verify whether forge force affects the defect free joint qualities (#4171AB, #4167B). When a setup of 1 ℃tilt, a T+3CT pin with a flute depth of 1.65 mm and a welding speed of 51 mm/min were applied, under the same forge force (69 KN), 160 rpm caused wormhole defects at AS near root, while 200 RPM caused wormhole defects at AS near mid-plane. The formation of wormhole defects inside the nugget might due to more material moved upward by a T+3CT pin with a flute depth of 1.65 mm, which is larger than the appropriate flute depth for sound material flow. It indicates that when rotating speed increased, wormhole defects moved upward, which might because

when rotating speed increased, the velocity at upper part of the pin increased more than at lower part of the pin (due to different pin diameters), which increased the possibility of worm holes forming there (-need more similar cases). When a setup of 1 °tilt, a T+3CT pin, a rotation rate of 160 rpm and a welding speed of 51 mm/min were applied, under the same forge force (69 KN), 0.9 mm deep counter-flow flute produced defect free joint, while 1.65 mm deep counter-flow (CT) flute still caused wormhole defects inside nugget. It indicates that, 1.65 mm CT flute was too deep to produce defect free welds. Based on current results, T+3CT with a flute depth of 0.9 mm is the best pin design for SSSP FSW.

In SSSP of AA7099, when a setup of 0 ° tilt and a welding speed of 51 mm/min are applied, tools with T+3F pin are more easily to cause surface defects, while tools with T+3CT pin are more likely to cause defects in the nugget, especially at AS near root. When a setup of 0 ° tilt, a welding speed of 51 mm/min, and a T+3F pin are applied, it should be focused on how to eliminate surface defects. When a setup of 0 ° tilt, a welding speed of 51 mm/min, and a T+3CT pin are applied, it should be focused on how to eliminate defects inside nuggets. Larger rotating speed leads to worse surface defects; counter-flow flutes with appropriate depth (0.9 mm) can reduce/eliminate surface defects and produce joints without volumetric defects inside the nugget. It indicates that, to get FSW welds with good welding quality, low tool rotation rate, T+3CT pin with a flute depth of 0.9 mm are recommended.

In SSSP of AA7050, when a setup of 0 ° tilt, the T+3F tool with a flat depth of 1.7 mm, a welding speed of 51 mm/min and a forge force of 66.7 KN are applied, both 200 RPM and 160 RPM caused bad surface defects, which might due to the setup of 0 ° tilt and the T+3F tool, which are not effective to eliminate surface defects in SSSP.

In SSSP of AA6061, when a setup of 1 °tilt, the T+3CT tool with a flute depth of 0.9 mm, a welding speed of 203 mm/min are applied, under the same forge force (66.7 KN), all the rotation rates of 480 RPM, 400 RPM and 320 RPM can produce defect free SSSP joints; with the same rotation rate of 320 RPM, appropriate forge forces (66.7 KN, 62.3 KN and 53.4 KN)can produce defect free joints, while too low forge forces (44.5 KN and 35.6 KN) cause volumetric defects (holes at bottom AS) inside the nuggets.

Defect investigation results indicate that, pin features and base metals have different effects on material flow in SSSP. When a setup of 1 °tilt, a flat/flute depth of 0.9 mm, a rotating rate of 160 rpm and a welding speed of 51 mm/min were applied, T+3CT is recommended for SSSP to enhance material vertical movements, improve weldability and produce defect free joints. Keep other parameters the same, SSSP in AA7099 and AA7050 share the similar defects in defective extent and locations, which might due to similar strength of the parent metals. Relative to AA7099 and AA7050, SSSP in AA6061 allows much larger FSW speeds and has a much better weldability to produce defect free joints with good surface finish, which might because that AA6061 base metal is much softer relative to the other two 7XXX alloys.

4.4.1.3 Nugget

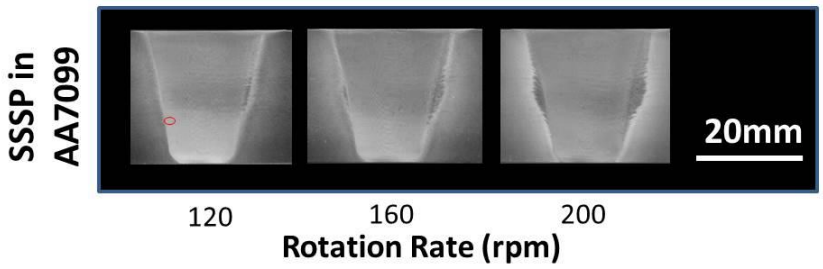

Figure 4.105 Macro Transverse Cross Sections of SSSP in AA7099: 1 °tilt, T+3CT, 0.9 mm deep flutes, 51 mm/min, 69 KN, different rotation rates

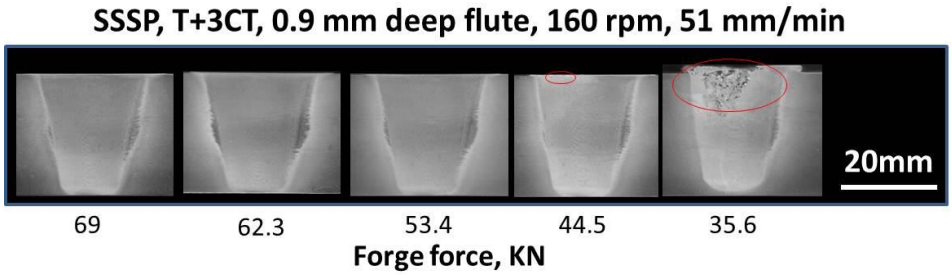

Figure 4.16 Macro Transverse Cross Sections of SSSP in AA7099: 1° tilt, T+3CT, 0.9 mm deep flute, 160 RPM, 51 mm/min, different forge forces (first appears in section 4.2)

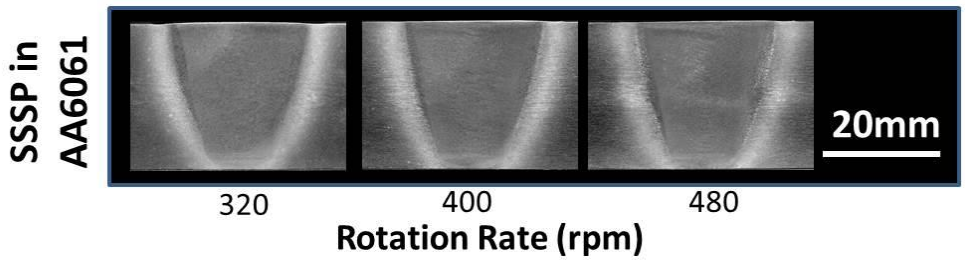

Figure 4.106 Macro Transverse Cross Sections of SSSP in AA6061: 1° tilt, T+3CT, 0.9 mm deep flats, 203 mm/min, 66.7 KN, different rotation rates

Figure 4.105 shows macro transverse cross sections of SSSP in AA7099 produced with different rotation rates. Higher rotation rates caused larger TMAZ area. Figure 4.16 (which has appeared in section 4.2) shows macro transverse cross sections of SSSP in AA7099 produced with different forge forces. Higher forge force caused a little larger TMAZ area, especially at mid-plane RS. Figure 4.106 shows macro transverse cross sections of SSSP in AA6061 produced with different rotation rates. Higher rotation rates caused larger TMAZ area.

Figure 4.107 shows macro transverse cross sections of SSSP in AA6061 produced with different forge forces. Higher forge force caused a little larger TMAZ area, especially at mid-plane RS, and a less tapered nugget. Figure 4.108 shows macro transverse cross sections of SSSP in different alloys. It indicates that, in SSSP of AA7099,

AA7050 and AA6061, higher rotating speed caused larger TMAZ area. The four SSSP in AA7099 and AA7050 were produced by the T+3F pin, while the two SSSP in AA6061 were produced by a T+3CT pin, therefore the two SSSP joints in AA6061 had more tapered nuggets. Under the same speeds, relative to SSSP in AA7050, SSSP in AA7099 had a little larger TMAZ area, especially at mid-plane, which might due to different properties of the parent metals.

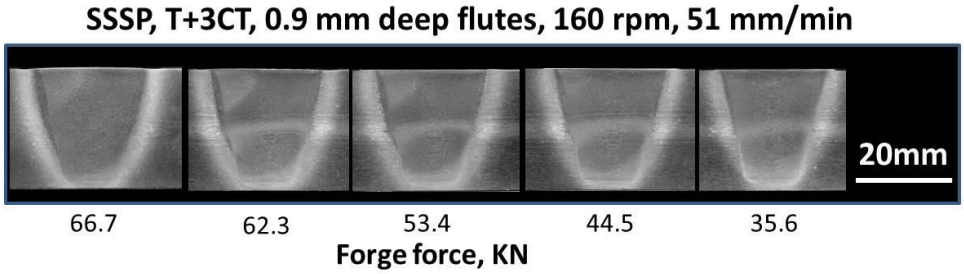

Figure 4.107 Macro Transverse Cross Sections of SSSP in AA6061: 1° tilt, T+3CT, 0.9 mm deep flats, 320 RPM, 203 mm/min, different forge forces

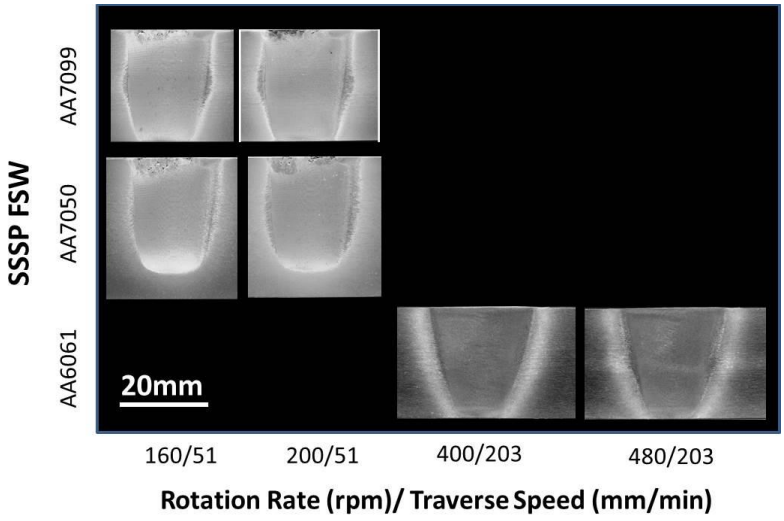

Figure 4.108 Macro Transverse Cross Sections of SSSP in different alloys

4.4.2 Process Responses

Process response parameters include in plane reaction forces (F_x, F_y and the resultant force F_{xy}), torque, power, peak temperature measured at pin center (which was

also considered as the peak temperature measured at center NG due to the pretty close positions) and grain size (GS) measured at center NG. Process response parameters were collected and calculated. Process response parameters as a function of tool rotation rate are summarized and shown in Figure 4.109for comparable SSSP joints in AA7099 and AA7050 produced with the same welding speed of 51 mm/min. Process response parameters as a function of applied forge force are summarized and shown in Figure 4.110 for comparable SSSP joints in AA7099 and AA6061 produced by a T+3CT tool with a setup of 1° tilt, a flute depth of 0.9 mm deep flute, a welding speed of 51 mm/min for AA7099 and a welding speed of 203 mm/min for AA6061. Figure 4.111 show temperatures at center pin as a function of power input for comparable SSSP joints in AA7099 and AA6061 produced by a T+3CT tool with a setup of 1° tilt, a flute depth of 0.9 mm deep flute, a welding speed of 51 mm/min for AA7099 and a welding speed of 203 mm/min for AA6061. Various symbols represent for different FSW conditions including pin types, tilt angle, and rotation rates. Here all welds were produced with normal TBCs, which are in air environment nearby the work piece surface and the steel backing plate applying underneath the work piece bottom. All SSSP joints of AA7099 and AA6061 were performed on 25.4 mm thick parent plates, while SSSP joints of AA7050 were performed on 30 mm thick parent plates. All pins were 24.9 mm long.

Figure 4.109 shows that:

(1) In SSSP of AA7099 produced by the T+3F tool with a setup of 0° and a flat depth of 1.7 mm, under the same forge force, when the rotation rate increased from 160 rpm to 200 rpm, in-plane forces were affected little, torque decreased a little (-12%), power increased a little (9%), and GS at center nugget increased (52%).

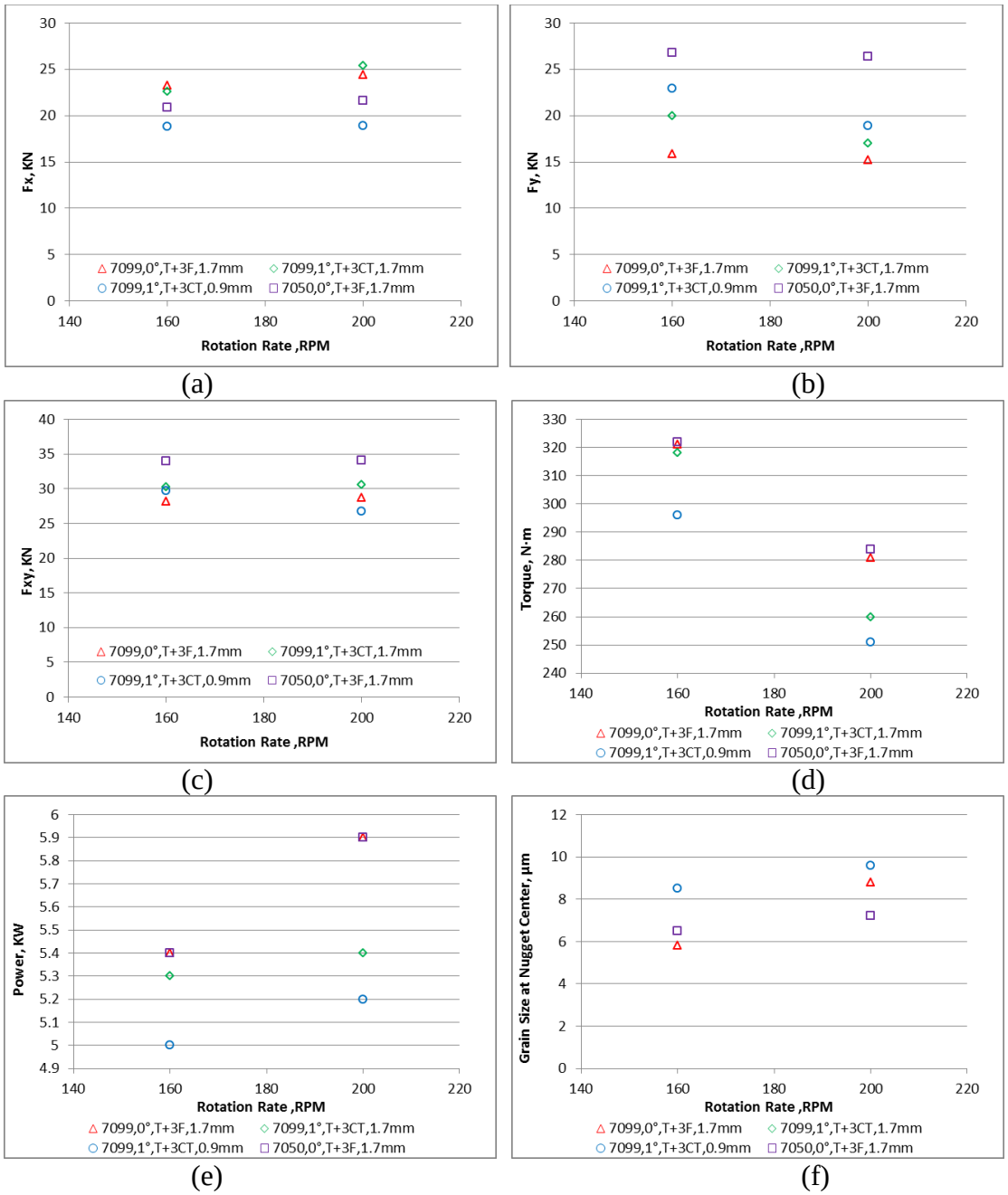

Figure 4.109 Reaction forces, torque, power and GS as functions of tool rotation rate for comparable SSSP joints in AA7099 and AA7050: the same welding speed of 51 mm/min

(2) In SSSP of AA7099 produced by the T+3CT tool with a setup of 1° and a flute depth of 1.7 mm, under the same forge force, when the rotation rate increased from 160 rpm to 200 rpm, F_x increased a little (12%), F_y decreased a little (-15%), F_{xy} was affected little, torque decreased a little (-18%), and power was affected little.

(3) In SSSP of AA7099 produced by the T+3CT tool with a setup of 1° and a flute depth of 0.9 mm, under the same forge force, when the rotation rate increased from 160 rpm to 200 rpm, F_x was affected little, F_y and F_{xy} decreased a little (-10~17%), torque decreased a little (-15%), power and temperature at pin center were affected little, and GS at center nugget increased a little (13%).

(4) In SSSP of AA7050 produced by the T+3F tool with a setup of 0° and a flat depth of 0.9 mm, under the same forge force, when the rotation rate increased from 160 rpm to 200 rpm, in-plane forces were affected little, torque decreased a little (-12%), power increased (9%) and GS at center nugget increased a little (11%).

(5) In SSSP of AA7099 produced by the T+3CT tool with a flute depth of 1.7 mm and a rotation rate of 160 rpm, relative to the setup of 0° , when the setup of 1° was applied, F_x was affected little, F_y increased (26%), F_{xy} increased slightly (7%), torque and power were affected little.

(6) In SSSP of AA7099 produced by the T+3CT tool with a flute depth of 1.7 mm and a rotation rate of 200 rpm, relative to the setup of 0° , when the setup of 1° was applied, F_x decreased slightly (-7%), F_y increased (32%), F_{xy} increased slightly (5%), torque increased a little (13%), and power decreased a little (-10%).

(7) In SSSP of AA7099 produced by the T+3CT tool with setup of 1° and a rotation rate of 160 rpm, relative to the flute depth of 1.7 mm, when the flute depth of 0.9 mm was applied, F_x decreased a little (-17%), F_y increased a little (15%), F_{xy} was affected little, torque (-7%) and power (-6%) decreased slightly.

(8) In SSSP of AA7099 produced by the T+3CT tool with setup of 1° and a rotation rate of 200 rpm, relative to the flute depth of 1.7 mm, when the flute depth of 0.9

mm was applied, F_x decreased (-26%), F_y increased a little (11%), F_{xy} decreased a little (-13%), torque and power were affected little.

(9) In SSSP joints produced by the T+3F tool with setup of 0° , a flat depth of 1.7 mm and a rotation rate of 160 or 200 rpm, relative to AA7050, in AA7099, F_x increased a little (11~13%), F_y decreased (-41~42%), F_{xy} decreased a little (-16~17%), and torque and power were affected little.

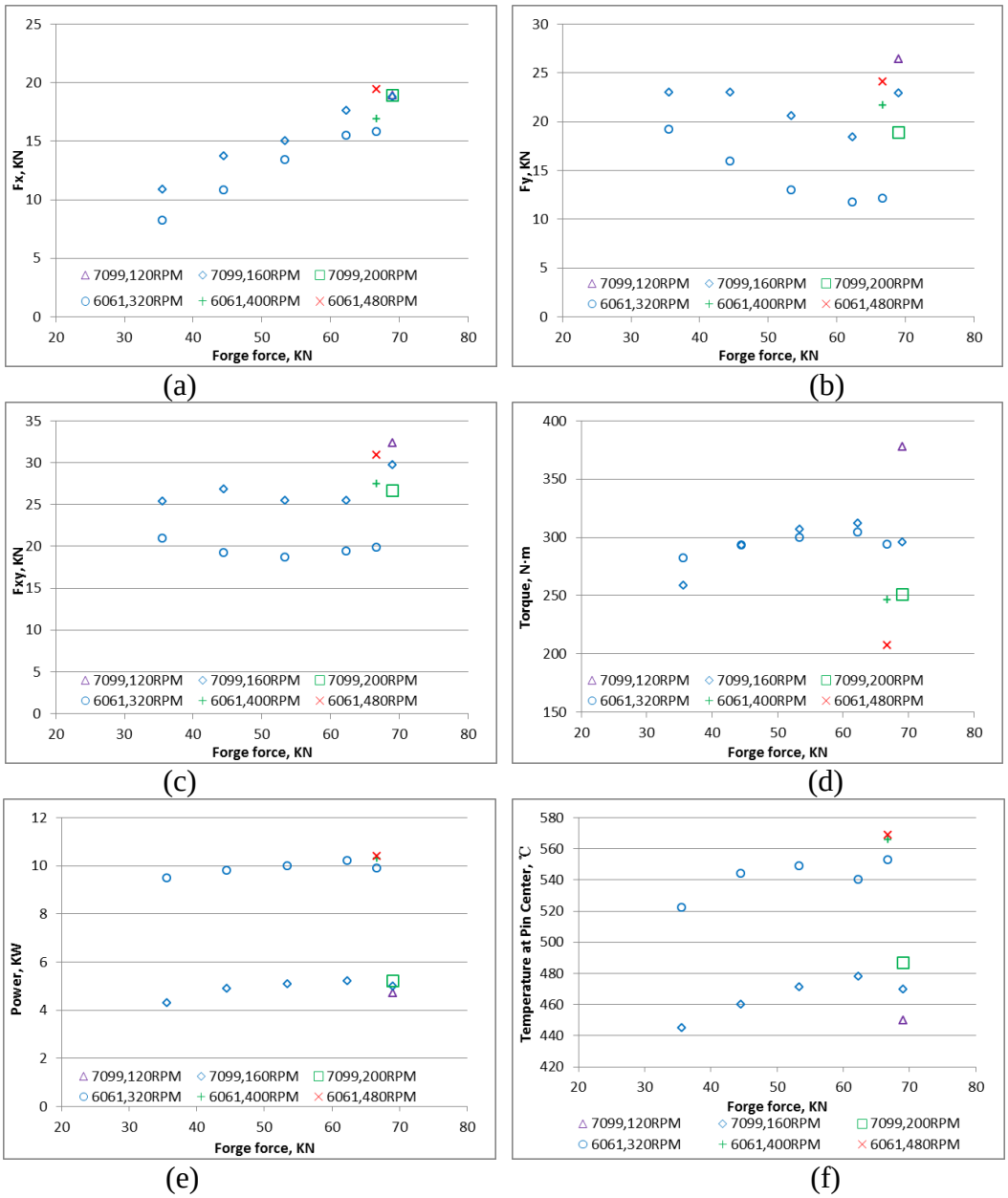

(a) (b) (c) (d) (e) (f)

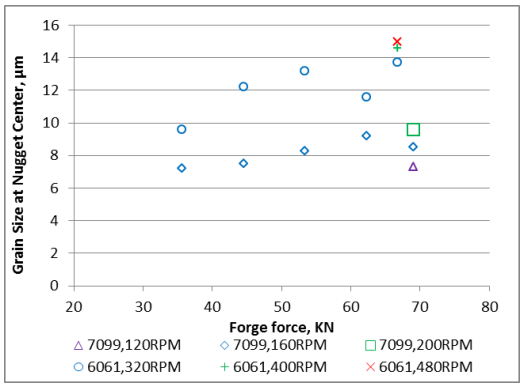

(g)

Figure 4.110 Reaction forces, torque, power, peak T and GS as functions of tool rotation rate for comparable SSSP joints in AA7099 and AA6061: 1° tilt, T+3CT, 0.9 mm deep flute, the welding speed of 51 mm/min for AA7099 and 203 mm/min for AA6061

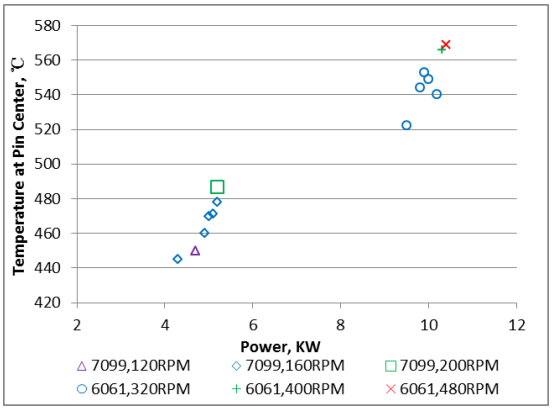

Figure 4.111 T at center pin as a function of power input for comparable SSSP joints in AA7099 and AA6061: 1° tilt, T+3CT, 0.9 mm deep flute, the welding speed of 51 mm/min for AA7099 and 203 mm/min for AA6061

Figure 4.110 and Figure 4.111 show that:

(1) In SSSP of AA7099 produced by the T+3CT tool with a setup of 1° , a flute depth of 0.9 mm and a welding speed of 51 mm/min, under the same forge force of 69 KN, when the rotation rate increased, Fx were similar, Fy decreased a little, Fxy decreased slightly, torque decreased with a decreasing slope, power increased slightly with a decreasing slope, temperature at pin center increased slightly with a decreasing

slope, and grain size at center nugget increased a little with a decreasing slope. When the power increased, temperature at pin center increased.

(2) In SSSP of AA7099 produced by the T+3CT tool with a setup of 1° , a flute depth of 0.9 mm and a welding speed of 51 mm/min, under the same rotation rate of 160 rpm, when the forge force increased, F_x increased, F_y decreased then increased after arriving the minimum at the medium forge force; F_{xy} were similar when the forge force was within the medium forge force and increased when the forge force was beyond the medium forge force; torque increased with a decreasing slope then decreased after arriving the maximum at the medium forge force; power slightly increased with a decreasing slope then slightly decreased after arriving the maximum at the medium forge force; temperature at center pin and grain size at center nugget increased with a decreasing slope then decreased after arriving the maximum at the medium forge force. When the power increased, temperature at pin center increased.

(3) In SSSP of AA6061 produced by the T+3CT tool with a setup of 1° , a flute depth of 0.9 mm and a welding speed of 203 mm/min, under the same forge force of 66.7 KN, when the rotation rate increased, F_x increased with an increasing slope, F_y and then F_{xy} increased with a decreasing slope, torque decreased a little, power increased slightly with a decreasing slope, temperature at pin center increased slightly with a decreasing slope, and grain size at center nugget increased a little with a decreasing slope. When the power increased, temperature at pin center increased with a smaller slope than that of SSSP in AA7099.

(4) In SSSP of AA6061 produced by the T+3CT tool with a setup of 1° , a flute depth of 0.9 mm and a welding speed of 203 mm/min, under the same rotation rate of 320

rpm, when the forge force increased, F_x increased, F_y decreased then increased after arriving the minimum at the medium forge force; F_{xy} decreased slightly when the forge force was within the medium forge force and increased slightly when the forge force was beyond the medium forge force; torque increased with a decreasing slope then decreased after arriving the maximum at the medium forge force; relative to AA7099, torque of SSSP in AA6061 increased a little slower and decreased a little faster; power slightly increased then slightly decreased after arriving the maximum at the medium forge force; temperature at center pin and grain size at center nugget increased with a decreasing slope then decreased at the medium forge force and increased again, arriving the maximum at the largest forge force. When the power increased, temperature at pin center increased then decreased after arriving at the maximum.

4.5 Simulation Work

4.5.1 Explanation of Schmidt model

In this research, the Thermal Pseudo-Mechanical model (TPM model, proposed by Schmidt et al. [103],[91]) implemented in COMSOL MULTIPHYSICS 4.0/4.4 has been adopted to investigate the thermal distribution in the FSW joints produced with different process variants: CSSP, SSSP, CSDP, and SSDP.

In FSW process, heat is generated by the plastic deformation of material caused by the tool shoulder and tool pin.

$$q = \alpha\omega\gamma\tau(T) \qquad \text{Eq (4.1)}$$

Heat generated during FSW process is mostly transferred by heat conduction (from tool to workpiece and from workpiece to the backing plate) and dissipated by heat convection (from domains to the ambient). The heat conduction between the workpiece

and the backing plate is expressed in the form of heat convection. Heat transfer from one domain to another is simulated by the implicit heat transfer equation 4.2.

$$k\left(\frac{\partial T}{\partial x}+\frac{\partial T}{\partial y}+\frac{\partial T}{\partial z}\right)=h(T_1-T_2) \qquad \text{Eq (4.2)}$$

Equation 4.1 is the equation of local heat generation strength in FSW process, which has been discussed previously. Equation 4.2 is the implicit heat transfer to simulate heat transfer from one domain to another.

Here, q is the local strength of heat source (J) generated on the tool surface. ω is the tool angular velocity (rad/s). "*r"* is the radial distance (m) from the simulated location to tool rotation axis. T is the temperature (K). $\tau(T)$ is the temperature dependent flow stress (MPa) of the involved workpiece material. *"k" is the* thermal conductivity (W/(m K)). T_1 is the temperature of the domain from where heat transfers to another domain with the temperature of T_2. "h" is the heat transfer coefficient (W/(m^2 K)) depending on the thermal properties and other conditions of respective domains. α is the contact condition between the workpiece and the tool, ranging from 0 to 1. Schmidt [91] adopted the contact condition α (ranging from 0 to 1) between the work piece and the tool to describe the heat generation. If it's in the fully sticking condition, α equals to 1; while if it's in the fully sliding condition, α equals to 0.

4.5.2 Motivation and Goals

During FSW, the weld joint material undergoes intense thermo-mechanical deformation and temperature cycle. In precipitation hardened aluminum alloys, thermal history in the joint cross section significantly affects the microstructural distribution, which affects the relevant joint properties. Thermal history a joint goes through is the most effective key to understand effects of weld parameters on joint properties. Therefore,

temperature history especially at weld nugget and heat affected zone, which is determined by primary control parameters like weld speeds and forge force, are of utmost significance in study of FSW joint properties. Understanding and finally establishing the relationship between control parameters and temperature history probably realize the tailoring of desired specific properties in FSW joints. Temperature history can be experimentally measured by imbedding TCs inside the tool and/or theoretically simulated by software. Unfortunately, it is hardly possible to measure actual transient temperatures in the deformation zone. Therefore thermal history of FSW with different process variants will be theoretically simulated based on reliable simulation model to investigate the effect of process variants, material properties such as flow stress, thermal conductivity, heat capacity, TBCs, variations in control parameters like rotation rate and welding speed on thermal distribution and power generation.

4.5.3 Details of Simulation

4.5.3.1 Details of Simulated Joints

Table 4.1 Summary of Experimental Control and Response Parameters

FSW Type	Rotation Speed, RPM	Welding Speed, mm/s	F_z, KN	Power, KW	Temperature, ℃
CSSP	160	0.85	46.7	5.3	484
SSSP	160	0.85	62.3	5.2	477
CSDP-1	160	1.7	42.3	4.2	433
CSDP-2	160	1.7	40	4.2	444
SSDP-1	160	1.7	35.8	4.3	424
SSDP-2	160	1.7	35.8	4.1	430

Among the welds studied in this dissertation, simulation work has been performed on selected comparable joints listed in Table 4.1. Those bead-on-plate welds were performed on AA7099-T7651 plates. Experimental process control and response

parameters are listed in Table 4.1. DP-1 means the 1_{st} pass of the dual pass weld, and DP-2 means the 2_{nd} pass of the weld.

Table 4.2 Summary of Tool Parameters

FSW Type	Taper Angle, °	Pin Material	Shoulder Diameter, mm	Pin Top Diameter, mm	Pin Length, mm
CSSP	9	MP159	35.6	19.1	25.0
SSSP	8	MP159	31.8	19.1	25.0
CSDP	8	H13 Steel	25.4	15.9	12.7
SSDP	8	MP159	31.8	15.9	12.7

Information of tools applied in FSW in this paper has been listed in Table 4.2. Single pass welds were performed by tool pins with a flat/flute depth of 0.89 mm, and a thread pitch of 1.75 mm/thread. Dual pass welds were performed by tool pins with a flat/flute depth of 1.35 mm, and a thread pitch of 2.12 mm/thread.

Single pass welds were performed on 25.4 mm thick plates while the dual pass welds were made on 24.9 mm thick plates machined from the 25.4 mm thick base metal. The thinner plates for dual pass welding were utilized to facilitate the use of a tool originally designed for welding 12.5 mm thick plate while producing some overlap between the first and second pass weld regions. In each case, final weldment dimensions were 203 mm wide by 610 mm long. A 914 mm x 152 mm x 8 mm backing plate (steel BP) made of O1 tool steel was used to make welds in the lab air.

4.5.3.2 Simulation of FSW speeds

During simulation, the tool shoulder is ascribed a velocity field equivalent to the tool rotation rate in CSFSW while equal to zero in SSFSW. The tool pin is ascribed a velocity field equivalent to the tool rotation rate, and the plate is ascribed a linear velocity equal to the welding speed. In the simulation, pin rotates CCT, and workpiece moves in

positive X direction. Therefore according to the adopted coordinate system, when Y>0, it is the advancing side (AS); when Y<0, it is the retreating side (RS).

4.5.3.3 Evaluation and Calibration of TPM model

Experimental values and measured results of temperature and power will be used to evaluate the model reliability and calibrate the model. Then reliable thermal distribution results will be studied to investigate the relationship between process variants and temperature history.

4.5.4 Selection of material properties

4.5.4.1 Contact Condition α

The contact condition α is a function of the ratio of the uniform shoulder pressure σ_z to the local and temperature dependent yield stress, referring to that of AA7449 [112]. In this research, α_1 is the contact condition between the workpiece and the tool shoulder, while α_2 is the contact condition between the workpiece and the tool pin. In SSSP, α_1 is 0, while α_2 is 1. In CSSP, α_1 varies from 0 to 1, while α_2 is 1. In SSDP-1, α_1 is 0, while α_2 varies from 0 to 1. In SSDP-2, α_1 is 0, while α_2 adopts the optimized value based on simulation results of SSDP-1. In CSDP-1, α_1 varies from 0 to 1, and α_2 varies from 0 to 1. In CSDP-2, α_1 adopts the optimized value based on simulation results of CSDP-1, while α_2 varies from 0 to 1.

4.5.4.2 Thermal conductivity of workpiece in T7 and W conditions

In SPFSW, before the FSW process, the whole workpiece is the base metal in T7 condition with the thermal conductivity referring to AA7075 [68]. In DPFSW, before the FSW process of the 1st pass, the whole workpiece is also the base metal in T7 condition; after the FSW process of the 1st pass, material in the welded area of the workpiece has

experienced intense mechanical and thermal cycles, considered as in the W condition, resulting in different thermal conductivities from the material in T7 condition under the same temperature. To simulate this change, the rectangular area (with the same area of the pin's cross section, the red area as shown in Figure 4.114c) underneath the pin is considered as in the W condition with different thermal conductivity K_w which is needed to be determined, while other area in the workpiece is considered as still in T7 condition. In this research, $K_w(T)$ (thermal conductivity in W condition) is assumed to be some certain value (ΔK) substracted from the $K(T)$ (thermal conductivity in T7 condition), which means $K_w=K-\Delta K$.

Table 4.3 Thermal conductivity, heat capacity and density of materials adopted in the Simulation [68],[123]

Property	Workpiece	Tool shoulder (H13 Steel)	Tool Probe (MP159)	Backing Plate (O1 tool steel)
Thermal Conductivity, W/(m·℃)	(0.1265T+153.4) a_3	28	14.7	28
Heat Capacity, J/(Kg·℃)	0.8509T+825.7	490	421	490
Density, Kg/m^3	2850	7750	8330	7750

The function of $K(T)$ has been listed in Table 4.3, along with heat capacity and density of materials adopted in the simulation [68],[123]. a_3 ranging from 0.7~1 is the coefficient multiplying with $K(T)$ to adjust the thermal conductivity of workpiece in T7 condition. ΔK varies from 0 to 100 W/(m·K). For example, when ΔK equals to 20 W/(m·K), then K_w is assumed to be 20 W/(m·K) less than the K, which means $K_w=K-20=0.1265T+133.4$. In this research, in SSSP, CSSP, SSDP-1 and CSDP-1, material in the whole workpiece is AA7099 in T7 condition with the thermal conductivity

of *K*. In SSDP-2 and CSDP-2, the rectangular area (red area as shown in Figure 4.114c) underneath the pin is considered as in the W condition with different thermal conductivity K_w (ΔK varies from 0 to 100 W/(m K)), while other area in the workpiece is considered as still in T7 condition with the thermal conductivity of *K*.

4.5.4.3 Temperature dependent flow stress of workpiece: $a_4 \cdot \tau(T)$

Temperature dependent flow stress of workpiece $\tau(T)$ is listed in Table 4.4 [68]. a_4 ranging from 0.7~1 is the coefficient multiplying with $\tau(T)$ to adjust the flow stress of workpiece in simulation. Boundary convection coefficients of interfaces adopted in the simulation are listed in Table 4.5. The different heat transfer coefficients have been applied to the entire top surface of the simulated workpiece.

Table 4.4 Temperature dependent flow stress of workpiece adopted in Simulation [68]

Temperature, °C	Standard Flow Stress, MPa	Adjusted Flow Stress, MPa
25	450	450
400	120	$120(1-a_4)$
425	100	$100(1-a_4)$
450	80	$80(1-a_4)$
475	60	$60(1-a_4)$
500	30	$30(1-a_4)$
532	0	0

Table 4.5 Boundary convection coefficients of interfaces adopted in the Simulation. Convection coefficients between boundaries and air refer to Maxx's report [112].

Interfaces	Boundary convection coefficients: $W/(m^2 K)$
Backing plate & underneath FSW table	700
Backing plate & air	10
Workpiece & air	10
Lower shoulder & air	100
Upper shoulder & air	700
Top of upper shoulder & other adjacent parts	900
Thermal management on workpiece surface	h=10, 200 or 5000

4.5.4.4 Simulation Approaches

The following parameters will be adjusted while keeping other factors the same to investigate effects of variables on thermal distribution and power:

(1) Contact condition on shoulder α_1, ranging from 0 to 1.

(2) Contact condition on pin α_2, ranging from 0 to 1.

(3) Temperature dependent thermal conductivity of workpiece in T7 condition: a_3 $k(T)$, here a_3=0.7, 0.8, 0.9, 1.

(4) Temperature dependent thermal conductivity of workpiece in W condition: $k(T)$- ΔK, here ΔK varies from 0 to 100 W/(m K).

(5) T dependent flow stress of workpiece: $a_4 \cdot \tau(T)$, here a_4=0.7, 0.8, 0.9, 1.

(6) Rotation rate at constant welding speed: 5~30.2 rad/s.

(7) Welding speed at constant rotation rate for SP: 0.85, 1.275, 1.7, 2.125 mm/s.

(8) Welding speed at constant rotation rate for DP: 1.7, 2.125, 2.55, 2.975, 3.4, 3.825, 4.25 mm/s.

(9) Different speeds with the same APR (rotating rate/welding speed) for SP:

①16.76 rad/s & 0.85 mm/s; ②25.14 rad/s & 1.275 mm/s;

③33.52 rad/s & 1.7mm/s; ④41.9 rad/s &2.125 mm/s

(10) Different sets of speeds with the same APR for DP-1:

①16.76 rad/s & 1.7 mm/s; ②20.95 rad/s & 2.125 mm/s;

③25.14 rad/s & 2.55 mm/s; ④29.33 rad/s &2.975 mm/s;

⑤33.52 rad/s & 3.4 mm/s; ⑥37.71 rad/s &3.825 mm/s;

⑦41.9 rad/s & 4.25 mm/s.

(11) Different heat transfer coefficients at workpiece surface, W/(m^2 K):

① h=10 corresponds approximately to convection to still air;

② h=200 corresponds approximately to convection to forced air;

③ h=5000 corresponds approximately to convection associated with vigorous water spray.

4.5.5 Simulation Procedures

4.5.5.1 Data Collecting

Data like process control parameters of FSW like rotation rate, welding speed and forge force, geometries, properties like density, heat capacity and thermal conductivity of all domains, temperature dependent flow stress, temperature dependent thermal conductivity of workpiece has been collected to build the TPM model. Contact conditions between workpiece and shoulder/pin haven been determined during simulation. Experimental values of response variables like temperature and power have also been collected to evaluate the model reliability and calibrate the model.

4.5.5.2 TPM model building

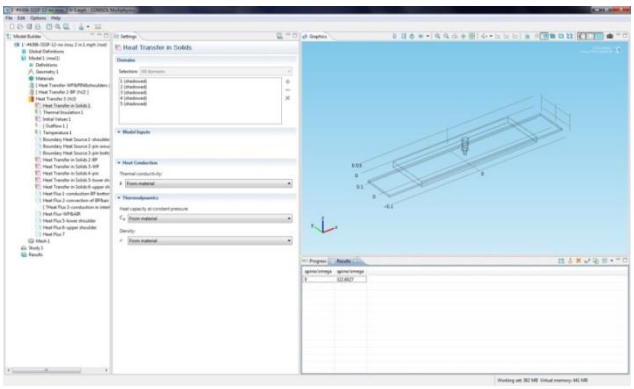

Figure 4.112 A snapshot of COMSOL Graphical User Interface

COMSOL graphical user interface with typical geometries in different domains is shown in Figure 4.112. In this simulation, different domains to be built include the upper

shoulder (US), the lower shoulder (LS), the pin, the workpiece (WP), and the backing plate (BP), as shown in Figure 4.113.Terms of area heat generation are applied over the interface between the workpiece material and the tool shoulder ($q_{shoulder}$), and the interfaces between the workpiece material and the tool probe (q_{pina} around pin and q_{pinb} at pin bottom), as shown in Figure 4.113. Typical cross sections in y-z plane of TPM model of (a) SP, (b) DP-1 and (c) DP-2 are shown in Figure 4.114. In CSFSW, both the rotating shoulder and the probe are assigned a velocity field equal to the tool rotation rate. In SSFSW, the stationary shoulder has a velocity of zero, while the rotating probe is assigned a velocity field equivalent to the tool rotation rate. In both CSFSW and SSFSW, the workpiece is assigned a linear velocity equal to the tool travelling speed.

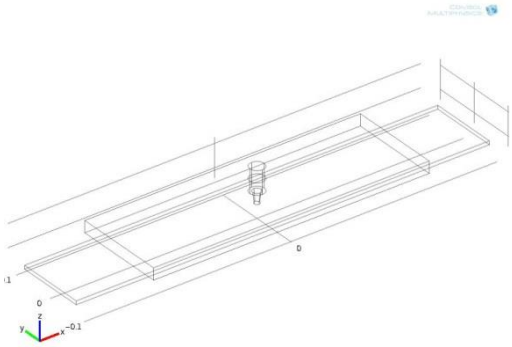

(a) Global TPM model of SPFSW

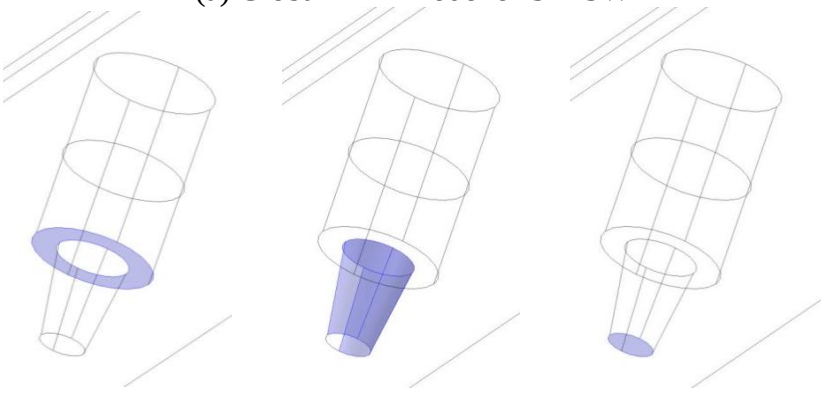

(b) Shoulder (c) Pin around (d) Pin bottom

Figure 4.113 Typical TPM model for SPFSW: (a) global TPM model, interface of (b) WP and tool shoulder, (c) WP and tool pin around, and (d) WP and tool pin bottom. Heat generation terms are applied in shoulder/WP and pin/WP interfaces (blue areas)

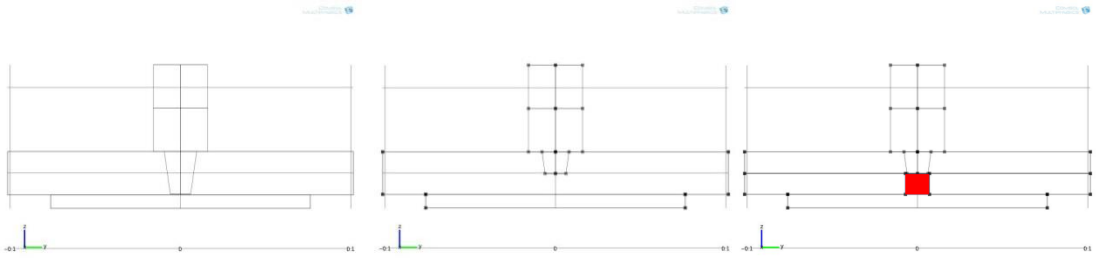

(a) SP (b) DP-1 (c) DP-2

Figure 4.114 Typical Cross Sections in y-z plane of TPM model: (a) SP, (b) DP-1 and (c) DP-2

4.5.5.3 Definition of Heat Generation

Terms of area heat generation are applied over the interface (blue areas as shown in Figure 4.112) between the workpiece material and the tool shoulder ($q_{shoulder}$), and the interfaces between the workpiece material and the tool probe around pin (q_{pina}) and at pin bottom (q_{pinb}). When contact conditions on shoulder and pin are constants, heat generated at different interfaces of tool and workpiece is stated as following:

Heat generated by shoulder $q_s=a_1\ \omega r\tau(T);$

Heat generated by pin around $q_{pina}=a_2\ \omega r\tau(T);$

Heat generated by pin bottom $q_{pinb}=a_2\ \omega r\tau(T)$.

Here a_1 is the contact condition between shoulder and workpiece, and a_2 is the average contact condition between pin and workpiece. Constant values between 0~1 can be assigned depending on specific conditions. Contact condition of shoulder and workpiece a_1 in SS is 0 (fully sliding).

4.5.5.4 Mesh

Free tetrahedral element is applied to mesh the 3D model. Since the tool shoulder and pin have the similar scale of geometry, while the workpiece and backing plate have the similar scale of geometry, different free tetrahedral elements with normal densities

have been applied in tool shoulder and pin with an average mesh size of 54 mm, while in workpiece and backing plate with an average mesh size of 6 mm. Since that in area nearby the tool shoulder and pin the gradients of temperature and strain are known to be higher, finer mesh near the heat source while coarser mesh in the exterior are applied, as shown in Figure 4.115.

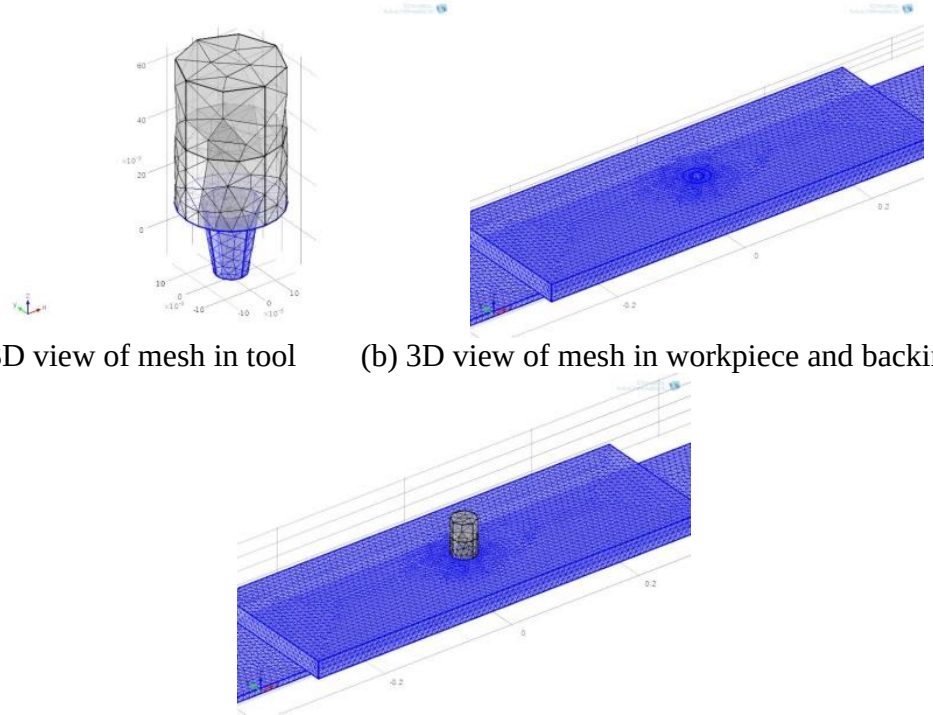

(a) 3D view of mesh in tool (b) 3D view of mesh in workpiece and backing plate

(c) 3D view of mesh in the global model

Figure 4.115 Snapshot of meshed geometry inside COMSOL

4.5.5.5 Run the Model

When the model is built, click the “calculate” button to run the simulation. COMSOL software keeps calculating the temperature distribution in steady state. After satisfactory convergence is reached, a thermal field is available in all domains of the model as shown in Figure 4.116. Then results of heat generation at different interfaces of tool and workpiece, temperature distribution and so on can be plotted and exported for further study.

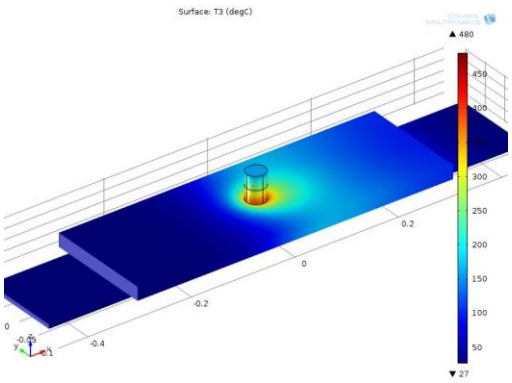

(a) 3D view of the thermal field

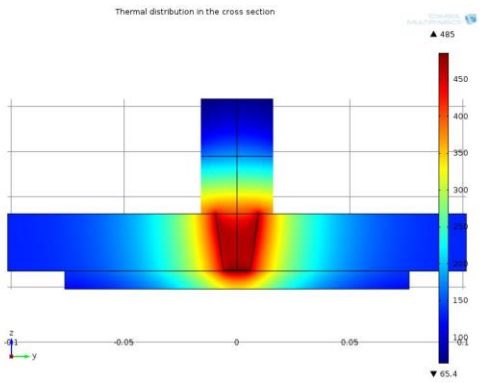

(b) 2D view of the thermal field in YZ plane

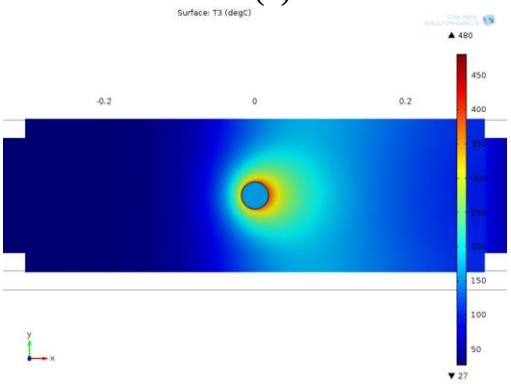

(c) 2D view of the thermal field in XY plane

Figure 4.116 Thermal field of the TPM model obtained through simulation

4.5.6 Simulation Results and Discussion

4.5.6.1 Study 1: Calibrate the TPM model

Goal of this study is to calibrate the model and determine properties and parameters adopted in the simulation to build a reliable model, yielding reasonable results. Results of simulated and experimental temperature and power have been plotted in Figure 4.117~Figure 4.120.

Figure 4.117 shows the measured and simulated temperature at pin center and power of the SSSP joint #4306, respectively. Here alpha on the shoulder α_1 equals to 0. It shows that, as for the SSSP joint #4306, when α_2 ranges from 0.3 to 0.5, the simulation yields reasonable and reliable simulated results with acceptable differences relative to experimental results. When α_2 equals to 0.4, relative to measured values, the simulation

yields currently the best results: simulated power is 6% larger, simulated temperature at pin center is 4% lower. It shows that the selection of material properties is reasonable, and the model for the SSSP joint is reliable. α_2 with a value of 0.4 will be adopted in the following simulation of CSSP joint #4299.

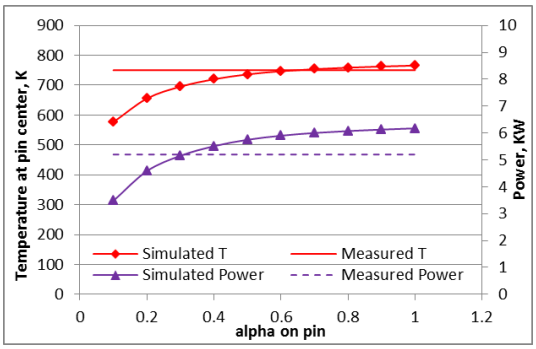

Figure 4.117 Simulated and measured temperature and power as a function of alpha on pin in SSSP: alpha on shoulder is 0

Figure 4.117 also shows that, in SSSP, with the increasing contact condition on pin (less slip), simulated power and then temperature at pin center increased with decreasing slopes. Under the same speeds, power enjoys the same trend with torque. Therefore with the increasing contact condition on pin, simulated torque increased with a decreasing slope, possibly due to that on one hand, more power is required to soften the workpiece material around pin while on the other hand, the softer material will yield lower flow stress, resulting in the torque and power increase with decreasing slopes.

Figure 4.118 shows the measured and simulated temperature at pin center and power of the CSSP joint #4299, respectively. Here alpha on the pin α_2 equals to 0.4. It shows that, as for the CSSP joint #4299, when α_1 ranges from 0 to 0.1, the simulation yields reasonable and reliable results with acceptable differences relative to experimental results. When α_1 equals to 0.07, relative to measured values, the simulation yields currently the best results: simulated power is 10% larger, simulated temperature at pin

center is 4% lower. It shows that the selection of material properties is reasonable, and the model for the CSSP joint is reliable.

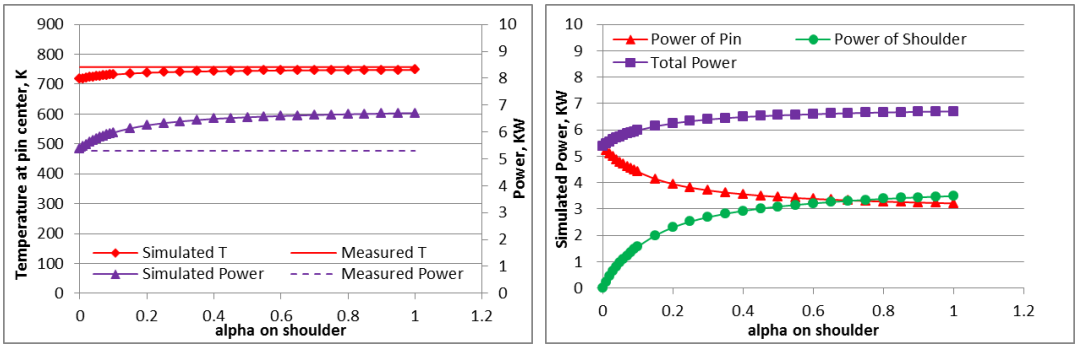

(a) (b)

Figure 4.118 (a) Simulated and measured temperature and power as a function of alpha on shoulder, and (b) simulated power generated by pin, shoulder, and total power in CSSP: alpha on pin is 0.4

Figure 4.118 also shows that, in CSSP, with the increasing contact condition on shoulder (less slip), simulated temperature at pin center increased slightly, simulated power of pin decreased with a decreasing slope, simulated power of shoulder increased with a decreasing slope, while total simulated power increased with a decreasing slope. For this gage, when alpha on shoulder is less than about 0.7, pin power is always larger than shoulder power and the difference decreases when alpha on shoulder increases; when alpha on shoulder is larger than about 0.7, shoulder power is slightly larger than pin power and the difference increases slightly when alpha on shoulder increases.

Figure 4.119 shows the measured and simulated temperature at pin center and power of the SSDP-1 joint #4309, respectively. Here alpha on the shoulder α_1 equals to 0. It shows that, as for the SSDP-1 joint #4309, when α_2 ranges from 0.4 to 0.7, the simulation yields reasonable and reliable simulated results with acceptable differences relative to experimental results. When α_2 equals to 0.5, relative to measured values, the simulation yields currently the best results: simulated power is 5% larger, simulated

temperature at pin center is 10% lower. It shows that the selection of material properties is reasonable, and the model for the SSDP-1 joint is reliable. α_2 with a value of 0.5 will be adopted in the following simulation of CSDP-1 joint #4302. Figure 4.119 also shows that, in SSDP-1, with the increasing contact condition on pin (less slip), simulated power and then temperature at pin center increased with decreasing slopes.

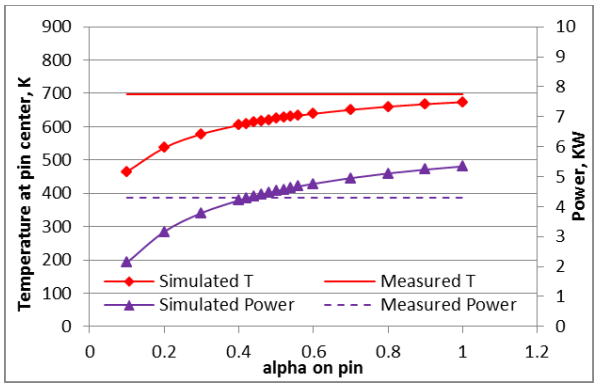

Figure 4.119 Simulated and measured temperature and power as a function of alpha on pin in SSDP-1: alpha on shoulder is 0

Figure 4.120 shows the measured and simulated temperature at pin center and power of the CSDP-1 joint #4302, respectively. Here alpha on the pin α_2 equals to 0.5. It shows that, as for the CSDP-1 joint #4302, when α_1 ranges from 0 to 0.1, the simulation yields reasonable and reliable results with acceptable differences relative to experimental results. It shows that the selection of material properties is reasonable, and the model for the CSDP-1 joint is reliable.

Figure 4.120 also shows that, in CSDP-1, with the increasing contact condition on shoulder (less slip), simulated temperature at pin center increased slightly, simulated power of pin decreased with a decreasing slope, simulated power of shoulder increased with a decreasing slope, while total simulated power increased with a decreasing slope.

For this gage, pin power is always larger than shoulder power and the difference decreases when alpha on shoulder increases.

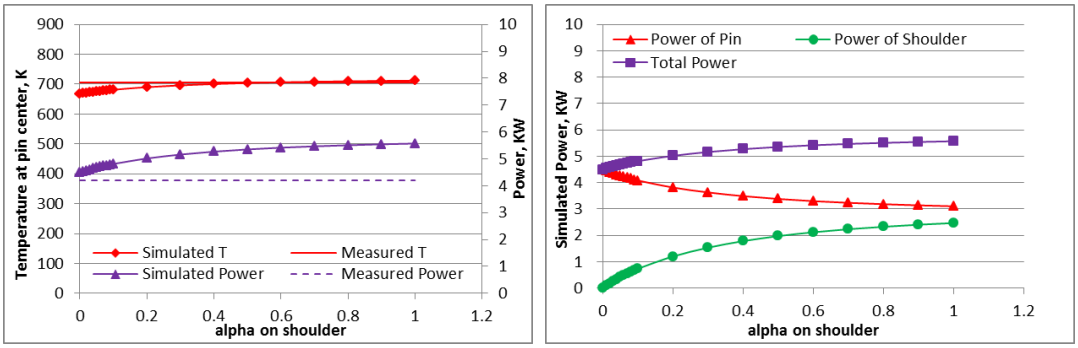

(a) (b)

Figure 4.120 (a) Simulated and measured temperature and power as a function of alpha on shoulder, and (b) simulated power generated by pin, shoulder, and total power in CSDP-1: alpha on pin is 0.5

Since that in DP-2 joints, workpiece underneath the tool has been changed from T7 condition to W condition due to the 1st pass weld, which results in uncertainties and changes of properties like temperature dependent flow stress and thermal conductivity, heat capacity and so on, simulation of DP-2 joints will not be considered and discussed here in study 1~3. Study 4 is to investigate the effect of changes in temperature dependent thermal conductivity of workpiece in W condition on simulated temperature and power. Based on the above study, it shows that the selection of material properties and coefficients is reasonable, and the built TPM model is reliable. In the following study, the model will be used to investigate effects and trends as discussed previously.

4.5.6.2 Study 2: Effects of adjusted Variables

Goal of this study is to investigate effects of temperature dependent thermal conductivity $k(T)$ and flow stress $\tau(T)$ of workpiece, rotation rate, welding speed, different sets of speeds with the same APR and different thermal managements applied on workpiece surface on simulated temperature and power. The same contact conditions

of shoulder and pin have been adopted when the same shoulder is applied. In SSSP and SSDP-1, α_1 equals to 0, and α_2 equals to 0.5. In CSSP and CSDP-1, α_1 equals to 0.1, and α_2 equals to 0.5. In SSSP, CSSP, SSDP-1 and CSDP-1, when standard values of variables like flow stress etc. are applied, differences of simulated temperature at pin center from measured results are -2% (2% smaller), -2%, -5% and -3%, respectively, while differences of simulated power from measured results are -11%, -16%, 5% and 15% (15% larger), respectively. Here negative value means the simulated result is lower, while positive value means the simulated result is larger, compared with measured results. Those simulated results especially the power results may be not very close to the experimental results. However, trends generated by those models are reliable and useful.

Figure 4.121(a~j) show the simulated temperature at pin center, simulated pin power, shoulder power and total simulated power as functions of separately adjusted variables in the simulation of SP joints.

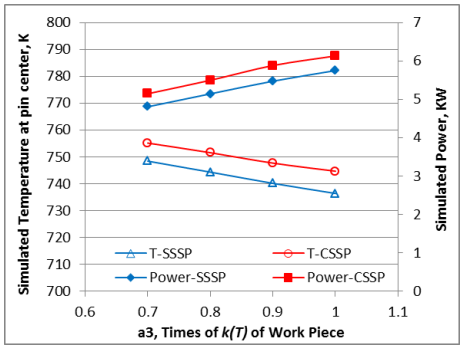

(a)

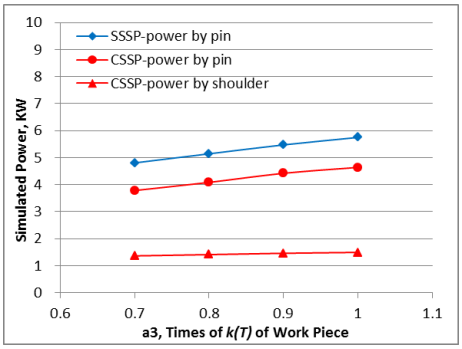

(b)

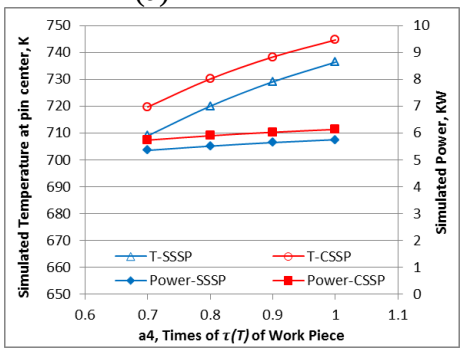

(c)

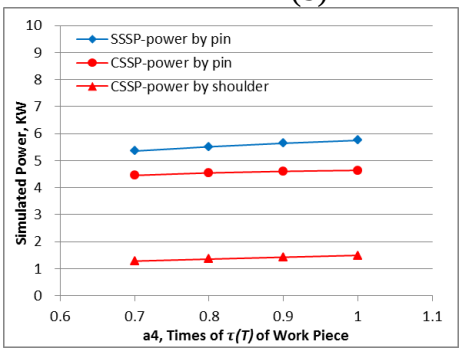

(d)

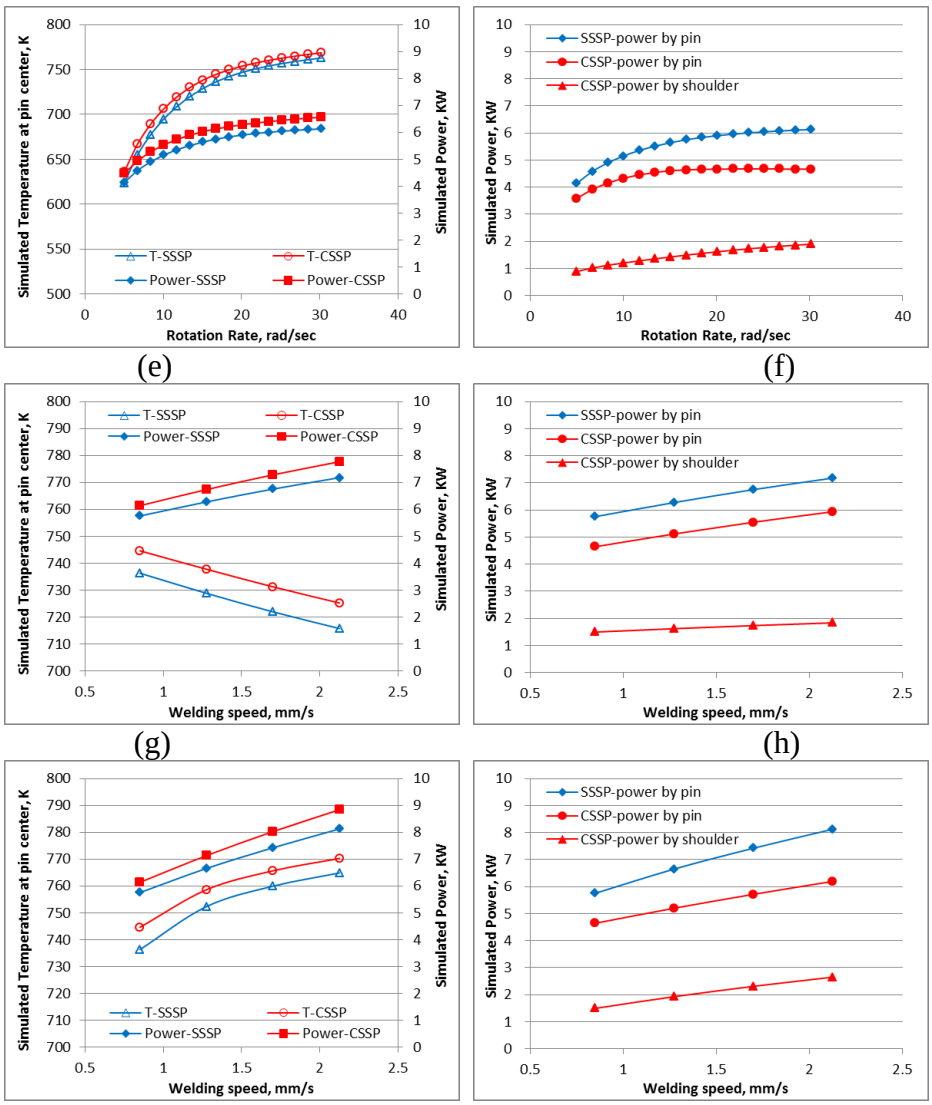

Figure 4.121 Simulated T at pin center and power as functions of adjusted variables in SP

Figure 4.121(a~b) shows that, in SP, with the increasing of thermal conductivity *k(T)* of workpiece, simulated temperature at pin center decreased slightly, while simulated total power increased. In CSSP, simulated pin power increased, while simulated shoulder power was similar. Under the same thermal conductivity, relative to SSSP, in CSSP, simulated temperature at pin center is about 10℃ higher, and simulated total power is about 7% larger. Under the same thermal conductivity, in CSSP, simulated pin power is much larger than simulated shoulder power.

Figure 4.121(c~d) shows that, in SP, with the increasing of flow stress *(T)* of workpiece, simulated temperature at pin center and power increased slightly. In CSSP, both simulated pin power and shoulder power increased slightly. Under the same flow stress, relative to SSSP, in CSSP, simulated temperature at pin center is about 10℃ higher, and simulated total power is about 7% larger. Under the same flow stress, in CSSP, simulated pin power is much larger than simulated shoulder power.

Figure 4.121e~f) shows that, in SP, keeping the welding speed constant, with the increasing of rotation rate, simulated temperature at pin center and power increased with a decreasing slope. Results conform to what is expected from actual welds showing a plateau in power and probe temperature at high rotation rate. In CSSP, simulated pin power increased with a decreasing slope, while simulated shoulder power increased. Under the same rotation rate, relative to SSSP, in CSSP, simulated temperature at pin center is 10℃ higher, and simulated total power is 7% larger. Under the same rotation rate, in CSSP, simulated pin power is much larger than simulated shoulder power.

Figure 4.121(g~h) shows that, in SP, keeping the rotation rate constant, with the increasing of welding speed, simulated temperature at pin center decreased slightly, and simulated total power increased. In CSSP, simulated pin power increased, while simulated shoulder power was similar. Under the same welding speed, relative to SSSP, in CSSP, simulated temperature at pin center is about 10℃ higher, and simulated total power is about 7% larger. Under the same welding speed, in CSSP, simulated pin power is much larger than simulated shoulder power.

Figure 4.121(i~j) shows that, in SP, keeping the APR (rotation rate/welding speed) constant, with the increasing of speeds, simulated temperature at pin center increased

slightly, and simulated total power increased. It's also consistent with experimental observation. In CSSP, both simulated pin power and shoulder power increased. Under the same speeds, relative to SSSP, in CSSP, simulated temperature at pin center is about 7℃ higher, and simulated total power is about 7% larger. Under the same welding speed, in CSSP, simulated pin power is much larger than simulated shoulder power.

Generally, Figure 4.121 shows that, in SP, the effect of increasing thermal conductivity of workpiece is to decrease temperature at pin center slightly and increase power; the effect of increasing flow stress of workpiece is to increase temperature at pin center and power slightly; the effect of increasing rotation rate while keeping welding speed constant is to increase temperature at pin center and power with decreasing slopes; the effect of increasing welding speed while keeping rotation rate constant is to decrease temperature at pin center slightly and increase power; the effect of increasing speeds while keeping the APR constant is to increase temperature at pin center slightly and increase power. It indicates that the above variables affect temperature at pin center slightly, while affect power at some extent, especially the rotation rate, welding speed, and then thermal conductivity of workpiece. Figure 4.121 also shows that, relative to SSSP, in CSSP, simulated temperature at pin center is about 7~10℃ higher, and simulated total power is about 7% larger; In CSSP, simulated pin power is much larger than simulated shoulder power which might due to the selected values of contact conditions on pin (0.5) and shoulder (0.1) in CSSP.

Figure 4.122(a~j) show the simulated temperature at pin center, simulated pin power, shoulder power and total simulated power as functions of separately adjusted variables in the simulation of DP-1 joints.

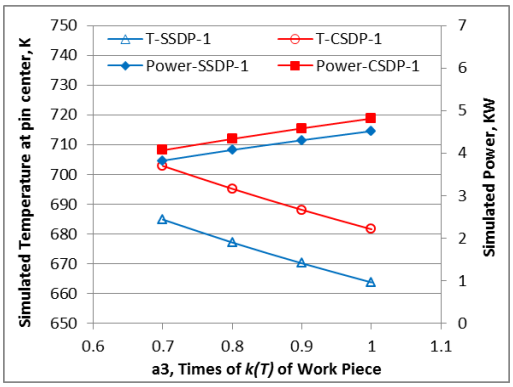

(a)

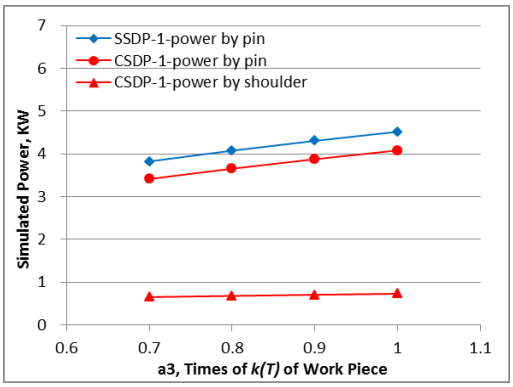

(b)

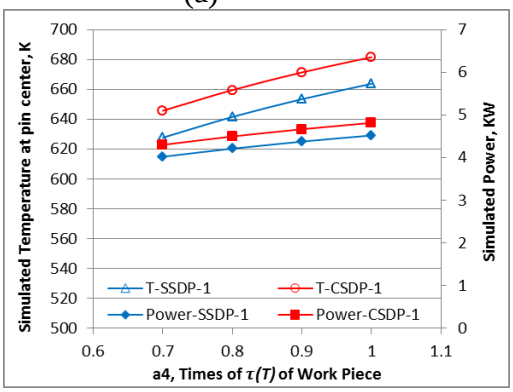

(c)

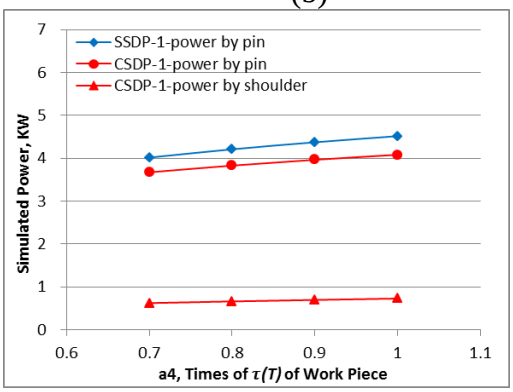

(d)

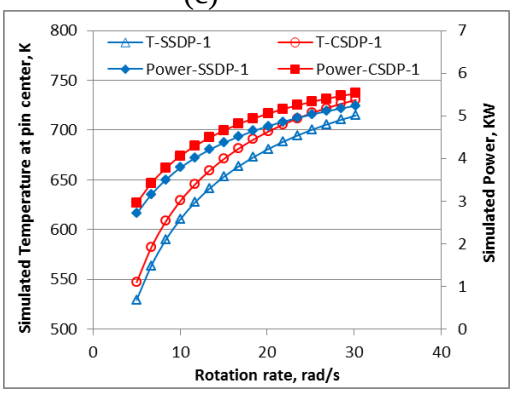

(e)

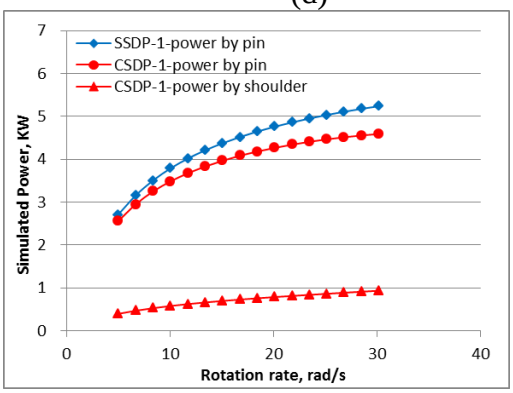

(f)

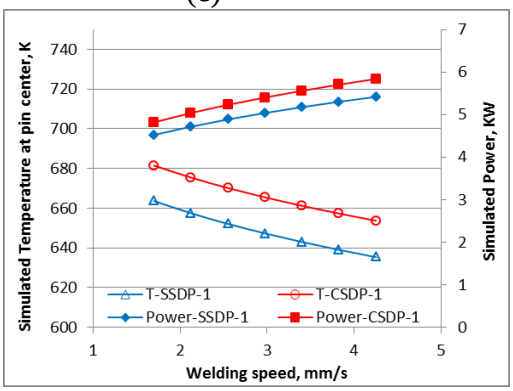

(g)

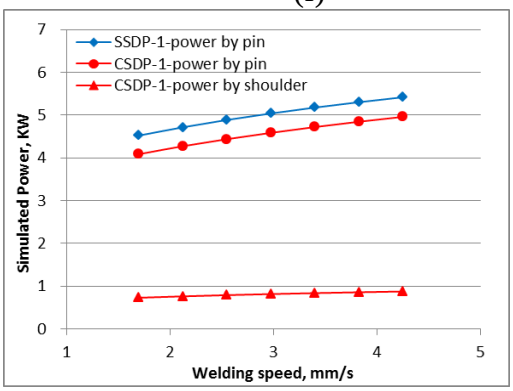

(h)

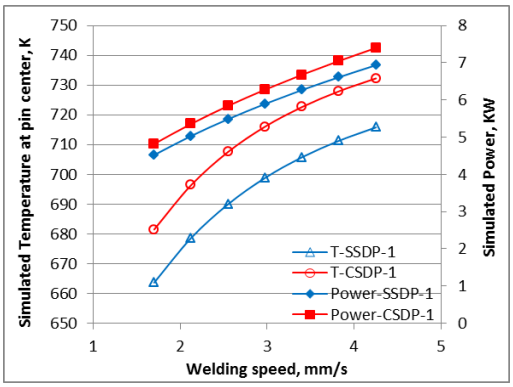

(i) The same APR

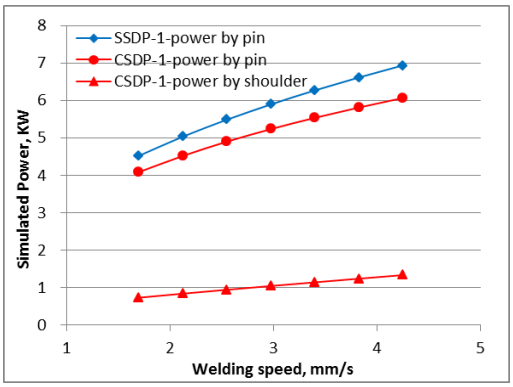

(j) The same APR

Figure 4.122 Simulated temperature at pin center and power as functions of adjusted variables in DP-1 joints

Figure 4.122(a~b) shows that, in DP-1, with the increasing of thermal conductivity *k(T)* of workpiece, simulated temperature at pin center decreased slightly, while simulated total power increased. In CSDP-1, simulated pin power increased, while simulated shoulder power was similar. Under the same thermal conductivity, relative to SSDP-1, in CSDP-1, simulated temperature at pin center is about 18℃ higher, and simulated total power is about 6% larger. Under the same thermal conductivity, in CSDP-1, simulated pin power is much larger than simulated shoulder power.

Figure 4.122(c~d) shows that, in DP-1, with the increasing of flow stress *(T)* of workpiece, simulated temperature at pin center increased slightly, and simulated power increased. In CSDP-1, simulated pin power increased, and simulated shoulder power was similar. Under the same flow stress, relative to SSDP-1, in CSDP-1, simulated temperature at pin center is about 18℃ higher, and simulated total power is about 6% larger. Under the same flow stress, in CSDP-1, simulated pin power is much larger than simulated shoulder power.

Figure 4.122(e~f) shows that, in DP-1, keeping the welding speed constant, with the increasing of rotation rate, simulated T at pin center and power increased with a

decreasing slope. Results conform to what is expected from actual welds showing a plateau in power and probe T at high rotation rate. In CSDP-1, simulated pin power increased with a decreasing slope, while simulated shoulder power increased. Under the same rotation rate, relative to SSDP-1, in CSDP-1, simulated T at pin center is about 18℃ higher, and simulated total power is about 7% larger. Under the same rotation rate, in CSDP-1, simulated pin power is much larger than simulated shoulder power.

Figure 4.122(g~h) shows that, in DP-1, keeping the rotation rate constant, with the increasing of welding speed, simulated T at pin center decreased slightly, and simulated total power increased. In CSDP-1, simulated pin power increased, while simulated shoulder power was similar. Under the same welding speed, relative to SSDP-1, in CSDP-1, simulated T at pin center is about 18℃ higher, and simulated total power is about 8% larger. Under the same welding speed, in CSDP-1, simulated pin power is much larger than simulated shoulder power.

Figure 4.122(i~j) shows that, in DP-1, keeping the APR (rotation rate/welding speed) constant, with the increasing of speeds, simulated T at pin center increased slightly, and simulated total power increased. It's also consistent with experimental observation. In CSDP-1, both simulated pin power and shoulder power increased. Under the same speeds, relative to SSDP-1, in CSDP-1, simulated T at pin center is about 16℃ higher, and simulated total power is about 7% larger. Under the same welding speed, in CSDP-1, simulated pin power is much larger than simulated shoulder power.

Generally, Figure 4.122 shows similar results of DP-1 with SP: in DP-1, the effect of increasing thermal conductivity of workpiece is to decrease temperature at pin center slightly and increase power; the effect of increasing flow stress of workpiece is to

increase temperature at pin center slightly and increase power; the effect of increasing rotation rate while keeping welding speed constant is to increase temperature at pin center and power with decreasing slopes; the effect of increasing welding speed while keeping rotation rate constant is to decrease temperature at pin center slightly and increase power; the effect of increasing speeds while keeping the APR constant is to increase temperature at pin center slightly and increase power. It indicates that the above variables affect temperature at pin center slightly, while affect power at some extent, especially the rotation rate, welding speed, and then thermal conductivity of workpiece. Figure 4.122 also shows that, relative to SSDP-1, in CSDP-1, simulated temperature at pin center is about 16~18℃ higher, and simulated total power is about 7% larger; In CSDP-1, simulated pin power is much larger than simulated shoulder power, which is different from the current opinion that heat generated by the rotating shoulder dominates during FSW process.

4.5.6.3 Study 3: Effects of Thermal Boundary Conditions

Goal of this study is to investigate effects of the welding speed and thermal management applied on the workpiece surface on thermal distribution, HAZ width, transverse temperature profiles, HAZ temperature history, time of temperature staying among 200~350℃ (relative temperature in HAZ) and power at various depths. The different convection coefficients have been applied to the entire top surface of the simulated workpiece.

Figure 4.123 shows the way to determine the HAZ width and time of temperature staying among 200~350℃. First, plot the 2D temperature contour plot in XY plane as shown in Figure 4.123(a). Here pin rotates CCT, and workpiece moves in positive X

direction. Therefore in this graph, advancing side (AS) is at the side when Y>0, while retreating side (RS) is at the side when Y<0. Determine the points (x,y) at which the 350 ℃ isotherm is tangent to the welding direction at AS (as indicated by the solid black line in Figure 4.123(a)) and RS, then HAZ width is obtained. These y-values will correspond approximately to the HAZ minimum hardness location. Secondly, extract the temperature history data of the located positions at either AS or RS, and plot it as a function of x and convert x to time through welding speed, as shown in Figure 4.123(b), and calculate relevant time using arbitrary 200-350 ℃ range.

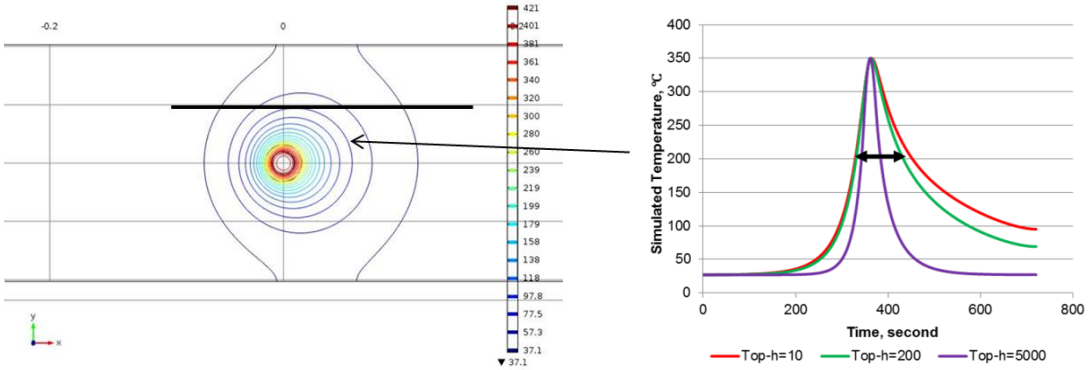

(a) 2D isothermal contour plot in XY plane (b) Simulated temperature as a function of time

Figure 4.123 Determination of HAZ width and time of T staying among 200~350˚C

4.5.6.3.1 3D and 2D thermal distributions

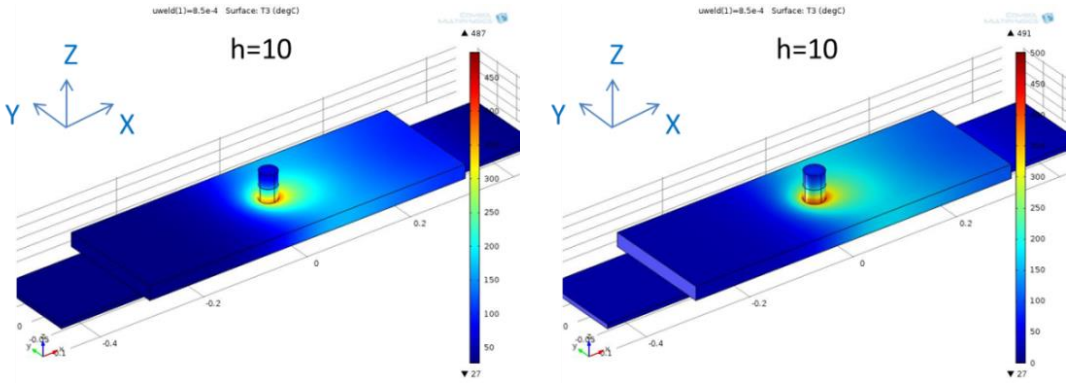

(a) SSSP: h=10 (b) CSSP: h=10

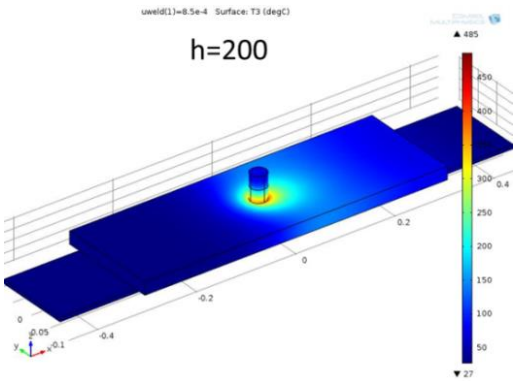

(c) SSSP: h=200

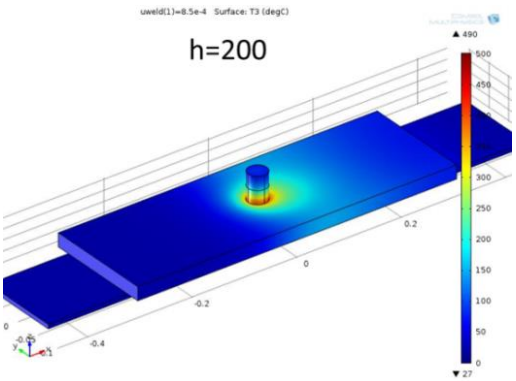

(d) CSSP: h=200

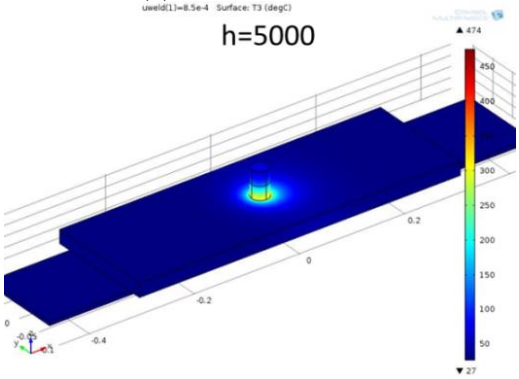

(e) SSSP: h=5000

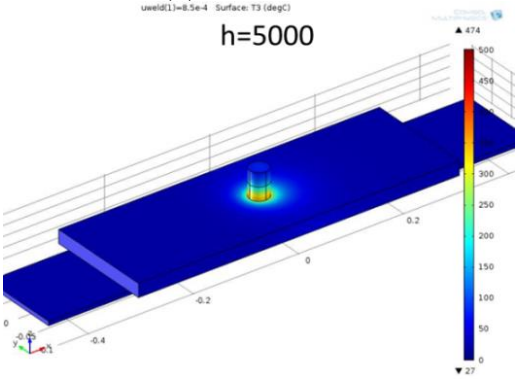

(f) CSSP: h=5000

Figure 4.124 Typical 3D view of T field obtained from TPM model of SP joints

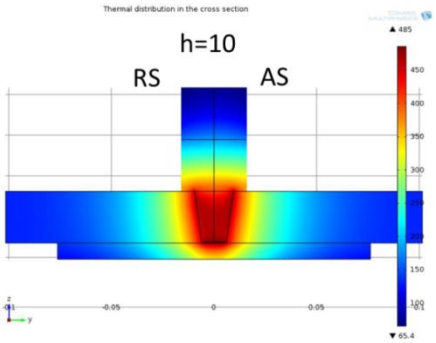

(a) SSSP: h=10

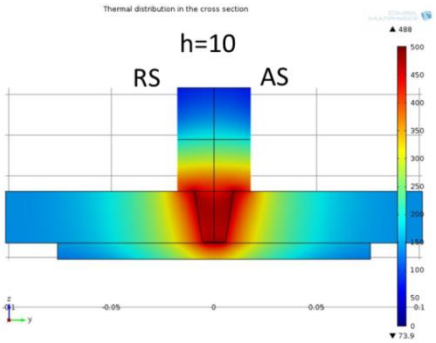

(b) CSSP: h=10

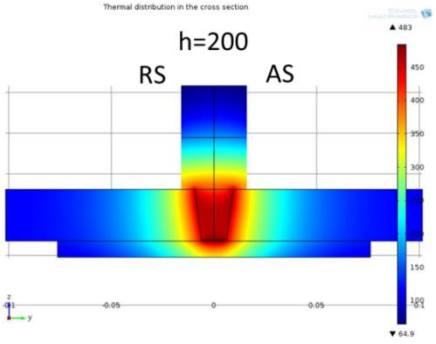

(c) SSSP: h=200

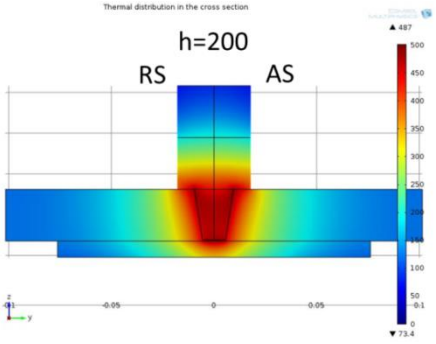

(d) CSSP: h=200

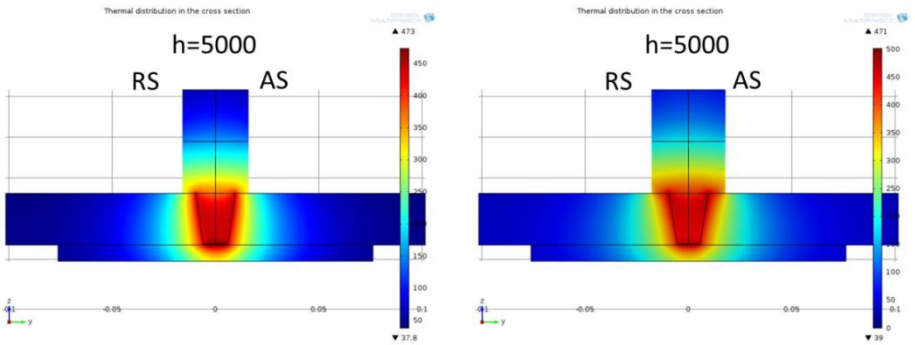

(e) SSSP: h=5000 (f) CSSP: h=5000

Figure 4.125 Typical contour plots of temperature at transverse cross-section obtained from TPM model of SP joints

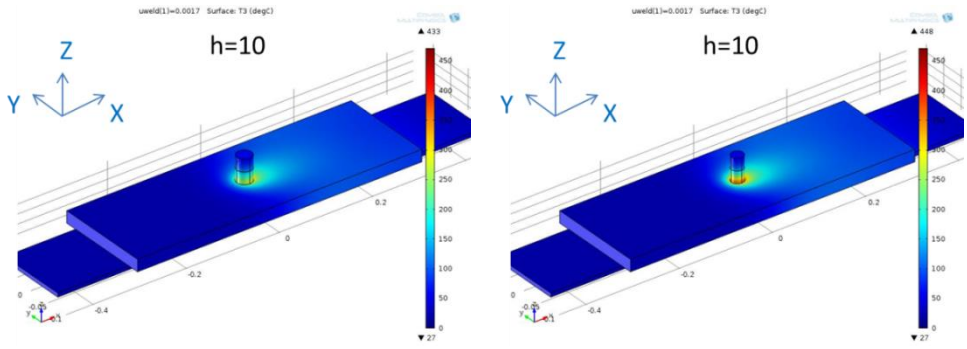

(a) SSDP-1: h=10 (b) CSDP-1: h=10

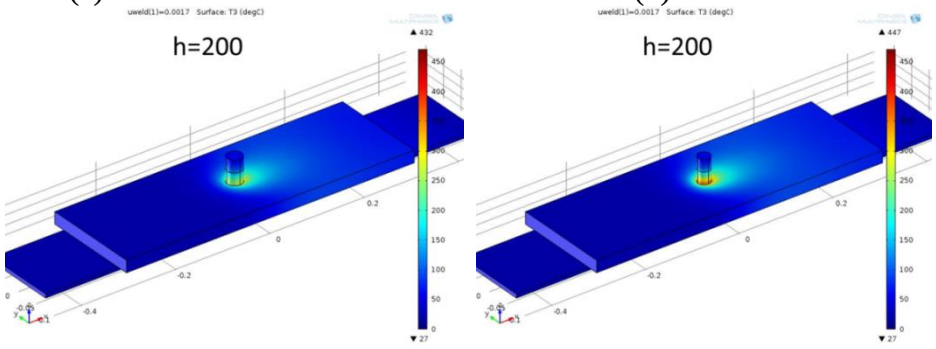

(c) SSDP-1: h=200 (d) CSDP-1: h=200

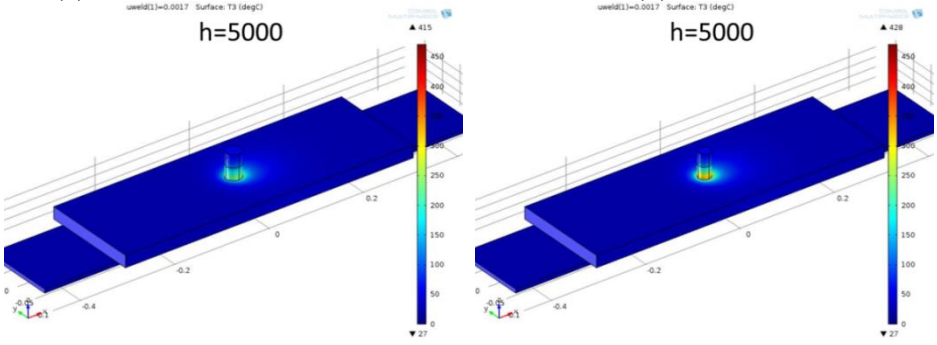

(e) SSDP-1: h=5000 (f) CSDP-1: h=5000

Figure 4.126 Typical 3D view of T field obtained from TPM model of DP-1 joints

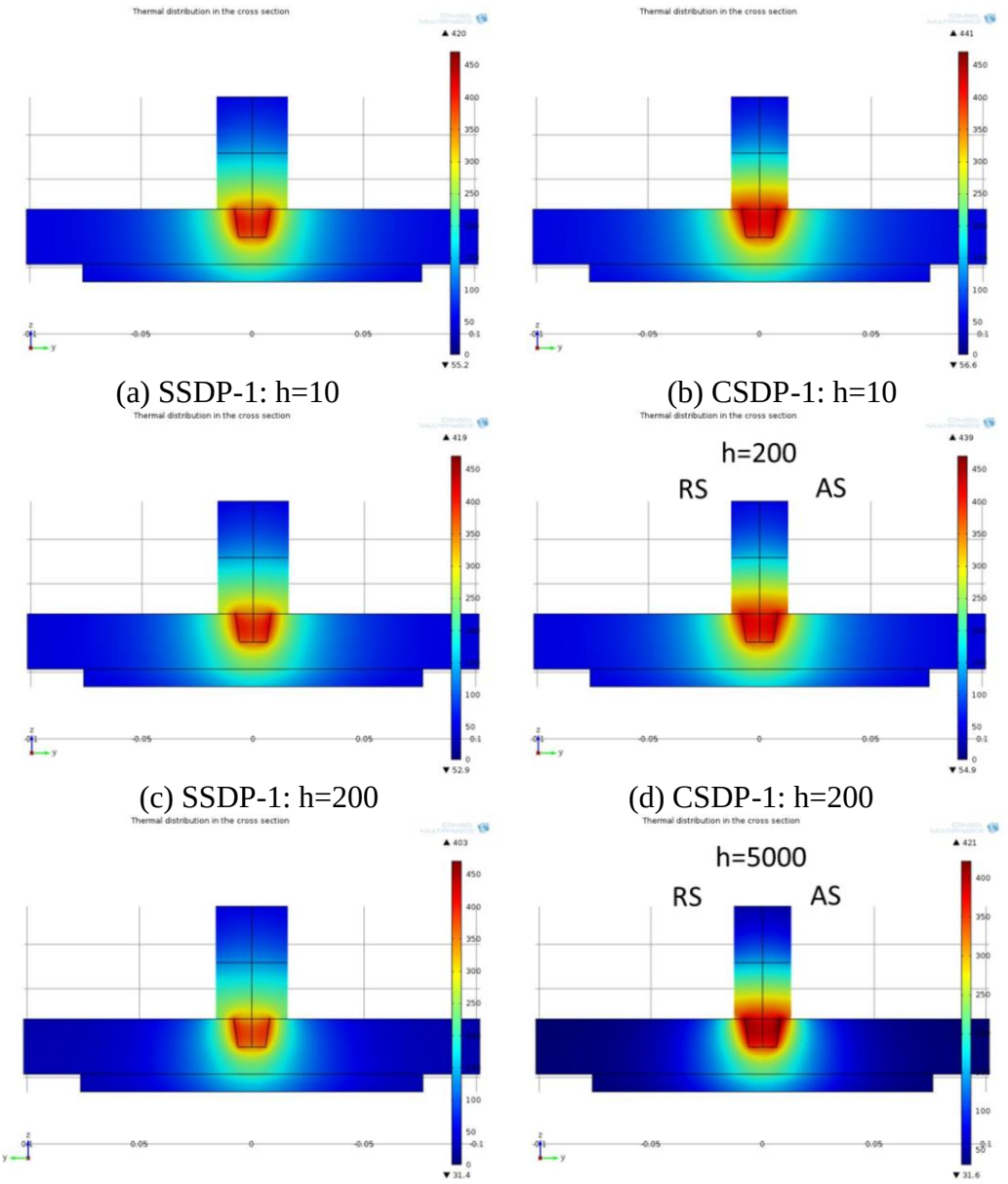

(a) SSDP-1: h=10 (b) CSDP-1: h=10

(c) SSDP-1: h=200 (d) CSDP-1: h=200

(e) SSDP-1: h=5000 (f) CSDP-1: h=5000

Figure 4.127 Typical contour plots of temperature at transverse cross-section obtained from TPM model of DP-1 joints

Figure 4.124 and Figure 4.125 show typical 3D view of T field and 2D contour plots of T at transverse cross-section obtained from TPM models of SP joints. Figure 4.126 and Figure 4.127 show typical 3D view of temperature field and 2D contour plots of temperature at transverse cross-section obtained from TPM models of DP-1 joints.

Figure 4.124~Figure 4.127 show that, in both SP and DP-1, different h (heat transfer coefficient) at workpiece surface caused different thermal distributions on workpiece surface and on transverse cross section: higher h, then less tapered NG shape, and narrower HAZ area especially near weld crown. For the highest h, there is significant difference in the shape of the near crown isotherms compared to lower h.

4.5.6.3.2 Simulated Temperature at pin center and Power

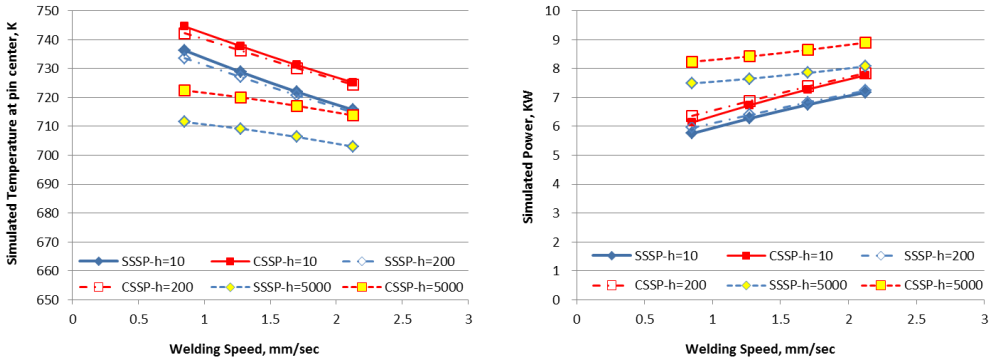

(a) Temperature at pin center (b) Power

Figure 4.128 Simulated (a) T at pin center and (b) power as a function of welding speed with different h applied at workpiece surface obtained from TPM model of SP joints

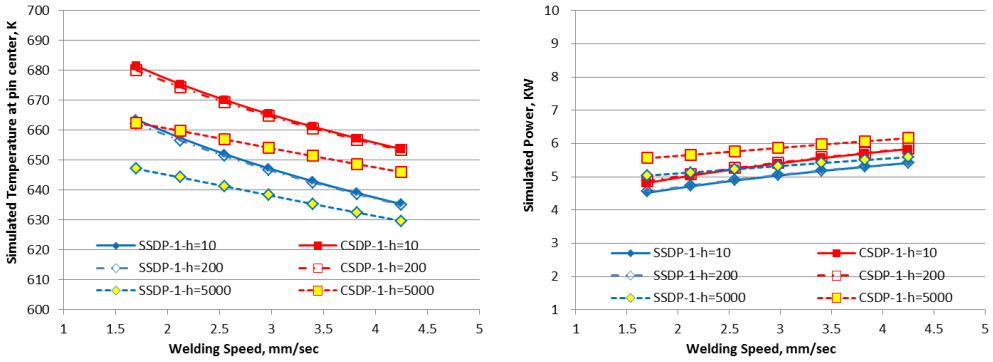

(a) Temperature at pin center (b) Power

Figure 4.129 Simulated (a) T at pin center and (b) power as a function of welding speed with different h applied at workpiece surface obtained from TPM model of DP-1 joints

Figure 4.128 shows the simulated (a) temperature at pin center and (b) power as a function of welding speed with different h applied at workpiece surface obtained from

TPM models of SP joints. Figure 4.129 shows the simulated (a) temperature at pin center and (b) power as a function of welding speed with different h applied at workpiece surface obtained from TPM models of DP-1 joints.

Figure 4.128~Figure 4.129 show that, when welding speed increased, in both SP and DP-1, T decreased slightly, while power increased, which effects decreased when thermal managements with higher heat transfer coefficient applied on the workpiece surface. Higher heat transfer coefficient at the workpiece surface decreased T and increased power. However, effects of higher heat transfer coefficient at the workpiece surface on decreasing T and increasing power are smaller in DP-1 than those in SP.

4.5.6.3.3 HAZ Width at various depths

Figure 4.130 shows the HAZ width as a function of welding speed with different h applied at workpiece surface (a) at crown, (b) at mid-plane and (c) at root obtained from TPM model of SP joints. Figure 4.130 shows that, in both SSSP and CSSP, when welding speed increased, HAZ width decreased, and the decreasing slope was smaller when higher h was applied. At the same welding speed and h, HAZ width decreased from pin top to root. Relative to SS, in SP, CS resulted in wider HAZ especially at crown, and had little effect on HAZ width at root.

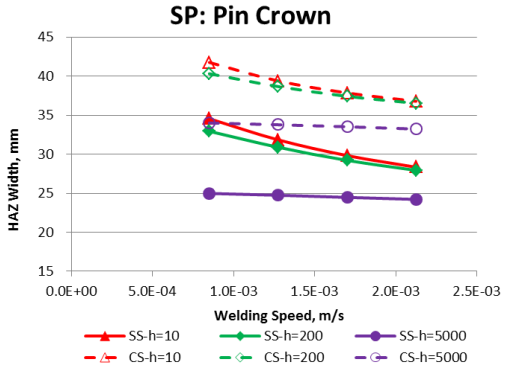

(a) Crown

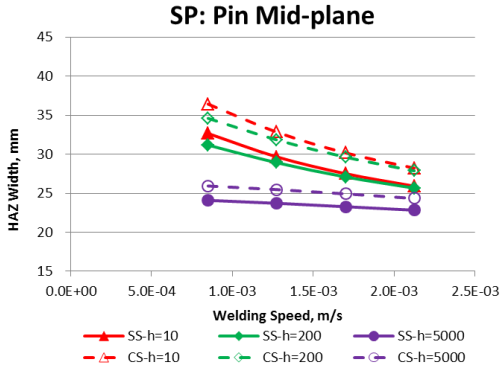

(b) Mid-plane

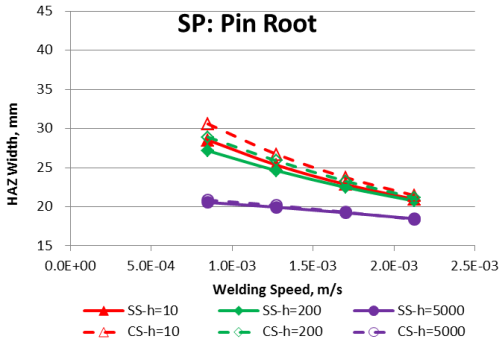

(c) Root

Figure 4.130 HAZ width as a function of welding speed with different h applied at workpiece surface obtained from TPM model of SP joints: (a) at crown, (b) at mid-plane and (c) at root

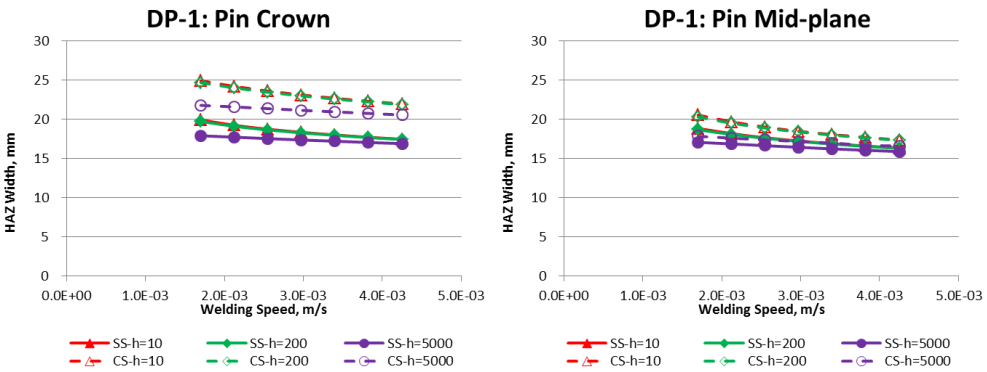

(a) Crown (b) Mid-plane

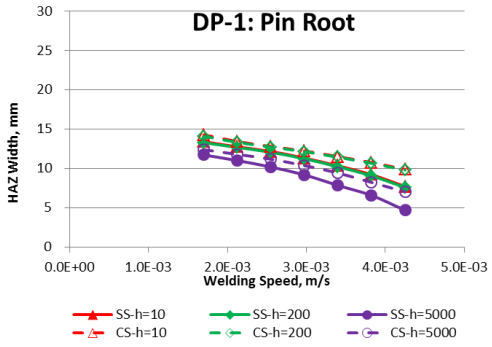

(c) Root

Figure 4.131 HAZ width as a function of welding speed with different h applied at workpiece surface obtained from TPM model of DP-1 joints: (a) at crown, (b) at mid-plane and (c) at root

Figure 4.131 shows the HAZ width as a function of welding speed with different h applied at workpiece surface (a) at crown, (b) at mid-plane and (c) at root obtained

from TPM model of DP-1 joints. Figure 4.131 shows that, in both SSDP-1 and CSDP-1, when welding speed increased, HAZ width decreased slightly. At the same welding speed and h, HAZ width decreased slightly from pin top to root. Relative to SS, in DP-1, CS resulted in a little wider HAZ especially at crown, and affected HAZ width at root little.

Figure 4.130 and Figure 4.131 also show that, relative to SP, in DP-1, h has much less effect on HAZ width.

4.5.6.3.4 Transverse Temperature Profile at pin center

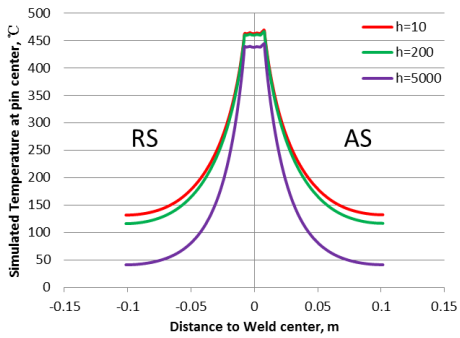

(a) SSSP: 0.85 mm/s

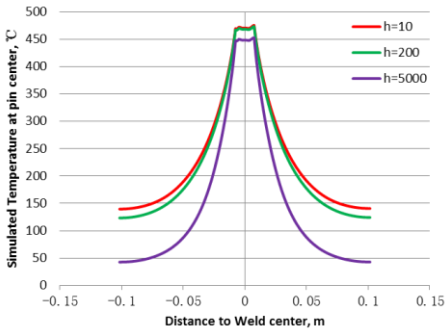

(b) CSSP: 0.85 mm/s

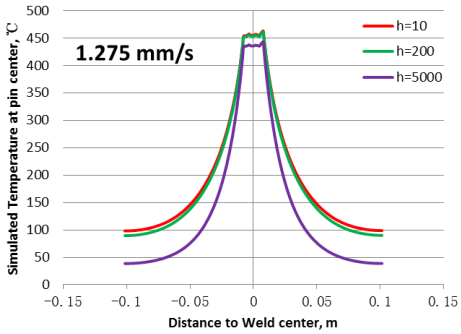

(c) SSSP: 1.275 mm/s

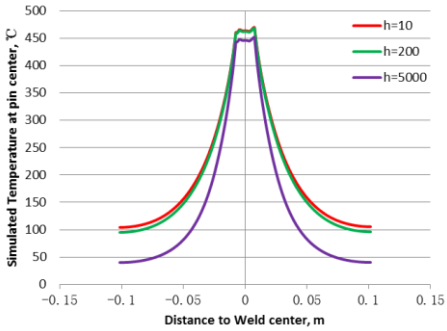

(d) CSSP: 1.275 mm/s

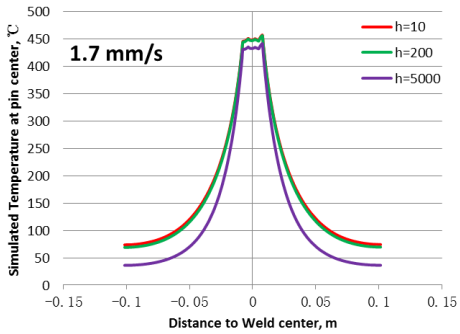

(e) SSSP: 1.7 mm/s

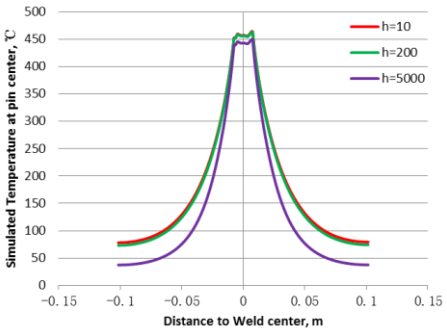

(f) CSSP: h=1.7 mm/s

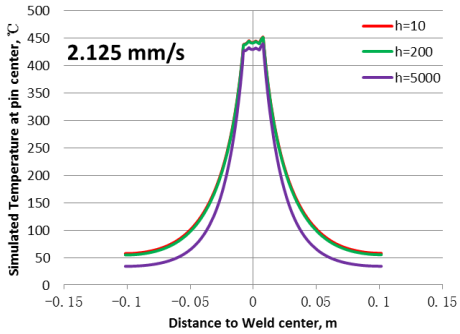

(g) SSSP: 2.125 mm/s

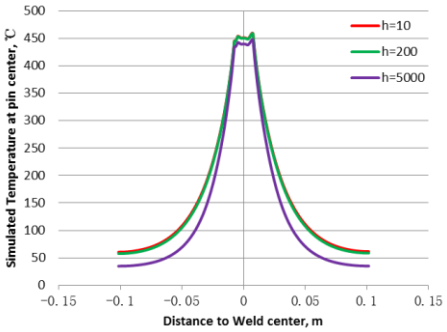

(h) CSSP: h=2.125 mm/s

Figure 4.132 Simulated T at pin center as a function of distance to weld center with different welding speeds and h applied at WP surface obtained from TPM model of SP

Figure 4.132 shows the simulated temperature at pin center as a function of distance to weld center with different welding speeds and h applied at workpiece surface obtained from TPM model of SP joints. Figure 4.133 shows the simulated temperature at pin center as a function of distance to weld center with different welding speeds and h applied at workpiece surface obtained from TPM model of DP-1 joints.

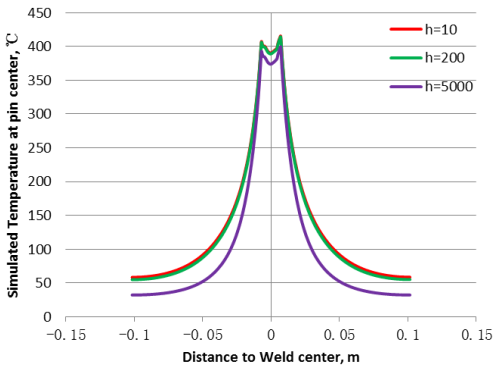

(a) SSDP-1: 1.7 mm/s

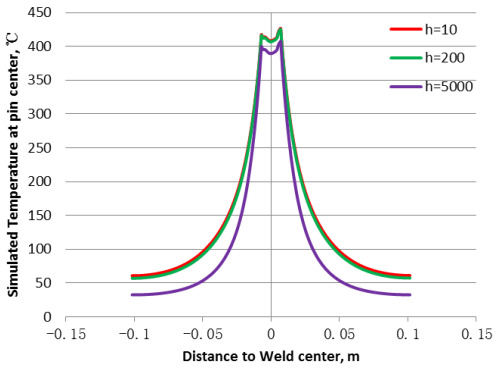

(b) CSDP-1: 1.7 mm/s

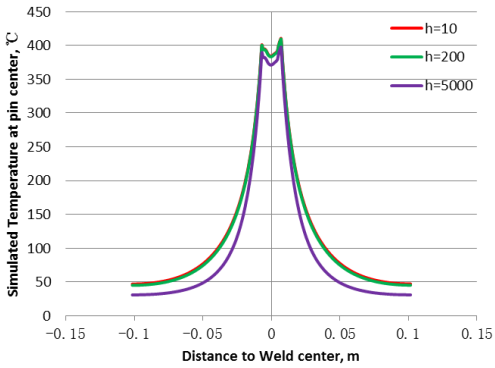

(c) SSDP-1: 2.125 mm/s

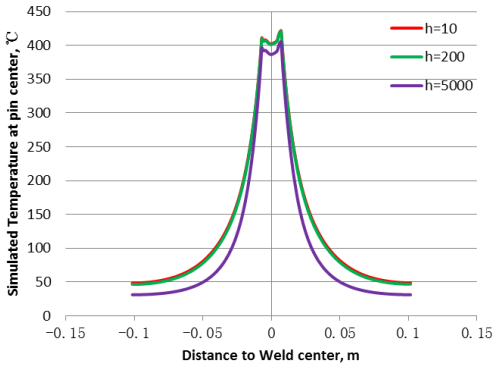

(d) CSDP-1: 2.125 mm/s

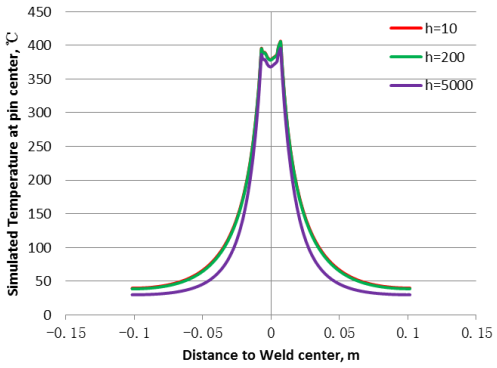

(e) SSDP-1: 2.55 mm/s

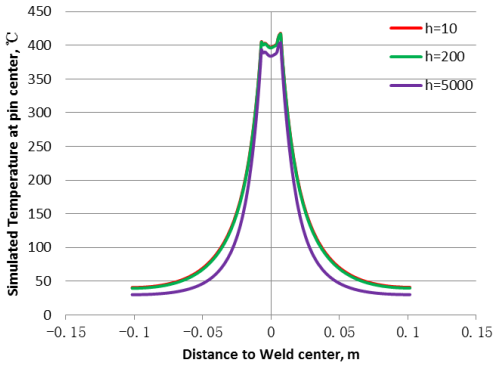

(f) CSDP-1: h=2.55 mm/s

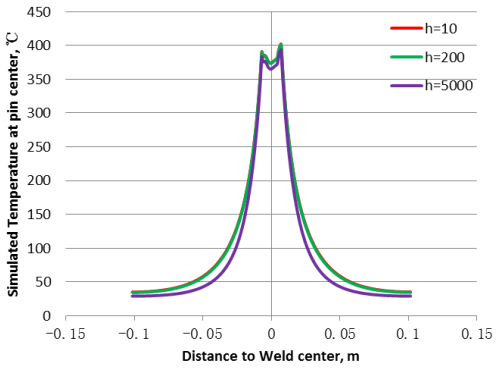

(g) SSDP-1: 2.975 mm/s

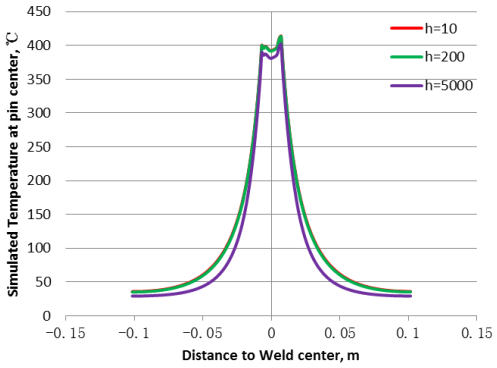

(h) CSDP-1: h=2.975 mm/s

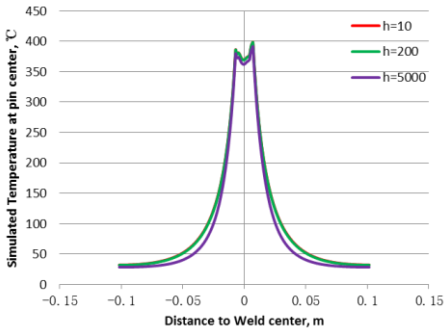

(i) SSDP-1: 3.4 mm/s

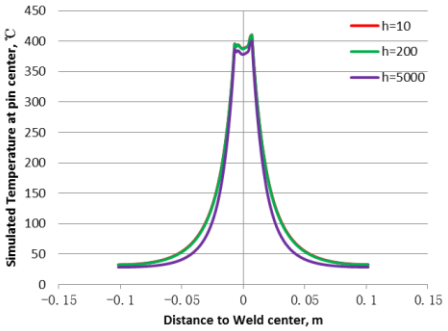

(j) CSDP-1: 3.4 mm/s

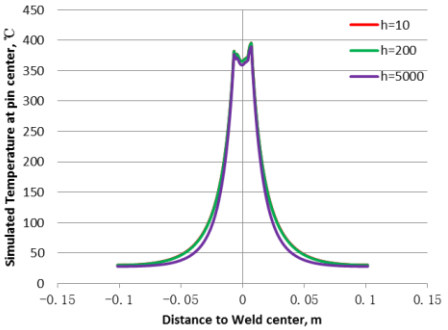

(k) SSDP-1: 3.825 mm/s

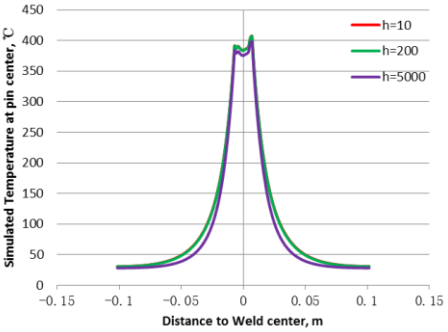

(l) CSDP-1: h=3.825 mm/s

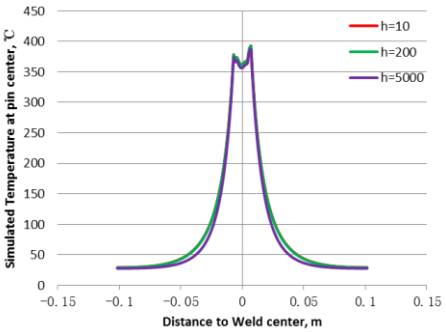

(m) SSDP-1: 4.25 mm/s

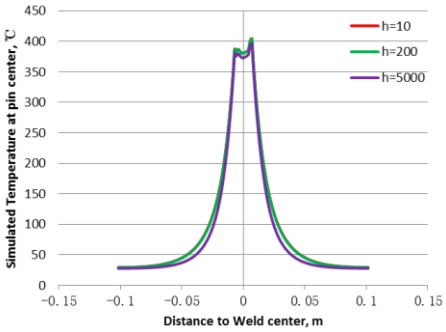

(n) CSDP-1: h=4.25 mm/s

Figure 4.133 Simulated temperature at pin center as a function of distance to weld center with different welding speeds and h applied at workpiece surface obtained from TPM model of DP-1 joints

Figure 4.132 and Figure 4.133 show that, in both SP and DP-1, under the same welding speed, different h at workpiece surface caused different thermal distributions on transverse cross section: higher h, then lower temperature at the same distance to weld center. The effect of h on probe mid-plane temperature is relatively small. With the same h and rotation rate, higher welding speed reduced the effect of h, and decreased the temperature at pin center. Temperature is slightly asymmetric at AS and RS. Relative to SP, in DP-1, h has much less effect on transverse temperature profile.

4.5.6.3.5 HAZ Temperature history at various depths

Figure 4.134~Figure 4.137 show the HAZ temperature history as a function of process time at various depths with different welding speed and h applied at workpiece surface obtained from TPM model of SP joints. Figure 4.138~Figure 4.144 show the HAZ temperature history as a function of process time at various depths with different welding speed and h applied at workpiece surface obtained from TPM model of DP-1 joints.

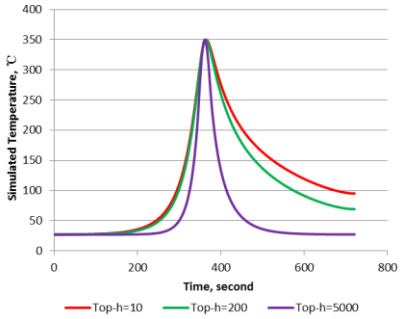

(a) SSSP: 0.85 mm/s, crown

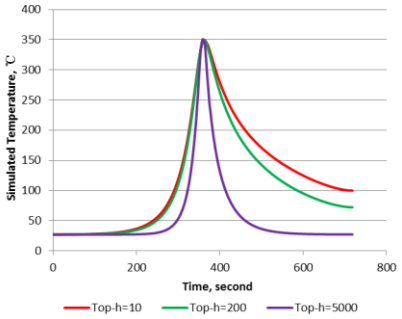

(b) CSSP: 0.85 mm/s, crown

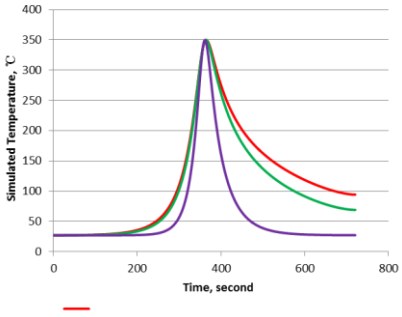

(c) SSSP: 0.85 mm/s, mid-plane

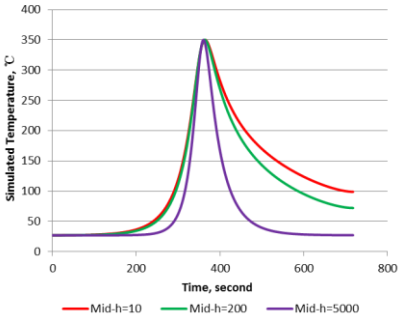

(d) CSSP: 0.85 mm/s, mid-plane

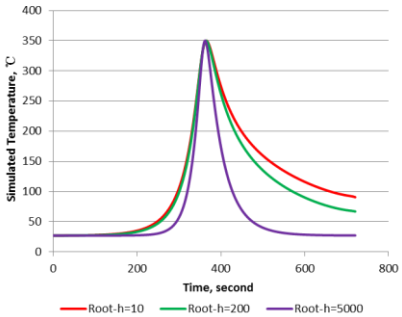

(e) SSSP: 0.85 mm/s, root

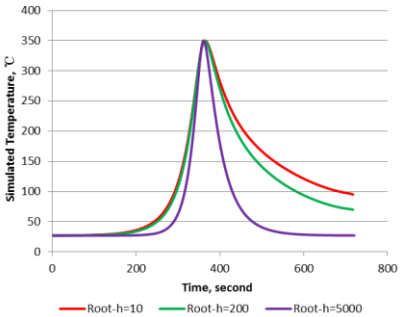

(f) CSSP: 0.85 mm/s, root

Figure 4.134 HAZ T history as a function of process time at various depths with different h applied at WP surface obtained from TPM model of SP: welding speed 0.85 mm/s

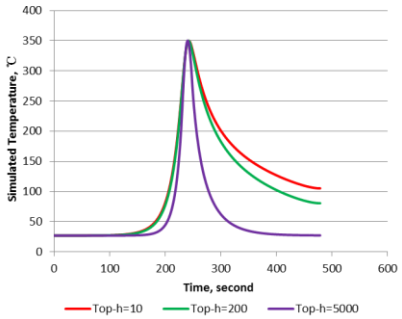

(a) SSSP: 1.275 mm/s, crown

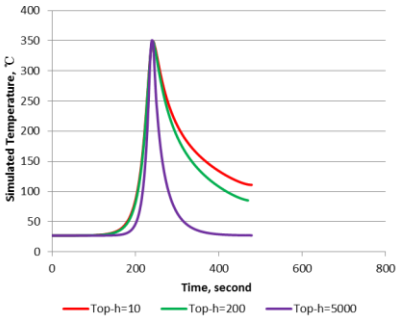

(b) CSSP: 1.275 mm/s, crown

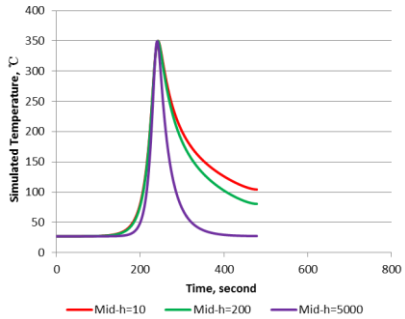

(c) SSSP: 1.275 mm/s, mid-plane

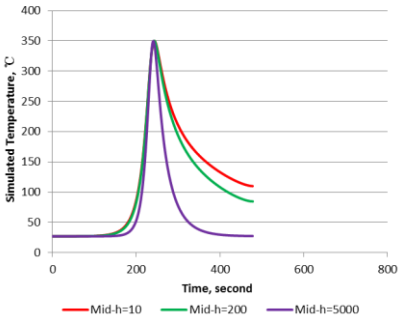

(d) CSSP: 1.275 mm/s, mid-plane

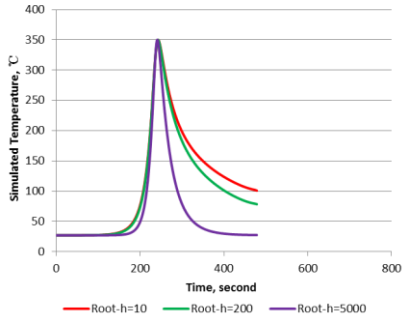

(e) SSSP: 1.275 mm/s, root

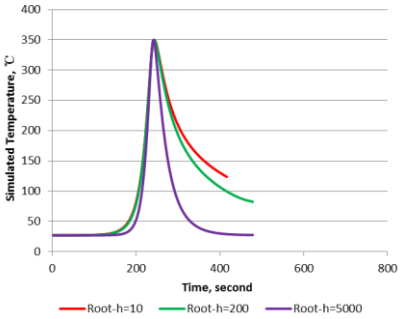

(f) CSSP: 1.275 mm/s, root

Figure 4.135 HAZ T history as a function of process time at various depths with different h applied at WP surface obtained from TPM model of SP: a welding speed of 1.275 mm/s

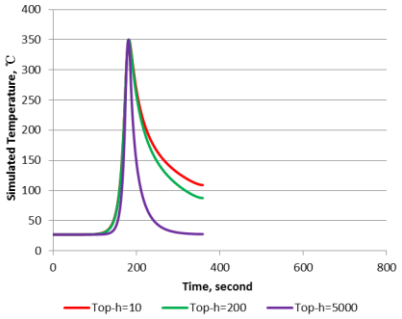

(a) SSSP: 1.7 mm/s, crown

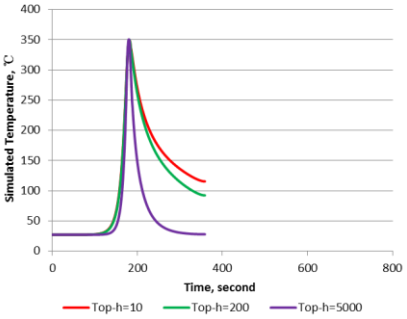

(b) CSSP: 1.7 mm/s, crown

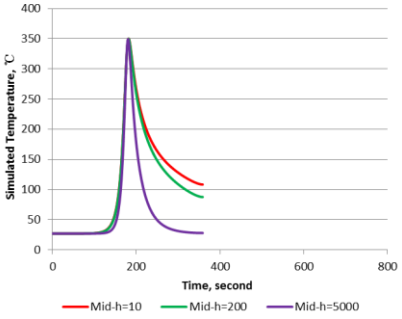

(c) SSSP: 1.7 mm/s, mid-plane

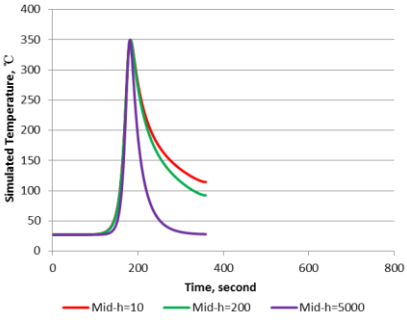

(d) CSSP: 1.7 mm/s, mid-plane

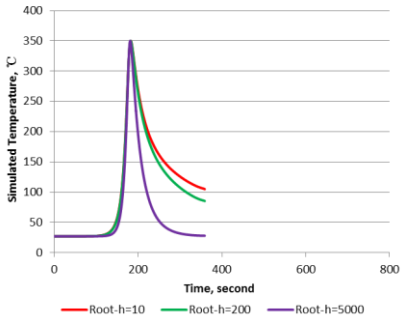

(e) SSSP: 1.7 mm/s, root

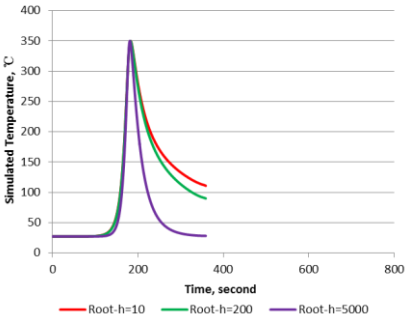

(f) CSSP: 1.7 mm/s, root

Figure 4.136 HAZ T history as a function of process time at various depths with different h applied at WP surface obtained from TPM model of SP: a welding speed of 1.7 mm/s

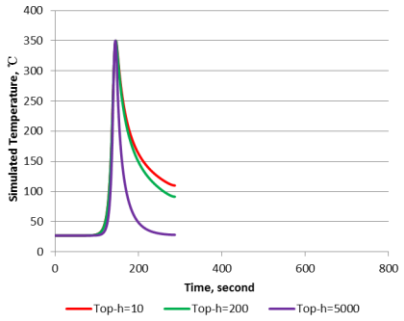

(a) SSSP: 2.125 mm/s, crown

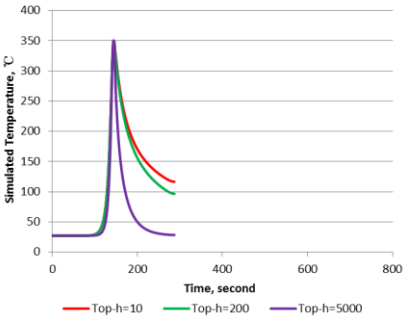

(b) CSSP: 2.125 mm/s, crown

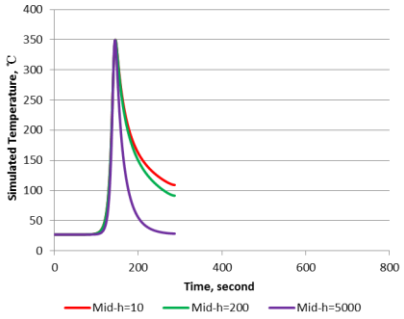

(c) SSSP: 2.125 mm/s, mid-plane

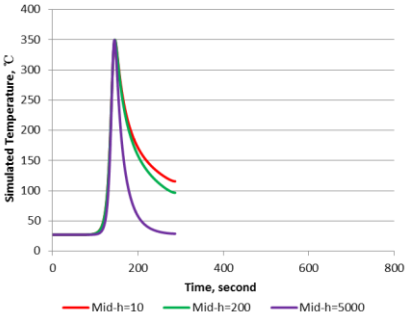

(d) CSSP: 2.125 mm/s, mid-plane

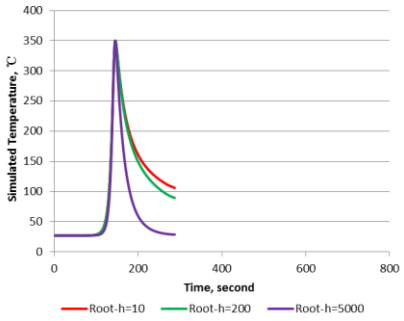

(e) SSSP: 2.125 mm/s, root

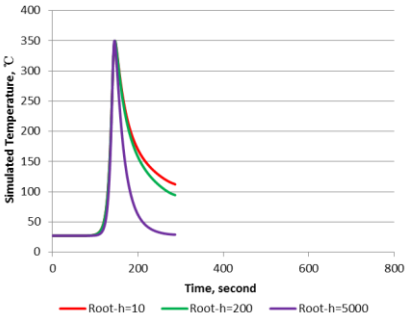

(f) CSSP: 2.125 mm/s, root

Figure 4.137 HAZ T history as a function of process time at various depths with different h applied at WP surface obtained from TPM model of SP: a welding speed of 2.125 mm/s

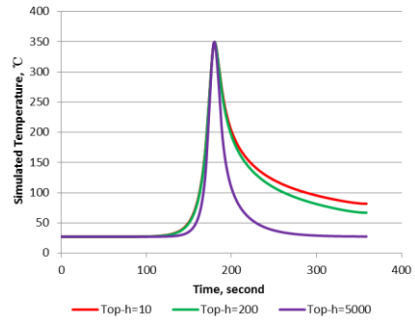

(a) SSDP-1: 1.7 mm/s, crown

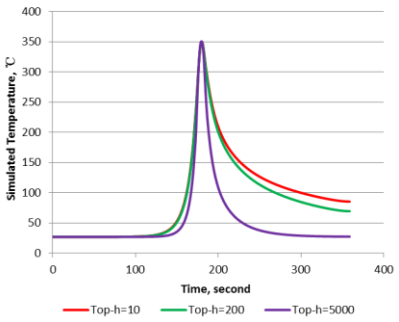

(b) CSDP-1: 1.7 mm/s, crown

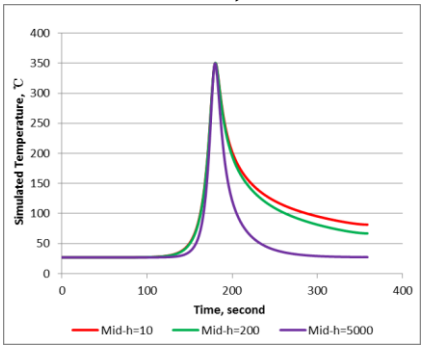

(c) SSDP-1: 1.7 mm/s, mid-plane

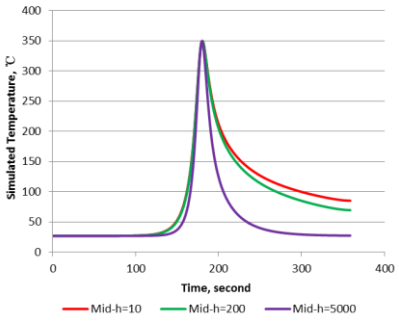

(d) CSDP-1: 1.7 mm/s, mid-plane

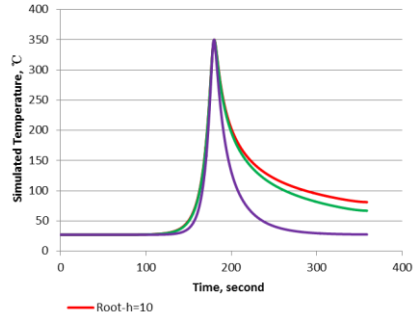

(e) SSDP-1: 1.7 mm/s, root

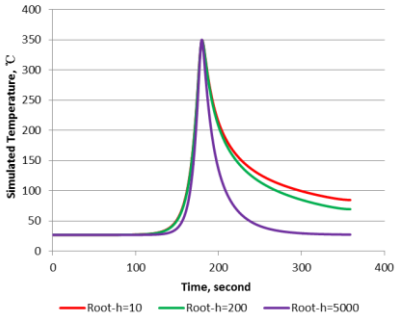

(f) CSDP-1: 1.7 mm/s, root

Figure 4.138 HAZ T history as a function of process time at various depths with different h applied at WP surface obtained from TPM model of DP-1: a welding speed of 1.7 mm/s

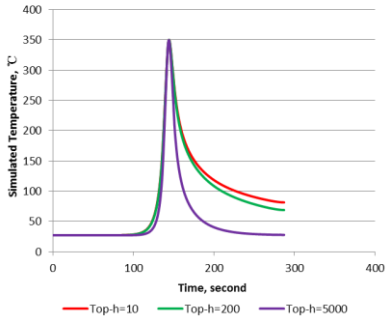

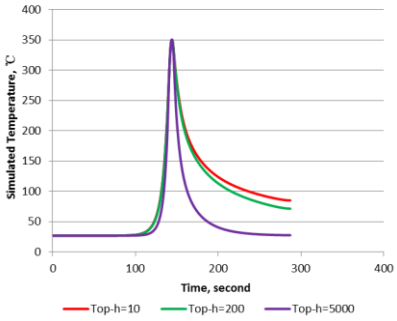

(a) SSDP-1: 2.125 mm/s, crown

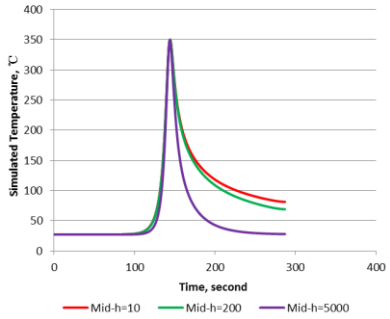

(b) CSDP-1: 2.125 mm/s, crown

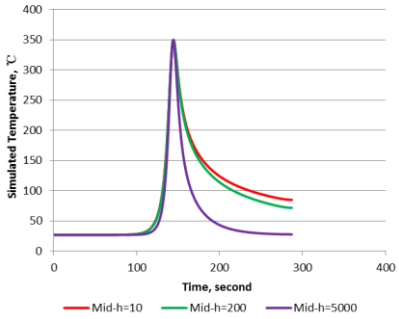

(c) SSDP-1: 2.125 mm/s, mid-plane

(d) CSDP-1: 2.125 mm/s, mid-plane

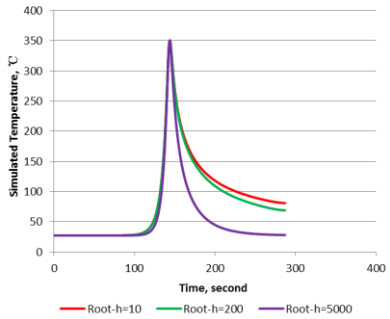

(e) SSDP-1: 2.125 mm/s, root

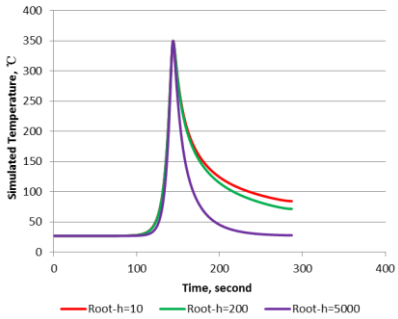

(f) CSDP-1: 2.125 mm/s, root

Figure 4.139 HAZ T history as a function of process time at various depths with different h applied at WP surface obtained from TPM model of DP-1: welding speed 2.125 mm/s

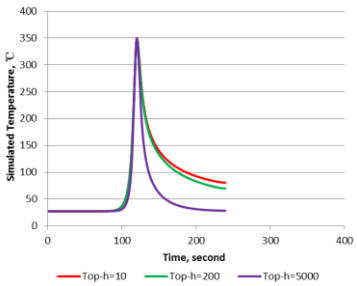

(a) SSDP-1: 2.55 mm/s, crown

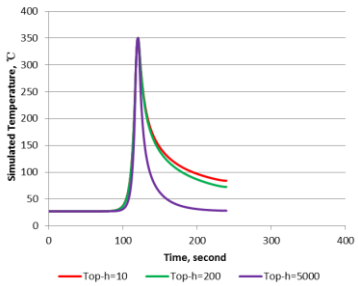

(b) CSDP-1: 2.55 mm/s, crown

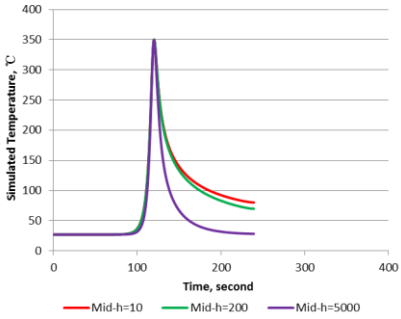

(c) SSDP-1: 2.55 mm/s, mid-plane

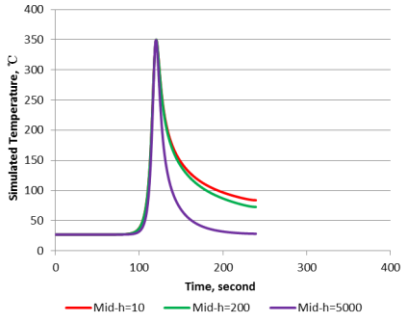

(d) CSDP-1: 2.55 mm/s, mid-plane

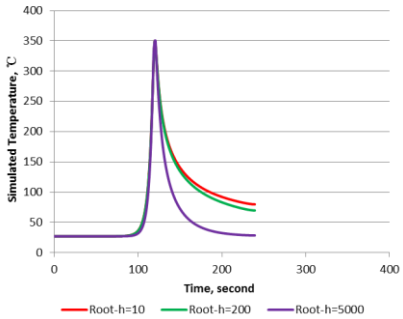

(e) SSDP-1: 2.55 mm/s, root

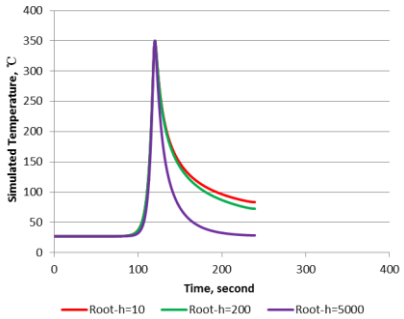

(f) CSDP-1: 2.55 mm/s, root

Figure 4.140 HAZ T history as a function of process time at various depths with different h applied at WP surface obtained from TPM model of DP-1: welding speed of 2.55 mm/s

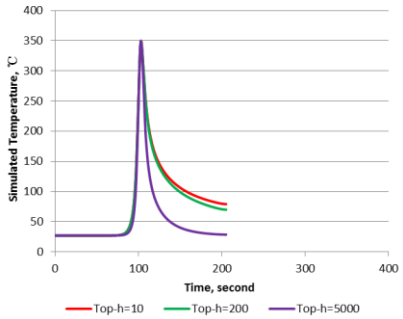

(a) SSDP-1: 2.975 mm/s, crown

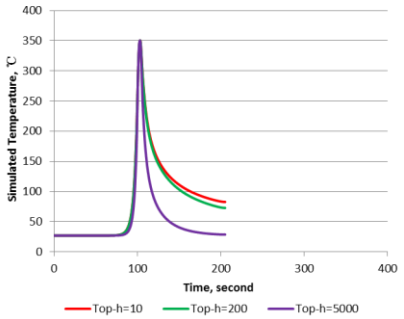

(b) CSDP-1: 2.975 mm/s, crown

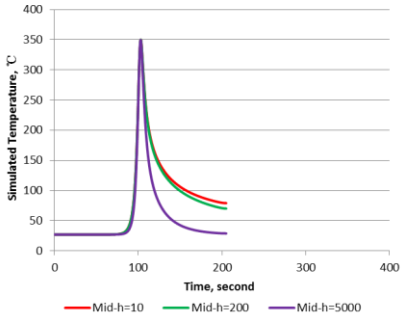

(c) SSDP-1: 2.975 mm/s, mid-plane

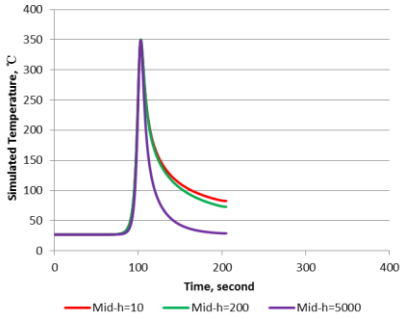

(d) CSDP-1: 2.975 mm/s, mid-plane

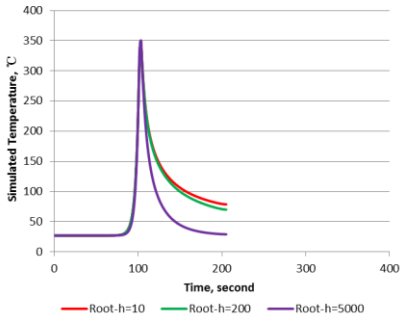

(e) SSDP-1: 2.975 mm/s, root

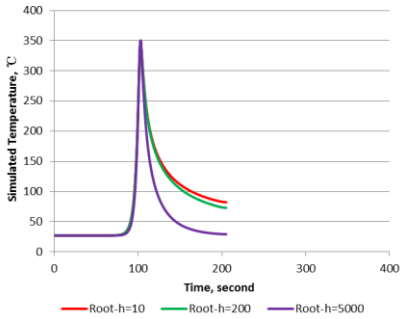

(f) CSDP-1: 2.975 mm/s, root

Figure 4.141 HAZ T history as a function of process time at various depths with different h applied at WP surface obtained from TPM model of DP-1: welding speed 2.975 mm/s

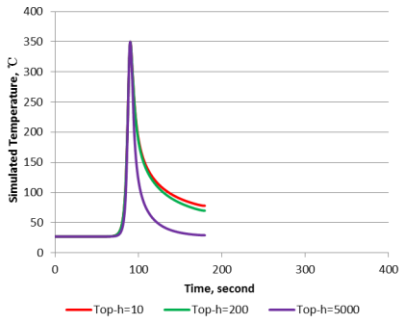

(a) SSDP-1: 3.4 mm/s, crown

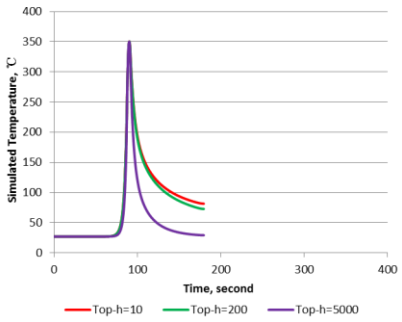

(b) CSDP-1: 3.4 mm/s, crown

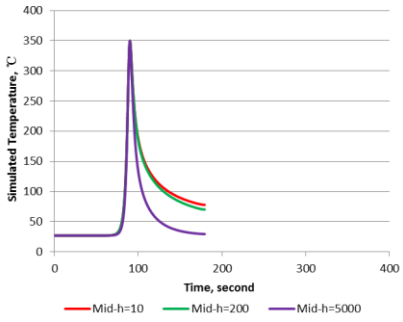

(c) SSDP-1: 3.4 mm/s, mid-plane

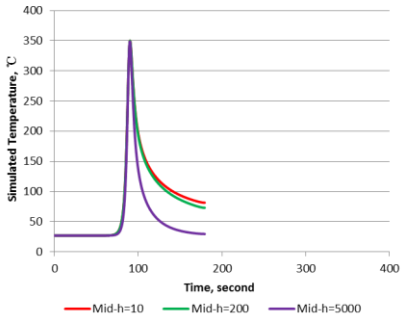

(d) CSDP-1: 3.4 mm/s, mid-plane

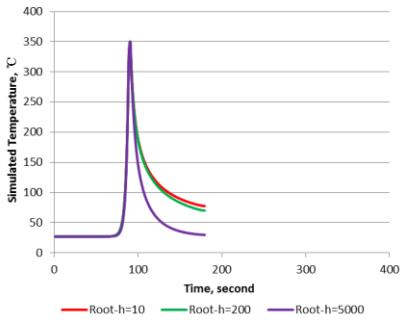

(e) SSDP-1: 3.4 mm/s, root

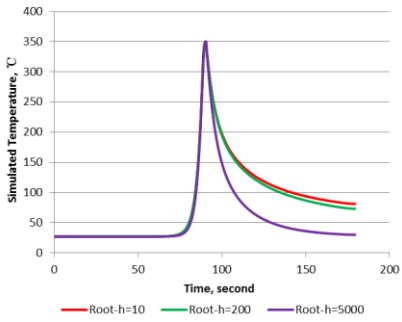

(f) CSDP-1: 3.4 mm/s, root

Figure 4.142 HAZ T history as a function of process time at various depths with different h applied at WP surface obtained from TPM model of DP-1: a welding speed of 3.4 mm/s

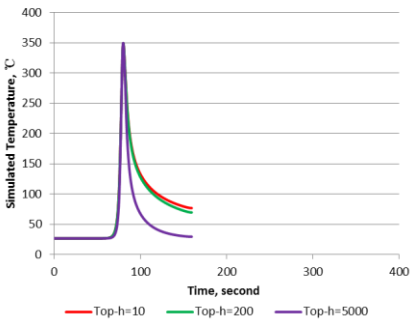

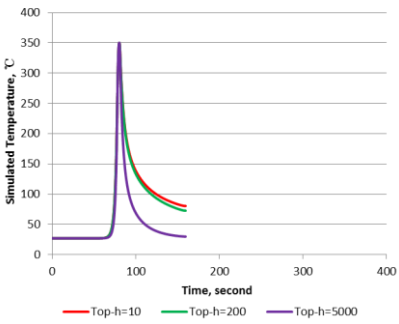

(a) SSDP-1: 3.825 mm/s, crown

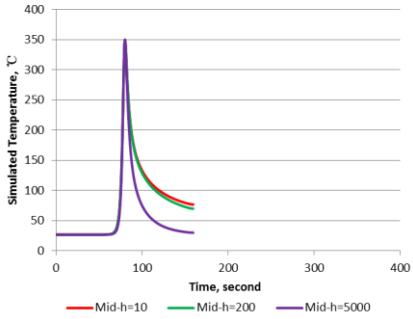

(b) CSDP-1: 3.825 mm/s, crown

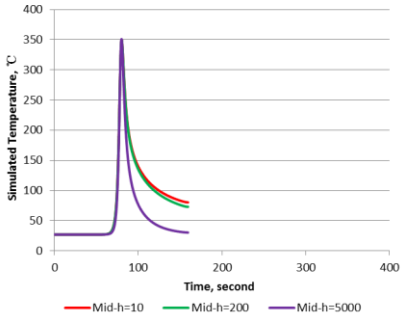

(c) SSDP-1: 3.825 mm/s, mid-plane

(d) CSDP-1: 3.825 mm/s, mid-plane

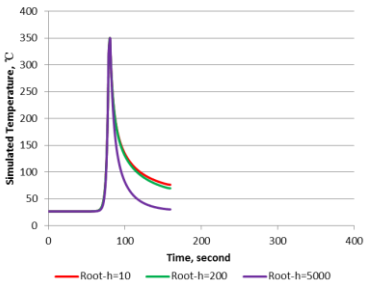

(e) SSDP-1: 3.825 mm/s, root

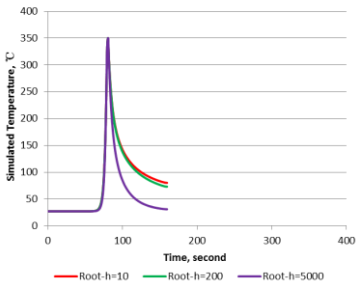

(f) CSDP-1: 3.825 mm/s, root

Figure 4.143 HAZ T history as a function of process time at various depths with different h applied at WP surface obtained from TPM model of DP-1: welding speed 3.825 mm/s

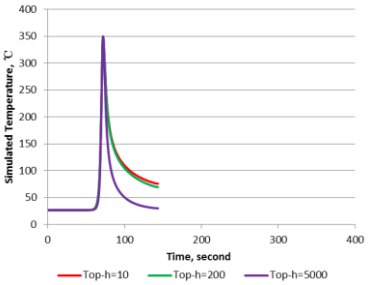

(a) SSDP-1: 4.25 mm/s, crown

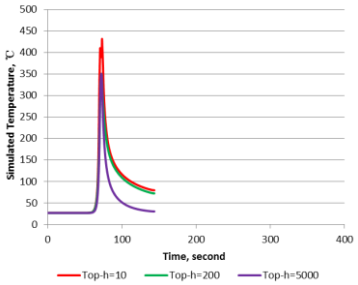

(b) CSDP-1: 4.25 mm/s, crown

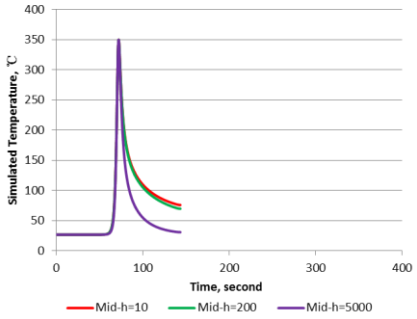

(c) SSDP-1: 4.25 mm/s, mid-plane

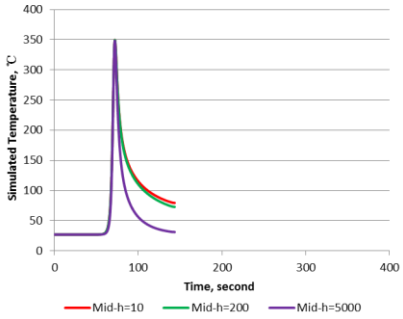

(d) CSDP-1: 4.25 mm/s, mid-plane

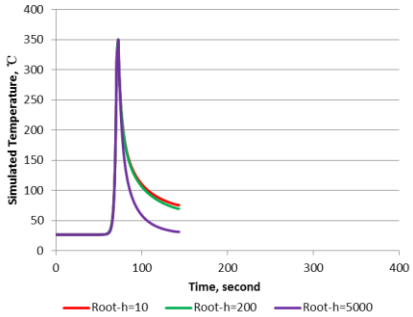

(e) SSDP-1: 4.25 mm/s, root

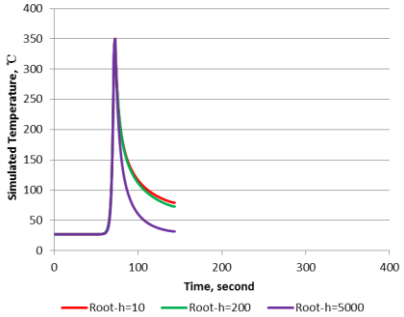

(f) CSDP-1: 4.25mm/s, root

Figure 4.144 HAZ T history as a function of process time at various depths with different h applied at WP surface obtained from TPM model of DP-1: welding speed 4.25 mm/s

Figure 4.134~Figure 4.144 show that, in both SP and DP-1, with the same welding speed and h, far field thermal histories at various depths are similar. With the same h, when welding speed increased, heating and cooling rates increased. At the same depth from weld crown, different h at workpiece surface caused different thermal histories: higher h, then higher heating and cooling rates.

4.5.6.3.6 Time of Temperature staying among 200~350℃ at various depths

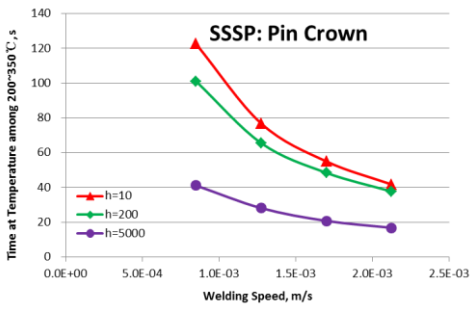

(a) SSSP: crown

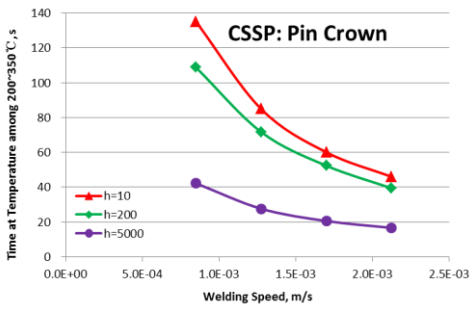

(b) CSSP: crown

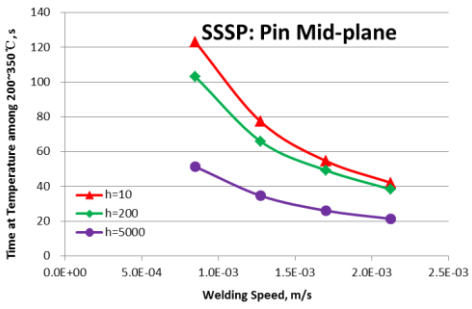

(c) SSSP: mid-plane

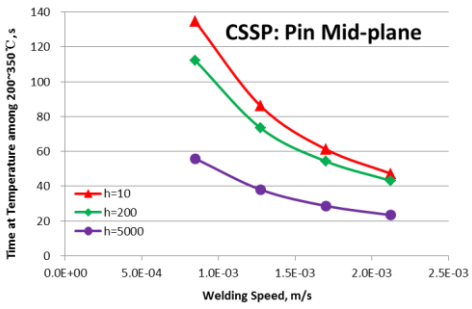

(d) CSSP: mid-plane

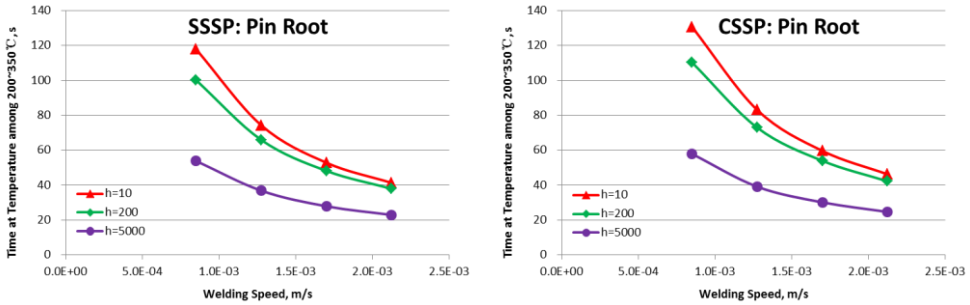

(e) SSSP: root (f) CSSP: root

Figure 4.145 Time of T staying among 200~350˚C with different h applied at WP: SP

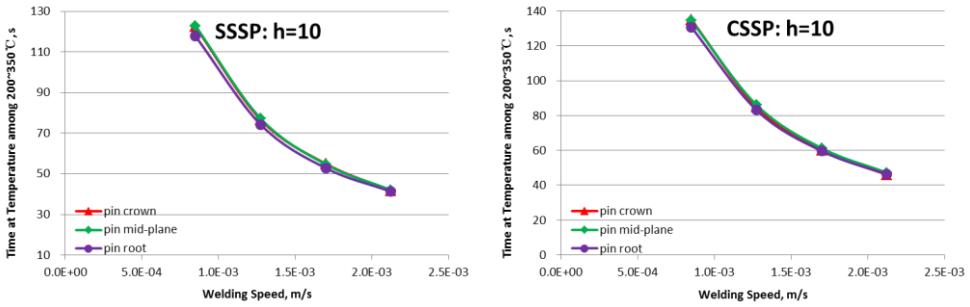

(a) SSSP: h=10 (b) CSSP: h=10

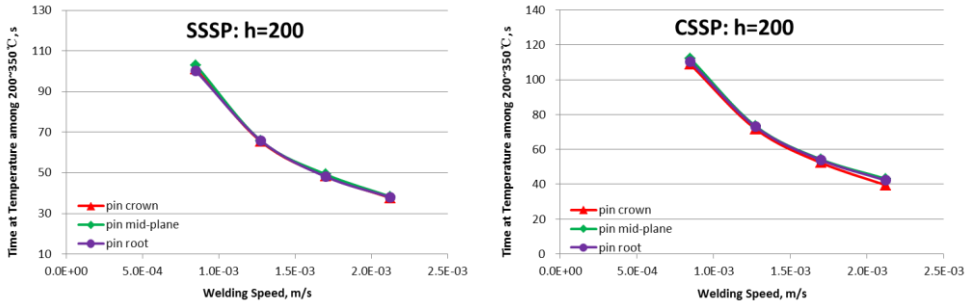

(c) SSSP: h=200 (d) CSSP: h=200

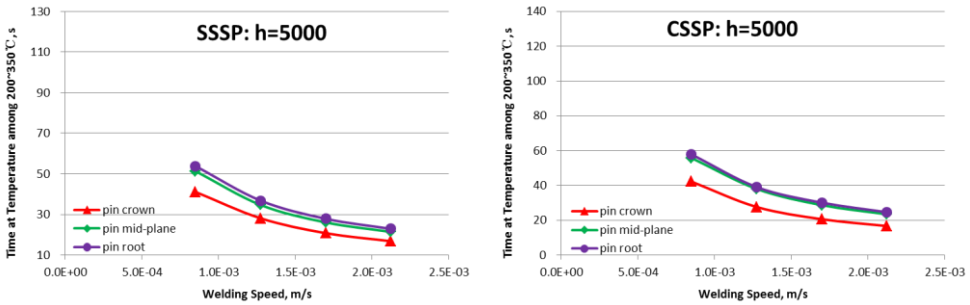

(e) SSSP: h=5000 (f) CSSP: h=5000

Figure 4.146 Time of T staying among 200~350˚C at various depths: SP

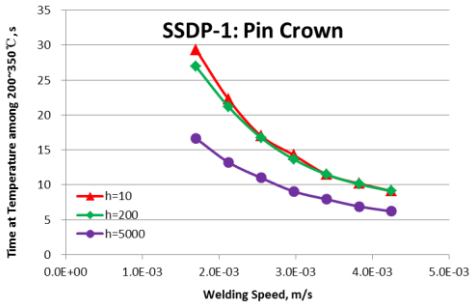

(a) SSDP-1: crown

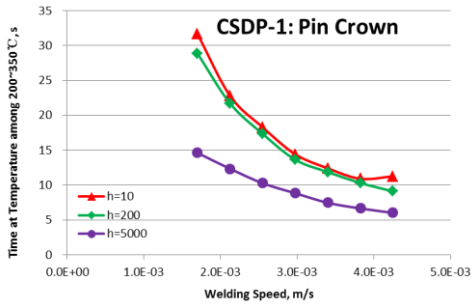

(b) CSDP-1: crown

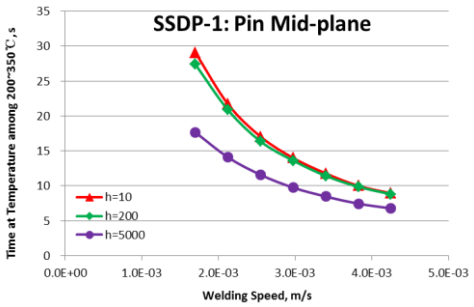

(c) SSDP-1: mid-plane

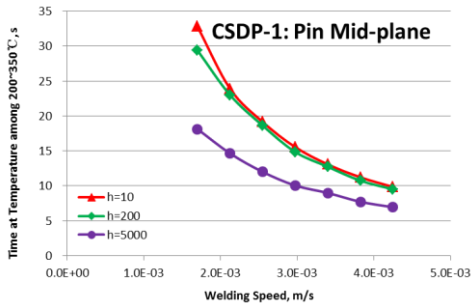

(d) CSDP-1: mid-plane

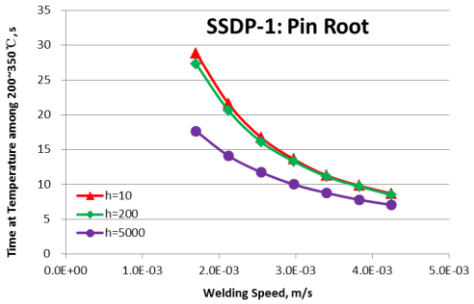

(e) SSDP-1: root

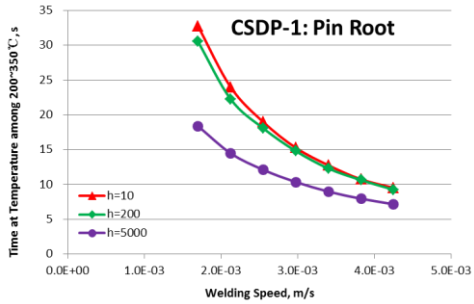

(f) CSDP-1: root

Figure 4.147 Time of T staying among 200~350˚C with different h: DP-1

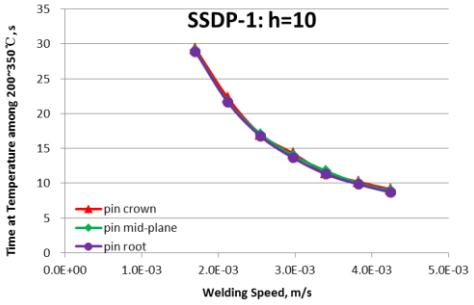

(a) SSDP-1: h=10

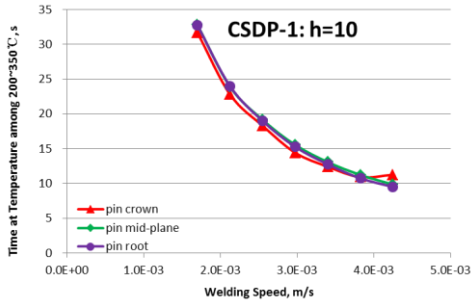

(b) CSDP-1: h=10

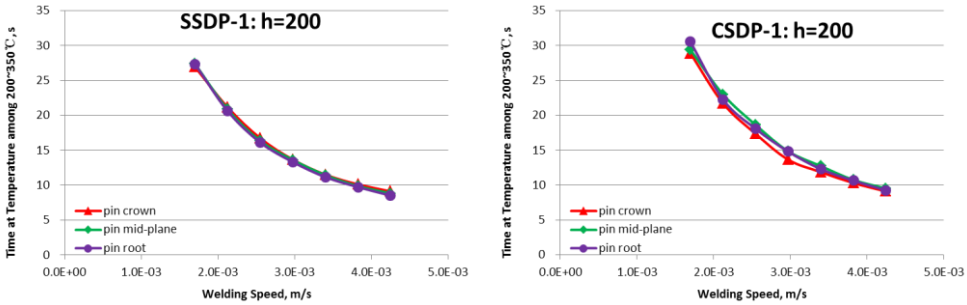

(c) SSDP-1: h=200 (d) CSDP-1: h=200

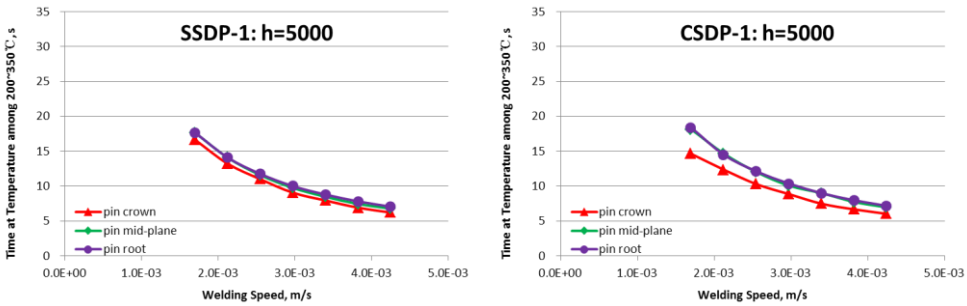

(e) SSDP-1: h=5000 (f) CSDP-1: h=5000

Figure 4.148 Time of T staying among 200~350℃ at various depths: DP-1

Figure 4.145 and Figure 4.146 show the time of T staying among 200~350℃ as a function of welding speed at various depths with different h applied at workpiece surface obtained from TPM model of SP joints. Figure 4.147 and Figure 4.148 show the time of temperature staying among 200~350℃ as a function of welding speed at various depths with different h applied at workpiece surface obtained from TPM model of DP-1 joints.

Figure 4.145~Figure 4.148 show that, in both SP and DP-1, with the same h, when welding speed increased, time of temperature staying among 200~350℃ decreased with decreasing slopes. Time decreased slower when higher h was applied. With the same welding speed, when h increased, time of temperature staying among 200~350℃ decreased, and the decreasing effect reduced when distance from weld crown increased.

4.5.6.4 Study 4: Effect of thermal conductivity of workpiece in W condition on thermal distribution and power of DP-2

In DPFSW, before the FSW process of the 1st pass, the whole workpiece is the base metal in T7 condition; after the FSW process of the 1st pass, material in the welded area of the workpiece has experienced intense mechanical and thermal cycles, considered as in the W condition, resulting in different thermal conductivities from the material in T7 condition under the same T. To simulate this change, the rectangular area (with the same area of the pin's cross section, the red area as shown in Figure 4.114c) underneath the pin is considered as in the W condition with different thermal conductivity K_w which is needed to be determined, while other area in the workpiece is considered as still in T7 condition. In this research, K_w (thermal conductivity in W condition) is assumed to be some certain value (ΔK) substracted from the K (thermal conductivity in T7 condition), which means $K_w=K-\Delta K$. ΔK varies from 0 to 100 W/(m K). For example, when ΔK equals to 20 W/(m K), then K_w is assumed to be 20 W/(m K) less than the K, which means $K_w=K-20=0.1265T+133.4$. In this research, in SSDP-2 and CSDP-2, the rectangular area (red area as shown in Figure 4.114c) underneath the pin is considered as in the W condition with different thermal conductivity K_w (ΔK varies from 0 to 100 W/(m K)), while other area in the workpiece is considered as still in T7 condition with the thermal conductivity of K.

Table 4.1 shows the summary of experimental control and response parameters of simulated joints. It shows that, in DP joints, under the same speeds, relative to DP-1, in DP-2, T at pin center is about 10℃ lower, while power is similar. FSW time recorded in the weld log shows that, there was enough time gap for the plate to cool down to ambient

T after the 1st pass weld and before the 2nd pass weld. The approximate 10℃ lower T at pin center of DP-2 is assumed to because of the change in thermal conductivity ΔK of the area underneath the pin. ΔK ranging from 0 to 100 W/(m·K) has been applied in the simulation model of DP-2 joints to investigate effect of change in thermal conductivity ΔK on T change and power in DP-2 relative to DP-1. Figure 4.149 (a) and (b) show the simulated T at pin center and power of DP joints as a function of ΔK, respectively.

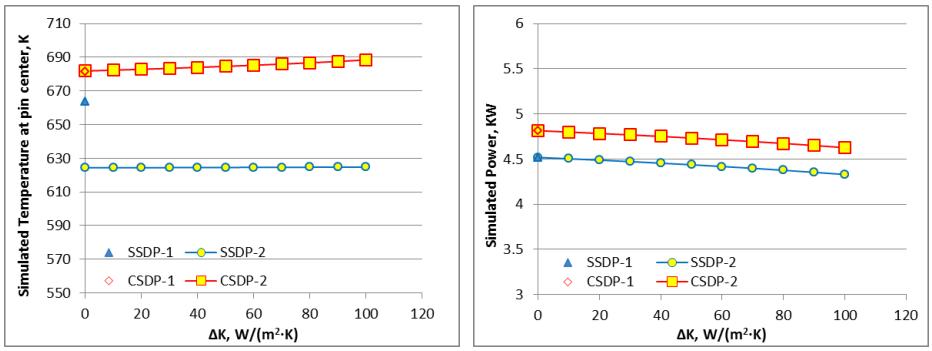

(a) Temperature at pin center (b) Power

Figure 4.149 Simulated T at pin center and power of DP joints as a function of ΔK

Figure 4.149 shows the simulated (a) T at pin center and (b) power of DP joints as a function of ΔK. It shows that, in SSDP, relative to DP-1, with the same speeds, in DP-2, simulated T at pin center is about 40℃ lower, while simulated power is similar; In CSDP, relative to DP-1, with the same speeds, in DP-2, simulated temperature at pin center and power are similar. It also shows that, in DP-2, with the decreasing of thermal conductivity of workpiece in W condition K_w (increasing of ΔK), simulated T at pin center was affected little, while simulated power decreased slightly. This study indicates that the change in thermal conductivity of workpiece in W condition is not the reason resulting about 10℃ lower T in DP-2 relative to DP-1. Some other possible factors like changes in flow stress, heat capacity and so on could be considered in future work to figure out the reason.

CHAPTER 5

SUMMARY, CONCLUSIONS AND FUTURE WORK

5.1 Summary

In this research, different thermal managements in FSW have been applied and investigated to further understand CSFSW and SSFSW mechanical and metallurgical process, produce high quality thick plate SSFSW joint on 7xxx aluminum alloys, as well as investigate the influence of control parameters, thermal distribution and history in welded joint's response parameters, metallurgical and mechanical properties. Thermal managements mainly include modifying thermal boundary conditions at the workpiece surface (in air or water spray) and underneath the workpiece (backing plates with different thermal conductivity) and adopting process variants like conventional shoulder (CS), stationary shoulder (SS), single pass (SP) and dual pass (DP).

Literature review has been presented in chapter 2 for depicting a thorough background and reviewing relevant studies in several aspects. First, basic background of FSW like history of invention and developments, process advantages and disadvantages relative to other joining technologies, process parameters, and weld microstructure are reviewed to provide this research work a general background. Then to offer a general idea about the crucial mechanism in FSW and how to tailor the process variables to obtain sound and defect-free weld joints depend on specific applications, effects of

primary control parameters (like tool rotation rate, travelling speed, and forge force) on response parameters (torque, temperature), thermal history and properties, effects of temperature and its transients on weld properties, as well as temperature measuring methods are reviewed. Thermal managements in FSW especially the modification of thermal boundary conditions are also reviewed to better understand the thermal managements applied in this research. Finally, state of the art of FSW modeling is reviewed to widen and deepen our understanding of simulation about FSW process.

Currently this research of FSW is mainly conducted by experiments, post experiment analysis and simulation. The experimental devices, procedures, materials (detailed chemistry compositions, general precipitation sequences and properties), procedures, welding setup, welding preparation, data acquisition, metallography sample preparation, and various testing methods used in this process are illustrated. In this research, FSW with various thermal managements and process variants in 24.9mm and 25.4mm thick AA7099-T7651 aluminum alloy plates has been produced and studied. To understand single pass FSW in different aluminum alloys, welds of 32mm thick AA7050-T7451 and 25.4mm thick AA6061-T651 aluminum alloy plates have also been investigated. Generally, different types of FSW process with different combinations of each thermal management are applied as follows: Conventional Shoulder Single Pass Half penetration (CSSPH) FSW, Stationary Shoulder Single Pass Half penetration (SSSPH) FSW, Conventional Shoulder Single Pass full penetration (CSSP) FSW, Stationary Shoulder Single Pass full penetration (SSSP) FSW, Conventional Shoulder Dual Pass full penetration (CSDP) FSW, and Stationary Shoulder Dual Pass full penetration (SSDP) FSW.

Weldability, macro and micro structure, effect of control parameters and thermal managements (CS&SS; WS&CBP; SP&DP) on response parameters and properties, influence of thermal distribution and history in welded joint metallurgical and mechanical properties are investigated and discussed in several categories: (a) CSSP and SSSP, (b) CSSPH and SSSPH, (c) CSDP and SSDP and (d) SSSP in different aluminum alloys. Comparison study is performed to further understand FSW mechanism in aluminum alloys.

5.2 Conclusions

By comprehensive analysis all the results from experiments and numerical simulations, several conclusions and trends are summarized and highlighted as following:

(1) Effects of speeds, process variants and TBCs on weldability, torque, power, temperature, time of temperature staying around 350℃, and strength:

a) Keeping other parameters the same, when rotation rate increased, weldability was improved, nugget boundaries become blurry, required forge force decreases, torque decreased with an decreasing slope, while power, temperature at pin center and grain size at center nugget increased, showing a plateau in power and probe temperature at high RPM.

b) Keeping other parameters the same, when welding speed increased, weldability decreased, required forge force and in plane forces increases, torque and power increased, while temperature at pin center decreased slightly. Time of temperature staying around 350℃ decreased, HAZ minimum hardness and thereby the UTS increased significantly.

c) Keeping other parameters the same, relative to CS, SS decreased the weldability especially in single pass full penetration FSW, decreased torque and power slightly, decreased temperature at pin center, affected time of temperature staying around 350℃ little, increased HAZ minimum hardness and thereby the UTS.

d) Keeping other parameters the same, relative to single pass full penetration FSW, the 1st and 2nd pass of dual pass FSW improved weldability significantly, decreased torque and power significantly, decreased temperature at pin center, decreased time of temperature staying around 350℃, increased HAZ minimum hardness and thereby the UTS.

e) Keeping other parameters the same, relative to FSW produced with the original TBCs (in air, with steel backing plate), the application of water spray (WS) increased torque and power, decreased temperature at pin center slightly, decreased time of temperature staying around 350℃, increased HAZ minimum hardness and thereby the UTS (7%).

f) Keeping other parameters the same, relative to FSW produced with the original TBCs (in air, with steel backing plate), the application of composite backing plate (CBP) increased torque and power, decreased temperature at pin center slightly, and affected the UTS little.

(2) Ways to improve the min hardness and thereby, the UTS of FSW joints in thick plate 7XXX alloys include:

a) Adopting dual pass full penetration (DP) FSW instead of single pass full penetration (SP) FSW: relative to SP, keeping other parameters the same, DP allows higher welding speed which increases the UTS; and remains the material at temperature around 350℃ relatively shorter, which will also benefit the joint strength.

b) Adopting stationary shoulder (SS) FSW which decreased temperature at pin center, increased HAZ minimum hardness and thereby the UTS.

c) Adopting the device of water spray (WS) to obtain higher cooling rate, which will result in larger HAZ minimum hardness and thereby joint strength.

(3) Advantages of DP relative to SP:

Relative to SP, DP allows higher speeds, decreases torque, power and T in each pass, and increases joint strength. DP also requires less on robust machinery due to smaller forces and torques required and generated during FSW.

(4) How much do tool shoulder and pin contribute to the total heat generation?

In CSFSW joints, power contribution from pin is not as small as most researchers claimed. On the contrary, in these welds, pin contribution to heat generation is significant and larger than shoulder. It's also worthy to note that, added heat from shoulder decreases the energy input from pin.

(5) Effects of stationary shoulder (SS) technique:

Relative to CS, SS enjoys advantages like producing better surface finish, avoiding overheating in SP, increasing UTS in DP, and improving

homogeneity in thermal distribution. SS also has several disadvantages like limiting application of higher speeds especially in SP, requiring larger forge force, then leading to larger in-plane forces (especially X forces). Relative to CS, SS affects torque and power little for a given IPM/RPM combination, and affects through thickness HV and microstructure little.

(6) In SSSPH, under the same forge force and rotating rate, pin feature had little influence in torque and power;

(7) In SSSP, compared with 0 °tilt, 1 °tilt can significantly eliminate defects on surface and inside the nugget, produce defect free welds by providing more consolidation/forge at back of the shoulder. In DP, compared with 0 °tilt, 1 °tilt has little effect on process parameters like required forge force, in-plane forces, torque, and power.

(8) The studied like thermal conductivity and flow stress of workpiece affect temperature at pin center slightly, while affect power at some extent.

(9) The change in thermal conductivity of workpiece in W condition is not the reason resulting about measured 10℃ lower temperature in DP-2 relative to DP-1.

(10) Compared with SSSP of AA7099 (and AA7050), SSSP of AA6061 allows much higher process speed, requires similar forge force, and leads to smaller in-plane forces, similar torque, larger power, temperature and then GS; Under the same forge force, when rotation rate increases, in SSSP of AA6061 torque decreases slower, power, then temperature and GS increased slower.

5.3 Recommendations for future Work

Based on above analysis and current understanding of FSW, future work is proposed as following: (1) fractography study to ascertain reason(s) for failure in specimens broken in longitudinal tensile testing, to ascertain whether the tested samples have been overheated, to ascertain reason(s) for about 10℃ difference in temperature at center NG in DP-1 and DP-2, and to study effects of different process variants employed in SPFSW like CS, SS, DP-1 and DP-2 on fracture, microstructure and properties, and (2) further calibration of TPM model by obtaining more accurate temperature dependent flow stress of AA7099-T7651; and investigation effects of TBC modification at WP bottom through simulation.

BIBLIOGRAPHY

[1] B. Irving, "Interest in welded aluminum automobiles gathers momentum worldwide: Aluminium welding," *Weld. J.*, vol. 77, no. 6, pp. 31–35, 1998.

[2] "Welding," *Wikipedia, the free encyclopedia*. 04-Dec-2015.

[3] M. R. Johnsen, "Friction stir welding takes off at Boeing," *Weld. J.*, vol. 78, no. 2, pp. 35–39, 1999.

[4] "Application of friction stir welding in the shipbuilding industry," 05-Dec-2015. [Online]. Available: http://www.twi-global.com/technical-knowledge/published-papers/application-of-friction-stir-welding-in-the-shipbuilding-industry-february-2000/. [Accessed: 05-Dec-2015].

[5] Holroyd, "Friction Stir Welding Applications & Uses," *Holroyd*, 05-Dec-2015. .

[6] P. Upadhyay and A. P. Reynolds, "Effects of thermal boundary conditions in friction stir welded AA7050-T7 sheets," *Mater. Sci. Eng. A*, vol. 527, no. 6, pp. 1537–1543, 2010.

[7] A. P. Reynolds, W. Tang, Z. Khandkar, J. A. Khan, and K. Lindner, "Relationships between weld parameters, hardness distribution and temperature history in alloy 7050 friction stir welds," *Sci. Technol. Weld. Join.*, vol. 10, no. 2, pp. 190–199, 2005.

[8] T. Long, W. Tang, and A. P. Reynolds, "Process response parameter relationships in aluminium alloy friction stir welds," *Sci. Technol. Weld. Join.*, vol. 12, no. 4, pp. 311–317, 2007.

[9] P. L. Threadgill, A. J. Leonard, H. R. Shercliff, and P. J. Withers, "Friction stir welding of aluminium alloys," *Int. Mater. Rev.*, vol. 54, no. 2, pp. 49–93, Mar. 2009.

[10] H. J. Zhang, H. J. Liu, and L. Yu, "Effect of Water Cooling on the Performances of Friction Stir Welding Heat-Affected Zone," *J. Mater. Eng. Perform.*, vol. 21, no. 7, pp. 1182–1187, Oct. 2011.

[11] X. Huang, J. Scheming, and A. P. Reynolds, "FSW of High Strength 7XXX Aluminum Using Four Process Variants," in *Friction Stir Welding and Processing VIII*, R. S. Mishra, M. W.honey, Y. Sato, and Y. Hovanski, Eds. John Wiley & Sons, Inc., 2015, pp. 89–98.

[12] P. L. Threadgill, "Terminology in friction stir welding," *Sci. Technol. Weld. Join.*, vol. 12, no. 4, pp. 357–360, May 2007.

[13] A. Oosterkamp, L. D. Oosterkamp, and A. Nordeide, "Kissing bond'phenomena in solid-state welds of aluminum alloys," *Weld. J.-N. Y.-*, vol. 83, no. 8, p. 225–S, 2004.

[14] R. F. Tylecote, *The Solid Phase Welding of Metals', St*. Martin's Press, New York, 1968.

[15] H. Lawrence and V. Vlack, "Elements of materials science and engineering," *Addison-Wesley*, 1975.

[16] R. LI, J. LI, J. XIONG, F. ZHANG, K. ZHAO, and C. JI, "Friction heat production and atom diffusion behaviors during Mg-Ti rotating friction welding process," *Trans. Nonferrous Met. Soc. China*, vol. 22, no. 11, pp. 2665–2671, Nov. 2012.
[17] S. W. Kallee, E. D. Nicholas, and W. M. Thomas, "Friction Stir Welding- Invention, Innovations and Applications," *Kei Kinzoku YosetsuJournal Light Met. Weld. Constr.*, vol. 43, no. 11, pp. 34–35, 2005.
[18] J. F. Hinrichs, J. S. Noruk, W. M. McDonald, and R. J. Heideman, "Challenges of Welding Aluminium Alloys for Automotive Structures," *Svetsaren*, vol. 50, no. 3, pp. 7–9, 1995.
[19] M. A. Sutton, A. P. Reynolds, D.-Q. Wang, and C. R. Hubbard, "A study of residual stresses and microstructure in 2024-T3 aluminum friction stir butt welds," *J. Eng. Mater. Technol.*, vol. 124, no. 2, pp. 215–221, 2002.
[20] R. S. Mishra and M. W. Mahoney, *Friction Stir Welding and Processing*. ASM International, 2007.
[21] A. Gerlich, P. Su, and T. H. North, "Peak temperatures and microstructures in aluminium and magnesium alloy friction stir spot welds," *Sci. Technol. Weld. Join.*, vol. 10, no. 6, pp. 647–652, 2005.
[22] W. J. Arbegast, "Friction stir welding after a decade of development," *Weld. J.*, vol. 85, no. 3, pp. 28–35, 2006.
[23] M. J. Peel, A. Steuwer, P. J. Withers, T. Dickerson, Q. Shi, and H. Shercliff, "Dissimilar friction stir welds in AA5083-AA6082. Part I: Process parameter effects on thermal history and weld properties," *Metall. Mater. Trans. A*, vol. 37, no. 7, pp. 2183–2193, Jul. 2006.
[24] A. P. Reynolds, "Flow visualization and simulation in FSW," *Scr. Mater.*, vol. 58, no. 5, pp. 338–342, Mar. 2008.
[25] J. Yan, M. A. Sutton, and A. P. Reynolds, "Process–structure–property relationships for nugget and heat affected zone regions of AA2524–T351 friction stir welds," *Sci. Technol. Weld. Join.*, vol. 10, no. 6, pp. 725–736, 2005.
[26] C. Blignault, D. G. Hattingh, G. H. Kruger, T. I. Van Niekerk, and M. N. James, "Friction stir weld process evaluation by multi-axial transducer," *Measurement*, vol. 41, no. 1, pp. 32–43, 2008.
[27] D. G. Hattingh, C. Blignault, T. I. Van Niekerk, and M. N. James, "Characterization of the influences of FSW tool geometry on welding forces and weld tensile strength using an instrumented tool," *J. Mater. Process. Technol.*, vol. 203, no. 1, pp. 46–57, 2008.
[28] E. Boldsaikhan, "The use of feedback forces for nondestructive evaluation of friction stir welding," South Dakota School of Mines and Technology, Rapid City, 2008.
[29] M. Song and R. Kovacevic, "Thermal modeling of friction stir welding in a moving coordinate system and its validation," *Int. J. Mach. Tools Manuf.*, vol. 43, no. 6, pp. 605–615, 2003.
[30] J. Ouyang, E. Yarrapareddy, and R. Kovacevic, "Microstructural evolution in the friction stir welded 6061 aluminum alloy (T6-temper condition) to copper," *J. Mater. Process. Technol.*, vol. 172, no. 1, pp. 110–122, 2006.
[31] A. Fehrenbacher, *Closed-loop control of temperature in friction stir welding*. Madison, 2008.

[32] P. Kalya, *Modeling and control of friction stir welding*. MISSOURI UNIVERSITY OF SCIENCE AND TECHNOLOGY, 2007.
[33] A. Kosugi, I. Matsuya, and I. Ihara, "Feasibility Study on Noncontact Monitoring of Temperature Distributions of Rotating Tool," in *Applied Mechanics and Materials*, 2013, vol. 372, pp. 336–339.
[34] W. Woo *et al.*, "In situ neutron diffraction measurements of temperature and stresses during friction stir welding of 6061-T6 aluminium alloy," *Sci. Technol. Weld. Join.*, vol. 12, no. 4, pp. 298–303, May 2007.
[35] M. W. Mahoney, C. G. Rhodes, J. G. Flintoff, W. H. Bingel, and R. A. Spurling, "Properties of friction-stir-welded 7075 T651 aluminum," *Metall. Mater. Trans. A*, vol. 29, no. 7, pp. 1955–1964, 1998.
[36] W. Tang, X. Guo, J. C. McClure, L. E. Murr, and A. Nunes, "Heat input and temperature distribution in friction stir welding," *J. Mater. Process. Manuf. Sci.*, vol. 7, pp. 163–172, 1998.
[37] Ø. Frigaard, Ø. Grong, and O. T. Midling, "A process model for friction stir welding of age hardening aluminum alloys," *Metall. Mater. Trans. A*, vol. 32, no. 5, pp. 1189–1200, 2001.
[38] Y. J. Kwon, N. Saito, and I. Shigematsu, "Friction stir process as a new manufacturing technique of ultrafine grained aluminum alloy," *J. Mater. Sci. Lett.*, vol. 21, no. 19, pp. 1473–1476, 2002.
[39] Y. S. Sato, M. Urata, and H. Kokawa, "Parameters controlling microstructure and hardness during friction-stir welding of precipitation-hardenable aluminum alloy 6063," *Metall. Mater. Trans. A*, vol. 33, no. 3, pp. 625–635, 2002.
[40] R. W. Fonda and S. G. Lambrakos, "Analysis of friction stir welds using an inverse problem approach," *Sci. Technol. Weld. Join.*, vol. 7, no. 3, pp. 177–181, 2002.
[41] Y. J. Chao, X. Qi, and W. Tang, "Heat transfer in friction stir welding—experimental and numerical studies," *J. Manuf. Sci. Eng.*, vol. 125, no. 1, pp. 138–145, 2003.
[42] C. M. Chen and R. Kovacevic, "Finite element modeling of friction stir welding—thermal and thermomechanical analysis," *Int. J. Mach. Tools Manuf.*, vol. 43, no. 13, pp. 1319–1326, Oct. 2003.
[43] K. A. Hassan, P. B. Prangnell, A. F. Norman, D. A. Price, and S. W. Williams, "Effect of welding parameters on nugget zone microstructure and properties in high strength aluminium alloy friction stir welds," *Sci. Technol. Weld. Join.*, vol. 8, no. 4, pp. 257–268, 2003.
[44] A. Simar, T. Pardoen, B. de Meester de Betzenbroeck, and others, "Influence of friction stir welding parameters on the power input and the temperature distribution in aluminium alloys," in *5th International Symposium on Friction Stir Welding*, 2004.
[45] W. M. Thomas and E. D. Nicholas, "Friction stir welding for the transportation industries," *Mater. Des.*, vol. 18, no. 4, pp. 269–273, 1997.
[46] K. J. Colligan, P. J. Konkol, J. J. Fisher, and J. R. Pickens, "Friction stir welding demonstrated for combat vehicle construction," *Weld. J.*, vol. 82, no. 3, pp. 34–40, 2003.
[47] S. Rajakumar, C. Muralidharan, and V. Balasubramanian, "Influence of friction stir welding process and tool parameters on strength properties of AA7075-T6 aluminium alloy joints," *Mater. Des.*, vol. 32, no. 2, pp. 535–549, Feb. 2011.

[48] A. Simar *et al.*, "A multiscale multiphysics investigation of aluminum friction stir welds," PhD Thesis, Universite Catholique De Louvain, Louvain-la-Neuve, Belgium, 2006.
[49] D. Rosenthal, "Mathematical theory of heat distribution during welding and cutting," *Weld. J.*, vol. 20, no. 5, p. 220s–234s, 1941.
[50] T. J. Lienert, W. L. Stellwag Jr, B. B. Grimmett, and R. W. Warke, "Friction stir welding studies on mild steel," *Weld. J.-N. Y.-*, vol. 82, no. 1, p. 1–S, 2003.
[51] J. L. Covington, "Experimental and numerical investigation of tool heating during friction stir welding," 2005.
[52] L. Cederqvist, "Friction stir welding of copper canisters using power and temperature control," Lund University, 2011.
[53] A. Fehrenbacher, N. A. Duffie, N. J. Ferrier, F. E. Pfefferkorn, and M. R. Zinn, "Toward automation of friction stir welding through temperature measurement and closed-loop control," *J. Manuf. Sci. Eng.*, vol. 133, no. 5, p. 51008, 2011.
[54] R. Brown, W. Tang, and A. P. Reynolds, "Multi-pass friction stir welding in alloy 7050-T7451: Effects on weld response variables and on weld properties," *Mater. Sci. Eng. A*, vol. 513, pp. 115–121, 2009.
[55] T. W. Nelson, R. J. Steel, and W. J. Arbegast, "In situ thermal studies and post-weld mechanical properties of friction stir welds in age hardenable aluminium alloys," *Sci. Technol. Weld. Join.*, vol. 8, no. 4, pp. 283–288, 2003.
[56] P. Upadhyay and A. P. Reynolds, "Thermal Management in Friction-Stir Welding of Precipitation-Hardened Aluminum Alloys," *JOM*, vol. 67, no. 5, pp. 1022–1031, 2015.
[57] C. B. Fuller, M. W. Mahoney, M. Calabrese, and L. Micona, "Evolution of microstructure and mechanical properties in naturally aged 7050 and 7075 Al friction stir welds," *Mater. Sci. Eng. A*, vol. 527, no. 9, pp. 2233–2240, 2010.
[58] A. J. Leonard, "Microstructure and ageing behaviour of FSWs in aluminium alloys 2014A-T651 and 7075-T651," in *Proc. 2nd Int. Symp. on Friction Stir Welding, Gothenburg, Sweden*, 2000.
[59] K. V. Jata, K. K. Sankaran, and J. J. Ruschau, "Friction-stir welding effects on microstructure and fatigue of aluminum alloy 7050-T7451," *Metall. Mater. Trans. A*, vol. 31, no. 9, pp. 2181–2192, 2000.
[60] Y. S. Sato, H. Kokawa, M. Enomoto, and S. Jogan, "Microstructural evolution of 6063 aluminum during friction-stir welding," *Metall. Mater. Trans. A*, vol. 30, no. 9, pp. 2429–2437, 1999.
[61] R. Y. Hwang and C. P. Chou, "The study on microstructural and mechanical properties of weld heat affected zone of 7075-T651 aluminum alloy," *Scr. Mater.*, vol. 38, no. 2, pp. 215–221, 1997.
[62] D. Godard, P. Archambault, E. Aeby-Gautier, and G. Lapasset, "Precipitation sequences during quenching of the AA 7010 alloy," *Acta Mater.*, vol. 50, no. 9, pp. 2319–2329, 2002.
[63] J.-Q. Su, T. W. Nelson, R. Mishra, and M. Mahoney, "Microstructural investigation of friction stir welded 7050-T651 aluminium," *Acta Mater.*, vol. 51, no. 3, pp. 713–729, 2003.
[64] G. Sha and A. Cerezo, "Early-stage precipitation in Al–Zn–Mg–Cu alloy (7050)," *Acta Mater.*, vol. 52, no. 15, pp. 4503–4516, 2004.

[65] L.-E. Svensson, L. Karlsson, H. Larsson, B. Karlsson, M. Fazzini, and J. Karlsson, "Microstructure and mechanical properties of friction stir welded aluminium alloys with special reference to AA 5083 and AA 6082," *Sci. Technol. Weld. Join.*, vol. 5, no. 5, pp. 285–296, 2000.
[66] J.-Q. Su, T. W. Nelson, and C. J. Sterling, "Microstructure evolution during FSW/FSP of high strength aluminum alloys," *Mater. Sci. Eng. A*, vol. 405, no. 1, pp. 277–286, 2005.
[67] M. Dumont, A. Steuwer, A. Deschamps, M. Peel, and P. J. Withers, "Microstructure mapping in friction stir welds of 7449 aluminium alloy using SAXS," *Acta Mater.*, vol. 54, no. 18, pp. 4793–4801, 2006.
[68] P. Upadhyay, "Thermal management in friction stir welding of aluminum alloys," UNIVERSITY OF SOUTH CAROLINA, 2012.
[69] R. S. Mishra and Z. Y. Ma, "Friction stir welding and processing," *Mater. Sci. Eng. R Rep.*, vol. 50, no. 1–2, pp. 1–78, Aug. 2005.
[70] C. H. Martens, "weld strengthening process," 3282748, Nov-1966.
[71] S. Benavides, Y. Li, L. E. Murr, D. Brown, and J. C. McClure, "Low-temperature friction-stir welding of 2024 aluminum," *Scr. Mater.*, vol. 41, no. 8, pp. 809–815, Sep. 1999.
[72] S. Benavides, "Low-temperature friction-stir welding," *ETD Collect. Univ. Tex. El Paso*, pp. 1–77, Jan. 2000.
[73] E. M. van der Aa, M. J. M. Hermans, I. M. Richardson, N. M. van der Pers, and R. Delhez, "Experimental study of the influence of a trailing heat sink on the welding residual stress distribution," in *Materials science forum*, 2006, vol. 524, pp. 479–484.
[74] D. G. Richards, P. B. Prangnell, P. J. Withers, S. W. Williams, T. Nagy, and S. Morgan, "Efficacy of active cooling for controlling residual stresses in friction stir welds," *Sci. Technol. Weld. Join.*, vol. 15, no. 2, pp. 156–165, 2010.
[75] P. Staron, M. Koçak, and S. Williams, "Residual stresses in friction stir welded Al sheets," *Appl. Phys. A*, vol. 74, no. 1, pp. s1161–s1162, Dec. 2002.
[76] G. Luan, G. Li, C. Li, and C. Dong, "DC-LSND friction stir welding," in *7th International Friction Stir Welding Symposium, Osaka*, 2008.
[77] D. Sakurada, K. Katoh, and H. Tokisue, "Underwater friction welding of 6061 aluminum alloy," *J.-Jpn. Inst. LIGHT Met.*, vol. 52, no. 1, pp. 2–6, 2002.
[78] J.-Q. Su, T. W. Nelson, and C. J. Sterling, "Friction stir processing of large-area bulk UFG aluminum alloys," *Scr. Mater.*, vol. 52, no. 2, pp. 135–140, 2005.
[79] D. C. Hofmann and K. S. Vecchio, "Submerged friction stir processing (SFSP): An improved method for creating ultra-fine-grained bulk materials," *Mater. Sci. Eng. A*, vol. 402, no. 1, pp. 234–241, 2005.
[80] L. Fratini, G. Buffa, and R. Shivpuri, "In-process heat treatments to improve FS-welded butt joints," *Int. J. Adv. Manuf. Technol.*, vol. 43, no. 7–8, pp. 664–670, 2009.
[81] M. Hosseini and H. D. Manesh, "Immersed friction stir welding of ultrafine grained accumulative roll-bonded Al alloy," *Mater. Des.*, vol. 31, no. 10, pp. 4786–4791, 2010.
[82] T. Bloodworth, "On the immersed friction stir welding of AA6061-T6: a metallurgic and mechanical comparison to friction stir welding," Vanderbilt University, 2009.

[83] K. J. Colligan, *Friction stir welding with simultaneous cooling*. Google Patents, 2003.
[84] G. Kohn, Y. Greenberg, I. Makover, and A. Munitz, "Laser-assisted friction stir welding," *Weld. J.-N. Y.-*, vol. 81, no. 2, pp. 46–46, 2002.
[85] B. Cabage, "New way to weld," *Oak Ridge Natl. Lab. Report.*, no. 84, 2006.
[86] P. Sinclair, "Heated friction stir welding: an investigation into how preheating aluminum 6061 affects process forces," Vanderbilt University, 2009.
[87] M. J. C. Rosales, N. G. Alcantara, J. Santos, and R. Zettler, "The backing bar role in heat transfer on aluminium alloys friction stir welding," in *Materials Science Forum*, 2010, vol. 636, pp. 459–464.
[88] P. Su, A. Gerlich, T. H. North, and G. J. Bendzsak, "Energy utilisation and generation during friction stir spot welding," *Sci. Technol. Weld. Join.*, vol. 11, no. 2, pp. 163–169, 2006.
[89] D. Bakavos and P. B. Prangnell, "Effect of reduced or zero pin length and anvil insulation on friction stir spot welding thin gauge 6111 automotive sheet," *Sci. Technol. Weld. Join.*, vol. 14, no. 5, pp. 443–456, 2009.
[90] H. Wu, Y. C. Chen, D. Strong, and P. Prangnell, "Assessment of the Advantages of Static Shoulder FSW for Joining Aluminium Aerospace Alloys," *Mater. Sci. Forum*, vol. 783–786, pp. 1770–1775, May 2014.
[91] H. Schmidt, J. Hattel, and J. Wert, "An analytical model for the heat generation in friction stir welding," *Model. Simul Mater Sci Eng*, vol. 12, pp. 143–157, Jan. 2004.
[92] Y. J. Chao, S. Liu, and C.-H. Chien, "Friction stir welding of al 6061-T6 thick plates: Part II-numerical modeling of the thermal and heat transfer phenomena," *J. Chin. Inst. Eng.*, vol. 31, no. 5, pp. 769–779, 2008.
[93] Shercliff HR, Colegrove PA; Chapter 10: Process Modeling. In Friction Stir Welding and Processing, Rajiv SM, Mahoney MW (Editors), ASM International, 2007.
[94] M. Z. H. Khandkar, J. A. Khan, and A. P. Reynolds, "Prediction of temperature distribution and thermal history during friction stir welding: input torque based model," *Sci. Technol. Weld. Join.*, vol. 8, no. 3, pp. 165–174, Jun. 2003.
[95] C. T. Canaday, M. A. Moore, W. Tang, and A. P. Reynolds, "Through thickness property variations in a thick plate AA7050 friction stir welded joint," *Mater. Sci. Eng. A*, vol. 559, pp. 678–682, Jan. 2013.
[96] P. Upadhyay and A. Reynolds, "Effect of Backing Plate Thermal Property on Friction Stir Welding of 25-mm-Thick AA6061," *Metall. Mater. Trans. A*, vol. 45, no. 4, pp. 2091–2100, Nov. 2013.
[97] D. M. Neto and P. Neto, "Numerical modeling of friction stir welding process: a literature review," *Int. J. Adv. Manuf. Technol.*, vol. 65, no. 1–4, pp. 115–126, 2013.
[98] M. J. Russell, C. Blignault, N. L. Horrex, and C. S. Wiesner, "Recent developments in the friction stir welding of titanium alloys," *Weld. World*, vol. 52, no. 9–10, pp. 12–15, 2008.
[99] H. J. Liu, J. Q. Li, and W. J. Duan, "Friction stir welding characteristics of 2219-T6 aluminum alloy assisted by external non-rotational shoulder," *Int. J. Adv. Manuf. Technol.*, vol. 64, no. 9–12, pp. 1685–1694, 2013.
[100] H. Wu, Y.-C. Chen, D. Strong, and P. Prangnell, "Stationary shoulder FSW for joining high strength aluminum alloys," *J. Mater. Process. Technol.*, vol. 221, pp. 187–196, 2015.

[101] Md. Reza-E-Rabby. QUANTIFICATION OF THE EFFECT OF TOOL GEOMETRIC FEATURES ON ASPECTS OF FRICTION STIR WELDING. University of South Carolina, 2015.
[102] W. M. Thomas, E. D. Nicholas, J. C. Needhan, M. G. Murch, P. Temple-Smith, and C. J. Dawes, "International patent application PCT/GB92/02203 and GB patent application 9125978.8," *UK Pat. Off. Lond.*, vol. 6, 1991.
[103] H. B. Schmidt and J. H. Hattel, "Thermal modelling of friction stir welding," *Scr. Mater.*, vol. 58, no. 5, pp. 332–337, 2008.
[104] J. Hilgert, H. N. B. Schmidt, J. F. Dos Santos, and N. Huber, "Thermal models for bobbin tool friction stir welding," *J. Mater. Process. Technol.*, vol. 211, no. 2, pp. 197–204, 2011.
[105] R. Nandan, G. G. Roy, and T. Debroy, "Numerical simulation of three-dimensional heat transfer and plastic flow during friction stir welding," *Metall. Mater. Trans. A*, vol. 37, no. 4, pp. 1247–1259, 2006.
[106] R. Nandan, B. Prabu, A. De, and T. Debroy, "Improving reliability of heat transfer and materials flow calculations during friction stir welding of dissimilar aluminum alloys," *Weld. J.-N. Y.-*, vol. 86, no. 10, p. 313, 2007.
[107] P. Ulysse, "Three-dimensional modeling of the friction stir-welding process," *Int. J. Mach. Tools Manuf.*, vol. 42, no. 14, pp. 1549–1557, 2002.
[108] P. A. Colegrove and H. R. Shercliff, "Experimental and numerical analysis of aluminium alloy 7075-T7351 friction stir welds," *Sci. Technol. Weld. Join.*, vol. 8, no. 5, pp. 360–368, 2003.
[109] P. A. Colegrove, H. R. Shercliff, and R. Zettler, "Model for predicting heat generation and temperature in friction stir welding from the material properties," *Sci. Technol. Weld. Join.*, vol. 12, no. 4, pp. 284–297, 2007.
[110] X. Deng and S. Xu, "Two-dimensional finite element simulation of material flow in the friction stir welding process," *J. Manuf. Process.*, vol. 6, no. 2, pp. 125–133, 2004.
[111] M. Song and R. Kovacevic, "Heat transfer modelling for both workpiece and tool in the friction stir welding process: a coupled model," *Proc. Inst. Mech. Eng. Part B J. Eng. Manuf.*, vol. 218, no. 1, pp. 17–33, 2004.
[112] Maxime BARRA, Understanding and simulation of the heat flow during FSW - Effect of the forge force and of the alloy , report.
[113] W.J. Arbegast. Modeling friction stir joining as a metal working process. In Z Jin, editor, Hot deformation of aluminum alloys III: 2003 TMS Annual Meeting, San Diego, California, March 2-6, 2003. Minerals, Metals and Materials Society, 2003.
[114] G. G. Roy, R. Nandan, and T. DebRoy, "Dimensionless correlation to estimate peak temperature during friction stir welding," *Sci. Technol. Weld. Join.*, vol. 11, no. 5, pp. 606–608, Sep. 2006.
[115] N. Balasubramanian, B. Gattu, and R. S. Mishra, "Process forces during friction stir welding of aluminium alloys," *Sci. Technol. Weld. Join.*, vol. 14, no. 2, pp. 141–145, Feb. 2009.
[116] Prabhanjana Kalya, K Krishnamurthy, and R Mishra. Specific energy and temperaturemechanisticmodelsforfrictionstirprocessingofAL-F357. InRajivS.Mishra, Murray W. Mahoney, and Thomas J. Lienert, editors, Friction stir welding and

processing IV: proceedings TMS 2007 Annual Meeting & Exhibition,. John Wiley & Sons, Orlando, Florida, USA, May 2007.
[117] A. P. Reynolds and Maxime Barra. Addition of the forge force effect in simulation of FSW by the thermal pseudo-mechanical model, 2011.
[118] Henrick Schmidt. Modeling of Thermomechanical Condition in Friction stir welding. Ph.D. thesis, Department of Manufacturing Engineering and Management,DTU,Denmark, 2004.
[119] Rajiv Mishra, Hugh R Shercliff, Paul A Colegrove, and Mahoney Murrey. Process modelling. In Handbook of aluminum: Alloy production and materials manufacturing, pages 187–218. CRC Press, April 2003.
[120] Mir Zahedul Huq Khandkar. Thermo-Mechanical Modeling of friction stir welding. PhD thesis, Univeristy of South Carolina, Columbia SC, 2005.
[121] A. Arora, R. Nandan, A. P. Reynolds, and T. DebRoy, "Torque, power requirement and stir zone geometry in friction stir welding through modeling and experiments," *Scr. Mater.*, vol. 60, no. 1, pp. 13–16, Jan. 2009.
[122] P. A. Colegrove and H. R. Shercliff, "Development of Trivex friction stir welding tool Part 2 – three-dimensional flow modelling," *Sci. Technol. Weld. Join.*, vol. 9, no. 4, pp. 352–361, Aug. 2004.
[123] Online materials information resource of AA7099-T7651 – KaiserSelect – https://online.kaiseraluminum.com/
[124] Online materials information resource of AA6061-T6 – MatWeb. http://asm.matweb.com/.
[125] Online materials information resource of AA7050-T7451 – MatWeb. http://asm.matweb.com/.
[126] Aluminum Alloys –Effects of Alloying Elements –Total Materia. http://www.totalmateria.com/.
[127] Online materials information resource of AA7050 – Kaiser Aluminum – https://kaiseraluminum.com/.
[128] N. A. Belov, D. G. Eskin, and A. A. Aksenov, *Multicomponent phase diagrams: applications for commercial aluminum alloys: applications for commercial aluminum alloys*. Elsevier, 2005.
[129] L. Backerud, G. Chai, and J. Tamminen, "Solidification Characteristics of Aluminum Alloys. Vol. 2. Foundry Alloys," *Am. Foundrymens Soc. Inc 1990*, p. 266, 1990.
[130] I. Dutta and S. M. Allen, "A calorimetric study of precipitation in commercial aluminium alloy 6061," *J. Mater. Sci. Lett.*, vol. 10, no. 6, pp. 323–326, 1991.
[131] G. A. Edwards, K. Stiller, G. L. Dunlop, and M. J. Couper, "The precipitation sequence in Al–Mg–Si alloys," *Acta Mater.*, vol. 46, no. 11, pp. 3893–3904, 1998.
[132] R. P. Wahi and M. Von Heimendahl, "On the Occurrence of the Metastable Phase β″ in an Al Si Mg Alloy," *Phys. Status Solidi A*, vol. 24, no. 2, pp. 607–612, Aug. 1974.
[133] J. P. Lynch, L. M. Brown, and M. H. Jacobs, "Microanalysis of age-hardening precipitates in aluminium alloys," *Acta Metall.*, vol. 30, no. 7, pp. 1389–1395, Jul. 1982.

[134] G. B. Burger, A. K. Gupta, P. W. Jeffrey, and D. J. Lloyd, "Microstructural control of aluminum sheet used in automotive applications," *Mater. Charact.*, vol. 35, no. 1, pp. 23–39, 1995.
[135] M. H. Jacobs, "The structure of the metastable precipitates formed during ageing of an Al-Mg-Si alloy," *Philos. Mag.*, vol. 26, no. 1, pp. 1–13, 1972.
[136] D. J. Chakrabarti and D. E. Laughlin, "Phase relations and precipitation in Al–Mg–Si alloys with Cu additions," *Prog. Mater. Sci.*, vol. 49, no. 3, pp. 389–410, 2004.
[137] S. Esmaeili, X. Wang, D. J. Lloyd, and W. J. Poole, "On the precipitation-hardening behavior of the Al-Mg-Si-Cu alloy AA6111," *Metall. Mater. Trans. A*, vol. 34, no. 3, pp. 751–763, 2003.
[138] C. Gallais, A. Denquin, Y. Bréchet, and G. Lapasset, "Precipitation microstructures in an AA6056 aluminium alloy after friction stir welding: characterisation and modelling," *Mater. Sci. Eng. A*, vol. 496, no. 1, pp. 77–89, 2008.
[139] W. F. Miao and D. E. Laughlin, "Effects of Cu content and preaging on precipitation characteristics in aluminum alloy 6022," *Metall. Mater. Trans. A*, vol. 31, no. 2, pp. 361–371, 2000.
[140] M. Tamizifar and G. W. Lorimer, "Aluminum alloys: their physical and mechanical properties," in *Proc. 3rd Int. Conf. Aluminum, edited by L. Arnberg, O. Lohne, E. Nes and N. Ryum*, 1992, vol. 1, p. 220.
[141] D. K. Chatterjee and K. M. Entwistle, "A Study of the Effect of Magnesium Loss and of the Addition of Copper on the Aging of Aluminum-Magnesium-Silicon Alloys," *J Inst Met Feb 1973 101 53-59*, 1973.
[142] R. J. Livak, "The Effects of Copper and Chromium on the Aging Response of Dilute Al-Mg-Si Alloys," *Metall. Mater. Trans. A*, vol. 13, no. 7, pp. 1318–1321, 1982.
[143] H. Suzuki, M. Kanno, and G. Itoh, "A Consideration on Two-Step Aging in Al–Mg–Si Alloy," *J. Jpn. Inst. Light Met.*, vol. 30, no. 11, pp. 609–6616, 1980.
[144] T. Sakurai and T. Eto, "Aluminum alloys: their physical and mechanical properties," in *Proc. 3rd Int. Conf. Aluminum, edited by L. Arnberg, O. Lohne, E. Nes and N. Ryum (Norwegian Institute of Technology and SINTEF Metallurgy, Trondheim, 1992) Vol*, 1992, vol. 1, p. 208.
[145] D. J. Chakrabarti, B. K. Cheong, D. E. Laughlin, and S. K. Das, "Automotive alloys II," in *Proc. TMS Annual Meeting, San Antonio, TX, ed. Subodh K. Das,(TMS, Warrendale, 1998) pp*, 1998, pp. 27–44.
[146] S. D. Dumolt, D. E. Laughlin, and J. C. Williams, "Formation of a modified β′ phase in aluminum alloy 6061," *Scr. Metall.*, vol. 18, no. 12, pp. 1347–1350, 1984.
[147] L. Sagalowicz, G. Hug, D. Bechet, P. Sainfort, and G. Lapasset, "A study of the structural precipitation in the Al-Mg-Si-Cu system," in *Proceedings of the 4th International Conference on Aluminum Alloys*, 1994.
[148] P. Lequeu, K. P. Smith, and A. Daniélou, "Aluminum-copper-lithium alloy 2050 developed for medium to thick plate," *J. Mater. Eng. Perform.*, vol. 19, no. 6, pp. 841–847, 2010.
[149] ASTM: '*Standard Test Method for Determining Average Grain Size*', in 'Annual Book of ASTM Standard Section 3: Metals Test Method and Analytical Procedure', 313-338; 2007, PA, USA, ASTM International.

[150] ASTM International and American Society for Testing & Materials. *Standard test method for microindentation hardness of materials*. In Annual Book of ASTM Standards: Section Three: Metals Test Methods and Analytical Procedures, pages 487–507. American Society for Testing & Materials, 2007.
[151] ASTM E290-97a, *Standard Test Method for Bend Testing of Material for Ductility*, ASTM International, West Conshohocken, PA, 1997, www.astm.org
[152] M. A. Sutton, J. J. Orteu, and H. Schreier, *Image correlation for shape, motion and deformation measurements: basic concepts, theory and applications*. Springer Science & Business Media, 2009.
[153] C. Solutions, "Vic 2D reference manual," *Correl. Solut. Columbia*, 2009.
[154] ASTM International and American Society for Testing & Materials. *Standard Test Methods of Tension Testing of Metallic Materials*. In Annual Book of ASTM Standards: Section Three: Metals Test Methods and Analytical Procedures, pages 137. American Society for Testing & Materials, 1991.
[155] W. Cheng and I. Finnie, "The crack compliance method for residual stress measurement," *Weld. World*, vol. 28, no. 5, pp. 103–110, 1990.
[156] H.-J. Schindler, W. Cheng, and I. Finnie, "Experimental determination of stress intensity factors due to residual stresses," *Exp. Mech.*, vol. 37, no. 3, pp. 272–277, 1997.
[157] M. B. Prime, "Residual stress measurement by successive extension of a slot: the crack compliance method," *Appl. Mech. Rev.*, vol. 52, no. 2, pp. 75–96, 1999.
[158] H.-J. Schindler, "Experimental determination of crack closure by the cut compliance technique," *ASTM Spec. Tech. Publ.*, vol. 1343, pp. 175–190, 1999.
[159] A. International, *Standard Test Method for Measurement of Fatigue Crack Growth Rates*. ASTM International, 2011.
[160] E. Committee and others, "Test Method for Linear-Elastic Plane-Strain Fracture Toughness KIc of Metallic Materials," *ASTM Int.*, 2009.

APPENDIX A - SUMMARY OF FSW TOOL PARAMETERS

Tool No.	FSW	θ , °	Pin Feature	D_1, mm	Pin Material
1-1	SSSPH	8	T+3F	1.35	H-13
1-2	CSDP	8	T+3F	1.35	H-13
1-3	CSDP	8	T+3F	1.35	H-13
2	SSSPH	8	T+3C	1.35	MP-159
3	SSSPH&DP	8	T+3CT	1.35	MP-159
4	CSSPH	8	T+3F	1.35	MP-159
5-1	SSSP	9	T+3F	1.65	MP-159
5-2	SSSP	9	T+3F	1.40	MP-159
5-3	SSSP	9	T+3F	0.89	MP-159
5-4	CSSP	9	T+3F	0.89	MP-159
6	SSSP	8	T+3CT	0.89	MP-159
7-1	SSSP	8	T+3CT	1.65	MP-159
7-2	SSSP	8	T+3CT	1.35	MP-159
8	CSDP	8	T+3CT	1.35	H-13
Tool No.	D_2, mm	D_3, mm	D_4, mm	L, mm	Thread Pitch, mm
1-1	31.75	15.88	12.31	12.7	2.12
1-2	31.75	15.88	12.31	12.7	2.12
1-3	25.4	15.88	12.31	12.7	2.12
2	31.75	15.88	12.31	12.7	2.12
3	31.75	15.88	12.31	12.7	2.12
4	25.4	15.88	12.31	12.7	2.12
5-1	31.75	19.05	11.13	25.0	1.75
5-2	31.75	19.05	11.13	25.0	1.75
5-3	31.75	19.05	11.13	25.0	1.75
5-4	35.56	19.05	11.13	25.0	1.75
6	31.75	19.05	12.01	25.0	1.75
7-1	31.75	19.05	12.01	25.0	1.75
7-2	31.75	19.05	12.01	25.0	1.75
8	25.4	15.88	12.31	12.7	2.12

θ : Taper Angle of pin; D_1: Flat/Flute Depth; D_2: Shoulder Diameter;
D_3: Pin Top Diameter; D_4: Pin Tip Diameter; L: Pin Length

APPENDIX B - SUMMARY OF TBCS AND FSW CONTROL PARAMETERS

Weld No.	Alloy	FSW	Back Plate	Water Spray	Tool No.	Rotating Speed, RPM	Welding Speed, mm/min	Forge Force, KN
3957A	7099	SSSPH	Steel	No	1-1	500	102	46.7
3957B	7099	SSSPH	Steel	No	1-1	400	102	53.4
3957C	7099	SSSPH	Steel	No	1-1	300	102	55.6
3957D	7099	SSSPH	Steel	No	1-1	200	102	55.6
3958A	7099	SSSPH	Steel	No	1-1	300	102	64.5
3958B	7099	SSSPH	Steel	No	1-1	200	102	64.5
3958C	7099	SSSPH	Steel	No	1-1	160	102	64.5
3960A	7099	SSSPH	Steel	No	3	300	102	64.5
3960B	7099	SSSPH	Steel	No	3	200	102	64.5
3960C	7099	SSSPH	Steel	No	3	160	102	64.5
3961A	7099	SSSPH	Steel	No	2	300	102	64.5
3961B	7099	SSSPH	Steel	No	2	200	102	64.5
3961C	7099	SSSPH	Steel	No	2	160	102	64.5
4094A	7099	CSSPH	Steel	No	4	240	102	33.4
4094B	7099	CSSPH	Steel	No	4	200	102	37.8
4094C	7099	CSSPH	Steel	No	4	160	102	40
4098A	7099	CSSPH	Steel	No	N/A	240	102	28.9
4098B	7099	CSSPH	Steel	No	N/A	200	102	33.4
4098C	7099	CSSPH	Steel	No	N/A	160	102	37.8
4227A	7099	CSSPH	Steel	No	8	320	203	46.7
4227B	7099	CSSPH	Steel	No	8	240	203	57.8
3963A	7099	SSSP	Steel	No	5-3	200	51	73.4
3963B	7099	SSSP	Steel	No	5-3	160	51	73.4
3964A	7099	SSSP	Steel	No	5-2	300	51	73.4
3964B	7099	SSSP	Steel	No	5-2	200	51	73.4
3964C	7099	SSSP	Steel	No	5-2	160	51	73.4
3965A	7099	SSSP	Steel	No	5-1	200	51	71.2
3965B	7099	SSSP	Steel	No	5-1	160	51	71.2
3973A	7099	SSSP	Steel	No	7-2	200	51	69.0

3973B	7099	SSSP	Steel	No	7-2	160	51	69.0
3974A	7099	SSSP	Steel	No	7-2	300	51	69.0
3974B	7099	SSSP	Steel	No	7-2	240	51	69.0
3975A	7099	SSSP	Steel	No	7-1	240	51	69.0
3975B	7099	SSSP	Steel	No	7-1	200	51	69.0
4106A	7099	SSSP	Steel	No	7-1	120	51	69.0
4106B	7099	SSSP	Steel	No	7-1	80	25	69.0
4107A	7099	SSSP	Steel	No	5-1	120	51	77.8
4107B	7099	SSSP	Steel	No	5-1	80	25	82.3
4114	7099	SSSP	Steel	No	7-1	200	51	69.0
4115	7099	SSSP	Steel	No	5-1	200	51	69.0
4116	7099	SSSP	Steel	No	7-1	160	51	69.0
4167A	7099	SSSP	Steel	No	6	200	51	69.0
4167B	7099	SSSP	Steel	No	6	160	51	69.0
4167C	7099	SSSP	Steel	No	6	120	51	69.0
4171A	7099	SSSP	Steel	No	6	160	51	62.3
4171B	7099	SSSP	Steel	No	6	160	51	53.4
4171C	7099	SSSP	Steel	No	6	160	51	44.5
4171D	7099	SSSP	Steel	No	6	160	51	35.6
4306	7099	SSSP	Steel	No	6	160	51	62.3
4153A	7099	CSSP	Steel	No	5-4	200	51	48.9
4153B	7099	CSSP	Steel	No	5-4	160	51	48.9
4153C	7099	CSSP	Steel	No	5-4	120	51	48.9
4154A	7099	CSSP	Steel	No	5-4	100	51	53.4
4154B	7099	CSSP	Steel	No	5-4	80	51	53.4
4154C	7099	CSSP	Steel	No	5-4	120	102	64.5
4155A	7099	CSSP	Steel	No	5-4	180	102	60.1
4155B	7099	CSSP	Steel	No	5-4	160	102	60.1
4155C	7099	CSSP	Steel	No	5-4	140	102	64.5
4155D	7099	CSSP	Steel	No	5-4	100	102	73.4
4156A	7099	CSSP	Steel	No	5-4	100	51	55.6
4156B	7099	CSSP	Steel	No	5-4	120	102	66.7
4163	7099	CSSP	Composite	Yes	5-4	100	102	57.8
4164	7099	CSSP	Composite	Yes	5-4	160	102	82.3
4165	7099	CSSP	Composite	No	5-4	160	102	64.5
4166	7099	CSSP	Steel	Yes	5-4	160	102	77.8
4299	7099	CSSP	Steel	No	5-4	160	51	46.7
4315	7099	CSSP	Steel	No	5-4	160	51	55.6
4300	7099	CSSP	Steel	No	5-4	160	102	66.7
4309	7099	SSDP-1	Steel	No	3	160	102	35.8
4311	7099	SSDP-2	Steel	No	3	160	102	35.8
4310	7099	SSDP-1	Steel	No	3	200	203	43.5
4312	7099	SSDP-2	Steel	No	3	200	203	43.5
4226A	7099	CSDP-1	Steel	No	8	200	102	40
4226B	7099	CSDP-1	Steel	No	8	160	102	44.5

4228A	7099	CSDP-2	Steel	No	8	240	152	44.5
4228B	7099	CSDP-2	Steel	No	8	180	152	46.7
4229	7099	CSDP-1	Steel	No	8	160	102	40
4230	7099	CSDP-2	Steel	No	8	160	102	40
4231	7099	CSDP-2	Steel	No	8	160	102	37.8
4232A	7099	CSDP-1	Steel	No	1-3	160	152	48.9
4232B	7099	CSDP-1	Steel	No	1-3	200	203	53.4
4233A	7099	CSDP-2	Steel	No	1-3	160	152	46.7
4233B	7099	CSDP-2	Steel	No	1-3	200	203	51.2
4237	7099	CSDP-1	Steel	Yes	1-3	200	203	53.4
4238	7099	CSDP-2	Steel	Yes	1-3	200	203	48.9
4241	7099	CSDP-1	Steel	No	1-2	200	203	57.8
4242	7099	CSDP-2	Steel	No	1-2	200	203	55.6
4243	7099	CSDP-1	Steel	Yes	1-2	200	203	55.6
4244	7099	CSDP-2	Steel	Yes	1-2	200	203	55.6
4302	7099	CSDP-1	Steel	No	1-3	160	102	42.3
4304	7099	CSDP-2	Steel	No	1-3	160	102	40
4301	7099	CSDP-1	Steel	No	1-3	200	203	55.6
4303	7099	CSDP-2	Steel	No	1-3	200	203	53.4
3966A	7050	SSSP	Steel	No	5-1	200	51	66.7
3966B	7050	SSSP	Steel	No	5-1	160	51	66.7
4168A	6061	SSSP	Steel	No	6	480	203	66.7
4168B	6061	SSSP	Steel	No	6	400	203	66.7
4169	6061	SSSP	Steel	No	6	320	203	66.7
4170A	6061	SSSP	Steel	No	6	320	203	62.3
4170B	6061	SSSP	Steel	No	6	320	203	53.4
4170C	6061	SSSP	Steel	No	6	320	203	44.5
4170D	6061	SSSP	Steel	No	6	320	203	35.6

APPENDIX C - SUMMARY OF DEFECT EXAMINATION RESULTS

Weld No.	Alloy	FSW	Defect Examination Results
3957A	7099	SSSPH	Defective: Surface defect
3957B	7099	SSSPH	Defective: Surface defect
3957C	7099	SSSPH	Defective: Surface defect
3957D	7099	SSSPH	Defective: Surface defect
3958A	7099	SSSPH	Defective: a little SD at AS; Defect free in nugget
3958B	7099	SSSPH	Defect free
3958C	7099	SSSPH	Defect free
3960A	7099	SSSPH	Defect free
3960B	7099	SSSPH	Defect free
3960C	7099	SSSPH	Defect free
3961A	7099	SSSPH	Defective: Surface defect
3961B	7099	SSSPH	Defective: Surface defect
3961C	7099	SSSPH	Defective: Surface defect
4309	7099	SSDP	Defect free
4310	7099	SSDP	Defect free
4094A	7099	CSSPH	Defective
4094B	7099	CSSPH	Defect free
4094C	7099	CSSPH	Defective: cracks and wormholes near AS between mid-plane and crown
4098A	7099	CSSPH	Defective
4098B	7099	CSSPH	Defective: cracks and wormholes near AS between mid-plane and crown

4098C	7099	CSSPH	Defect free
4226A	7099	CSDP	Defective: small hole at mid-plane AS
4226B	7099	CSDP	Defect free
4227A	7099	CSDP	Defective: SD; Large holes between mid-plane&bottom
4227B	7099	CSDP	Defective: SD; holes between mid-plane and bottom
4229	7099	CSDP	Defect free
4232A	7099	CSDP	Defect free
4232B	7099	CSDP	Defect free
4302	7099	CSDP	Defect free
4301	7099	CSDP	Defect free
3963A	7099	SSSP	Defective: Surface defect
3963B	7099	SSSP	Defective: Surface defect
3964A	7099	SSSP	Defective: Surface defect
3964B	7099	SSSP	Defective: Surface defect
3964C	7099	SSSP	Defective: Surface defect
3965A	7099	SSSP	Defective: Surface defect
3965B	7099	SSSP	Defective: Surface defect
3973A	7099	SSSP	Defective: SD; Cracks at mid-plane AS
3973B	7099	SSSP	Defective: Cracks at mid-plane AS
3974A	7099	SSSP	Defective: Surface defect
3974B	7099	SSSP	Defective: SD; cracks near root
3975A	7099	SSSP	Defective: SD; cracks near root at AS
3975B	7099	SSSP	Defective: cracks near root at AS
4106A	7099	SSSP	Defective: Hole defects near bottom center
4106B	7099	SSSP	Defective: Large hole defects at bottom AS
4107A	7099	SSSP	Defective: SD; Little defects at top AS
4107B	7099	SSSP	Defective: SD; Little defects at top AS
4114	7099	SSSP	Defective: small hole defects at mid-AS
4115	7099	SSSP	Defective: Surface defect
4116	7099	SSSP	Defective: small cracks at bottom AS
4167A	7099	SSSP	Defective: overheated?

4167B	7099	SSSP	Defect free
4167C	7099	SSSP	Defective: small hole between mid-plane and bottom AS
4171A	7099	SSSP	Defect free
4171B	7099	SSSP	Defect free
4171C	7099	SSSP	Defective: Surface defect
4171D	7099	SSSP	Defective: SD from crown to mid-plane
4306	7099	SSSP	Defect free
4153A	7099	CSSP	SD; Worm holes at top & mid-plane from AS to RS
4153B	7099	CSSP	Defective: SD; Small hole at mid-plane RS
4153C	7099	CSSP	SD; Small holes between crown and mid-plane AS
4154A	7099	CSSP	Defective: Small holes at AS near crown
4154B	7099	CSSP	Worm holes between crown and mid-plane AS
4154C	7099	CSSP	Defective: Worm holes at center AS
4155A	7099	CSSP	Defective: overheated?
4155B	7099	CSSP	Defective: overheated?
4155C	7099	CSSP	Defective: overheated?
4155D	7099	CSSP	Defective: Holes near center AS
4156A	7099	CSSP	Defective: Small holes at AS near crown
4156B	7099	CSSP	Defective: Worm holes at center AS
4163	7099	CSSP	Defective. Aborted due to too large torque
4164	7099	CSSP	Defective: overheated?
4165	7099	CSSP	Defective: overheated?
4166	7099	CSSP	Defective: overheated?
4299	7099	CSSP	Defective: Worm holes at mid
4315	7099	CSSP	Defective: Worm holes at center near root
4300	7099	CSSP	Defect free
4309	7099	SSDP	Defect free
4311	7099	SSDP	Defect free
4310	7099	SSDP	Defect free
4312	7099	SSDP	Defective: Worm holes at mid AS near crown
4226A	7099	CSDP	Defective: small hole at mid AS

4226B	7099	CSDP	Defect free
4227A	7099	CSDP	Defective: SD; Large holes between mid-plane& bottom
4227B	7099	CSDP	Defective: SD; holes between mid-plane and bottom
4228A	7099	CSDP	Defective: large holes between mid-plane and bottom
4228B	7099	CSDP	Defective: holes and cracks at mid-plane near AS
4229	7099	CSDP	Defect free
4230	7099	CSDP	Defect free
4231	7099	CSDP	Defect free
4232A	7099	CSDP	Defect free
4232B	7099	CSDP	Defect free
4233A	7099	CSDP	Defect free
4233B	7099	CSDP	Defect free
4237	7099	CSDP	Defective: small holes at AS near crown and mid-plane
4238	7099	CSDP	Defect free
4241	7099	CSDP	Defect free
4242	7099	CSDP	Defect free
4243	7099	CSDP	Defective: holes near mid-plane AS
4244	7099	CSDP	Defective: surface defect at AS
4302	7099	CSDP	Defect free
4304	7099	CSDP	Defect free
4301	7099	CSDP	Defect free
4303	7099	CSDP	Defect free
3966A	7050	SSSP	Defective: Surface defect
3966B	7050	SSSP	Defective: Surface defect
4168A	6061	SSSP	Defect free
4168B	6061	SSSP	Defect free
4169	6061	SSSP	Defect free
4170A	6061	SSSP	Defect free
4170B	6061	SSSP	Defect free
4170C	6061	SSSP	Defective: Holes at bottom AS
4170D	6061	SSSP	Defective: Holes at bottom AS